

**Physicochemical and Pharmacokinetic Characterization
of Carbohydrate Mimetics**

Inauguraldissertation

zur

Erlangung der Würde eines Doktors der Philosophie

vorgelegt der

Philosophisch-Naturwissenschaftlichen Fakultät

der Universität Basel

von

Simon Kleeb

aus Eriswil, BE, Schweiz

Basel, 2015

Originaldokument gespeichert auf dem Dokumentenserver der Universität Basel

edoc.unibas.ch

Genehmigt von der Philosophisch-Naturwissenschaftlichen Fakultät auf Antrag von

Prof. Dr. Beat Ernst, Institut für molekulare Pharmazie, Universität Basel

Dr. Manfred Kansy, F. Hoffmann-La Roche AG, Basel

Basel, den 18. Juni 2013

Prof. Dr. Jörg Schibler

Dekan

Acknowledgements

This thesis was only possible thanks to the support from many people to whom I am sincerely grateful.

First, I would like to thank Prof. Beat Ernst for entrusting me with challenging tasks in the broad area of pharmacokinetics, for offering me a workplace equipped with all I could wish, and for many fruitful discussions not only about pharmacokinetics and carbohydrate mimetics.

Several people from the laboratory deserve special thanks. I am particularly grateful to Dr. Matthias Wittwer for his great efforts in establishing several assays and methods which I could adapt for my own work and on which I was able to build up my further projects. I would also like to thank him for making me familiar with the challenges of LC-MS analytics and for supporting me with many advices during the first year of my PhD studies. My sincere thanks go to Jacqueline Bezençon for taking over the project and for many interesting questions, discussions, and helpful solutions. Furthermore, I would like to express my gratitude to Dr. Katharina Mayer, Dr. Lijuan Pang, Wojciech Schönemann, Dr. Oliver Schwardt, and Dr. Xiaohua Jiang for synthesizing all the test compounds – a crucial prerequisite for the success of my thesis. Many thanks go to my master students Florentina Schädler, Philipp Dätwyler, and Marcel Lindegger for their great effort in the laboratory and for their big contribution to my projects. Finally, I would also like to thank all other members, past or present, of the Institute of Molecular Pharmacy, for their help, the many stimulating discussions, and for all the adventures and activities we experienced together.

I would like to express my gratitude to Dr. Manfred Kansy for being the co-referee in the thesis-committee. At Roche, I am furthermore thankful to Dr. Christoph Funk and his collaborators for sharing their knowledge and experience in implementing the assays addressing drug metabolism.

Finally, I would like to thank my family for their many encouraging words and their constant help and support not only during my PhD studies.

Preface

The work described in this thesis was conducted by Simon Kleeb from November 2009 until May 2013 at the Institute of Molecular Pharmacy, University of Basel, under the supervision of Prof. Dr. Beat Ernst.

Parts of the thesis have been published in peer reviewed journals. These articles are included in the thesis and are termed as *Papers*. Manuscripts that have not yet been submitted for publication are marked as *Manuscripts*. Further work is described in *Chapters*. Prior to each section, the contribution of the author to the respective project is mentioned. On account of clarity, the references are listed at the end of each section.

Articles published in peer-reviewed journals:

Kleeb, S.*; Pang, L.*; Mayer, K.*; Eris, D.*; Sigl, A.*; Preston, R. C.; Zihlmann, P.; Sharpe, T.; Jakob, R. P.; Abgottspon, D.; Hutter, A. S.; Scharenberg, M.; Jiang, X.; Navarra, G.; Rabbani, S.; Smiesko, M.; Lüdin, N.; Bezençon, J.; Schwaradt, O.; Maier, T.; Ernst, B. FimH antagonists: bioisosteres to improve the in vitro and in vivo PK/PD profile. *J. Med. Chem.* **2015**, *58*, 2221-2239.

Pang, L.*; Kleeb, S.*; Lemme, K.*; Rabbani, S.*; Scharenberg, M.; Zalewski, A.; Schädler, F.; Schwaradt, O.; Ernst, B. FimH antagonists: structure-activity and structure-property relationships for biphenyl α -D-mannopyranosides. *ChemMedChem* **2012**, *7*, 1404-1422.

Jiang, X.*; Abgottspon, D.*; Kleeb, S.*; Rabbani, S.; Scharenberg, M.; Wittwer, M.; Haug, M.; Schwaradt, O.; Ernst, B. Antiadhesion therapy for urinary tract infections – a balanced PK/PD profile proved to be key for success. *J. Med. Chem.* **2012**, *55*, 4700-4713.

Schwaradt, O.; Rabbani, S.; Hartmann, M.; Abgottspon, D.; Wittwer, M.; Kleeb, S.; Zalewski, A.; Smiesko, M.; Cutting, B.; Ernst, B. Design, synthesis and biological evaluation of mannosyl triazoles as FimH antagonists. *Bioorg. Med. Chem.* **2011**, *19*, 6454-6473.

Klein, T.*; Abgottspon, D.*; Wittwer, M.*; Rabbani, S.*; Herold, J.*; Jiang, X.; Kleeb, S.; Lüthi, C.; Scharenberg, M.; Bezençon, J.; Gubler, E.; Pang, L.; Smiesko, M.; Cutting, B.; Schwaradt, O.; Ernst, B. FimH antagonists for the oral treatment of urinary tract infections: from design and synthesis to in vitro and in vivo evaluation. *J. Med. Chem.* **2010**, *53*, 8627-8641.

* contributed equally

Posters presented at scientific meetings:

Kleeb, S.; Pang, L.; Abgottspon, D.; Ernst, B. Development of orally available FimH antagonists for the treatment of urinary tract infections. *XXIInd International Symposium on Medicinal Chemistry EFMC/ISMC 2012*, Berlin, Germany.

Kleeb, S.; Wittwer, M.; Ernst, B. Development of orally available FimH antagonists for the treatment of urinary tract infections. *Gordon Research Conference on Drug Metabolism 2011*, Holderness, MA, USA.

Kleeb, S.; Wittwer, M.; Ernst, B. Ester prodrugs: how the chemical structure influences the hydrolysis rate. *Annual Research Meeting of the Department of Pharmaceutical Sciences 2011*, Basel, Switzerland.

Wittwer, M.; Kleeb, S.; Bezençon, J.; Gubler, E.; Cutting, B.; Ernst, B. PADMET-platform: pharmacokinetic profiling of glycomimetics. *Swiss Pharma Science Day 2010*, Bern, Switzerland.

Abstract

Urinary tract infection by uropathogenic *Escherichia coli* is one of the most frequent infectious diseases requiring an antibiotic treatment. Since the recurrent exposure to antibiotics leads to the emergence of antibacterial resistance, alternative prevention and treatment strategies are urgently needed.

The interaction of the bacterial lectin FimH with mannosylated glycoproteins on the surface of the bladder mucosa is the initial step triggering the infection. Biaryl α -D-mannopyranosides were identified as potent FimH antagonists preventing this first contact.

The present thesis describes the development of two biaryl mannosides, that are, the biphenyl mannoside bearing a *para*-carboxylate on the terminal ring of the aglycone and the 5-nitroindoliny phenyl mannoside, towards drug-likeness. For this purpose, various approaches, such as the introduction of ester or phosphate prodrugs, the replacement of essential substituents with bioisosteres, the optimization of the substitution pattern, or the introduction of aromatic heterocycles, were explored. Several assays addressing the characterization of the physicochemical and *in vitro* pharmacokinetic properties, *i.e.* pK_a , lipophilicity, aqueous solubility, membrane permeability, plasma protein binding, chemical and metabolic stability, were implemented for the identification of the most successful strategies providing high oral bioavailability, metabolic stability, and sustained renal clearance as major route of drug elimination.

As a result of our thorough studies, two approaches proved most advantageous for the development of orally available FimH antagonists: first, the prodrug approach, *i.e.* the introduction of an alkyl promoiety masking the carboxylic acid substituent of the biphenyl mannoside or the creation of phosphate monoester prodrugs conferring high aqueous solubility, and second, the replacement of the carboxylic acid with bioisosteres providing optimal physicochemical properties for oral absorption and renal excretion.

Abbreviations

ABC-transporter	ATP-binding cassette transporter
ADMET	absorption, distribution, metabolism, excretion, toxicity
ALP	alkaline phosphatase
ATP	adenosine 5'-triphosphate
AUC	area under the curve
BBB	blood brain barrier
BChE	butyrylcholinesterase
BNPP	bis(4-nitrophenyl) phosphate
<i>C</i>	concentration
Caco-2 cells	human colorectal adenocarcinoma cells
CES	carboxylesterase
CL'_{int}	intrinsic clearance
CRD	carbohydrate recognition domain
CYP450	cytochrome P450
<i>D</i>	distribution coefficient
DMEM	Dulbecco's Modified Eagle's Medium
DMSO	dimethyl sulfoxide
DPBS	Dulbecco's Phosphate Buffered Saline
ER	endoplasmic reticulum
FBS	fetal bovine serum
f_b	fraction bound
f_u	fraction unbound
GFR	glomerular filtration rate
GSE	general solubility equation
hCE1	human carboxylesterase 1
hCE2	human carboxylesterase 2
hERG	human Ether-à-go-go-Related Gene
HLM	human liver microsomes
HPLC	high-performance liquid chromatography
IC ₅₀	half maximal inhibitory concentration
<i>J</i>	drug flux (mass per area per time)
K_a	acid dissociation constant

Abbreviations

LC-MS	liquid chromatography-mass spectrometry
MAD	maximum absorbable dose
MDCK cells	Madin Darby Canine Kidney cells
MeCN	acetonitrile
MeOH	methanol
MP	melting point
MTT	thiazolyl blue tetrazolium bromide
NADPH	nicotinamide adenine dinucleotide phosphate
NMR	nuclear magnetic resonance
OAT	organic anion transporter
OCT	organic cation transporter
OD	optical density
P	partition coefficient
PAMPA	parallel artificial membrane permeability assay
PDB	protein data bank
P_{app}	apparent permeability
P_e	effective permeability
PPB	plasma protein binding
PSA	polar surface area
RLM	rat liver microsomes
S	solubility
S9 fraction	supernatant obtained from differential centrifugation at 9000g
SGA	spectral gradient analysis
SITT	small intestinal transit time
SIWV	small intestinal water volume
SLC	solute carrier
$t_{1/2}$	half-life
TEER	transepithelial electrical resistance
TRIS	Tris(hydroxymethyl)aminomethane
UDP	uridine 5'-diphosphate
UDPGA	uridine 5'-diphosphoglucuronic acid
UPEC	uropathogenic <i>Escherichia coli</i>
UTI	urinary tract infection
UV/Vis spectroscopy	ultraviolet-visible spectroscopy

Table of contents

1. Introduction.....	11
1.1. Urinary tract infection.....	11
1.1.1. Pathogens and the infection cycle.....	11
1.1.2. Type I pilus – structure and assembly.....	12
1.1.3. The bacterial lectin FimH.....	13
1.2. FimH antagonists.....	13
1.3. Drug delivery to the urinary bladder: pharmacokinetic aspects.....	14
1.3.1. Oral bioavailability.....	14
1.3.2. Metabolic stability.....	17
1.3.3. Renal excretion.....	17
1.4. Carbohydrate derivatives: absorption and disposition.....	18
1.4.1. Strategies for achieving ‘drug-likeness’.....	18
1.5. ADME profiling.....	20
1.5.1. Physicochemical parameters.....	20
1.5.2. Absorption.....	22
1.5.3. Distribution.....	23
1.5.4. Metabolism.....	24
1.5.5. Excretion.....	25
1.6. Aims of the thesis.....	27
2. Results and discussion.....	35
2.1. Outline.....	35
2.2. <i>Paper 1</i>	37
FimH antagonists for the oral treatment of urinary tract infections: from design and synthesis to <i>in vitro</i> and <i>in vivo</i> evaluation	
2.3. <i>Chapter 2</i>	53
FimH antagonists: ester prodrugs with improved oral bioavailability	
2.4. <i>Manuscript 3</i>	85
FimH antagonists – solubility vs. oral availability	
2.5. <i>Paper 4</i>	123
FimH Antagonists: Structure-activity and structure-property relationships for biphenyl α -D-mannopyranosides	

2.6.	<i>Manuscript 5</i>	143
	Urinary tract infection – which FimH conformation is therapeutically relevant?	
2.7.	<i>Paper 6</i>	179
	FimH antagonists: bioisosteres to improve the <i>in vitro</i> and <i>in vivo</i> PK/PD profile	
2.8.	<i>Chapter 7</i>	199
	Prodrugability of carbohydrates – investigations on FimH antagonists	
2.9.	<i>Paper 8</i>	225
	Antiadhesion therapy for urinary tract infections – a balanced PK/PD profile proved to be key for success	
2.10.	<i>Manuscript 9</i>	241
	FimH antagonists – phosphate prodrugs improve oral bioavailability	
2.11.	<i>Paper 10</i>	269
	Design, synthesis and biological evaluation of mannosyl triazoles as FimH antagonists	
3.	Summary and outlook.....	291

1 Introduction

1.1 Urinary tract infection

Urinary tract infection (UTI) is one of the most frequent bacterial infections worldwide, which affects millions of people – particularly women – every year and accounts for high medical costs.¹ As many as 60% of women experience at least one UTI episode during their lifetime, and approximately 30-40% of patients suffer from at least one recurrence.² Acute, uncomplicated lower urinary tract infection, commonly referred to as cystitis or bladder infection, requires an antibiotic treatment to tackle the symptoms, which are dysuria, frequent and urgent urination, bacteriuria, and pyuria, and to prevent more devastating or even life threatening complications like pyelonephritis and urosepsis.³ The first-line treatment for uncomplicated UTI is a three-day antibiotic treatment with a combination of trimethoprim-sulfamethoxazole or with fluoroquinolone (*e.g.* ciprofloxacin).⁴ However, the repeated use of antibacterial chemotherapeutics can lead to the emergence of antimicrobial resistance and, as a consequence, to treatment failure.⁵ Increasing resistance faces a limited number of marketed antiinfectives, which manifests the need for novel, non-antibiotic strategies to prevent and treat UTI.

1.1.1 Pathogens and the infection cycle

About 80-85% of manifest episodes of UTI are caused by uropathogenic *Escherichia coli* (UPEC). About 5-15% are caused by *Staphylococcus saprophyticus*, whereas *Klebsiella pneumoniae* and *Proteus mirabilis* occur in small numbers.⁶

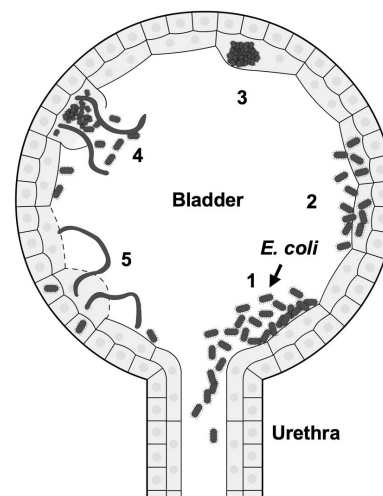


Figure 1.1. Infection cycle of uropathogenic *E. coli* (UPEC) in the lower urinary tract (adopted from Ref. 9). Initial bacterial adhesion (1) to the urothelial cells is mediated by type 1 pili binding to mannosylated glycoproteins on the cell surface. UPEC consequently invade into the cells (2) where they start replicating and forming intracellular biofilms (3), which protect them from host defense mechanisms and antibiotic treatment. UPECs are released as filamentous structures upon exfoliation of bladder epithelial cells (4) and spread in the surrounding tissue where they can infect further urothelial cells (5).

UPEC undergo a well-defined infection cycle within the host (Figure 1.1).⁷⁻⁹ Bacterial adherence to the epithelial cells in the lower urinary tract is the first step of the pathogenesis (1). This interaction is mediated by bacterial type 1 pili, which target the mannosylated glycoprotein uroplakin Ia on the surface of the urinary bladder mucosa.¹⁰ This initial step of adhesion prevents UPEC from being removed from the bladder by micturition and, at the same time, initiates the invasion into the bladder epithelial cells (2). Once within the host cells, UPEC start replicating and forming intracellular biofilms (3), which protect them from host defense mechanisms and antibiotic treatment. In response to the infection, the epithelial cells start exfoliating (4), whereupon the bacteria leave the cells as filamentous structures and spread in the environment (5), where they can infect surrounding urothelial cells.

1.1.2 Type I pilus – structure and assembly

The type 1 pilus, mediating the initial contact of the bacterium to the host cell, is composed of a helical rod formed by 500 to 3000 copies of the main structural subunit FimA and of a linear tip fibrillum formed by FimG and FimF and by the mannose specific adhesin FimH.¹¹

The pilus rod is assembled through a chaperone-usher pathway (Figure 1.2). Each subunit has an incomplete immunoglobulin-like fold, with a missing C-terminal beta strand. During the assembly in the bacterial periplasm, the subunit is bound to the chaperone protein FimC, which donates the missing beta strand and stabilizes the subunit. Upon the delivery to FimD – the usher – it is released from FimC and linked to the next subunit, which itself donates the missing beta strand.¹²

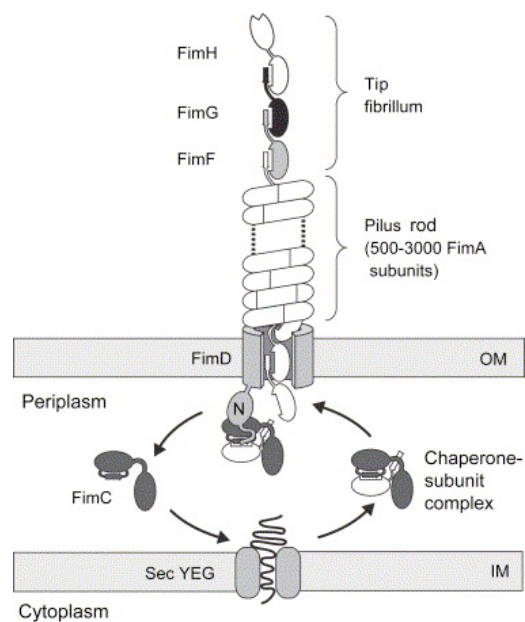


Figure 1.2. Schematic representation of type 1 pili and their assembly through the chaperone-usher pathway (adopted from Ref. 12). The chaperone protein FimC in the periplasm binds pilus subunits, accelerates the folding, and delivers the subunits to the transmembrane assembly platform FimD – the usher – for their incorporation into the pilus. The bacterial lectin FimH is located on the tip of the pilus.

1.1.3 The bacterial lectin FimH

The adhesin FimH located at the tip of the type 1 pilus consists of two immunoglobulin-like domains: the N-terminal lectin domain (residues 1 – 156) and – connected by a short linker – the C-terminal pilin domain (residues 160 – 279).¹³ The lectin domain encloses the carbohydrate recognition domain (CRD) binding to the oligomannosides present on the cell surface, whereas the pilin domain anchors the adhesin into the pilus and regulates the switch between the low- and high-affinity states of the lectin domain.¹⁴ The CRD, as characterized from the crystal structure of FimH with α -D-mannose (PDB code 1KLF),¹⁵ consists of a deep, negatively charged pocket which accommodates the mannose by means of an extended hydrogen bond network. The entrance to the binding site is composed of three hydrophobic amino acids (Tyr 48, Tyr 137, and Ile 52) and is therefore referred to as the “tyrosine gate”. When FimH was crystallized with *n*-butyl α -D-mannopyranoside (PDB code 1UWF), the butyl moiety provided van der Waals interactions with the tyrosine gate.¹⁶ This observations sparked the development of α -D-mannopyranosides with hydrophobic aglycones as FimH antagonists.

1.2 FimH antagonists

The inhibition of the initial bacterial adherence by FimH antagonists is a promising approach to tackle the resistance problem of the current antibiotic treatment strategies.¹⁷ Besides being efficacious, these anti-adhesive compounds should however fulfill a set of requirements: they must be orally available, inexpensive, and safe and should not induce antimicrobial resistance mechanisms.

In the late 1970s, Sharon and coworkers identified methyl α -D-mannopyranoside (**1**) as an inhibitor of the bacterial adherence to the epithelial cells.¹⁸ However, only weak interactions in the milli- to micromolar range were observed. For the further improvement, two different approaches were explored. First, multivalent mannosides showing nanomolar affinities to the carbohydrate recognition domain (CRD) were identified¹⁹⁻²¹ and second, the affinity of monovalent α -D-mannopyranosides was optimized by modifications of the aglycone portion. Bouckaert and coworkers investigated different alkyl α -D-mannopyranosides as potential FimH antagonists and identified a length of seven carbon atoms, such as present in *n*-heptyl α -D-mannopyranoside (**2**), to be optimal for target affinity.¹⁶ Otherwise, aromatic glycosides were described, such as *p*-nitrophenyl α -D-mannopyranoside (**3**) showing a 30 times higher inhibitory effect than methyl α -D-mannopyranoside.²²⁻²⁴ Extension of the aromatic aglycone

led to squaric acid monoamide derivatives (\rightarrow **4**),^{25, 26} biphenyl mannosides modified with a carboxylic acid substituent (\rightarrow **5a-f**),²⁷⁻³⁰ and indolyl phenyl mannosides (\rightarrow **6**).³¹ These structures show a high affinity in the nanomolar range because of additional hydrophobic interactions of the aglycone with the aromatic residues of the tyrosine gate. However, the binding modes can differ. The aglycones of the alkyl mannosides, for example, reside between Tyr48 and Tyr137 of the tyrosine gate.¹⁶ By contrast, the bulky aromatic aglycones adopt a different conformation, in which the interaction occurs only with Tyr48, as suggested by the X-ray crystal structure of FimH co-crystallized with the biphenyl mannoside **5a**.²⁷ Electron withdrawing substituents on the terminal ring of the biaryl aglycone, *e.g.* the carboxylic acid present in the biphenyl derivatives **5a-f**^{27, 28, 30} or the nitro group in antagonist **6**³¹, furthermore enforce the π - π stacking interactions with the electron rich Tyr48. A representative set of the most important monovalent FimH antagonists are summarized in Figure 1.3.

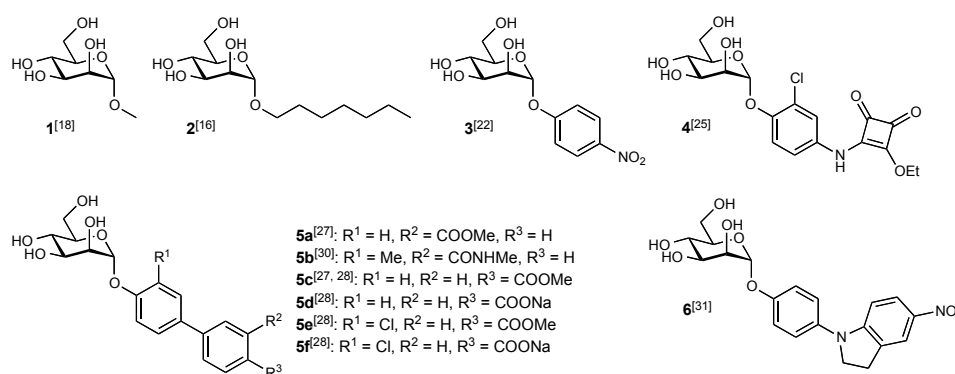


Figure 1.3. Alkyl and aryl α -D-mannopyranosides identified as potent FimH antagonists.

1.3 Drug delivery to the urinary bladder: pharmacokinetic aspects

For reasons of convenience, oral dosing is basically the preferential route of drug application for the treatment of UTI. Oral bioavailability, metabolic stability, and renal excretion are therefore key issues for delivering orally dosed FimH antagonists to the urinary bladder.

1.3.1 Oral bioavailability

Oral bioavailability, defined by the U.S. Food and Drug Administration as ‘the rate and extent to which the active ingredient or active moiety is absorbed from a drug product and becomes available at the site of action’,³² relies first on the rapid and quantitative dissolution

of the applied dose in the intestine, second on the transfer across the membranes lining the intestine by means of passive diffusion or carrier-mediated transport, and third on the stability against metabolic modifications during the absorption in the enterocytes and during the first pass through the liver.^{33, 34} This subchapter sets the focus on aqueous solubility and membrane permeability, which are the key determinants of absorption in the small intestine.³⁵ Metabolic stability will be exposed in the subsequent section.

Aqueous solubility. Since only drug molecules dissolved in the aqueous intestinal fluids are available for absorption, rapid and quantitative dissolution of the orally administered dose is the first requirement for achieving oral bioavailability. Aqueous solubility, *i.e.* the maximum amount of drug which can remain in solution under equilibrium conditions, primarily depends on the crystallinity of the solute, its interaction with the aqueous solvent, and the conditions predominant in the medium, *e.g.* pH, temperature, and the presence of solubilizing components.³⁶ Melting point (*MP*) and lipophilicity as quantified by the octanol-water partition coefficient ($\log P$) are key physicochemical determinants of solubility, the former as descriptor of the lattice energy lost in the dissolution process, the latter accounting for the interaction of the solute with water.³⁷ Combining *MP* (in degree centigrade) and $\log P$, the general solubility equation (GSE, Equation 1) estimates the molar solubility (*S*) of nonelectrolytic solid drug in aqueous medium.

$$\log S_w^{solid} = 0.5 - 0.01(MP - 25) - \log P \quad (1)$$

Membrane permeability. Passive diffusion and carrier-mediated transport both contribute to the intestinal absorption, with passive diffusion as the primary mechanism.³⁸ Diffusion by either the paracellular route or the transcellular pathway is a concentration gradient driven mass transport, which is not saturable. The route between the cells is basically reserved for small, hydrophilic molecules.³³ The ease to permeate the intestinal mucosa on the transcellular route (*i.e.* the membrane permeability) relies on the physicochemical properties of the whole molecule. In their seminal publication, Lipinski *et al.* introduced key physicochemical predictors of permeability, that are, molecular weight, number of hydrogen bond donor groups, number of hydrogen bond acceptor groups, and lipophilicity as quantified by the octanol-water partition coefficient ($\text{clog } P$).³⁹ Moreover, Veber *et al.* revealed a positive influence of increasing molecular rigidity, as measured by the rotatable bond count, and a negative impact of increasing polar surface area (PSA) on permeability.⁴⁰

In contrast to passive diffusion, carrier-mediated transcellular permeation is substrate specific and saturable. There exist two types of carrier-mediated permeation: facilitated diffusion and active transport. Facilitated diffusion means the spontaneous transfer of polar molecules or ions through transmembrane carrier proteins along a concentration gradient. Active transport means the carrier-mediated transfer of substrate across the membrane against the concentration gradient under consumption of energy provided by adenosine-5'-triphosphate (ATP). Intestinal epithelial cells express in their apical membrane several transporters of the solute carrier (SLC) superfamily supporting drug uptake, as well as ATP-dependent efflux pumps interfering with drug absorption.⁴¹

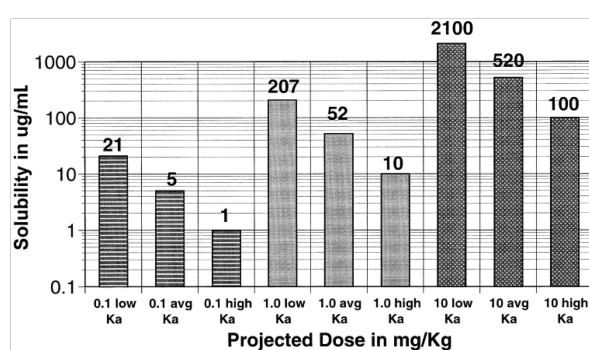


Figure 1.4. Minimum acceptable solubility in $\mu\text{g/mL}$ (adapted from Ref. 44). The columns represent the minimum solubility for low, medium and high permeability (k_a) compounds at a projected clinical dose of 0.1, 1.0, and 10 mg/kg body weight. The left three columns are for a 0.1 mg/kg dose, the middle three columns are for a 1.0 mg/kg dose, and the right three columns are for a 10 mg/kg dose. Within each group, the left column represents low permeability, the middle column represents medium permeability, and the right column represents high permeability. For the absorption of a 1.0 mg/kg dose of a drug with medium permeability, minimum solubility of 52 $\mu\text{g/mL}$ is needed.

Intestinal absorption. The absorptive flux per time per area (J) is proportional to the product of the permeability of the mucosa to the drug and the concentration gradient between the intestinal lumen and the portal blood (Equation 2):

$$J = P_e \times \Delta C \quad (2)$$

where P_e is the effective permeability, and ΔC is the concentration gradient across the mucosa.^{34, 42} The maximum drug concentration in the intestinal lumen, in turn, is delimited by its aqueous solubility. The concept of maximum absorbable dose (MAD)⁴² integrates the different aspects of drug absorption and is defined as follows (Equation 3):

$$MAD = S \times k_a \times SIWV \times SITT \quad (3)$$

where S is the aqueous solubility, k_a is the intestinal absorption rate constant as determined from intestinal perfusion experiments, $SIWV$ is the small intestinal water volume (around 250 mL), and $SITT$ is the small intestinal transit time (around 270 min).⁴³ By rearranging Equation 3, Lipinski defined the minimum solubility required for quantitative intestinal absorption of low, medium, and high permeability compounds at projected doses of 0.1, 1.0, or 10 mg/kg body weight (Figure 1.4).⁴⁴

1.3.2 Metabolic stability

Drug metabolism includes various enzyme-mediated biotransformation reactions which lead towards more hydrophilic and water-soluble molecules than the parent compound.⁴⁵ Intestinal and hepatic first pass metabolism impairs the compound availability in the bloodstream and promotes, in case of the FimH antagonists, undesired, non-renal clearance which prevents the antagonist from reaching the therapeutic target in the urinary bladder.⁴⁶ Drug metabolism is mediated by phase I (hydrolysis, oxidation, or reduction) or phase II (conjugation) reactions. The cytochrome P450 (CYP450) enzyme superfamily, which catalyzes mono-oxygenase reactions, plays a dominating role in phase I biotransformation. Smith *et al.* defined three key determinants for CYP450 mediated metabolism,⁴⁷ which are:

1. The topography of the active site.
2. The degree of steric hindrance of the access of the iron-oxygen complex to the possible sites of metabolism.
3. The possible ease of electron or hydrogen abstraction from the various carbons or heteroatoms of the substrate.

1.3.3 Renal excretion

Renal excretion, *i.e.* the transfer of drug from the bloodstream into the urine, equals the sum of different mechanisms including glomerular filtration, tubular secretion and tubular reabsorption.⁴⁸ The rate of glomerular filtration (GFR) corresponds to about 10% of the renal blood flow at the glomerulus of the nephron (about 125 mL/min in a 70-kg young male), and the primary criterion determining whether a molecule enters the ultrafiltrate is its molecular size.⁴⁹ Consequently, drug molecules bound to plasma proteins are predominantly rejected by the glomerular sieve, whereas the fraction of unbound drug enters the ultrafiltrate. Clearance by glomerular filtration therefore equals the product of GFR and plasma free fraction (f_u).⁵⁰

Secretion from the plasma into the proximal tubular lumen is primarily carrier mediated and, as a consequence, substrate specific and saturable. Organic cation transporters (OCT) and

organic anion transporters (OAT) localized on the basolateral membrane of the proximal tubule cells constitute the majority of the key carrier involved in secretion.⁴¹ By contrast, tubular reabsorption from the primary urine into plasma primarily depends on passive permeation. The extensive tubular water reuptake from the ultrafiltrate creates a concentration gradient, which drives the diffusion through the membranes.⁵¹ The octanol-water distribution coefficient at pH 7.4 ($\log D_{7.4}$) was identified as key predictor for passive tubular reuptake^{47, 52} and for plasma protein binding,⁵³ which in turn determines the $\text{GFR} \cdot f_u$ factor of the glomerular filtration.

1.4 Carbohydrate derivatives: absorption and disposition

In recent years, only few carbohydrate derived drugs have reached the market despite the importance of carbohydrate-protein interactions not only for the establishment of UTI but for a vast array of biological processes.⁵⁴ The pharmacokinetic properties inherent in carbohydrates and carbohydrate mimetics scarcely fit the requirements for oral bioavailability described above. Because of their high polarity, they are barely capable to cross the intestinal membranes by the passive transcellular pathway. Moreover, once systemically available, the polar carbohydrate derivatives suffer from rapid renal excretion, unless binding to blood plasma components is possible. As a consequence, carbohydrate derivatives require a parenteral application (*e.g.* low-molecular weight heparins and fondaparinux⁵⁵ used as coagulants) or they exert their therapeutic effects in the small intestine and do therefore not need to be absorbed into circulation upon oral dosing (*e.g.* voglibose⁵⁶, miglitol⁵⁷, acarbose⁵⁸ used as α -glycosidase inhibitors).

1.4.1 Strategies for achieving ‘drug-likeness’

For achieving ‘drug-likeness’,⁵⁹ the pharmacokinetic profile of the carbohydrate derivatives needs to be adjusted towards enhanced lipophilicity, which conduces to both membrane permeability and plasma protein binding.⁶⁰ However, these modifications should not constrain aqueous solubility, which is basically favored by high polarity, or increase the propensity to metabolic biotransformations. Strategies for optimizing the pharmacokinetic profile are modifications of the substitution pattern,⁶¹ the bioisosteric replacement of crucial groups,⁶² or the prodrug approach.⁶³

Bioisosteres. Exploring bioisosteres, *i.e.* structurally distinct moieties that are similarly recognized by the drug target, is an appealing strategy for altering the physicochemical properties of a lead compound (*e.g.* lipophilicity or pK_a).⁶⁴ Classical bioisosteres include structurally simple mono-, di-, trivalent atoms or groups as well as ring equivalents, whereas nonclassical bioisosteres extend the concept to elements that comprise a different number of atoms and exhibit different steric and electronic properties compared to the functionality being emulated. Meanwell comprehensively reviewed classical and nonclassical bioisosteres recently used in the drug design.⁶² The angiotensin receptor II-antagonist Losartan (Figure 1.5) is a marketed drug where a bioisosteric replacement was successfully applied to optimize the pharmacokinetic properties.⁶⁵ The replacement of a terminal carboxylic acid group with an isosteric tetrazole ring conferred the required oral activity and duration of action.

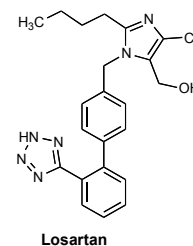


Figure 1.5. Bioisosteres. During development of the angiotensin receptor II-antagonist Losartan, oral bioavailability was achieved by replacing the terminal carboxylic acid group with an isosteric tetrazole ring.⁶⁵

Prodrugs. Bioreversible derivatives that are enzymatically reconverted to the active parent compound have become an established tool for improving the intestinal absorption potential by increasing membrane permeability or aqueous solubility.⁶⁶

Poor membrane permeability can be overcome by masking polar moieties of the molecule. The most common prodrug approach is therefore the esterification of an acid group with an alkyl alcohol that, upon absorption from the intestine, is cleaved by hepatic or plasma-borne esterases. Beaumont *et al.* comprehensively reviewed the prerequisites for a successful ester prodrug approach.⁶³ One example of a marketed ester prodrug is oseltamivir phosphate used as neuraminidase inhibitor in the prevention of influenza virus infections (Figure 1.6a). Starting from a carbohydrate lead, the structure was optimized by eliminating polar groups and metabolic “soft spots” and by finally designing an ester prodrug to reach oral bioavailability.⁶⁷ Upon absorption, the ester is hydrolyzed to the active carboxylate RO64-0802 with an absolute bioavailability of 80%.⁶⁸ The active principle can be detected in the plasma within 30 minutes after application of the prodrug and reaches maximal concentrations after 3-4 hours.⁶⁹

Aqueous solubility of a candidate molecule can be enhanced by adding a phosphate promoiety, which is rapidly cleaved by the endogenous alkaline phosphatase enzyme in the intestinal lumen upon dissolution, but before absorption.⁷⁰ Although there are many marketed phosphate prodrugs for parenteral administration, only few of them have been developed exclusively for oral administration.⁷¹ Fosamprenavir calcium (Figure 6b), an orally administered prodrug, is a phosphate ester of the HIV protease inhibitor Amprenavir. The prodrug shows better water solubility and as a consequence higher oral bioavailability than the pharmacologically active parent compound.⁷²

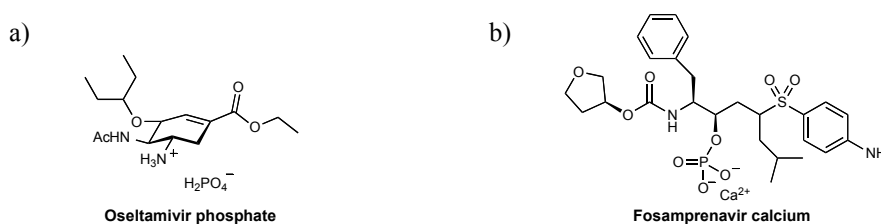


Figure 1.6. Prodrugs. (a) For improving the permeability through the intestinal membranes, the polar carboxylic acid moiety of Oseltamivir was masked by an ethyl ester.⁶⁷ (b) The aqueous solubility of Amprenavir, an HIV-protease inhibitor, was improved by a phosphate ester approach (Fosamprenavir calcium).⁷²

1.5 ADME profiling

A thorough pharmaceutical profiling during the lead identification and optimization process supports the identification of the most promising strategies for achieving ‘drug-likeness’ and enables the research team to specifically address unfavorable pharmacokinetic properties of the lead structure.⁷³ Current profiling methods *in silico* and *in vitro* cover specific pharmacokinetic aspects of absorption, distribution, metabolism, or excretion and are therefore referred to as ADME studies, or they set the focus on the physicochemical properties which are the underlying descriptors for these processes. The following section summarizes the most common parameters and the corresponding *in vitro* assays. An excellent overview of the concepts can also be gained from Kerns *et al.*,⁴⁵ furthermore presenting information on *in silico* and *in vivo* approaches.

1.5.1 Physicochemical parameters

Lipophilicity. The tendency of a compound to partition into a nonpolar matrix versus an aqueous matrix has been correlated to various drug properties, including permeability, absorption, distribution, plasma protein binding, metabolism, elimination, and toxicity.⁶⁰

Traditionally, the partitioning is determined between octanol and aqueous buffer and quantified as partition coefficient ($\log P$) or distribution coefficient ($\log D$). The partition coefficient describes the partitioning at a pH where all of the compound molecules are in the neutral form, whereas $\log D$ is determined for ionizable compounds at a specified pH. In general, ions have a lower affinity for the nonpolar phase than the unionized portion. Unlike the partition coefficient, $\log D$ therefore depends on the pH of the aqueous buffer, on the pK_a of the compound, and on whether the compound is an acid or a base.⁷⁴ For predicting a compound's lipophilicity, various *in silico* tools have been developed.⁷⁵ The CLOGP methods predict the $\log P$ of a substance by first breaking it up into substructures with experimentally determined $\log P$ and then calculating the sum of the individual contributions. Otherwise, the MLOGP method introduced by Moriguchi estimates the lipophilicity based on 13 parameters determined for each compound individually.⁷⁶ The gold standard for the experimental determination of $\log D$ is the shake-flask approach,⁷⁷ where an aqueous compound solution and *n*-octanol are brought together and vigorously shaken. Upon separation, the concentrations of analyte are determined in both phases and the ratio of the concentrations is calculated to obtain the coefficient. Further methods commonly used for $\log D$ determination include reversed-phase HPLC,⁷⁸ capillary electrophoresis,⁷⁹ and pH-metric approaches.⁸⁰

Aqueous solubility. The maximum concentration that a compound reaches in a solvent at equilibrium with solid compound is a key property, because low solubility compromises the outcome of activity or property assays *in vitro* as well as the oral bioavailability *in vivo* (*vide supra*).⁸¹ It is important to distinguish between 'kinetic' and 'thermodynamic' solubility. For determining the kinetic solubility, the compound is entirely dissolved in an organic solvent (*e.g.* DMSO) and then titrated to the aqueous buffer until precipitation can be observed. The equilibrium between dissolved and solid compound is usually not reached, because the precipitates can be in a metastable crystalline form. Typically, the kinetic solubility is determined in early drug discovery as a high throughput assay by use of one of the following methods: the direct UV method,⁸² where the concentration of solute upon filtration is determined against a single point standard, or the nephelometric and the turbidimetric methods,^{39, 83} which directly measure the precipitation of the added compound from the solution once it exceeds the solubility. For determining the thermodynamic solubility,⁷⁴ solid compound is directly added to aqueous buffer and stirred until it reaches an equilibrium between dissolved and solid state. Upon filtration, the concentration of solute in the

supernatant is determined by LC-MS. The thermodynamic solubility is usually assessed for crystalline material at later stages of drug discovery and development and is most relevant for formulation and clinical development.

pK_a . The negative logarithm of the acid dissociation constant (K_a) indicates a compound's ionizability, *i.e.* it defines the fractions of ionized and neutral species of an acid or a base in aqueous solution at a given pH. In general, ionized molecules are more polar than neutral molecules. Therefore, the pK_a of a drug affects various properties, such as the aqueous solubility at a given pH, the permeability through biological membranes, the plasma protein binding, or the excretion via the bile or the kidney.⁸⁴ Different *in silico* tools have been developed for pK_a prediction. Commercially available software were comprehensively reviewed by Balogh *et al.*⁸⁵ and Liao and Nicklaus.⁸⁶ Methods for the experimental pK_a determination include spectral gradient analysis (SGA),⁸⁷ NMR spectroscopy,⁸⁸ capillary electrophoresis,⁸⁹ or potentiometric titration.⁹⁰

1.5.2 Absorption

Along with the concentration gradient through the intestinal mucosa primarily determined by the applied dose or the compound's solubility, permeability is a key factor of the absorptive flux. Several assays exist for assessing the ability to permeate the membrane at an early stage of drug discovery and development. Currently, two approaches are commonly applied: First, artificial membrane permeation methods which model passive diffusion mechanisms; second, cell layer methods that consider passive diffusion, active uptake, efflux, and paracellular permeation.

Parallel artificial membrane permeability assay (PAMPA): Introduced by Kansy *et al.*, PAMPA is a cost-effective high throughput assay for passive diffusion assessment.⁹¹ In brief, test compound dissolved in buffer is placed in a 96-well plate - the 'donor plate'. The filter membranes of a 96-well filter plate - the 'acceptor plate' - are infused with a phospholipid-solvent mixture, which soaks into the holes of the filter and forms the artificial membrane. Donor and acceptor plate are assembled and blank buffer is placed in the wells of the filter plate, on top of the artificial barrier. This 'sandwich' is maintained at a constant temperature and humidity for a predefined period (1 to 18 h), such that diffusion can occur. The effective permeability is calculated from the compound flux, the concentration gradient between the donor and acceptor compartments and the filter area. Since the first application, the assay parameters have been varied with the aim to better mimic the physiological conditions and to

speed up the procedure.⁹² For example, the lipid composition has been modified to adapt *in vivo* brush-border membrane conditions, additives have been given to the acceptor well solution to maintain sink conditions, or stirring plates have been placed in the donor compartments in order to compress the thickness of the aqueous boundary layer located next to the artificial membrane.

Cell layer methods. Cell based approaches are more time-consuming than PAMPA but consider passive diffusion as well as carrier-mediated transport and therefore provide enhanced information on permeability mechanisms. The human colorectal adenocarcinoma (Caco-2) cell line is the best-known cell line for the assay.⁹³ Furthermore, the Madin Darby Canine Kidney (MDCK) cell line has been used primarily for passive diffusion studies.⁹⁴ Caco-2 cells are cultivated on filter-support inlets of multiwell plates, where they grow to confluence, develop the microvilli morphology on the apical surface and express transporter proteins as well as metabolizing enzymes.⁹⁵ The compound flux can be studied in the apical to basolateral direction or *vice versa* for modeling membrane diffusion or active transport processes (see section 1.5.5 below).

1.5.3 Distribution

Drug distribution, as quantified by the volume of distribution, is related to the extent of drug binding in tissues *vs.* the extent of binding in plasma (the central compartment). Binding in plasma can easily be determined *in vitro* by measuring the plasma protein binding (PPB), whereas tissue binding has not been accessible *in vitro* so far. Besides PPB, experimental log *D* and pK_a have been identified as key predictors for modeling the volume of distribution of neutral and basic small molecules.⁹⁶ Furthermore, membrane barriers, *e.g.* the blood brain barrier (BBB), determine the compound distribution into specific tissues. Approaches for predicting BBB permeation include artificial membrane permeability methods (PAMPA-BBB),⁹⁷ cell-based methods,⁹⁸ or *in vivo* brain uptake studies, amongst others.

Plasma protein binding. The fraction bound to plasma proteins is not only a key descriptor for drug distribution but also strongly influences the drug clearance because only unbound drug is accessible to the enzymatic bioconversion or to the filtration in the renal glomeruli.⁹⁹ Different methods have been established to determine the fraction of drug bound to plasma proteins *in vitro*. The equilibrium dialysis method represents the ‘gold standard’.¹⁰⁰ In brief, two chambers – one filled with plasma with the added test compound, the other filled with blank buffer – are separated by a dialysis membrane which is permeable for free drug

molecules but impermeable for plasma proteins. The system is incubated for a predefined period until the concentrations of free drug on each side of the membrane are in equilibrium. To determine the fraction unbound in plasma (f_u), the concentration of drug in the buffer chamber at equilibrium is divided by the total drug concentration in the plasma chamber. For increasing the experimental throughput, the equilibrium dialysis method has been miniaturized to a 96-well format.^{101, 102} Further approaches for the PPB determination include ultrafiltration, ultracentrifugation, HPLC, microdialysis, or surface plasmon resonance, amongst others.^{100, 103, 104}

1.5.4 Metabolism

Metabolic bioconversion is mediated by a vast array of enzymes, which are associated to different body tissues and involve various co-factors into the enzymatic reaction.⁴⁷ The most prominent enzymes in phase I reactions are monooxygenases of the cytochrome P450 family, which are associated to the endoplasmic reticulum (ER) of different tissues (*e.g.* hepatocytes or enterocytes). Phase II reactions are mediated by, amongst others, UDP-glucuronosyltransferases to form glucuronide metabolites, sulfotransferases to form sulfate metabolites, or glutathione-S-transferases to form glutathione conjugates.

Different computational tools have been developed to predict the cytochrome P450 mediated drug metabolism, *i.e.* the most likely metabolic labile sites of a drug candidate, CYP substrate specificities, the rate and extent of the metabolic turnover, as well as inhibitors and inducers of individual isozymes. Tools and commercial software available for the prediction of metabolism were comprehensively reviewed by Crivori and Poggesi.¹⁰⁵

Metabolic stability studies. High stability towards phase I modifications and phase II conjugations is usually aspired to provide sufficiently high drug levels for the pharmacological effect.³³ In the case of prodrugs, high susceptibility to the enzyme-mediated bioactivation is however desirable.⁶³ Metabolic stability studies are conducted *in vitro* with liver and intestinal microsomes, S9 fraction, hepatocytes, liver slices, or plasma.^{106, 107} Microsomes are prepared by differential centrifugation of a liver or intestine tissue homogenate and contain the metabolizing enzymes that are bound to the endoplasmic reticulum, *e.g.* the cytochrome P450 oxidizing enzymes, enzymes of the carboxylesterase superfamily, or phase II conjugating enzymes such as the UDP-glucuronosyltransferases.⁴⁵ The assessment of CYP-mediated monooxygenation requires the addition of NADPH,¹⁰⁸ the glucuronidation requires uridine diphosphate glucuronic acid (UDPGA),¹⁰⁹ whereas the

carboxylesterase-activity does not rely on a co-factor.¹¹⁰ Microsomes are most commonly used for metabolic stability screenings during early drug discovery. For this purpose, test compound is dissolved in a buffered aqueous solution containing microsomes and the respective co-factor. Aliquots are removed from the mixture at specific time points for determination of remaining parent compound. The metabolic stability is usually reported as metabolic half-life ($t_{1/2}$) or as intrinsic clearance (CL'_{int}).¹⁰⁸

At a later stage of discovery and development, when phase I and II stability are of interest, either S9 fraction, hepatocytes, or liver slices are used. The S9 fraction, *i.e.* the supernatant obtained from differential centrifugation of liver homogenate at 9000g, contains both the cellular cytosol and the endoplasmic reticulum with the associated metabolizing enzymes.⁴⁵ Hepatocytes – either in suspension or used as ‘sandwich culture hepatocytes’ – are prepared from fresh livers and are useful when the interplay of metabolism and cellular uptake is of interest. They contain a complete ensemble of metabolizing enzymes of all isotypes, co-factors, cellular components, and membrane permeation mechanisms. The most complex systems are ‘precision-cut’ liver slices, *i.e.* sections of the whole liver tissue. They represent all of the natural liver metabolizing systems, including transporters, enzymes, and co-factors, and are particularly useful for in-depth studies of selected compounds.

Plasma also contains enzymes that convert drugs, *e.g.* esterases.¹¹¹ Metabolic liability studies with plasma therefore play an important role in the development of ester prodrugs. For assessing plasma stability, test compound dissolved in aqueous buffer is mixed with plasma and incubated at 37°C. Aliquots are removed at specific time points. The parent compound remaining after incubation is quantified by LC-MS for the calculation of the metabolic half-life ($t_{1/2}$).¹⁰⁷

1.5.5 Excretion

Renal and hepatobiliary excretion are the two main routes of drug excretion in the human body. Polar drugs or metabolites are predominantly renally excreted, whereas apolar compounds, which are not susceptible to bioconversion, prefer the hepatobiliary route. The rate of renal excretion depends on the glomerular filtration primarily restricted by the PPB as well as on the passive or transporter-mediated tubular reabsorption and secretion.⁵⁰ Hepatobiliary excretion relies on the compound uptake from the sinusoid into the hepatocytes and the subsequent excretion into the bile, either by passive diffusion or active carrier-mediated transport.⁴⁷

Transporter studies. Given the importance of carrier-mediated mechanisms for absorption, distribution, and excretion, various methods to assess transport have been developed. Currently applied methods include membrane based assay systems (*i.e.* ATPase assay, membrane vesicle transport assay) and cell-based assays which involve either polarized cell lines without recombinant transporters (*e.g.* Caco-2, MDCK), transfected cell lines, or primary cells.¹¹²

The ATPase assay is used to evaluate the interactions of substrates with ABC transporters. Substrate-dependent ATPase activity in cell membrane preparations or purified membrane proteins is detected by a colorimetric analysis of the inorganic phosphate release during the transport process.¹¹³ Inverted plasma membrane vesicles are primarily used to study the efflux activity by ABC transporters. Inverted membrane vesicles are prepared from cells expressing the transport proteins of interest (*e.g.* baculovirus-infected insect cells). When they are added to a compound solution, substrate accumulates within the vesicles and can be detected upon washing and lysis.¹¹⁴

The cell-based assay systems are performed using either a cell suspension or a confluent cell monolayer cultured on a permeable membrane support matrix. When cells in suspension are exposed to the test compound, transporter substrate accumulates within the cells and can be quantified upon washing and lysis.¹¹⁵ Transporter studies involving a cell monolayer are done by applying a test compound to either the apical or basolateral side of the confluent cell layer and measuring the resulting transmembrane flux.¹¹⁶ Active uptake or efflux can be identified by the appearance of bi-directional differences in the apparent permeability.¹¹⁶ Primary hepatocytes are furthermore cultured in a sandwich configuration between two layers of gelled collagen, where they reestablish a structurally and functionally normal bile canalicular network and express sinusoidal and canclicular transporter proteins. Sandwich-cultured hepatocytes are used to study hepatic uptake, metabolism, and biliary excretion in one assay.¹¹⁷

1.6 Aims of the thesis

The present thesis is embedded in the development process of a highly active and orally available FimH antagonist. The goal of the thesis was the physicochemical and *in vitro* pharmacokinetic characterization of biaryl α -D-mannopyranosides within a development cycle (Figure 1.7) which explores several optimization strategies, such as prodrug and bioisostere approaches. *In vitro* assays predictive for drug absorption, distribution, metabolism, and excretion were implemented with the aim to comprehensively characterize the candidate molecules and to guide their development towards ‘drug-likeness’.

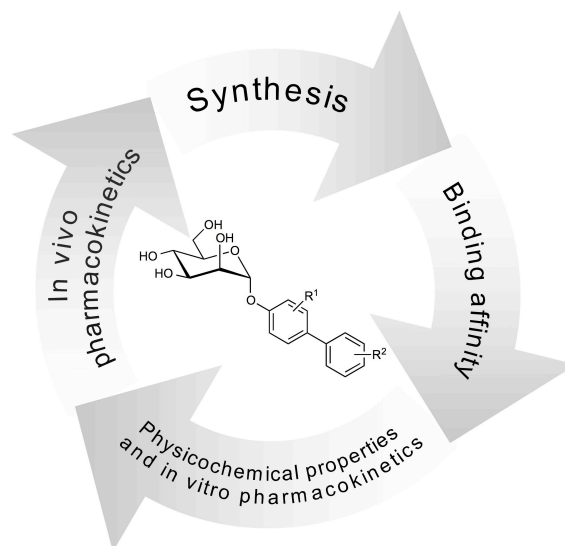


Figure 1.7. Pharmacodynamic and pharmacokinetic optimization of biaryl α -D-mannopyranoside FimH antagonists.

REFERENCES

1. Foxman, B.; Barlow, R.; D'Arcy, H.; Gillespie, B.; Sobel, J. D. Urinary tract infection: self-reported incidence and associated costs. *Ann Epidemiol* **2000**, *10*, 509-515.
2. Fihn, S. D. Clinical practice. Acute uncomplicated urinary tract infection in women. *N Engl J Med* **2003**, *349*, 259-266.
3. Hooton, T. M.; Besser, R.; Foxman, B.; Fritsche, T. R.; Nicolle, L. E. Acute uncomplicated cystitis in an era of increasing antibiotic resistance: a proposed approach to empirical therapy. *Clin Infect Dis* **2004**, *39*, 75-80.
4. Nicolle, L.; Anderson, P. A.; Conly, J.; Mainprize, T. C.; Meuser, J.; Nickel, J. C.; Senikas, V. M.; Zhanel, G. G. Uncomplicated urinary tract infection in women. Current practice and the effect of antibiotic resistance on empiric treatment. *Can Fam Physician* **2006**, *52*, 612-618.
5. Sanchez, G. V.; Master, R. N.; Karlowsky, J. A.; Bordon, J. M. In vitro antimicrobial resistance of urinary *Escherichia coli* isolates among U.S. outpatients from 2000 to 2010. *Antimicrob Agents Chemother* **2012**, *56*, 2181-2183.
6. Ronald, A. The etiology of urinary tract infection: traditional and emerging pathogens. *Am J Med* **2002**, *113 Suppl 1A*, 14S-19S.
7. Mulvey, M. A.; Schilling, J. D.; Martinez, J. J.; Hultgren, S. J. Bad bugs and beleaguered bladders: interplay between uropathogenic *Escherichia coli* and innate host defenses. *Proc Natl Acad Sci U S A* **2000**, *97*, 8829-8835.
8. Wiles, T. J.; Kulesus, R. R.; Mulvey, M. A. Origins and virulence mechanisms of uropathogenic *Escherichia coli*. *Exp Mol Pathol* **2008**, *85*, 11-19.
9. Abgottspon, D.; Ernst, B. In vivo evaluation of FimH antagonists - a novel class of antimicrobials for the treatment of urinary tract infection. *Chimia (Aarau)* **2012**, *66*, 166-169.
10. Zhou, G.; Mo, W. J.; Sebbel, P.; Min, G.; Neubert, T. A.; Glockshuber, R.; Wu, X. R.; Sun, T. T.; Kong, X. P. Uroplakin Ia is the urothelial receptor for uropathogenic *Escherichia coli*: evidence from in vitro FimH binding. *J Cell Sci* **2001**, *114*, 4095-103.
11. Schilling, J. D.; Mulvey, M. A.; Hultgren, S. J. Structure and function of *Escherichia coli* type 1 pili: new insight into the pathogenesis of urinary tract infections. *J Infect Dis* **2001**, *183 Suppl 1*, S36-40.
12. Capitani, G.; Eidam, O.; Glockshuber, R.; Grütter, M. G. Structural and functional insights into the assembly of type 1 pili from *Escherichia coli*. *Microbes Infect* **2006**, *8*, 2284-2290.
13. Choudhury, D.; Thompson, A.; Stojanoff, V.; Langermann, S.; Pinkner, J.; Hultgren, S. J.; Knight, S. D. X-ray structure of the FimC-FimH chaperone-adhesin complex from uropathogenic *Escherichia coli*. *Science* **1999**, *285*, 1061-1066.
14. Le Trong, I.; Aprikian, P.; Kidd, B. A.; Forero-Shelton, M.; Tchesnokova, V.; Rajagopal, P.; Rodriguez, V.; Interlandi, G.; Klevit, R.; Vogel, V.; Stenkamp, R. E.; Sokurenko, E. V.; Thomas, W. E. Structural basis for mechanical force regulation of the adhesin FimH via finger trap-like beta sheet twisting. *Cell* **2010**, *141*, 645-655.
15. Hung, C. S.; Bouckaert, J.; Hung, D.; Pinkner, J.; Widberg, C.; DeFusco, A.; Auguste, C. G.; Strouse, R.; Langermann, S.; Waksman, G.; Hultgren, S. J. Structural basis of tropism of *Escherichia coli* to the bladder during urinary tract infection. *Mol Microbiol* **2002**, *44*, 903-915.
16. Bouckaert, J.; Berglund, J.; Schembri, M.; De Genst, E.; Cools, L.; Wuhler, M.; Hung, C. S.; Pinkner, J.; Slättegård, R.; Zavialov, A.; Choudhury, D.; Langermann, S.; Hultgren, S. J.; Wyns, L.; Klemm, P.; Oscarson, S.; Knight, S. D.; De Greve, H. Receptor binding studies disclose a novel class of high-affinity inhibitors of the *Escherichia coli* FimH adhesin. *Mol Microbiol* **2005**, *55*, 441-455.
17. Sharon, N. Carbohydrates as future anti-adhesion drugs for infectious diseases. *Biochim Biophys Acta* **2006**, *1760*, 527-537.
18. Ofek, I.; Mirelman, D.; Sharon, N. Adherence of *Escherichia coli* to human mucosal cells mediated by mannose receptors. *Nature* **1977**, *265*, 623-625.

19. Imberty, A.; Chabre, Y. M.; Roy, R. Glycomimetics and glycodendrimers as high affinity microbial anti-adhesins. *Chemistry* **2008**, *14*, 7490-7499.
20. Pieters, R. J. Maximising multivalency effects in protein-carbohydrate interactions. *Org Biomol Chem* **2009**, *7*, 2013-2025.
21. Hartmann, M.; Lindhorst, T. K. The bacterial lectin FimH, a target for drug discovery - carbohydrate inhibitors of type 1 fimbriae-mediated bacterial adhesion. *Eur. J. Org. Chem.* **2011**, 3583-3609.
22. Firon, N.; Ofek, I.; Sharon, N. Interaction of mannose-containing oligosaccharides with the fimbrial lectin of *Escherichia coli*. *Biochem Biophys Res Commun* **1982**, *105*, 1426-1432.
23. Firon, N.; Ofek, I.; Sharon, N. Carbohydrate specificity of the surface lectins of *Escherichia coli*, *Klebsiella pneumoniae*, and *Salmonella typhimurium*. *Carbohydr Res* **1983**, *120*, 235-249.
24. Firon, N.; Ashkenazi, S.; Mirelman, D.; Ofek, I.; Sharon, N. Aromatic alpha-glycosides of mannose are powerful inhibitors of the adherence of type 1 fimbriated *Escherichia coli* to yeast and intestinal epithelial cells. *Infect Immun* **1987**, *55*, 472-476.
25. Sperling, O.; Fuchs, A.; Lindhorst, T. K. Evaluation of the carbohydrate recognition domain of the bacterial adhesin FimH: Design, synthesis and binding properties of mannoside ligands. *Org Biomol Chem* **2006**, *4*, 3913-3922.
26. Grabosch, C.; Hartmann, M.; Schmidt-Lassen, J.; Lindhorst, T. K. Squaric acid monoamide mannosides as ligands for the bacterial lectin FimH: covalent inhibition or not? *Chembiochem* **2011**, *12*, 1066-1074.
27. Han, Z.; Pinkner, J. S.; Ford, B.; Obermann, R.; Nolan, W.; Wildman, S. A.; Hobbs, D.; Ellenberger, T.; Cusumano, C. K.; Hultgren, S. J.; Janetka, J. W. Structure-based drug design and optimization of mannoside bacterial FimH antagonists. *J Med Chem* **2010**, *53*, 4779-4792.
28. Klein, T.; Abgottspon, D.; Wittwer, M.; Rabbani, S.; Herold, J.; Jiang, X.; Kleeb, S.; Lüthi, C.; Scharenberg, M.; Bezençon, J.; Gubler, E.; Pang, L.; Smiesko, M.; Cutting, B.; Schwardt, O.; Ernst, B. FimH antagonists for the oral treatment of urinary tract infections: from design and synthesis to in vitro and in vivo evaluation. *J Med Chem* **2010**, *53*, 8627-8641.
29. Cusumano, C. K.; Pinkner, J. S.; Han, Z.; Greene, S. E.; Ford, B. A.; Crowley, J. R.; Henderson, J. P.; Janetka, J. W.; Hultgren, S. J. Treatment and Prevention of Urinary Tract Infection with Orally Active FimH Inhibitors. *Sci Transl Med* **2011**, *3*, 109ra115.
30. Han, Z.; Pinkner, J. S.; Ford, B.; Chorell, E.; Crowley, J. M.; Cusumano, C. K.; Campbell, S.; Henderson, J. P.; Hultgren, S. J.; Janetka, J. W. Lead optimization studies on FimH antagonists: discovery of potent and orally bioavailable ortho-substituted biphenyl mannosides. *J Med Chem* **2012**, *55*, 3945-3959.
31. Jiang, X.; Abgottspon, D.; Kleeb, S.; Rabbani, S.; Scharenberg, M.; Wittwer, M.; Haug, M.; Schwardt, O.; Ernst, B. Antiadhesion therapy for urinary tract infections--a balanced PK/PD profile proved to be key for success. *J Med Chem* **2012**, *55*, 4700-4713.
32. Guidance for industry, bioavailability and bioequivalence studies for orally administered drug products - general considerations. U.S. Department of Health and Human Services, Food and Drug Administration, Center for Drug Evaluation and Research (CDER), **2003**.
33. van De Waterbeemd, H.; Smith, D. A.; Beaumont, K.; Walker, D. K. Property-based design: optimization of drug absorption and pharmacokinetics. *J Med Chem* **2001**, *44*, 1313-1333.
34. Burton, P. S.; Goodwin, J. T.; Vidmar, T. J.; Amore, B. M. Predicting drug absorption: how nature made it a difficult problem. *J Pharmacol Exp Ther* **2002**, *303*, 889-895.
35. Amidon, G. L.; Lennernäs, H.; Shah, V. P.; Crison, J. R. A theoretical basis for a biopharmaceutic drug classification: the correlation of in vitro drug product dissolution and in vivo bioavailability. *Pharm Res* **1995**, *12*, 413-420.
36. Dressman, J. B.; Thelen, K.; Jantratid, E. Towards quantitative prediction of oral drug absorption. *Clin Pharmacokinet* **2008**, *47*, 655-667.

37. Jain, N.; Yalkowsky, S. H. Estimation of the aqueous solubility I: application to organic nonelectrolytes. *J Pharm Sci* **2001**, *90*, 234-252.
38. Sugano, K.; Kansy, M.; Artursson, P.; Avdeef, A.; Bendels, S.; Di, L.; Ecker, G. F.; Faller, B.; Fischer, H.; Gerebtzoff, G.; Lennernaes, H.; Senner, F. Coexistence of passive and carrier-mediated processes in drug transport. *Nat Rev Drug Discov* **2010**, *9*, 597-614.
39. Lipinski, C. A.; Lombardo, F.; Dominy, B. W.; Feeney, P. J. Experimental and computational approaches to estimate solubility and permeability in drug discovery and development settings. *Adv Drug Deliv Rev* **2001**, *46*, 3-26.
40. Veber, D. F.; Johnson, S. R.; Cheng, H. Y.; Smith, B. R.; Ward, K. W.; Kopple, K. D. Molecular properties that influence the oral bioavailability of drug candidates. *J Med Chem* **2002**, *45*, 2615-2623.
41. Giacomini, K. M.; Huang, S. M.; Tweedie, D. J.; Benet, L. Z.; Brouwer, K. L.; Chu, X.; Dahlin, A.; Evers, R.; Fischer, V.; Hillgren, K. M.; Hoffmaster, K. A.; Ishikawa, T.; Keppler, D.; Kim, R. B.; Lee, C. A.; Niemi, M.; Polli, J. W.; Sugiyama, Y.; Swaan, P. W.; Ware, J. A.; Wright, S. H.; Yee, S. W.; Zamek-Gliszczynski, M. J.; Zhang, L. Membrane transporters in drug development. *Nat Rev Drug Discov* **2010**, *9*, 215-236.
42. Johnson, K. C.; Swindell, A. C. Guidance in the setting of drug particle size specifications to minimize variability in absorption. *Pharm Res* **1996**, *13*, 1795-1798.
43. Curatolo, W. Physical chemical properties of oral drug candidates in the discovery and exploratory development settings. *Pharm. Sci. Technol. Today* **1998**, *1*, 387-393.
44. Lipinski, C. A. Drug-like properties and the causes of poor solubility and poor permeability. *J Pharmacol Toxicol Methods* **2000**, *44*, 235-249.
45. Kerns, E. H.; Di, L. *Drug-like properties : concepts, structure design and methods: from ADME to toxicity optimization*. Academic Press: Amsterdam, London, **2008**.
46. Pond, S. M.; Tozer, T. N. First-pass elimination. Basic concepts and clinical consequences. *Clin Pharmacokinet* **1984**, *9*, 1-25.
47. Smith, D. A.; Jones, B. C.; Walker, D. K. Design of drugs involving the concepts and theories of drug metabolism and pharmacokinetics. *Med Res Rev* **1996**, *16*, 243-266.
48. Masereeuw, R.; Russel, F. G. Mechanisms and clinical implications of renal drug excretion. *Drug Metab Rev* **2001**, *33*, 299-351.
49. Walton, K.; Dorne, J. L.; Renwick, A. G. Species-specific uncertainty factors for compounds eliminated principally by renal excretion in humans. *Food Chem Toxicol* **2004**, *42*, 261-274.
50. Feng, B.; LaPerle, J. L.; Chang, G.; Varma, M. V. Renal clearance in drug discovery and development: molecular descriptors, drug transporters and disease state. *Expert Opin Drug Metab Toxicol* **2010**, *6*, 939-952.
51. Fagerholm, U. Prediction of human pharmacokinetics - renal metabolic and excretion clearance. *J Pharm Pharmacol* **2007**, *59*, 1463-1471.
52. Varma, M. V.; Feng, B.; Obach, R. S.; Troutman, M. D.; Chupka, J.; Miller, H. R.; El-Kattan, A. Physicochemical determinants of human renal clearance. *J Med Chem* **2009**, *52*, 4844-4852.
53. Obach, R. S.; Lombardo, F.; Waters, N. J. Trend analysis of a database of intravenous pharmacokinetic parameters in humans for 670 drug compounds. *Drug Metab Dispos* **2008**, *36*, 1385-1405.
54. Ernst, B.; Magnani, J. L. From carbohydrate leads to glycomimetic drugs. *Nat Rev Drug Discov* **2009**, *8*, 661-677.
55. Petitou, M.; Duchaussoy, P.; Herbert, J. M.; Duc, G.; El Hajji, M.; Branellec, J. F.; Donat, F.; Necciari, J.; Cariou, R.; Bouthier, J.; Garrigou, E. The synthetic pentasaccharide fondaparinux: first in the class of antithrombotic agents that selectively inhibit coagulation factor Xa. *Semin Thromb Hemost* **2002**, *28*, 393-402.
56. Chen, X.; Zheng, Y.; Shen, Y. Voglibose (Basen, AO-128), one of the most important alpha-glucosidase inhibitors. *Curr Med Chem* **2006**, *13*, 109-116.

57. Campbell, L. K.; Baker, D. E.; Campbell, R. K. Miglitol: assessment of its role in the treatment of patients with diabetes mellitus. *Ann Pharmacother* **2000**, *34*, 1291-1301.
58. Truscheit, E.; Frommer, W.; Junge, B.; Mueller, L.; Schmidt, D. D.; Wingender, W. Chemistry and biochemistry of microbial alpha-glucosidase inhibitors. *Angew. Chem. Int. Ed. Engl.* **1981**, *20*, 744-761.
59. Leeson, P. D.; Springthorpe, B. The influence of drug-like concepts on decision-making in medicinal chemistry. *Nat Rev Drug Discov* **2007**, *6*, 881-890.
60. Waring, M. J. Lipophilicity in drug discovery. *Expert Opin Drug Discov* **2010**, *5*, 235-248.
61. Ishikawa, M.; Hashimoto, Y. Improvement in aqueous solubility in small molecule drug discovery programs by disruption of molecular planarity and symmetry. *J Med Chem* **2011**, *54*, 1539-1554.
62. Meanwell, N. A. Synopsis of some recent tactical application of bioisosteres in drug design. *J Med Chem* **2011**, *54*, 2529-2591.
63. Beaumont, K.; Webster, R.; Gardner, I.; Dack, K. Design of ester prodrugs to enhance oral absorption of poorly permeable compounds: challenges to the discovery scientist. *Curr Drug Metab* **2003**, *4*, 461-485.
64. Lima, L. M.; Barreiro, E. J. Bioisosterism: a useful strategy for molecular modification and drug design. *Curr Med Chem* **2005**, *12*, 23-49.
65. Wexler, R. R.; Carini, D. J.; Duncia, J. V.; Johnson, A. L.; Wells, G. J.; Chiu, A. T.; Wong, P. C.; Timmermans, P. B. Rationale for the chemical development of angiotensin II receptor antagonists. *Am J Hypertens* **1992**, *5*, 209S-220S.
66. Rautio, J.; Kumpulainen, H.; Heimbach, T.; Oliyai, R.; Oh, D.; Järvinen, T.; Savolainen, J. Prodrugs: design and clinical applications. *Nat Rev Drug Discov* **2008**, *7*, 255-270.
67. Kim, C. U.; Lew, W.; Williams, M. A.; Liu, H.; Zhang, L.; Swaminathan, S.; Bischofberger, N.; Chen, M. S.; Mendel, D. B.; Tai, C. Y.; Laver, W. G.; Stevens, R. C. Influenza neuraminidase inhibitors possessing a novel hydrophobic interaction in the enzyme active site: design, synthesis, and structural analysis of carbocyclic sialic acid analogues with potent anti-influenza activity. *J Am Chem Soc* **1997**, *119*, 681-690.
68. Taylor, N. R.; von Itzstein, M. Molecular modeling studies on ligand binding to sialidase from influenza virus and the mechanism of catalysis. *J Med Chem* **1994**, *37*, 616-624.
69. He, G.; Massarella, J.; Ward, P. Clinical pharmacokinetics of the prodrug oseltamivir and its active metabolite Ro 64-0802. *Clin Pharmacokinet* **1999**, *37*, 471-484.
70. Stella, V. J.; Nti-Addae, K. W. Prodrug strategies to overcome poor water solubility. *Adv Drug Deliv Rev* **2007**, *59*, 677-694.
71. Heimbach, T.; Oh, D. M.; Li, L. Y.; Rodríguez-Hornedo, N.; Garcia, G.; Fleisher, D. Enzyme-mediated precipitation of parent drugs from their phosphate prodrugs. *Int J Pharm* **2003**, *261*, 81-92.
72. Wire, M. B.; Shelton, M. J.; Studenberg, S. Fosamprenavir : clinical pharmacokinetics and drug interactions of the amprenavir prodrug. *Clin Pharmacokinet* **2006**, *45*, 137-168.
73. Kerns, E. H.; Di, L. Pharmaceutical profiling in drug discovery. *Drug Discov Today* **2003**, *8*, 316-323.
74. Kerns, E. H. High throughput physicochemical profiling for drug discovery. *J Pharm Sci* **2001**, *90*, 1838-1858.
75. Mannhold, R.; van de Waterbeemd, H. Substructure and whole molecule approaches for calculating log P. *J Comput Aided Mol Des* **2001**, *15*, 337-54.
76. Moriguchi, I.; Hirono, S.; Liu, Q.; Nakagome, I.; Matsushita, Y. Simple method of calculating octanol/water partition coefficient. *Chem. Pharm. Bull.* **1992**, *40*, 127-130.
77. Dearden, J. C.; Bresnen, G. M. The measurement of partition coefficients. *Quant. Struct.-Act. Relat.* **1988**, *7*, 133-144.

78. Minick, D. J.; Frenz, J. H.; Patrick, M. A.; Brent, D. A. A comprehensive method for determining hydrophobicity constants by reversed-phase high-performance liquid chromatography. *J Med Chem* **1988**, *31*, 1923-1933.
79. Poole, S. K.; Durham, D.; Kibbey, C. Rapid method for estimating the octanol--water partition coefficient (log P_{ow}) by microemulsion electrokinetic chromatography. *J Chromatogr B Biomed Sci Appl* **2000**, *745*, 117-126.
80. Slater, B.; McCormack, A.; Avdeef, A.; Comer, J. E. pH-metric log P. 4. Comparison of partition coefficients determined by HPLC and potentiometric methods to literature values. *J Pharm Sci* **1994**, *83*, 1280-1283.
81. Di, L.; Fish, P. V.; Mano, T. Bridging solubility between drug discovery and development. *Drug Discov Today* **2012**, *17*, 486-495.
82. Avdeef, A. High-throughput measurements of solubility profiles. In *Pharmacokinetic Optimization in Drug Research; Biological, Physicochemical and Computational Strategies*, Testa, B.; van de Waterbeemd, H.; Folkers, G.; Guy, R., Eds. Helvetica Chimica Acta: Zurich, **2001**; pp 305-326.
83. Bevan, C. D.; Lloyd, R. S. A high-throughput screening method for the determination of aqueous drug solubility using laser nephelometry in microtiter plates. *Anal Chem* **2000**, *72*, 1781-1787.
84. Kerns, E. H.; Di, L. Physicochemical profiling: overview of the screens. *Drug Discov. Today Technol.* **2004**, *1*, 343-348.
85. Balogh, G. T.; Gyarmati, B.; Nagy, B.; Molnar, L.; Keseru, G. M. Comparative evaluation of in silico pK_a prediction tools on the gold standard dataset. *QSAR Comb. Sci.* **2009**, *28*, 1148-1155.
86. Liao, C.; Nicklaus, M. C. Comparison of nine programs predicting pK_a values of pharmaceutical substances. *J Chem Inf Model* **2009**, *49*, 2801-2812.
87. Box, K.; Bevan, C.; Comer, J.; Hill, A.; Allen, R.; Reynolds, D. High-throughput measurement of pK_a values in a mixed-buffer linear pH gradient system. *Anal Chem* **2003**, *75*, 883-892.
88. Handloser, C. S.; Chakrabarty, M. R.; Mosher, M. W. Experimental determination of pK_a values by use of NMR chemical shift. *J. Chem. Educ.* **1973**, *50*, 510-511.
89. Ishihama, Y.; Nakamura, M.; Miwa, T.; Kajima, T.; Asakawa, N. A rapid method for pK_a determination of drugs using pressure-assisted capillary electrophoresis with photodiode array detection in drug discovery. *J Pharm Sci* **2002**, *91*, 933-942.
90. Avdeef, A. pH-metric log P. II: Refinement of partition coefficients and ionization constants of multiprotic substances. *J Pharm Sci* **1993**, *82*, 183-190.
91. Kansy, M.; Senner, F.; Gubernator, K. Physicochemical high throughput screening: parallel artificial membrane permeation assay in the description of passive absorption processes. *J Med Chem* **1998**, *41*, 1007-1010.
92. Kansy, M.; Avdeef, A.; Fischer, H. Advances in screening for membrane permeability: high-resolution PAMPA for medicinal chemists. *Drug Discov. Today Technol.* **2004**, *1*, 349-355.
93. Artursson, P.; Karlsson, J. Correlation between oral drug absorption in humans and apparent drug permeability coefficients in human intestinal epithelial (Caco-2) cells. *Biochem Biophys Res Commun* **1991**, *175*, 880-885.
94. Irvine, J. D.; Takahashi, L.; Lockhart, K.; Cheong, J.; Tolan, J. W.; Selick, H. E.; Grove, J. R. MDCK (Madin-Darby canine kidney) cells: A tool for membrane permeability screening. *J Pharm Sci* **1999**, *88*, 28-33.
95. Hubatsch, I.; Ragnarsson, E. G.; Artursson, P. Determination of drug permeability and prediction of drug absorption in Caco-2 monolayers. *Nat Protoc* **2007**, *2*, 2111-2119.
96. Lombardo, F.; Obach, R. S.; Shalaeva, M. Y.; Gao, F. Prediction of volume of distribution values in humans for neutral and basic drugs using physicochemical measurements and plasma protein binding data. *J Med Chem* **2002**, *45*, 2867-2876.
97. Di, L.; Kerns, E. H.; Fan, K.; McConnell, O. J.; Carter, G. T. High throughput artificial membrane permeability assay for blood-brain barrier. *Eur J Med Chem* **2003**, *38*, 223-232.

98. Garberg, P.; Ball, M.; Borg, N.; Cecchelli, R.; Fenart, L.; Hurst, R. D.; Lindmark, T.; Mabondzo, A.; Nilsson, J. E.; Raub, T. J.; Stanimirovic, D.; Terasaki, T.; Oberg, J. O.; Osterberg, T. In vitro models for the blood-brain barrier. *Toxicol In Vitro* **2005**, *19*, 299-334.
99. Schmidt, S.; Gonzalez, D.; Derendorf, H. Significance of protein binding in pharmacokinetics and pharmacodynamics. *J Pharm Sci* **2010**, *99*, 1107-1122.
100. Oravcová, J.; Böhs, B.; Lindner, W. Drug-protein binding sites. New trends in analytical and experimental methodology. *J Chromatogr B Biomed Appl* **1996**, *677*, 1-28.
101. Kariv, I.; Cao, H.; Oldenburg, K. R. Development of a high throughput equilibrium dialysis method. *J Pharm Sci* **2001**, *90*, 580-587.
102. Banker, M. J.; Clark, T. H.; Williams, J. A. Development and validation of a 96-well equilibrium dialysis apparatus for measuring plasma protein binding. *J Pharm Sci* **2003**, *92*, 967-974.
103. Rich, R. L.; Day, Y. S.; Morton, T. A.; Myszka, D. G. High-resolution and high-throughput protocols for measuring drug/human serum albumin interactions using BIACORE. *Anal Biochem* **2001**, *296*, 197-207.
104. Zhang, F.; Xue, J.; Shao, J.; Jia, L. Compilation of 222 drugs' plasma protein binding data and guidance for study designs. *Drug Discov Today* **2012**, *17*, 475-485.
105. Crivori, P.; Poggesi, I. Computational approaches for predicting CYP-related metabolism properties in the screening of new drugs. *Eur J Med Chem* **2006**, *41*, 795-808.
106. Lin, J. H.; Rodrigues, A. D. In vitro models for early studies or drug metabolism. In *Pharmacokinetic Optimization in Drug Research; Biological, Physicochemical and Computational Strategies*, Testa, B.; van de Waterbeemd, H.; Folkers, G.; Guy, R., Eds. Helvetica Chimica Acta: Zurich, **2001**; pp 217-243.
107. Di, L.; Kerns, E. H.; Hong, Y.; Chen, H. Development and application of high throughput plasma stability assay for drug discovery. *Int J Pharm* **2005**, *297*, 110-119.
108. Obach, R. Prediction of human clearance of twenty-nine drugs from hepatic microsomal intrinsic clearance data: An examination of in vitro half-life approach and nonspecific binding to microsomes. *Drug Metab Dispos* **1999**, *27*, 1350-1359.
109. Kilford, P. J.; Stringer, R.; Sohal, B.; Houston, J. B.; Galetin, A. Prediction of drug clearance by glucuronidation from in vitro data: use of combined cytochrome P450 and UDP-glucuronosyltransferase cofactors in alamethicin-activated human liver microsomes. *Drug Metab Dispos* **2009**, *37*, 82-89.
110. Imai, T.; Taketani, M.; Shii, M.; Hosokawa, M.; Chiba, K. Substrate specificity of carboxylesterase isozymes and their contribution to hydrolase activity in human liver and small intestine. *Drug Metab Dispos* **2006**, *34*, 1734-1741.
111. Li, B.; Sedlacek, M.; Manoharan, I.; Boopathy, R.; Duysen, E. G.; Masson, P.; Lockridge, O. Butyrylcholinesterase, paraoxonase, and albumin esterase, but not carboxylesterase, are present in human plasma. *Biochem Pharmacol* **2005**, *70*, 1673-1684.
112. Zhang, Y.; Bachmeier, C.; Miller, D. W. In vitro and in vivo models for assessing drug efflux transporter activity. *Adv Drug Deliv Rev* **2003**, *55*, 31-51.
113. Borgnia, M. J.; Eytan, G. D.; Assaraf, Y. G. Competition of hydrophobic peptides, cytotoxic drugs, and chemosensitizers on a common P-glycoprotein pharmacophore as revealed by its ATPase activity. *J Biol Chem* **1996**, *271*, 3163-3171.
114. Glavinas, H.; Krajcsi, P.; Cserepes, J.; Sarkadi, B. The role of ABC transporters in drug resistance, metabolism and toxicity. *Curr Drug Deliv* **2004**, *1*, 27-42.
115. Kerns, E. H.; Hill, S. E.; Detlefsen, D. J.; Volk, K. J.; Long, B. H.; Carboni, J.; Lee, M. S. Cellular uptake profile of paclitaxel using liquid chromatography tandem mass spectrometry. *Rapid Commun Mass Spectrom* **1998**, *12*, 620-624.
116. Polli, J. W.; Wring, S. A.; Humphreys, J. E.; Huang, L.; Morgan, J. B.; Webster, L. O.; Serabjit-Singh, C. S. Rational use of in vitro P-glycoprotein assays in drug discovery. *J Pharmacol Exp Ther* **2001**, *299*, 620-628.

117. Liu, X.; Chism, J. P.; LeCluyse, E. L.; Brouwer, K. R.; Brouwer, K. L. Correlation of biliary excretion in sandwich-cultured rat hepatocytes and in vivo in rats. *Drug Metab Dispos* **1999**, *27*, 637-644.

2 Results and discussion

2.1 Outline

Optimization of the biphenyl mannoside. In line with most carbohydrate-derived compounds, the biphenyl α -D-mannopyranoside FimH antagonist **5d** is highly hydrophilic, which hampers intestinal absorption and promotes rapid clearance of the systemically available fraction via the kidneys (for details refer to *Paper 1* in the following section). Renal excretion as the major route of elimination is basically aspired. However, too fast clearance leads to high peak levels in the urine and a rapid decrease beyond antiadhesive concentrations, implying the need for a frequent dosing to maintain the therapeutic effect in the bladder. The optimization of the lead structure **5d** towards higher oral bioavailability and sustained excretion relies on diverse modifications summarized in Figure 2.1 and described in the following chapters:

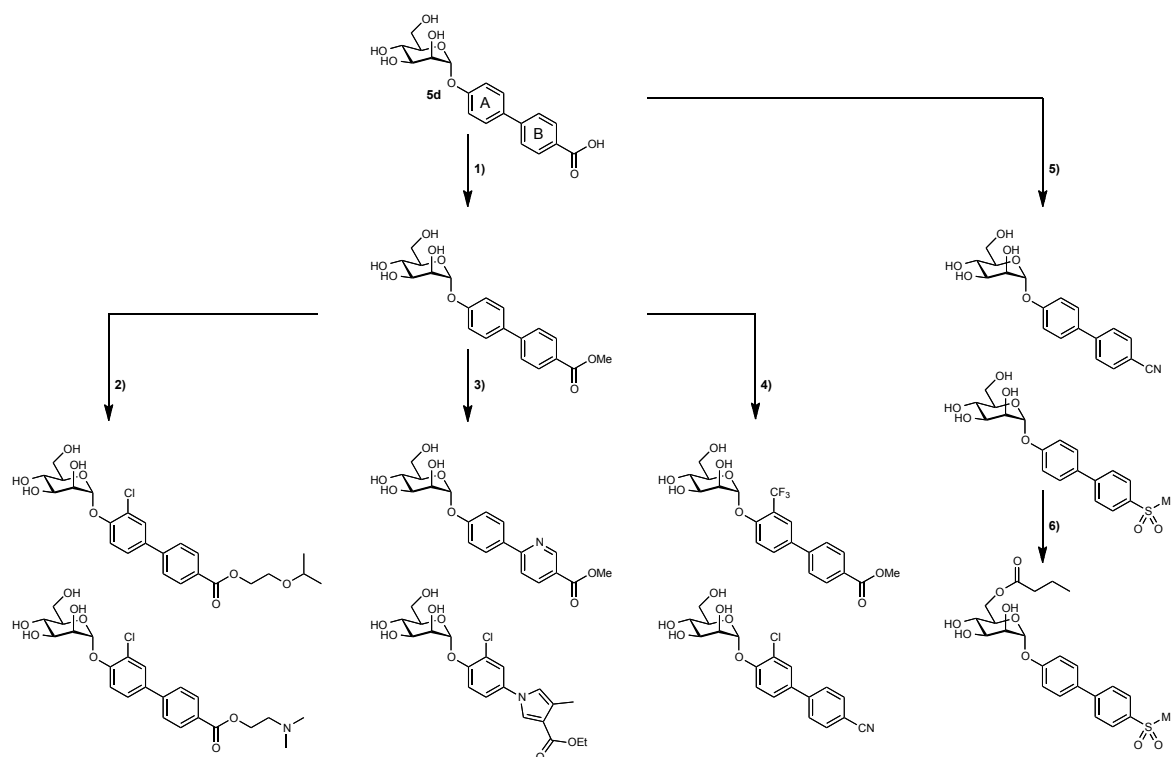


Figure 2.1. Modifications to the biphenyl α -D-mannopyranoside lead structure **5d** by 1) introduction of a methyl ester prodrug masking the polar carboxyl acid substituent on the terminal ring of the biphenyl aglycone, 2) optimization of the alkyl prodrug moiety of the ester prodrug, 3) introduction of aromatic heterocycles as terminal ring of the biaryl aglycone, 4) optimization of the substitution patterns of ring A and B, 5) introduction of bioisosteres replacing the carboxylic acid moiety, and 6) introduction of acyl prodrug moieties on the mannose portion.

- 1) Introduction of a methyl ester prodrug which masks the polar carboxylic acid substituent on the terminal ring (B) of the biphenyl aglycone (*Paper 1*).
- 2) Optimization of the alkyl promoiety of the ester prodrug (*Chapter 2*).
- 3) Introduction of aromatic heterocycles as terminal ring (B) of the biaryl aglycone (*Manuscript 3*).
- 4a) Optimization of the *ortho*-substituent on ring A of the biphenyl aglycone (*Paper 4*).
- 4b) Optimization of the substitution pattern on the terminal ring (B) of the biphenyl aglycone following the *Topliss* approach (*Manuscript 5*).
- 5) Replacement of the carboxylic acid moiety by bioisosteres (*Paper 6*).
- 6) Introduction of acyl promoiety on the mannose portion (*Chapter 7*).

Optimization of the indolinyl phenyl mannoside. In contrast to the biphenyl derivatives, the indolinyl phenyl α -D-mannopyranoside FimH antagonist **6** shows elevated lipophilicity, promoting the permeation through the membranes lining the small intestine. However low aqueous solubility impairs the initial dissolution step in the intestinal fluids and therefore the intestinal absorption (for details refer to *Paper 8*). The optimization of the indolinyl phenyl mannoside **6** towards higher aqueous solubility follows a phosphate ester prodrug strategy depicted in Figure 2.2 and described in detail in *Manuscript 9*.

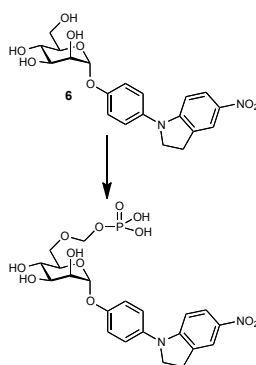


Figure 2.2. Modifications to the indolinyl phenyl α -D-mannopyranoside lead structure **6** by introduction of a phosphate promoiety.

Characterization of diverse aryl mannosides. The physicochemical profiles of diverse FimH antagonists with aglycones of increased flexibility, including triazolyl-methyl and -ethyl α -D-mannopyranosides, *N*-linked mannosyl triazoles, and triazolyl-methyl-*C*-mannosides, are described in *Paper 10*.

2.2 **Paper 1: FimH antagonists for the oral treatment of urinary tract infections: from design and synthesis to in vitro and in vivo evaluation**

This publication describes the identification of biphenyl α -D-mannopyranosides as potent FimH-antagonists and the experimental determination of the basic physicochemical and pharmacokinetic properties. Furthermore an ester prodrug approach is introduced as an appealing strategy for achieving oral bioavailability.

Contribution to the project:

Simon Kleeb established and performed the metabolic stability assays and interpreted the resulting data. Furthermore, he contributed to the writing of the experimental section about the determination of the pharmacokinetic properties.

This paper was published in the *Journal of Medicinal Chemistry*:

Klein, T.*; Abgottspon, D.*; Wittwer, M.*; Rabbani, S.*; Herold, J.* Jiang, X.; Kleeb, S.; Lüthi, C.; Scharenberg, M.; Bezençon, J.; Gubler, E.; Pang, L.; Smiesko, M.; Cutting, B.; Schwardt, O.; Ernst, B. FimH antagonists for the oral treatment of urinary tract infections: from design and synthesis to in vitro and in vivo evaluation. *J. Med. Chem.* **2010**, *53*, 8627-8641.

* These authors contributed equally to the project.

© 2010 American Chemical Society

FimH Antagonists for the Oral Treatment of Urinary Tract Infections: From Design and Synthesis to in Vitro and in Vivo Evaluation

Tobias Klein,[†] Daniela Abgottspon,[†] Matthias Wittwer,[†] Said Rabbani,[†] Janno Herold,[†] Xiaohua Jiang, Simon Kleeb, Christine Lüthi, Meike Scharenberg, Jacqueline Bezençon, Erich Gubler, Lijuan Pang, Martin Smiesko, Brian Cutting, Oliver Schwarardt, and Beat Ernst*

Institute of Molecular Pharmacy, Pharmacenter, University of Basel, Klingelbergstrasse 50, CH-4056 Basel, Switzerland.

[†]These authors contributed equally to the project

Received August 4, 2010

Urinary tract infection (UTI) by uropathogenic *Escherichia coli* (UPEC) is one of the most common infections, particularly affecting women. The interaction of FimH, a lectin located at the tip of bacterial pili, with high mannose structures is critical for the ability of UPEC to colonize and invade the bladder epithelium. We describe the synthesis and the in vitro/in vivo evaluation of α -D-mannosides with the ability to block the bacteria/host cell interaction. According to the pharmacokinetic properties, a prodrug approach for their evaluation in the UTI mouse model was explored. As a result, an orally available, low molecular weight FimH antagonist was identified with the potential to reduce the colony forming units (CFU) in the urine by 2 orders of magnitude and in the bladder by 4 orders of magnitude. With FimH antagonist **16b**, the great potential for the effective treatment of urinary tract infections with a new class of orally available antiinfectives could be demonstrated.

Introduction

Urinary tract infection (UTI⁶) is one of the most common infections, affecting millions of people each year. Particularly affected are women, who have a 40–50% risk to experience at least one symptomatic UTI episode at some time during their life. In addition, more than half of them experience a relapse of the infection within 6 months.^{1,2}

Although UTIs rarely cause severe diseases such as pyelonephritis or urosepsis, they are associated with high incidence rate and consume considerable healthcare resources.³ Uropathogenic *Escherichia coli* (UPEC) are the primary cause of UTIs, accounting for 70–95% of the reported cases. Symptomatic UTIs require antimicrobial treatment, often resulting in the emergence of resistant microbial flora. As a consequence, treatment of consecutive infections becomes increasingly difficult because the number of antibiotics is limited and the resistance of *E. coli* is increasing, especially in patients with diabetes, urinary tract anomaly, paraplegy, and those with permanent urinary catheter. Therefore, a new approach for the prevention and treatment of UTI with inexpensive, orally

applicable therapeutics with a low potential for resistance would have a great impact on patient care, public health care, and medical expenses.

UPEC strains express a number of well-studied virulence factors used for a successful colonization of their host.^{3–5} One important virulence factor is located on type 1 pili, allowing UPEC to adhere and invade host cells within the urinary tract. It enables UPEC to attach to oligomannosides, which are part of the glycoprotein uroplakin Ia on the urinary bladder mucosa. This initial step prevents the rapid clearance of *E. coli* from the urinary tract by the bulk flow of urine and at the same time enables the invasion of the host cells.^{3,6}

Type 1 pili are the most prevalent fimbriae encoded by UPEC, consisting of the four subunits FimA, FimF, FimG, and FimH, the latter located at the tip of the pili.⁷ As a part of the FimH subunit, a carbohydrate-recognizing domain (CRD) is responsible for bacterial interactions with the host cells within the urinary tract.⁶ The crystal structure of the FimH-CRD was solved⁸ and its complexes with *n*-butyl α -D-mannopyranoside⁹ and Man α (1–3)[Man α (1–6)]Man¹⁰ recently became available.

Previous studies showed that vaccination with FimH adhesin inhibits colonization and subsequent *E. coli* infection of the urothelium in humans.^{11,12} In addition, adherence and invasion of host cells by *E. coli* can also be prevented by α -D-mannopyranosides, which are potent antagonists of interactions mediated by type 1 pili.¹³ Whereas α -D-mannopyranosides efficiently prevent adhesion of *E. coli* to human urothelium, they are not exhibiting a selection pressure to induce antimicrobial resistance. Furthermore, environmental contamination is less problematic compared to antibiotics.¹⁴

More than two decades ago, Sharon and co-workers have investigated various mannosides and oligomannosides as

*To whom correspondence should be addressed. Phone: +41 61 267 1551. Fax: +41 61 267 1552. E-mail: beat.ernst@unibas.ch.

^a Abbreviations: AUC, area under the curve; Caco-2 cells, Caucasian colon adenocarcinoma cells; CFU, colony forming units; CRD, carbohydrate recognition domain; DC-SIGN, dendritic cell-specific intercellular adhesion molecule-3-grabbing nonintegrin; CES, carboxylesterase; IC₅₀, half maximal inhibitory concentration; iv, intravenous; D, distribution coefficient; GPE, guinea pig erythrocytes; LC-MS, liquid chromatography–mass spectrometry; MBP, mannose-binding protein; PAMPA, parallel artificial membrane permeation assay; P_{app} , apparent permeability; P_e , effective permeation; po, peroral; PPB, plasma protein binding; PSA, polar surface area; S, solubility; SAR, structure–activity relationship; sGF, simulated gastric fluid; sIF, simulated intestinal fluid; TEER, transepithelial resistance; UPEC, uropathogenic *E. coli*; UTI, urinary tract infection.

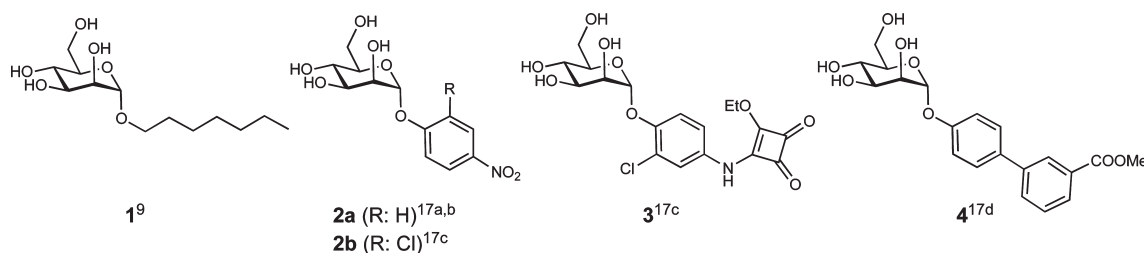
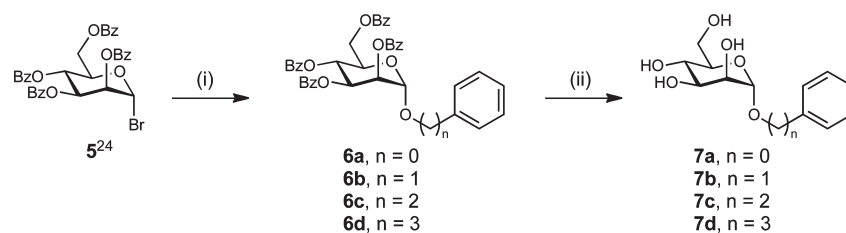


Figure 1. Known alkyl (**1**) and aryl (**2–4**) α -D-mannosides exhibiting nanomolar affinities.

Scheme 1. Phenyl α -D-Mannosides **7a–7d** with Spacers of Different Lengths between the Carbohydrate Moiety and the Phenyl Substituent^a



^a (i) $\text{Ph}(\text{CH}_2)_n\text{OH}$, $\text{Hg}(\text{CN})_2$, HgBr_2 , DCM, 2 h to 7 d, rt, 57–99%; (ii) NaOMe, MeOH, 6–16 h, rt, 48–91%.

potential antagonists for type 1 fimbriae-mediated bacterial adhesion.¹⁵ However, for these mannosides, only weak interactions in the milli- to micromolar range were observed. In contrast, numerous reports on glycoconjugate dendrimers with nanomolar affinities have been published.¹⁶ However, on the basis of their large molecular weight and high polarity, they are predicted to exhibit only poor intestinal absorption and are therefore not amenable for oral dosing. Recently, some isolated reports on high affinity monovalent FimH antagonists were published¹⁷ and, in one case, a systematic structure–activity relationship (SAR) profile was established.^{17d} In summary,^{8,9,15–19} long chain alkyl and aryl mannosides (selected examples are presented in Figure 1) displayed the highest affinity, likely due to hydrophobic interactions with two tyrosines and one isoleucine forming the entrance to the binding site, the so-called “tyrosine gate”.¹⁸ Because binding affinities were obtained from diverse assay formats,^{9,17c,20} a direct comparison of the affinities is difficult. On the basis of various crystal structures of methyl-⁸ and *n*-butyl α -D-mannoside¹⁸ as well as oligomannose-3⁹ bound to FimH, Han et al. recently presented a rationale for the design of arylmannosides with increased affinities.^{17d}

To date, a few reports on the *in vivo* potential of methyl α -D-mannoside^{10,21,22} and *n*-heptyl α -D-mannoside (**1**)¹⁰ are available. In all cases, the FimH antagonists were directly instilled into the bladder concomitantly with uropathogenic *E. coli* (UPEC). In this communication, we present for the first time nanomolar FimH antagonists exhibiting appropriate pharmacokinetic properties for *iv* and oral treatment of urinary tract infections.

Results and Discussion

Identification of Lead Mannoside. In most of the reported FimH antagonists, aromatic aglycones have been applied.¹⁷ However, only limited information on the optimal spacer length between the mannose moiety and the aromatic substituent is available. Generally, the aromatic moiety is directly fused to the anomeric oxygen.^{17a–d} Extended spacers containing one^{17b,d} or two^{17e} methylene moieties were also reported,

however, the corresponding antagonists are not really comparable to each other because different assay formats were used for their evaluation. For the identification of the optimal spacer length, we therefore synthesized mannosides **7a–d** (Scheme 1). In a competitive binding assay,²³ mannoside **7a** showed a slightly higher affinity (Table 1, entry 2) compared with **7b–7d** (see Table 1, entries 3–5), confirming recent data for **7a** and **7b**.^{17d}

From the crystal structure of *n*-butyl α -D-mannoside bound to FimH,¹⁸ it becomes obvious that the hydrophobic rim formed by Tyr48, Tyr137, and Ile52 is not reached by an anomeric phenyl group. An extension by a second aromatic ring, i.e. a biphenyl α -D-mannoside, however, should be compatible for π – π stacking. Indeed, some recently published representatives of this compound class show excellent affinities.^{17d}

To achieve an optimal fit with the hydrophobic binding site of FimH, the conformation of the biphenyl aglycone in **1** was modified by different substitution patterns on ring A (Figure 2). Because electron poor aromatic rings substantially improve the binding affinities of FimH antagonists (a 10-fold improvement is reported for **2B** vs **2A**^{17c}), chloro substituents on ring A were used for the spatial exploration of the binding site. With substituents in *ortho*-position, only a minor change of the dihedral angle Φ_1 is observed (-3.3° to -0.7°). However, by an increased rotational barrier, the conformational flexibility is limited. The dihedral angle Φ_2 between the conjugated aromatic rings results from an interplay between π -conjugation and steric effects.^{24,25} By migrating the substituent to the *meta*-position, the torsion angle Φ_2 is substantially influenced. Whereas unsubstituted biphenyls show a global twisted minimum at a torsion angle Φ_2 of approximately 39° ,²⁶ substituents in the *meta*-position favor an increase of Φ_2 to 60° . Details of the conformational analyses are summarized in the Supporting Information.

Design Strategy for Intestinal Absorption and Renal Elimination. Besides high affinity, drug-like pharmacokinetic properties are a prerequisite for a successful *in vivo* application. In the present case, orally available FimH antagonists

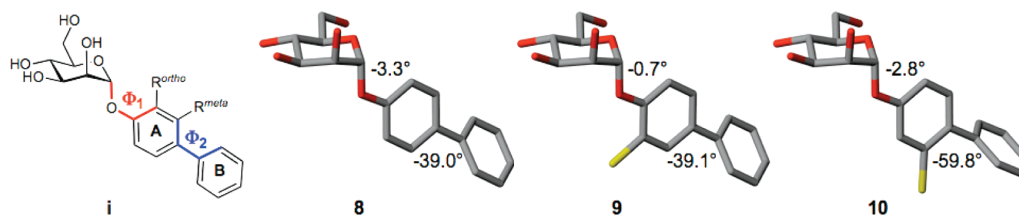


Figure 2. Conformational changes of the biphenyl aglycone by chloro substitutions in *ortho*- and *meta*-position of ring A.

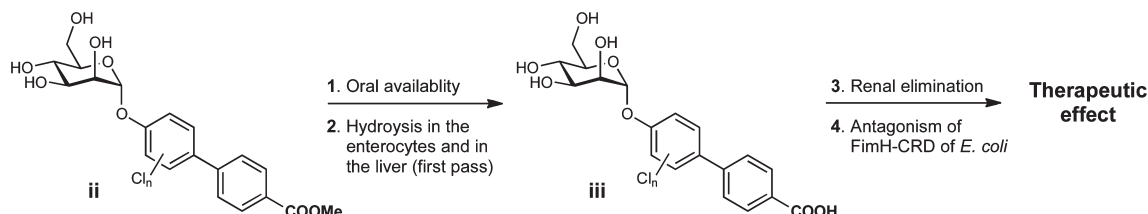


Figure 3. FimH antagonists with the pharmacodynamic and pharmacokinetic properties required for a therapeutic application. (1) For the prediction of oral availability, the PAMPA³⁰ and the Caco-2 cell assay³¹ are applied. (2) The hydrolysis of ester **ii** to carboxylate **iii** is evaluated by mouse liver microsomes. (3) Renal excretion is estimated based on a positive correlation with polar descriptors (polar surface area, H-bond donors, H-bond acceptors, rotatable bonds).³² (4) The potential of FimH antagonists is assessed with a target-based assay²³ and a function-based cellular assay.³³ For the evaluation of the therapeutic effect, a urinary tract infection mouse model (UTI mouse model in C3H/HeN mice) is applied.

that, once in circulation, are metabolically stable and undergo fast renal elimination, are required. This pharmacokinetic profile results from various serial and/or simultaneous processes that include dissolution, intestinal absorption, plasma protein binding, metabolic clearance, body distribution as well as renal and other clearance mechanisms. Because intestinal absorption and renal elimination are related to opposed properties, i.e. lipophilicity for intestinal absorption and hydrophilicity for renal elimination, a prodrug approach²⁷ was envisaged (Figure 3). Ester **ii** is expected to undergo intestinal absorption²⁸ and, later on, efficient hydrolysis to carboxylate **iii** by esterases²⁹ present in enterocytes lining the small intestine and in the liver.

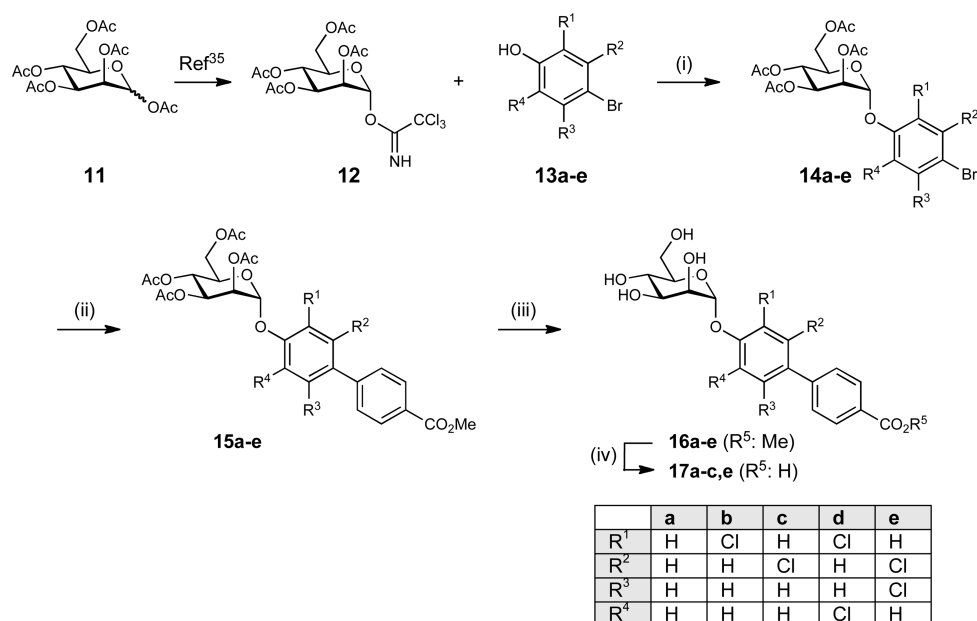
For renal clearance, the net result of glomerular filtration, active tubular secretion, and reabsorption, carboxylate **iii** should exhibit low lipophilicity ($\log D_{7.4}$) and favorable polar descriptor values (polar surface area (PSA), H-bond capacity and rotatable bonds).³² By contrast, lipophilic compounds are efficiently reabsorbed (as the passive reabsorption process occurs throughout the length of the nephron, whereas the secretion predominantly occurs at the proximal tubule). The estimated negative $\log D_{7.4}$ for antagonists of type **iii** is expected to fulfill these specifications for an efficient renal elimination and a low reabsorption. Finally, once arrived at the site of action in the bladder, the antagonist binds to the carbohydrate recognition domain (CRD) located on the bacterial pili, thus interfering with the adhesion of *E. coli* to oligosaccharide structures on urothelial cells.³⁴ To identify antagonists with the pharmacokinetic properties required for oral absorption and fast renal elimination, it was planned to determine PK parameters such as $\log D_{7.4}$, pK_a , solubility, plasma protein binding, metabolic stability, and oral availability using the parallel artificial membrane permeation assay (PAMPA)³⁰ and the Caco-2 cell assay.³¹

Synthesis of FimH Antagonists. The aglycone in the α -1-position of D-mannose plays a ternary role, i.e. it mediates the lipophilic contact with the hydrophobic tyrosine gate, contains the elements required for intestinal absorption and, after metabolic cleavage of the prodrug, for a fast renal elimination.

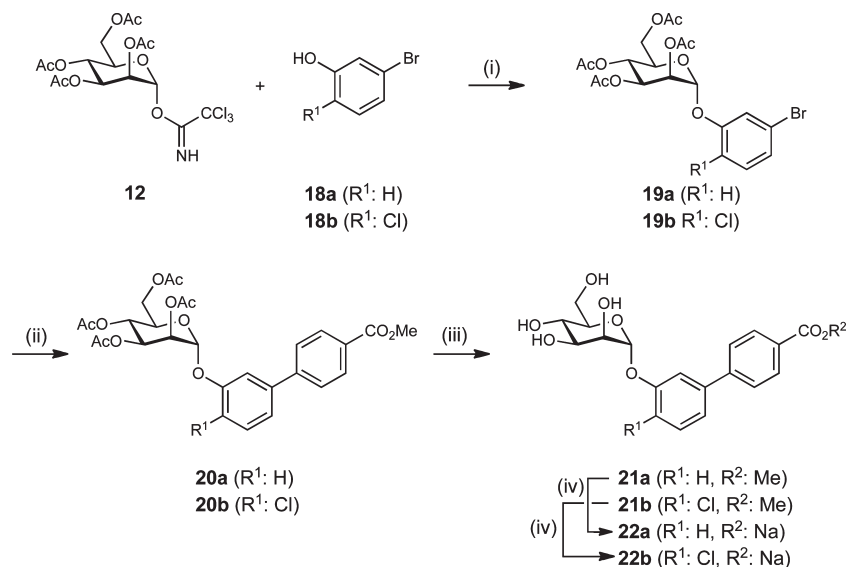
The syntheses of the *para*-substituted biphenyls **16a–e** and **17a–c,e** are outlined in Scheme 2. Lewis acid promoted glycosylation of the halogenated phenols **13a–e** with trichloroacetimidate **12**³⁵ yielded the phenyl α -D-mannosides **14a–e**. In a palladium-catalyzed Suzuki coupling with 4-methoxycarbonylphenylboronic acid, the biphenyls **15a–e** were obtained. For the deprotection of the mannose moiety, Zemplén conditions were applied (\rightarrow **16a–e**). Finally, the methyl esters were saponified, yielding the sodium salts **17a–c,e**.

In a similar approach, two *meta*-substituted biphenyls in their ester form (\rightarrow **21a,b**) and as free acids (\rightarrow **22a,b**) were obtained (see Scheme 3).

Binding Affinities and Activities. For the biological *in vitro* evaluation of the FimH antagonists, two assay formats have been developed. For an initial characterization, a cell-free competitive binding assay²³ and, later on, a cell-based aggregation assay,³³ were applied. Whereas in the cell-free competitive binding assay only the CRD of the pili was used, the complete pili are present in the cell-based assay format. Furthermore, both formats are competitive assays, i.e. the analyzed antagonists compete with mannosides for the binding site. In the cell-free competitive binding assay, the competitors are polymer-bound trimannosides, whereas in the aggregation assay, the antagonist competes with more potent oligo- and polysaccharide chains present on the surface of erythrocytes.³⁶ Therefore, lower IC_{50} values are expected for the cell-free competitive binding assay. In addition, switching from the cell-free target-based assay to the function-based assay generally leads to a reduction of potency by several orders of magnitude. The interaction is further complicated by the existence of a high- and a low-affinity state of the CRD of FimH. Aprikian et al. experimentally demonstrated that in full-length fimbriae the pilin domain stabilizes the CRD domain in the low-affinity state, whereas the CRD domain alone adopts the high-affinity state.³⁷ It was recently shown that the pilin domain allosterically causes a twist in the β -sandwich fold of the CRD domain, resulting in a loosening of the binding pocket.³⁸ On

Scheme 2^a

^a (i) TMSOTf, toluene, rt, 5 h (42–77%); (ii) 4-methoxycarbonylphenylboronic acid, Cs₂CO₃, Pd(PPh₃)₄, dioxane, 120°C, 8 h (28–85%); (iii) NaOMe, MeOH, rt, 4–24 h (22–86%); (iv) NaOMe, MeOH, rt, then NaOH/H₂O, rt, 16–24 h (63–94%).

Scheme 3^a

^a (i) TMSOTf, toluene, rt, 5 h (67–70%); (ii) 4-methoxycarbonylphenylboronic acid, Cs₂CO₃, Pd(PPh₃)₄, dioxane, 120°C, 8 h or Pd₂(dba)₃, S-Phos, dioxane, 80°C, overnight (46–56%); (iii) NaOMe, MeOH, rt, 24 h (52–67%); (iv) NaOMe, MeOH, rt, then NaOH/H₂O, rt, 24 h (75–95%).

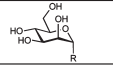
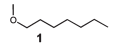
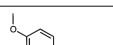
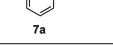
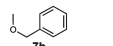
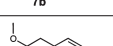
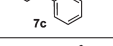
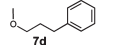
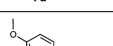
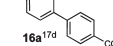
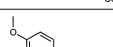
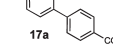
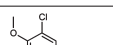
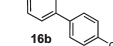
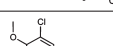
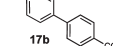
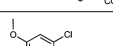
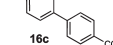
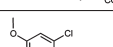
the basis of these findings, we expect a loss of affinity of our antagonists toward full-length fimbriae, when compared to the CRD domain alone.

Cell-Free Competitive Binding Assay. The cell-free inhibition assay is based on the interaction of a biotinylated polyacrylamide glycopolymer with the FimH-CRD as previously reported.²³ A recombinant protein consisting of the carbohydrate recognition domain of FimH linked with a thrombin cleavage site to a 6His-tag (FimH-CRD-Th-6His) was expressed in *E. coli* strain HM125 and purified by affinity chromatography. The IC₅₀ values of the test compounds were determined in microtiter plates coated with

FimH-CRD-Th-6His. Complexation of the biotinylated glycopolymer with streptavidin coupled to horseradish peroxidase allowed the quantification of the binding properties of FimH antagonists (Figure 4a). To ensure comparability with different antagonists, the reference compound *n*-heptyl α -D-mannopyranoside (**1**)³³ was tested in parallel in each individual microtiter plate. The affinities are reported relative to *n*-heptyl α -D-mannopyranoside (**1**) as rIC₅₀ in Table 1.

The most active representatives from the ester group are **16a** (Table 1, entry 6) and **16b** (entry 8) with affinities in the low nanomolar range, which is an approximately 10-fold improvement compared to reference compound **1**. The

Table 1. Pharmacodynamic and Pharmacokinetic Parameters of FimH Antagonists^{a,b}

		IC ₅₀ binding assay [nM]	rIC ₅₀	IC ₅₀ Aggrego- metry assay [μM]	PAMPA log P _e [log10 ⁶ cm/s]/ %Mm	Caco-2 P _{app} [10 ⁻⁶ cm/s]	log D _{7.4}	pK _a	log S [μg/mL]/ pH	PPB [%]
1		73±7.9	1.0	77.14±8.7	-4.89/21	nd	1.65	-	>3000	81
2		150±11.5	1.9	nd	nd/nd	nd	nd	-	>3000	nd
3		364±16.8	4.6	nd	nd/nd	nd	nd	-	nd	nd
4		210±11.2	2.6	nd	nd/nd	nd	nd	-	nd	nd
5		253±13.4	3.2	nd	nd/nd	nd	nd	-	nd	nd
6		10.4±1.2	0.14	42±7	-4.7/<20%	4.23	2.14	-	33.8/6.51	93
7		17.1±2.2	0.15	45±8	np	nd	<-1.5	3.88	>3000/6.61	73
8		4.8±1.2	0.06	9±2.7	-4.6/41.00	2.05	2.32	-	11.9/6.53	94
9		6.7±2.1	0.09	10±2.3	np/3.5	nd	-0.77	3.98	>3000/6.50	89
10		22.0±8.4	0.30	41 ¹⁾	-4.72/67.6	nd	2.42	-	11.5/6.50	95
11		27.6±3.9	0.38	17 ¹⁾	np	nd	-1.33	3.95	>3000/6.50	83
12		16.0±0.8	0.22	14 ¹⁾	-4.29/54.3	3.32	2.31	-	4.6/6.53	98
13		15.3±0.4	0.07	nd	-4.40/70.2	5.81	3.10	-	22.7/6.53	94
14		23.9±2.2	0.19	nd	nd/nd	nd	nd	nd	nd	nd
15		20.0±4.3	0.27	33 ¹⁾	-5.01/60.7	4.88	2.02	-	37.6/6.52	92
16		38.7±5.2	0.53	45 ¹⁾	np/9.7	nd	<-1.5	3.60	>3000/6.50	81
17		11.8±0.1	0.16	31 ¹⁾	-4.69/51.7	1.63	1.70	-	24.3/6.54	96
18		29.2±0.7	0.40	nd	np/nr	0.55	<-1.5	3.41	>3000/6.5	87

^a Single determination; P_e , effective permeation; P_{app} , apparent permeability; np, no permeation; nr, no retention; nd, not determined. ^b The IC₅₀s were determined with the cell-free competitive binding assay.²³ The rIC₅₀ of each substance was calculated by dividing the IC₅₀ of the compound of interest by the IC₅₀ of the reference compound **1** (entry 1). This leads to rIC₅₀ values below 1.00 for derivatives binding better than **1** and rIC₅₀ values above 1.00 for compounds with a lower affinity than **1**. The aggregation of *E. coli* and GPE were determined in the aggregometry assay.³³ Passive permeation through an artificial membrane and retention therein was determined by PAMPA (parallel artificial membrane permeation assay).³⁰ The permeation through cell monolayers was assessed by a Caco-2 assay.³¹ Distribution coefficients (log *D* values) were measured by a miniaturized shake flask procedure.⁴⁴ pK_a values were determined by NMR spectroscopy.⁴⁵ Plasma protein binding (PPB) was assessed by a miniaturized equilibrium dialysis protocol.⁴⁶ Thermodynamic solubility (*S*) was measured by an equilibrium shake flask approach.⁴⁷

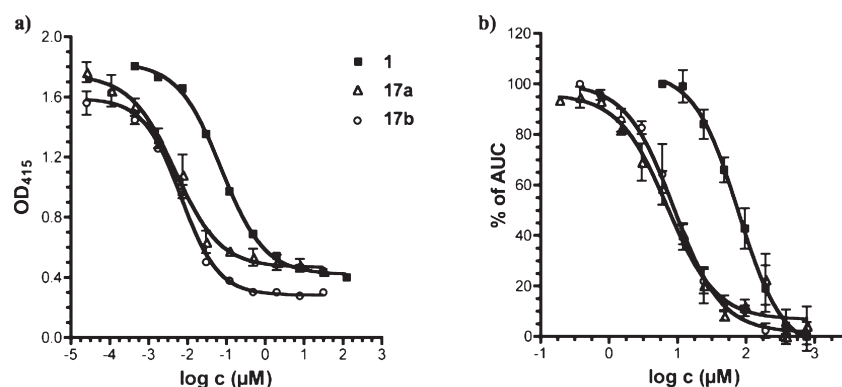


Figure 4. Affinities were determined in two different competitive assay formats. (a) a cell-free competitive binding assay²³ and (b) a cell-based aggregometry assay.³³ For antagonists **17a**, **17b**, and the reference compound **1**, IC₅₀ values in the nM and µM range, respectively, were obtained. The 1000-fold difference between the two assay formats is due to the different competitors used as well as the different affinity states present in FimH, i.e. the high-affinity state present in the CRD used in the cell-free competitive binding assay and the low-affinity state present in the pili of *E. coli* used in the aggregometry assay.

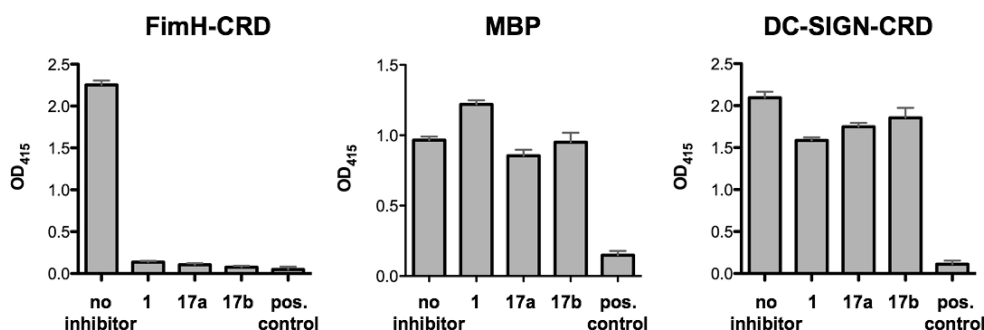


Figure 5. Competitive binding assay using FimH-CRD-Th-6His, DC-SIGN-CRD-IgG-Fc,⁴³ and MBP to evaluate the selectivity of compounds **1**, **17a**, and **17b**. Inhibitory capacities of the compounds were tested at a concentration of 1 mM. As positive control, D-mannose at a concentration of 50 mM was used.

corresponding carboxylic acids **17a** (entry 7) and **17b** (entry 9) exhibited a small reduction in affinity but are still 5-fold more active than reference compound **1**. All the remaining antagonists listed in Table 1 are slightly less active. For the in vivo examination, antagonists **17a** and **17b** were therefore foreseen for iv application and the prodrug **16b** for oral application.

Target selectivity is a further important issue. Mammalian mannose receptors are part of various biological processes, e.g. in cell–cell adhesion (DC-SIGN, dendritic cell-specific intercellular adhesion molecule-3-grabbing nonintegrin),³⁹ in the regulation of serum glycoprotein homeostasis (mannose receptor)⁴⁰ or in the innate and adaptive immune system by recognizing molecular patterns on pathogens (e.g., mannose-binding protein, mannose receptor, DC-SIGN).^{39,41,42} Non-specific interactions to the various mannose receptors by FimH inhibitors would have a profound impact on these processes. We therefore determined the affinity of reference compound **1** and the two antagonists **17a** and **17b** for two additional mannose binding proteins, DC-SIGN,^{39,43} and MBP (mannose-binding protein)⁴² (Figure 5). In both cases, affinities above 1 mM, i.e. a decrease of more than 5 orders of magnitude, was detected.

Aggregometry Assay. The potential of the biphenyl mannosides to disaggregate *E. coli* from guinea pig erythrocytes (GPE) was determined by a function-based aggregometry assay.³³ Antagonists were measured in triplicates, and the corresponding IC₅₀ values were calculated by plotting the

area under the curve (AUC) of disaggregation against the concentration of the antagonists. *n*-Heptyl α -D-mannopyranoside (**1**) was used again as reference compound and exhibits an IC₅₀ of $77.14 \pm 8.7 \mu\text{M}$. Antagonists **17a** and **17b** showed IC₅₀ values of $45 \pm 8 \mu\text{M}$ and $10 \pm 2.3 \mu\text{M}$, respectively (Figure 4b). In general, the activities obtained from the aggregometry assay are approximately 1000-fold lower than the affinities determined in the target-based competitive assay (discussion see above).

In Vitro Pharmacokinetic Characterization of FimH Antagonists. For an application in the UTI mouse model, iv or po available FimH antagonists are required that, once absorbed to circulation, are metabolically stable and undergo fast renal elimination. Sufficient bioavailability requires a combination of high solubility and permeability to maximize absorption and low hepatic clearance to minimize first pass extraction. Furthermore, for efficient renal elimination, active and/or passive membrane permeability and low reabsorption in the renal tubuli is required. From the series of FimH antagonists with nanomolar in vitro activities (see Table 1), representatives with appropriate pharmacokinetic properties were selected for in vivo experiments based on the parameters shown below.

Oral Absorption and Renal Excretion. For the evaluation of oral absorption and renal excretion of the esters **16** and **21** as well as the acids **17** and **22** physicochemical parameters such as pK_a values, lipophilicity (distribution coefficients, log *D*_{7.4}), solubility, and permeability were determined

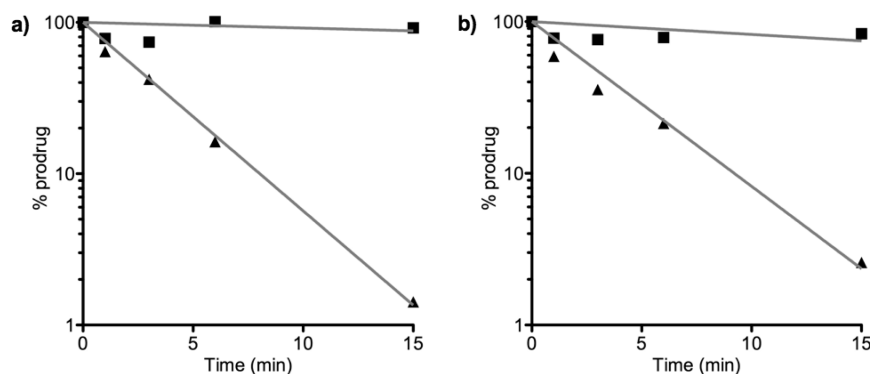


Figure 6. Incubation of (a) **16a** and (b) **16b** with pooled mouse liver microsomes (0.25 mg of protein/mL), in absence (▲) and in presence (■) of the specific carboxylesterase inhibitor bis(4-nitrophenyl) phosphate (BNPP).

(Table 1). Not surprisingly, the acids **17** and **22** showed $\log D_{7.4}$ values in the range of -1 to -2 and pK_a values of approximately 4. While these parameters are beneficial for renal excretion,³² oral absorption by passive diffusion seems unlikely. Indeed, when the permeation through an artificial membrane (PAMPA³⁰) was studied, neither significant permeation ($\log P_e$, P_e : effective permeation) nor membrane retention could be detected. Whereas for a successful oral absorption $\log P_e$ should be above -5.7 and/or the membrane retention above 80%,⁴⁸ the corresponding values for the carboxylic acids **17** and **22** are far from being in this range (see Table 1, e.g. entries 7 and 9). However, $\log D_{7.4}$ values and PAMPA results were markedly improved for the esters **16** and **21** (Table 1, e.g. entries 6 and 8), suggesting that these FimH antagonists are orally absorbed. This assumption was fully confirmed in a cell-based permeation assay with Caco-2 cells.³¹ For renal excretion, Varma et al.³¹ correlated low lipophilicity and the presence of a charged state at physiological pH positively with enhanced elimination. On the basis of $\log D_{7.4}$ and pK_a summarized in Table 1, the carboxylates **17** and **22** fulfill these requirements. Overall, these results support the prodrug approach: (i) oral application of the esters **16** and **21** and (ii) renal elimination of the corresponding acids **17** and **22**.

Solubility. A major problem of the antagonists **16** and **21** is their insufficient solubility, ranging from 4.6 to 37.6 $\mu\text{g/mL}$. Even though the solubility issue can be addressed by appropriate formulations, further structural modifications to improve solubility are necessary. Opposite to the esters, the corresponding carboxylates **17** and **22** showed excellent solubility (> 3 mg/mL). This enables their iv application in physiological solutions (PBS) in the UTI model without further needs to develop suitable formulations (see below).

Stability in Simulated Gastrointestinal Fluids. To exclude degradation in the gastrointestinal tract prior to absorption, the stability of **1**, **16b**, and **17b** in simulated gastric fluid (sGF) and simulated intestinal fluid (sIF) was determined. All three antagonists proved to be sufficiently stable with more than 80% of the initial concentrations found after two hours.

Metabolic Stability. Because the prodrug approach is only applicable when the esters **16a** and **16b** are rapidly metabolically cleaved into the corresponding acids, their propensity to enzymatic hydrolysis by carboxylesterase (CES) was studied. Mammalian CESs are localized in the endoplasmic reticulum of the liver and most other organs.²⁹ Because of the excellent affinity of the corresponding acids **17a** and

17b to FimH, we concentrated our metabolic studies on the ester prodrugs **16a** and **16b**, which were incubated with pooled male mouse liver microsomes to study the hydrolysis and the release of the metabolites. Preliminary experiments involving low substrate concentrations (2 μM) and a concentration of the microsomal protein of 0.25 mg/mL showed a fast degradation of the ester prodrugs (Figure 6). Addition of the specific CES inhibitor bis(4-nitrophenyl) phosphate (BNPP) prevented ester degradation, suggesting that the metabolic transformation can be attributed to CESs.⁴⁹

On the basis of these *in vitro* results, we also expect fast hydrolysis of the esters *in vivo* at the first liver passage. Current studies are focusing on the kinetic parameters of the enzymatic ester cleavage.

To reach the minimal therapeutic concentration in the bladder (approximately 1 $\mu\text{g/mL}$, as estimated from a cell-based infection assay⁵⁰), the FimH antagonists **17a** and **17b** should be efficiently renally eliminated and not further metabolically processed. Therefore, the metabolic fate of the free carboxylic acids **17a** and **17b** was examined. A common method to predict a compound's propensity to phase I metabolism is its incubation with liver microsomes in presence of NADPH.⁵¹ Under these conditions, *in vitro* incubations of the free carboxylic acids **17a** and **17b** with pooled male mouse liver microsomes (0.5 mg microsomal protein/mL) did not show significant compound depletion over a period of 30 min, suggesting a high stability against cytochrome P450 mediated metabolism *in vivo*. However, phase II metabolic pathways such as glucuronidation remain to be studied in details.

Plasma Protein Binding (PPB). Compared to the corresponding esters **16** and **21**, the antagonists **17** and **22** exhibit 5–20% lower plasma protein binding, typically in the range of 73–89%. This rather low PPB beneficially influences renal excretion because, in line with the free drug hypothesis,⁵² molecules bound to plasma proteins evade metabolism and excretion. However, for a concluding statement, the kinetics of PPB, i.e. association and dissociation rate constants, have to be determined because PPB alone is not necessarily predictive for distribution, metabolism, and clearance.^{53,54}

In Vivo Pharmacokinetics and Treatment Studies. The two mannose derivatives methyl α -D-mannoside and *n*-heptyl α -D-mannoside (**1**) were previously tested in the UTI mouse model.^{10,21,22} In all three studies, the FimH antagonists were first preincubated with the bacterial suspension, followed by transurethral inoculation. To efficiently reduce infection,

Antagonist	Compartment	C_{\max} ($\mu\text{g/mL}$)	AUC_{0-24} ($\mu\text{g} \times \text{h/mL}$)	PPB
1	plasma	35 ± 14.1	34.3 ± 33.3	81%
	urine	951.4 ± 249.6	2469.3 ± 636.4	
17a	plasma	34.4 ± 11.8	19.3 ± 6.2	73%
	urine	509.6 ± 427.5	139.9 ± 118.8	
17b	plasma	39.4 ± 15.7	20.8 ± 7.3	89%
	urine	588.4 ± 218.2	209.6 ± 72.3	

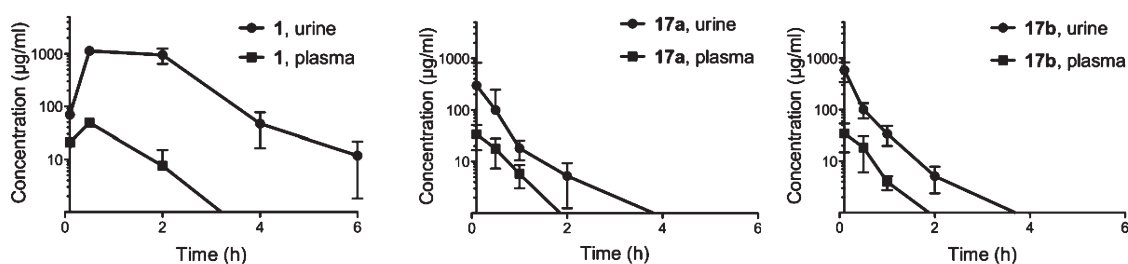


Figure 7. Determination of antagonist concentration in urine and plasma after a single iv application of 50 mg/kg. The data (table and graphs) show time-dependent urine and plasma concentrations of **1**, **17a**, and **17b**.

large amounts of methyl α -D-mannoside had to be applied (up to 1 M).²¹ For *n*-heptyl α -D-mannoside (**1**), an approximately one \log_{10} unit reduction of bacterial counts in the bladder was reached with lower, but still millimolar, concentration.¹⁰ In the previously presented studies, the FimH antagonists were exclusively instilled into the bladder, which is obviously not suitable for a therapeutic application. The aim of our project was therefore the identification of FimH antagonists suitable for iv or preferably po applications. Before infection studies in a mouse disease model could be performed, the in vivo pharmacokinetic parameters (C_{\max} , AUC) had to be determined to ensure the antagonists availability in the target organ (bladder).

Pharmacokinetics of a Single iv Application in C3H/HeN Mice. Plasma and urine concentrations of the FimH antagonists **1**, **17a**, and **17b** after iv application were determined. With a single dose of 50 mg/kg, the control compound **1** exhibited availability in the bladder over a period of 6 h after administration ($n = 4$), whereas at similar doses, **17a** and **17b** showed lower urine concentrations over a reduced time period (max 2 h) ($n = 6$). In Figure 7, the pharmacokinetic parameters are summarized. Overall, for all three compounds, higher availability of the antagonists in the urine was observed compared to the plasma. Because plasma protein binding is of comparable scale for the three compounds (see Table 1 and Figure 7), it similarly influences urine concentrations.

Pharmacokinetics of a Single po Application in C3H/HeN Mice. Aiming for an orally available FimH antagonist, the prodrug **16b** and its metabolite **17b** were tested. Because of the in vitro pharmacokinetic properties of **17b** (Table 1, entry 9), its low oral bioavailability after the administration of a single po dose (50 mg/kg) was not surprising. For the determination of the availability of a similar dose of **16b** at the target organ (bladder), plasma and urine concentrations were determined over a period of 24 h ($n = 6$) (Figure 8). Because **16b** was designed as a prodrug expected to be rapidly

Antagonist applied	Antagonist detected	Compartment	$\text{AUC}_{0-24 \text{ p.o.}}$ ($\mu\text{g} \times \text{h/mL}$)
17b	17b	Plasma	n.d.
		Urine	2.7 ± 3.2
16b	16b	Plasma	1.02 ± 0.32
		Urine	1.89 ± 0.37
	17b	Plasma	2.1 ± 0.61
		Urine	21.69 ± 3.88

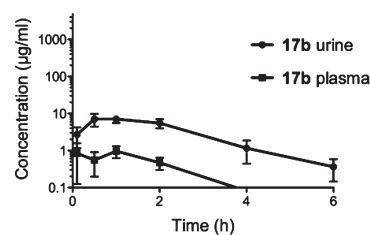


Figure 8. Determination of antagonist concentration in urine and plasma after a single po application of 50 mg/kg of antagonists **16b** and **17b**. The data (table and graph) show their time-dependent urine and plasma concentrations. When **17b** was orally applied, its plasma concentration was below the detection level, and only a small portion was present in the urine. However, after the application of the prodrug **16b**, metabolite **17b** was predominantly detected due to fast metabolic hydrolysis of **16b**. However, minor amounts of **16b** are still traceable in plasma as well as urine; nd, not detectable.

hydrolyzed, plasma and urine samples were analyzed not only for **16b** but also for its metabolite **17b**. **16b** was present only in minor concentrations in both plasma and urine. However, although the AUC of metabolite **17b** in urine is reduced by 90% compared to the iv application, its minimal therapeutic concentration can be maintained over a period of 2 to 3 h.

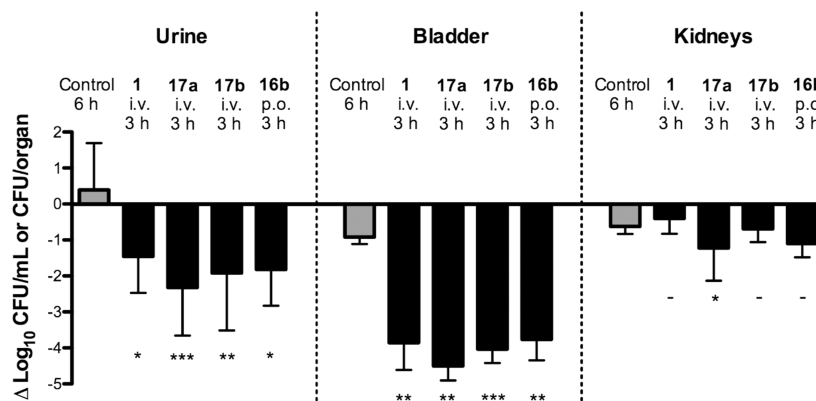


Figure 9. Treatment efficacy of the reference compound (**1**) and three FimH antagonists (**17a**, **17b**, **16b**) at a dosage of 50 mg/kg in the UTI mouse model after 3 h of infection, compared to a 6 h infection study ($n = 6$). **1**, **17a**, and **17b** were applied iv into the tail vein, whereas **16b** was applied orally. As baseline (reference), the mean counts of the 3 h infection were subtracted from the results of the tested antagonists and the 6 h control group. P values were calculated by comparing the treatment groups with the 3 h control group. (*) $P < 0.05$, (**) $P < 0.01$, (***) $P < 0.001$, (-) not significant (determined by Mann–Whitney test).

UTI Mouse Model: Treatment Study. Before treatment studies were started, the optimal infection profile was established. A 3 h infection exhibited the highest infection level in the C3H/HeN mouse strain. At longer infection times, e.g. 6 h, the control group showed indeed higher bacterial counts in the urine, however, the bladder and kidney counts already decreased due to self-clearance of the infection in the UTI mouse model.⁵⁵ For the in vivo UTI treatment studies (Figure 9), antagonists **1**, **17a**, **17b**, and **16b** were applied followed by infection with UPEC (UTI89). For each antagonist, a group of six animals was used. The animals were sacrificed 3 h after inoculation and urine and homogenized organs (bladder, kidneys) were examined for bacterial counts. The mean value in the untreated reference group ($n = 6$) showed 1.8×10^6 CFU/mL in the urine, 1.4×10^8 CFU in the bladder and 9.7×10^6 CFU in the kidneys. The bar diagram in Figure 9 summarizes the bacterial counts after iv (**1**, **17a**, and **17b**) and po (**16b**) treatment. The baseline represents the values obtained for the control group after 3 h and was used as reference for CFU reductions. **1** showed the lowest inhibition of growth in the urine with $1.5 \log_{10}$ CFU reduction and an approximately $4 \log_{10}$ reduction of bacterial counts in the bladder. After iv application of **17a**, a substantial decrease in the bacterial count was obtained ($> 2 \log_{10}$ CFU reduction in the urine and $4.5 \log_{10}$ reduction in the bladder). A slightly lower reduction was observed when **17b** was applied iv (a decrease of $2 \log_{10}$ CFU in the urine and $4 \log_{10}$ for bladder counts). Interestingly, almost the same reduction of the bacterial count was detected with orally applied **16b**.

In general, urine samples showed higher bacterial counts compared to the bladder. This could be due to the difficulties during urine sampling. We observed that infected C3H/HeN mice void considerably less urine (5–50 μ L) compared to healthy mice (50–100 μ L). As a consequence, the lower urine volume leads to a higher concentration of bacteria in the collected urine and therefore to higher bacterial counts compared to the bladder.

In all treated animals, bacterial counts were only marginally reduced in the kidneys. This lower response to the treatment with FimH antagonists is probably due to different bacterial adhesion mechanisms in bladder and kidney. Whereas in the bladder adhesion is mediated by type I pili (via the CRD of FimH), P pili-dependent interactions are crucial for the adhesion in the kidneys.⁶

Summary and Conclusions

With the objective to develop an oral treatment of urinary tract infections, we have synthesized a series of potent small molecular weight FimH antagonists. Starting from the known antagonist phenyl α -D-mannopyranoside (**7a**), two equally potent classes of biphenyl α -D-mannopyranoside, those with an ester function (**16** and **21**) and those with a carboxylate (**17** and **22**) on the terminal aromatic ring, were synthesized. According to their pharmacokinetic properties, the acids **17** and **22** were not expected to be orally absorbed, a prediction that was also confirmed by an in vivo PK study. Therefore, a prodrug approach was envisaged. On the basis of permeation assays (PAMPA and Caco-2), the esters **16** and **22** were expected to exhibit oral availability. Moreover, metabolic studies with mouse liver microsomes proposed fast in vivo hydrolysis of orally applied **16b** to the corresponding carboxylate **17b**. In vivo PK studies in mice finally confirmed the in vitro prediction of a fast renal elimination of **17b** to the target organ, the bladder. When orally applied **16b** was tested in the UTI mouse model, it reduced the colony forming units (CFU) in the urine by 2 orders of magnitude and in the bladder by 4 orders of magnitude. As a result, a low molecular weight FimH antagonist suitable for the oral treatment of urinary tract infections was identified.

However, a number of parameters remain to be improved. Because the solubilities of the esters **16** and **22** are in the low μ g/mL range, an iv application was impossible and the suspension in DMSO/1% Tween 80 used for oral dosing is not optimal. In addition, due to fast renal elimination, the minimal therapeutic concentration of **17b** in the bladder could only be maintained for 2–3 h. Because high plasma protein binding was observed, an unfavorable kinetic of dissociation of the active principle from plasma proteins followed by fast renal elimination might be the reason for these findings. An improvement of the corresponding pharmacokinetic parameters should positively influence the duration of action. Furthermore, a detailed analysis of the metabolic pathway of **16b** and its metabolite **17b** will elucidate their overall metabolic fate. Finally, a detailed PK/PD profile in the mouse model will elucidate the full potential of FimH antagonists for the therapy of urinary tract infections (UTI).

Experimental Section

General Methods. NMR spectra were recorded on a Bruker Avance DMX-500 (500 MHz) spectrometer. Assignment of ^1H

and ^{13}C NMR spectra was achieved using 2D methods (COSY, HSQC, TOCSY). Chemical shifts are expressed in ppm using residual CHCl_3 , CHD_2OD , and HDO as references. Optical rotations were measured using Perkin-Elmer polarimeter 341. Electron spray ionization mass spectra (ESI-MS) were obtained on a Waters micromass ZQ. HRMS analysis were carried out using a Bruker Daltonics micrOTOF spectrometer equipped with a TOF hexapole detector. Microanalyses were performed at the Department of Chemistry, University of Basel, Switzerland. Microwave-assisted reactions were carried out with a CEM Discover and Explorer. Reactions were monitored by TLC using glass plates coated with silica gel 60 F₂₅₄ (Merck) and visualized by using UV light and/or by heating to 140 °C for 5 min with a molybdate solution (a 0.02 M solution of ammonium cerium sulfate dihydrate and ammonium molybdate tetrahydrate in aqueous 10% H_2SO_4). Column chromatography was performed on a CombiFlash Companion (Teledyne-ISCO, Inc.) using RediSep normal phase disposable flash columns (silica gel). Reversed phase chromatography was performed on LiChroprepRP-18 (Merck, 40–63 μm). Commercially available reagents were purchased from Fluka, Aldrich, Merck, AKSci, ASDI, or Alfa Aesar. Methanol (MeOH) was dried by refluxing with sodium methoxide and distilled immediately before use. Toluene was dried by filtration over Al_2O_3 (Fluka, type 5016 A basic). Dioxane was dried by distillation from sodium/benzophenone.

4-Bromophenyl 2,3,4,6-Tetra-O-acetyl- α -D-mannopyranoside (14a). To a stirred solution of **12** (1.17 g, 3.00 mmol) and 4-bromophenol (**13a**, 623 mg, 3.60 mmol) in toluene (12 mL), TMSOTf (65 μL , 0.36 mmol) was added dropwise under argon. The mixture was stirred at rt for 5 h and then diluted with toluene (15 mL) and washed with satd aq NaHCO_3 . The organic layer was separated, and the aqueous layer was extracted three times with toluene. The combined organic layers were dried over Na_2SO_4 and concentrated in vacuo. The residue was purified by flash chromatography on silica (petroleum ether/EtOAc, 19:1 to 1.5:1) to yield **14a** (1.17 g, 74%) as a white solid.

$[\alpha]_{\text{D}}^{20} +80.8$ (*c* 1.00, CHCl_3). ^1H NMR (500 MHz, CDCl_3): δ 2.06 (s, 9H, 3 COCH_3), 2.19 (s, 3H, COCH_3), 4.06 (m, 2H, H-5, H-6a), 4.27 (dd, *J* = 5.6, 12.4 Hz, 1H, H-6b), 5.36 (t, *J* = 10.2 Hz, 1H, H-4), 5.43 (dd, *J* = 1.8, 3.5 Hz, 1H, H-2), 5.48 (d, *J* = 1.7 Hz, 1H, H-1), 5.53 (dd, *J* = 3.5, 10.1 Hz, 1H, H-3), 6.98, 7.41 (AA', BB' of AA'BB', *J* = 9.0 Hz, 4H, C_6H_4). ^{13}C NMR (125 MHz, CDCl_3): δ 20.71, 20.73, 20.74, 20.9 (4 COCH_3), 62.1 (C-6), 65.9 (C-4), 68.8 (C-3), 69.2 (C-2), 69.3 (C-5), 95.9 (C-1), 115.6, 118.3, 132.6, 154.7 (6C, C_6H_4), 170.0 (4C, 4 CO).

4-Bromo-2-chlorophenyl 2,3,4,6-tetra-O-acetyl- α -D-mannopyranoside (14b). According to the procedure described for **14a**, compound **12** (2.38 g, 4.84 mmol) and 4-bromo-2-chlorophenol (**13b**, 1.20 g, 5.80 mmol) were treated with TMSOTf (107 mg, 0.484 mmol) to yield **14b** (1.54 g, 59%) as a white solid.

$[\alpha]_{\text{D}}^{20} +60.6$ (*c* 0.40, CHCl_3). ^1H NMR (500 MHz, CDCl_3): δ 2.02, 2.04, 2.18 (3s, 12H, 4 COCH_3), 4.05 (dd, *J* = 2.3, 12.2 Hz, 1H, H-6a), 4.10 (ddd, *J* = 2.7, 5.3, 9.6 Hz, 1H, H-5), 4.24 (dd, *J* = 5.4, 12.2 Hz, 1H, H-6b), 5.35 (t, *J* = 10.1 Hz, 1H, H-4), 5.48 (m, 2H, H-1, H-2), 5.56 (dd, *J* = 3.2, 10.1 Hz, 1H, H-3), 7.03 (d, *J* = 8.8 Hz, 1H, C_6H_3), 7.30 (dd, *J* = 2.4, 8.8 Hz, 1H, C_6H_3), 7.53 (d, *J* = 2.4 Hz, 1H, C_6H_3). ^{13}C NMR (125 MHz, CDCl_3): δ 20.9, 21.1 (4C, 4 COCH_3), 62.3 (C-6), 65.9 (C-4), 68.9 (C-3), 69.4 (C-2), 70.1 (C-5), 96.9 (C-1), 115.9, 118.4, 125.7, 130.8, 133.3, 150.6 (C_6H_3), 169.9, 170.0, 170.1, 170.7 (4 CO). ESI-MS calcd for $\text{C}_{20}\text{H}_{22}\text{BrClNaO}_{10}$ [*M* + *Na*]⁺ 559.0; found 559.0; Anal. Calcd for $\text{C}_{20}\text{H}_{22}\text{BrClO}_{10}$: C 44.67, H 4.12. Found: C 45.08, H 4.14.

Methyl 4'-(2,3,4,6-Tetra-O-acetyl- α -D-mannopyranosyloxy)-biphenyl-4-carboxylate (15a). A Schlenk tube was charged with **14a** (503 mg, 1.00 mmol), 4-methoxycarbonylphenylboronic acid (224 mg, 1.24 mmol), *S*-Phos (20.5 mg, 0.05 mmol), cesium carbonate (1.17 g, 3.6 mmol), $\text{Pd}_2(\text{dba})_3$ (10.4 mg, 0.01 mmol), and a stirring bar. The tube was closed with a rubber septum and was evacuated and flushed with argon. This procedure was

repeated once, and then freshly degassed dioxane (5 mL) was added under a stream of argon. The reaction tube was quickly sealed and the contents were stirred at 80 °C overnight. The reaction mixture was cooled to rt, diluted with EtOAc (10 mL), washed with satd aq NaHCO_3 (5 mL) and brine (5 mL), and dried over Na_2SO_4 . The solvents were removed in vacuo, and the residue was purified by flash chromatography on silica (petroleum ether/EtOAc, 3:1 to 3:2) to give **15a** (474 mg, 85%) as a white solid.

$[\alpha]_{\text{D}}^{20} +80.8$ (*c* 1.00, CHCl_3). ^1H NMR (500 MHz, CDCl_3): δ 2.02, 2.03, 2.04, 2.19 (4s, 12H, COCH_3), 3.91 (s, 3H, OCH_3), 4.08 (m, 2H, H-6a, H-5), 4.27 (dd, *J* = 5.2, 12.2 Hz, 1H, H-6b), 5.37 (t, *J* = 10.1 Hz, 1H, H-4), 5.45 (dd, *J* = 1.8, 3.4 Hz, 1H, H-2), 5.56 (m, 2H, H-1, H-3), 7.16 (AA' of AA'BB', *J* = 8.7 Hz, 2H, C_6H_4), 7.57 (m, 4H, C_6H_4), 8.07 (BB' of AA'BB', *J* = 8.4 Hz, 2H, C_6H_4). ^{13}C NMR (125 MHz, CDCl_3): δ 20.74, 20.75, 20.77, 21.0 (4 COCH_3), 52.2 (OCH_3), 62.1 (C-6), 65.9 (C-4), 68.9 (C-3), 69.3, 69.4 (C-2, C-5), 95.8 (C-1), 116.9, 126.7, 128.5, 128.7, 130.2, 134.8, 144.8, 155.7 (12C, 2 C_6H_4), 167.0, 169.8, 170.0, 170.1, 170.6 (5 CO). ESI-MS calcd for $\text{C}_{28}\text{H}_{30}\text{NaO}_{12}$ [*M* + *Na*]⁺ 581.2; found 581.0.

Methyl 4'-(2,3,4,6-Tetra-O-acetyl- α -D-mannopyranosyloxy)-3'-chlorobiphenyl-4-carboxylate (15b). A microwave tube was charged with bromide **14b** (720 mg, 1.34 mmol), 4-methoxycarbonylphenylboronic acid (289 mg, 1.61 mmol), cesium carbonate (1.31 g, 4.02 mmol), and $\text{Pd}(\text{PPh}_3)_4$ (77.4 mg, 0.067 mmol). The tube was sealed with a Teflon septum, evacuated through a needle, and flushed with argon. Degassed dioxane (1.5 mL) was added and the closed tube was degassed in an ultrasonic bath for 15 min, flushed again with argon for 20 min, and exposed to microwave irradiation at 120 °C for 500 min. The solvent was evaporated in vacuo. The residue was dissolved in DCM (10 mL), washed with brine (2 \times 10 mL), dried over Na_2SO_4 , and concentrated in vacuo. The residue was purified by flash chromatography on silica (petroleum ether/EtOAc, 5:1 to 0.5:1) to yield **15b** (333 mg, 42%) as a white foam.

$[\alpha]_{\text{D}}^{20} +66.3$ (*c* 1.06, CHCl_3). ^1H NMR (500 MHz, CDCl_3): δ 2.03, 2.06, 2.20 (3s, 12H, COCH_3), 3.92 (s, 3H, OCH_3), 4.08 (dd, *J* = 2.4, 12.3 Hz, 1H, H-6a), 4.17 (m, 1H, H-5), 4.28 (dd, *J* = 5.4, 12.3 Hz, 1H, H-6b), 5.39 (t, *J* = 10.6 Hz, 1H, H-4), 5.54 (dd, *J* = 1.9, 3.4 Hz, 1H, H-2), 5.59 (d, *J* = 1.8 Hz, 1H, H-1), 5.62 (dd, *J* = 3.5, 10.1 Hz, 1H, H-3), 7.24 (s, 1H, C_6H_3), 7.44 (dd, *J* = 2.2, 8.5 Hz, 1H, C_6H_3), 7.57 (AA' of AA'BB', *J* = 8.5 Hz, 2H, C_6H_4), 7.65 (d, *J* = 2.2 Hz, 1H, C_6H_3), 8.08 (BB' of AA'BB', *J* = 8.5 Hz, 2H, C_6H_4). ^{13}C NMR (125 MHz, CDCl_3): δ 20.9, 21.0, 21.1 (4C, 4 COCH_3), 52.5 (OCH_3), 62.3 (C-6), 66.0 (C-4), 69.0 (C-3), 69.5 (C-2), 70.0 (C-5), 96.8 (C-1), 117.4, 126.7, 126.9, 129.5, 130.5, 136.4, 143.6, 151.3 (12C, C_6H_3 , C_6H_4), 167.0, 169.9, 170.0, 170.2, 170.7 (5 CO). ESI-MS calcd for $\text{C}_{28}\text{H}_{29}\text{ClNaO}_{12}$ [*M* + *Na*]⁺ 615.1; found 615.2. Anal. Calcd for $\text{C}_{28}\text{H}_{29}\text{ClO}_{12}$: C 56.71, H 4.93. Found: C 56.79, H 4.92.

Methyl 4'-(α -D-Mannopyranosyloxy)-biphenyl-4-carboxylate (16a).^{17d} To a solution of **15a** (170 mg, 0.304 mmol) in MeOH (3 mL) was added freshly prepared 1 M NaOMe in MeOH (100 μL) under argon. The mixture was stirred at rt until the reaction was complete (monitored by TLC), then neutralized with Amberlyst-15 (H^+) ion-exchange resin, filtered, and concentrated in vacuo. The residue was purified by reversed-phase chromatography (RP-18, $\text{H}_2\text{O}/\text{MeOH}$, 1:0–1:1) to give **16a** (90 mg, 76%) as white solid.

$[\alpha]_{\text{D}}^{20} +82.8$ (*c* 0.2, MeOH). ^1H NMR (500 MHz, CD_3OD): δ 3.62 (m, 1H, H-5), 3.72 (m, 3H, H-4, H-6a, H-6b), 3.92 (m, 4H, H-3, OCH_3), 4.03 (s, 1H, H-2), 5.55 (s, 1H, H-1), 7.24 (AA' of AA'BB', *J* = 8.0 Hz, 2H, C_6H_4), 7.64 (AA' of AA'BB', *J* = 7.5 Hz, 2H, C_6H_4), 7.71 (BB' of AA'BB', *J* = 8.0 Hz, 2H, C_6H_4), 8.07 (BB' of AA'BB', *J* = 7.5 Hz, 2H, C_6H_4). ^{13}C NMR (125 MHz, CD_3OD): δ 52.6 (OCH_3), 62.7 (C-6), 68.3 (C-4), 72.0 (C-2), 72.4 (C-3), 75.5 (C-5), 100.1 (C-1), 118.2, 127.7, 131.1, 135.1, 146.6, 158.2, 160.3 (12C, 2 C_6H_4), 166.1 (CO). HR-MS calcd for $\text{C}_{20}\text{H}_{22}\text{NaO}_8$ [*M* + *Na*]⁺ 413.1212; found 413.1218.

Methyl 3'-Chloro-4'-(α -D-mannopyranosyloxy)-biphenyl-4-carboxylate (16b). According to the procedure described for **16a**, compound **16b** was prepared from **15b** (764 mg, 1.29 mmol). Yield: 69 mg, 12%.

$[\alpha]_D^{+97.4}$ (*c* 1.01, MeOH). $^1\text{H NMR}$ (500 MHz, CD_3OD): δ 3.64 (m, 1H, H-5), 3.72 (m, 1H, H-6a), 3.78 (m, 2H, H-4, H-6b), 3.91 (s, 3H, OCH_3), 4.00 (dd, $J=3.4, 9.5$ Hz, 1H, H-3), 4.11 (dd, $J=1.8, 3.1$ Hz, 1H, H-2), 5.60 (d, $J=1.1$ Hz, 1H, H-1), 7.46 (d, $J=8.6$ Hz, 1H, C_6H_3), 7.58 (dd, $J=2.2, 8.6$ Hz, 1H, C_6H_3), 7.69 (AA' of AA'BB', $J=8.4$ Hz, 2H, C_6H_4), 7.72 (d, $J=2.2$ Hz, 1H, C_6H_3), 8.08 (BB' of AA'BB', $J=8.4$ Hz, 2H, C_6H_4). $^{13}\text{C NMR}$ (125 MHz, CD_3OD): δ 52.7 (OCH_3), 62.8 (C-6), 68.3 (C-4), 71.9 (C-2), 72.5 (C-3), 76.2 (C-5), 100.8 (C-1), 118.7, 125.58, 127.8, 127.9, 129.9, 130.3, 131.3, 136.4, 145.3, 153.5 (12C, C_6H_3 , C_6H_4), 168.4 (CO). HR-MS calcd for $\text{C}_{20}\text{H}_{21}\text{ClNaO}_8$ [$\text{M} + \text{Na}$] $^+$ 447.0823; found 447.082.

Sodium 4'-(α -D-Mannopyranosyloxy)-biphenyl-4-carboxylate (17a). To a solution of **15a** (228 mg, 0.408 mmol) in MeOH (6.0 mL) was added 1 M NaOMe in MeOH (60 μL) at rt. The reaction mixture was stirred at rt for 4 h, and then NaOH (82 mg) in water (6 mL) was added and stirring was continued at rt overnight. The reaction mixture was concentrated in vacuo, and the residue was purified by reversed-phase chromatography (RP-18, $\text{H}_2\text{O}/\text{MeOH}$, 1:0–1:1) to afford **17a** (96 mg, 63%) as a white solid.

$[\alpha]_D^{+103}$ (*c* 0.10, MeOH). $^1\text{H NMR}$ (500 MHz, CD_3OD): δ 3.60 (m, 1H, H-5), 3.72 (m, 3H, H-6a, H-6b, H-4), 3.89 (dd, $J=3.4, 9.5$ Hz, 1H, H-3), 4.00 (dd, $J=1.8, 3.3$ Hz, 1H, H-2), 5.51 (s, 1H, H-1), 7.19, 7.60 (AA', BB' of AA'BB', $J=8.7$ Hz, 4H, C_6H_4), 8.01 (d, $J=8.2$ Hz, 2H, C_6H_4), 8.46 (s, 2H, C_6H_4). $^{13}\text{C NMR}$ (125 MHz, CD_3OD): δ 63.2 (C-6), 68.9 (C-4), 72.6 (C-2), 73.0 (C-3), 76.1 (C-5), 100.7 (C-1), 118.7, 128.0, 129.9, 131.8 (12C, 2 C_6H_4). HR-MS calcd for $\text{C}_{19}\text{H}_{20}\text{NaO}_8$ [$\text{M} + \text{H}$] $^+$ 399.1056; found 399.1052.

Sodium 3'-Chloro-4'-(α -D-mannopyranosyloxy)-biphenyl-4-carboxylate (17b). To a solution of **15b** (380 mg, 0.641 mmol) in MeOH (10 mL) was added 1 M NaOMe in MeOH (300 μL). After stirring at rt for 24 h, 0.5 M aq NaOH (18 mL) was added and stirring continued for another 24 h. The solution was concentrated in vacuo and the residue was purified by reversed-phase chromatography (RP-18, $\text{H}_2\text{O}/\text{MeOH}$, 1:0–1:1) to yield **17b** (222 mg, 80%) as a white solid.

$[\alpha]_D^{+61.6}$ (*c* 1.00, H_2O). $^1\text{H NMR}$ (500 MHz, D_2O): δ 3.66 (m, 1H, H-5), 3.73 (m, 2H, H-6a, H-6b), 3.79 (t, $J=9.8$ Hz, 1H, H-4), 4.07 (dd, $J=3.4, 9.8$ Hz, 1H, H-3), 4.14 (d, $J=1.4$ Hz, 1H, H-2), 5.47 (bs, 1H, H-1), 7.04 (d, $J=8.6$ Hz, 1H, C_6H_3), 7.24 (d, $J=8.6$ Hz, 1H, C_6H_3), 7.37 (AA' of AA'BB', $J=8.1$ Hz, 2H, C_6H_4), 7.41 (bs, 1H, C_6H_3), 7.86 (BB' of AA'BB', $J=8.1$ Hz, 2H, C_6H_4). $^{13}\text{C NMR}$ (125 MHz, D_2O): δ 60.6 (C-6), 66.5 (C-4), 69.0 (C-2), 70.5 (C-3), 73.9 (C-5), 98.6 (C-1), 117.5, 123.9, 126.2, 126.4, 128.4, 129.6, 135.2, 135.3, 141.0, 150.4 (12C, C_6H_3 , C_6H_4), 175.0 (CO). HR-MS calcd for $\text{C}_{19}\text{H}_{18}\text{ClNaO}_8$ [$\text{M} + \text{H}$] $^+$ 433.0666; found 433.0670.

Competitive Binding Assay. A recombinant protein consisting of the CRD of FimH linked with a thrombin cleavage site to a 6His-tag (FimH-CRD-Th-6His) was expressed in *E. coli* strain HM125 and purified by affinity chromatography.²³ To determine the affinity of the various FimH antagonists, a competitive binding assay described previously²³ was applied. Microtiter plates (F96 MaxiSorp, Nunc) were coated with 100 $\mu\text{L}/\text{well}$ of a 10 $\mu\text{g}/\text{mL}$ solution of FimH-CRD-Th-6His in 20 mM HEPES, 150 mM NaCl, and 1 mM CaCl_2 , pH 7.4 (assay buffer) overnight at 4 $^\circ\text{C}$. The coating solution was discarded and the wells were blocked with 150 $\mu\text{L}/\text{well}$ of 3% BSA in assay buffer for 2 h at 4 $^\circ\text{C}$. After three washing steps with assay buffer (150 $\mu\text{L}/\text{well}$), a 4-fold serial dilution of the test compound (50 $\mu\text{L}/\text{well}$) in assay buffer containing 5% DMSO and streptavidin-peroxidase coupled Man- α (1-3)-[Man- α (1-6)]-Man- β (1-4)-GlcNAc- β (1-4)-GlcNAc β polyacrylamide (TM-PAA) polymer (50 $\mu\text{L}/\text{well}$ of a 0.5 $\mu\text{g}/\text{mL}$ solution) were added. On each individual microtiter plate, *n*-heptyl α -D-mannopyranoside (**1**) was tested in parallel.

The plates were incubated for 3 h at 25 $^\circ\text{C}$ and 350 rpm and then carefully washed four times with 150 $\mu\text{L}/\text{well}$ assay buffer. After the addition of 100 $\mu\text{L}/\text{well}$ of 2,2'-azino-di-(3-ethylbenzthiazoline-6-sulfonic acid) (ABTS)-substrate, the colorimetric reaction was allowed to develop for 4 min and then stopped by the addition of 2% aqueous oxalic acid before the optical density (OD) was measured at 415 nm on a microplate-reader (Spectramax 190, Molecular Devices, California, USA). The IC_{50} values of the compounds tested in duplicates were calculated with prism software (GraphPad Software, Inc., La Jolla, California, USA). The IC_{50} defines the molar concentration of the test compound that reduces the maximal specific binding of TM-PAA polymer to FimH-CRD by 50%. The relative IC_{50} (rIC_{50}) is the ratio of the IC_{50} of the test compound to the IC_{50} of *n*-heptyl α -D-mannopyranoside (**1**).

Selectivity for FimH vs Mannose-Binding Protein and DC-SIGN. Recombinant FimH-CRD-Th-6His (10 $\mu\text{g}/\text{mL}$), DC-SIGN-CRD-Fc-IgG³⁹ (2.5 $\mu\text{g}/\text{mL}$), and mannose-binding protein⁴² (MBP, 10 $\mu\text{g}/\text{mL}$, R&D Systems, Minneapolis, MN) were each diluted in assay buffer (20 mM HEPES, pH 7.4, 150 mM NaCl, and 10 mM CaCl_2) and were coated on microtiter plates (F96 MaxiSorp, Nunc) with 100 $\mu\text{L}/\text{well}$ overnight at 4 $^\circ\text{C}$. The further steps were performed as described above.

Aggregometry Assay. The aggregometry assay was carried out as previously described.³³ In short, the percentage of aggregation of *E. coli* UTI89 with guinea pig erythrocytes (GPE) was quantitatively determined by measuring the optical density at 740 nm and 37 $^\circ\text{C}$ under stirring at 1000 rpm using an APACT 4004 aggregometer (Endotell AG, Allschwil, Switzerland). Bacteria were cultivated as described below (see in vivo models). GPE were separated from guinea pig blood (Charles River Laboratories, Sulzfeld, Germany) using Histopaque (density of 1.077 g/mL at 24 $^\circ\text{C}$, Sigma-Aldrich, Buchs, Switzerland). Prior to the measurements, the cell densities of *E. coli* and GPE were adjusted to an OD_{600} of 4, corresponding to 1.9×10^8 CFU/mL and 2.2×10^6 cells/mL, respectively. For the calibration of the instrument, the aggregation of protein-poor plasma (PPP) using PBS alone was set as 100% and the aggregation of protein-rich plasma (PRP) using GPE as 0%. After calibration, measurements were performed with 250 μL of GPE and 50 μL of bacterial suspension and the aggregation monitored over 600 s. After the aggregation phase of 600 s, 25 μL of antagonist in PBS was added to each cuvette and disaggregation was monitored for 1400 s. UTI89 $\Delta\text{fimA-H}$ was used as negative control.

Determination of the Pharmacokinetic Parameters. Materials. Dimethyl sulfoxide (DMSO), 1-octanol, pepsin, pancreatin, reduced nicotinamide adenine dinucleotide phosphate (NADPH), Dulbecco's Modified Eagle's Medium (DMEM) high glucose, and bis(4-nitrophenyl) phosphate (BNPP) were purchased from Sigma-Aldrich (Sigma-Aldrich, St. Louis MO, USA). PAMPA System Solution, GIT-0 Lipid Solution, and Acceptor Sink Buffer were ordered from pIon (pIon, Woburn MA, USA). L-Glutamine-200 mM (100 \times) solution, MEM nonessential amino acid (MEM-NEAA) solution, fetal bovine serum (FBS), and DMEM without sodium pyruvate and phenol red were bought from Invitrogen (Invitrogen, Carlsbad CA, USA). Human plasma was bought from Biopredic (Biopredic, Rennes, France) and acetonitrile (MeCN) from Acros (Acros Organics, Geel, Belgium). Pooled male mouse liver microsomes were purchased from BD Bioscience (BD Bioscience, Woburn, MA, USA). Magnesium chloride was bought from Fluka (Fluka Chemie GmbH, Buchs, Switzerland). Tris(hydroxymethyl)-aminomethane (TRIS) was obtained from AppliChem (AppliChem, Darmstadt, Germany). The Caco-2 cells were kindly provided by Prof G. Imanidis, FHNW, Muttens, and originated from the American Type Culture Collection (Rockville, MD, USA).

log $D_{7.4}$ Determination. The in silico prediction tool ALOGPS 2.1⁵⁶ was used to estimate the log *P* values of the compounds. Depending on these values, the compounds were classified into three categories: hydrophilic compounds (log *P*

Table 2

compound type	log <i>P</i>	ratios (1-octanol:buffer)
hydrophilic	<0	30:140, 40:130
moderately lipophilic	0–1	70:110, 110:70
lipophilic	>1	3:180, 4:180

below zero), moderately lipophilic compounds (log *P* between zero and one) and lipophilic compounds (log *P* above one). For each category, two different ratios (volume of 1-octanol to volume of buffer) were defined as experimental parameters (Table 2):

Equal amounts of phosphate buffer (0.1 M, pH 7.4) and 1-octanol were mixed and shaken vigorously for 5 min to saturate the phases. The mixture was left until separation of the two phases occurred, and the buffer was retrieved. Stock solutions of the test compounds were diluted with buffer to a concentration of 1 μM. For each compound, six determinations, i.e., three determinations per 1-octanol:buffer ratio, were performed in different wells of a 96-well plate. The respective volumes of buffer containing analyte (1 μM) were pipetted to the wells and covered by saturated 1-octanol according to the chosen volume ratio. The plate was sealed with aluminum foil, shaken (1350 rpm, 25 °C, 2 h) on a Heidolph Titramax 1000 plate-shaker (Heidolph Instruments GmbH & Co. KG, Schwabach, Germany) and centrifuged (2000 rpm, 25 °C, 5 min, 5804 R Eppendorf centrifuge, Hamburg, Germany). The aqueous phase was transferred to a 96-well plate for analysis by liquid chromatography–mass spectrometry (LC-MS).

log *D*_{7.4} was calculated from the 1-octanol:buffer ratio (*o:b*), the initial concentration of the analyte in buffer (1 μM), and the concentration of the analyte in buffer (*c*_B) with equilibration:

$$\log D_{7.4} = \log\left(\frac{1 \mu\text{M} - c_B}{c_B} \times \frac{1}{o:b}\right)$$

The average of the three log *D*_{7.4} values per 1-octanol:buffer ratio was calculated. If the two mean values obtained for a compound did not differ by more than 0.1 unit, the results were accepted.

Parallel Artificial Membrane Permeation Assay (PAMPA). log *P*_e was determined in a 96-well format with the PAMPA³⁰ permeation assay. For each compound, measurements were performed at three pH values (5.0, 6.2, 7.4) in quadruplicates. For this purpose, 12 wells of a deep well plate, i.e., four wells per pH value, were filled with 650 μL of System Solution. Samples (150 μL) were withdrawn from each well to determine the blank spectra by UV-spectroscopy (SpectraMax 190, Molecular Devices, Silicon Valley CA, USA). Then, analyte dissolved in DMSO was added to the remaining System Solution to yield 50 μM solutions. To exclude precipitation, the optical density was measured at 650 nm, with 0.01 being the threshold value. Solutions exceeding this threshold were filtrated. Afterward, samples (150 μL) were withdrawn to determine the reference spectra. A further 200 μL were transferred to each well of the donor plate of the PAMPA sandwich (pIon, Woburn MA, USA, P/N 110 163). The filter membranes at the bottom of the acceptor plate were impregnated with 5 μL of GIT-0 Lipid Solution and 200 μL of Acceptor Sink Buffer were filled into each acceptor well. The sandwich was assembled, placed in the GutBox, and left undisturbed for 16 h. Then, it was disassembled and samples (150 μL) were transferred from each donor and acceptor well to UV-plates. Quantification was performed by both UV-spectroscopy and LC-MS. log *P*_e values were calculated with the aid of the PAMPA Explorer Software (pIon, version 3.5).

Colorectal Adenocarcinoma Cells (Caco-2 Cells) Permeation Assay. The cells were cultivated in tissue culture flasks (BD Biosciences, Franklin Lakes NJ, USA) with DMEM high glucose medium, containing 1% L-glutamine solution, 1% MEM-NEAA solution, and 10% FBS. The cells were kept at

37 °C in humidified air containing 8% CO₂, and the medium was changed every second to third day. When approximately 90% confluence was reached, the cells were split in a 1:10 ratio and distributed to new tissue culture flasks. At passage numbers between 60 and 65, they were seeded at a density of 5.33 × 10⁵ cells per well to Transwell 6-well plates (Corning Inc., Corning NY, USA) with 2.5 mL of culture medium in the basolateral compartment and 1.5 mL (days 1–10) or 1.8 mL (from day 10 on) in the basolateral compartment. The medium was renewed on alternate days. Experiments were performed between days 19 and 21 postseeding. DMEM without sodium pyruvate and phenol red was used as transport medium for experiments. Previous to the experiment, the integrity of the Caco-2 monolayers was evaluated by measuring the transepithelial resistance (TEER) in transport medium (37 °C) with an Endohm tissue resistance instrument (World Precision Instruments Inc., Sarasota, FL, USA). Only wells with TEER values higher than 300 Ωcm² were used. Experiments were performed in triplicates. Transport medium (10 μL) from the apical compartments of three wells were replaced by the same volume of compound stock solutions (10 mM). The Transwell plate was then shaken (250 rpm) in the incubator. Samples (100 μL) were withdrawn after 5, 15, 30, 60, and 120 min from the basolateral compartment and concentrations were analyzed by HPLC. Apparent permeability coefficients (*P*_{app}) were calculated according to the following equation

$$P_{\text{app}} = \frac{dQ}{dt} \times \frac{1}{A \times c_0}$$

where *dQ/dt* is the permeability rate, *A* the surface area of the monolayer, and *c*₀ the initial concentration in the donor compartment.³¹ After the experiment, TEER values were assessed again for every well and results from wells with values below 300 Ωcm² were discarded.

p*K*_a Values. The p*K*_a values were determined as described elsewhere.⁴⁵ Briefly, the pH of a sample solution was gradually changed and the chemical shift of protons adjacent to ionizable centers was monitored by ¹H nuclear magnetic resonance (NMR) spectroscopy. The shift was plotted against the pH of the respective sample, and the p*K*_a was read out from the inflection point of the resulting sigmoidal curve.

Plasma Protein Binding (PPB). The dialysis membranes (HTDialysis LCC, Gales Ferry, CT, USA; MWCO 12–14 K) were prepared according to company instructions. The human plasma was centrifuged (5800 rpm, 25 °C, 10 min), the pH of the centrifugate (without floating plasma lipids) was adjusted to 7.5, and analyte was added to yield 10 μM solutions. Equal volumes (150 μL) of phosphate buffer (0.1 M, pH 7.5) and analyte-containing plasma were transferred to the separated compartments of the assembled 96-well high throughput dialysis block (HTDialysis LCC, Gales Ferry, CT, USA). Measurements were performed in triplicates. The plate was covered with a sealing film and incubated (5 h, 37 °C). Buffer and plasma compartment were processed separately. From the buffer compartments, 90 μL were withdrawn and 10 μL of blank plasma were added. From the plasma compartments, 10 μL were withdrawn and 90 μL of blank buffer were added. After protein precipitation with 300 μL ice-cooled MeCN, the solutions were mixed, centrifuged (3600 rpm, 4 °C, 11 min), and 50 μL of the supernatant were retrieved. Analyte concentrations were determined by LC-MS. The fraction bound (*f*_b) was calculated as follows:

$$f_b = 1 - \frac{c_b}{c_p}$$

where *c*_b is the concentration in the buffer and *c*_p the concentration in the plasma compartment. Values were accepted if the recovery of analyte was between 80 and 120%.

Thermodynamic Solubility. Microanalysis tubes (Labo-Tech J. Stofer LTS AG, Muttenz, Switzerland) were charged with

1 mg of solid substance and 250 μ L of phosphate buffer (50 mM, pH 6.5). The samples were briefly shaken by hand and then sonicated for 15 min and vigorously shaken (600 rpm, 25 °C, 2 h) on a Eppendorf Thermomixer Comfort. Afterward, the samples were left undisturbed for 24 h. After measuring the pH, the saturated solutions were filtered through a filtration plate (MultiScreen HTS, Millipore, Billerica MA, USA) by centrifugation (1500 rpm, 25 °C, 3 min). Prior to concentration determination by LC-MS, the filtrates were diluted (1:1, 1:10 and 1:100 or, if the results were outside of the calibration range, 1:1000 and 1:10000). The calibration was based on six values ranging from 0.1 to 10 μ g/mL.

Stability in Simulated Gastrointestinal Fluids. Simulated gastric fluid (sGF) and simulated intestinal fluid (sIF) were prepared according to the United States Pharmacopeia (USP 28). sGF contained sodium chloride (200 mg), pepsin (320 mg), and 37% aq HCl (0.7 mL) in bidistilled water (100 mL). sIF consisted of monopotassium phosphate (680 mg), 0.2 M NaOH (7.7 mL), and pancreatin (1 g) in bidistilled water (100 mL). sIF was adjusted to pH 6 by adding 0.2 M NaOH. sGF and sIF were preheated (37 °C), and the compounds were added to yield 10 μ M solutions. Incubations were performed on a Eppendorf Thermomixer Comfort (500 rpm, 37 °C). Before starting the experiment ($t = 0$ min) and after an incubation time of 15, 30, 60, and 120 min, samples (20 μ L) were withdrawn, precipitated with ice-cooled MeCN, and centrifuged (3600 rpm, 4 °C, 10 min). The concentrations of analyte in the supernatant were analyzed by LC-MS. Stability was expressed as percentage remaining compound relative to the initial concentration.

In Vitro Metabolism: Ester Hydrolysis. Incubations were performed in a 96-well format on a Eppendorf Thermomixer Comfort. Each compound was incubated with a reaction mixture (270 μ L) consisting of pooled male mouse liver microsomes in the presence of TRIS buffer (0.1 M, pH 7.4) and MgCl₂ (2 mM). After preheating (37 °C, 500 rpm, 10 min), the incubation was initiated by adding 30 μ L of compound solution (20 μ M) in TRIS buffer. The final concentration of the compounds was 2 μ M, and the microsomal concentration was 0.25 mg/mL. At the beginning of the experiment ($t = 0$ min) and after an incubation time of 1, 3, 6, and 15 min, samples (50 μ L) were transferred to 150 μ L of ice-cooled MeCN, centrifuged (3600 rpm, 4 °C, 10 min), and 80 μ L of supernatant were transferred to a 96-well plate for LC-MS analysis. Metabolic degradation was assessed as percentage remaining compound versus incubation time. Control experiments were performed in parallel by preincubating the microsomes with the specific carboxylesterase inhibitor BNPP (1 mM) for 5 min before addition of the antagonists.

In Vitro Metabolism: Cytochrome P450-Mediated Metabolism. Incubations consisted of pooled male mouse liver microsomes (0.5 mg microsomal protein/mL), compounds (2 μ M), MgCl₂ (2 mM), and NADPH (1 mM) in a total volume of 300 μ L TRIS buffer (0.1 M, pH 7.4) and were performed in a 96-well plate on a Thermomixer Comfort. Compounds and microsomes were preincubated (37 °C, 700 rpm, 10 min) before NADPH was added. Samples (50 μ L) at $t = 0$ min and after an incubation time of 5, 10, 20, and 30 min were quenched with 150 μ L of ice-cooled acetonitrile, centrifuged (3600 rpm, 4 °C, 10 min), and 80 μ L of each supernatant were transferred to a 96-well plate for LC-MS analysis. Control experiments without NADPH were performed in parallel.

LC-MS Measurements. Analyses were performed using a 1100/1200 series HPLC system coupled to a 6410 triple quadrupole mass detector (Agilent Technologies, Inc., Santa Clara, CA, USA) equipped with electrospray ionization. The system was controlled with the Agilent MassHunter Workstation Data Acquisition software (version B.01.04). The column used was an Atlantis T3 C18 column (2.1 mm \times 50 mm) with a 3 μ m particle size (Waters Corp., Milford, MA, USA). The mobile phase consisted of two eluents: solvent A (H₂O, containing 0.1%

formic acid, v/v) and solvent B (acetonitrile, containing 0.1% formic acid, v/v), both delivered at 0.6 mL/min. The gradient was ramped from 95% A/5% B to 5% A/95% B over 1 min, and then held at 5% A/95% B for 0.1 min. The system was then brought back to 95% A/5% B, resulting in a total duration of 4 min. MS parameters such as fragmentor voltage, collision energy, polarity were optimized individually for each drug, and the molecular ion was followed for each compound in the multiple reaction monitoring mode. The concentrations of the analytes were quantified by the Agilent Mass Hunter Quantitative Analysis software (version B.01.04).

In Vivo Pharmacokinetic and Disease Model. Bacteria. The clinical *E. coli* isolate UTI89⁵⁵ (UTI89wt) were kindly provided by the group of Prof. Urs Jenal, Biocenter, University of Basel. Microorganisms were stored at –70 °C and before experiment incubated for 24 h under static conditions at 37 °C in 10 mL of Luria–Bertani broth (Becton, Dickinson and Company, Le Pont de Claix, France) using 50 mL tubes. Prior to each experiment, the microorganisms were washed twice and resuspended in phosphate buffered saline (PBS, Hospital Pharmacy at the University Hospital Basel, Switzerland). Bacterial concentrations were determined by plating serial 1:10 dilutions on blood agar, followed by colony counting with 20–200 colonies after overnight incubation at 37 °C.

Animals. Female C3H/HeN mice weighting between 19 and 25 g were obtained from Charles River (Sulzfeld, Germany) and were housed four to a cage. Mice were kept under specific-pathogen-free conditions in the Animal House of the Department of Biomedicine, University Hospital Basel, and animal experimentation guidelines according to the regulations of Swiss veterinary law were followed. After seven days of acclimatization, 9- to 10-week old mice were used for the PK and infection studies. During the studies, animals were allowed free access to chow and water. Three days before infection studies and during infection, 5% D-(+)-glucose (AppliChem, Baden-Dättwil, Switzerland) was added to the drinking water to increase the number of bacterial counts in the urine and kidneys.⁵⁷

Pharmacokinetic Studies. Single-dose pharmacokinetic studies were performed by iv and po application of the FimH antagonists at a concentration of 50 mg/kg followed by urine and plasma sampling. For iv application, the antagonists (**1**, **17a**, **17b**) were diluted in 100 μ L of PBS and injected into the tail vein. For po application, antagonist **1** was diluted in 200 μ L of PBS and antagonists **17b** and **16b** were first dissolved in DMSO (20 \times) and then slowly diluted to the final concentration (1 \times) in 1% Tween-80/PBS to obtain a suspension. Antagonists were applied iv by injection into the tail vein and po using a gavage followed by blood and urine sampling (10 μ L) after 6 min, 30 min, 1 h, 2 h, 4 h, 6 h, 8 h, and 24 h. Before analysis, proteins in blood and urine samples were precipitated using methanol (Acros Organics, Basel, Switzerland) and centrifuged for 11 min at 13000 rpm. The supernatant was transferred into a 96-well plate (0.5 mL, polypropylene, Agilent Technologies, Basel, Switzerland) and analyzed by LC-MS as described above.

UTI Mouse Model. Mice were infected as previously described.⁵⁷ In brief, before infection, all remaining urine was depleted from the bladder by gentle pressure on the abdomen. Mice were anesthetized with 2.5 vol% isoflurane/oxygen mixture (Attane, Minrad Inc., Buffalo, NY, USA) and placed on their back. Anesthetized mice were inoculated transurethrally with the bacterial suspension by use of a 2 cm polyethylene catheter (Intramedic polyethylene tubing, inner diameter 0.28 mm, outer diameter 0.61 mm, Beckton Dickinson, Allschwil, Switzerland), which was placed on a syringe (Hamilton Gastight Syringe 50 μ L, removable 30G needle, BGB Analytik AG, Boeckten, Switzerland). The catheter was gently inserted through the urethra until it reached the top of the bladder, followed by slow injection of 50 μ L of bacterial suspension at a concentration of approximately 10⁹ to 10¹⁰ CFU/mL.

Antagonist Treatment Studies. FimH antagonists were applied iv in 100 μ L of PBS into the tail vein or po as a suspension by the help

of a gavage, 10 min (**17a**, **17b**, **16b**) or 1 h before infection (**1**). Three h after the onset of infection, urine was collected by gentle pressure on the abdomen and then the mouse was sacrificed with CO₂. Organs were removed aseptically and homogenized in 1 mL of PBS by using a tissue lyser (Retsch, Haan, Germany). Serial dilutions of urine, bladder, and kidneys were plated on Levine Eosin Methylene Blue Agar plates (Beckton Dickinson, Le Pont de Claix, France). CFU counts were determined after overnight incubation at 37 °C and expressed as CFU/mL for the urine and CFU/bladder and CFU/2 kidneys for the organs.

Acknowledgment. We thank Professor Rudi Glockshuber (ETH Zürich, Switzerland) for gratefully providing the plasmid pNT-FimH used for the cloning of the FimH CRD and *E. coli* strain HM 125. We thank Dr. Manfred Kansy and Dr. Christoph Funk, F. Hoffmann-La Roche AG, Basel, Switzerland, for supporting us with their expertise when we established the PADMET platform, and to Prof. Angelo Vedani, University of Basel, Switzerland, for fruitful discussions on conformational issues. We further appreciate the support by Prof. Dr. med. Radek Skoda, Department of Biomedicine, University Hospital Basel, Switzerland, for giving us access to the animal facility and Prof. Niels Frimodt-Møller, Statens Serum Institut, Copenhagen, Denmark for the introduction to the in vivo model. We thank Prof G. Imanidis, FHNW, Muttens, Switzerland, for providing the Caco-2 cells, and Dr. M. Schneider, Department of Pharmaceutical Sciences, University of Basel, Switzerland, for his help during the assay build-up. We are grateful to Prof. Urs Jenal, Biocenter of the University of Basel, Switzerland, for the clinical *E. coli* isolate UTI89 and the FimH knock out strain UTI89Δ*fimA-H*. Finally, we thank the Swiss National Science Foundation (project K-32K1-120904) for their financial support.

Supporting Information Available: ¹H NMR spectra and HPLC traces for the target compounds **16a–e**, **17a–c,e**, **21a,b**, and **22a,b** and experimental and spectroscopic details for compounds **6a–d**, **7a–d**, **14c–e**, **15c–e**, **17c,e**, **19a,b**, **20a,b**, and **21a,b**. This material is available free of charge via the Internet at <http://pubs.acs.org>.

References

- Fihn, S. D. Clinical practice. Acute uncomplicated urinary tract infection in women. *N. Engl. J. Med.* **2003**, *349*, 259–266.
- Hooton, T. M. Recurrent urinary tract infection in women. *Int. J. Antimicrob. Agents* **2001**, *17*, 259–268.
- Wiles, T. J.; Kulesus, R. R.; Mulvey, M. A. Origins and virulence mechanisms of uropathogenic *Escherichia coli*. *Exp. Mol. Pathol.* **2008**, *85*, 11–19.
- Gouin, S. G.; Wellens, A.; Bouckaert, J.; Kovensky, J. Synthetic Multimeric Heptyl Mannosides as Potent Antiadhesives of Uropathogenic *Escherichia coli*. *ChemMedChem* **2009**, *4*, 749–755.
- Rosen, D. A.; Hung, C. S.; Kline, K. A.; Hultgren, S. J. Streptozocin-induced diabetic mouse model of urinary tract infection. *Infect. Immun.* **2008**, *76*, 4290–4298.
- Mulvey, M. A. Adhesion and entry of uropathogenic *Escherichia coli*. *Cell Microbiol.* **2002**, *4*, 257–271.
- Capitani, G.; Eidam, O.; Glockshuber, R.; Grutter, M. G. Structural and functional insights into the assembly of type 1 pili from *Escherichia coli*. *Microbes Infect.* **2006**, *8*, 2284–2290.
- Choudhury, D.; Thompson, A.; Stojanoff, V.; Langermann, S.; Pinkner, J.; Hultgren, S. J.; Knight, S. D. X-ray structure of the FimC–FimH chaperone–adhesin complex from uropathogenic *Escherichia coli*. *Science* **1999**, *285*, 1061–1066.
- Bouckaert, J.; Berglund, J.; Schembri, M.; Genst, E. D.; Cools, L.; Wuhrer, M.; Hung, C. S.; Pinkner, J.; Slättergard, R.; Zavalov, A.; Choudhury, D.; Langermann, S.; Hultgren, S. J.; Wyns, L.; Klemm, P.; Oscarson, S.; Knight, S. D.; Greve, H. D. Receptor binding studies disclose a novel class of high-affinity inhibitors of the *Escherichia coli* FimH adhesin. *Mol. Microbiol.* **2005**, *55*, 441–455.
- Wellens, A.; Garofalo, C.; Nguyen, H.; Van Gerven, N.; Slättergard, R.; Hernalsteens, J.-P.; Wyns, L.; Oscarson, S.; De Greve, H.; Hultgren, S.; Bouckaert, J. Intervening with urinary tract infections using anti-adhesives based on the crystal structure of the FimH–oligomannose-3 complex. *PLoS ONE* **2008**, *3*, 4–13.
- Langermann, S.; Molloy, R.; Burlein, J. E.; Palaszynski, S. R.; Auguste, C. G.; DeFusco, A.; Strouse, R.; Schenerman, M. A.; Hultgren, S. J.; Pinkner, J. S.; Winberg, J.; Guldevall, L.; Soderhall, M.; Ishikawa, K.; Normark, S.; Koenig, S. Vaccination with FimH adhesin protects cynomolgus monkeys from colonization and infection by uropathogenic *Escherichia coli*. *J. Infect. Dis.* **2000**, *181*, 774–778.
- Langermann, S.; Palaszynski, S.; Barnhart, M.; Auguste, G.; Pinkner, J. S.; Burlein, J.; Barren, P.; Koenig, S.; Leath, S.; Jones, C. H.; Hultgren, S. J. Prevention of mucosal *Escherichia coli* infection by FimH-adhesin-based systemic vaccination. *Science* **1997**, *276*, 607–611.
- Bouckaert, J.; Mackenzie, J.; de Paz, J. L.; Chipwaza, B.; Choudhury, D.; Zavalov, A.; Mannerstedt, K.; Anderson, J.; Pierard, D.; Wyns, L.; Seeberger, P. H.; Oscarson, S.; De Greve, H.; Knight, S. D. The affinity of the FimH fimbrial adhesin is receptor-driven and quasi-independent of *Escherichia coli* pathotypes. *Mol. Microbiol.* **2006**, *61*, 1556–1568.
- Sharon, N. Carbohydrates as future anti-adhesion drugs for infectious diseases. *Biochim. Biophys. Acta* **2006**, *1760*, 527–537.
- (a) Firon, N.; Ofek, I.; Sharon, N. Interaction of mannose-containing oligosaccharides with the fimbrial lectin of *Escherichia coli*. *Biochem. Biophys. Res. Commun.* **1982**, *105*, 1426–1432. (b) Firon, N.; Ofek, I.; Sharon, N. Carbohydrate specificity of the surface lectins of *Escherichia coli*, *Klebsiella pneumoniae* and *Salmonella typhimurium*. *Carbohydr. Res.* **1983**, *120*, 235–249. (c) Sharon, N. Bacterial lectins, cell–cell recognition and infectious disease. *FEBS Lett.* **1987**, *217*, 145–157.
- (a) Neeser, J.-R.; Koellreutter, B.; Wuersch, P. Oligomannoside-type glycopeptides inhibiting adhesion of *Escherichia coli* strains mediated by type 1 pili: preparation of potent inhibitors from plant glycoproteins. *Infect. Immun.* **1986**, *52*, 428–436. (b) Lindhorst, T. K. Artificial multivalent sugar ligands to understand and manipulate carbohydrate–protein interactions. *Top. Curr. Chem.* **2002**, *218*, 201–235 (review); (c) Patel, A.; Lindhorst, T. K. A modular approach for the synthesis of oligosaccharide mimetics. *Carbohydr. Res.* **2006**, *341*, 1657–1668. (d) Nagahori, N.; Lee, R. T.; Nishimura, S.-L.; Pagé, S.; Roy, R.; Lee, Y. C. Inhibition of adhesion of type 1 fimbriated *Escherichia coli* to highly mannosylated ligands. *ChemBioChem* **2002**, *3*, 836–844. (e) Appeldoorn, C. C. M.; Joosten, J. A. F.; Maate, F. A.; Dobrindt, U.; Hacker, J.; Liskamp, R. M. J.; Khan, A. S.; Pieters, R. J. Novel multivalent mannose compounds and their inhibition of the adhesion of type 1 fimbriated uropathogenic *E. coli*. *Tetrahedron Asymmetry* **2005**, *16*, 361–372. (f) Touaibia, M.; Wellens, A.; Shiao, T. C.; Wang, Q.; Sirois, S.; Bouckaert, J.; Roy, R. Mannosylated G(0) dendrimers with nanomolar affinities to *Escherichia coli* FimH. *ChemMedChem* **2007**, *2*, 1190–1201.
- (a) Firon, N.; Ashkenazi, S.; Mirelman, D.; Ofek, I.; Sharon, N. Aromatic alpha-glycosides of mannose are powerful inhibitors of the adherence of type 1 fimbriated *Escherichia coli* to yeast and intestinal epithelial cells. *Infect. Immun.* **1987**, *55*, 472–476. (b) Lindhorst, T. K.; Kötter, S.; Kubisch, J.; Krallmann-Wenzel, U.; Ehlers, S.; Kren, V. Effect of p-substitution of aryl α-D-mannosides on inhibiting mannose-sensitive adhesion of *Escherichia coli*—synthesis and testing. *Eur. J. Org. Chem.* **1998**, 1669–1674. (c) Sperling, O.; Fuchs, A.; Lindhorst, T. K. Evaluation of the carbohydrate recognition domain of the bacterial adhesin FimH: design, synthesis and binding properties of mannoside ligands. *Org. Biomol. Chem.* **2006**, *4*, 3913–3922. (d) Han, Z.; Pinker, J. S.; Ford, B.; Obermann, R.; Nolan, W.; Wildman, S. A.; Hobbs, D.; Ellenberger, T.; Cusumano, C. K.; Hultgren, S. J.; Janetka, J. W. Structure-Based Drug Design and Optimization of Mannoside Bacterial FimH Antagonists. *J. Med. Chem.* **2010**, *53*, 4779–4792. (e) Berglund, J.; Bouckaert, J.; De Greve, H.; Knight, S. Anti-adhesive compounds to prevent and treat bacterial infections. International Patent Application PCT/US 2005/089733, 2005.
- Hung, C. S.; Bouckaert, J.; Hung, D.; Pinkner, J.; Widberg, C.; Defusco, A.; Auguste, C. G.; Strouse, R.; Langermann, S.; Waksman, G.; Hultgren, S. J. Structural basis of tropism of *Escherichia coli* to the bladder during urinary tract infection. *Mol. Microbiol.* **2002**, *44*, 903–918.
- Ernst, B.; Magnani, J. L. From carbohydrate leads to glycomimetic drugs. *Nature Rev. Drug Discovery* **2009**, *8*, 661–677.
- (a) Lindhorst, T. K.; Kieburg, C.; Krallmann-Wenzel, U. Inhibition of the type 1 fimbriae-mediated adhesion of *Escherichia coli* to erythrocytes by multiantennary α-mannosyl clusters: the effect of multivalency. *Glycoconjugate J.* **1998**, *15*, 605–613. (b) Dubber, M.; Sperling, O.; Lindhorst, T. K. Oligomannoside mimetics by glycosylation of octopus glycosides and their investigation as inhibitors of type 1

- fimbriae-mediated adhesion of *Escherichia coli*. *Org. Biomol. Chem.* **2006**, *4*, 3901–3912. (c) Touaibia, M.; Wellens, A.; Shiao, T. C.; Wang, Q.; Sirois, S.; Bouckaert, J.; Roy, R. Mannosylated G0 dendrimers with nanomolar affinities to *Escherichia coli* FimH. *ChemMedChem* **2007**, *2*, 1190–1201.
- (21) Aronson, M.; Medalia, O.; Schori, L.; Mirelman, D.; Sharon, N.; Ofek, I. Prevention of colonization of the urinary tract of mice with *Escherichia coli* by blocking of bacterial adherence with methyl α -D-mannopyranoside. *J. Infect. Dis.* **1979**, *139*, 329–332.
- (22) Svanborg Eden, C.; Freter, R.; Hagberg, L.; Hull, R.; Leffer, H.; Schoolnik, G. Inhibition of experimental ascending urinary tract infection by an epithelial cell-surface receptor analog. *Nature* **1982**, *298*, 560–562.
- (23) Rabbani, S.; Jiang, X.; Schwardt, O.; Ernst, B. Expression of the carbohydrate recognition domain of FimH and development of a competitive binding assay. *Anal. Biochem.* **2010**, *407*, 188–195.
- (24) Ness, R. K.; Fletcher, H. G.; Hudson, C. S. Reaction of 2,3,4,6-tetrabenzoyl- α -D-glucopyranosyl bromide and 2,3,4,6-tetrabenzoyl- α -D-mannopyranosyl bromide with methanol. Certain benzoylated derivatives of D-glucose and D-mannose. *J. Am. Chem. Soc.* **1950**, *72*, 2200–2205.
- (25) Sancho-Garcia, J. C.; Cornil, J. Anchoring the Torsional Potential of Biphenyl at the ab Initio Level: The Role of Basis Set versus Correlation Effects. *J. Chem. Theory Comput.* **2005**, *1*, 581–589.
- (26) Eaton, V. J.; Steele, D. Dihedral angle of biphenyl in solution and the molecular force field. *J. Chem. Soc., Faraday Trans. 2* **1973**, *1601*–1608.
- (27) Albert, A. Chemical aspects of selective toxicity. *Nature* **1958**, *182*, 421–422.
- (28) Winiwarter, S.; Bonham, N. M.; Ax, F.; Hallberg, A.; Lennernäs, H.; Karlén, A. Correlation of Human Jejunal Permeability (in Vivo) of Drugs with Experimentally and Theoretically Derived Parameters. A Multivariate Data Analysis Approach. *J. Med. Chem.* **1998**, *41*, 4939–4949.
- (29) Taketani, M.; Shii, M.; Ohura, K.; Ninomiya, S.; Imai, T. Carboxylesterase in the liver and small intestine of experimental animals and human. *Life Sci.* **2007**, *81*, 924–932.
- (30) Kansy, M.; Senner, F.; Gubernator, K. Physicochemical High Throughput Screening: Parallel Artificial Membrane Permeation Assay in the Description of Passive Absorption Processes. *J. Med. Chem.* **1998**, *41*, 1007–1010.
- (31) Artursson, P.; Karlsson, J. Correlation between oral drug absorption in humans and apparent drug permeability coefficients in human intestinal epithelial (Caco-2) cells. *Biochem. Biophys. Res. Com.* **1991**, *175*, 880–885.
- (32) Varma, M. V. S.; Feng, B.; Obach, R. S.; Troutman, M. D.; Chupka, J.; Miller, H. R.; El-Kattan, A. Physicochemical Determinants of Human Renal Clearance. *J. Med. Chem.* **2009**, *52*, 4844–4852.
- (33) Abgottspon, D.; Rölli, G.; Hosch, L.; Steinhuber, A.; Jiang, X.; Schwardt, O.; Cutting, B.; Smiesko, M.; Jenal, U.; Ernst, B.; Trampuz, A. Development of an Aggregation Assay to Screen FimH Antagonists. *J. Microbiol. Methods* **2010**, *82*, 249–255.
- (34) Zhou, G.; Mo, W.-J.; Sebbel, P.; Min, G.; Neubert, T. A.; Glockshuber, R.; Wu, X.-R.; Sun, T.-T.; Kong, X.-P. Uroplakin Ia is the urothelial receptor for uropathogenic *Escherichia coli*: evidence from in vitro FimH binding. *J. Cell Sci.* **2001**, *114*, 4095–4103.
- (35) (a) Kartha, K. P. R.; Field, R. A. Iodine: a versatile reagent in carbohydrate chemistry. IV. Per-O-acetylation, regioselective acylation and acetolysis. *Tetrahedron* **1997**, *53*, 11753–11766. (b) Chittaboina, S.; Hodges, B.; Wang, Q. A facile route for the regioselective deacetylation of peracetylated carbohydrates at anomeric position. *Lett. Org. Chem.* **2006**, *3*, 35–38. (c) Mori, M.; Ito, Y.; Ogawa, T. Total synthesis of the mollu-series glycosyl ceramides α -D-Manp-(1 \rightarrow 3)- β -D-Manp-(1 \rightarrow 4)- β -D-Glcp-(1 \rightarrow 1)-Cer and α -D-Manp-(1 \rightarrow 3)-[β -D-Xylp-(1 \rightarrow 2)]- β -D-Manp-(1 \rightarrow 4)- β -D-Glcp-(1 \rightarrow 1)-Cer. *Carbohydr. Res.* **1990**, *195*, 199–224. (d) Egusa, K.; Kusumoto, S.; Fukase, K. Solid-phase synthesis of a phytoalexin elicitor pentasaccharide using a 4-azido-3-chlorobenzyl group as the key for temporary protection and catch-and-release purification. *Eur. J. Org. Chem.* **2003**, 3435–3445.
- (36) Giampapa, C. S.; Abraham, S. N.; Chiang, T. M.; Beachey, E. H. Isolation and characterization of a receptor for type 1 fimbriae of *Escherichia coli* from guinea pig erythrocytes. *J. Biol. Chem.* **1988**, *263*, 5362–5367.
- (37) Aprikian, P.; Tchesnokova, V.; Kidd, B.; Yakovenko, O.; Yarov-Yarovoy, V.; Trinchina, E.; Vogel, V.; Thomas, W.; Sokurenko, E. Interdomain interaction in the FimH adhesin of *Escherichia coli* regulates the affinity to mannose. *J. Biol. Chem.* **2007**, *282*, 23437–23446.
- (38) Trong, I. L.; Aprikian, P.; Kidd, B. A.; Forero-Shelton, M.; Tchesnokova, V.; Rajagopal, P.; Rodriguez, V.; Interlandi, G.; Klevit, R.; Vogel, V.; Stenkamp, R. E.; Sokurenko, E. V.; Thomas, W. E. Structural basis for mechanical force regulation of the adhesin FimH via finger trap-like beta sheet twisting. *Cell* **2010**, *141*, 645–655.
- (39) Khoo, U. S.; Chan, K. Y. K.; Chan, V. S. F.; Lin, C. L. S. DC-SIGN and L-SIGN: the SIGNs for infection. *J. Mol. Med.* **2008**, *86*, 861–874.
- (40) Lee, S. J.; Evers, S.; Roeder, D.; Parlow, A. F.; Risteli, J.; Risteli, L.; Lee, Y. C.; Feizi, T.; Langen, H.; Nussenzweig, M. C. Mannose receptor-mediated regulation of serum glycoprotein homeostasis. *Science* **2002**, *295*, 1898–1901.
- (41) East, L.; Isacke, C. M. The mannose receptor family. *Biochim. Biophys. Acta* **2002**, *1572*, 364–386.
- (42) Dommett, R. M.; Klein, N.; Turner, M. W. Mannose-binding lectin in innate immunity: past, present and future. *Tissue Antigens* **2006**, *68*, 193–209.
- (43) Scharenberg, M. Expression and purification of DC-SIGN-CRD-Fc-IgG. Unpublished results.
- (44) Dearden, J. C.; Bresnen, J. G. M. The measurement of partition coefficients. *QSAR Comb. Sci.* **1988**, *7*, 133–144.
- (45) Wittwer, M.; Bezençon, J.; Cutting, B.; Wagner, B.; Kansy, M.; Ernst, B. pK_a determination by ¹H-NMR spectroscopy—an old methodology revisited. Unpublished results.
- (46) Banker, M. J.; Clark, T. H.; Williams, J. A. Development and validation of a 96-well equilibrium dialysis apparatus for measuring plasma protein binding. *J. Pharm. Sci.* **2003**, *92*, 967–974.
- (47) Kerns, E. H. High throughput physicochemical profiling for drug discovery. *J. Pharm. Sci.* **2001**, *90*, 1838–1858.
- (48) Avdeef, A.; Bendels, S.; Di, L.; Faller, B.; Kansy, M.; Sugano, K.; Yamauchi, Y. Parallel artificial membrane permeability assay (PAMPA)-critical factors for better predictions of absorption. *J. Pharm. Sci.* **2007**, *96*, 2893–2909.
- (49) Brandt, E.; Heymann, E.; Mentlein, R. Selective inhibition of rat liver carboxylesterases by various organophosphorus diesters in vivo and in vitro. *Biochem. Pharmacol.* **1980**, *29*, 1927–1931.
- (50) Scharenberg, M.; Abgottspon, D. Personal communication.
- (51) Obach, R. S. Prediction of human clearance of twenty-nine drugs from hepatic microsomal intrinsic clearance data: an examination of in vitro half-life approach and nonspecific binding to microsomes. *Drug Metab. Dispos.* **1999**, *27*, 1350–1359.
- (52) Trainor, G. L. The importance of plasma protein binding in drug discovery. *Expert Opin. Drug Discovery* **2007**, *2*, 51–64.
- (53) Weisiger, R. A. Dissociation from albumin: a potentially rate-limiting step in the clearance of substances by the liver. *Proc. Natl. Acad. Sci. U.S.A.* **1985**, *82*, 1563–1567.
- (54) Urien, S.; Tillement, J.-P.; Barre, J., The significance of plasma protein binding in drug research. In *Pharmacokinetic Optimization in Drug Research: Biological, Physicochemical, and Computational Strategies*; Wiley-VCH: Weinheim, Germany, 2001; pp 189–197.
- (55) Mulvey, M. A.; Schilling, J. D.; Hultgren, S. J. Establishment of a persistent *Escherichia coli* reservoir during the acute phase of a bladder infection. *Infect. Immun.* **2001**, *69*, 4572–4579.
- (56) (a) VCCLAB, *Virtual Computational Chemistry Laboratory*; <http://www.vcclab.org>, 2005; (b) Tetko, I. V.; Gasteiger, J.; Todeschini, R.; Mauri, A.; Livingstone, D.; Ertl, P.; Palyulin, V. A.; Radchenko, E. V.; Zefirov, N. S.; Makarenko, A. S.; Tanchuk, V. Y.; Prokopenko, V. V. Virtual computational chemistry laboratory—design and description. *J. Comput.-Aided Mol. Des.* **2005**, *19*, 453–463.
- (57) Kern, M. B.; Frimodt-Møller, N.; Espersen, F. Effects of Sulfo-methizole and Amdinocillin against *Escherichia coli* Strains (with Various Susceptibilities) in an Ascending Urinary Tract Infection Model. *Antimicrob. Agents Chemother.* **2003**, *47*, 1002–1009.

2.3 Chapter 2: FimH antagonists: ester prodrugs with improved oral bioavailability

The following chapter extends the ester prodrug strategy for optimizing the oral absorption potential of the biphenyl α -D-mannopyranosides. A broad set of simple and functionalized alkyl promoieties are introduced and their effects on the oral absorption potential are exposed in detail. Particular attention is paid to the characterization of the bioconversion of the prodrugs to the parent compound by different microsome-associated and plasma-borne hydrolases.

Contribution to the project:

Simon Kleeb performed all experiments regarding the physicochemical and *in vitro* pharmacokinetic characterization of the diverse ester prodrugs. In particular, he implemented various assays for exploring the enzyme-mediated transformation of the prodrugs to the pharmacologically active parent compound. Overall, he was responsible for the writing of the entire chapter with the exception of the synthesis section.

Wojciech Schönemann synthesized all the tested compounds and was responsible for the writing of the synthesis section.

Abbreviations: BChE, butyrylcholinesterase; BNPP, bis(4-nitrophenyl) phosphate; Caco-2 cells, colorectal adenocarcinoma cells; CES, carboxylesterase; CRD, carbohydrate-recognition domain; D , octanol-water distribution coefficient; ER, endoplasmic reticulum; hCE1, human carboxylesterase isotype 1; hCE2, human carboxylesterase isotype 2; HLM, human liver microsomes; P , octanol-water partition coefficient; P_{app} , apparent permeability; P_e , effective permeability; PAMPA, parallel artificial membrane permeability assay; RLM, rat liver microsomes, UPEC, uropathogenic *Escherichia coli*; UTI, urinary tract infection.

Introduction

Urinary tract infection (UTI), which is characterized by dysuria, frequent and urgent urination, bacteriuria, or pyuria, is one of the most common bacterial infections. Around 60% of women have at least one UTI in their lifetime and most episodes are caused by uropathogenic *Escherichia coli* (UPEC).^[1] UTI requires an antibiotic treatment to tackle the symptoms and to prevent potentially devastating complications like pyelonephritis and urosepsis.^[2] However, recurrent infections with subsequent antibiotic exposure can result in antimicrobial resistance. This often leads to treatment failure and reduces the range of therapeutic options.^[3] Therefore, efficient non-antibiotic treatment strategies are urgently needed.

The pathogenesis of UTI relies on bacterial lectins which recognize carbohydrate ligands located on the endothelial cells of the urinary tract.^[4] P-piliated UPEC cause pyelonephritis by binding to galabiose-containing ligands on the kidney epithelium, while mannose-binding type 1 pili promote cystitis by targeting uroplakin Ia on the mucosal surface of the urinary bladder.^[5] The bacterial adhesion prevents rapid clearance of UPEC from the urinary tract by the bulk flow of urine and enables the colonization of the host cells.^[6] The bacterial lectin FimH expressed at the tip of type I pili encloses a carbohydrate recognition domain (CRD) which targets the mannosylated glycoproteins on the cell surface, and a pilin domain regulating the switch between the low and high affinity states of the CRD.^[7, 8]

The inhibition of the bacteria-cell interaction by FimH antagonists is a promising approach tackling the resistance problem of the current antibiotic treatment strategies. More than two decades ago, Sharon and coworkers investigated various mannosides as antagonists for type 1 fimbriae-mediated specific bacterial adhesion.^[9-11] Since then, two different approaches have been explored for the further improvement of the antiadhesive effects. First, multivalent mannosides^[12-14] were investigated and second, monovalent high-affinity antagonists^[15-21] were designed based on the structural information obtained from crystal structures of FimH co-crystallized with alkyl and aryl α -D-mannopyranosides.^[15, 22-25] Only recently, the first in vivo studies performed in a mouse model were published, describing antibacterial effects in the bladder upon oral administration of biphenyl α -D-mannopyranosides.^[18, 26] In either of the reported cases, high dose (≥ 50 mg/kg body weight) was however necessary to maintain the minimal therapeutic concentration in the urine due to unfavorable physicochemical properties of the antagonists for an oral treatment.^[18, 21]

In order to reach the urinary bladder, an orally applied FimH antagonist needs to be absorbed from the intestinal lumen into the bloodstream and subsequently excreted via the kidneys. Permeability through the intestinal mucosa usually improves with an increase in lipophilicity.^[27, 28] By contrast, renal excretion is favored in the case of hydrophilic molecules, the polar character of which limits the reabsorption from the primary urine in the renal tubules and reduces the propensity to non-renal elimination pathways.^[29, 30] This chapter presents an ester prodrug concept (Figure 1) combining lipophilicity, conferred by an alkyl promoiety, and hydrophilicity, provided by the free carboxylate upon enzyme-mediated hydrolysis of the ester in hepatocytes or in plasma.^[31, 32]

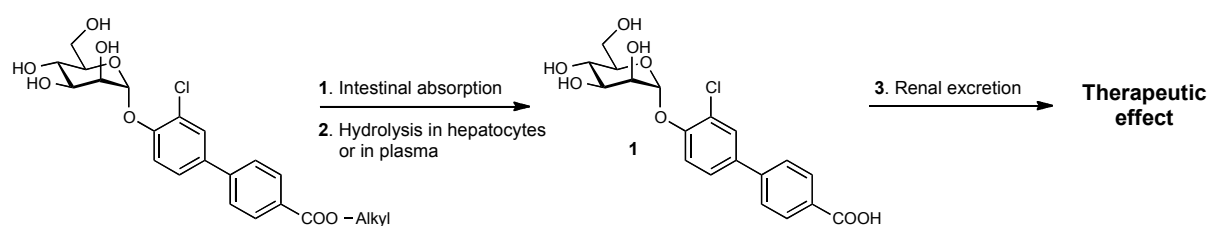
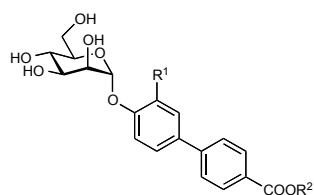
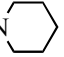



Figure 1. Ester prodrug concept enabling oral bioavailability and renal excretion for the biphenyl α -D-mannopyranoside FimH antagonist **1**.

Results and Discussion

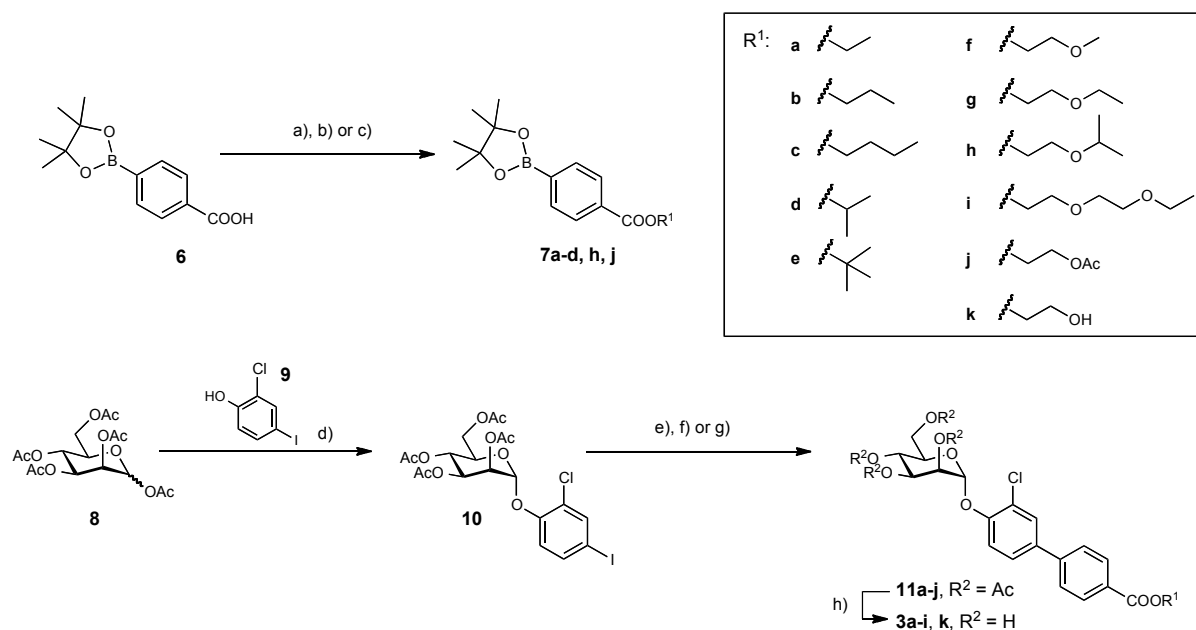
In a recent publication, we described the biphenyl α -D-mannopyranoside **1** exhibiting nanomolar affinity towards the isolated FimH-CRD and treatment efficacy in a mouse disease model.^[18] Moreover, we showed that esterification of the polar carboxylate with a methyl promoiety (\rightarrow **2**) is a promising approach for achieving oral bioavailability. Nevertheless, the levels of the parent compound in plasma detected upon oral administration of the prodrug were moderate when compared to the concentrations reached by intravenous application. Therefore, we expanded the ester prodrug strategy in order to optimize the oral absorption potential. In a first step, we synthesized a set of simple alkyl esters (\rightarrow **3a-e**, Table 1) and characterized their intestinal absorption potential. Based on these findings we then optimized the prodrug by (a) introducing alkyl promoieties functionalized with oxygenated or nitrogenated substituents (\rightarrow **3f-i**, **k-n**) and by (b) replacing the *ortho*-chloro substituent of the biphenyl aglycone with a trifluoromethyl group (\rightarrow **4**, **5I**).

Table 1. Ester prodrugs for optimizing oral bioavailability of the biphenyl α -D-mannopyranosides **1** and **4**.

cpd	R ¹	R ²	cpd	R ¹	R ²	cpd	R ¹	R ²
1 ^[18]	Cl	H	3f	Cl	CH ₂ CH ₂ OCH ₃	4 ^[21]	CF ₃	H
2 ^[18]	Cl	CH ₃	3g	Cl	CH ₂ CH ₂ OCH ₂ CH ₃	5l	CF ₃	CH ₂ CH ₂ N(CH ₃) ₂
3a	Cl	CH ₂ CH ₃	3h	Cl	CH ₂ CH ₂ OCH(CH ₃) ₂			
3b	Cl	CH ₂ CH ₂ CH ₃	3i	Cl	CH ₂ CH ₂ OCH ₂ CH ₂ OCH ₂ CH ₃			
3c	Cl	(CH ₂) ₃ CH ₃	3k	Cl	CH ₂ CH ₂ OH			
3d	Cl	CH(CH ₃) ₂	3l	Cl	CH ₂ CH ₂ N(CH ₃) ₂			
3e	Cl	C(CH ₃) ₃	3m	Cl	CH ₂ CH ₂ - N 			
			3n	Cl	CH ₂ CH ₂ - N 			

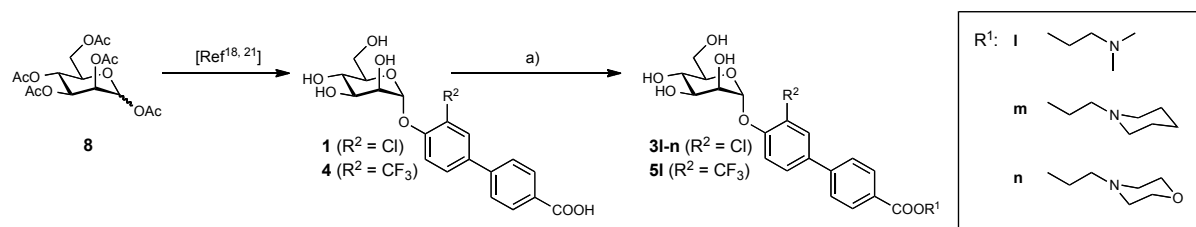
Synthesis

The synthesis of alkyl and oxygen-containing heteroalkyl esters is depicted in Scheme 1. The glycosylation between commercially available **8** and phenol **9** was performed in presence of Lewis acid affording α -D-mannoside **10**. The boronate ester intermediates **7a-d**, **f**, **g** were obtained by treating **6** with thionyl chloride and excess of corresponding alcohol. The alcohols applied in the case of **7h-j** were coupled with carboxylic acid by Steglich esterification.^[33] All boronate ester intermediates were purified by MPLC on silica gel and characterized except **7f**, **7g** and **7i**, from which only major impurities were removed before using them in the next step. The compound **7e** was purchased from Frontier Scientific, Inc. chemical company. The compound **10** underwent palladium-mediated Suzuki coupling reaction^[34] together with **7a-j** yielding biphenyls **11a-j**. In order to avoid transesterification, deacetylation was done in a mixture of chloroform and corresponding alcohol together with its alkoxide. In the case of more complex alcohols, bulky *tert*-butanol with potassium *tert*-butoxide was applied.



Scheme 1. a) R¹-OH, SOCl₂, 60 °C, 2-6 h, 42-65% (**7a-c**); b) R¹-OH, DIC, DMAP, CH₂Cl₂, 0 °C → rt, 1-4 h, 43-69% (**7h, j**); c) iPrOH, SOCl₂, Et₃N, CHCl₃, 60 °C, 5 h, 32% (**7d**); d) BF₃·Et₂O, CH₂Cl₂, 4 Å MS, 40 °C, 76 h, 62%; e) **7a-e, 7h** or **7j**, PdCl₂(dppf)·CH₂Cl₂, K₃PO₄, DMF, 80 °C, 2-6 h, 55-81% (**11a-e, h, j**); f) i. **6**, R¹-OH, SOCl₂, 60 °C, 4-6 h; ii. PdCl₂(dppf)·CH₂Cl₂, K₃PO₄, DMF, 80 °C, 4-5.5 h, 47-52% (**11f, g**); g) i. **6**, R¹-OH, DIC, DMAP, CH₂Cl₂, 0 °C → rt, 3.5 h; ii. PdCl₂(dppf)·CH₂Cl₂, K₃PO₄, DMF, 80 °C, 5 h, 44% (**11i**); h) R¹-ONa/R¹-OH or *t*-BuOK/*t*-BuOH, CHCl₃, rt, 2-25 h, 25-69%.

The synthesis of nitrogen-containing ester analogs was performed in a different manner to avoid possible deactivation of the catalyst^[35] during Suzuki coupling reaction. Esterification was performed directly on compound **1** or **4** (Scheme 2). The crude products **3l-n** and **5l** were purified by means of preparative HPLC resulting in moderate yields.



Scheme 2. a) R¹-OH, COMU, DIPEA, DMF, rt, 4-31 h, 14-53%.

Physicochemical and in vitro pharmacokinetic characterization

For estimating the oral absorption potential of the various ester prodrugs as well as their propensity to enzyme-mediated bioactivation, we conducted aqueous solubility, lipophilicity, permeability, and metabolic stability studies (for experimental data refer to Table 2). Aqueous solubility was of interest because the orally applied dose needs to be dissolved in the intestinal fluids prior to absorption.^[36] Lipophilicity was quantified by means of the octanol-water distribution coefficient at pH 7.4 ($\log D_{7.4}$).^[37] The parallel artificial membrane permeability assay (PAMPA) was performed to estimate the prodrugs' ability to diffuse through the intestinal membranes,^[38] while bi-directional permeation studies across a colorectal adenocarcinoma (Caco-2) cell monolayer were implemented to reveal active influx and efflux processes.^[39] Furthermore, the prodrugs were incubated with rat and human liver microsomes (RLM, HLM) for estimating their susceptibility to hydrolases localized in the endoplasmic reticulum of hepatocytes,^[40] while incubations with human plasma were performed to investigate the involvement of plasma-borne enzymes in ester hydrolysis.^[41]

Table 2. Pharmacokinetic parameters of different ester prodrugs of the FimH antagonists **1** and **4**. PAMPA, parallel artificial membrane permeability assay; P_e , effective permeability; P_{app} , apparent permeability; RLM, rat liver microsomes; HLM, human liver microsomes; n.d., not determined. The Caco-2 assay was performed at an initial compound concentration (c_0) of 62.5 μ M. Microsomal stability was determined with pooled male rat liver microsomes (0.125 mg/mL) and pooled human liver microsomes (0.125 mg/mL) at pH 7.4 and 37 °C. Plasma stability was determined with human plasma (50%) at pH 7.4 and 37 °C.

cpd	PAMPA $\log P_e$ [cm/s]/pH	Caco-2 P_{app} [10^{-6} cm/s]		$\log D_{7.4}$	Solubility [μ g/mL]/pH	RLM $t_{1/2}$ [min]	HLM $t_{1/2}$ [min]	Plasma $t_{1/2}$ [min]
		a→b	b→a					
1 ^[18]	no permeation	0.2±0.0	0.4±0.0	< -1.5	>3000 / 6.61	---	---	---
2 ^[18]	-4.6	5.3±0.6	18±1	2.32	11.9 / 6.53	3.1	36	>120
3a	-4.5±0.1 / 7.4	n.d.	n.d.	n.d.	3.9±0.1 / 7.4	n.d.	n.d.	n.d.
3b	-4.5±0.1 / 7.4	n.d.	n.d.	n.d.	2.2±0.5 / 7.4	n.d.	n.d.	n.d.
3c	-4.6 / 7.4	n.d.	n.d.	n.d.	0.8±0.2 / 7.4	n.d.	n.d.	n.d.
3d	-4.4±0.1 / 7.4	n.d.	n.d.	n.d.	14±1 / 7.4	n.d.	n.d.	n.d.
3e	-4.4±0.1 / 7.4	n.d.	n.d.	n.d.	3.8±0.6 / 7.4	n.d.	n.d.	n.d.
3k	-6.6±0.1 / 7.4	0.6±0.1	9.6±0.6	1.8±0.1	>160 / 7.4	>120	>120	>120

3f	-4.9±0.0 / 7.4	4.5±0.4	18±1	2.3±0.0	121±4 / 7.4	4.1	47	57
3g	-4.9±0.2 / 7.4	11±1	19±1	2.7±0.0	137±14 / 7.4	5.9	101	66
3h	-4.5±0.1 / 7.4	8.3±0.7	36±4	3.1±0.1	90±6 / 7.4	1.9	16	57
3i	-5.1±0.1 / 7.4	4.6±0.6	36±7	2.1±0.1	147±6 / 7.4	5.1	33	33
3l	-6.4±0.0 / 5.0 -6.2±0.1 / 7.4	0.9±0.1	27±0	1.6±0.0	>160 / 3.0 >160 / 7.4	>120	>120	6.2
3m	-5.5±0.0 / 5.0 -5.1±0.0 / 7.4	1.0±0.3	33±2	2.4±0.1	79±8 / 3.0 57±4 / 7.4	49	>120	3.7
3n	-6.3±0.2 / 5.0 -5.6±0.0 / 7.4	0.6±0.2	35±5	2.2±0.1	>120 / 3.0 >120 / 7.4	32	>120	86
4	-8.4±1.3 / 5.0 -8.6±1.6 / 7.4	n.d.	n.d.	-0.8±0.1	15±1 / 3.0 >200 / 7.4	---	---	---
5l	-6.7±0.2 / 5.0 -6.4±0.0 / 7.4	1.6	37	1.7±0.0	>160 / 3.0 >160 / 7.4	80	n.d.	17

Oral absorption. As previously reported, low aqueous solubility (< 20 µg/mL) is a primary drawback constraining oral absorption of the methyl ester **2**.^[18, 42] Moreover, carrier-mediated efflux at the apical enterocyte membrane – revealed by the bi-directional Caco-2 permeation assay – probably interferes with the intestinal uptake of the prodrug, in spite of promising membrane permeability suggested by PAMPA ($\log P_e = -4.6$).^[43, 44] Therefore, we expanded the alkyl promoiety with the aim to increase solubility and permeability.

In the first step, esters with simple alkyl promoiety (**3a-e**) were introduced, trending towards slightly higher effective permeability ($\log P_e$), as determined by PAMPA. Nevertheless, replacing the methyl promoiety with an ethyl, propyl, butyl, isopropyl, or *tert*-butyl group further reduced the aqueous solubility of the prodrug and, as a consequence, its intestinal absorption potential.^[36]

In order to counteract decreasing aqueous solubility, we introduced in the next step ethyl promoiety functionalized with oxygenated or nitrogenated substituents.^[45] These esters (**3f-i, k-n**) were indeed more soluble than the initial methyl ester **2** and the prodrugs **3a-e**. Moreover, the 2-ethoxyethyl ester **3g** and the 2-isopropoxyethyl ester **3h** displayed a higher $\log D_{7.4}$ than the methyl ester, suggesting an increase in membrane permeability. On the other hand, the tertiary amines present in the compounds **3l** and **3n** induced a decrease in $\log D_{7.4}$ but a strong increase in aqueous solubility. The moderate lipophilicity of the 2-(dimethylamino)ethyl ester **3l** could in turn be slightly raised by replacing the *ortho*-chloro

substituent on the first aromatic ring of the biphenyl aglycone with a trifluoromethyl moiety (\rightarrow **5I**). Effective permeability deduced from PAMPA ($\log P_e$) correlated with $\log D_{7.4}$, such that the most lipophilic ester **3h** showed optimal $\log P_e$ for membrane permeation (-4.5).^[43] In the case of the esters **3I-n** and **5I** bearing an amine functional group, we observed, moreover, a strong dependence of $\log P_e$ on the pH of the compound solution in the donor compartment of the PAMPA.

A bi-directional Caco-2 permeability screening at low initial compound concentrations in the donor chamber ($c_0 = 62.5 \mu\text{M}$) classified all heteroalkyl esters as apparent substrates of efflux transporters.^[44] Passive diffusion driven by the concentration gradient across the cell monolayer and active efflux given for intrinsic carrier substrates are considered as key determinants of the apparent net flux.^[46] Accordingly, the moderately permeable aminoalkyl esters, such as compound **3I**, diffused slowly but were strongly recognized by the efflux carriers, resulting in a high efflux ratio ($b \rightarrow a/a \rightarrow b$). Since **3I** is well soluble in aqueous medium, the initial concentration (c_0) in the donor chambers could, however, be expanded to $825 \mu\text{M}$, which increased the gradient and apparently saturated the transporter activity (Figure 2). As a result, apparent permeability ($P_{\text{app}, a-b}$) in the range for successful oral absorption was achieved.

In contrast to the 2-aminoethyl esters, the highly permeable esters **3f-h** diffused more rapidly, which led to a lower efflux ratio and promising $P_{\text{app}, a-b}$ under the screening conditions ($c_0 = 62.5 \mu\text{M}$). However, for the ester **3h** exhibiting the least favorable efflux ratio among those esters, the attempt to saturate the transporters was not successful due to insufficient aqueous solubility ($90 \mu\text{g/mL}$).

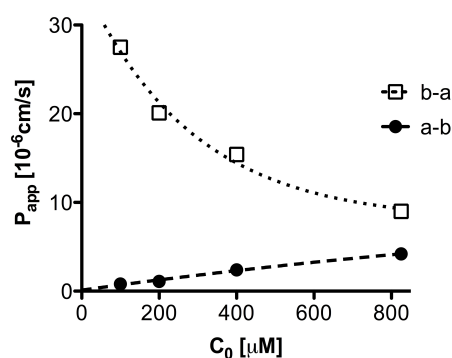


Figure 2. Apparent permeability (P_{app}) of ester **3I** through a Caco-2 cell monolayer. The assay was performed at different initial compound concentrations in the donor compartment (c_0), ranging from $100 \mu\text{M}$ to $825 \mu\text{M}$. $P_{\text{app}}(a \rightarrow b)$, permeability in the absorptive direction; $P_{\text{app}}(b \rightarrow a)$, permeability in the secretory direction.

Enzyme-mediated bioactivation. Besides solubility and permeability, propensity to enzyme-mediated bioactivation was a key feature of our ester prodrug concept.^[31] Hydrolysis of the ester bond can be mediated by plasma-borne enzymes or by isozymes of the carboxylesterase (CES) superfamily associated to the endoplasmic reticulum of various tissues.^[41, 47] The isozyme hCE1, highly expressed in hepatocytes but scarcely observed in enterocytes, and the isozyme hCE2, present in both hepatocytes and enterocytes, have been identified as major human CES.^[40] Since the prodrug approach might only be successful if hydrolysis takes place in the bloodstream or in the liver and not in the intestine during absorption, high chemical stability of the ester bond and substrate specificity for plasma-borne hydrolases or hCE1 was aspired.

Incubations of the esters **3f-i**, **k-n**, and **5l** in buffer without active enzyme (pH 7.4, 37 °C) showed a negligible degradation within one hour, suggesting high chemical stability of the ester bond. With regard to the enzyme-mediated bioactivation, we identified different esterases to be involved in the conversion of the oxygen-containing esters **3f-i**, **k** and the amine-bearing esters **3l-n** and **5l** to the active parent compounds.

When we incubated the oxyethyl esters **3f-h**, **k** (initial concentration, $c_0 = 2 \mu\text{M}$ in TRIS-HCl 0.1 M, pH 7.4) with RLM (0.125 mg/mL, total incubation time = 60 min), we observed the previously described relationship between the lipophilicity of the ester and its propensity to hydrolysis by microsome-associated hydrolases.^[48, 49] The 2-hydroxyethyl ester **3k**, *i.e.* the least lipophilic compound among the oxyethyl esters, remained stable during the entire incubation ($t_{1/2} > 120$ min). By contrast, the 2-methoxyethyl **3f**, 2-ethoxyethyl **3g**, and 2-isopropoxyethyl **3h** esters were all susceptible to degradation by microsome-associated enzymes, with the most lipophilic **3h** showing the shortest metabolic half-life. Nonetheless, the observed high rates of biotransformation by murine hydrolases did not correlate with the turnover by human enzymes. In fact, the incubations with HLM under similar assay conditions revealed important species differences in the observed half-lives (see Table 2), which need to be considered when predicting the rates of bioconversion in human from *in vivo* animal experiments.^[50]

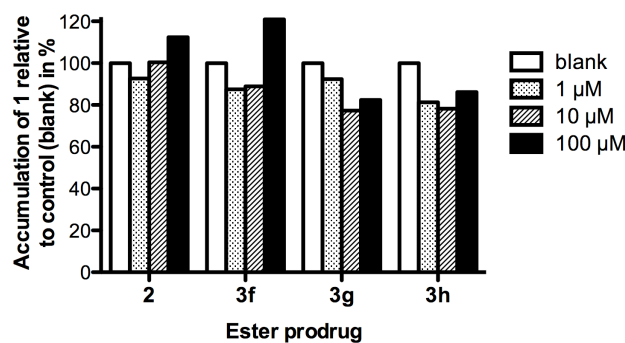


Figure 3. Human liver microsome mediated hydrolysis of ester prodrug **2**, **3f**, **3g**, and **3h** in presence of Loperamide hydrochloride, a specific inhibitor of the human carboxylesterase isotype 2 (hCE2). The bars represent the accumulation of the parent compound **1** in the incubation with inhibitor (1 μM, 10 μM, 100 μM) relative to the accumulation in the control experiment without Loperamide (blank).

When bis(4-nitrophenyl) phosphate (BNPP, 1 mM) – an inhibitor of all CES isozymes – was added to the microsomal incubations of the esters **3f-h**, a strong decrease in the rates of hydrolysis was observed. These results suggest that enzymes of the CES superfamily are the main contributors to the bioactivation of these prodrugs.^[40] Otherwise, treating the HLM with Loperamide (1 – 100 μM) – a specific inhibitor of the human CES isotype 2 (hCE2) – did not affect the rates of hydrolysis (Figure 3), which attributes the observed enzymatic turnover primarily to the hCE1 isozyme.^[51]

In contrast to the 2-oxyethyl esters, all 2-aminoethyl prodrugs **3i-n** and **5i** showed low susceptibility to hydrolysis by microsome-associated esterases. Indeed, the cationic tertiary amine present in these esters is supposed to establish strong interactions with negatively charged residues in the active site gorge of the CES and, as a consequence, to inhibit the hydrolytic activity.^[49] By contrast, the 2-(dimethylamino)ethyl esters **3i**, **5i**, and the 2-(piperidin-1-yl)ethyl ester **3m** were rapidly cleaved by plasma-borne enzymes. Since the 2-aminoethyl carboxylate present in these prodrugs is structurally related to choline esters, we postulated that they were recognized by the butyrylcholinesterase (BChE) present in human plasma.^[52, 53] The metabolic turnover could indeed be inhibited by the specific cholinesterase inhibitor Neostigmine bromide (Figure 4), which confirms the strong contribution of BChE to the observed hydrolysis.^[54] Against our expectations, the 2-morpholinoethyl promoiety in **3n**, known from marketed ester prodrugs (*e.g.* Micophenolate mofetil),^[55] was scarcely cleaved by microsomal or plasma-associated enzymes.

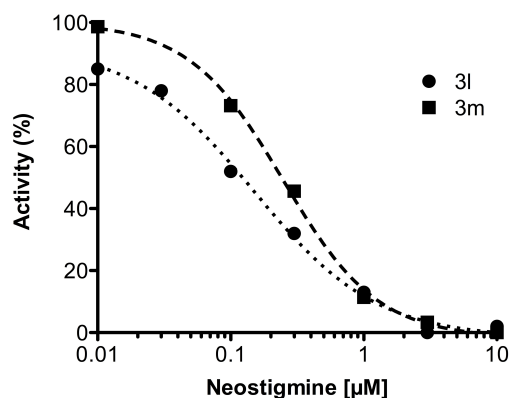


Figure 4. Hydrolysis of the 2-(dimethylamino)ethyl ester **3l** and the 2-(piperidin-1-yl)ethyl ester **3m** by plasma-associated esterases in presence of the specific butyrylcholinesterase inhibitor Neostigmine bromide (0.01 - 10 μM). The activity was calculated by dividing the metabolic $t_{1/2}$ observed in presence of inhibitor by the metabolic $t_{1/2}$ of the control experiment without inhibitor.

In summary, the prodrug approach proved successful to mask the polar character of the carboxylic acid and hence to increase permeability of the biphenyl α -D-mannopyranoside **1**. As opposed to merely aliphatic motifs present in **3a-e**, the oxyalkyl promoieties in **3f-h** enhanced both permeability and solubility. Nonetheless, aqueous solubility was still insufficient to reach concentrations necessary for efflux transporter saturation. Moreover, we suspect that, despite hydrolysis by hepatic CES, further metabolic modifications within the hepatocytes (*e.g.* glucuronidation of the free acid) or hepatobiliary excretion may take place and constrain the systemic availability of the active principle.^[31] Otherwise, the 2-aminoethyl derivatives showed high aqueous solubility, compensating for moderate permeability and providing a promising overall absorption potential. Furthermore, the well soluble esters **3l** and **5l** displayed high propensity to hydrolysis by plasma-borne enzymes, which suggests rapid and quantitative conversion of the prodrug to the polar active principle within the bloodstream and thus low compound loss during the first pass through the liver.^[31]

With regard to the rate of enzyme-mediated bioactivation, rapid conversion, such as observed for the prodrugs **3h**, **3l** or **5l**, is not necessarily advantageous since it favors rapid compound clearance from circulation, *i.e.* high initial concentrations in the bladder but only short-acting therapeutic effects. We therefore hypothesize that the slightly prolonged metabolic $t_{1/2}$ of the prodrug **3g** would allow to maintain the minimal therapeutic concentration in the urine for a longer period of time, thus reducing the dosing frequency.

Summary and Conclusion

The physicochemical profile of most biaryl α -D-mannosides described as potent and selective FimH antagonists is unfavorable for an oral therapy. In a former publication, we introduced an ester prodrug approach rendering the biphenyl mannoside **1** orally available. The goal of the present study was to optimize the properties of the promoiety in order to enhance the intestinal uptake and the delivery of the pharmacologically active parent compound to the therapeutic target in the urinary bladder.

Introducing alkyl promoieties (*i.e.* ethyl, propyl, isopropyl, butyl, isopropyl, or *tert*-butyl) was little successful due to markedly reduced aqueous solubility of the final molecules. By contrast, alkyl promoieties functionalized with oxygenated or nitrogenated substituents proved advantageous for masking the polar carboxylic acid substituent of the biphenyl aglycone and for raising the aqueous solubility of the prodrug. With regard to the enzymatic bioactivation, we identified different esterases responsible for the hydrolysis of the alkoxyethyl esters and the aminoethyl derivatives. The first mentioned class of esters was recognized by the ER-associated CES expressed in hepatocytes. The latter group of prodrugs was rapidly cleaved by the plasma-borne BChE, which implies immediate availability of the active principle in the bloodstream and lower non-renal clearance by phase II metabolic reactions or hepatobiliary excretion.

With respect to all ADME parameters determined *in vitro*, the prodrugs **3g** and **5l** showed the most promising profiles. The 2-(dimethylamino)ethyl ester derivative **5l** displayed high solubility, moderate permeability, and rapid hydrolysis mediated by the cholinesterase, which can lower the risk of non-renal clearance but also shorten the dosing interval of the treatment. On the other hand, the 2-ethoxyethyl ester derivative **3g** exhibited moderate solubility, high permeability, and slightly prolonged $t_{1/2}$, which may be beneficial in terms of dose regimen but also may increase the propensity to hepatic clearance. In order to prove the advantages and drawbacks of the optimized structures, *in vivo* pharmacokinetic studies in mice should be conducted as a next step.

Experimental Section

Synthesis

General methods. NMR spectra were recorded on a Bruker Avance DMX-500 (500 MHz) spectrometer. Assignment of ^1H and ^{13}C NMR spectra was achieved using 2D methods (COSY, HSQC, HMBC). Chemical shifts are expressed in ppm using residual CHCl_3 , CHD_2OD or HDO as references. Optical rotations were measured using Perkin-Elmer Polarimeter 341. Electron spray ionization mass spectra (ESI-MS) were obtained on a Waters micromass ZQ Mass Spectrometer. The LC-HRMS analysis were carried out using a Agilent 1100 LC equipped with a photodiode array detector and a Micromass QTOF I equipped with a 4 GHz digital-time converter. Reactions were monitored by TLC using glass plates coated with silica gel 60 F₂₅₄ (Merck) and visualized by using UV light and/or by charring with a molybdate solution (a 0.02 M solution of ammonium cerium sulfate dihydrate and ammonium molybdate tetrahydrate in aqueous 10% H_2SO_4). MPLC separations were carried out on a CombiFlash Companion or R_f from Teledyne Isco equipped with RediSep normal-phase. LC-MS separations were carried out on a Waters system equipped with sample manager 2767, pump 2525, PDA 2996, column SunFire™ Prep C₁₈ OBD™ (5 μm , 19 x 150 mm), and Micromass ZQ. All compounds used for biological assays are at least of 95% purity based on HPLC analytical results. Commercially available reagents were purchased from Aldrich, Alfa Aesar, Acros Organics or Frontier Scientific. Solvents were purchased from Sigma-Aldrich or Acros and were dried prior to use where indicated. Methanol (MeOH), ethanol (EtOH), *n*-propanol (PrOH), isopropanol (*i*-PrOH), *n*-butanol (BuOH) and *tert*-butanol (*t*-BuOH) were dried by storing with activated molecular sieves 3Å or 4Å for at least one day. Dichloromethane (DCM) was dried by filtration over Al_2O_3 (Fluka, type 5016 A basic) and stored over activated molecular sieves 4Å. Molecular sieves 3Å and 4Å were activated in vacuo at 200 °C for 30 min immediately before use.

General procedure A for Suzuki coupling reaction. A round-bottom flask was charged with **10**, boronate **6** or **7** and K_3PO_4 , then evacuated and flushed with argon. Anhydrous DMF (0.5-4 mL) was added and the mixture was degassed in an ultrasonic bath for 10 min followed by the addition of $\text{PdCl}_2(\text{dppf})\cdot\text{CH}_2\text{Cl}_2$. The reaction was stirred at 80 °C under argon until completion (2-6 h). After cooling to rt, the mixture was diluted with EtOAc (30-50 mL) and washed with satd aq NaHCO_3 (2 x 20 mL) and H_2O (2 x 20 mL). The organic layer was dried over Na_2SO_4 , concentrated in vacuo and purified by MPLC on silica gel to afford **11a-j**.

General procedure B for deacetylation. To a solution of protected mannoside **11** in a mixture of dry alcohol and chloroform, freshly prepared sodium alkoxide or potassium *tert*-butoxide was added. The mixture was stirred at rt under argon until completion (2-25 h). Then, the mixture was neutralized with Amberlyst-15 (H^+) ion-exchange resin, filtered and concentrated in vacuo. The crude product was purified by MPLC on silica gel to afford **3a-i, k**.

General procedure C for esterification of compounds 1 and 4. To a solution of **1** or **4**, the corresponding alcohol and DIPEA in DMF, was added COMU. The mixture was stirred at rt under argon until completion (4-31 h) and then concentrated in vacuo. The residue was dissolved in MeOH (1 mL) or MeCN (1 mL), passed through a nylon membrane syringe filter (pore size 0.45 μm) and purified by LC-MS ($\text{H}_2\text{O}/\text{MeCN} + 0.2\% \text{HCO}_2\text{H}$) to afford **31-n** and **51** as solids after lyophilization from H_2O .

4-Ethoxycarbonylphenylboronic acid pinacol ester (7a). A round-bottom flask was charged with **6** (60 mg, 0.235 mmol), evacuated and flushed with argon. Then, dry EtOH (0.6 mL) and SOCl_2 (41 μL , 0.282 mmol, 2.4 eq) were added. The mixture was stirred at 60 $^\circ\text{C}$ for 2 h. The reaction mixture was concentrated in vacuo and purified by MPLC on silica gel (petroleum ether/EtOAc, 9:1) to afford **7a** (43 mg, 66%) as a colorless oil. Analytical data are in accordance with literature data.^[56]

4-Propoxycarbonylphenylboronic acid pinacol ester (7b). Prepared according to the procedure for **7a** from **6** (39 mg, 0.152 mmol) with SOCl_2 (12 μL , 0.152 mmol, 1.0 eq) in dry PrOH (0.3 mL). After stirring for 6 h, the reaction mixture was diluted with EtOAc (40 mL) and washed with satd aq NaHCO_3 (20 mL). The organic layer was dried over Na_2SO_4 , concentrated in vacuo and purified by MPLC on silica gel (petroleum ether/EtOAc, 9:1) to afford **7b** (23 mg, 52%) as a colorless oil. ^1H NMR (500 MHz, CDCl_3): $\delta = 7.95$ (d, $J = 8.2$ Hz, 2H, Ar-H), 7.79 (d, $J = 8.2$ Hz, 2H, Ar-H), 4.21 (t, $J = 6.7$ Hz, 2H, OCH_2), 1.76-1.69 (m, 2H, CH_2), 1.28 (s, 12H, 2 $\text{C}(\text{CH}_3)_2$), 0.96 (t, $J = 7.4$ Hz, 3H, CH_3); ^{13}C NMR (125 MHz, CDCl_3): $\delta = 166.92$ (CO), 134.84, 132.91, 128.76 (6C, Ar-C), 84.36 (2C, 2 $\text{C}(\text{CH}_3)_2$), 66.82 (OCH_2), 25.08 (4C, 2 $\text{C}(\text{CH}_3)_2$), 22.31 (CH_2), 10.72 (CH_3); elemental analysis: Calcd (%) for $\text{C}_{16}\text{H}_{23}\text{BO}_4$: C 66.23, H 7.99, found: C 66.15, H 8.01.

4-Butoxycarbonylphenylboronic acid pinacol ester (7c). Prepared according to the procedure for **7a** from **6** (47 mg, 0.188 mmol) with SOCl_2 (17 μL , 0.232 mmol, 1.2 eq) in dry BuOH (0.4 mL). After stirring for 6 h, the mixture was concentrated in vacuo and purified by MPLC on silica gel (petroleum ether/EtOAc, 9:1) to afford **7c** (37 mg, 65%) as a colorless oil. ^1H NMR (500 MHz, CDCl_3): $\delta = 7.94$ (d, $J = 8.2$ Hz, 2H, Ar-H), 7.79 (d, $J = 8.1$ Hz, 2H, Ar-H), 4.25 (t, $J = 6.7$ Hz, 2H, OCH_2), 1.71-1.66 (m, 2H, CH_2), 1.44-1.37 (m, 2H, CH_2), 1.28 (s, 12H, 2 $\text{C}(\text{CH}_3)_2$), 0.91 (t, $J = 7.4$ Hz, 3H, CH_3); ^{13}C NMR (125 MHz, CDCl_3): $\delta = 166.93$ (CO), 134.84, 132.91, 128.75 (6C, Ar-C), 84.36 (2C, 2 $\text{C}(\text{CH}_3)_2$), 65.13 (OCH_2), 30.97 (CH_2), 25.08 (4C, 2 $\text{C}(\text{CH}_3)_2$), 19.47 (CH_2), 13.97 (CH_3); ESI-MS: m/z : Calcd for $\text{C}_{17}\text{H}_{25}\text{BNaO}_4$ $[\text{M}+\text{Na}]^+$: 327.17, found: 326.98.

4-Isopropoxycarbonylphenylboronic acid pinacol ester (7d). To a solution of **6** (39 mg, 0.152 mmol) in CHCl_3 (1 mL) was added SOCl_2 (28 μL , 0.380 mmol, 2.5 eq). The reaction mixture was stirred at 60 $^\circ\text{C}$ under argon. Dry *i*-PrOH (1 mL) and Et_3N (23 μL , 0.167 mmol, 1.1 eq) were added after 2 h. When the reaction was complete (2.5 h), the mixture was concentrated in vacuo and the residue purified by MPLC on silica gel (petroleum ether/EtOAc, 9:1) to afford **7d** (14 mg, 32%) as a

colorless oil. ^1H NMR (500 MHz, CDCl_3): δ = 7.94 (d, J = 8.2 Hz, 2H, Ar-H), 7.78 (d, J = 8.1 Hz, 2H, Ar-H), 5.18 (hept, J = 6.3 Hz, 1H, OCH), 1.71-1.66 (m, 2H, CH_2), 1.44-1.37 (m, 2H, CH_2), 1.31-1.29 (m, 18H, 2 $\text{C}(\text{CH}_3)_2$, $\text{CH}(\text{CH}_3)_2$); ^{13}C NMR (125 MHz, CDCl_3): δ = 166.37 (CO), 134.79, 133.33, 128.74 (6C, Ar-C), 84.36 (2C, 2 $\text{C}(\text{CH}_3)_2$), 68.67 (OCH), 25.10 (4C, 2 $\text{C}(\text{CH}_3)_2$), 22.16 (2C, $\text{CH}(\text{CH}_3)_2$); ESI-MS: m/z : Calcd for $\text{C}_{16}\text{H}_{23}\text{BNaO}_4$ [$\text{M}+\text{Na}$] $^+$: 313.16, found: 312.99.

4-(2-Isopropoxyethoxycarbonyl)phenylboronic acid pinacol ester (7h). To a solution of **6** (100 mg, 0.391 mmol) in dry DCM (2 mL) under argon were added 2-isopropoxyethanol (91 μL , 0.782 mmol, 2.0 eq) and a catalytic amount of DMAP (4 mg, 0.033 mmol, 0.08 eq). Then, DIC (91 μL , 0.587 mmol, 1.5 eq) was added at 0 $^\circ\text{C}$, the reaction was allowed to reach rt and stirred for 1 h. The reaction mixture was diluted with EtOAc (40 mL) and washed with 0.1 N HCl (10 mL), satd aq NaHCO_3 (20 mL) and H_2O (20 mL). The organic layer was dried over Na_2SO_4 , concentrated in vacuo and purified by MPLC on silica gel (DCM/MeOH, 99:1) to afford **7h** (70 mg, 53%) as a colorless oil. ^1H NMR (500 MHz, CDCl_3): δ = 8.03 (d, J = 8.3 Hz, 2H, Ar-H), 7.86 (d, J = 8.1 Hz, 2H, Ar-H), 4.46-4.43 (m, 2H, COCH_3), 3.77-3.75 (m, 2H, CH_2O), 3.66 (hept, J = 6.1 Hz, 1H, OCH), 1.35 (s, 12H, 2 $\text{C}(\text{CH}_3)_2$), 1.18 (d, J = 6.1 Hz, 6H, $\text{CH}(\text{CH}_3)_2$); ^{13}C NMR (125 MHz, CDCl_3): δ = 166.78 (CO), 134.76, 132.52, 128.82 (6C, Ar-C), 84.30 (2C, 2 $\text{C}(\text{CH}_3)_2$), 72.20 (OCH), 66.09 (CH_2O), 64.71 (COCH_2), 25.02 (4C, 2 $\text{C}(\text{CH}_3)_2$), 22.19 (2C, $\text{CH}(\text{CH}_3)_2$); elemental analysis: Calcd (%) for $\text{C}_{18}\text{H}_{27}\text{BO}_5$: C 64.69, H 8.14, found: C 65.05, H 8.21.

4-(2-Acetoxyethoxycarbonyl)phenylboronic acid pinacol ester (7j). Prepared according to the procedure for **7h** from **6** (100 mg, 0.403 mmol) and 2-hydroxyethyl acetate^[57] (0.150 mL) with DIC (94 μL , 0.605 mmol, 1.5 eq) and DMAP (4 mg, 0.033 mmol, 0.08 eq) in dry DCM (2 mL) to afford **7j** (71 mg, 53%) as a colorless oil. ^1H NMR (500 MHz, CD_3OD): δ = 8.00 (d, J = 8.2 Hz, 2H, Ar-H), 7.84 (d, J = 8.2 Hz, 2H, Ar-H), 4.53-4.51 (m, 2H, CH_2), 4.43-4.41 (m, 2H, CH_2), 2.06 (s, 3H, COCH_3), 1.36 (s, 12H, 2 $\text{C}(\text{CH}_3)_2$); ^{13}C NMR (125 MHz, CD_3OD): δ = 172.63, 167.70 (2 CO), 135.69, 129.64 (6C, Ar-C), 85.53 (2C, 2 $\text{C}(\text{CH}_3)_2$), 64.17, 63.44 (2 OCH_2), 25.20 (4C, 2 $\text{C}(\text{CH}_3)_2$), 20.66 (COCH_3); ESI-MS: m/z : Calcd for $\text{C}_{17}\text{H}_{23}\text{BNaO}_6$ [$\text{M}+\text{Na}$] $^+$: 357.15, found: 357.04.

Ethyl 4'-(2,3,4,6-tetra-*O*-acetyl- α -D-mannopyranosyloxy)-3'-chlorobiphenyl-4-carboxylate (11a). Prepared according to general procedure A from **10** (83 mg, 0.142 mmol) and **7a** (43 mg, 0.156 mmol, 1.1 eq) with K_3PO_4 (93 mg, 0.411 mmol, 3.0 eq) and $\text{PdCl}_2(\text{dppf})\cdot\text{CH}_2\text{Cl}_2$ (3.4 mg, 4.2 μmol , 0.03 eq) in anhydrous DMF (0.5 mL). Purified by MPLC on silica gel (petroleum ether/EtOAc, 7:3). Yield: 62 mg (62%) as colorless oil. $[\alpha]_D^{20}$ +66.4 (c 1.00, CHCl_3); ^1H NMR (500 MHz, CDCl_3): δ = 8.02 (d, J = 8.4 Hz, 2H, Ar-H), 7.59 (d, J = 2.2 Hz, 1H, Ar-H), 7.51 (d, J = 8.4 Hz, 2H, Ar-H), 7.39 (dd, J = 2.2, 8.6 Hz, 1H, Ar-H), 7.18 (d, J = 8.6 Hz, 1H, Ar-H), 5.58-5.54 (m, 2H, H-1, H-3), 5.48 (dd, J = 1.8, 3.4 Hz, 1H, H-2), 5.33 (t, J = 10.1 Hz, 1H, H-4), 4.32 (q, J = 7.1 Hz, 2H, OCH_2), 4.22 (dd, J = 5.3, 12.3 Hz, 1H, H-6a), 4.12 (ddd, J = 2.1, 5.2, 10.1 Hz, 1H, H-5), 4.03 (dd, J = 2.2, 12.4 Hz,

1H, H-6b), 2.14, 2.00, 1.97, 1.96 (4 s, 12H, 4 COCH₃), 1.34 (t, $J = 7.1$ Hz, 3H, CH₃); ¹³C NMR (125 MHz, CDCl₃): $\delta = 170.61, 170.10, 169.92, 169.91, 166.45$ (5 CO), 151.27, 143.48, 136.33, 130.36, 129.79, 129.44, 126.83, 126.64, 125.03, 117.39 (12C, Ar-C), 96.79 (C-1), 69.99 (C-5), 69.47 (C-2), 68.92 (C-3), 65.96 (C-4), 62.25 (C-6), 61.22 (OCH₂), 21.02, 20.86, 20.84, 20.82 (4 COCH₃), 14.51 (CH₃); elemental analysis: Calcd (%) for C₂₉H₃₁ClO₁₂: C 57.38, H 5.15, found: C 57.62, H 5.32.

Propyl 4'-(2,3,4,6-tetra-O-acetyl- α -D-mannopyranosyloxy)-3'-chlorobiphenyl-4-carboxylate (11b). Prepared according to general procedure A from **10** (35 mg, 0.060 mmol) and **7b** (19 mg, 0.065 mmol, 1.1 eq) with K₃PO₄ (39 mg, 0.179 mmol, 3.0 eq) and PdCl₂(dppf)·CH₂Cl₂ (2.3 mg, 2.8 μ mol, 0.05 eq) in DMF (0.5 mL). Purified by MPLC on silica gel (petroleum ether/EtOAc, 1:0-0:1). Yield: 26 mg (70%) as colorless oil. $[\alpha]_D^{20} +68.2$ (c 0.87, CHCl₃); ¹H NMR (500 MHz, CDCl₃): $\delta = 8.03$ (d, $J = 8.4$ Hz, 2H, Ar-H), 7.60 (d, $J = 2.2$ Hz, 1H, Ar-H), 7.52 (d, $J = 8.4$ Hz, 2H, Ar-H), 7.39 (dd, $J = 2.2, 8.6$ Hz, 1H, Ar-H), 7.19 (d, $J = 8.5$ Hz, 1H, Ar-H), 5.57 (dd, $J = 3.5, 10.1$ Hz, 1H, H-3), 5.54 (d, $J = 1.5$ Hz, 1H, H-1), 5.49 (dd, $J = 1.9, 3.4$ Hz, 1H, H-2), 5.34 (t, $J = 10.1$ Hz, 1H, H-4), 4.25-4.21 (m, 3H, H-6a, OCH₂), 4.12 (ddd, $J = 2.1, 5.2, 10.1$ Hz, 1H, H-5), 4.03 (dd, $J = 2.2, 12.3$ Hz, 1H, H-6b), 2.15, 2.01, 1.98, 1.97 (4 s, 12H, 4 COCH₃), 1.78-1.71 (m, 2H, CH₂), 0.98 (t, $J = 7.4$ Hz, 3H, CH₃); ¹³C NMR (125 MHz, CDCl₃): $\delta = 170.66, 170.16, 169.97, 169.96, 166.57$ (5 CO), 151.32, 143.54, 136.40, 130.41, 129.86, 129.49, 126.90, 126.68, 125.09, 117.43 (12C, Ar-C), 96.84 (C-1), 70.03 (C-5), 69.52 (C-2), 68.96 (C-3), 66.85 (OCH₂), 66.01 (C-4), 62.29 (C-6), 22.33 (CH₂), 21.07, 20.90, 20.88, 20.86 (4 COCH₃), 10.72 (CH₃); ESI-MS: m/z : Calcd for C₃₀H₃₇ClNO₁₂ [M+NH₄]⁺: 638.20, found: 638.07.

Butyl 4'-(2,3,4,6-tetra-O-acetyl- α -D-mannopyranosyloxy)-3'-chlorobiphenyl-4-carboxylate (11c). Prepared according to general procedure A from **10** (52 mg, 0.090 mmol) and **7c** (30 mg, 0.099 mmol, 1.1 eq) with K₃PO₄ (59 mg, 0.270 mmol, 3.0 eq) and PdCl₂(dppf)·CH₂Cl₂ (3.9 mg, 4.5 μ mol, 0.05 eq) in DMF (0.5 mL). Purified by MPLC on silica gel (petroleum ether/EtOAc, 7:3). Yield: 33 mg (58%) as pink oil. $[\alpha]_D^{20} +105.1$ (c 1.10, CHCl₃); ¹H NMR (500 MHz, CDCl₃): $\delta = 8.03$ (d, $J = 8.4$ Hz, 2H, Ar-H), 7.61 (d, $J = 2.2$ Hz, 1H, Ar-H), 7.54 (d, $J = 8.4$ Hz, 2H, Ar-H), 7.41 (dd, $J = 2.2, 8.6$ Hz, 1H, Ar-H), 7.19 (d, $J = 8.6$ Hz, 1H, Ar-H), 5.57 (dd, $J = 3.5, 10.1$ Hz, 1H, H-3), 5.54 (d, $J = 1.6$ Hz, 1H, H-1), 5.49 (dd, $J = 1.9, 3.4$ Hz, 1H, H-2), 5.34 (t, $J = 10.1$ Hz, 1H, H-4), 4.28 (t, $J = 6.6$ Hz, 2H, OCH₂), 4.22 (dd, $J = 5.3, 12.3$ Hz, 1H, H-6a), 4.12 (ddd, $J = 2.2, 5.2, 10.1$ Hz, 1H, H-5), 4.04 (dd, $J = 2.2, 12.3$ Hz, 1H, H-6b), 2.15, 2.01, 1.98, 1.97 (4 s, 12H, 4 COCH₃), 1.73-1.67 (m, 2H, CH₂), 1.46-1.39 (m, 2H, CH₂), 0.92 (t, $J = 7.4$ Hz, 3H, CH₃); ¹³C NMR (125 MHz, CDCl₃): $\delta = 170.67, 170.17, 169.98, 169.97, 166.58$ (5 CO), 151.33, 143.54, 136.41, 130.42, 129.87, 129.50, 126.90, 126.68, 125.09, 117.44 (12C, Ar-C), 96.85 (C-1), 70.04 (C-5), 69.53 (C-2), 68.96 (C-3), 66.02 (C-4), 65.16 (OCH₂), 62.30 (C-6), 31.00 (CH₂), 21.07, 20.91, 20.88, 20.87 (4 COCH₃), 19.49 (CH₂), 13.98 (CH₃); HRMS: m/z : Calcd for C₃₁H₃₅ClNaO₁₂ [M+Na]⁺: 657.1715, found: 657.1711.

Isopropyl 4'-(2,3,4,6-tetra-*O*-acetyl- α -D-mannopyranosyloxy)-3'-chlorobiphenyl-4-carboxylate (11d). Prepared according to general procedure A from **10** (26 mg, 0.044 mmol) and **7d** (14 mg, 0.048 mmol, 1.1 eq) with K₃PO₄ (29 mg, 0.132 mmol, 3.0 eq) and PdCl₂(dppf)·CH₂Cl₂ (1.5 mg, 1.8 μ mol, 0.04 eq) in DMF (0.5 mL). Purified by MPLC on silica gel (petroleum ether/EtOAc, 7:3). Yield: 22 mg (81%) as colorless oil. $[\alpha]_D^{20} +57.5$ (*c* 1.05, CHCl₃); ¹H NMR (500 MHz, CDCl₃): δ = 8.02 (d, *J* = 8.5 Hz, 2H, Ar-H), 7.61 (d, *J* = 2.2 Hz, 1H, Ar-H), 7.53 (d, *J* = 8.5 Hz, 2H, Ar-H), 7.40 (dd, *J* = 2.2, 8.6 Hz, 1H, Ar-H), 7.19 (d, *J* = 8.3 Hz, 1H, Ar-H), 5.57 (dd, *J* = 3.5, 10.1 Hz, 1H, H-3), 5.54 (d, *J* = 1.6 Hz, 1H, H-1), 5.49 (dd, *J* = 1.9, 3.4 Hz, 1H, H-2), 5.34 (t, *J* = 10.1 Hz, 1H, H-4), 5.20 (hept, *J* = 6.3 Hz, 1H, OCH), 4.22 (dd, *J* = 5.3, 12.3 Hz, 1H, H-6a), 4.12 (ddd, *J* = 2.2, 5.2, 10.1 Hz, 1H, H-5), 4.03 (dd, *J* = 2.3, 12.2 Hz, 1H, H-6b), 2.15, 2.01, 1.98, 1.97 (4 s, 12H, 4 COCH₃), 1.38 (d, *J* = 6.3 Hz, 6H, CH(CH₃)₂); ¹³C NMR (125 MHz, CDCl₃): δ = 170.67, 170.17, 169.98, 169.97, 166.00 (5 CO), 151.30, 143.44, 136.46, 130.39, 130.26, 129.49, 126.84, 126.68, 125.08, 117.43 (12C, Ar-C), 96.84 (C-1), 70.03 (C-5), 69.52 (C-2), 68.97 (C-3), 68.71 (OCH), 66.02 (C-4), 62.30 (C-6), 22.17 (2C, CH(CH₃)₂), 21.07, 20.91, 20.88, 20.87 (4 COCH₃); HRMS: *m/z*: Calcd for C₃₀H₃₃ClNaO₁₂ [M+Na]⁺: 643.1558, found: 643.1554.

***tert*-Butyl 4'-(2,3,4,6-tetra-*O*-acetyl- α -D-mannopyranosyloxy)-3'-chlorobiphenyl-4-carboxylate (11e).** Prepared according to general procedure A from **10** (27 mg, 0.047 mmol) and 4-*tert*-butyloxycarbonylphenyl boronic pinacol ester (**7e**, 16 mg, 0.052 mmol, 1.1 eq) with K₃PO₄ (31 mg, 0.141 mmol, 3.0 eq) and PdCl₂(dppf)·CH₂Cl₂ (1.6 mg, 1.9 μ mol, 0.04 eq) in DMF (0.5 mL). Purified by MPLC on silica gel (petroleum ether/EtOAc, 7:3). Yield: 22 mg (74%) as colorless oil. $[\alpha]_D^{20} +64.9$ (*c* 1.09, CHCl₃); ¹H NMR (500 MHz, CDCl₃): δ = 7.97 (d, *J* = 8.4 Hz, 2H, Ar-H), 7.59 (d, *J* = 2.2 Hz, 1H, Ar-H), 7.49 (d, *J* = 8.4 Hz, 2H, Ar-H), 7.38 (dd, *J* = 2.2, 8.6 Hz, 1H, Ar-H), 7.18 (d, *J* = 8.8 Hz, 1H, Ar-H), 5.57 (dd, *J* = 3.5, 10.1 Hz, 1H, H-3), 5.55 (d, *J* = 1.5 Hz, 1H, H-1), 5.49 (dd, *J* = 1.9, 3.4 Hz, 1H, H-2), 5.34 (t, *J* = 10.1 Hz, 1H, H-4), 4.22 (dd, *J* = 5.3, 12.3 Hz, 1H, H-6a), 4.12 (ddd, *J* = 2.1, 5.3, 10.1 Hz, 1H, H-5), 4.03 (dd, *J* = 2.2, 12.3 Hz, 1H, H-6b), 2.15, 2.01, 1.98, 1.97 (4 s, 12H, 4 COCH₃), 1.54 (s, 9H, C(CH₃)₃); ¹³C NMR (125 MHz, CDCl₃): δ = 170.68, 170.18, 169.99, 169.98, 165.68 (5 CO), 151.26, 143.16, 136.55, 131.39, 130.30, 129.48, 126.77, 126.67, 125.08, 117.45 (12C, Ar-C), 96.86 (C-1), 81.40 (C(CH₃)₃), 70.04 (C-5), 69.54 (C-2), 68.98 (C-3), 66.04 (C-4), 62.31 (C-6), 28.43 (3C, C(CH₃)₃), 21.09, 20.92, 20.90, 20.88 (4 COCH₃); ESI-MS: *m/z*: Calcd for C₃₁H₃₅ClNaO₁₂ [M+Na]⁺: 657.17, found: 657.13.

2-Methoxyethyl 4'-(2,3,4,6-tetra-*O*-acetyl- α -D-mannopyranosyloxy)-3'-chloro-biphenyl-4-carboxylate (11f). 4-(2-Methoxyethoxycarbonyl)phenylboronic acid pinacol ester (**7f**) was prepared according to the procedure for **7a** from **6** (25 mg, 0.104 mmol) with SOCl₂ (11 μ L, 0.151 mmol, 1.5 eq) in 2-methoxyethanol (0.4 mL). The reaction mixture was concentrated in vacuo after 4 h. The crude product was used directly for the coupling reaction according to general procedure A with **10**

(55 mg, 0.095 mmol), K_3PO_4 (61 mg, 0.285 mmol, 3.0 eq) and $PdCl_2(dppf)\cdot CH_2Cl_2$ (3.1 mg, 3.8 μ mol, 0.04 eq) in DMF (1 mL). Purified by MPLC on silica gel (petroleum ether/EtOAc, 3:2). Yield: 32 mg (52% over two steps) as colorless oil. $[\alpha]_D^{20} +60.9$ (*c* 1.26, $CHCl_3$); 1H NMR (500 MHz, $CDCl_3$): δ = 8.05 (d, *J* = 8.4 Hz, 2H, Ar-H), 7.60 (d, *J* = 2.2 Hz, 1H, Ar-H), 7.52 (d, *J* = 8.4 Hz, 2H, Ar-H), 7.39 (dd, *J* = 2.2, 8.6 Hz, 1H, Ar-H), 7.19 (d, *J* = 8.9 Hz, 1H, Ar-H), 5.56 (dd, *J* = 3.5, 10.1 Hz, 1H, H-3), 5.54 (d, *J* = 1.5 Hz, 1H, H-1), 5.49 (dd, *J* = 1.9, 3.4 Hz, 1H, H-2), 5.34 (t, *J* = 10.1 Hz, 1H, H-4), 4.43-4.42 (m, 2H, CH_2), 4.22 (dd, *J* = 5.3, 12.3 Hz, 1H, H-6a), 4.12 (ddd, *J* = 2.2, 5.2, 10.1 Hz, 1H, H-5), 4.03 (dd, *J* = 2.2, 12.3 Hz, 1H, H-6b), 3.68-3.67 (m, 2H, CH_2), 3.37 (s, 3H, OCH_3), 2.14, 2.01, 1.98, 1.97 (4 s, 12H, 4 $COCH_3$); ^{13}C NMR (125 MHz, $CDCl_3$): δ = 170.58, 170.07, 169.89, 169.88, 166.39 (5 CO), 151.26, 143.64, 136.25, 130.51, 129.41, 129.30, 126.81, 126.60, 125.00, 117.34 (12C, Ar-C), 96.74 (C-1), 70.69 (CH_2), 69.95 (C-5), 69.42 (C-2), 68.87 (C-3), 65.92 (C-4), 64.24 (CH_2), 62.20 (C-6), 59.19 (OCH_3), 20.98, 20.82, 20.79, 20.78 (4 $COCH_3$); ESI-MS: *m/z*: Calcd for $C_{30}H_{33}ClNaO_{13}$ $[M+Na]^+$: 659.15, found: 659.12.

2-Ethoxyethyl 4'-(2,3,4,6-tetra-*O*-acetyl- α -D-mannopyranosyloxy)-3'-chloro-biphenyl-4-carboxylate (11g). 4-(2-Ethoxyethoxycarbonyl)phenylboronic acid pinacol ester (**7g**) was prepared according to the procedure for **7a** from **6** (40 mg, 0.161 mmol) with $SOCl_2$ (35 μ L, 0.484 mmol, 3.0 eq) in 2-ethoxyethanol (0.6 mL). After 6 h, the reaction mixture was diluted with DCM (40 mL) and washed with H_2O (4 x 30 mL). The organic layer was dried over Na_2SO_4 and concentrated in vacuo. The crude product was used directly in the coupling reaction according to general procedure A with **10** (47 mg, 0.081 mmol), K_3PO_4 (53 mg, 0.242 mmol, 3.0 eq) and $PdCl_2(dppf)\cdot CH_2Cl_2$ (3.3 mg, 4.1 μ mol, 0.05 eq) in DMF (2 mL). Purified by MPLC on silica gel (petroleum ether/EtOAc, 1:0-0:1). Yield: 25 mg (47% over two steps) as colorless oil. $[\alpha]_D^{20} +54.5$ (*c* 1.15, $CHCl_3$); 1H NMR (500 MHz, $CDCl_3$): δ = 8.12 (d, *J* = 8.4 Hz, 2H, Ar-H), 7.67 (d, *J* = 2.2 Hz, 1H, Ar-H), 7.59 (d, *J* = 8.4 Hz, 2H, Ar-H), 7.46 (dd, *J* = 2.2, 8.6 Hz, 1H, Ar-H), 7.27-7.25 (m, 1H, Ar-H), 5.64 (dd, *J* = 3.5, 10.1 Hz, 1H, H-3), 5.62 (d, *J* = 1.7 Hz, 1H, H-1), 5.56 (dd, *J* = 1.9, 3.4 Hz, 1H, H-2), 5.41 (t, *J* = 10.1 Hz, 1H, H-4), 4.50-4.48 (m, 2H, CH_2), 4.30 (dd, *J* = 5.3, 12.3 Hz, 1H, H-6a), 4.20 (ddd, *J* = 2.2, 5.2, 10.1 Hz, 1H, H-5), 4.11 (dd, *J* = 2.2, 12.2 Hz, 1H, H-6b), 3.80-3.78 (m, 2H, CH_2), 3.60 (q, *J* = 7.0 Hz, 2H, OCH_2CH_3), 2.22, 2.08, 2.05, 2.04 (4 s, 12H, 4 $COCH_3$), 1.24 (t, *J* = 7.0 Hz, 3H, CH_3); ^{13}C NMR (125 MHz, $CDCl_3$): δ = 170.59, 170.09, 169.91, 169.89, 166.43 (5 CO), 151.28, 143.62, 136.29, 130.52, 129.43, 129.42, 126.83, 126.62, 125.02, 117.35 (12C, Ar-C), 96.77 (C-1), 69.96 (C-5), 69.45 (C-2), 68.89 (C-3), 68.56 (CH_2), 66.85 (OCH_2CH_3), 65.94 (C-4), 64.49 (CH_2), 62.22 (C-6), 21.00, 20.84, 20.81, 20.80 (4 $COCH_3$), 15.30 (CH_3); ESI-MS: *m/z*: Calcd for $C_{31}H_{35}ClNaO_{13}$ $[M+Na]^+$: 673.17, found: 673.19.

2-Isopropoxyethyl 4'-(2,3,4,6-tetra-*O*-acetyl- α -D-mannopyranosyloxy)-3'-chloro-biphenyl-4-carboxylate (11h). Prepared according to general procedure A from **10** (105 mg, 0.180 mmol) and **7h**

(60 mg, 0.180 mmol, 1.0 eq) with K_3PO_4 (118 mg, 0.540 mmol, 3.0 eq) and $PdCl_2(dppf) \cdot CH_2Cl_2$ (7.3 mg, 9.0 μ mol, 0.05 eq) in DMF (2 mL). Purified by MPLC on silica gel (petroleum ether/EtOAc, 1:0-0:1). Yield: 67 mg (56%) as colorless oil. $[\alpha]_D^{20} +55.6$ (*c* 1.10, $CHCl_3$); 1H NMR (500 MHz, $CDCl_3$): δ = 8.11 (d, *J* = 8.4 Hz, 2H, Ar-H), 7.67 (d, *J* = 2.2 Hz, 1H, Ar-H), 7.59 (d, *J* = 8.4 Hz, 2H, Ar-H), 7.46 (dd, *J* = 2.2, 8.6 Hz, 1H, Ar-H), 7.26 (d, *J* = 8.4 Hz, 1H, Ar-H), 5.63 (dd, *J* = 3.5, 10.1 Hz, 1H, H-3), 5.61 (d, *J* = 1.3 Hz, 1H, H-1), 5.55 (dd, *J* = 1.8, 3.3 Hz, 1H, H-2), 5.40 (t, *J* = 10.1 Hz, 1H, H-4), 4.47-4.45 (m, 2H, CH_2), 4.29 (dd, *J* = 5.3, 12.3 Hz, 1H, H-6a), 4.20 (ddd, *J* = 2.1, 5.2, 10.0 Hz, 1H, H-5), 4.10 (dd, *J* = 2.1, 12.2 Hz, 1H, H-6b), 3.78-3.76 (m, 2H, CH_2), 3.67 (hept, *J* = 6.1 Hz, 1H, OCH), 2.21, 2.07, 2.05, 2.04 (4 s, 12H, 4 $COCH_3$), 1.22 (d, *J* = 6.1 Hz, 6H, $CH(CH_3)_2$); ^{13}C NMR (125 MHz, $CDCl_3$): δ = 170.59, 170.09, 169.91, 169.89, 166.43 (5 CO), 151.28, 143.59, 136.30, 130.49, 129.49, 129.44, 126.83, 126.61, 125.03, 117.36 (12C, Ar-C), 96.78 (C-1), 72.20 (OCH), 69.97 (C-5), 69.45 (C-2), 68.89 (C-3), 66.12 (CH_2), 65.95 (C-4), 64.76 (CH_2), 62.22 (C-6), 22.21 (2C, $CH(CH_3)_2$), 21.00, 20.84, 20.81, 20.80 (4 $COCH_3$); ESI-MS: *m/z*: Calcd for $C_{32}H_{37}ClNaO_{13}$ $[M+Na]^+$: 687.18, found: 687.23.

2-(2-Ethoxyethoxy)ethyl 4'-(2,3,4,6-tetra-*O*-acetyl- α -D-mannopyranosyloxy)-3'-chlorobiphenyl-4-carboxylate (11i). 4-(2-(2-Ethoxyethoxy)ethoxycarbonyl)phenyl-boronic acid pinacol ester (**7i**) was prepared according to the procedure for **7h** from **6** (75 mg, 0.196 mmol) and 2-(2-ethoxyethoxy)ethanol (40 μ L, 0.196 mmol, 1.0 eq) with DIC (54 μ L, 0.235 mmol, 1.2 eq) and DMAP (2 mg, 0.016 mmol, 0.08 eq) in DCM (2 mL). The crude product was pre-purified by MPLC on silica gel (DCM/MeOH, 99:1) and used directly in the coupling reaction according to general procedure A with **10** (79 mg, 0.135 mmol), K_3PO_4 (89 mg, 0.405 mmol, 3.0 eq) and $PdCl_2(dppf) \cdot CH_2Cl_2$ (5.5 mg, 6.8 μ mol, 0.05 eq) in DMF (2 mL). Purified by MPLC on silica gel (petroleum ether/EtOAc, 3:2). Yield: 60 mg (44% over two steps) as colorless oil. $[\alpha]_D^{20} +58.6$ (*c* 1.15, $CHCl_3$); 1H NMR (500 MHz, $CDCl_3$): δ = 8.06-8.04 (m, 2H, Ar-H), 7.60 (d, *J* = 2.2 Hz, 1H, Ar-H), 7.53-7.51 (m, 2H, Ar-H), 7.39 (dd, *J* = 2.3, 8.6 Hz, 1H, Ar-H), 7.19 (m, 1H, Ar-H), 5.57 (dd, *J* = 3.5, 10.1 Hz, 1H, H-3), 5.54 (d, *J* = 1.7 Hz, 1H, H-1), 5.49 (dd, *J* = 1.9, 3.4 Hz, 1H, H-2), 5.34 (t, *J* = 10.1 Hz, 1H, H-4), 4.45-4.43 (m, 2H, CH_2), 4.22 (dd, *J* = 5.3, 12.3 Hz, 1H, H-6a), 4.12 (ddd, *J* = 2.2, 5.2, 10.1 Hz, 1H, H-5), 4.03 (dd, *J* = 2.2, 12.3 Hz, 1H, H-6b), 3.80-3.78 (m, 2H, CH_2), 3.65-3.63 (m, 2H, CH_2), 3.56-3.54 (m, 2H, CH_2), 3.47 (q, *J* = 7.0 Hz, 2H, OCH_2CH_3), 2.15, 2.01, 1.98, 1.97 (4 s, 12H, 4 $COCH_3$), 1.14 (t, *J* = 7.0 Hz, 3H, CH_3); ^{13}C NMR (125 MHz, $CDCl_3$): δ = 170.60, 170.10, 169.91, 169.90, 166.40 (5 CO), 151.28, 143.63, 136.28, 130.52, 129.44, 129.40, 126.83, 126.62, 125.02, 117.35 (12C, Ar-C), 96.77 (C-1), 70.92, 70.00 (2C, 2 CH_2), 69.96 (C-5), 69.45 (C-2), 69.39 (CH_2), 68.89 (C-3), 66.86 (OCH_2CH_3), 65.94 (C-4), 64.37 (CH_2), 62.22 (C-6), 21.00, 20.84, 20.82, 20.80 (4 $COCH_3$), 15.29 (CH_3); ESI-MS: *m/z*: Calcd for $C_{33}H_{39}ClNaO_{14}$ $[M+Na]^+$: 717.19, found: 717.27.

2-Acetoxyethyl 4'-(2,3,4,6-tetra-*O*-acetyl- α -D-mannopyranosyloxy)-3'-chloro-biphenyl-4-carboxylate (11j). Prepared according to general procedure A from **10** (120 mg, 0.205 mmol) and **7j** (69 mg, 0.205 mmol, 1.0 eq) with K₃PO₄ (135 mg, 0.618 mmol, 3.0 eq) and PdCl₂(dppf)·CH₂Cl₂ (8.4 mg, 10.3 μ mol, 0.05 eq) in DMF (2 mL). Purified by MPLC on silica gel (petroleum ether/EtOAc, 3:2). Yield: 79 mg (58%) as colorless oil. $[\alpha]_D^{20}$ +43.9 (*c* 0.75, CHCl₃); ¹H NMR (500 MHz, CDCl₃): δ = 8.11 (d, *J* = 8.4 Hz, 2H, Ar-H), 7.67 (d, *J* = 2.2 Hz, 1H, Ar-H), 7.60 (d, *J* = 8.4 Hz, 2H, Ar-H), 7.46 (dd, *J* = 2.3, 8.6 Hz, 1H, Ar-H), 7.27 (m, 1H, Ar-H), 5.64 (dd, *J* = 3.5, 10.1 Hz, 1H, H-3), 5.62 (d, *J* = 1.7 Hz, 1H, H-1), 5.56 (dd, *J* = 1.9, 3.4 Hz, 1H, H-2), 5.41 (t, *J* = 10.1 Hz, 1H, H-4), 4.54-4.53 (m, 2H, CH₂), 4.45-4.43 (m, 2H, CH₂), 4.30 (dd, *J* = 5.3, 12.3 Hz, 1H, H-6a), 4.19 (ddd, *J* = 2.2, 5.2, 10.1 Hz, 1H, H-5), 4.11 (dd, *J* = 2.2, 12.3 Hz, 1H, H-6b), 2.22, 2.11, 2.08, 2.05, 2.04 (5 s, 15H, 5 COCH₃); ¹³C NMR (125 MHz, CDCl₃): δ = 171.01, 170.61, 170.12, 169.93, 169.90, 166.19 (6 CO), 151.35, 143.86, 136.21, 130.53, 129.46, 129.05, 126.93, 126.64, 125.07, 117.37 (12C, Ar-C), 96.79 (C-1), 69.99 (C-5), 69.46 (C-2), 68.90 (C-3), 65.95 (C-4), 62.97, 62.33 (2C, 2 CH₂), 62.23 (C-6), 21.02, 21.00, 20.85, 20.83, 20.82 (5 COCH₃); HRMS: *m/z*: Calcd for C₃₁H₃₃ClNaO₁₄ [M+Na]⁺: 687.1457, found: 687.1450.

Ethyl 3'-chloro-4'-(α -D-mannopyranosyloxy)biphenyl-4-carboxylate (3a). Prepared according to general procedure B from **11a** (18 mg, 0.030 mmol) with 1 M EtONa/EtOH (160 μ L) in EtOH/CHCl₃ (4 mL, 1:1). Purified by MPLC on silica gel (DCM/MeOH, 17:3). Yield: 9 mg (69%) as a white solid. $[\alpha]_D^{20}$ +105.0 (*c* 0.60, MeOH); ¹H NMR (500 MHz, CD₃OD): δ = 8.07 (d, *J* = 8.5 Hz, 2H, Ar-H), 7.73 (d, *J* = 2.3 Hz, 1H, Ar-H), 7.70 (d, *J* = 8.5 Hz, 2H, Ar-H), 7.59 (dd, *J* = 2.3, 8.6 Hz, 1H, Ar-H), 7.49 (d, *J* = 8.7 Hz, 1H, Ar-H), 5.61 (d, *J* = 1.6 Hz, 1H, H-1), 4.38 (q, *J* = 7.1 Hz, 2H, OCH₂), 4.12 (dd, *J* = 1.8, 3.3 Hz, 1H, H-2), 4.00 (dd, *J* = 3.4, 9.5 Hz, 1H, H-3), 3.80-3.71 (m, 3H, H-4, H-6a, H-6b), 3.65 (ddd, *J* = 2.4, 5.4, 9.8 Hz, 1H, H-5), 1.40 (t, *J* = 7.1 Hz, 3H, CH₃); ¹³C NMR (125 MHz, CD₃OD): δ = 167.86 (CO), 153.35, 145.15, 136.26, 131.15, 130.50, 129.76, 127.79, 127.74, 125.38, 118.61 (12C, Ar-C), 100.73 (C-1), 76.02 (C-5), 72.40 (C-3), 71.84 (C-2), 68.22 (C-4), 62.66 (C-6), 62.19 (OCH₂), 14.61 (CH₃); HRMS: *m/z*: Calcd for C₂₁H₂₃ClNaO₈ [M+Na]⁺: 461.0979, found: 461.0972.

Propyl 3'-chloro-4'-(α -D-mannopyranosyloxy)biphenyl-4-carboxylate (3b). Prepared according to general procedure B from **11b** (22 mg, 0.035 mmol) with 1 M PrONa/PrOH (150 μ L) in PrOH/CHCl₃ (2 mL, 1:1). Purified by MPLC on silica gel (DCM/MeOH, 17:3). Yield: 9 mg (56%) as a white solid. $[\alpha]_D^{20}$ +90.0 (*c* 0.90, MeOH); ¹H NMR (500 MHz, CD₃OD): δ = 8.08 (d, *J* = 8.5 Hz, 2H, Ar-H), 7.74 (d, *J* = 2.3 Hz, 1H, Ar-H), 7.72 (d, *J* = 8.5 Hz, 2H, Ar-H), 7.59 (dd, *J* = 2.3, 8.6 Hz, 1H, Ar-H), 7.47 (d, *J* = 8.7 Hz, 1H, Ar-H), 5.61 (d, *J* = 1.5 Hz, 1H, H-1), 4.29 (t, *J* = 6.6 Hz, 2H, OCH₂), 4.12 (dd, *J* = 1.8, 3.3 Hz, 1H, H-2), 4.02 (dd, *J* = 3.4, 9.5 Hz, 1H, H-3), 3.81-3.71 (m, 3H, H-4, H-6a, H-6b), 3.65 (ddd, *J* = 2.4, 5.5, 9.9 Hz, 1H, H-5), 1.85-1.78 (m, 2H, CH₂), 1.06 (t, *J* = 7.4 Hz, 3H, CH₃); ¹³C NMR (125 MHz, CD₃OD): δ = 167.91 (CO), 153.35, 145.16, 136.28, 131.14, 130.47, 129.76, 127.80,

127.76, 125.37, 118.61 (12C, Ar-C), 100.73 (C-1), 76.02 (C-5), 72.40 (C-3), 71.84 (C-2), 68.22 (C-4), 67.74 (OCH₂), 62.66 (C-6), 23.18 (CH₂), 10.80 (CH₃); HRMS: *m/z*: Calcd for C₂₂H₂₅ClNaO₈ [M+Na]⁺: 475.1136, found: 475.1131.

Butyl 3'-chloro-4'-(α -D-mannopyranosyloxy)biphenyl-4-carboxylate (3c). Prepared according to general procedure B from **11c** (33 mg, 0.052 mmol) with 1 M BuONa/BuOH (200 μ L) in BuOH/CHCl₃ (3 mL, 2:1). An additional portion of 1 M BuONa/BuOH (200 μ L) was added after 2 h. Purified by MPLC on silica gel (DCM/MeOH, 9:1). Yield: 9 mg (37%) as a white solid. $[\alpha]_D^{20}$ +78.5 (*c* 0.95, MeOH); ¹H NMR (500 MHz, CD₃OD): δ = 8.07 (d, *J* = 8.5 Hz, 2H, Ar-H), 7.74 (d, *J* = 2.2 Hz, 1H, Ar-H), 7.71 (d, *J* = 8.5 Hz, 2H, Ar-H), 7.60 (dd, *J* = 2.3, 8.6 Hz, 1H, Ar-H), 7.47 (d, *J* = 8.7 Hz, 1H, Ar-H), 5.61 (d, *J* = 1.3 Hz, 1H, H-1), 4.34 (t, *J* = 6.5 Hz, 2H, OCH₂), 4.12 (dd, *J* = 1.8, 3.3 Hz, 1H, H-2), 4.00 (dd, *J* = 3.5, 9.5 Hz, 1H, H-3), 3.80-3.71 (m, 3H, H-4, H-6a, H-6b), 3.65 (ddd, *J* = 2.4, 5.5, 9.8 Hz, 1H, H-5), 1.81-1.75 (m, 2H, CH₂), 1.55-1.48 (m, 2H, CH₂), 1.01 (t, *J* = 7.4 Hz, 3H, CH₃); ¹³C NMR (125 MHz, CD₃OD): δ = 167.91 (CO), 153.36, 145.17, 136.29, 131.15, 130.48, 129.77, 127.80, 127.76, 125.38, 118.61 (12C, Ar-C), 100.73 (C-1), 76.02 (C-5), 72.40 (C-3), 71.84 (C-2), 68.22 (C-4), 65.99 (OCH₂), 62.66 (C-6), 31.94, 20.33 (2 CH₂), 14.08 (CH₃); HRMS: *m/z*: Calcd for C₂₃H₂₇ClNaO₈ [M+Na]⁺: 489.1292, found: 489.1291.

Isopropyl 3'-chloro-4'-(α -D-mannopyranosyloxy)biphenyl-4-carboxylate (3d). Prepared according to general procedure B from **11d** (21 mg, 0.034 mmol) with 1 M *i*-PrONa/*i*-PrOH (200 μ L) in *i*-PrOH/CHCl₃ (1.5 mL, 2:1). An additional portion of 0.5 M *i*-PrONa/*i*-PrOH (500 μ L) was added after 6.5 h. Purified by MPLC on silica gel (DCM/MeOH, 9:1). Yield: 9.5 mg (62%) as a white solid. $[\alpha]_D^{20}$ +89.4 (*c* 0.90, MeOH); ¹H NMR (500 MHz, CD₃OD): δ = 8.06 (d, *J* = 8.5 Hz, 2H, Ar-H), 7.73 (d, *J* = 2.3 Hz, 1H, Ar-H), 7.70-7.69 (m, 2H, Ar-H), 7.61 (dd, *J* = 2.3, 8.7 Hz, 1H, Ar-H), 7.47 (d, *J* = 8.7 Hz, 1H, Ar-H), 5.61 (d, *J* = 1.6 Hz, 1H, H-1), 5.23 (hept, *J* = 6.3 Hz, 1H, OCH), 4.12 (dd, *J* = 1.8, 3.3 Hz, 1H, H-2), 4.00 (dd, *J* = 3.4, 9.5 Hz, 1H, H-3), 3.81-3.71 (m, 3H, H-4, H-6a, H-6b), 3.64 (ddd, *J* = 2.4, 5.4, 9.8 Hz, 1H, H-5), 1.38 (d, *J* = 6.3 Hz, 6H, CH(CH₃)₂); ¹³C NMR (125 MHz, CD₃OD): δ = 167.38 (CO), 153.34, 145.07, 136.31, 131.10, 130.85, 129.76, 127.78, 127.70, 125.37, 118.61 (12C, Ar-C), 100.73 (C-1), 76.02 (C-5), 72.40 (C-3), 71.84 (C-2), 69.87 (OCH), 68.22 (C-4), 62.66 (C-6), 22.14 (2C, CH(CH₃)₂); HRMS: *m/z*: Calcd for C₂₂H₂₅ClNaO₈ [M+Na]⁺: 475.1136, found: 475.1132.

***tert*-Butyl 3'-chloro-4'-(α -D-mannopyranosyloxy)biphenyl-4-carboxylate (3e).** Prepared according to general procedure B from **11e** (17 mg, 0.027 mmol) with *t*-BuOK (49 mg, 0.441 mmol, 16 eq) in *t*-BuOH/CHCl₃ (2 mL, 3:1). Purified by MPLC on silica gel (DCM/MeOH, 9:1). Yield: 8 mg (63%) as a colorless solid. $[\alpha]_D^{20}$ +82.4 (*c* 0.40, MeOH); ¹H NMR (500 MHz, CD₃OD): δ = 8.01 (d, *J* = 8.5 Hz, 2H, Ar-H), 7.73 (d, *J* = 2.2 Hz, 1H, Ar-H), 7.67 (d, *J* = 8.5 Hz, 2H, Ar-H), 7.59 (dd, *J* = 2.3, 8.6 Hz, 1H, Ar-H), 7.47 (d, *J* = 8.7 Hz, 1H, Ar-H), 5.61 (d, *J* = 1.3 Hz, 1H, H-1), 4.12 (dd, *J* = 1.8, 3.2 Hz, 1H, H-2), 4.00 (dd, *J* = 3.4, 9.5 Hz, 1H, H-3), 3.81-3.71 (m, 3H, H-4, H-6a, H-6b), 3.64 (ddd, *J* = 2.4,

5.4, 9.6 Hz, 1H, H-5), 1.61 (s, 9H, C(CH₃)₃); ¹³C NMR (125 MHz, CD₃OD): δ = 167.13 (CO), 153.29, 144.78, 136.39, 131.99, 131.02, 129.74, 127.76, 127.60, 125.36, 118.61 (12C, Ar-C), 100.74 (C-1), 82.35 (C(CH₃)₃), 76.01 (C-5), 72.40 (C-3), 71.84 (C-2), 68.22 (C-4), 62.66 (C-6), 28.43 (3C, C(CH₃)₃); HRMS: *m/z*: Calcd for C₂₃H₂₇ClNaO₈ [M+Na]⁺: 489.1292, found: 489.1286.

2-Methoxyethyl 3'-chloro-4'-(α-D-mannopyranosyloxy)biphenyl-4-carboxylate (3f). Prepared according to general procedure B from **11f** (16 mg, 0.025 mmol) with *t*-BuOK (56 mg, 0.502 mmol, 20 eq) in *t*-BuOH/CHCl₃ (6 mL, 5:1). An additional portion of *t*-BuOH (3 mL) was added after 17 h and additional portions of *t*-BuOK were added after 17 h (40 eq) and 22 h (8 eq). Purified by MPLC on silica gel (DCM/MeOH, 9:1). Yield: 3 mg (25%) as a white wax. [α]_D²⁰ +92.3 (*c* 0.30, MeOH); ¹H NMR (500 MHz, CD₃OD): δ = 8.10 (d, *J* = 8.5 Hz, 2H, Ar-H), 7.75 (d, *J* = 2.3 Hz, 1H, Ar-H), 7.72 (d, *J* = 8.5 Hz, 2H, Ar-H), 7.61 (dd, *J* = 2.3, 8.6 Hz, 1H, Ar-H), 7.48 (d, *J* = 8.7 Hz, 1H, Ar-H), 5.61 (d, *J* = 1.6 Hz, 1H, H-1), 4.48-4.46 (m, 2H, CH₂), 4.12 (dd, *J* = 1.8, 3.3 Hz, 1H, H-2), 4.00 (dd, *J* = 3.4, 9.5 Hz, 1H, H-3), 3.80-3.71 (m, 5H, CH₂, H-4, H-6a, H-6b), 3.64 (ddd, *J* = 2.3, 5.4, 9.7 Hz, 1H, H-5), 3.43 (s, 3H, OCH₃); ¹³C NMR (125 MHz, CD₃OD): δ = 167.75 (CO), 153.38, 145.30, 136.27, 131.29, 130.19, 129.78, 127.82, 127.77, 125.39, 118.62 (12C, Ar-C), 100.73 (C-1), 76.03 (C-5), 72.40 (C-3), 71.84 (C-2), 71.65 (CH₂), 68.22 (C-4), 65.17 (CH₂), 62.66 (C-6), 59.18 (OCH₃); HRMS: *m/z*: Calcd for C₂₂H₂₅ClNaO₉ [M+Na]⁺: 491.1085, found: 491.1080.

2-Ethoxyethyl 3'-chloro-4'-(α-D-mannopyranosyloxy)biphenyl-4-carboxylate (3g). Prepared according to general procedure B from **11g** (12.5 mg, 0.019 mmol) with *t*-BuOK (51 mg, 0.432 mmol, 23 eq) in *t*-BuOH/CHCl₃ (6 mL, 5:1). An additional portion of *t*-BuOK (23 eq) was added after 19 h. Purified by MPLC on silica gel (DCM/MeOH, 9:1). Yield: 6 mg (67%) as a colorless solid. [α]_D²⁰ +70.1 (*c* 0.55, MeOH); ¹H NMR (500 MHz, CD₃OD): δ = 8.11-8.09 (m, 2H, Ar-H), 7.74 (d, *J* = 2.3 Hz, 1H, Ar-H), 7.72-7.71 (m, 2H, Ar-H), 7.60 (dd, *J* = 2.3, 8.6 Hz, 1H, Ar-H), 7.47 (d, *J* = 8.7 Hz, 1H, Ar-H), 5.61 (d, *J* = 1.6 Hz, 1H, H-1), 4.47-4.45 (m, 2H, CH₂), 4.12 (dd, *J* = 1.8, 3.4 Hz, 1H, H-2), 4.00 (dd, *J* = 3.4, 9.5 Hz, 1H, H-3), 3.81-3.71 (m, 5H, H-4, H-6a, H-6b, CH₂), 3.65 (m, 1H, H-5), 3.61 (q, *J* = 7.0 Hz, 2H, OCH₂CH₃), 1.22 (t, *J* = 7.0 Hz, 3H, CH₃); ¹³C NMR (125 MHz, CD₃OD): δ = 167.77 (CO), 153.37, 145.27, 136.27, 131.28, 130.22, 129.78, 127.82, 127.76, 125.38, 118.61 (12C, Ar-C), 100.73 (C-1), 76.02 (C-5), 72.40 (C-3), 71.84 (C-2), 69.56 (CH₂), 68.22 (C-4), 67.67 (OCH₂CH₃), 65.40 (CH₂), 62.22 (C-6), 15.44 (CH₃); ESI-MS: *m/z*: Calcd for C₂₃H₂₇ClNaO₉ [M+Na]⁺: 505.1241, found: 505.1234.

2-Isopropoxyethyl 3'-chloro-4'-(α-D-mannopyranosyloxy)biphenyl-4-carboxylate (3h). Prepared according to general procedure B from **11h** (48 mg, 0.072 mmol) with *t*-BuOK (42 mg, 0.361 mmol, 5.0 eq) in *t*-BuOH/CHCl₃ (5.5 mL, 10:1). Additional portions of *t*-BuOK were added every 30 min (5.0 eq, 5.0 eq and 1.0 eq). Purified by MPLC on silica gel (DCM/MeOH, 9:1). Yield: 24 mg (67%) as a white solid. [α]_D²⁰ +74.6 (*c* 0.30, MeOH); ¹H NMR (500 MHz, CD₃OD): δ = 8.09 (d, *J* = 8.5 Hz,

2H, Ar-H), 7.74 (d, $J = 2.2$ Hz, 1H, Ar-H), 7.71 (d, $J = 8.5$ Hz, 2H, Ar-H), 7.60 (dd, $J = 2.3, 8.6$ Hz, 1H, Ar-H), 7.47 (d, $J = 8.7$ Hz, 1H, Ar-H), 5.61 (d, $J = 1.4$ Hz, 1H, H-1), 4.45-4.43 (m, 2H, CH₂), 4.12 (dd, $J = 1.8, 3.2$ Hz, 1H, H-2), 4.00 (dd, $J = 3.4, 9.5$ Hz, 1H, H-3), 3.81-3.69 (m, 6H, CH₂, H-4, H-6a, H-6b, OCH), 3.65 (ddd, $J = 2.3, 5.4, 9.7$ Hz, 1H, H-5), 1.08 (d, $J = 6.1$ Hz, 6H, CH(CH₃)₂); ¹³C NMR (125 MHz, CD₃OD): $\delta = 167.79$ (CO), 153.37, 145.26, 136.26, 131.26, 130.62, 129.77, 127.81, 127.76, 125.38, 118.61 (12C, Ar-C), 100.73 (C-1), 76.02 (C-5), 73.45 (OCH), 72.40 (C-3), 71.83 (C-2), 68.21 (C-4), 67.22 (CH₂), 65.70 (CH₂), 62.66 (C-6), 22.38 (2C, CH(CH₃)₂); HRMS: m/z : Calcd for C₂₄H₂₉ClNaO₉ [M+Na]⁺: 519.1398, found: 519.1395.

2-(2-Ethoxyethoxy)ethyl 3'-chloro-4'-(α -D-mannopyranosyloxy)biphenyl-4-carboxylate (3i).

Prepared according to general procedure B from **11i** (14 mg, 0.020 mmol) with *t*-BuOK (4 mg, 0.034 mmol, 1.7 eq) in *t*-BuOH (2 mL). An additional portion of *t*-BuOK (1.7 eq) was added after 2.5 h. Purified by MPLC on silica gel (DCM/MeOH, 9:1). Yield: 4.2 mg (40%) as a white wax. $[\alpha]_D^{20} +76.4$ (*c* 0.40, MeOH); ¹H NMR (500 MHz, CD₃OD): $\delta = 8.11$ -8.09 (m, 2H, Ar-H), 7.74 (d, $J = 2.3$ Hz, 1H, Ar-H), 7.72-7.70 (m, 2H, Ar-H), 7.60 (dd, $J = 2.3, 8.6$ Hz, 1H, Ar-H), 7.48 (d, $J = 8.7$ Hz, 1H, Ar-H), 5.61 (d, $J = 1.7$, 1H, H-1), 4.49-4.46 (m, 2H, CH₂), 4.12 (dd, $J = 1.8, 3.4$ Hz, 1H, H-2), 4.00 (dd, $J = 3.4, 9.5$ Hz, 1H, H-3), 3.86-3.84 (m, 2H, CH₂), 3.80-3.69 (m, 5H, H-6a, H-6b, H-4, OCH₂), 3.65 (ddd, $J = 2.4, 5.4, 9.8$ Hz, 1H, H-5), 3.62-3.60 (m, 2H, CH₂), 3.53 (q, $J = 7.0$ Hz, 2H, OCH₂CH₃), 1.17 (t, $J = 7.0$ Hz, 3H, CH₃); ¹³C NMR (125 MHz, CD₃OD): $\delta = 167.76$ (CO), 153.37, 145.27, 136.26, 131.30, 130.24, 129.77, 127.81, 127.75, 125.38, 118.61 (12C, Ar-C), 100.73 (C-1), 76.02 (C-5), 72.40 (C-3), 71.84 (C-2), 71.68, 70.92, 70.22 (3C, CH₂), 68.22 (C-4), 67.62 (CH₂), 65.35 (OCH₂CH₃), 62.66 (C-6), 15.41 (CH₃); HRMS: m/z : Calcd for C₂₅H₃₁ClNaO₁₀ [M+Na]⁺: 549.1503, found: 549.1498.

2-Hydroxyethyl 3'-chloro-4'-(α -D-mannopyranosyloxy)biphenyl-4-carboxylate (3k). Prepared according to general procedure B from **11j** (36 mg, 0.054 mmol) with *t*-BuOK (32 mg, 0.271 mmol, 5.0 eq) in *t*-BuOH/CHCl₃ (5.5 mL, 10:1). Additional portions of *t*-BuOK (10 eq) were added after 2 h and 24 h. Purified by MPLC on silica gel (DCM/MeOH, 9:1). Yield: 8 mg (32%) as a white wax. $[\alpha]_D^{20} +79.5$ (*c* 0.65, MeOH); ¹H NMR (500 MHz, CD₃OD): $\delta = 8.13$ (d, $J = 8.5$ Hz, 2H, Ar-H), 7.74 (d, $J = 2.3$ Hz, 1H, Ar-H), 7.71 (d, $J = 8.5$ Hz, 2H, Ar-H), 7.60 (dd, $J = 2.3, 8.6$ Hz, 1H, Ar-H), 7.47 (d, $J = 8.7$ Hz, 1H, Ar-H), 5.61 (d, $J = 1.6$ Hz, 1H, H-1), 4.41-4.39 (m, 2H, CH₂), 4.12 (dd, $J = 1.8, 3.3$ Hz, 1H, H-2), 4.00 (dd, $J = 3.4, 9.5$ Hz, 1H, H-3), 3.89-3.87 (m, 2H, CH₂), 3.80-3.71 (m, 3H, H-4, H-6a, H-6b), 3.65 (ddd, $J = 2.4, 5.4, 9.7$ Hz, 1H, H-5); ¹³C NMR (125 MHz, CD₃OD): $\delta = 167.93$ (CO), 153.36, 145.23, 136.29, 131.35, 130.29, 129.77, 127.80, 127.72, 125.38, 118.62 (12C, Ar-C), 100.73 (C-1), 76.02 (C-5), 72.40 (C-3), 71.83 (C-2), 68.22 (C-4), 67.63 (CH₂), 62.66 (C-6), 61.16 (CH₂); HRMS: m/z : Calcd for C₂₁H₂₃ClNaO₉ [M+Na]⁺: 477.0928, found: 477.0921.

2-(Dimethylamino)ethyl 3'-chloro-4'-(α -D-mannopyranosyloxy)biphenyl-4-carboxylate (3l).

Prepared according to general procedure C from **1** (19 mg, 0.044 mmol) and 2-

(dimethylamino)ethanol (13 μL , 0.132 mmol, 3.0 eq) with DIPEA (23 μL , 0.132 mmol, 3.0 eq) and COMU (39 mg, 0.088 mmol, 2.0 eq) in DMF (2 mL). Purified by preparative LC-MS (RP-18, $\text{H}_2\text{O}/\text{MeCN}$, 19:1-3:7, + 0.2% HCOOH). Yield: 8.2 mg (39%) as a white solid. $[\alpha]_D^{20} +62.7$ (c 0.75, MeOH); ^1H NMR (500 MHz, CD_3OD): δ = 8.15 (d, J = 8.4 Hz, 2H, Ar-H), 7.75-7.73 (m, 3H, Ar-H), 7.60 (dd, J = 2.2, 8.6 Hz, 1H, Ar-H), 7.48 (d, J = 8.7 Hz, 1H, Ar-H), 5.61 (d, J = 1.5 Hz, 1H, H-1), 4.69-4.67 (m, 2H, CH_2), 4.11 (dd, J = 1.8, 3.3 Hz, 1H, H-2), 4.00 (dd, J = 3.4, 9.5 Hz, 1H, H-3), 3.80-3.71 (m, 3H, H-4, H-6a, H-6b), 3.64 (ddd, J = 2.4, 5.5, 9.7 Hz, 1H, H-5), 3.57-3.55 (m, 2H, CH_2), 2.97 (s, 6H, $\text{N}(\text{CH}_3)_2$); ^{13}C NMR (125 MHz, CD_3OD): δ = 167.18 (CO), 153.46, 145.69, 136.03, 131.54, 129.77, 129.38, 127.83, 125.41, 118.61 (12C, Ar-C), 100.69 (C-1), 76.03 (C-5), 72.39 (C-3), 71.82 (C-2), 68.21 (C-4), 62.66 (C-6), 60.42, 57.65 (2 CH_2), 44.16 (2C, $\text{N}(\text{CH}_3)_2$); HRMS: m/z : Calcd for $\text{C}_{23}\text{H}_{29}\text{ClNO}_8$ $[\text{M}+\text{H}]^+$: 482.1582, found: 482.1578.

2-Piperidinoethyl 3'-chloro-4'-(α -D-mannopyranosyloxy)biphenyl-4-carboxylate (3m). Prepared according to general procedure C from **1** (46 mg, 0.112 mmol) and 1-(2-hydroxyethyl)piperidine (59 μL , 0.448 mmol, 4.0 eq) with DIPEA (58 μL , 0.336 mmol, 3.0 eq) and COMU (99 mg, 0.224 mmol, 2.0 eq) in DMF (4 mL). Purified by preparative LC-MS (RP-18, $\text{H}_2\text{O}/\text{MeCN}$, 19:1-1:19, + 0.2% HCOOH). Yield: 7.8 mg (13%) as a yellowish solid. $[\alpha]_D^{20} +64.3$ (c 0.25, MeOH); ^1H NMR (500 MHz, CD_3OD): δ = 8.12 (d, J = 8.4 Hz, 2H, Ar-H), 7.75-7.73 (m, 3H, Ar-H), 7.61 (dd, J = 2.2, 8.6 Hz, 1H, Ar-H), 7.48 (d, J = 8.7 Hz, 1H, Ar-H), 5.62 (d, J = 1.4 Hz, 1H, H-1), 4.62-4.60 (m, 2H, CH_2), 4.12 (dd, J = 1.8, 3.2 Hz, 1H, H-2), 4.00 (dd, J = 3.4, 9.5 Hz, 1H, H-3), 3.81-3.71 (m, 3H, H-4, H-6a, H-6b), 3.64 (ddd, J = 2.4, 5.5, 9.6 Hz, 1H, H-5), 3.23 (m, 2H, CH_2N), 3.02 (br s, 4H, 2 NCH_2), 1.81-1.76 (m, 4H, 2 CH_2), 1.62-1.60 (m, 2H, $(\text{CH}_2)_2\text{CH}_2$); ^{13}C NMR (125 MHz, CD_3OD): δ = 167.23 (CO), 153.47, 145.69, 136.03, 131.49, 129.78, 129.44, 127.86, 127.83, 125.42, 118.62 (12C, Ar-C), 100.70 (C-1), 76.04 (C-5), 72.40 (C-3), 71.82 (C-2), 68.22 (C-4), 62.67 (C-6), 60.19 (CH_2), 57.01 (CH_2N), 54.93 (2 NCH_2), 24.31 (2C, 2 CH_2), 22.65 ($(\text{CH}_2)_2\text{CH}_2$); HRMS: m/z : Calcd for $\text{C}_{26}\text{H}_{33}\text{ClNO}_8$ $[\text{M}+\text{H}]^+$: 522.1895, found: 522.1889.

2-Morpholinoethyl 3'-chloro-4'-(α -D-mannopyranosyloxy)biphenyl-4-carboxylate (3n). Prepared according to general procedure C from **1** (20 mg, 0.049 mmol) and 4-(2-hydroxyethyl)morpholine (18 μL , 0.147 mmol, 3.0 eq) with DIPEA (25 μL , 0.146 mmol, 3.0 eq) and COMU (42 mg, 0.095 mmol, 2.0 eq) in DMF (2 mL). Pre-purified by MPLC on silica gel (DCM/MeOH , 8:2) followed by purification by preparative LC-MS (RP-18, $\text{H}_2\text{O}/\text{MeCN}$, 19:1-1:19, + 0.2% HCOOH). Yield: 3.2 mg (13%) as a yellowish solid. $[\alpha]_D^{20} +72.5$ (c 0.35, MeOH); ^1H NMR (500 MHz, CD_3OD): δ = 8.12 (d, J = 8.4 Hz, 2H, Ar-H), 7.75-7.72 (m, 3H, Ar-H), 7.61 (dd, J = 2.2, 8.6 Hz, 1H, Ar-H), 7.48 (d, J = 8.7 Hz, 1H, Ar-H), 5.61 (d, J = 1.4 Hz, 1H, H-1), 4.59-4.57 (m, 2H, OCH_2), 4.12 (dd, J = 1.8, 3.3 Hz, 1H, H-2), 4.00 (dd, J = 3.4, 9.5 Hz, 1H, H-3), 3.81-3.71 (m, 7H, 2 CH_2O , H-4, H-6a, H-6b), 3.64 (ddd, J = 2.3, 5.4, 9.6 Hz, 1H, H-5), 3.13-3.11 (m, 2H, CH_2N), 2.92 (m, 4H, 2 NCH_2); ^{13}C NMR (125 MHz,

CD₃OD): δ = 167.53 (CO), 153.43, 145.47, 136.17, 131.37, 129.93, 129.78, 127.81, 125.41, 118.62 (12C, Ar-C), 100.72 (C-1), 76.04 (C-5), 72.40 (C-3), 71.83 (C-2), 68.22 (C-4), 66.78 (2C, 2 CH₂O), 62.67 (C-6), 61.95 (OCH₂), 57.94 (CH₂N), 54.55 (2C, 2 NCH₂); HRMS: m/z : Calcd for C₂₅H₃₁ClNO₉ [M+H]⁺: 524.1687, found: 524.1684.

2-(Dimethylamino)ethyl 3'-trifluoromethyl-4'-(α -D-mannopyranosyloxy)-biphenyl-4-carboxylate (5I). Prepared according to general procedure C from **4**^[21] (60 mg, 0.135 mmol) and 2-(dimethylamino)ethanol (82 μ L, 0.810 mmol, 6.0 eq) with DIPEA (69 μ L, 0.405 mmol, 3.0 eq) and COMU (119 mg, 0.270 mmol, 2.0 eq) in DMF (4 mL). Purified by preparative LC-MS (RP-18, H₂O/MeCN, 19:1-1:19, + 0.2% HCOOH). Yield: 37 mg (53%) as a white solid. $[\alpha]_D^{20}$ +80.9 (*c* 1.00, MeOH); ¹H NMR (500 MHz, CD₃OD): δ = 8.17 (d, *J* = 8.4 Hz, 2H, Ar-H), 7.91-7.89 (m, 2H, Ar-H), 7.76 (d, *J* = 8.4 Hz, 2H, Ar-H), 7.61 (d, *J* = 8.4 Hz, 1H, Ar-H), 5.66 (d, *J* = 1.2 Hz, 1H, H-1), 4.66-4.64 (m, 2H, OCH₂), 4.06 (dd, *J* = 1.8, 3.3 Hz, 1H, H-2), 3.94 (dd, *J* = 3.4, 9.5 Hz, 1H, H-3), 3.81-3.71 (m, 3H, H-4, H-6a, H-6b), 3.58 (ddd, *J* = 2.3, 5.6, 9.6 Hz, 1H, H-5), 3.45-3.43 (m, 2H, CH₂N), 2.87 (s, 6H, N(CH₃)₂); ¹³C NMR (125 MHz, CD₃OD): δ = 167.23 (CO), 155.61, 145.55, 134.59, 133.46, 131.58, 129.67, 127.89, 126.46, 126.41, 126.07, 123.90, 121.00, 120.76, 120.51, 117.83 (13C, Ar-C, CF₃), 100.27 (C-1), 76.13 (C-5), 72.24 (C-3), 71.73 (C-2), 68.11 (C-4), 62.68 (C-6), 60.95 (OCH₂), 57.79 (CH₂N), 44.41 (2C, N(CH₃)₂); HRMS: m/z : Calcd for C₂₄H₂₉F₃NO₈ [M+H]⁺: 516.1845, found: 516.1840.

Physicochemical and *in vitro* pharmacokinetic studies

Materials: Dimethyl sulfoxide (DMSO), 1-propanol, 1-octanol, Dulbecco's Modified Eagle's Medium (DMEM) high glucose, Penicillin-Streptomycin (solution stabilized, with 10'000 units Penicillin and 10 mg Streptomycin/mL), L-glutamine solution (200 mM), magnesium chloride, bis(4-nitrophenyl) phosphate (BNPP), Loperamide hydrochloride, and Neostigmine bromide were purchased from Sigma-Aldrich (St. Louis, MI, USA). PRISMA HT universal buffer, GIT-0 Lipid Solution, and Acceptor Sink Buffer were ordered from pIon (Woburn, MA, USA). MEM non-essential amino acids solution 10 mM (100X), fetal bovine serum (FBS), and DMEM without sodium pyruvate and phenol red were bought from Invitrogen (Carlsbad, CA, USA). Acetonitrile (MeCN) and methanol (MeOH) were ordered from Acros Organics (Geel, Belgium). Human plasma was purchased from Biopredic (Rennes, France). Pooled male rat liver microsomes (Sprague Dawley), and pooled human liver microsomes were ordered from BD Bioscience (Woburn, MA, USA). The Caco-2 cells were kindly provided by Prof G. Imanidis, FHNW, Muttentz, Switzerland and originated from the American Type Culture Collection (Rockville, MD, USA).

Aqueous solubility. Solubility was determined in a 96-well format using the μ SOL Explorer solubility analyzer (pIon, version 3.4.0.5). For each compound, measurements were performed at two pH values (3.0, 7.4) in triplicate. Six wells of a deep well plate, *i.e.* three wells per pH value, were

filled with 300 μL of PRISMA HT universal buffer adjusted to pH 3.0 or 7.4 by adding the requested amount of NaOH (0.5 M). Aliquots (3 μL) of a compound stock solution (40-100 mM in DMSO) were added and thoroughly mixed. The final sample concentration was 0.4-1.0 mM, the residual DMSO concentration was 1.0% (v/v) in the buffer solutions. After 15 h, the solutions were filtrated (0.2 μm 96-well filter plates) using a vacuum to collect manifold (Whatman Ltd., Maidstone, UK) to remove any precipitates. Equal amounts of filtrate and 1-propanol were mixed and transferred to a 96-well plate for UV/Vis detection (190 to 500 nm, SpectraMax 190, Molecular Devices, Silicon Valley, CA, USA). The amount of material dissolved was calculated by comparison with UV/Vis spectra obtained from reference samples, which were prepared by dissolving compound stock solution in a 1:1 mixture of buffer and 1-propanol (final concentrations 0.067-0.167 mM).

log $D_{7.4}$ determination. The in silico prediction tool ALOGPS^[58] was used to estimate the log P values of the compounds. Depending on these values, the compounds were classified into three categories: hydrophilic compounds (log P below zero), moderately lipophilic compounds (log P between zero and one) and lipophilic compounds (log P above one). For each category, two different ratios (volume of 1-octanol to volume of buffer) were defined as experimental parameters (Table 3).

Table 3. Compound classification based on estimated log P values.

compound type	log P	ratios (1-octanol: buffer)
hydrophilic	< 0	30:140, 40:130
moderately lipophilic	0 - 1	70:110, 110:70
lipophilic	> 1	3:180, 4:180

Equal amounts of phosphate buffer (0.1 M, pH 7.4) and 1-octanol were mixed and shaken vigorously for 5 min to saturate the phases. The mixture was left until separation of the two phases occurred, and the buffer was retrieved. Stock solutions of the test compounds were diluted with buffer to a concentration of 1 μM . For each compound, six determinations, *i.e.* three determinations per 1-octanol:buffer ratio, were performed in different wells of a 96-well plate. The respective volumes of buffer containing analyte (1 μM) were pipetted to the wells and covered by saturated 1-octanol according to the chosen volume ratio. The plate was sealed with aluminium foil, shaken (1350 rpm, 25 °C, 2 h) on a Heidolph Titramax 1000 plate-shaker (Heidolph Instruments GmbH & Co. KG, Schwabach, Germany) and centrifuged (2000 rpm, 25 °C, 5 min, 5804 R Eppendorf centrifuge, Hamburg, Germany). The aqueous phase was transferred to a 96-well plate for analysis by liquid chromatography-mass spectrometry (LC-MS, see below).

The log $D_{7.4}$ coefficients were calculated from the 1-octanol:buffer ratio (o:b), the initial concentration of the analyte in buffer (1 μM), and the concentration of the analyte in buffer (c_B) with Equation 1:

$$\log D_{7.4} = \log \left(\frac{1\mu M - c_B}{c_B} \times \frac{1}{o:b} \right) \quad (1)$$

The average of the three $\log D_{7.4}$ values per 1-octanol:buffer ratio was calculated. If the two means obtained for a compound did not differ by more than 0.1 units, the results were accepted.

Parallel artificial membrane permeability assay (PAMPA). Effective permeability ($\log P_e$) was determined in a 96-well format with the PAMPA.^[38] For each compound, measurements were performed at two pH values (5.0, 7.4) in quadruplicate. Eight wells of a deep well plate, *i.e.* four wells per pH-value, were filled with 650 μ L of PRISMA HT universal buffer adjusted to pH 5.0 or 7.4 by adding the requested amount of NaOH (0.5 M). Samples (150 μ L) were withdrawn from each well to determine the blank spectra by UV-spectroscopy (190 to 500 nm, SpectraMax 190). Then, analyte dissolved in DMSO (10 mM) was added to the remaining buffer to yield 50 μ M solutions. To exclude precipitation, the optical density was measured at 650 nm, with 0.01 being the threshold value. Solutions exceeding this threshold were filtrated. Afterwards, samples (150 μ L) were withdrawn to determine the reference spectra. Further 200 μ L was transferred to each well of the donor plate of the PAMPA sandwich (pIon, P/N 110 163). The filter membranes at the bottom of the acceptor plate were infused with 5 μ L of GIT-0 Lipid Solution and 200 μ L of Acceptor Sink Buffer was filled into each acceptor well. The sandwich was assembled, placed in the GutBoxTM, and left undisturbed for 16 h. Then, it was disassembled and samples (150 μ L) were transferred from each donor and acceptor well to UV-plates. Quantification was done by UV/Vis-spectroscopy. Effective permeability ($\log P_e$) was calculated from the compound flux deduced from the UV/Vis spectra, the filter area, and the initial sample concentration in the donor well with the aid of the PAMPA Explorer Software (pIon, version 3.5).

Colorectal adenocarcinoma (Caco-2) cell permeation assay. Caco-2 cells were cultivated in tissue culture flasks (BD Biosciences, Franklin Lakes, NJ, USA) with DMEM high glucose medium, containing L-glutamine (2 mM), nonessential amino acids (0.1 mM), Penicillin (100 U/mL), Streptomycin (100 μ g/mL), and fetal bovine serum (10%). The cells were kept at 37 °C in humidified air containing 5% CO₂, and the medium was changed every second day. When approximately 90% confluence was reached, the cells were split in a 1:10 ratio and distributed to new tissue culture flasks. At passage numbers between 60 and 65, they were seeded at a density of 5.3×10^5 cells per well to Transwell 6-well plates (Corning Inc., Corning, NY, USA) with 2.5 mL of culture medium in the basolateral and 2 mL in the apical compartment. The medium was renewed on alternate days. Permeation experiments were performed between days 19 and 21 post seeding. Previously to the experiment, the integrity of the Caco-2 monolayers was evaluated by measuring the transepithelial electrical resistance (TEER) with an Endohm tissue resistance instrument (World Precision Instruments Inc., Sarasota, FL, USA). Only wells with TEER values higher than 250 Ω cm² were used. To inhibit carboxylesterase activity, the Caco-2 cell monolayers were pre-incubated with bis(4-

nitrophenyl) phosphate (BNPP, 200 μM) dissolved in transport medium (DMEM without sodium pyruvate and phenol red) for 40 min.^[59] Experiments were performed in the apical-to-basolateral (absorptive) and basolateral-to-apical (secretory) directions in triplicate. Transport medium was withdrawn from the donor compartments of three wells and replaced by the same volume of compound stock solutions (in DMSO) to reach an initial sample concentration of 62.5 μM , 100 μM , 200 μM , 400 μM , or 825 μM . The Transwell plate was shaken (600 rpm, 37 °C) on a Heidolph Titramax 1000 plate-shaker. Samples (40 μL) were withdrawn from the donor and acceptor compartments 30 min after initiation of the experiment and the concentrations were determined by LC-MS (see below). Apparent permeability (P_{app}) was calculated according to Equation 2:

$$P_{\text{app}} = \frac{dQ}{dt} \times \frac{1}{A \times c_0} \quad (2)$$

where dQ/dt is the compound flux (mol s^{-1}), A the surface area of the monolayer (cm^2), and c_0 the initial concentration in the donor compartment (mol cm^{-3}).^[44] After the experiment, TEER values were assessed again for each well and results from wells with values below 250 $\Omega \text{ cm}^2$ were discarded.

In vitro metabolism: microsomal stability

Metabolic stability study. Incubations were performed in triplicate in a 96-well format on an Eppendorf Thermomixer Comfort. The reaction mixture (270 μL) consisting of liver microsomes (0.139 $\mu\text{g/mL}$), TRIS-HCl buffer (0.1 M, pH 7.4) and MgCl_2 (2 mM) was preheated (37 °C, 500 rpm, 10 min), and the incubation was initiated by adding 30 μL of compound solution (20 μM) in TRIS-HCl buffer. The final concentration of the compound was 2 μM , and the microsomal concentration was 0.125 mg/mL. At the beginning of the experiment ($t = 0$ min) and after an incubation time of 5, 10, 20, 40, and 60 min, samples (40 μL) were transferred to 120 μL of ice-cooled MeCN or MeOH and centrifuged (3600 rpm, 4 °C, 10 min). Then, 80 μL of supernatant was transferred to a 96-well plate for LC-MS analysis (see below). The metabolic half-life ($t_{1/2}$) was calculated from the slope of the linear regression from the log percentage remaining compound versus incubation time relationship. Control experiments were performed in parallel by preincubating the microsomes with the specific carboxylesterase inhibitor BNPP (1 mM) for 5 min before addition of the compound solution.^[40]

Inhibition study. Test compounds were dissolved in DMSO to 1 mM and then diluted with TRIS-HCl buffer (0.1 M, pH 7.4) containing MgCl_2 (2 mM) to a concentration of 6 μM . Loperamide hydrochloride was dissolved in DMSO to 20 mM, 2 mM, and 0.2 mM and then diluted with TRIS-HCl buffer containing MgCl_2 to a concentration of 750 μM , 75 μM , and 7.5 μM . Human liver microsomes were suspended in TRIS-HCl buffer containing MgCl_2 to a concentration of 30 $\mu\text{g/mL}$. Compound solution (100 μL) and microsome suspension (200 μL) mixed with Loperamide solution or blank buffer (50 μL) were preheated (37 °C, 500 rpm, 15 min) in separate wells of a 96-well plate.

The incubation was initiated by transferring 200 μL of microsome suspension containing Loperamide to the compound solution. The final compound concentration was 2 μM , the microsomal concentration was 20 $\mu\text{g}/\text{ml}$, and the Loperamide concentration was 100 μM , 10 μM , 1 μM , and 0 μM (blank). At the beginning of the experiment ($t = 0$ min) and after an incubation time of 10, 20, 30, 45, and 60 min, samples (20 μL) were transferred to 60 μL of ice-cooled MeOH and analysed by LC-MS (see below). The metabolic turnover was assessed as accumulation of product **1** versus incubation time.

***In vitro* metabolism: plasma stability**

Metabolic stability study. Incubations were performed in triplicates in a 96-well format according to the procedure described by Di et al.^[58] Human plasma was centrifuged (4 $^{\circ}\text{C}$, 3000 rpm, 10 min) to remove particulates before use. Compounds were dissolved in DMSO to 80 μM and then diluted with phosphate buffer (0.1 M, pH 7.4) to a concentration of 8 μM . Plasma (156 μL) was mixed with phosphate buffer (84 μL) and preheated (37 $^{\circ}\text{C}$, 500 rpm, 10 min). The incubation was initiated by adding 80 μL of compound solution. The final compound concentration was 2 μM and the plasma concentration was 50% in buffer pH 7.4. At the beginning of the experiment ($t = 0$ min) and after an incubation time of 15, 30, 60, and 120 min, samples (50 μL) were transferred to 150 μL of ice-cooled MeOH, frozen (-20 $^{\circ}\text{C}$, 10 min) and centrifuged (3600 rpm, 4 $^{\circ}\text{C}$, 10 min). The supernatant (80 μL) was transferred to a 96-well plate for LC-MS analysis (see below). The metabolic half-life ($t_{1/2}$) was calculated from the slope of the linear regression from the log percentage remaining compound versus incubation time relationship. To monitor non-enzymatic compound degradation, incubations in absence of human plasma were run in parallel.

Inhibition study. Human plasma and test compound were processed as described above. Neostigmine bromide was dissolved in DMSO to 10 mM, 3 mM, 1 mM, 0.3 mM, 0.1 mM, 0.03 mM, and 0.01 mM and then diluted with phosphate buffer (0.1 M, pH 7.4) to a concentration of 80 μM , 24 μM , 8 μM , 2.4 μM , 0.8 μM , 0.24 μM , and 0.08 μM . Human plasma (156 μL) mixed with phosphate buffer (44 μL) was preheated (37 $^{\circ}\text{C}$, 500 rpm, 10 min). Then, Neostigmine bromide solution or blank buffer (40 μL) was added for preincubation (37 $^{\circ}\text{C}$, 500 rpm, 5 min). The incubation was initiated by adding 80 μL of compound solution. The final compound concentration was 2 μM , the plasma concentration was 50% in buffer pH 7.4, and the Neostigmine bromide concentration was 10 μM , 3 μM , 1 μM , 0.3 μM , 0.1 μM , 0.03 μM , 0.01 μM , and 0 μM (blank). At the beginning of the experiment ($t = 0$ min) and after an incubation time of 5, 10, 30, and 60 min, samples (50 μL) were transferred to 150 μL of ice-cooled MeOH, frozen (-20 $^{\circ}\text{C}$, 10 min), and centrifuged (3600 rpm, 4 $^{\circ}\text{C}$, 10 min). The supernatant (80 μL) was transferred to a 96-well plate for LC-MS analysis (see below). Metabolic activity was calculated from the slope of the linear regression from the log percentage remaining compound versus incubation time relationship.

LC-MS measurements. Analyses were performed using a 1100/1200 Series HPLC System coupled to a 6410 Triple Quadrupole mass detector (Agilent Technologies, Inc., Santa Clara, CA, USA) equipped with electrospray ionization. The system was controlled with the Agilent MassHunter Workstation Data Acquisition software (version B.01.04). The column used was an Atlantis® T3 C18 column (2.1 x 50 m) with a 3- μ m particle size (Waters Corp., Milford, MA, USA). The mobile phase consisted of eluent A: H₂O containing 0.1% formic acid (for **1**, **3f-i**, **3l-n**, **4**, and **5l**), or 10 mM ammonium acetate, pH 5.0 in 95:5 H₂O:MeCN (for **2**, **3a-e**, **3k**); and eluent B: MeCN containing 0.1% formic acid. The flow rate was maintained at 0.6 mL/min. The gradient was ramped from 95% A/5% B to 5% A/95% B over 1 min, and then hold at 5% A/95% B for 0.1 min. The system was then brought back to 95% A/5% B, resulting in a total duration of 4 min. MS parameters such as fragmentor voltage, collision energy, polarity were optimized individually for each drug, and the molecular ion was followed for each compound in the multiple reaction monitoring mode. The concentrations of the analytes were quantified by the Agilent Mass Hunter Quantitative Analysis software (version B.01.04).

References

- [1] T. M. Hooton, R. Besser, B. Foxman, T. R. Fritsche, L. E. Nicolle, *Clin. Infect. Dis.* **2004**, *39*, 75-80.
- [2] S. D. Fihn, *N. Engl. J. Med.* **2003**, *349*, 259-266.
- [3] G. V. Sanchez, R. N. Master, J. A. Karlowsky, J. M. Bordon, *Antimicrob. Agents Chemother.* **2012**, *56*, 2181-2183.
- [4] N. Sharon, *Biochim. Biophys. Acta* **2006**, *1760*, 527-537.
- [5] B. Westerlund-Wikström, T.K. Korhonen, *Int. J. Med. Microbiol.* **2005**, *295*, 479-486.
- [6] T. J. Wiles, R. R. Kulesus, M. A. Mulvey, *Exp. Mol. Pathol.* **2008**, *85*, 11-19.
- [7] J. D. Schilling, M. A. Mulvey, S. J. Hultgren, *J. Infect. Dis.* **2001**, *183 Suppl. 1*, S36-40.
- [8] G. Capitani, O. Eidam, R. Glockshuber, M. G. Grütter, *Microbes Infect.* **2006**, *8*, 2284-2290.
- [9] N. Firon, I. Ofek, N. Sharon, *Biochem. Biophys. Res. Commun.* **1982**, *105*, 1426-1432.
- [10] N. Firon, I. Ofek, N. Sharon, *Carbohydr. Res.* **1983**, *120*, 235-249.
- [11] N. Firon, S. Ashkenazi, D. Mirelman, I. Ofek, N. Sharon, *Infect. Immun.* **1987**, *55*, 472-476.
- [12] R. J. Pieters, *Org. Biomol. Chem.* **2009**, *7*, 2013-2025.
- [13] A. Imberty, Y. M. Chabre, R. Roy, *Chem. Eur. J.* **2008**, *14*, 7490-7499.
- [14] M. Hartmann, T.K. Lindhorst, *Eur. J. Org. Chem.* **2011**, 3583-3609.
- [15] J. Bouckaert, J. Berglund, M. Schembri, E. D. Genst, L. Cools, M. Wuhrer, C. S. Hung, J. Pinkner, R. Slättergard, A. Zavialov, D. Choudhury, S. Langermann, S. J. Hultgren, L. Wyns, P. Klemm, S. Oscarson, S. D. Knight, H. D. Greve, *Mol. Microbiol.* **2005**, *55*, 441-455.
- [16] O. Sperling, A. Fuchs, T. K. Lindhorst, *Org. Biomol. Chem.* **2006**, *4*, 3913-3922.
- [17] Z. Han, J. S. Pinkner, B. Ford, R. Obermann, W. Nolan, S. A. Wildman, D. Hobbs, T. Ellenberger, C. K. Cusumano, S. J. Hultgren, J. W. Janetka, *J. Med. Chem.* **2010**, *53*, 4779-4792.
- [18] T. Klein, D. Abgottspon, M. Wittwer, S. Rabbani, J. Herold, X. Jiang, S. Kleeb, C. Lüthi, M. Scharenberg, J. Bezençon, E. Gubler, L. Pang, M. Smiesko, B. Cutting, O. Schwardt, B. Ernst, *J. Med. Chem.* **2010**, *53*, 8627-8641.
- [19] O. Schwardt, S. Rabbani, M. Hartmann, D. Abgottspon, M. Wittwer, S. Kleeb, A. Zalewski, M. Smiesko, B. Cutting, B. Ernst, *Bioorg. Med. Chem.* **2011**, *19*, 6454-6473.

- [20] X. Jiang, D. Abgottspon, S. Kleeb, S. Rabbani, M. Scharenberg, M. Wittwer, M. Haug, O. Schwardt, B. Ernst, *J. Med. Chem.* **2012**, *55*, 4700-4713.
- [21] L. Pang, S. Kleeb, K. Lemme, S. Rabbani, M. Scharenberg, A. Zalewski, F. Schädler, O. Schwardt, B. Ernst, *ChemMedChem.* **2012**, *7*, 1404-1422.
- [22] D. Choudhury, A. Thompson, V. Stojanoff, S. Langermann, J. Pinkner, S. J. Hultgren, S. D. Knight, *Science* **1999**, *285*, 1061-1066.
- [23] C.-S. Hung, J. Bouckaert, D. Hung, J. Pinkner, C. Widberg, A. DeFusco, C. G. Auguste, R. Strouse, S. Langermann, G. Waksman, S. J. Hultgren, *Mol. Microbiol.* **2002**, *44*, 903-915.
- [24] A. Wellens, C. Garofalo, H. Nguyen, N. Van Gerven, R. Slättergard, J.-P. Hernalsteens, L. Wyns, S. Oscarson, H. De Greve, S. Hultgren, J. Bouckaert, *PLoS One* **2008**, *3*, 4-13.
- [25] A. Wellens, M. Lahmann, M. Touaibia, J. Vaucher, S. Oscarson, R. Roy, H. Remaut, J. Bouckaert, *Biochemistry* **2012**, *51*, 4790-4799.
- [26] Z. Han, J. S. Pinkner, B. Ford, E. Chorell, J. M. Crowley, C. K. Cusumano, S. Campbell, J. P. Henderson, S. J. Hultgren, J. W. Janetka, *J. Med. Chem.* **2012**, *55*, 3945-3959.
- [27] S. Winiwarter, N. M. Bonham, F. Ax, A. Hallberg, H. Lennernäs, A. Karlén, *J. Med. Chem.* **1998**, *41*, 4939-4949.
- [28] M. J. Waring, *Expert Opin. Drug Discov.* **2010**, *5*, 235-248.
- [29] H. van de Waterbeemd, D. A. Smith, K. Beaumont, D. K. Walker, *J. Med. Chem.* **2001**, *44*, 1313-1333.
- [30] M. V. S. Varma, B. Feng, R. S. Obach, M. D. Troutman, J. Chupka, H. R. Miller, A. El-Kattan, *J. Med. Chem.* **2009**, *52*, 4844-4852.
- [31] K. Beaumont, R. Webster, I. Gardner, K. Dack, *Curr. Drug Metab.* **2003**, *4*, 461-485.
- [32] P. Ettmayer, G. L. Amidon, B. Clement, B. Testa, *J. Med. Chem.* **2004**, *47*, 2393-2404.
- [33] B. Neises, W. Steglich, *Angew. Chem. Int. Ed.* **1978**, *17*, 522-524.
- [34] N. Miyaura, A. Suzuki, *Chem. Rev.* **1995**, *95*, 2457-2483.
- [35] S. Caron, S. S. Massett, D. E. Bogle, M. J. Castaldi, T. F. Braish, *Org. Process Res. Dev.* **2001**, *5*, 254-256.
- [36] C. A. Lipinski, *J. Pharmacol. Toxicol. Methods* **2000**, *44*, 235-249.
- [37] J. C. Dearden, G. M. Bresnen, *QSAR Comb. Sci.* **1988**, *7*, 133-144.
- [38] M. Kansy, F. Senner, K. Gubernator, *J. Med. Chem.* **1998**, *41*, 1007-1010.
- [39] P. Artursson, J. Karlsson, *Biochem. Biophys. Res. Commun.* **1991**, *175*, 880-885.
- [40] M. Taketani, M. Shii, K. Ohura, S. Ninomiya, T. Imai, *Life Sci.* **2007**, *81*, 924-932.
- [41] B. Li, M. Sedlacek, I. Manoharan, R. Boopathy, E. G. Duysen, P. Masson, O. Lockridge, *Biochem. Pharmacol.* **2005**, *70*, 1673-1684.
- [42] M. Ishikawa, Y. Hashimoto, *J. Med. Chem.* **2011**, *54*, 1539-1554.
- [43] A. Avdeef, S. Bendels, L. Di, B. Faller, M. Kansy, K. Sugano, Y. Yamauchi, *J. Pharm. Sci.* **2007**, *96*, 2893-2909.
- [44] I. Hubatsch, E. G. E. Ragnarsson, P. Artursson, *Nat. Protoc.* **2007**, *2*, 2111-2119.
- [45] B. Testa, J. M. Mayer, *Hydrolysis in Drug and Prodrug Metabolism, Chemistry, Biochemistry, and Enzymology*, Helvetica Chimica Acta, Zurich, **2003**, pp. 425-434.
- [46] A. Seelig, G. Gerebtzoff, *Expert Opin. Drug. Metab. Toxicol.* **2006**, *2*, 733-752.
- [47] B. M. Liederer, R. T. Borchardt, *J. Pharm. Sci.* **2006**, *95*, 1177-1195.
- [48] J. M. Hatfield, M. Wierdl, R. M. Wadkins, P. M. Potter, *Expert Opin. Drug Metab. Toxicol.* **2008**, *4*, 1153-1165.
- [49] G. Vistoli, A. Pedretti, A. Mazzolari, B. Testa, *Bioorg. Med. Chem.* **2010**, *18*, 320-329.
- [50] Y. Naritomi, S. Terashita, S. Kimura, A. Suzuki, A. Kagayama, Y. Sugiyama, *Drug Metab. Dispos.* **2001**, *29*, 1316-1324.
- [51] C. Jewell, C. Ackermann, N. A. Payne, G. Fate, R. Voorman, F. M. Williams, *Drug Metab. Dispos.* **2007**, *35*, 2015-2022.
- [52] Y. Nicolet, O. Lockridge, P. Masson, J. C. Fontecilla-Camps, F. Nachon, *J. Biol. Chem.* **2003**, *278*, 41141-41147.
- [53] S. Darvesh, D. A. Hopkins, C. Geula, *Nat. Rev. Neurosci.* **2003**, *4*, 131-138.
- [54] K. Y. Sunew, R. G. Hicks, *Anesthesiology* **1978**, *49*, 188-191.

- [55] N. Fujiyama, M. Miura, S. Kato, T. Sone, M. Isobe, S. Satoh, *Drug Metab. Dispos.* **2010**, *38*, 2210-2217.
- [56] M. Murata, S. Watanabe, Y. Masuda, *J. Org. Chem.*, **1997**, *62*, 6458-6459.
- [57] B. Das, P. Thirupathi, *J. Mol. Catal. A. Chem.*, **2007**, *269*, 12-16.
- [58] a) VCCLAB, Virtual Computational Chemistry Laboratory, 2005, <http://www.vcclab.org> (accessed April 8, 2013); b) I. V. Tetko, J. Gasteiger, R. Todeschini, A. Mauri, D. Livingstone, P. Ertl, V. A. Palyulin, E. V. Radchenko, N. S. Zefirov, A. S. Makarenko, V. Y. Tanchuk, V. V. Prokopenko, *J. Comput. Aided Mol. Des.* **2005**, *19*, 453-463.
- [59] K. Ohura, T. Nozawa, K. Murakami, T. Imai, *J. Pharm. Sci.* **2011**, *100*, 3985-3994.

2.4 **Manuscript 3: FimH antagonists – solubility vs. oral availability**

This manuscript addresses the low aqueous solubility of the methyl ester prodrugs by two approaches: First, by disrupting the molecular planarity and symmetry with modified substitution pattern on the biphenyl moiety and, second, by increasing the polar surface area with heterocyclic biaryl aglycones. Solubility and *in vitro* permeability studies were performed to identify ester prodrugs with oral availability; and microsomal stability studies were done to estimate the propensity to enzyme-mediated bioactivation. Surprisingly, those esters containing a phenyl-*1H*-pyrrole aglycone show high microsomal stability and therefore do not act as prodrugs but are renally excreted unchanged.

Contribution to the project:

Simon Kleeb was responsible for the characterization of the physicochemical and *in vitro* pharmacokinetic properties of the diverse biaryl α -D-mannopyranosides. Moreover, he contributed to the writing of the manuscript except for the sections about synthesis and the *in vivo* pharmacokinetic study.

This manuscript is in preparation for *ChemMedChem*.

FimH Antagonists – Solubility vs. Oral Availability

Lijuan Pang,⁺ Simon Kleeb,⁺ Said Rabbani, Jacqueline Bezençon, Anja Sigl, Deniz Eris, Martin Smiesko, Oliver Schwardt, and Beat Ernst*

Institute of Molecular Pharmacy, Pharmacenter, University of Basel, Klingelbergstr. 50, 4056 Basel, Switzerland

⁺ These authors equally contributed to this work.

* Corresponding author, e-mail: beat.ernst@unibas.ch

Keywords: Aqueous solubility, ester prodrug, FimH antagonist, oral bioavailability

Abbreviations: Caco-2 cells, colorectal adenocarcinoma cells; CES, carboxylesterase; CRD, carbohydrate recognition domain; HPLC, high performance liquid chromatography; IC₅₀, half maximal inhibitory concentration; LC-MS, liquid chromatography mass spectrometry; MAD, maximum absorbable dose; PAMPA, parallel artificial membrane permeability assay; *P*, octanol-water partition coefficient; *P*_{app}, apparent permeability; *P*_e, effective permeability; RLM, rat liver microsomes; UPEC, uropathogenic *Escherichia coli*; UTI, urinary tract infection.

Abstract

Urinary tract infections (UTI) caused by uropathogenic *Escherichia coli* are frequent infectious diseases requiring antibiotic treatment. Since recurrent antibiotic exposure can induce antimicrobial resistance, efficient non-antibiotic prevention and treatment strategies are urgently needed. The first step of the pathogenesis of UTI is the bacterial adherence to the urothelial host cell, mediated by the mannose-binding adhesin FimH, which is located at the tip of bacterial pili. Biphenyl α -D-mannopyranosides with an electron-withdrawing carboxylate on the terminal aromatic ring of the aglycone were identified as potent FimH antagonists. In a preliminary study, oral availability of these charged FimH antagonists could be established by an ester prodrug approach, although for the price of a dramatically reduced solubility. In this article, the solubility problem of the ester prodrug is addressed by disrupting the molecular planarity and symmetry of the biphenyl aglycone by means of the substitution pattern and by introducing heteroatoms. With the parallel artificial membrane permeability assay (PAMPA) and the Caco-2 assay ester prodrugs with oral availability were identified. Surprisingly, those containing a phenyl-*1H*-pyrrole aglycone show high microsomal stability and therefore do not act as prodrugs but are renally excreted unchanged. Their potential for passive reabsorption leads to elevated urine concentration for up to 6 h. The best candidate, the nanomolar FimH antagonist **41f** therefore represents a promising candidate for oral application in UTI treatment.

Introduction

Urinary tract infections (UTIs) – also known as acute cystitis or bladder infections – are among the most prevalent infectious diseases worldwide. UTIs affect millions of people every year and account for significant morbidity and high medical costs.^[1] Complicated UTIs require antibiotic treatment. Since recurrent antibiotic exposure leads to the ubiquitous problem of antimicrobial resistance, efficient non-antibiotic prevention and treatment strategies are urgently needed.^[2] More than 70% of UTIs are caused by uropathogenic *Escherichia coli* (UPEC).^[1a,3] The first step of the infection cycle is the bacterial adherence to the urothelial cell surface, which prevents UPEC from being cleared by micturition but also triggers the invasion into the cells.^[4] This initial contact is mediated by the bacterial adhesin FimH which is located at the tip of type 1 pili.^[5] FimH consists of an N-terminal carbohydrate recognition domain (CRD) and a C-terminal pilin domain. The CRD specifically recognizes mannosylated uroplakin Ia glycoproteins located on the urinary

bladder mucosa, whereas the pilin domain regulates the switch between the low- and high-affinity states of the CRD.^[6] Blocking the FimH-CRD with carbohydrates or mimetics thereof prevents the bacterial adherence as well as the subsequent infection and therefore is regarded as a potential opportunity for prevention and/or treatment of UTIs.^[7]

Over the last three decades, various mannosides and oligomannosides have been tested as potential antagonists for type 1 pili-mediated bacterial adhesion.^[8] The crystal structure of FimH was first solved in 1999,^[9] and since then, numerous crystallographic studies have been published, greatly facilitating the rational design of high-affinity ligands.^[10] As deduced from these studies, the FimH-CRD consists of a deep, negatively charged pocket which accommodates the mannopyranose moiety by an extended hydrogen bond network. At the entrance to this cavity, the amino acids Tyr48, Tyr137, and Ile52 form a hydrophobic rim, the ‘tyrosine gate’, perfectly suited to host aliphatic and aromatic aglycones.^[10a] As a consequence of these hydrophobic contacts, *n*-heptyl α -D-mannopyranoside (**1**, Figure 1) exhibits nanomolar affinity.^[10b] With aromatic aglycones, such as present in the antagonists **2-5**, further improvements were achieved.^[11] The high affinity of α -D-mannopyranosides with biphenyl (\rightarrow **3** & **4**) and indolanyl phenyl (\rightarrow **5**) aglycones could be rationalized by optimal π - π stacking interactions between the biaryl aglycone and the tyrosine gate.^[11d,e,i] Depending on the aglycone, different binding modes have been observed. The alkyl aglycone of *n*-butyl α -D-mannopyranoside interacts with both Tyr48 and Tyr137 of the tyrosine gate.^[10b] By contrast, the biphenyl aglycone present in antagonist **3** was shown to adopt an ‘out-docking mode’,^[11d] that means, it interacts only with Tyr48, probably due to limited flexibility of the biphenyl moiety. Moreover, *ortho*-substituents on ring A of the biphenyl aglycone, such as the *ortho*-chloro substituent in compound **4b**, proved beneficial to binding because of high shape complementarity within the binding pocket and therefore better van der Waals contacts.^[11j]

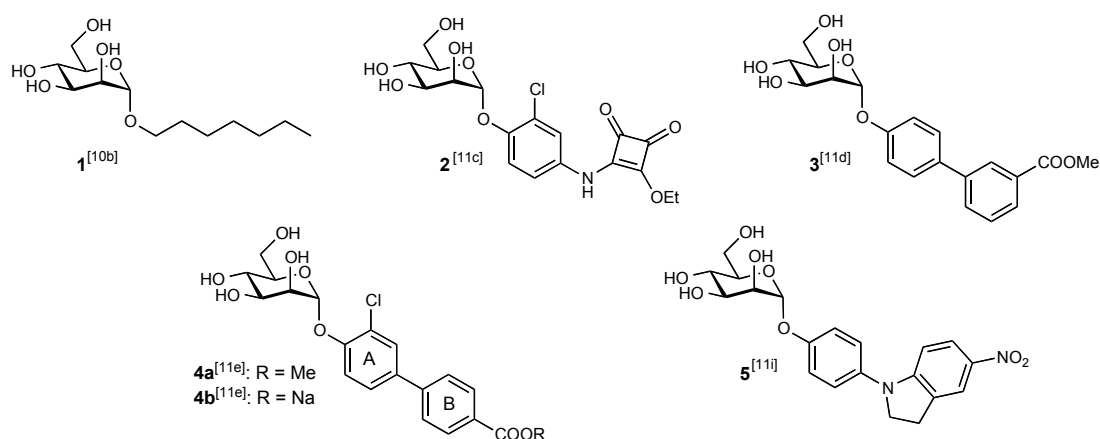


Figure 1. FimH antagonists: *n*-heptyl α -D-mannopyranoside (**1**) is used as reference compound; the squaric acid derivative **2**, the biphenyl derivatives **3-4**, and the indolinylphenyl derivative **5** exhibit nanomolar affinities.

For numerous diseases as *e.g.* UTI, oral administration of therapeutics is the standard care, because daily therapy is required. As described in our previous publication,^[11e] the carboxylic acid moiety in biphenyl α -D-mannoside **4b** – its electron-withdrawing potential is essential for an enhanced π - π stacking interaction – impairs the membrane permeability and, as a consequence, the potential for oral absorption. Otherwise, ester prodrug **4a** was shown to have markedly increased membrane permeability and to provide – upon absorption and enzyme-mediated hydrolysis – antagonist **4b**, which is perfectly suited for rapid renal excretion. Nonetheless, low aqueous solubility (12 $\mu\text{g/mL}$) was identified as a major drawback of prodrug **4a**, limiting the absorptive flux of the prodrug through the intestinal mucosa. According to the maximum absorbable dose (MAD) concept,^[12] aqueous solubility of at least 50 $\mu\text{g/mL}$ is required to achieve quantitative absorption of a 1 mg/kg dose of prodrug with medium permeability.

Results and Discussion

In the present study, the solubility issue of the ester prodrugs was addressed by two approaches: First, by disrupting the molecular planarity and symmetry with modified substitution pattern on the biphenyl moiety (Figure 2a) and second by increasing the polar surface area (PSA) with heterocyclic biaryl aglycones (Figure 2b).^[13] For improving oral availability, the carboxylic acid was replaced by the bioisosteric cyano group (Figure 2c).^[14]

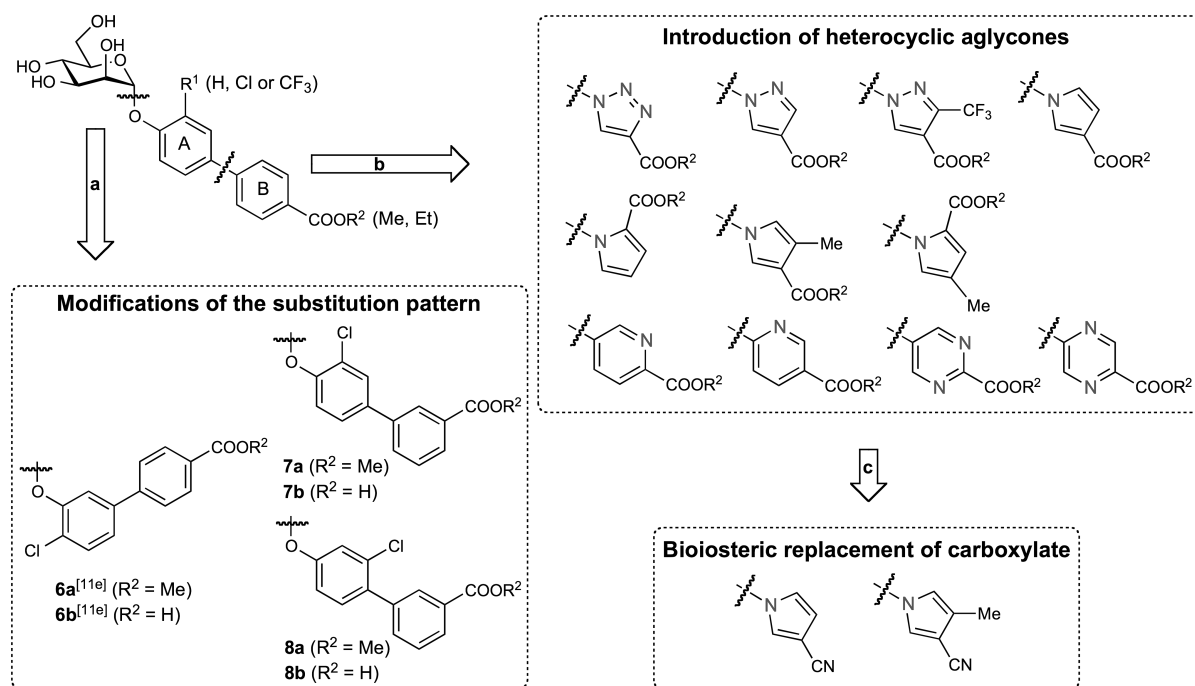


Figure 2. Modifications of the aglycone of FimH antagonists by (a) modifying the substitution pattern, (b) introducing heteroaryl aglycones and (c) replacing the carboxylate moiety with a bioisosteric cyano group.

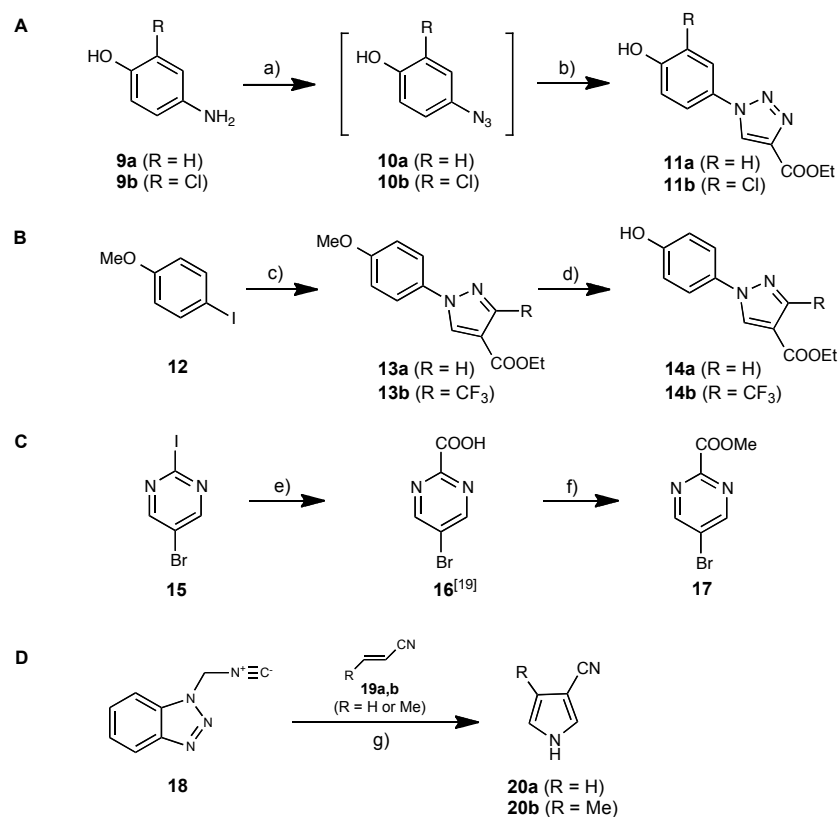
To evaluate the impact of these modifications on PK/PD properties, binding affinity to the FimH-CRD as well as the *in vitro/in vivo* pharmacokinetic properties predictive for oral bioavailability and metabolic stability were studied.

Synthesis

Biphenyl mannosides. Compounds **6a,b**, **7a,b** and **8a,b** (Figure 2a) were synthesized according to a previously described procedure (for synthesis and compound characterization see Supporting Information).^[11e]

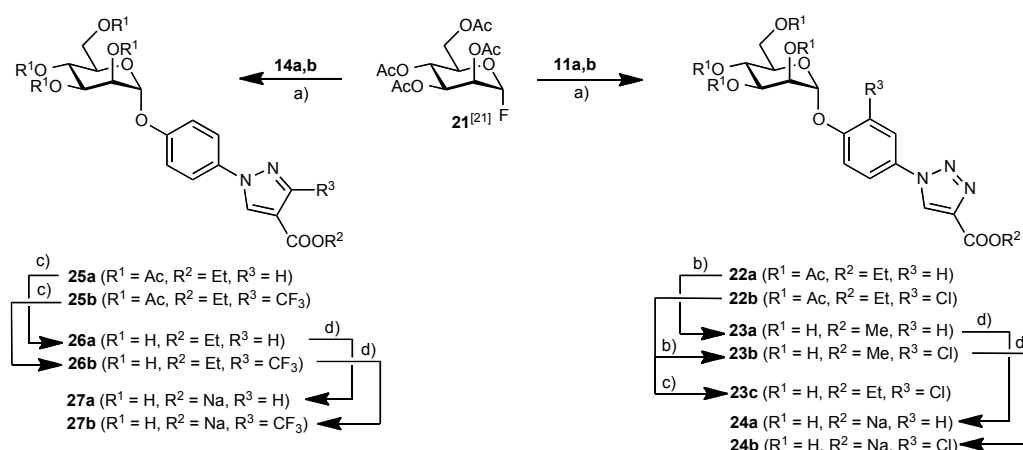
Synthesis of heteroaromatic building blocks (Scheme 1). Starting with the commercial aminophenols **9a,b**, the azidophenols **10a,b** were obtained via a diazotransfer reaction using freshly prepared triflyl azide in pyridine and copper (II) sulfate as catalyst.^[15] Because of instability, **10a,b** were used without purification in a subsequent copper (I)-catalyzed Huisgen cycloaddition^[16] with ethyl propiolate, yielding the triazolylphenols **11a,b** with high 1,4-regioselectivity (Scheme 1A). By using an Ullmann-type copper-diamine-catalyzed *N*-arylation,^[17] *1H*-pyrazole-4-carboxylate was coupled with 4-iodoanisole (**12**) in *N*-methyl-2-pyrrolidone (NMP) to furnish **13a**. Because of the low reactivity of the trifluoromethyl-substituted pyrazole, the coupling reaction was carried out under solvent-free condition to give **13b** in quantitative yield. Demethylation of **13a,b** with AlCl_3 gave the pyrazolyphenol

derivatives **14a,b**. Due to the instability of **14b** under $\text{AlCl}_3/n\text{Bu}_4\text{NI}$ conditions, a AlCl_3 /thiol combination was used to accelerate the reaction and to suppress byproduct formation (Scheme 1B).^[18] The pyrimidinyl derivative **17** was prepared via a $n\text{BuLi}$ -mediated carboxylation with CO_2 followed by esterification (Scheme 1C).^[19] To synthesize the cyano-substituted pyrroles **20a,b**, benzotriazol-1-ylmethyl isocyanide (BetMIC, **18**) was treated with the electron-deficient alkenes **19a,b** under basic heterocyclization conditions (Scheme 1D).^[20]



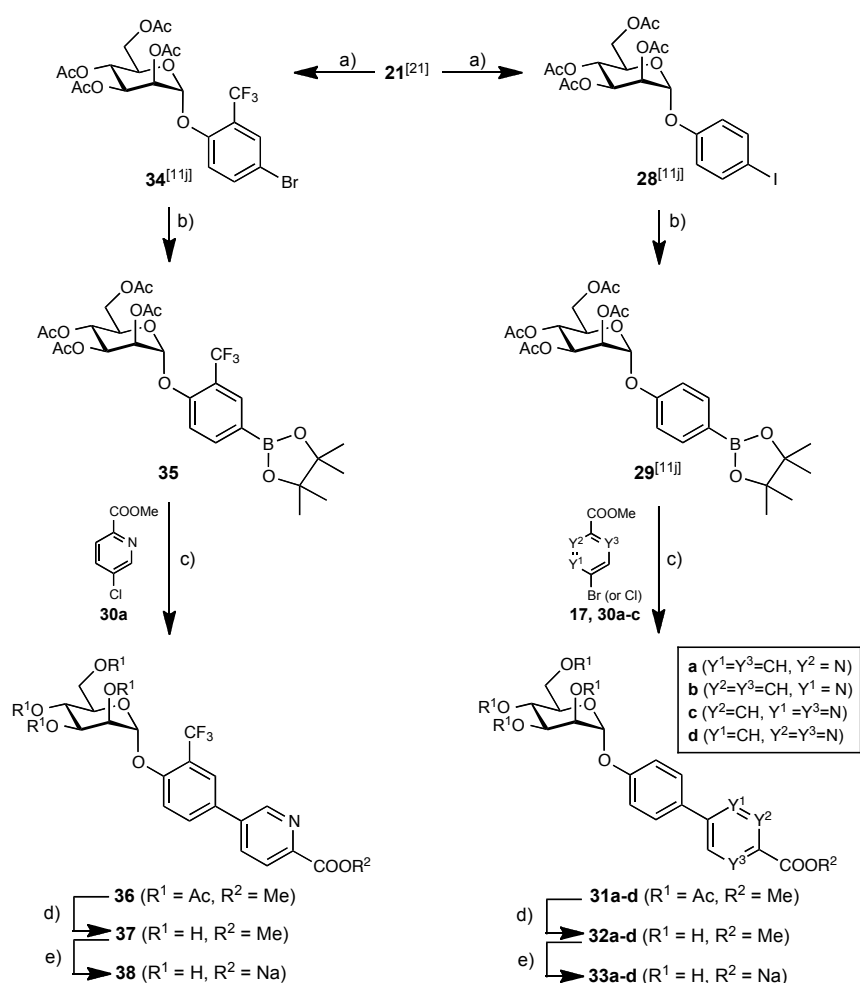
Scheme 1. a) TfN_3 , CuSO_4 , triethylamine, pyridine, 0 °C to rt, 2 h; b) ethyl propiolate, $\text{CuSO}_4 \cdot 5\text{H}_2\text{O}$, sodium ascorbate, $t\text{BuOH}/\text{H}_2\text{O}$ (1:1), rt, 30 min (yield for two steps: 77% for **11a**, 48% for **11b**); c) ethyl *1H*-pyrazole-4-carboxylate or ethyl 3-trifluoromethyl-*1H*-pyrazole-4-carboxylate, CuI , trans-*N,N'*-dimethyl-1,2-cyclohexanediamine, K_2CO_3 , NMP as solvent for **13a** and solvent free for **13b**, 110 °C, 24 h (80% for **13a**, quant. for **13b**); d) AlCl_3 , cat. $n\text{Bu}_4\text{NI}$, DCE (for **14a**), or 1-dodecanethiol without catalyst (for **14b**), 0 °C to rt (60% for **14a**, 26% for **14b**); e) i. $n\text{BuLi}$, hexane, toluene, -78 °C, 1 h; ii. CO_2 (g), -78 °C to rt, 7 h; f) conc. H_2SO_4 (0.8 eq), MeOH, reflux, overnight (37% for two steps); g) nitrile **19a,b**, $t\text{BuOK}$, THF, 0 °C to reflux, 2 h (60% for **20a**, 54% for **20b**).

Triazolylphenyl and pyrazolylphenyl mannosides (Schemes 2). Mannosylation of the phenols **11a,b** and **14a,b** (see Scheme 1A & B) with mannosyl fluoride **21**^[21] and BF₃·Et₂O as promoter, yielded exclusively the α-mannosides **22a,b** and **25a,b**. Deacetylation (→ **23a-c** and **26a,b**) followed by ester hydrolysis gave the test compounds **24a,b** and **27a,b**.



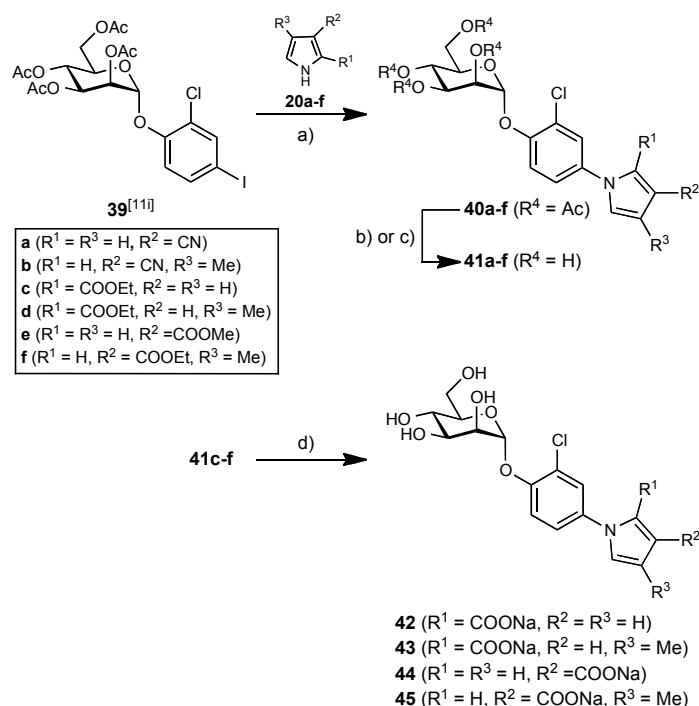
Scheme 2. a) BF₃·Et₂O, DCM, mol. sieves 4 Å, 0 °C to rt, overnight (79% for **22a**, 76% for **22b**, 98% for **25a**, 64% for **25b**); b) NaOMe, MeOH, rt, 4 h (74% for **23a**, 80% for **23b**); c) NaOEt, EtOH, rt, overnight (74% for **23c**, 95% for **26a**, 82% for **26b**); d) 0.2 N aq. NaOH, MeOH, rt, overnight (30% for **24a**, 90% for **24b**, 70% for **27a**, 79% for **27b**).

Pyridinylphenyl, pyrazinylphenyl, and pyrimidinylphenyl mannosides (Scheme 3). Mannosyl fluoride **21** was treated with 4-iodophenol or 4-bromo-2-trifluoromethylphenol in the presence of BF₃·Et₂O. The resulting iodide **28**^[11j] and bromide **34**^[11j] were transformed into the boronic acid pinacol esters **29**^[11j] and **35** under Miyaura-borylation conditions. In a palladium-catalyzed Miyaura-Suzuki coupling^[22] of the heteroaryl halides **17** (see Scheme 1C) and **30a-c** (commercially available) with boronic acid ester **29**, heteroarylphenyl mannosides **31a-d** were obtained in good to excellent yields. Similarly, mannoside **36** was prepared by coupling of ester **35** and pyridinylchloride **30a**. Deacetylation under Zemplén conditions (→ **32a-d**, **37**) followed by saponification of the methyl ester yielded the sodium salts **33a-d** and **38**.

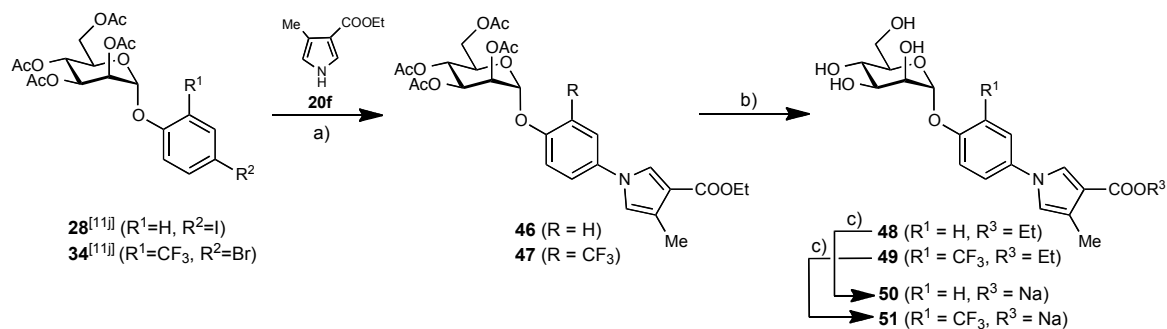


Scheme 3. a) 4-iodophenol or 4-bromo-2-trifluoromethylphenol, $\text{BF}_3 \cdot \text{Et}_2\text{O}$, DCM, mol. sieves 4 Å, 0 °C to rt, overnight (70% for **28**, 80% for **34**); b) bis(pinacolato)diborone, $\text{Pd}(\text{Cl}_2)\text{dppf} \cdot \text{CH}_2\text{Cl}_2$, KOAc, DMF, 85 °C, overnight (80% for **29**, 83% for **35**); c) $\text{Pd}(\text{Cl}_2)\text{dppf} \cdot \text{CH}_2\text{Cl}_2$, K_3PO_4 , DMF, 85 °C, overnight (60% for **31a**, 80% for **31b**, 68% for **31c**, 40% for **31d**, 57% for **36**); d) NaOMe, MeOH, rt, 4 h (36% for **32a**, 24% for **32b**, 36% for **32c**, 89% for **32d**, 60% for **37**); e) 0.2 N aq. NaOH, MeOH, rt, overnight (32% for **33a**, 48% for **33b**, 44% for **33c**, 60% for **33d**, 90% for **38**).

Pyrrolyphenyl mannosides (Schemes 4 & 5). In a copper catalyzed *N*-arylation, pyrroles **20a,b** (see Scheme 1D) and **20c-f** (commercial) were coupled with mannoside **39**^[11i] (*ortho*-Cl) to yield the pyrrolyphenyl mannosides **40a-f** (Scheme 4).^[18] Under similar conditions, mannosides **28** (without *ortho*-substituent) and **34** (*ortho*- CF_3) were coupled with pyrrole **20f** to yield **46** and **47** (Scheme 5). Because of partial deacetylation of the sugar moiety during *N*-arylation, the crude products were reacylated to facilitate purification. Deacetylation of the mannose moiety (\rightarrow **41a-f**, **48** and **49**) followed by saponification of the alkyl esters gave the test compounds **42-45**, **50** and **51**.



Scheme 4. a) i. CuI, (\pm)-*trans*-1,2-diaminocyclohexane, K₃PO₄, 1,4-dioxane, 110 °C, overnight; ii. Ac₂O, DMAP, pyridine, rt, overnight (44% for **40a**, 92% for **40b**, 33% for **40c**, 64% for **40d**, 99% for **40e**, 77% for **40f**); b) NaOMe, MeOH, rt, 4 h (65% for **41a**, 38% for **41b**, 83% for **41e**); c) NaOEt, EtOH, rt, overnight (91% for **41c**, 61% for **41d**, 93% for **41f**); d) NaOH, MeOH/H₂O (1:2), rt, 12-48 h (58% for **42**, 40% for **43**, 20% for **44**, 57% for **45**).



Scheme 5. a) i. CuI, (\pm)-*trans*-1,2-diaminocyclohexane, K₃PO₄, 1,4-dioxane, 110 °C, overnight; ii. Ac₂O, DMAP, pyridine, rt, overnight (94% for **46**, 49% for **47**); b) NaOEt, EtOH, rt, overnight (46% for **48**, 85% for **49**); c) NaOH, MeOH/H₂O (1:2), rt, 48 h (99% for **50**, 35% for **51**).

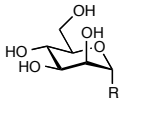
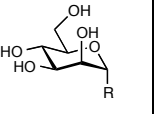
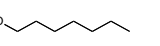
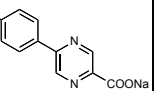
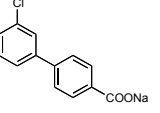
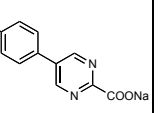
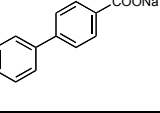
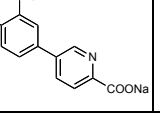
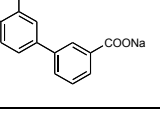
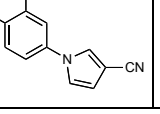
In vitro binding affinities

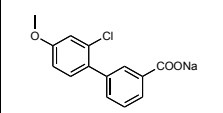
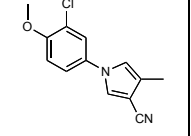
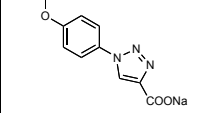
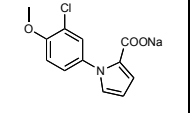
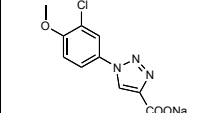
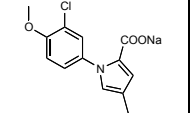
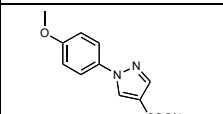
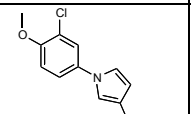
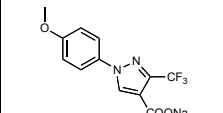
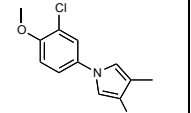
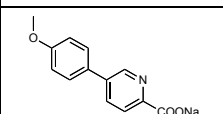
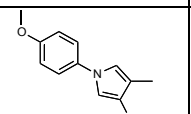
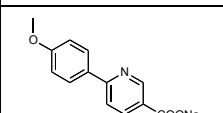
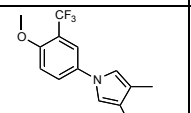
The hydrolyzed prodrugs, *i.e.* the free carboxylates (**6-8b**, **24a-b**, **27a-b**, **33a-d**, **38**, **42-45**, **50** and **51**) as well as the bioisosteric cyanides (**41a-b**), were evaluated in a cell-free competitive binding assay (Table 1).^[23]

Cell-free competitive binding assay.^[23] The cell-free competitive binding assay is based on the competitive interaction of the compound of interest and the biotinylated polyacrylamide glycopolymer TM-PAA (Man α 1-3(Man α 1-6)Man β 1-4GlcNAc β 1-4GlcNAc β -PAA) with the isolated CRD of FimH. Complexation of the biotinylated glycopolymer with streptavidin coupled to horseradish peroxidase allows for quantification of the binding affinity of the antagonists. For every compound the assay was performed twice with each concentration in duplicate. To ensure comparability between various antagonists, the reference compound *n*-heptyl α -D-mannopyranoside (**1**) was tested each time in parallel. The affinities are reported relative to **1** as rIC₅₀ in Table 1.

A comparison of the biphenyl mannoside antagonist **4b** (entry 2) with the regioisomers **6b**, **7b**, and **8b** (entries 3-5) indicates that changing the position of the carboxylic acid on the terminal ring B of the biphenyl aglycone as well as modifying the substitution pattern on ring A substantially reduced affinity. As previously reported, the *ortho*-chloro substituent present in the antagonists **4b** and **7b** provides additional van der Waals contacts leading to binding affinity in the low nanomolar range.^[11j]

Table 1. Pharmacodynamic parameters of FimH antagonists. The IC₅₀ values were determined with a cell-free competitive binding assay.^[23] The rIC₅₀ values were calculated by dividing the IC₅₀ of the compound of interest by the IC₅₀ of reference compound **1**. This leads to rIC₅₀ values below 1.0 for derivatives with higher affinity than reference **1** and rIC₅₀ above 1.0 for compounds with lower affinity than **1**.

Entry	Cpd		IC ₅₀ [nM]	rIC ₅₀	Entry	Cpd		IC ₅₀ [nM]	rIC ₅₀
		R					R		
1	1 ^[10b]		54.9	1	12	33c		39	0.73
2	4b ^[11e]		6.7	0.09	13	33d		35	0.60
3	6b ^[11e]		29	0.40	14	38		20	0.39
4	7b		12	0.19	15	41a		29	0.50

5	8b		53	0.97	16	41b		25	0.43
6	24a		16	0.30	17	42		75	1.37
7	24b		21	0.35	18	43		23	0.41
8	27a		111	2.02	19	44		25	0.45
9	27b		112	2.02	20	45		25	0.44
10	33a		16	0.30	21	50		65	1.18
11	33b		46	0.71	22	51		19	0.33

All heteroaryl mannosides (entries 6-22) showed IC_{50} values in the nanomolar range as well. Nonetheless, they were weaker binders than the optimized biphenyl mannoside **4b**, although *in silico* studies obtained with flexible docking (Glide software package^[24]) to the FimH-CRD suggested a similar ‘out-docking mode’ (Figure 3).

In comparison with the triazolylphenyl mannosides **24a,b** (entries 6 & 7) and the pyrrolylphenyl mannosides **41a,b**, **42-45**, **50** and **51** (entries 15-22), the pyrazolylphenyl analogues **27a,b** (entries 8 & 9) showed markedly lower affinity, even though we expected a similar conformation for all biaryl mannosides containing a five-membered aromatic heterocycle. Furthermore, a high impact of the substitution pattern on the binding affinity was observed for the various pyrrolylphenyl mannosides (entries 15-22). In agreement with previous observations,^[11g,j] the *ortho*-chloro and the *ortho*-trifluoromethyl substituents on ring A were beneficial to affinity (**50** vs. **45** & **51**, entries 20-22). The position of the electron-withdrawing carboxylic acid moiety in the heteroaromatic ring furthermore affected the binding affinity. In the 3-position (\rightarrow **44**, entry 19) it conferred three times higher affinity

than in the 2-position (\rightarrow **42**, entry 17). *In silico* docking studies indeed suggest that the 2-carboxylate forces the two rings of the aglycone in an orthogonal orientation and therefore disrupts the π - π stacking interactions between the heteroaromatic ring and Tyr48 of the tyrosine gate (\rightarrow **45**, Figure 3B). Otherwise, the additional 4-methyl substituent present in **43** (entry 18) could presumably provide an additional hydrophobic contact (Figure 3A).

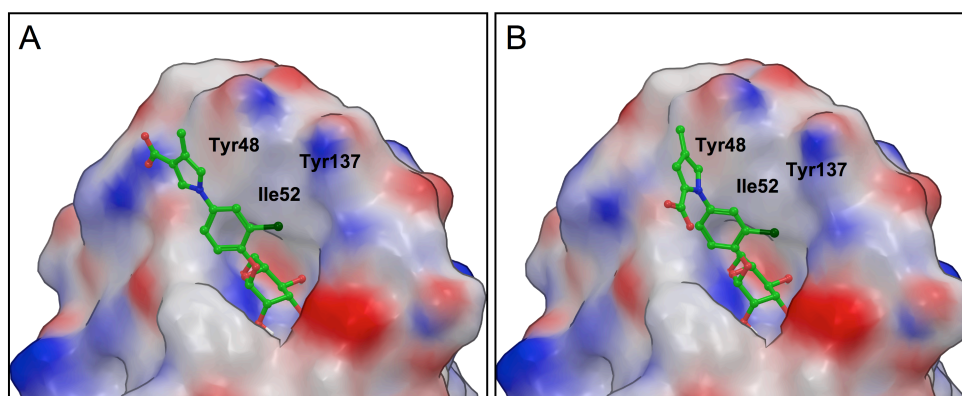
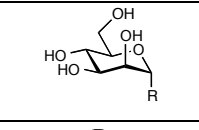
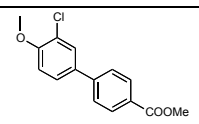
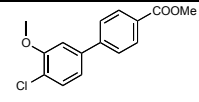


Figure 3. *In silico* docking studies obtained with flexible docking (Glide software package^[24]) to the FimH-CRD (PDB ID: 3MCY); top-scored binding modes of A) **43** (Table 1, entry 18) and B) **45** (entry 20).

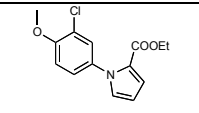
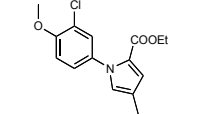
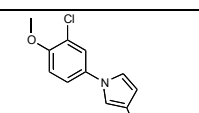
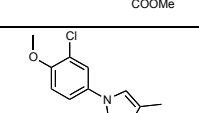
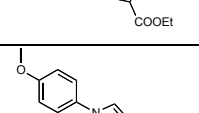
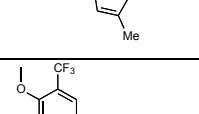
Physicochemical properties and *in vitro* pharmacokinetics

For assessing the potential for intestinal absorption, lipophilicity ($\log P$), aqueous solubility, and permeability through an artificial membrane (PAMPA, $\log P_e$) as well as a Caco-2 cell monolayer (P_{app}) were determined (Table 2).^[25-29] Furthermore, the esters were incubated with rat liver microsomes (RLM) for estimating their susceptibility to carboxylesterase (CES)-mediated hydrolysis.^[30] Mammalian CESs are localized in the endoplasmatic reticulum of the liver and most other organs. Table 2 indicates the metabolic half lives ($t_{1/2}$) as determinants of the rate of bioconversion to the respective acid.

Table 2. Physicochemical and pharmacokinetic parameters of FimH antagonists.

Entry	Cpd		$\log P^a$	Solubility [$\mu\text{g/mL}$] ^b	PAMPA $\log P_e$ [cm/s] ^c	Caco-2 P_{app} [10^{-6} cm/s] ^d		Microsomal stability $t_{1/2}$ [min] ^e
						a \rightarrow b	b \rightarrow a	
1	4a ^[11e]		2.3	11.9	-4.6	5.3 ± 0.6	17.5 ± 1.3	2.1
2	6a ^[11e]		1.7 ± 0.1	14 ± 0	-4.7	6.1 ± 1.2	21.1 ± 1.2	22

3	7a		2.7 ± 0.1	41 ± 3	-4.6 ± 0.2	6.7 ± 0.4	20.7 ± 2.5	84
4	8a		2.7 ± 0.1	134 ± 6	-4.5 ± 0.1	4.5 ± 0.3	10.8 ± 0.7	13
5	23a		-0.6 ± 0.0	> 180	-9.4 ± 0.3	n.d.	n.d.	38
6	23b		0.0 ± 0.0	> 150	-9.1 ± 1.8	n.d.	n.d.	32
7	23c		0.7 ± 0.0	> 150	-10	n.d.	n.d.	42
8	26a		0.9 ± 0.0	> 180	-6.6 ± 0.1	n.d.	n.d.	> 120
9	26b		2.1 ± 0.0	> 180	-5.7 ± 0.1	1.3 ± 0.1	12.4 ± 2.4	113
10	32a		0.2 ± 0.0	> 130	-7.5 ± 0.2	0.22 ± 0.05	2.3 ± 0.1	10
11	32b		1.0 ± 0.0	59 ± 6	-6.3 ± 0.0	0.64 ± 0.06	8.3 ± 0.4	11
12	32c		0.1 ± 0.1	> 150	-7.6 ± 0.0	0.24 ± 0.01	1.8 ± 0.2	11
13	32d		< -1.0	95 ± 6	-8.5 ± 0.1	0.16 ± 0.03	0.22 ± 0.05	24
14	37		1.3 ± 0.1	> 180	-8.6 ± 1.7	0.33 ± 0.04	7.2 ± 0.7	8.2
15	41a		1.5 ± 0.1	> 350	-8.8 ± 2.0	n.d.	n.d.	n.d.
16	41b		2.0 ± 0.1	69 ± 20	-6.3 ± 0.1	n.d.	n.d.	n.d.

17	41c		2.0 ± 0.0	> 180	-5.2 ± 0.0	n.d.	n.d.	> 120
18	41d		2.7 ± 0.0	34 ± 4	-4.8 ± 0.1	5.0 ± 0.2	35.6 ± 1.0	84
19	41e		2.1 ± 0.2	> 180	-6.0 ± 0.1	n.d.	n.d.	> 120
20	41f		2.8 ± 0.1	> 180	-4.8 ± 0.1	6.4 ± 0.7	30.0 ± 2.9	> 120
21	48		2.3 ± 0.0	> 180	-5.1 ± 0.1	1.5 ± 0.5	17.2 ± 0.6	> 120
22	49		3.0 ± 0.1	135 ± 6	-5.0 ± 0.2	5.0 ± 0.3	26.1 ± 1.5	> 120

[a] Octanol-water partition coefficients ($\log P$) were determined by a miniaturized shake flask procedure. The values are indicated as mean \pm SD of sextuplicate determinations.^[25] [b] Kinetic solubility was measured in a 96-well format in triplicate using the μ SOL Explorer solubility analyzer.^[26] [c] Permeation through an artificial membrane ($\log P_e$, effective permeability) was determined by PAMPA (parallel artificial membrane permeability assay) in quadruplicate.^[27] [d] Permeation through a Caco-2 cell monolayer (P_{app} , apparent permeability) was assessed in the absorptive (a \rightarrow b) and secretory (b \rightarrow a) directions in triplicate.^[28] [e] Microsomal stability was determined with pooled male rat liver microsomes (0.125 mg/mL) at pH 7.4 and 37 °C.^[29] n.d., not determined.

Biphenyl mannosides: Solubility, permeability, and metabolic stability. As observed in our previous study,^[11e] the biphenyl derivatives **4a** and **6a** (Table 2, entries 1 & 2) showed low aqueous solubility probably due to the symmetrical *para-para* substitution pattern. In order to disrupt this symmetry, the carboxylic acid moiety in **4a** was moved from the *para*- to the *meta*-position (\rightarrow **7a**, Table 2, entry 3), leading however only to moderately improved aqueous solubility. Moving the chloro substituent on ring A from the *ortho*- to the *meta*-position (\rightarrow **8a**, Table 2, entry 4) increased the dihedral angle (60.3° for **8a** vs. 39.6° for **7a**, Figure 4A; values calculated with MacroModel, version 9.9^[31]), resulting in the disruption of the molecular planarity and markedly enhanced aqueous solubility. Given the elevated solubility (134 μ g/mL) and the high effective permeability ($\log P_e$ -4.5), the prodrug **8a** was identified as the most promising biphenyl derivative for oral administration.

Incubation with rat liver microsomes induced a fast degradation of prodrug **4a** ($t_{1/2}$ 2.1 min, Table 2, entry 1). The esters of the biphenyl mannosides **6a** ($t_{1/2}$ 22 min, entry 2), **7a** ($t_{1/2}$ 84 min, entry 3), and **8a** ($t_{1/2}$ 13 min, entry 4) were less susceptible to the carboxylesterase (CES)-mediated metabolic turnover. The differing rates of hydrolysis may result from various reasons, *i.e.* the change in the molecular geometry and therefore in the accessibility of the ester by the serine hydrolase CES^[30] or differing electron-density on the carbonyl carbon. Since the first step of the catalytic mechanism relies on the nucleophilic attack by the hydroxyl group of the serine moiety,^[32] increasing electron-deficiency of the carbonyl carbon should lead to a higher propensity for hydrolysis. However, the calculated partial charges (δ) on the carbonyl carbons (AMSOL, Version 7.1^[33], data not shown) do not correlate with the propensities of the corresponding esters to hydrolysis. We therefore attributed the rate differences of the CES-mediated hydrolysis primarily to the differing geometry of the aglycones, which, in case of **4a**, orients the ester bond within the active site in an optimal position.

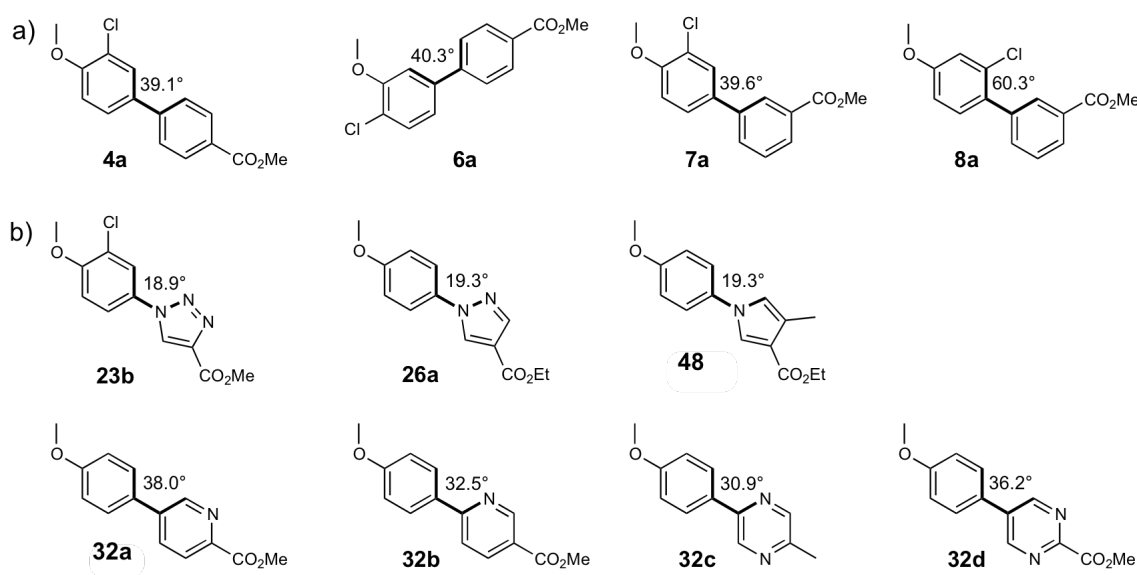


Figure 4. Dihedral angles between the aromatic rings of prominent biaryl α -D-mannopyranosides, A) biphenyl aglycones and B) heteroaryl aglycones. The values were calculated with MacroModel (version 9.9).^[31]

Heteroaryl mannosides: Solubility, permeability, and metabolic stability. In general, heterobiaryl mannosides (Table 2, entries 5-22) exhibited markedly higher aqueous solubility than biphenyl α -D-mannoside **4a**. When the nitrogen atom in ring B is moved from the *ortho*- (\rightarrow **32b**, entry 11) to the *meta*-position (\rightarrow **32a**, entry 10), the increase in steric hindrance (lone pair of N vs. C-H) leads to a larger internal dihedral angle (32.5° for **32b** vs. 38.0° for **32a**, Figure 4B), causing a disruption of the molecular planarity and hence to improved

solubility. A similar effect was observed for the antagonists **32d** (36.2°, entry 13) and **32c** (30.9°, entry 12). The five-membered heteroaryl mannosides in general excel in high solubility, either because of the increased polarity [\rightarrow triazoles **23a-c** (entries 5-7) and pyrazoles **26a,b** (entries 8 & 9)] or because of the disruption of molecular symmetry (\rightarrow pyrroles **41a-f**, **48**, **49**, entries 15-22).

As expected, the increase in polarity and solubility (\rightarrow **23a**, $\log P$ -0.6, entry 5) induces reduced permeability ($\log P_e$ -9.4), *i.e.* poor oral absorption.^[34] To enhance lipophilicity two strategies were followed: First, an *ortho*-chloro substituent was added to ring A of the biaryl aglycone (\rightarrow **23b**, entry 6) and, second, the methyl ester was replaced by an ethyl ester (\rightarrow **23c**, entry 7). However, both strategies were insufficient to substantially improve the oral absorption potential. For the pyrazolyphenyl derivative **26a** (entry 8), although slightly more lipophilic than the triazolyphenyl **23c** (entry 7), only low effective permeability ($\log P_e$ -6.6) was observed. Introduction of a trifluoromethyl substituent on the pyrazole moiety (\rightarrow **26b**, entry 9) further increased both lipophilicity and permeability but was still not sufficient for successful intestinal uptake.

By contrast, the pyrrolylphenyl mannosides **41a-f**, **48** and **49** (Table 2, entries 15-22) are among the most lipophilic and permeable biaryl derivatives. Starting from antagonist **41e** (entry 19), both parameters could be successively enhanced by introducing a methyl substituent in the 4-position of the pyrrole moiety (\rightarrow **48**, entry 21) and by modifying the *ortho*-substituent on ring A of the biaryl aglycone (\rightarrow **41f** and **49**, entries 20 & 22). For antagonists **41f** and **49**, effective permeability resulting from PAMPA ($\log P_e$ -4.8 and -5.0, respectively) suggested a high oral absorption potential. Moreover, the absorptive flux (apical \rightarrow basal) through the Caco-2 cell monolayer was outstandingly high. Although the ratio $P_{app,b-a}/P_{app,a-b}$ implied efflux-carrier activity, we expected high systemic availability of **41f** and **49** *in vivo*, notably because efflux transporters at human intestines are considered easily saturable when compounds are administered at elevated doses (*e.g.* > 100 mg).^[35] In the case of the pyrrolylphenyl derivatives **41c** and **41d** (entries 17 & 18), introducing a 4-methyl substituent increased permeability as well. In turn, it made **41d** the least soluble compound among all assessed heteroaryl mannosides. The bioisosteric replacement of the carboxylic moiety by a cyano group (\rightarrow **41a-b**, entries 15 & 16) resulted in PAMPA data indicating low permeability for both derivatives ($\log P_e$ -8.8 and -6.3, respectively).

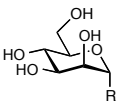
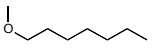
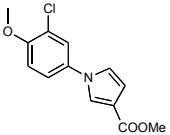
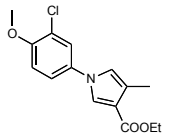
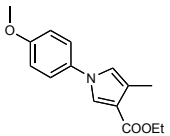
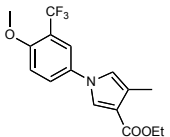
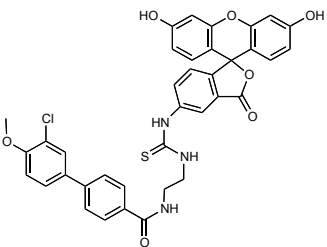
All heteroaryl derivatives with ester functions (Table 2, entries 5-14 and 17-22) were found to be less susceptible to CES-mediated bioconversion than the initial biphenyl mannoside **4a**. Nonetheless, the experimental half-lives suggest a strong relationship between the molecular structure of the heteroaryl moiety and the propensity to hydrolysis. All biphenyl and heterobiphenyl derivatives exhibit considerable propensity to enzyme-mediated hydrolysis. By contrast, the pyrrolylphenyl esters **41e,f**, **48**, and **49**, which were originally designed as prodrugs, surprisingly proved to be metabolically stable and not hydrolyzable by the carboxylesterases.

Binding affinity of selected esters

Since their lipophilicity ($\log P$), solubility, membrane permeation ($\log P_e$ and P_{app}) fulfill the requirements for an oral uptake, the binding affinities of these antagonists were determined in the cell-free competitive assay (see above) as well as in a competitive fluorescence polarization assay (Table 3). In both assays, *n*-heptyl mannoside (**1**) was used as a reference compound.

Competitive Fluorescence Polarization Assay.^[11k] For the rapid evaluation of binding affinity, a previously developed competitive binding assay based on fluorescence polarization (FP) was applied. A FimH variant consisting of the CRD linked to a His-tag by a thrombin cleaving site (FimH-CRD-Th-His₆, expressed and purified as previously described)^[23] was used. The antagonist of interest displaces the fluorescent-labeled competitor **52**^[11k] from the binding site, thereby reducing fluorescence polarization.^[36] Due to the long residence time of FimH antagonists ($t_{1/2} > 3.5$ h),^[37] a 24 h incubation time was applied before measurement of fluorescence polarization. IC₅₀ values were obtained by nonlinear least-squares regression (standard four-parameter IC₅₀ equation) and converted to K_D using a modified Cheng-Prusoff equation.^[36] The K_D values observed for the test compounds **41e,f**, **48** and **49** are summarized in Table 3. In general, the pyrrolylphenyl mannosides (entries 2-5) showed higher affinity than the reference compound **1**. The improved affinity for the *ortho*-substituted biaryls (Cl, **41f** and CF₃, **49**) was confirmed.

Table 3. Affinity of FimH antagonists to FimH-CRD-Th-His₆.^a The IC₅₀ values were determined with a cell-free competitive binding assay.^[23] The rIC₅₀ values were calculated by dividing the IC₅₀ of the compound of interest by the IC₅₀ of reference compound **1**. Dissociation constants (K_D) were determined in a competitive fluorescence polarization assay.^[11k,36] n.d., not determined.

Entry	Cpd		Binding Assay		FP-Assay K_D [nM]
			IC ₅₀ [nM]	rIC ₅₀	
1	1		54.9	1.0	28.3
2	41e		18.5	0.33	4.3
3	41f		25.2	0.46	7.5
4	48		24.9	0.45	24.6
5	49		36.9	0.72	6.0
6	52 ^[11k]		n.d.	n.d.	1.7

In vivo pharmacokinetic study. Antagonist **41f** exhibiting the best *in vitro* PK/PD profile was selected for an *in vivo* pharmacokinetic study. It was orally applied to three mice at a dose of 10 mg/kg. The concentration-time profiles are shown in Figure 5.

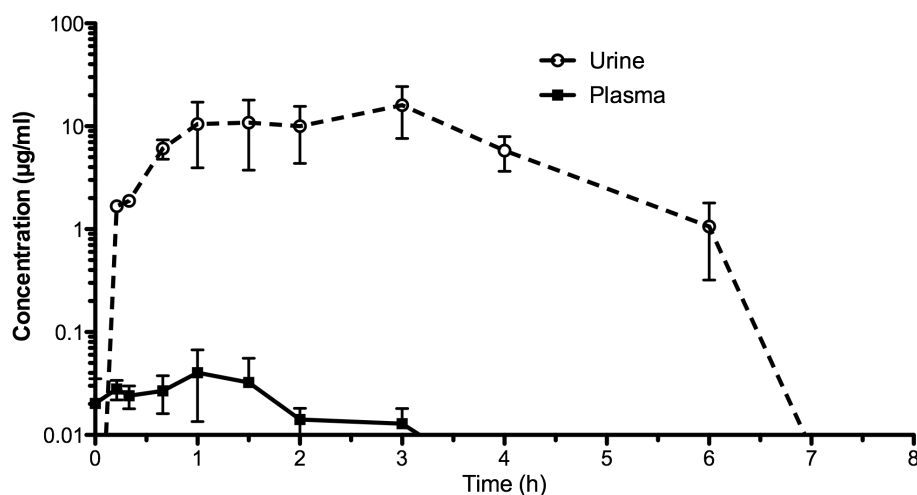


Figure 5. Urine (dashed line) and plasma (continuous line) concentration over time after an application of 10 mg/kg of **41f**. The detection limit for plasma samples was at 0.02 µg/ml, urine samples could be detected down to 0 µg/ml.

Generally, plasma concentrations of **41f** were low, barely exceeding the detection limit (0.02 µg/ml), with a peak between 40 min and 1.5 h after application and a C_{max} of only 0.04 µg/ml. Subsequently it dropped below the detection limit. In contrast, antagonist **41f** rapidly accumulates in the urine with a C_{max} ranging from 10 to 16 µg/ml at 1 to 3 h post application. After a stable concentration plateau, which is slightly shifted in time compared to plasma peak levels, **41f** was not detectable in urine 7 h post application. The total dose detected in urine corresponds to approximately 30% of the oral dose.

The accumulation in the urine, resulting in a relatively constant plateau concentration over a time-period of about 3 h, is related to several important interplaying mechanisms. Both, PAMPA^[27] and transport through a Caco-2 cell layer predict permeability for **41f** ($\log P_e$ -4.8 cm/s, and $P_{app,a-b}$ 6.4×10^{-6} cm/s, Table 2).^[38,39] However, absorption of **41f** is slowed down by the simultaneous efflux ($P_{app,b-a}$ 30×10^{-6} cm/s) by P-glycoprotein (P-gp),^[40] exceeding the uptake rate by a factor of approx. 5. Therefore, **41f** accumulates in the intestinal fluids, leading to P-gp saturation and, consequently, to a prolonged, but slow uptake. As this effect can influence plasma and urine drug levels only for a limited time, further mechanisms come into play. After absorption, antagonist **41f** remains in circulation only for a short period of time before it is filtered through the renal glomeruli in the kidneys. Its $\log P$ value ($\log P$ 2.8, entry 20, Table 2) implies a high reabsorption potential from the filtrate in the proximal tubuli, resulting in a delayed renal excretion.^[38,39,41] In summary, the observed PK profile of

41f results from a prolonged absorption due to P-gp mediated efflux combined with a delayed elimination via the kidneys due to reabsorption. These PK properties are beneficial for prevention or treatment of UTI, as high urine drug levels over an extended period of time limit the dosing frequency to few or even only one application a day.

Conclusions

Starting from prodrug **4a**, the present study aimed to optimize the pharmacokinetic properties of the biaryl mannoside in order to achieve high oral absorption of the ester prodrug and rapid enzyme-mediated release of the active principle. In this regard, our first approach, *i.e.* disruption of the molecular planarity and symmetry of the biphenyl mannoside by modifying the substitution pattern, proved successful. Compared to compound **4a**, the ester prodrug **8a** showed a tenfold increased solubility whereas membrane permeability remained unchanged. Moreover, hepatic esterases were shown to rapidly convert the ester to the polar parent compound **8b**. However, shifting the substituents on the aglycone markedly decreased the affinity to the FimH-CRD, overriding the gain in the intestinal uptake potential.

In a second approach, the improvement of the physicochemical properties by heterocyclic aglycones was studied. Thereby, triazole (**23a-c**), pyrazole (**26a,b**), and six-membered heterocyclic moieties (**32a-d** and **37**) proved highly beneficial to the aqueous solubility but in turn reduced lipophilicity and membrane permeability, which leads, overall, to poor oral absorption. By contrast, the pyrrolylphenyl mannosides – optimized by the introduction of a chloro or trifluoromethyl substituent on ring A and a methyl group on the heterocycle (**41f** and **49**) – exhibited sufficient permeability and aqueous solubility. However, incubations with rat liver microsomes, revealed low propensity to enzyme-mediated hydrolysis. Despite their high intestinal uptake potential, these esters therefore scarcely act as prodrugs facilitating the delivery of the active principles to the urinary bladder. Nonetheless, the introduction of a pyrrole moiety appears as a promising strategy for optimizing the oral absorption of biaryl mannoside analogues, which do not rely on an ester prodrug approach.

In summary, our study exemplifies the benefits of two approaches - rearrangement of the substitution pattern and introduction of aromatic heterocycles - on aqueous solubility. The high microsomal stability of the pyrrole derivatives indicates an action mode rather than a prodrug approach. For the esters **41f** and **49**, an optimal balance of pharmacodynamic, physicochemical and pharmacokinetic properties was obtained. According to the *in vivo* PK studies (see Figure 5), **41f** is a promising candidate to be tested in a UTI disease model.

Experimental Section

Synthesis. The synthesis of compounds **7a,b**, **8a,b**, **11a,b**, **13a,b**, **14a,b**, **17**, **20a,b**, **22b**, **23b,c**, **24b**, **25a,b**, **26a,b**, **27a,b**, **31b-d**, **32b-d**, **33b-d**, **40a-e**, **41a-e**, **42-44**, **47**, **49**, and **51**, including compound characterization data, can be found in the Supporting Information.

General Methods. NMR spectra were recorded on a Bruker Avance DMX-500 (500.1 MHz) spectrometer. Assignment of ^1H and ^{13}C NMR spectra was achieved using 2D methods (COSY, HSQC, HMBC). Chemical shifts are expressed in ppm using residual CHCl_3 , CHD_2OD or HDO as references. Optical rotations were measured using Perkin-Elmer Polarimeter 341. Electron spray ionization mass spectra (ESI-MS) were obtained on a Waters micromass ZQ. The LC/HRMS analysis were carried out using a Agilent 1100 LC equipped with a photodiode array detector and a Micromass QTOF I equipped with a 4 GHz digital-time converter. Microwave-assisted reactions were carried out with a CEM Discover and Explorer. Reactions were monitored by TLC using glass plates coated with silica gel 60 F₂₅₄ (Merck) and visualized by using UV light and/or by charring with a molybdate solution (a 0.02 M solution of ammonium cerium sulfate dihydrate and ammonium molybdate tetrahydrate in aqueous 10% H_2SO_4). MPLC separations were carried out on a CombiFlash Companion or Rf from Teledyne Isco equipped with RediSep normal-phase or RP-18 reversed-phase flash columns. LC-MS separations were done on a Waters system equipped with sample manager 2767, pump 2525, PDA 2525 and micromass ZQ. Size-exclusion chromatography was performed on Bio-Gel[®] P-2 Gel (45-90 mm) from Bio-Rad (Reinach, Switzerland). All compounds used for biological assays are at least of 98% purity based on HPLC analytical results. Commercially available reagents were purchased from Fluka, Aldrich, Alfa Aesar or Iris Biotech (Germany). Solvents were purchased from Sigma-Aldrich (Buchs, Switzerland) or Acros Organics (Geel, Belgium) and were dried prior to use where indicated. Methanol (MeOH) and ethanol (EtOH) were dried by refluxing with sodium methoxide or ethoxide and distilled immediately before use. Dichloromethane (DCM) was dried by filtration over Al_2O_3 (Fluka, type 5016 A basic). Molecular sieves 4Å were activated in vacuo at 500 °C for 1 h immediately before use.

General procedure A for the synthesis of mannosides 22a,b and 25a,b. To an ice-cold suspension of **21**^[21] (1.1 equiv), phenol **11a,b** or **14a,b** (1.0 equiv) and molecular sieves 4 Å (600 mg) in dry DCM (5 mL), $\text{BF}_3\cdot\text{Et}_2\text{O}$ (4.7 equiv) was added dropwise under argon. The mixture was stirred at 0 °C for 3 h, and then at rt overnight. The reaction mixture was filtered over Celite and the filtrate was diluted with DCM (50 mL), extracted with 0.5 N aq. NaOH (50 mL), water (50 mL) and brine (50 mL). The organic layer was dried over Na_2SO_4 and concentrated in vacuo. The residue was purified by MPLC on silica gel (petrol ether/EtOAc) to yield **22a,b** or **25a,b**.

General procedure B for the coupling of mannosylated phenyls with six-membered heterocyclic halides. A Schlenk tube was charged with heterocyclic halide **30a-c** or **17** (1.0 eq), boronate **29**^[11] or

35 (1.1 eq), Pd(dppf)Cl₂·CH₂Cl₂ (0.03 eq), K₃PO₄ (1.5 eq) and a stirring bar. The tube was closed with a rubber septum and was evacuated and flushed with argon. This procedure was repeated once, then anhydrous DMF (2 mL) was added under a stream of argon. The mixture was degassed in an ultrasonic bath and flushed with argon for 5 min, and then stirred at 80-85 °C overnight. The reaction mixture was cooled to rt, diluted with EtOAc (50 mL), and washed with water (50 mL) and brine (50 mL). The organic layer was dried over Na₂SO₄ and concentrated in vacuo. The residue was purified by MPLC on silica gel (petrol ether/EtOAc) to afford heteroarylphenyls **31a-d** or **36**.

General procedure C for the coupling of mannosylated phenyls with substituted pyrrolyl halides. A Schlenk tube was charged with phenyl halide **28**,^[11j] **34**^[11j] or **39**^[11j] (1.0 eq), pyrrolyl halide **20a-f** (1.2 eq), CuI (0.05 eq), (±)-*trans*-1,2-diaminocyclohexane (0.11 eq), K₃PO₄ (2.1 eq) and a stirring bar. The tube was closed with a rubber septum and was evacuated and flushed with argon. This procedure was repeated once, then anhydrous 1,4-dioxane (ca. 0.5 mL, 1 M to phenyl halide) was added under a stream of argon. The mixture was degassed in an ultrasonic bath and flushed with argon for 5 min, and then stirred at 110 °C for 24 h. The reaction mixture was cooled to rt, diluted with EtOAc (50 mL), and filtered through Celite. The filtrate was concentrated in vacuo and co-evaporated with toluene. The residue was acetylated with pyridine/acetic anhydride/DMAP, concentrated and purified by MPLC on silica gel (petrol ether/EtOAc) to afford pyrrolylphenyls **40a-f**, **46** or **47**.

General procedure D for deacetylation: To a solution of **22a,b**, **25a,b**, **31a-d**, **36**, **40a-f**, **46** or **47** (1.0 eq) in dry MeOH (5 mL) for producing methyl ester or in dry EtOH (5 mL) for producing ethyl ester, was added freshly prepared 1 M NaOMe/MeOH or NaOEt/EtOH (0.1 eq) under argon. The mixture was stirred at rt until the reaction was complete (monitored by TLC), then neutralized with Amberlyst-15 (H⁺) ion-exchange resin, filtered and concentrated in vacuo. The residue was purified by MPLC on silica gel (DCM/MeOH, 10:1 to 8:1 for methyl esters or DCM/EtOH, 3:1 for ethyl esters) to afford **23a-c**, **26a-b**, **32a-d**, **37**, **41a-f**, **48** or **49**.

General procedure E for saponification: To a solution of **22a,b**, **25a,b**, **31a-d**, **36**, **40a-f**, **46** or **47** (1.0 eq) in MeOH (5 mL) was added 1 M NaOMe/MeOH (0.1 eq) at rt. The reaction mixture was stirred at rt for 4 h and concentrated. The residue was treated with 0.5 M aq. NaOH (1 mL) for 24 h at rt. Then the pH was adjusted to 3-4 with Amberlyst-15 (H⁺) and the mixture was filtered and concentrated. The crude product was transformed into the sodium salt by passing through a small column of Dowex 50X8 (Na⁺ form) ion-exchange resin. After concentration the residue was purified by MPLC (RP-18, H₂O/MeOH, 1:0 to 2:1) followed by size-exclusion chromatography (P-2 gel, H₂O) to yield **24a,b**, **27a,b**, **33a-d**, **38**, **42-45**, **50** or **51** as white solids after final lyophilization from water.

Ethyl 1-[4-(2,3,4,6-tetra-*O*-acetyl- α -D-mannopyranosyloxy)phenyl]-1*H*-1,2,3-triazole-4-carboxylate (22a). Prepared according to general procedure A from **21** and **11a**. Yield: 341 mg

(79%) as colorless oil. R_f 0.30 (petrol ether/EtOAc, 1:1); $[\alpha]_D^{20} +76.7$ (c 0.90, MeOH); $^1\text{H NMR}$ (500 MHz, CDCl_3): $\delta = 8.47$ (s, 1H, triazole), 7.72-7.70 (m, 2H, Ar-H), 7.29-7.27 (m, 2H, Ar-H), 5.60 (d, $J = 1.7$ Hz, 1H, H-1), 5.56 (dd, $J = 3.0, 10.0$ Hz, 1H, H-3), 5.48 (dd, $J = 1.9, 3.0$ Hz, 1H, H-2), 5.40 (t, $J = 10.0$ Hz, 1H, H-4), 4.47 (dd, $J = 7.2, 14.2$ Hz, 2H, OCH_2), 4.29 (dd, $J = 5.4, 12.4$ Hz, 1H, H-6a), 4.11-4.07 (m, 2H, H-5, H-6b), 2.22, 2.07, 2.06, 2.05 (4 s, 12H, 4 COCH_3), 1.44 (t, $J = 7.2$ Hz, 3H, CH_3); $^{13}\text{C NMR}$ (126 MHz, CDCl_3): $\delta = 170.48, 170.01, 169.99, 169.69, 160.61$ (5 CO), 156.17, 140.87, 131.60, 125.52, 122.46, 117.62 (8C, Ar-C), 95.89 (C-1), 69.54 (C-5), 69.14 (C-2), 68.66 (C-3), 65.71 (C-4), 62.03 (C-6), 61.55 (OCH_2), 20.88, 20.71, 20.70 (4C, 4 COCH_3), 14.34 (CH_3); ESI-MS: m/z : Calcd for $\text{C}_{25}\text{H}_{30}\text{N}_3\text{O}_{12}$ $[\text{M}+\text{H}]^+$: 564.18, found: 564.20.

Methyl 1-[4-(α -D-mannopyranosyloxy)phenyl]-1H-1,2,3-triazole-4-carboxylate (23a). Prepared according to general procedure D from **22a**. Yield: 28 mg (74%) as white solid. R_f 0.20 (DCM/MeOH, 8:1); $[\alpha]_D^{20} +99.8$ (c 0.30, MeOH); $^1\text{H NMR}$ (500 MHz, CD_3OD): $\delta = 8.94$ (s, 1H, Ar-H), 7.72-7.69 (m, 2H, Ar-H), 7.25-7.23 (m, 2H, Ar-H), 5.48 (d, $J = 1.7$ Hz, 1H, H-1), 3.94 (dd, $J = 1.9, 3.4$ Hz, 1H, H-2), 3.85 (s, 3H, OCH_3), 3.81 (dd, $J = 3.5, 9.5$ Hz, 1H, H-3), 3.70-3.60 (m, 3H, H-4, H-6), 3.48 (ddd, $J = 2.4, 5.5, 9.7$ Hz, 1H, H-5); $^{13}\text{C NMR}$ (126 MHz, CD_3OD): $\delta = 162.33$ (CO), 158.64, 141.14, 132.38, 127.77, 123.47, 118.81 (8C, Ar-C), 100.26 (C-1), 75.77 (C-5), 72.34 (C-3), 71.82 (C-2), 68.27 (C-4), 62.68 (C-6), 52.66 (OCH_3); HRMS: m/z : Calcd for $\text{C}_{16}\text{H}_{19}\text{N}_3\text{NaO}_8$ $[\text{M}+\text{Na}]^+$: 404.1064, found: 404.1068.

Sodium 1-[4-(α -D-mannopyranosyloxy)phenyl]-1H-1,2,3-triazole-4-carboxylate (24a). Prepared according to general procedure E from **22a**. Yield: 5 mg (30%) as white solid. $[\alpha]_D^{20} +92.0$ (c 0.20, MeOH/ H_2O , 1:1); $^1\text{H NMR}$ (500 MHz, D_2O): $\delta = 8.40$ (s, 1H, Ar-H), 7.58-7.56 (m, 2H, Ar-H), 7.18-7.16 (m, 2H, Ar-H), 5.55 (d, $J = 1.4$ Hz, 1H, H-1), 4.08 (dd, $J = 1.9, 3.4$ Hz, 1H, H-2), 3.95 (dd, $J = 3.5, 9.5$ Hz, 1H, H-3), 3.73-3.57 (m, 4H, H-4, H-5, H-6); $^{13}\text{C NMR}$ (126 MHz, D_2O): $\delta = 167.44$ (CO), 156.00, 145.08, 131.02, 125.53, 122.73, 117.65 (8C, Ar-C), 97.98 (C-1), 73.41 (C-5), 70.26, 69.72, 66.51 (C-2, C-3, C-4), 60.60 (C-6); HRMS: m/z : Calcd for $\text{C}_{15}\text{H}_{17}\text{N}_3\text{NaO}_8$ $[\text{M}+\text{H}]^+$: 390.0908, found: 390.0905.

Methyl 5-[4-(2,3,4,6-tetra-*O*-acetyl- α -D-mannopyranosyloxy)phenyl]-picolinate (31a). Prepared according to general procedure B from **29**^[11] (120 mg, 0.21 mmol) and methyl 5-bromopicolinate (**30a**, 40 mg, 0.19 mmol). Yield: 62 mg (60%) as white solid. R_f 0.33 (petrol ether/EtOAc, 2:3); $[\alpha]_D^{20} +47.3$ (c 0.60, MeOH); $^1\text{H NMR}$ (500 MHz, CDCl_3): $\delta = 8.93$ (dd, $J = 0.5, 2.2$ Hz, 1H, Ar-H), 8.20 (dd, $J = 0.6, 8.2$ Hz, 1H, Ar-H), 7.99 (dd, $J = 2.4, 8.2$ Hz, 1H, Ar-H), 7.61-7.58 (m, 2H, Ar-H), 7.25-7.23 (m, 2H, Ar-H), 5.60 (d, $J = 1.8$ Hz, 1H, H-1), 5.59 (dd, $J = 3.6, 10.1$ Hz, 1H, H-3), 5.48 (dd, $J = 1.9, 3.5$ Hz, 1H, H-2), 5.41 (t, $J = 10.1$ Hz, 1H, H-4), 4.30 (dd, $J = 5.0, 12.4$ Hz, 1H, H-6a), 4.11-4.08 (m, 2H, H-5, H-6b), 4.04 (s, 3H, OCH_3), 2.23, 2.07, 2.06, 2.05 (4 s, 12H, 4 COCH_3); $^{13}\text{C NMR}$ (126 MHz, CDCl_3): $\delta = 170.49, 170.01, 169.99, 169.70, 165.61$ (5 CO), 156.25, 147.93, 146.20, 138.97,

134.70, 131.35, 128.69, 125.25, 117.22 (11C, Ar-C), 95.71 (C-1), 69.34 (C-2), 69.25 (C-5), 68.78 (C-3), 65.79 (C-4), 62.02 (C-6), 52.94 (OCH₃), 20.89, 20.71, 20.69, 20.68 (4 COCH₃); ESI-MS: *m/z*: Calcd for C₂₇H₃₀NO₁₂ [M+H]⁺: 560.18, found: 560.27.

Methyl 5-[4-(α -D-mannopyranosyloxy)phenyl]-picolinate (32a). Prepared according to general procedure D from **31a**. Yield: 15 mg (36%) as white solid. *R_f* 0.13 (DCM/MeOH, 8:1); [α]_D²⁰ +113.4 (*c* 0.20, MeOH); ¹H NMR (500 MHz, DMSO-*d*₆): δ = 9.18 (d, *J* = 2.2 Hz, 1H, Ar-H), 8.37 (dd, *J* = 2.2, 8.4 Hz, 1H, Ar-H), 8.20 (d, *J* = 8.9 Hz, 2H, Ar-H), 8.14 (d, *J* = 8.4 Hz, 1H, Ar-H), 7.29 (t, *J* = 5.8 Hz, 2H, Ar-H), 5.55 (d, *J* = 1.6 Hz, 1H, H-1), 5.15 (d, *J* = 4.2 Hz, 1H), 4.93 (d, *J* = 5.7 Hz, 1H), 4.87 (d, *J* = 5.6 Hz, 1H), 4.54 (t, *J* = 6.0 Hz, 1H), 3.96 (s, 3H, OCH₃), 3.92 (s, 1H), 3.76 (m, 1H), 3.66 (ddd, *J* = 1.9, 5.8, 11.6 Hz, 1H), 3.61-3.49 (m, 2H), 3.45 (m, 1H); ¹³C NMR (126 MHz, DMSO-*d*₆): δ = 165.20 (CO), 159.29, 158.04, 150.07, 137.81, 130.95, 128.57, 123.30, 119.25, 116.83 (11C, Ar-C), 98.55 (C-1), 75.10 (C-5), 70.59, 69.94, 66.59 (C-2, C-3, C-4), 60.94 (C-6), 52.32 (OCH₃); HRMS: *m/z*: Calcd for C₁₉H₂₁NNaO₈ [M+Na]⁺: 414.1159, found: 414.1162.

Sodium 5-[4-(α -D-mannopyranosyloxy)phenyl]-picolinate (33a). Prepared according to general procedure E from **31a**. Yield: 3 mg (32%) as white solid. [α]_D²⁰ +99.3 (*c* 0.20, MeOH/H₂O, 1:1); ¹H NMR (500 MHz, D₂O): δ = 8.63 (s, 1H, Ar-H), 7.96 (d, *J* = 8.0 Hz, 1H, Ar-H), 7.82 (d, *J* = 6.6 Hz, 1H, Ar-H), 7.56-7.54 (m, 2H, Ar-H), 7.13-7.11 (m, 2H, Ar-H), 5.54 (d, *J* = 1.4 Hz, 1H, H-1), 4.07 (m, 1H, H-2), 3.96 (dd, *J* = 3.5, 9.2 Hz, H-3), 3.70-3.58 (m, 4H, H-4, H-5, H-6); ¹³C NMR (126 MHz, D₂O): δ = 155.75, 146.29, 135.43, 131.05, 128.42, 123.82, 117.39 (11C, Ar-C), 97.91 (C-1), 73.33 (C-5), 70.31, 69.80, 66.51 (C-2, C-3, C-4), 60.59 (C-6); HRMS: *m/z*: Calcd for C₁₈H₁₉NNaO₈ [M+Na]⁺: 400.1003, found: 400.1003.

Methyl 5-[4-(2,3,4,6-tetra-*O*-acetyl- α -D-mannopyranosyloxy)-3-trifluoromethyl-phenyl]-picolinate (36). A Schlenk tube was charged with **34**^[10] (394 mg, 0.69 mmol), KOAc (203 mg, 2.07 mmol), bis(pinacolato)diboron (193 mg, 0.76 mmol) and Pd(dppf)Cl₂·CH₂Cl₂ (17 mg, 0.021 mmol). The tube was closed, evacuated and flushed with argon. Then anhydrous DMF (4 mL) was added under a stream of argon. The mixture was degassed in an ultrasonic bath and flushed with argon for 5 min, and then stirred at 85 °C overnight. The reaction mixture was cooled to rt and diluted with DCM/H₂O (100 mL, 1:1). The organic layer was washed with H₂O (50 mL) and brine (50 mL), dried over Na₂SO₄ and concentrated. The residue was passed through a short silica gel column (petrol ether/EtOAc, 2:1) to afford crude **35** (352 mg), which was used directly in the next step. Compound **36** was prepared according to general procedure B from crude **35** (352 mg, 0.57 mmol) and methyl 5-chloropyrazine-2-carboxylate (**30a**, 108 mg, 0.63 mmol). Yield: 205 mg (57%) as colorless oil. *R_f* 0.38 (petrol ether/EtOAc, 2:3); [α]_D²⁰ +64.5 (*c* 1.00, EtOAc); ¹H NMR (500 MHz, CDCl₃): δ = 8.92 (d, *J* = 2.1 Hz, 1H, Ar-H), 8.23 (d, *J* = 8.1 Hz, 1H, Ar-H), 8.00 (dd, *J* = 2.3, 8.1 Hz, 1H, Ar-H), 7.87 (d, *J* = 2.1 Hz, 1H, Ar-H), 7.77 (dd, *J* = 2.2, 8.6 Hz, 1H, Ar-H), 7.41 (d, *J* = 8.7 Hz, 1H, Ar-H), 5.72

(d, $J = 1.7$ Hz, 1H, H-1), 5.56 (dd, $J = 3.4, 10.1$ Hz, 1H, H-3), 5.50 (dd, $J = 1.9, 3.4$ Hz, 1H, H-2), 5.43 (t, $J = 10.1$ Hz, 1H, H-4), 4.30 (dd, $J = 5.1, 12.5$ Hz, 1H, H-6a), 4.16-4.02 (m, 6H, H-6b, H-5, OCH₃), 2.23, 2.06 (2s, 12H, 4 COCH₃); ¹³C NMR (126 MHz, CDCl₃): $\delta = 170.40, 169.94, 169.73, 169.62, 165.41$ (5 CO), 153.59, 147.93, 146.98, 137.80, 134.99, 132.06, 131.21, 126.32, 125.33, 116.15 (12C, Ar-C, CF₃), 95.71 (C-1), 70.06 (C-5), 69.10 (C-2), 68.52 (C-3), 65.48 (C-4), 61.95 (C-6), 53.03 (OCH₃), 20.85, 20.68 (4C, 4 COCH₃); ESI-MS: m/z : Calcd for C₂₈H₂₉F₃NO₁₂ [M+H]⁺: 628.16, found: 628.19.

Methyl 5-[4-(α -D-mannopyranosyloxy)-3-trifluoromethyl-phenyl]-picolinate (37). Prepared according to general procedure D from **36**. Yield: 15 mg (60%) as white solid. R_f 0.20 (DCM/MeOH, 8:1); $[\alpha]_D^{20} +104.9$ (c 0.40, MeOH); ¹H NMR (500 MHz, CD₃OD): $\delta = 8.95$ (dd, $J = 0.7, 2.1$ Hz, 1H, Ar-H), 8.25 (qd, $J = 1.5, 8.2$ Hz, 2H, Ar-H), 8.06-7.92 (m, 2H, Ar-H), 7.68 (m, 1H, Ar-H), 5.72 (d, $J = 1.6$ Hz, 1H, H-1), 4.09 (dd, $J = 1.8, 3.4$ Hz, 1H, H-2), 4.02 (s, 3H, OCH₃), 3.96 (dd, $J = 3.4, 9.5$ Hz, 1H, H-3), 3.86-3.69 (m, 3H, H-4, H-6), 3.60 (ddd, $J = 2.3, 5.7, 9.7$ Hz, 1H, H-5); ¹³C NMR (126 MHz, CD₃OD): $\delta = 166.43$ (CO), 156.19, 148.61, 147.34, 139.82, 136.84, 133.76, 131.17, 126.81, 126.58, 118.09 (12C, Ar-C, CF₃), 100.31 (C-1), 76.24 (C-5), 72.25 (C-3), 71.71 (C-2), 68.11 (C-4), 62.70 (C-6), 53.28 (OCH₃); HRMS: m/z : Calcd for C₂₀H₂₀F₃NNaO₈ [M+Na]⁺: 482.1033, found: 482.0135.

Sodium 5-[4-(α -D-mannopyranosyloxy)-3-trifluoromethyl-phenyl]-picolinate (38). Prepared according to general procedure E from **36**. Yield: 40 mg (90%) as white solid. $[\alpha]_D^{20} +71.4$ (c 0.50, MeOH/H₂O, 1:1); ¹H NMR (500 MHz, CD₃OD): $\delta = 8.70$ (s, 1H, Ar-H), 8.00 (s, 2H, Ar-H), 7.86-7.77 (m, 2H, Ar-H), 7.53 (m, 1H, Ar-H), 5.58 (d, $J = 1.3$ Hz, 1H, H-1), 3.97 (dd, $J = 1.8, 3.3$ Hz, 1H, H-2), 3.85 (dd, $J = 3.4, 9.5$ Hz, 1H, H-3), 3.73-3.59 (m, 3H, H-4, H-6), 3.49 (m, 1H, H-5); ¹³C NMR (126 MHz, CD₃OD): $\delta = 172.52$ (CO), 155.69, 155.16, 147.65, 137.21, 136.17, 133.48, 132.31, 132.21, 126.48, 125.22, 118.01, 101.40 (12C, Ar-C, CF₃), 100.33 (C-1), 76.15 (C-5), 72.26 (C-3), 71.75 (C-2), 68.12 (C-4), 62.66 (C-6); HRMS: m/z : Calcd for C₁₉H₁₈F₃NNa₂O₈ [M+Na]⁺: 490.0696, found: 490.0713.

Ethyl 1-[4-(2,3,4,6-tetra-*O*-acetyl- α -D-mannopyranosyloxy)-3-chlorophenyl]-4-methyl-1*H*-pyrrole-3-carboxylate (40f). Prepared according to general procedure C from **39** and methyl 4-methyl-1*H*-pyrrole-3-carboxylate (**20f**). Yield: 240 mg (77%) as colorless oil. R_f 0.34 (petrol ether/EtOAc, 3:2); $[\alpha]_D^{20} +64.5$ (c 1.00, EtOAc); ¹H NMR (500 MHz, CDCl₃): $\delta = 7.55$ (d, $J = 2.5$ Hz, 1H, Ar-H), 7.46 (m, 1H, Ar-H), 7.28-7.20 (m, 2H, Ar-H), 6.76 (dd, $J = 1.0, 2.4$ Hz, 1H, Ar-H), 5.61 (dd, $J = 3.4, 10.0$ Hz, 1H, H-3), 5.57 (d, $J = 1.7$ Hz, 1H, H-1), 5.54 (dd, $J = 1.9, 3.4$ Hz, 1H, H-2), 5.41 (t, $J = 10.1$ Hz, 1H, H-4), 4.33-4.26 (m, 3H, H-6b, OCH₂), 4.19 (ddd, $J = 2.2, 5.3, 10.1$ Hz, 1H, H-5), 4.12 (m, 1H, H-6a), 2.31 (d, $J = 0.8$ Hz, 3H, CH₃), 2.21, 2.08, 2.05 (3 s, 12H, 4 COCH₃), 2.04 (s, 1H), 1.36 (t, $J = 7.1$ Hz, 3H, CH₃); ¹³C NMR (126 MHz, CDCl₃): $\delta = 170.41, 169.93, 169.77,$

169.73, 164.95 (5 CO), 149.71, 135.88, 125.46, 124.71, 123.48, 122.80, 119.68, 118.99, 117.93, 117.13 (Ar-C), 96.98 (C-1), 69.92 (C-5), 69.26 (C-2), 68.71 (C-3), 65.79 (C-4), 62.13 (C-6), 59.58 (OCH₂), 21.03, 20.85, 20.70, 20.68 (4 COCH₃), 14.51 (CH₃), 11.72 (CH₃); ESI-MS: *m/z*: Calcd for C₂₈H₃₂CINNaO₁₂ [M+Na]⁺: 632.15, found: 632.15.

Ethyl 1-[3-chloro-4-(α -D-mannopyranosyloxy)phenyl]-4-methyl-1*H*-pyrrole-3-carboxylate (41f). Prepared according to general procedure D from **40f**. Yield: 55 mg (93%) as white solid. *R_f* 0.29 (DCM/MeOH, 9:1); [α]_D²⁰ +89.1 (*c* 0.50, MeOH); ¹H NMR (500 MHz, CD₃OD): δ = 7.68 (d, *J* = 2.5 Hz, 1H, Ar-H), 7.58 (d, *J* = 2.7 Hz, 1H, Ar-H), 7.47 (d, *J* = 8.9 Hz, 1H, Ar-H), 7.39 (dd, *J* = 2.7, 8.9 Hz, 1H, Ar-H), 6.95 (d, *J* = 1.0 Hz, 1H, Ar-H), 5.58 (d, *J* = 1.4 Hz, 1H, H-1), 4.28 (q, *J* = 7.1 Hz, 2H, OCH₂), 4.14 (dd, *J* = 1.8, 3.2 Hz, 1H, H-2), 4.01 (dd, *J* = 3.4, 9.5 Hz, 1H, H-3), 3.86-3.72 (m, 3H, H-4, H-6), 3.67 (m, 1H, H-5), 2.29 (s, 3H, CH₃), 1.37 (t, *J* = 7.1 Hz, 3H, CH₃); ¹³C NMR (126 MHz, CD₃OD): δ = 166.98 (CO), 151.75, 136.28, 126.11, 125.75, 124.16, 123.19, 120.88, 120.51, 119.26, 117.60 (Ar-C), 101.01 (C-1), 76.04 (C-5), 72.36 (C-3), 71.78 (C-2), 68.19 (C-4), 62.66 (C-6), 60.74 (OCH₂), 14.77 (CH₃), 11.96 (CH₃); HRMS: *m/z*: Calcd for C₂₀H₂₄CINNaO₈ [M+Na]⁺: 464.1083, found: 464.1086.

Sodium 1-[3-chloro-4-(α -D-mannopyranosyloxy)phenyl]-4-methyl-1*H*-pyrrole-3-carboxylate (45). Prepared according to general procedure E from **40f**. Yield: 30 mg (57%) as white solid. ¹H NMR (500 MHz, CD₃OD): δ = 7.69 (d, *J* = 2.5 Hz, 1H, Ar-H), 7.60 (d, *J* = 2.6 Hz, 1H, Ar-H), 7.48 (d, *J* = 8.9 Hz, 1H, Ar-H), 7.42 (dd, *J* = 2.7, 8.9 Hz, 1H, Ar-H), 6.97 (d, *J* = 1.2 Hz, 1H, Ar-H), 5.57 (d, *J* = 1.4 Hz, 1H, H-1), 4.13 (dd, *J* = 1.8, 3.2 Hz, 1H, H-2), 4.00 (dd, *J* = 3.4, 9.5 Hz, 1H, H-3), 3.87-3.70 (m, 3H, H-4, H-6), 3.66 (ddd, *J* = 2.2, 5.5, 9.6 Hz, 1H, H-5), 2.30 (s, 3H, CH₃); ¹³C NMR (126 MHz, CD₃OD): δ = 168.95 (CO), 151.77, 136.47, 126.41, 125.80, 124.42, 123.25, 120.95, 120.51, 119.34, 118.09 (Ar-C), 101.08 (C-1), 76.08 (C-5), 72.39 (C-3), 71.82 (C-2), 68.23 (C-4), 62.69 (C-6), 11.92 (CH₃); HRMS: *m/z*: Calcd for C₁₈H₂₀CINNaO₈ [M+H]⁺: 436.0770, found: 436.0773.

Ethyl 1-[4-(2,3,4,6-tetra-*O*-acetyl- α -D-mannopyranosyloxy)phenyl]-4-methyl-1*H*-pyrrole-3-carboxylate (46). Prepared according to general procedure C from **28** and methyl 4-methyl-1*H*-pyrrole-3-carboxylate (**20f**). Yield: 293 mg (94%) as colorless oil. *R_f* 0.47 (petrol ether/EtOAc, 3:2); [α]_D²⁰ +63.7 (*c* 2.20, EtOAc); ¹H NMR (500 MHz, CDCl₃): δ = 7.36 (d, *J* = 2.4 Hz, 1H, Ar-H), 7.20 (d, *J* = 8.8 Hz, 1H, Ar-H), 7.15 (dd, *J* = 2.5, 8.7 Hz, 1H, Ar-H), 6.91 (d, *J* = 1.6 Hz, 1H, Ar-H), 6.67 (d, *J* = 0.9 Hz, 1H, Ar-H), 5.62 (dd, *J* = 3.5, 10.0 Hz, 1H, H-3), 5.57 (d, *J* = 1.6 Hz, 1H, H-1), 5.53 (dd, *J* = 1.9, 3.4 Hz, 1H, H-2), 5.40 (t, *J* = 10.1 Hz, 1H, H-4), 4.31 (dd, *J* = 5.3, 12.3 Hz, 1H, H-6a), 4.20 (ddd, *J* = 2.2, 5.2, 10.1 Hz, 1H, H-5), 4.18-4.08 (m, 3H, OCH₂, H-6b), 2.21, 2.11, 2.08, 2.07, 2.05 (5 s, 15H, 4 COCH₃, CH₃), 1.23 (t, *J* = 7.1 Hz, 3H, CH₃); ¹³C NMR (126 MHz, CDCl₃): δ = 170.52, 169.91, 169.75, 160.32 (5C, 5 CO), 150.69, 136.26, 128.55, 128.10, 125.80, 123.86, 123.18, 120.00, 119.90, 116.17 (Ar-C), 96.86 (C-1), 69.83 (C-5), 69.32 (C-2), 68.75 (C-3), 65.81 (C-4), 62.08

(C-6), 59.90 (OCH₂), 20.85, 20.71, 20.68, 14.27, 11.43 (6C, 4 COCH₃, 2 CH₃); ESI-MS: *m/z*: Calcd for C₂₈H₃₃NNaO₁₂ [M+Na]⁺: 598.19, found: 598.16.

Ethyl 1-[4-(α -D-mannopyranosyloxy)phenyl]-4-methyl-1*H*-pyrrole-3-carboxylate (48). Prepared according to general procedure D from **46**. Yield: 87 mg (46%) as white solid. *R_f* 0.30 (DCM/MeOH, 8:1); [α]_D²⁰ +109.7 (*c* 0.80, MeOH); ¹H NMR (500 MHz, CD₃OD): δ = 7.67 (d, *J* = 2.5 Hz, 1H, Ar-H), 7.46-7.41 (m, 2H, Ar-H), 7.27-7.22 (m, 2H, Ar-H), 6.95 (dd, *J* = 1.0, 2.4 Hz, 1H, Ar-H), 5.52 (d, *J* = 1.6 Hz, 1H, H-1), 4.29 (q, *J* = 7.1 Hz, 2H, OCH₂), 4.04 (dd, *J* = 1.8, 3.4 Hz, 1H, H-2), 3.92 (dd, *J* = 3.4, 9.4 Hz, 1H, H-3), 3.84-3.70 (m, 3H, H-4, H-6), 3.62 (ddd, *J* = 2.4, 5.4, 9.7 Hz, 1H, H-5), 2.30 (d, *J* = 0.9 Hz, 3H, CH₃), 1.37 (t, *J* = 7.1 Hz, 3H, CH₃); ¹³C NMR (126 MHz, CD₃OD): δ = 167.22 (CO), 156.53, 135.97, 126.23, 123.86, 122.85, 120.73, 118.92, 117.13 (8C, Ar-C), 100.47 (C-1), 75.57 (C-5), 72.41 (C-3), 71.95 (C-2), 68.35 (C-4), 62.72 (C-6), 60.68 (OCH₂), 14.80, 11.98 (2 CH₃); HRMS: *m/z*: Calcd for C₂₀H₂₅NNaO₈ [M+Na]⁺: 430.1472, found: 430.1474.

Sodium 1-[4-(α -D-mannopyranosyloxy)phenyl]-4-methyl-1*H*-pyrrole-3-carboxylate (50). Prepared according to general procedure E from **46**. Yield: 93 mg (99%) as white solid. [α]_D²⁰ +97.0 (*c* 0.70, MeOH/H₂O, 1:2); ¹H NMR (500 MHz, D₂O): δ = 7.51 (d, *J* = 2.4 Hz, 1H, Ar-H), 7.42 (d, *J* = 8.9 Hz, 2H, Ar-H), 7.22 (d, *J* = 8.9 Hz, 2H, Ar-H), 6.93 (s, 1H, Ar-H), 5.60 (s, 1H, H-1), 4.19 (m, 1H, H-2), 4.07 (dd, *J* = 3.4, 8.9 Hz, 1H, H-3), 3.90-3.68 (m, 4H, H-4, H-5, H-6), 2.27 (s, 3H, CH₃); ¹³C NMR (125 MHz, D₂O): δ = 174.29 (CO), 153.52, 135.00, 123.89, 121.84, 121.78, 121.56, 119.09, 118.07 (10C, Ar-C), 98.45 (C-1), 73.40 (C-5), 70.39 (C-3), 69.88 (C-2), 66.58 (C-4), 60.65 (C-6), 10.97 (CH₃); HRMS: *m/z*: Calcd for C₁₈H₂₁NNaO₈ [M+Na]⁺: 402.1159, found: 402.1159.

Cell-free competitive binding assay.

A recombinant protein consisting of the CRD of FimH linked with a thrombin cleavage site to a 6His-tag (FimH-CRD-Th-6His) was expressed in *E. coli* strain HM125 and purified by affinity chromatography.^[23] To determine the affinity of the various FimH antagonists, a competitive binding assay as described previously was applied.^[23] Microtiter plates (F96 MaxiSorp, Nunc) were coated with 100 μ L/well of a 10 μ g/mL solution of FimH-CRD-Th-6His in 20 mM HEPES, 150 mM NaCl, and 1 mM CaCl₂, pH 7.4 (assay buffer) overnight at 4 °C. The coating solution was discarded and the wells were blocked with 150 μ L/well of 3% BSA in assay buffer for 2 h at 4 °C. After three washing steps with assay buffer (150 μ L/well), a 4-fold serial dilution of the test compound (50 μ L/well) in assay buffer containing 5% DMSO and streptavidin-peroxidase coupled to Man- α (1-3)[Man- α (1-6)]-Man- β (1-4)-GlcNAc- β (1-4)-GlcNAc β polyacrylamide (TM-PAA) polymer (50 μ L/well of a 0.5 μ g/mL solution) were added. On each individual microtiter plate, *n*-heptyl α -D-mannopyranoside (**1**) was tested in parallel. The plates were incubated for 3 h at 25 °C and 350 rpm and then carefully washed four times with 150 μ L/well assay buffer. After the addition of 100 μ L/well of 2,2'-azino-di-

(3-ethylbenzthiazoline-6-sulfonic acid) (ABTS)-substrate, the colorimetric reaction was allowed to develop for 4 min and then was stopped by the addition of 2% aq. oxalic acid before the optical density (OD) was measured at 415 nm on a microplate-reader (Spectramax 190, Molecular Devices, Silicon Valley, CA, USA). The IC₅₀ values of the compounds tested in duplicates were calculated with prism software (GraphPad Software, Inc., La Jolla, CA, USA). The IC₅₀ defines the molar concentration of the test compound that reduces the maximal specific binding of TM-PAA polymer to FimH-CRD by 50%. The relative IC₅₀ (rIC₅₀) is the ratio of the IC₅₀ of the test compound to the IC₅₀ of *n*-heptyl α -D-mannopyranoside (**1**).

K_D determination with fluorescence polarization assay.

The fluorescently labeled ligand **52**^[11k] was used for the competitive fluorescence polarization assay. A serial dilution of non-labeled FimH antagonist with final concentrations ranging from 0-10 μ M was titrated into 96-well NBSTM plates to a final volume of 200 μ L containing a constant concentration of protein (final concentration 25 nM) and FITC-labeled ligand **52** which was fixed at a higher concentration in competitive binding assays to obtain higher fluorescence intensities (final concentration 20 nM). Prior to measuring the fluorescence polarization, the plates were incubated on a shaker for 24 h at rt until the reaction reached its equilibrium. The IC₅₀ value was determined with Prism (GraphPad Software Inc., La Jolla, CA, USA) by applying a standard four-parameter IC₅₀ function. The obtained IC₅₀ values were converted into their corresponding K_D values using the following derivation of the Cheng-Prusoff equation (Equation 1):^[36]

$$K_D = \frac{I_{50}}{\frac{L_{50}}{K_D} + \frac{P_0}{K_D} + 1} \quad (1)$$

where I_{50} and L_{50} are the concentrations of inhibitor and ligand at half-maximal inhibition, respectively, and P_0 is the free concentration of protein in the absence of inhibitor. This variation of the Cheng-Prusoff equation is applied to competition assays with tight-binding inhibitors. However, the K_D for antagonists, which have a higher affinity towards FimH than the labeled ligand could not be accurately determined with this equation.^[36]

Physicochemical properties and in vitro pharmacokinetics

Materials. Dimethyl sulfoxide (DMSO), 1-propanol, 1-octanol, Dulbecco's Modified Eagle's Medium (DMEM) high glucose, penicillin-streptomycin (solution stabilized, with 10'000 units penicillin and 10 mg streptomycin/mL), L-glutamine solution (200 mM), magnesium chloride, ammonium acetate, and bis(4-nitrophenyl) phosphate (BNPP) were purchased from Sigma-Aldrich (Buchs, Switzerland). PRISMA HT universal buffer, GIT-0 Lipid Solution, and Acceptor Sink Buffer were ordered from pIon (Woburn, MA, USA). MEM non-essential amino acids solution 10 mM (100X), fetal bovine serum (FBS), and DMEM without sodium pyruvate and phenol red were bought

from Invitrogen (Carlsbad, CA, USA). Acetonitrile (MeCN) and methanol (MeOH) were ordered from Acros Organics (Geel, Belgium). Pooled male rat liver microsomes (Sprague Dawley) were ordered from BD Bioscience (Franklin Lakes, NJ, USA). The Caco-2 cells were kindly provided by Prof G. Imanidis, FHNW, MuttENZ, Switzerland and originated from the American Type Culture Collection (Rockville, MD, USA).

log P determination. The in silico prediction tool ALOGPS^[42] was used to estimate the octanol-water partition coefficient ($\log P$) of the compounds. Depending on these values, the compounds were classified into three categories: hydrophilic compounds ($\log P < 0$), moderately lipophilic compounds ($\log P$ between 0 and 1) and lipophilic compounds ($\log P > 1$). For each category, two different ratios (volume of 1-octanol to volume of buffer) were defined as experimental parameters (Table 4).

Table 4. Parameters for the experimental determination of lipophilicity.

Compound type	$\log P$	ratios (1-octanol: buffer)
hydrophilic	< 0	30:140, 40:130
moderately lipophilic	0 - 1	70:110, 110:70
lipophilic	> 1	3:180, 4:180

Equal amounts of phosphate buffer (0.1 M, pH 7.4) and 1-octanol were mixed and shaken vigorously for 5 min to saturate the phases. The mixture was left until separation of the two phases occurred, and the buffer was retrieved. Stock solutions of the test compounds were diluted with buffer to a concentration of 1 μM . For each compound, six determinations, *i.e.* three determinations per 1-octanol:buffer ratio, were performed in different wells of a 96-well plate. The respective volumes of buffer containing analyte (1 μM) were pipetted to the wells and covered by saturated 1-octanol according to the chosen volume ratio. The plate was sealed with aluminium foil, shaken (1350 rpm, 25 °C, 2 h) on a Heidolph Titramax 1000 plate-shaker (Heidolph Instruments GmbH & Co. KG, Schwabach, Germany) and centrifuged (2000 rpm, 25 °C, 5 min, 5804R Eppendorf centrifuge, Hamburg, Germany). The aqueous phase was transferred to a 96-well plate for analysis by liquid chromatography-mass spectrometry (LC-MS, see below). The partition coefficient ($\log P$) was calculated from the 1-octanol:buffer ratio (o:b), the initial concentration of the analyte in buffer (1 μM), and the concentration of the analyte in buffer (c_B) according to Equation 2:

$$\log P = \log\left(\frac{1\mu\text{M} - c_B}{c_B} \times \frac{1}{o:b}\right) \quad (2)$$

The average of the three $\log P$ values per 1-octanol:buffer ratio was calculated. If the two means obtained for a compound did not differ by more than 0.1 units, the results were accepted.

Aqueous solubility. Solubility was determined in a 96-well format using the μSOL Explorer solubility analyzer (pIon, version 3.4.0.5). For each compound, measurements were performed in

triplicate. Three wells of a deep well plate were filled with 300 μL of PRISMA HT universal buffer, adjusted to pH 7.4 by adding the requested amount of NaOH (0.5 M). Aliquots (3 μL) of a compound stock solution (40-100 mM in DMSO) were added and thoroughly mixed. The final sample concentration was 0.4-1.0 mM, the residual DMSO concentration was 1.0% (v/v). Fifteen hours after initiation of the experiment, the solutions were filtrated (0.2 μm 96-well filter plates) using a vacuum to collect manifold (Whatman Ltd., Maidstone, UK) and to remove any precipitates. Equal amounts of filtrate and 1-propanol were mixed and transferred to a 96-well plate for UV/Vis detection (190 to 500 nm, SpectraMax 190, Molecular Devices, Silicon Valley, CA, USA). The amount of material dissolved was calculated by comparison with the spectra obtained from reference samples, which were prepared by dissolving the compound stock solution in a 1:1 mixture of buffer and 1-propanol (final concentrations 0.067-0.167 mM).

Parallel artificial membrane permeability assay (PAMPA). Effective permeability ($\log P_e$) was determined in a 96-well format with PAMPA.^[27] For each compound, measurements were performed in quadruplicate. Four wells of a deep well plate were filled with 650 μL of PRISMA HT universal buffer, adjusted to pH 7.4 by adding the requested amount of NaOH (0.5 M). Samples (150 μL) were withdrawn from each well to determine the blank spectra by UV/Vis-spectroscopy (190 to 500 nm, SpectraMax 190). The analyte dissolved in DMSO was added to the remaining buffer to yield 50 μM solutions. To exclude precipitation, the optical density (OD) was measured at 650 nm, and solutions exceeding OD 0.01 were filtrated. Afterwards, samples (150 μL) were withdrawn to determine the reference spectra. Further 200 μL were transferred to each well of the donor plate of the PAMPA sandwich (pIon, P/N 110 163). The filter membranes at the bottom of the acceptor plate were infused with 5 μL of GIT-0 Lipid Solution, and 200 μL of Acceptor Sink Buffer were filled into each acceptor well. The sandwich was assembled, placed in the GutBoxTM, and left undisturbed for 16 h. Then, it was disassembled and samples (150 μL) were withdrawn from each donor and acceptor well for detection of the UV/Vis spectra. Effective permeability ($\log P_e$) was calculated from the compound flux deduced from the spectra, the filter area, and the initial sample concentration in the donor well with the aid of the PAMPA Explorer Software (pIon, version 3.5).

Colorectal adenocarcinoma (Caco-2) cell permeation assay. Caco-2 cells were cultivated in tissue culture flasks (BD Biosciences, Franklin Lakes, NJ, USA) with DMEM high glucose medium, containing L-glutamine (2 mM), non-essential amino acids (0.1 mM), penicillin (100 U/mL), streptomycin (100 $\mu\text{g}/\text{mL}$), and fetal bovine serum (10%). The cells were kept at 37 °C in humidified air containing 5% CO_2 , and the medium was changed every second day. When approximately 90% confluence was reached, the cells were split in a 1:10 ratio and distributed to new tissue culture flasks. At passage numbers between 60 and 65, they were seeded at a density of 5.3×10^5 cells per well to Transwell 6-well plates (Corning Inc., Corning, NY, USA) with 2.5 mL of culture medium in the basolateral and 2 mL in the apical compartment. The medium was renewed on alternate days.

Permeation experiments were performed between days 19 and 21 post seeding. Previously to the experiment, the integrity of the Caco-2 monolayers was evaluated by measuring the transepithelial electrical resistance (TEER) with an Endohm tissue resistance instrument (World Precision Instruments Inc., Sarasota, FL, USA). Only wells with TEER values higher than $250 \Omega \text{ cm}^2$ were used. To inhibit carboxylesterase activity, the Caco-2 cell monolayers were pre-incubated with bis(4-nitrophenyl) phosphate (BNPP, $200 \mu\text{M}$) dissolved in transport medium (DMEM without sodium pyruvate and phenol red) for 40 min.^[43] Experiments were performed in the apical-to-basolateral (absorptive) and basolateral-to-apical (secretory) directions in triplicates. Transport medium was withdrawn from the donor compartments and replaced by the same volume of compound stock solution (10 mM in DMSO) to reach an initial sample concentration of $62.5 \mu\text{M}$. The Transwell plate was shaken (600 rpm , $37 \text{ }^\circ\text{C}$) on a Heidolph Titramax 1000 plate-shaker. Samples ($40 \mu\text{L}$) were withdrawn from the donor and acceptor compartments 30 min after initiation of the experiment and the concentrations were determined by LC-MS (see below). Apparent permeability (P_{app}) was calculated according to Equation 3:

$$P_{\text{app}} = \frac{dQ}{dt} \times \frac{1}{A \times c_0} \quad (3)$$

where dQ/dt is the compound flux (in mol s^{-1}), A is the surface area of the monolayer (in cm^2), and c_0 is the initial concentration in the donor compartment (in mol cm^{-3}).^[44] After the experiment, TEER values were assessed again and results from wells with values below $250 \Omega \text{ cm}^2$ were discarded.

Microsomal stability assay. Incubations were performed in duplicate in a 96-well format on an Eppendorf Thermomixer Comfort. The reaction mixture ($270 \mu\text{L}$) consisting of liver microsomes ($0.139 \mu\text{g/mL}$), TRIS-HCl buffer (0.1 M , $\text{pH } 7.4$) and MgCl_2 (2 mM) was preheated ($37 \text{ }^\circ\text{C}$, 500 rpm , 10 min), and the incubation was initiated by adding $30 \mu\text{L}$ of compound solution ($20 \mu\text{M}$ in TRIS-HCl buffer). The final concentration of the compound was $2 \mu\text{M}$, and the microsomal concentration was 0.125 mg/mL . At the beginning of the experiment ($t = 0 \text{ min}$) and after an incubation time of 5, 10, 20, 40, and 60 min, samples ($40 \mu\text{L}$) were transferred to $120 \mu\text{L}$ of ice-cooled MeOH and centrifuged (3600 rpm , $4 \text{ }^\circ\text{C}$, 10 min , 5804 R Eppendorf centrifuge). Then, $80 \mu\text{L}$ of supernatant was transferred to a 96-well plate for analysis by LC-MS (see below). The metabolic half-life ($t_{1/2}$) was calculated from the slope of the linear regression from the log percentage remaining compound versus incubation time relationship. Control experiments were performed in parallel by preincubating the microsomes with the specific carboxylesterase inhibitor BNPP (1 mM) for 5 min before addition of the compound solution.^[45]

LC-MS measurements. Analyses were performed using an 1100/1200 Series HPLC System coupled to a 6410 Triple Quadrupole mass detector (Agilent Technologies, Inc., Santa Clara, CA, USA) equipped with electrospray ionization. The system was controlled with the Agilent MassHunter Workstation Data Acquisition software (version B.01.04). The column used was an Atlantis[®] T3 C18

column (2.1 × 50 mm) with a 3 µm particle size (Waters Corp., Milford, MA, USA). The mobile phase consisted of eluent A: H₂O containing 0.1% formic acid (for **23a-c**, **26a**, **32a-d**, **37**, **42a-f**) or 10 mM ammonium acetate, pH 5.0 in 95:5, H₂O:MeCN (for **4a**, **6-8a**, **26b**); and eluent B: MeCN, containing 0.1% formic acid. The flow rate was maintained at 0.6 mL/min. The gradient was ramped from 95% A/5% B to 5% A/95% B over 1 min, and then hold at 5% A/95% B for 0.1 min. The system was then brought back to 95% A/5% B, resulting in a total duration of 4 min. MS parameters such as fragmentor voltage, collision energy, polarity were optimized individually for each drug, and the molecular ion was followed for each compound in the multiple reaction monitoring mode. The concentrations of the analytes were quantified by the Agilent Mass Hunter Quantitative Analysis software (version B.01.04).

In vivo pharmacokinetic studies.

Eight-week-old female C3H/HeN mice from Harlan (Venray, The Netherlands) weighing between 19 and 25 g were used for the PK study. Three mice were put in one cage and kept under specific pathogen-free conditions in the Animal House of the Department of Biomedicine, University Hospital of Basel. All animal experimentation guidelines according to the regulations of the Swiss veterinary law were followed. The animals had free access to chow and water ad libitum and were kept in a 12 h/12 h light/dark cycle. After one week of acclimatization, the mice were used for the pharmacokinetic study. Compound **41f** was diluted in 5% DMSO in 1% Tween 80 in PBS and applied using an oral gavage at a dose of 10 mg/kg. Blood and urine samples (10 µL) were taken before the experiment (0 min) and at 6, 13, 20, 40 min, 1, 1.5, 2, 3, 4, 6, 8, and 24 h after administration. Samples were diluted in MeOH directly after sampling in a ratio of 1:5 to precipitate proteins. After centrifugation (11 min, 13000 rpm) the supernatant was transferred to a 96-well plate and analyzed by LC-MS as described before. The samples at 0 min were used to define the detection limit in plasma and urine.

Acknowledgement

The authors thank Prof. Dr. med. Radek Skoda, Department of Biomedicine, University Hospital Basel, Switzerland, for giving us access to the animal facility. The financial support by the Swiss National Science Foundation (SNF interdisciplinary grant K-32K1-120904) is gratefully acknowledged.

References

- [1] a) Hooton, T. M.; Stamm, W. E. Diagnosis and treatment of uncomplicated urinary tract infection. *Infect. Dis. Clin. North Am.* **1997**, *11*, 551-581; b) Wiles, T. J.; Kulesus, R. R.; Mulvey, M. A. Origins and virulence mechanisms of uropathogenic *Escherichia coli*. *Exp. Mol. Pathol.* **2008**, *85*, 11-19; c) Fihn, S. D. Acute uncomplicated urinary tract infection in women. *N. Engl. J. Med.* **2003**, *349*, 259-266.

- [2] a) Schilling, J. D.; Hultgren, S. J. Recent advances into the pathogenesis of recurrent urinary tract infections: the bladder as a reservoir for uropathogenic *Escherichia coli*. *Int. J. Antimicrob. Agents* **2002**, *19*, 457-460; b) Blango, M.; Mulvey, M. Persistence of uropathogenic *Escherichia coli* in the face of multiple antibiotics. *Agents Chemother.* **2010**, *54*, 1855-1863.
- [3] Svanborg, C.; Godaly, G. Bacterial virulence in urinary tract infection. *Infect. Dis. Clin. North Am.* **1997**, *11*, 513-529.
- [4] a) Mulvey, M. A. Adhesion and entry of uropathogenic *Escherichia coli*. *Cell Microbiol.* **2002**, *4*, 257-271; b) Eto, D. S.; Jones, T. A.; Sundsbak, J. L.; Mulvey, M. A. Integrin-mediated host cell invasion by type 1-piliated uropathogenic *Escherichia coli*. *PLoS Pathog.* **2007**, *3*, e100.
- [5] Capitani, G.; Eidam, O.; Glockshuber, R.; Grütter, M. G. Structural and functional insights into the assembly of type 1 pili from *Escherichia coli*. *Microbes Infect.* **2006**, *8*, 2284-2290.
- [6] Le Trong, I.; Aprikian, P.; Kidd, B. A.; Forero-Shelton, M.; Tchesnokova, V.; Rajagopal, P.; Rodriguez, V.; Interlandi, G.; Klevit, R.; Vogel, V.; Stenkamp, R. E.; Sokurenko, E. V.; Thomas, W. E. Structural basis for mechanical force regulation of the adhesin FimH via finger trap-like β sheet twisting. *Cell* **2010**, *141*, 645-655.
- [7] Sharon, N. Carbohydrates as future anti-adhesion drugs for infectious diseases. *Biochim. Biophys. Acta* **2006**, *1760*, 527-537.
- [8] a) Firon, N.; Ofek, I.; Sharon, N. Interaction of mannose-containing oligosaccharides with the fimbrial lectin of *Escherichia coli*. *Biochem. Biophys. Res. Commun.* **1982**, *105*, 1426-1432; b) Firon, N.; Ofek, I.; Sharon, N. Carbohydrate specificity of the surface lectins of *Escherichia coli*, *Klebsiella pneumoniae*, and *Salmonella typhimurium*. *Carbohydr. Res.* **1983**, *120*, 235-249; c) Sharon, N. Bacterial lectins, cell-cell recognition and infectious disease. *FEBS Lett.* **1987**, *217*, 145-157.
- [9] Choudhury, D.; Thompson, A.; Stojanoff, V.; Langermann, S.; Pinkner, J.; Hultgren, S. J.; Knight, S. D. X-ray structure of the FimC-FimH chaperone-adhesin complex from uropathogenic *Escherichia coli*. *Science* **1999**, *285*, 1061-1066.
- [10] a) Hung, C. S.; Bouckaert, J.; Hung, D.; Pinkner, J.; Widberg, C.; DeFusco, A.; Auguste, C. G.; Strouse, R.; Langermann, S.; Waksman, G.; Hultgren, S. J. Structural basis of tropism of *Escherichia coli* to the bladder during urinary tract infection. *Mol. Microbiol.* **2002**, *44*, 903-915; b) Bouckaert, J.; Berglund, J.; Schembri, M.; De Genst, E.; Cools, L.; Wuhler, M.; Hung, C. S.; Pinkner, J.; Slattegard, R.; Zavialov, A.; Choudhury, D.; Langermann, S.; Hultgren, S. J.; Wyns, L.; Klemm, P.; Oscarson, S.; Knight, S. D.; De Greve, H. Receptor binding studies disclose a novel class of high-affinity inhibitors of the *Escherichia coli* FimH adhesin. *Mol. Microbiol.* **2005**, *55*, 441-455; c) Wellens, A.; Garofalo, C.; Nguyen, H.; Van Gerven, N.; Slattegard, R.; Hernalsteens, J. P.; Wyns, L.; Oscarson, S.; De Greve, H.; Hultgren, S.; Bouckaert, J. Intervening with urinary tract infections using anti-adhesives based on the crystal structure of the FimH-oligomannose-3 complex. *PLoS ONE* **2008**, *3*, e2040; d) Wellens, A.; Lahmann, M.; Touaibia, M.; Vaucher, J.; Oscarson, S.; Roy, R.; Remaut, H.; Bouckaert, J. The tyrosine gate as a potential entropic lever in the receptor-binding site of the bacterial adhesin FimH. *Biochemistry* **2012**, *51*, 4790-4799.
- [11] a) Firon, N.; Ashkenazi, S.; Mirelman, D.; Ofek, I.; Sharon, N. Aromatic alpha-glycosides of mannose are powerful inhibitors of the adherence of type-1 fimbriated *Escherichia coli* to yeast and intestinal epithelial-cells. *Infect. Immun.* **1987**, *55*, 472-476; b) Lindhorst, T.; Kotter, S.; Kubisch, J.; Krallmann-Wenzel, U.; Ehlers, S.; Kren, V. Effect of p-substitution of aryl α -D-mannosides on inhibiting mannose-sensitive adhesion of *Escherichia coli* - Syntheses and testing. *Eur. J. Org. Chem.* **1998**, 1669-1674; c) Sperling, O.; Fuchs, A.; Lindhorst, T. K. Evaluation of the carbohydrate recognition domain of the bacterial adhesin FimH: Design, synthesis and binding properties of mannoside ligands. *Org. Biomol. Chem.* **2006**, *4*, 3913-3922; d) Han, Z. F.; Pinkner, J. S.; Ford, B.; Obermann, R.; Nolan, W.; Wildman, S. A.; Hobbs, D.; Ellenberger, T.; Cusumano, C. K.; Hultgren, S. J.; Janetka, J. W. Structure-based drug design and optimization of mannoside bacterial FimH antagonists. *J. Med. Chem.* **2010**, *53*, 4779-4792; e) Klein, T.; Abgottspon, D.; Wittwer, M.; Rabbani, S.; Herold, J.; Jiang, X. H.;

- Kleeb, S.; Luthi, C.; Scharenberg, M.; Bezencon, J.; Gubler, E.; Pang, L. J.; Smiesko, M.; Cutting, B.; Schwardt, O.; Ernst, B. FimH antagonists for the oral treatment of urinary tract infections: From design and synthesis to in vitro and in vivo evaluation. *J. Med. Chem.* **2010**, *53*, 8627-8641; f) Schwardt, O.; Rabbani, S.; Hartmann, M.; Abgottspon, D.; Wittwer, M.; Kleeb, S.; Zalewski, A.; Smieško, M.; Cutting, B.; Ernst, B. Design, synthesis and biological evaluation of mannosyl triazoles as FimH antagonists. *Bioorg. Med. Chem.* **2011**, *19*, 6454-6473; g) Cusumano, C. K.; Pinkner, J. S.; Han, Z.; Greene, S. E.; Ford, B. A.; Crowley, J. R.; Henderson, J. P.; Janetka, J. W.; Hultgren, S. J. Treatment and prevention of urinary tract infection with orally active FimH inhibitors. *Sci. Transl. Med.* **2011**, *3*, 109ra115; h) Han, Z. F.; Pinkner, J. S.; Ford, B.; Chorell, E.; Crowley, J. M.; Cusumano, C. K.; Campbell, S.; Henderson, J. P.; Hultgren, S. J.; Janetka, J. W. Lead optimization studies on FimH antagonists: Discovery of potent and orally bioavailable ortho-substituted biphenyl mannosides. *J. Med. Chem.* **2012**, *55*, 3945-3959; i) Jiang, X. H.; Abgottspon, D.; Kleeb, S.; Rabbani, S.; Scharenberg, M.; Wittwer, M.; Haug, M.; Schwardt, O.; Ernst, B. Antiadhesion therapy for urinary tract infections—a balanced PK/PD profile proved to be key for success. *J. Med. Chem.* **2012**, *55*, 4700-4713; j) Pang, L.; Kleeb, S.; Lemme, K.; Rabbani, S.; Scharenberg, M.; Zalewski, A.; Schadler, F.; Schwardt, O.; Ernst, B. FimH antagonists: Structure-activity and structure-property relationships for biphenyl α -D-mannopyranosides. *ChemMedChem* **2012**, *7*, 1404-1422; k) Kleeb, S.; Pang, L.; Mayer, K.; Eris, D.; Sigl, A.; Preston, R. C.; Zihlmann, P.; Sharpe, T.; Jakob, R. P.; Abgottspon, D.; Hutter, A. S.; Scharenberg, M.; Jiang, X.; Navarra, G.; Rabbani, S.; Smiesko, M.; Lüdin, N.; Bezençon, J.; Schwardt, O.; Maier, T.; Ernst, B. FimH antagonists: bioisosteres to improve the in vitro and in vivo PK/PD profile. *J. Med. Chem.* **2015**, *58*, 2221-2239.
- [12] a) Johnson, K. C.; Swindell, A. C. Guidance in the setting of drug particle size specifications to minimize variability in absorption. *Pharm. Res.* **1996**, *13*, 1795-1798; b) Lipinski, C. A. Drug-like properties and the causes of poor solubility and poor permeability. *J. Pharmacol. Toxicol. Methods* **2000**, *44*, 235-249.
- [13] Ishikawa, M.; Hashimoto, Y. Improvement in aqueous solubility in small molecule drug discovery programs by disruption of molecular planarity and symmetry. *J. Med. Chem.* **2011**, *54*, 1539-1554.
- [14] Meanwell, N. A. Synopsis of some recent tactical application of bioisosteres in drug design. *J. Med. Chem.* **2011**, *54*, 2529-2591.
- [15] Yan, R.; Yang, F.; Wu, Y.; Zhang, L.; Ye, X. An efficient and improved procedure for preparation of triflyl azide and application in catalytic diazotransfer reaction. *Tetrahedron Lett.* **2005**, *46*, 8993-8995.
- [16] Rostovtsev, V.; Green, L.; Fokin, V.; Sharpless, K. A stepwise Huisgen cycloaddition process: Copper(I)-catalyzed regioselective “ligation” of azides and terminal alkynes. *Angew. Chem. Int. Ed.* **2002**, *41*, 2596-2599.
- [17] Antilla, J.; Baskin, J.; Barder, T.; Buchwald, S. Copper-diamine-catalyzed *N*-arylation of pyrroles, pyrazoles, indazoles, imidazoles, and triazoles. *J. Org. Chem.* **2004**, *69*, 5578-5587.
- [18] a) Node, M.; Nishide, K.; Fujii, K.; Fujita, E. Hard acid and soft nucleophile system. 2. Demethylation of methyl esters of alcohol and phenol with an aluminum halide-thiol system. *J. Org. Chem.* **1980**, *45*, 4275-4277; b) Node, M.; Kumar, K.; Nishide, K.; Ohsugi, S.; Miyamoto, T. Odorless substitutes for foul-smelling thiols: Syntheses and applications. *Tetrahedron Lett.* **2001**, *42*, 9207-9210.
- [19] Le Bourdonnec, B.; Windh, R.; Leister, L.; Zhou, Q.; Ajello, C.; Gu, M.; Chu, G.; Tuthill, P.; Barker, W.; Koblish, M.; Wiant, D.; Graczyk, T.; Belanger, S.; Cassel, J.; Feschenko, M.; Brogdon, B.; Smith, S.; Derelanko, M.; Kutz, S.; Little, P.; DeHaven, R.; DeHaven-Hudkins, D.; Dolle, R. Spirocyclic delta opioid receptor agonists for the treatment of pain: Discovery of *N,N*-diethyl-3-hydroxy-4-(spiro[chromene-2,4'-piperidine]-4-yl) benzamide (ADL5747). *J. Med. Chem.* **2009**, *52*, 5685-5702.
- [20] Katritzky, A.; Cheng, D.; Musgrave, R. Syntheses of imidazoles and pyrroles: BetMIC and TosMIC as complementary reagents. *Heterocycles* **1997**, *44*, 67-70.

- [21] Scott, I. L.; Market, R. V.; DeOrazio, R. J.; Meckler, H.; Kogan, T. P. Stereospecific α -D-mannosylation. *Carbohydr. Res.* **1999**, *317*, 210-216.
- [22] Prieto, M.; Zurita, E.; Rosa, E.; Munoz, L.; Lloyd-Williams, P.; Giralt, E. Arylboronic acids and arylpinacolboronate esters in Suzuki coupling reactions involving indoles. Partner role swapping and heterocycle protection. *J. Org. Chem.* **2004**, *69*, 6812-6820.
- [23] Rabbani, S.; Jiang, X. H.; Schwardt, O.; Ernst, B. Expression of the carbohydrate recognition domain of FimH and development of a competitive binding assay. *Anal. Biochem.* **2010**, *407*, 188-195.
- [24] Glide, version 5.7, Schrödinger, LLC, New York, NY, **2011**.
- [25] Dearden, J. C.; Bresnen, G. M. The measurement of partition coefficients. *Quant. Struct.-Act. Rel.* **1988**, *7*, 133-144.
- [26] Avdeef, A. High-throughput measurements of solubility profiles. In *Pharmacokinetic Optimization in Drug Research; Biological, Physicochemical and Computational Strategies* (Eds.: Testa, B.; van de Waterbeemd, H.; Folkers, G.; Guy, R.), Verlag Helvetica Chimica Acta, Zurich, **2001**, pp 305-326.
- [27] Kansy, M.; Senner, F.; Gubernator, K. Physicochemical high throughput screening: Parallel artificial membrane permeation assay in the description of passive absorption processes. *J. Med. Chem.* **1998**, *41*, 1007-1010.
- [28] Artursson, P.; Karlsson, J. Correlation between oral-drug absorption in humans and apparent drug permeability coefficients in human intestinal epithelial (Caco-2) cells. *Biochem. Biophys. Res. Commun.* **1991**, *175*, 880-885.
- [29] Imai, T.; Taketani, M.; Shii, M.; Hosokawa, M.; Chiba, K. Substrate specificity of carboxylesterase isozymes and their contribution to hydrolase activity in human liver and small intestine. *Drug Metab. Dispos.* **2006**, *34*, 1734-1741.
- [30] a) Wadkins, R. M.; Morton, C. L.; Weeks, J. K.; Oliver, L.; Wierdl, M.; Danks, M. K.; Potter, P. M. Structural constraints affect the metabolism of 7-ethyl-10-[4-(1-piperidino)-1-piperidino]carbonyloxycamptothecin (CPT-11) by carboxylesterases. *Mol. Pharmacol.* **2001**, *60*, 355-362; b) Hatfield, J. M.; Wierdl, M.; Wadkins, R. M.; Potter, P. M. Modifications of human carboxylesterase for improved prodrug activation. *Expert Opin. Drug Metab. Toxicol.* **2008**, *4*, 1153-1165; c) Vistoli, G.; Pedretti, A.; Mazzolari, A.; Testa, B. In silico prediction of human carboxylesterase-1 (hCES1) metabolism combining docking analyses and MD simulations. *Bioorg. Med. Chem.* **2010**, *18*, 320-329.
- [31] MacroModel, version 9.9, Schrödinger, LLC, New York, NY, **2012**. Torsion angle measurements are based on the lowest-energy conformers.
- [32] Satoh, T.; Hosokawa, M. Structure, function and regulation of carboxylesterases. *Chem. Bio. Interact.* **2006**, *162*, 195-211.
- [33] a) AMSOL, version 7.1, by Hawkins, G. D.; Giesen, D. J.; Lynch, G. C.; Chambers, C. C.; Rossi, I.; Storer, J. W.; Li, J.; Thompson, J. D.; Winget, P.; Lynch, B. J.; Rinaldi, D.; Liotard, D. A.; Cramer, C. J.; Truhlar, D. G. University of Minnesota, Minneapolis, **2003**, based in part on AMPAC, version 2.1 by Liotard, D. A.; Healy, E. F.; Ruiz, J. M.; Dewar, M. J. S.; b) Storer, J.; Giesen, D.; Cramer, C.; Truhlar, D. Class-IV charge models – a new semiempirical approach in quantum-chemistry. *J. Comput. Aided Mol. Des.* **1995**, *9*, 87-110; c) Dewar, M.; Zoebisch, E.; Healy, E.; Stewart, J. The development and use of quantum mechanical molecular models. 76. AM1: A new general-purpose quantum mechanical molecular model. *J. Am. Chem. Soc.* **1985**, *107*, 3902-3909.
- [34] Avdeef, A.; Bendels, S.; Di, L.; Faller, B.; Kansy, M.; Sugano, K.; Yamauchi, Y. PAMPA – critical factors for better predictions of absorption. *J. Pharm. Sci.* **2007**, *96*, 2893-2909.
- [35] Lin, J. H. Drug-drug interaction mediated by inhibition and induction of P-glycoprotein. *Adv. Drug Deliv. Rev.* **2003**, *21*, 53-81.

-
- [36] Nikolovska-Coleska, Z.; Wang, R.; Fang, X.; Pan, H.; Tomita, Y.; Li, P.; Roller, P.; Krajewski, K.; Saito, N.; Stuckey, J.; Wang, S. Development and optimization of a binding assay for the XIAP BIR3 domain using fluorescence polarization. *Anal. Biochem.* **2004**, *332*, 261-273.
- [37] Scharenberg, M.; Jiang, X.; Pang, L.; Navarra, G.; Rabbani, S.; Binder, F.; Schwardt, O.; Ernst, B. Kinetic properties of carbohydrate-lectin interactions: FimH antagonists. *ChemMedChem* **2014**, *1*, 78-83.
- [38] Smith, D. A.; Jones, B. C.; Walker, D. K. Design of drugs involving the concepts and theories of drug metabolism and pharmacokinetics. *Med. Res. Rev.* **1996**, *16*, 243-266.
- [39] van de Waterbeemd, H.; Smith, D.; Beaumont, K.; Walker, D. Property-based design: Optimization of drug absorption and pharmacokinetics. *J. Med. Chem.* **2001**, *44*, 1313-1333.
- [40] van Breemen, R. B.; Li, Y. Caco-2 cell permeability assays to measure drug absorption. *Expert Opin. Drug. Metab. Toxicol.* **2005**, *1*, 175-185.
- [41] Varma, M. V.; Feng, B.; Obach, R. S.; Troutman, M. D.; Chupka, J.; Miller, H. R.; El-Kattan, A. Physicochemical determinants of human renal clearance. *J. Med. Chem.* **2009**, *52*, 4844-4852.
- [42] a) VCCLAB, Virtual Computational Chemistry Laboratory, **2005**, <http://www.vcclab.org> (accessed March 25, 2013); b) Tetko, I. V.; Gasteiger, J.; Todeschini, R.; Mauri, A.; Livingstone, D.; Ertl, P.; Palyulin, V. A.; Radchenko, E. V.; Zefirov, N. S.; Makarenko, A. S.; Tanchuk, V. Y.; Prokopenko, V. V. Virtual computational chemistry laboratory-design and description. *J. Comput. Aided Mol. Des.* **2005**, *19*, 453-463.
- [43] Ohura, K.; Sakamoto, H.; Ninomiya, S.; Imai, T. Development of a novel system for estimating human intestinal absorption using Caco-2 cells in the absence of esterase activity. *Drug Metab. Dispos.* **2010**, *38*, 323-331.
- [44] Hubatsch, I.; Ragnarsson, E. G.; Artursson, P. Determination of drug permeability and prediction of drug absorption in Caco-2 monolayers. *Nat. Protoc.* **2007**, *2*, 2111-2119.
- [45] Taketani, M.; Shii, M.; Ohura, K.; Ninomiya, S.; Imai, T. Carboxylesterase in the liver and small intestine of experimental animals and human. *Life Sci.* **2007**, *81*, 924-932.

2.5 **Paper 4: FimH antagonists: structure-activity and structure-property relationships for biphenyl α -D-mannopyranosides**

The following report explores diverse modifications of the biphenyl α -D-mannopyranoside, notably the introduction of *ortho*-substituents on the inner ring (A) of the biphenyl aglycone, the introduction of a methylene spacer between the anomeric oxygen and the biphenyl moiety, as well as the extension of the *para*-substituent on the terminal ring (B). The benefits of these approaches on the pharmacological activity and the physicochemical profile are thoroughly exposed.

Contribution to the project:

Simon Kleeb performed or supervised all experiments regarding the physicochemical and *in vitro* pharmacokinetic characterization and interpreted the resulting data. He furthermore described the determination of the pharmacokinetic parameters in the experimental section of the paper and revised the entire manuscript.

This paper was published in *ChemMedChem*:

Pang, L.*; Kleeb, S.*; Lemme, K.*; Rabbani, S.*; Scharenberg, M.; Zalewski, A.; Schädler, F.; Schwardt, O.; Ernst, B. FimH antagonists: structure-activity and structure-property relationships for biphenyl α -D-mannopyranosides. *ChemMedChem* **2012**, 7, 1404-1422.

* These authors contributed equally to the project.

© 2012 Wiley-VCH Verlag GmbH & Co. KGaA, Weinheim

DOI: 10.1002/cmdc.201200125

VIP

FimH Antagonists: Structure–Activity and Structure–Property Relationships for Biphenyl α -D-Mannopyranosides

Lijuan Pang, Simon Kleeb, Katrin Lemme, Said Rabbani, Meike Scharenberg, Adam Zalewski, Florentina Schädler, Oliver Schwardt, and Beat Ernst^{*[a]}

Urinary tract infections (UTIs) are caused primarily by uropathogenic *Escherichia coli* (UPEC), which encode filamentous surface-adhesive organelles called type 1 pili. FimH is located at the tips of these pili. The initial attachment of UPEC to host cells is mediated by the interaction of the carbohydrate recognition domain (CRD) of FimH with oligomannosides on urothelial cells. Blocking these lectins with carbohydrates or analogues thereof prevents bacterial adhesion to host cells and therefore offers a potential therapeutic approach for prevention and/or treatment of UTIs. Although numerous FimH antagonists have been developed so far, few of them meet the requirement for clinical application due to poor pharmacokinetics. Additionally, the binding mode of an antagonist to the

CRD of FimH can switch from an in-docking mode to an out-docking mode, depending on the structure of the antagonist. In this communication, biphenyl α -D-mannosides were modified to improve their binding affinity, to explore their binding mode, and to optimize their pharmacokinetic properties. The inhibitory potential of the FimH antagonists was measured in a cell-free competitive binding assay, a cell-based flow cytometry assay, and by isothermal titration calorimetry. Furthermore, pharmacokinetic properties such as $\log D$, solubility, and membrane permeation were analyzed. As a result, a structure–activity and structure–property relationships were established for a series of biphenyl α -D-mannosides.

Introduction

Urinary tract infections (UTIs), the most prevalent series of infectious diseases worldwide, affect millions of people and account for significant morbidity as well as high medical costs.^[1] The primary cause of UTIs are strains of uropathogenic *Escherichia coli* (UPEC), which make up 70–95% of reported cases.^[1a,2] UTIs are treated with antibiotics; however, recurrent infections by UPEC with subsequent antibiotic exposure can lead to the emergence of antimicrobial resistance.^[3]

Adhesion to host cells is the initial step of microbial infection. To gain an initial foothold within the bladder, UPEC strains encode filamentous surface-adhesive organelles called type 1 pili (fimbriae).^[4] They mediate bacterial attachment to uroplakin Ia, a glycoprotein located on urothelial cells. This initial step prevents the clearance of *E. coli* by the bulk flow of urine and facilitates the invasion of host cells.^[1b,5] A bacterial lectin known as FimH is located at the tips of type 1 pili. The carbohydrate recognition domain (CRD) of this lectin is responsible for binding to the complementary carbohydrate epitope of the host tissue. Blocking this lectin by a carbohydrate or a glycomimetic thereof offers a potential therapeutic approach for prevention and/or treatment of UTIs.^[6]

More than two decades ago, Sharon and co-workers explored various mannosides and oligomannosides as potential antagonists for type 1 pili-mediated bacterial adhesion and observed interactions in the micro- to millimolar range.^[7] The first crystal structure of FimH was solved in 1999,^[8] and since then, numerous crystallographic studies have been reported, greatly facilitating the design of high-affinity ligands.^[9] In summary,

the reported affinities can be rationalized on the basis of the structure of FimH: First, the binding pocket accommodates the mannose with the hydroxy groups forming an extended hydrogen bond network. Second, the entrance to the binding site, referred to as the “tyrosine gate”, is formed by three hydrophobic amino acids (Tyr48, Tyr137, and Ile52)^[9a] and can host aliphatic and aromatic aglycones.


As a consequence of hydrophobic contacts of the alkyl aglycone, *n*-heptyl α -D-mannopyranoside (**1**) exhibits nanomolar affinity.^[9b] With aromatic aglycones such as **2–5** (Figure 1), further improvements in affinity were observed.^[10] To explore the binding mode and to improve affinity as well as ADME properties, a series of biphenyl FimH antagonists were synthesized.

Results and Discussion

An unexpected docking mode was discovered upon co-crystallization of biphenyl mannoside **3** with the FimH CRD.^[10d] Whereas the alkyl aglycone of *n*-butyl α -D-mannopyranoside^[9b]

[a] L. Pang,⁺ S. Kleeb,⁺ Dr. K. Lemme,⁺ Dr. S. Rabbani,⁺ Dr. M. Scharenberg, A. Zalewski, F. Schädler, Dr. O. Schwardt, Prof. Dr. B. Ernst
Institute of Molecular Pharmacy, Pharmazentrum, University of Basel
Klingelbergstrasse 50, 4056 Basel (Switzerland)
E-mail: beat.ernst@unibas.ch

[*] These authors contributed equally to this work.

 Supporting information for this article is available on the WWW under <http://dx.doi.org/10.1002/cmdc.201200125>.

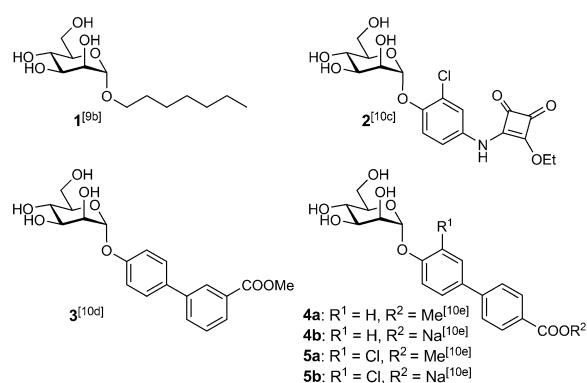


Figure 1. FimH antagonists: *n*-heptyl α -D-mannopyranoside (**1**) is used as reference compound; the squaric acid derivative **2** and biphenyl derivatives **3–5** exhibit nanomolar affinities.

interacts with both Tyr48 and Tyr137 of the tyrosine gate (in-docking mode),^[10f] the biphenyl aglycone adopts the out-docking mode; that is, it interacts only with Tyr48 (Figure 2A), probably due to insufficient flexibility; π - π stacking of the outer aromatic ring of the biphenyl aglycone (ring B) with Tyr48 is effected by induced fit: a substantial move of Tyr48. Moreover, further stabilization of the protein–ligand complex by polar interaction between the ester in the *meta* position of **3** and the side chain of Arg98 was proposed.^[10d]

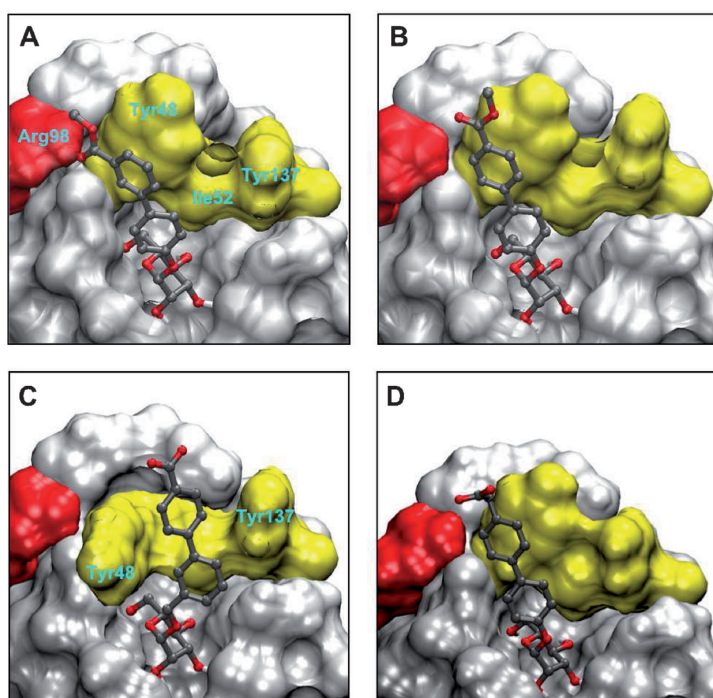


Figure 2. A) Crystal structure of biphenyl **3** (PDB ID: 3MCY)^[10d] bound to the FimH CRD. B–D) In silico docking studies obtained with flexible docking (Glide software package)^[11] to the same FimH CRD structure; top-scored binding mode of B) **4a**, C) **6**, and D) **7**.

In silico docking studies with biphenyl derivative **4a**^[10e] suggested a similar out-docking mode (Figure 2B). A close inspection revealed empty space between the *ortho* position of the aromatic ring adjacent to the anomeric center (ring A) and the protein surface. Indeed, with an *ortho*-chloro substituent (\rightarrow **5a**, Figure 1), affinity was substantially improved. Further studies with FimH antagonists that exhibit enhanced flexibility (e.g., compound **6**; Figure 2C and Figure 3) indicated a switch from the out-docking mode to the in-docking mode. However, whether an optimal π - π stacking within the tyrosine gate can be realized remains to be determined. Finally, docking studies also indicated that elongation of the carboxylate-bearing *para* substituent enables a polar interaction between the carboxylate and Arg98 (e.g., compound **7**; Figure 2D and Figure 3).

Starting from antagonist **4**, we explored three types of modifications (Figure 3):

- 1) For optimizing the van der Waals contact between the *ortho* position of ring A and the binding pocket, a series of substituents — F, CH₃, CF₃, OCH₃, cyclopropyl, and CN — were introduced as depicted in Scheme 1.
- 2) To determine whether the out-docking mode reported for **3**^[10d] results from insufficient flexibility, we increased the aglycone flexibility by introducing a methylene spacer between the anomeric oxygen and ring A of the biphenyl moiety (Scheme 2). This should decrease the conformational constraints to allow an optimized spatial arrangement of the aglycone in the tyrosine gate (\rightarrow **6**, Figure 2C); at the same time, water solubility should be improved as a result of the decreased stacking tendency derived from disruption of the symmetry of the aglycone.^[15]
- 3) To enable a polar interaction between the carboxylate substituent on ring B with Arg98 of FimH, we extended the *para* substituent of **4**, that is, we replaced it with either a flexible methyl ethanolate or a rigid methyl cyclopropanecarboxylate (Scheme 3). Biphenyl α -D-mannoside **24**^[10d] shows a three- to eightfold lower affinity for FimH than its counterparts with a methoxycarbonyl substituent at the *meta* (\rightarrow **3**)^[10d] or *para* positions (\rightarrow **4**)^[10e] of ring B (Table 1). Han et al. assigned the increased affinity of compound **3** to a polar interaction of the ester with Arg98 of FimH.^[10d] Because for spatial reasons the ester in the

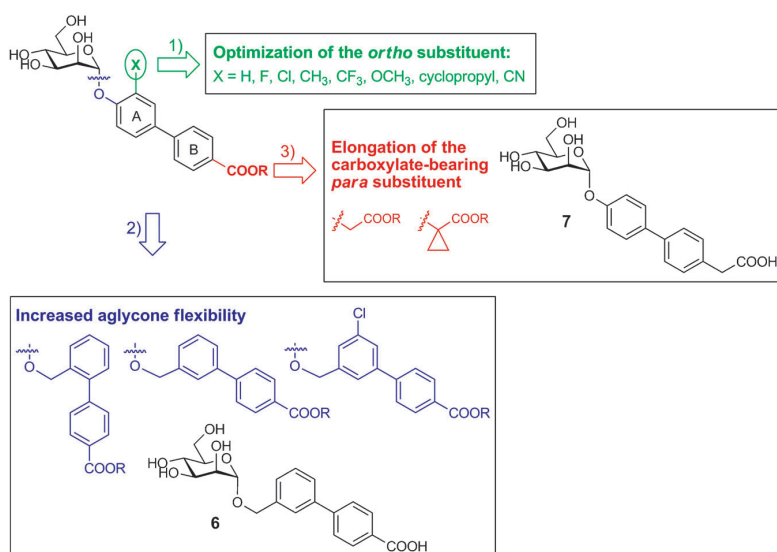


Figure 3. Modifications to the aglycone of FimH antagonists by 1) optimization of the *ortho* substituent, 2) an increase in the flexibility of the aglycone, and 3) elongation of the carboxylate-bearing *para* substituent.

para-substituted derivative **4** cannot establish a similar interaction with Arg98, the substantial improvement in affinity may result from solvation effects.

Synthesis

Optimization of *ortho* substituents (Scheme 1)

Mannosylation of phenols **9a–f** with mannosyl fluoride **8** and BF₃·OEt₂ as promoter yielded α -mannosides **10a–f** stereospecifically.^[12] Whereas the phenols **9a–d** and **9f** are commercially available, the cyclopropyl derivative **9e** was prepared via tandem carbolithiation/1,3-elimination according to Ocasio and Scanlan.^[13] In a palladium-catalyzed Miyaura–Suzuki coupling^[14] of **10a–f** with 4-methoxycarbonylphenylboronic acid (**11**), biphenyls **12a–f** were obtained in good to excellent yields. Deacetylation using Zemplén conditions (\rightarrow **13a–f**) followed by saponification of the methyl esters gave the test compounds **14a–e**. Owing to the instability of the cyano group under aqueous basic conditions, **14f** was synthesized by coupling **10f** with 4-carboxyphenylboronic acid pinacol ester (**15**) followed by transesterification under Zemplén conditions to avoid the final saponification with aqueous sodium hydroxide.

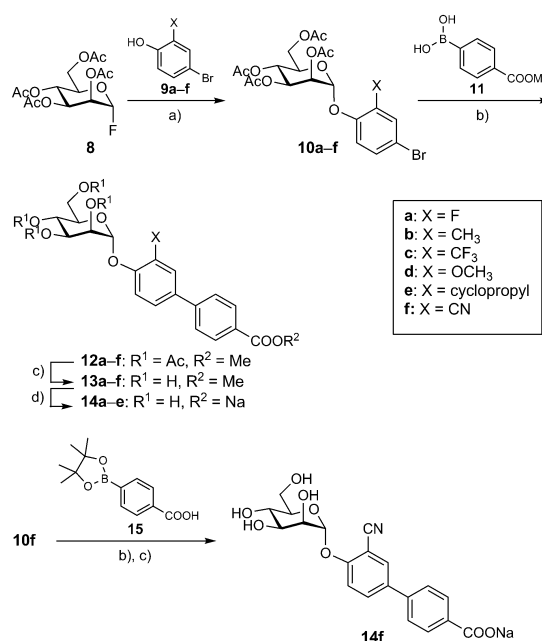
Increase in aglycone flexibility (Scheme 2)

Benzyl alcohols **16a–c** were first mannosylated with donor **8**^[12] to yield the benzyl mannosides **17a–c**. Subsequent cross-coupling with 4-methoxycarbonylphenylboronic acid (**11**) afforded acetates **18a,b** and **21**. Deacetylation of the mannose moiety

(\rightarrow **19a,b** and **22**) followed by saponification of the methyl esters gave compounds **6**, **20**, and **23**.

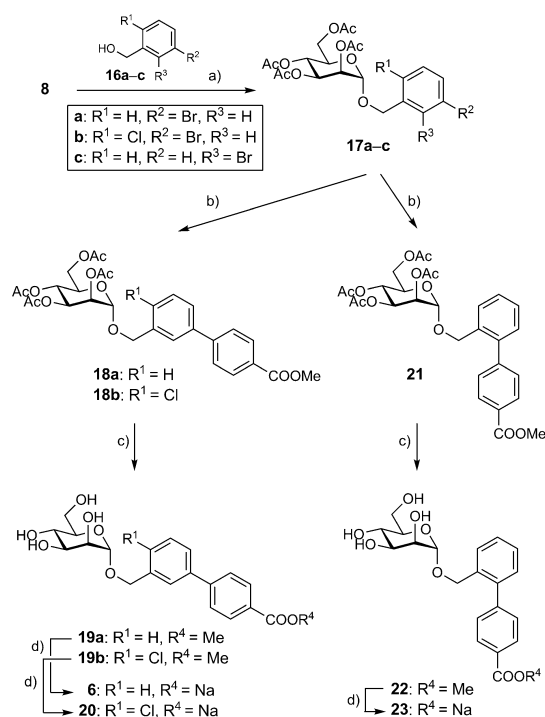
Elongation of the carboxylate-bearing *para* substituent (Scheme 3)

Peracetylated mannose **25** was treated with 4-iodophenol in the presence of BF₃·Et₂O. The resulting iodide **26** was transformed into boronic acid pinacol ester **27**, which was coupled with 4-bromophenylacetic acid methyl ester (**28**) and 4-bromophenylcyclopropylcarboxylic acid methyl ester (**32**) under Miyaura–Suzuki coupling conditions^[14] to yield biphenyls **29** and **33**. Deacetylation with sodium methoxide (\rightarrow

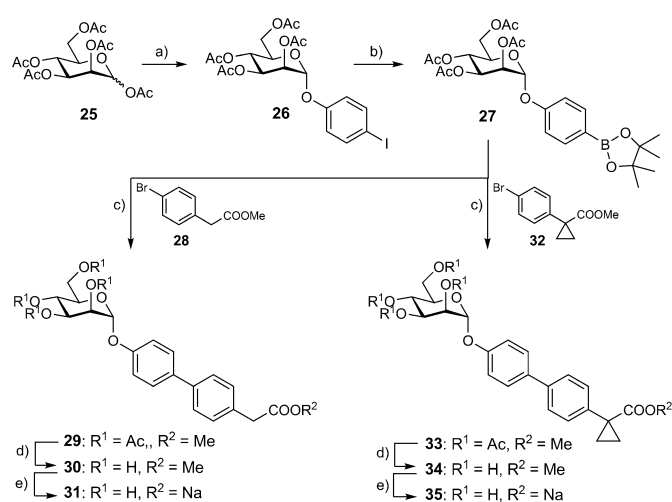


Scheme 1. Reagents and conditions: a) BF₃·Et₂O, CH₂Cl₂, 0 °C, 3 h (**10a–f**, 73–86%); b) Pd(Cl₂)dppf·CH₂Cl₂, K₃PO₄, DMF, 80 °C, overnight (**12a–f**, 55–91%); c) NaOMe, MeOH, RT, 4 h (**13a–e**, **14f**, 52–73%); d) 1. 0.2 N NaOH_(aq), MeOH, RT, overnight; 2. Dowex (Na⁺), size-exclusion chromatography (P-2 gel) (**14a–e**, 15–74%).

30 and **34**) followed by saponification of the methyl ester yielded the sodium salts **31** and **35**.



Scheme 2. Reagents and conditions: a) $\text{BF}_3 \cdot \text{Et}_2\text{O}$, CH_2Cl_2 , 0 °C, 3 h (**17a-c**, 34–48%); b) 4-methoxycarbonylphenylboronic acid (**11**), $\text{Pd}(\text{Cl}_2)\text{dppf} \cdot \text{CH}_2\text{Cl}_2$, K_3PO_4 , DMF, 80 °C, overnight (**18a,b** and **21**, 73–94%); c) NaOMe, MeOH, RT, 4 h (**19a,b** and **22**, 47–90%); d) 1. 0.2 N NaOH_{aq} , MeOH, RT, overnight; 2. Dowex (Na^+), size-exclusion chromatography (P-2 gel) (**6**, **20** and **23**, 10–96%).



Scheme 3. Reagents and conditions: a) 4-iodophenol, $\text{BF}_3 \cdot \text{Et}_2\text{O}$, CH_2Cl_2 , 40 °C, overnight (70%); b) bis(pinacolato)diboron, $\text{Pd}(\text{Cl}_2)\text{dppf} \cdot \text{CH}_2\text{Cl}_2$, KOAc, DMF, MW 120 °C, 2 h (50%); c) $\text{Pd}(\text{Cl}_2)\text{dppf} \cdot \text{CH}_2\text{Cl}_2$, K_3PO_4 , DMF, 80 °C, overnight (34–56%); d) NaOMe, MeOH, RT, 4 h (33–95%); e) 1. 0.2 N NaOH_{aq} , MeOH, RT, overnight; 2. Dowex (Na^+), size-exclusion chromatography (P-2 gel) (**31**: 40%; **35**: 23%).

Binding affinity and activity

The biphenyl α -D-mannosides with varying *ortho* substituents (**5a–b**, **13a–f**, **14a–f**), increased aglycone flexibility (**6**, **19**, **20**, **22**, **23**), and elongated carboxylate-bearing *para* substituents (**30**, **31**, **34**, **35**) were evaluated in vitro by two competitive assay formats (Table 1). All antagonists were tested in a cell-free competitive binding assay.^[16] Subsequently, the best candidates were investigated in a cell-based flow cytometry assay.^[17]

The cell-free competitive binding assay is based on the interaction of a biotinylated polyacrylamide glycopolymer as competitor with the isolated CRD of FimH. In contrast, the cell-based flow cytometry assay involves the infection of human urinary bladder epithelial carcinoma cells with GFP-labeled UPECs expressing the complete type 1 pili (see the Experimental Section below for details). The competitors in the former assay are thus polymer-bound trimannosides, whereas in the latter the antagonists compete with more potent high-mannose oligosaccharides present on uroplakin Ia, which is located on the surface of human urinary bladder cells.^[18,19] The interaction is further affected by the presence of high- and low-affinity states of the CRD of FimH. Aprikian et al. experimentally demonstrated that in full-length fimbriae, the pilin domain stabilizes the CRD domain in the low-affinity state, whereas the CRD domain alone adopts the high-affinity state.^[20] Furthermore, it was recently shown that shear stress can induce a conformational switch (twist in the β -sandwich fold of the CRD domain), resulting in improved affinity.^[21] Therefore, differing affinities were expected in the cell-based flow cytometry assay, in which full-length fimbriae are present, relative to the cell-free competitive binding assay.

Cell-free competitive binding assays^[16]

These assays were performed twice for every compound with each concentration in duplicate. To ensure comparability between various antagonists, the reference compound *n*-heptyl α -D-mannopyranoside **1**^[22] was tested each time in parallel. The affinities are reported relative to **1** as rIC_{50} in Table 1. A comparison of the affinities of compounds **4a** and **4b** with the *ortho*-substituted analogues **5a**, **13a–f** and **5b**, **14a–f** clearly demonstrates that *ortho* substituents on ring A indeed improve binding. However, the differences between the various substituted FimH antagonists are small. For a better understanding of these results, a more detailed analysis of the thermodynamic profile by isothermal titration calorimetry (ITC) was performed (see below). By increasing the flexibility of the aglycone, we expected a switch from the out-docking mode as present for antagonists **3** and **4** (Figure 2A,B) to the in-docking mode (represented by antagonist **6** in Figure 2C).^[10f] However, affinities for all six representatives with increased spacer length between carbohydrate and aglycone (Table 1: **6**, **19**, **20**, **22**, and **23**) were dramatically decreased. A similar tendency was observed

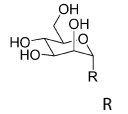
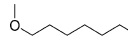
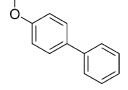
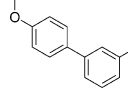
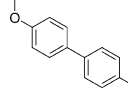
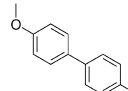
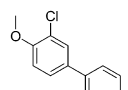
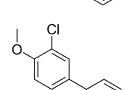
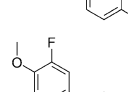
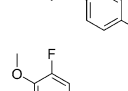
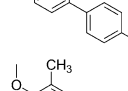
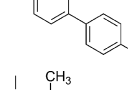
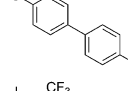
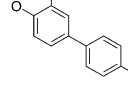
Table 1. Pharmacodynamic parameters of FimH antagonists.				
Compd		Binding assay		Flow cytometry
		IC ₅₀ [nM] ^[a]	rIC ₅₀ ^[b]	IC ₅₀ [μM] ^[a,c]
1 ^[10e]		73 ± 7.9	1	3.9 ± 1.6
24 ^[10d]		84.9	1.47	n.d.
3 ^[10d]		28.6	0.55	n.d.
4a ^[10e]		10.4 ± 1.2	0.14	n.d.
4b ^[10e]		17.1 ± 2.2	0.15	n.d.
5a		4.8 ± 1.2	0.06	n.d.
5b		6.7 ± 2.1	0.09	0.33 ± 0.05
13a		8.0	0.14	n.d.
14a		33.5	0.58	1.54 ± 0.31
13b		23.3	0.40	n.d.
14b		9.2	0.16	1.83 ± 0.14
13c		2.6	0.04	n.d.
14c		8.9	0.15	0.89 ± 0.10

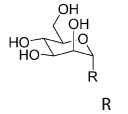
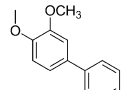
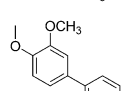
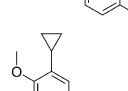
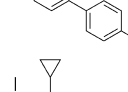
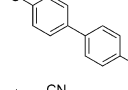
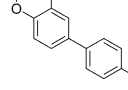
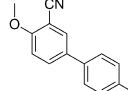
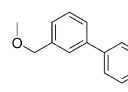
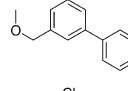
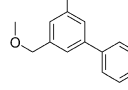
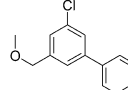
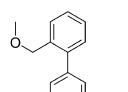
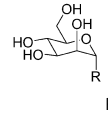
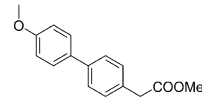
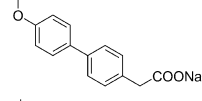
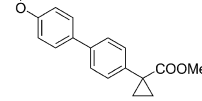
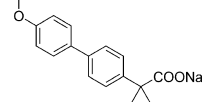
Table 1. (Continued)				
Compd		Binding assay		Flow cytometry
		IC ₅₀ [nM] ^[a]	rIC ₅₀ ^[b]	IC ₅₀ [μM] ^[a,c]
13d		3.5	0.06	n.d.
14d		4.8	0.08	1.95 ± 0.36
13e		31.7	0.55	n.d.
14e		63.0	1.09	4.85 ± 0.79
13f		22.5	0.39	n.d.
14f		33.9	0.58	n.d.
19a		56.1	0.97	n.d.
6		107.9	1.87	n.d.
19b		98.9	1.7	n.d.
20		142.2	2.44	n.d.
22		85.8	1.49	n.d.
23		642.0	11.14	n.d.

Table 1. (Continued)				
Compd		Binding assay		Flow cytometry
		IC ₅₀ [nM] ^[a]	rIC ₅₀ ^[b]	IC ₅₀ [μM] ^[a,c]
30		63.2	1.09	n.d.
31		70.5	1.21	n.d.
34		49.5	0.85	n.d.
35		62.5	1.07	n.d.

[a] IC₅₀ values were determined in a cell-free competitive binding assay.^[16]
 [b] The rIC₅₀ values were calculated by dividing the IC₅₀ of the compound of interest by that of reference compound **1**; this leads to rIC₅₀ values < 1 for derivatives that bind better than reference **1**, and rIC₅₀ values > 1 for compounds with lower affinity than **1**. [c] The anti-adhesion potential to human epithelial bladder cells was determined in the flow cytometry assay;^[17] n.d. = not determined.

for the biphenyls with an elongated carboxylate-bearing *para* substituent (Table 1: **30**, **31**, **34**, and **35**). It was previously described that the ester of **3** is placed within hydrogen bonding distance to form a polar interaction with Arg98 and Glu50.^[10d] However, an improvement of affinity provided by a similar polar interaction between Arg98 and the antagonists **31** and **35** could not be achieved, probably due to the high desolvation penalty of Arg98. Finally, it is important to note that the free acids (sodium salt) of the antagonists in general showed slightly lower affinities than their methyl ester counterparts, with the only exceptions of **13b** and **14b** (Table 1). However, because the esters are thought to act as prodrugs and to be rapidly cleaved after oral application,^[10e] the affinities of the carboxylates are relevant with regard to the therapeutic potential of the present FimH antagonists.

Cell-based flow cytometry assay^[17]

These assays were performed in duplicate/triplicate, and *n*-heptyl α -D-mannopyranoside **1** was used as reference compound with an IC₅₀ value of 3.9 ± 1.6 μM. The most potent antagonists **5b** and **14c** (Table 1) showed respective IC₅₀ values of 0.33 ± 0.05 and 0.89 ± 0.10 μM. In general, the activities obtained from the flow cytometry assay were ~50-fold lower than the affinities determined in the target-based competitive assay (see above).

Isothermal titration calorimetry

Because the biological *in vitro* evaluation only revealed small differences between affinities, ITC experiments were carried out to study the thermodynamic profile of the variously *ortho*-substituted biphenyl compounds **5b** and **14a–f** in binding to FimH. ITC directly measures the heat of interaction (change in enthalpy, ΔH) at a constant temperature on titrating two compounds of known concentration that form an equilibrium complex.^[23] It includes contributions from all equilibria that occur as the interacting molecules go from the free to the bound state, including those associated with solvent interactions and macromolecular conformational changes. The noncovalent interaction between a protein and a ligand can be quantified by the change in free energy (ΔG), consisting of the change in enthalpy (ΔH) and change in entropy (ΔS) [Eq. (1)].^[24] The binding energy under standard conditions (ΔG°), in which all reactants and products are at a concentration of 1 M, can be calculated from the dissociation constant, K_D [Eq. (2)]. With ITC, K_D and ΔH can be measured directly, whereas ΔG and the entropy term $T\Delta S$ are calculated according to Equations (1) and (2).

$$\Delta G = \Delta H - T\Delta S \quad (1)$$

$$\Delta G = RT \ln K_D \quad (2)$$

A favorable enthalpy term ΔH is associated with hydrogen bond formation, electrostatic, and dipole–dipole interactions at the overcompensation of the desolvation penalty.^[25] The entropy term ΔS reflects the overall change in the degrees of freedom of a system. It can be dissected into translational and rigid body rotational entropy,^[26] solvation entropy,^[27] and entropy costs related to conformational changes of protein and ligand [Eq. (3)].^[28] Whereas the formation of a protein–ligand complex is always associated with a decrease in translational and rotational freedom and therefore with entropy costs, the entropic contribution involving changes in solvation (ΔS_{solv}) and changes in rotational and vibrational entropy due to the loss of conformational flexibility (ΔS_{conf}) can differ both in sign and magnitude.^[29]

$$\Delta S = \Delta S_{\text{solv}} + \Delta S_{\text{trans/rot}} + \Delta S_{\text{conf}} \quad (3)$$

The FimH CRD was used for the ITC experiments. It was prepared from FimH-CRD-Th-His₆ (see *Competitive binding assay*, Experimental Section below) by incubation with thrombin, as described earlier.^[16]

The thermodynamic fingerprints of the various biphenyl derivatives (Table 2, Figure 4) reveal a significant improvement in the enthalpic term ($\Delta\Delta H$ -4.3 to -11.2 kJ mol⁻¹) for all substituted biphenyls (**5b**, **14a–f**) in comparison with the unsubstituted derivative **4b**. The largest enthalpy improvement was observed for the trifluoromethyl group (**14c**; Table 2). Interestingly, these largely improved enthalpic contributions are mostly compensated by entropic penalties ($-T\Delta\Delta S$ $+3.2$ to $+7.5$ kJ mol⁻¹), resulting in only marginally improved K_D values. In the best case, the trifluoromethyl derivative **14c**, a fourfold improvement in K_D was measured. Similar, but less pronounced

Table 2. Binding thermodynamics of FimH antagonists determined by ITC.

Compd	R	K_D [nM]	ΔG° [kJ mol ⁻¹]	ΔH° [kJ mol ⁻¹]	$-T\Delta S^\circ$ [kJ mol ⁻¹]	$N^{[a]}$	V_{vdW} [Å ³] ^[b]
4b	H	14.1	-44.8	-47.3	+2.5	1.00	7.2
5b	Cl	3.7	-48.1	-55.5	+7.4	1.01	22.4
14a	F	9.2	-45.9	-51.6	+5.7	1.00	13.3
14b	Me	4.8	-47.5	-56.2	+8.7	1.01	26.7
14c	CF ₃	3.2	-48.5	-58.5	+10.0	1.02	41.4
14d	OMe	7.7	-46.3	-52.5	+6.2	1.02	34.8
14e	cPr	6.9	-46.6	-46.7	+0.1	1.01	52.5
14f	CN	7.4	-46.4	-55.0	+8.6	1.01	29.7

[a] Molar ratio of protein/ligand. [b] van der Waals volumes (V_{vdW}) of the *ortho* substituent were calculated with the Phase volCalc utility.^[30]

effects were observed for most other *ortho* substituents. This trend was broken only by the cyclopropyl derivative **14e** ($\Delta\Delta H$ +0.7 kJ mol⁻¹, $-T\Delta\Delta S$ -2.4 kJ mol⁻¹; Table 2).

The influence of the *ortho* substituent on binding can be attributed to three factors. First, *ortho* substituents of appropriate volume establish an improved shape complementarity within the binding pocket, leading to a better van der Waals (vdW) contact and therefore an improvement in the enthalpy term ΔH . The improvement in enthalpy ($\Delta\Delta H$) correlates well with increasing vdW volumes of spherical *ortho* substituents (**5b**, **14a–c**; Figure 5). For non-spherical substituents (OMe, **14d**; cyclopropyl, **14e**; and CN, **14f**), the shape complementarity is not optimal, leading to only a decreased enthalpy contribution. However, better vdW contacts also lead to decreased conformational flexibility and therefore an entropic compensation by a less favorable ΔS_{conf} value. A second parameter is the desolvation enthalpy, which depends on the polarity of a spe-

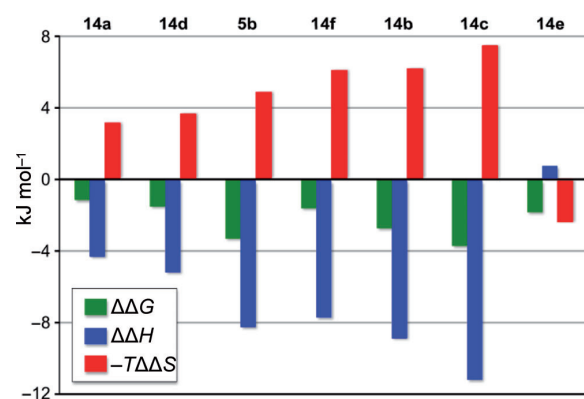


Figure 4. Enthalpy–entropy compensation, a property often reported for carbohydrate–lectin interactions,^[31] for *ortho*-substituted biphenyl α -D-mannopyranosides; $\Delta\Delta G$, $\Delta\Delta H$, and $T\Delta\Delta S$ values for **5b** and **14a–f** are plotted relative to the unsubstituted derivative **4b**.

cific *ortho* substituent and varies between -2.39 kJ mol⁻¹ for CH₃ and 19.31 kJ mol⁻¹ for CN.^[25] Finally, depending on the surface area of the *ortho* substituent, the entropy of solvation may change. In summary, the various effects are superimposed and of opposing contributions to the free binding energy ΔG .

Physicochemical and in vitro pharmacokinetic characterization

To estimate the oral bioavailability and renal elimination of acids **4b**, **5b**, **6**, **14a–f**, **20**, **23**, **31**, **35**, and the methyl esters **4a**, **5a**,

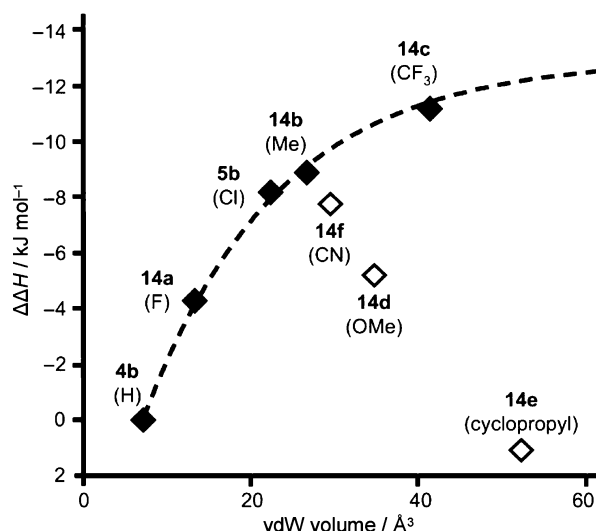


Figure 5. Correlation of $\Delta\Delta H$ (relative to antagonist **4b**) with the van der Waals volumes^[30] of *ortho* substituents.

13a–f, **19a–b**, **22**, **30** and **34**, several physicochemical parameters (lipophilicity, solubility) as well as permeability through an artificial membrane and a cell monolayer were determined (Table 3). The free acids of the antagonists assessed in this study (**4b**, **5b**, **6**, **14a–f**, **20**, **23**, **31**, and **35**) are generally hydrophilic and soluble at pH values > 5. All acids showed $\log D_{7.4}$ values below zero and are therefore thought to undergo considerable renal clearance,^[32] a prerequisite for FimH antagonists to reach their target in the urinary bladder. Permeation studies through an artificial membrane (PAMPA^[33]) indicated for all acids except **14a** effective permeation values ($\log P_e$) below -6.7, suggesting low absorption in the small intestine by passive permeation.^[34] However, the high absorption potential of the fluoro-substituted biphenyl **14a** predicted by

Table 3. Physicochemical and in vitro pharmacokinetic parameters of FimH antagonists.

Compd	PAMPA $\log P_e$ [$\log 10^{-6} \text{ cm s}^{-1}$]/pH ^[a]	Caco-2 P_{app} [$10^{-6} \text{ cm s}^{-1}$] ^[b]			$\log D_{7.4}$ ^[c]	Solubility [$\mu\text{g mL}^{-1}$]/pH ^[d]
		a→b	b→a	(b→a)/(a→b)		
1	-4.9	7.0±0.6	9.4±0.2	1.3	1.7	> 3000/6.5
24	-5.0±0.1/5.0 -4.9±0.1/6.2 -4.7±0.1/7.4	10.0±0.9	19.0±1.2	1.9	2.1±0.1	22±0/3.0 22±1/5.0 21±1/7.4
3	-4.9±0.0/5.0 -4.9±0.0/6.2 -4.9±0.0/7.4	2.2±0.2	17.6±0.4	8.0	2.0±0.0	> 150/3.0 > 150/5.0 > 150/7.4
4a	-4.7	1.5±0.0	6.4±0.4	4.3	2.1	14±1/3.0 13±1/5.0 12±1/7.4
4b	n.p.	n.d.	n.d.	n.d.	< -1.5	> 3000/6.6
5a	-4.6	5.3±0.6	17.5±1.3	3.3	2.3	16±2/3.0 15±0/5.0 17±2/7.4
5b	n.p.	0.2±0.0	0.4±0.0	1.6	-0.8	> 3000/6.5
13a	-4.8±0.0/5.0 -4.8±0.0/6.2 -4.8±0.0/7.4	5.6±0.7	22.0±0.6	4.0	2.7±0.1	22±1/3.0 24±3/5.0 17±6/7.4
14a	-5.8±0.1/5.0 -6.3±0.1/6.2 -7.4±0.1/7.4	0.2±0.1	0.2±0.0	0.8	< -1.5	30±3/3.0 > 100/5.0 > 100/7.4
13b	-4.5±0.1/5.0 -4.5±0.0/6.2 -4.6±0.1/7.4	6.2±1.3	22.7±1.2	3.6	2.4±0.2	7±0/3.0 7±0/5.0 7±0/7.4
14b	-8.6±1.7/5.0 -8.8±1.4/6.2 -8.7±1.5/7.4	n.d.	n.d.	n.d.	-0.6±0.1	34±3/3.0 > 200/5.0 > 200/7.4
13c	-4.4±0.0/5.0 -4.4±0.0/6.2 -4.5±0.1/7.4	9.2±0.1	16.9±1.5	1.8	2.8±0.1	17±1/3.0 15±1/5.0 16±1/7.4
14c	-8.4±1.3/5.0 -9.3±1.4/6.2 -8.6±1.6/7.4	n.d.	n.d.	n.d.	-0.8±0.1	15±1/3.0 140±6/5.0 > 200/7.4
13d	-5.4±0.0/5.0 -5.4±0.0/6.2 -5.4±0.0/7.4	4.2±0.7	16.4±1.2	3.9	1.8±0.1	24±0/3.0 24±1/5.0 26±1/7.4
14d	-8.5±0.6/5.0 -9.1±0.2/6.2 -9.2±0.4/7.4	n.d.	n.d.	n.d.	< -1.5	127±4/3/0 > 200/5.0 > 200/7.4
13e	-4.5±0.2/5.0 -4.4±0.0/6.2 -4.4±0.1/7.4	6.1±0.6	17.9±1.2	3.0	2.9±0.1	14±2/3.0 13±0/5.0 14±1/7.4
14e	-9.3±1.3/5.0 -8.7±1.5/6.2 -8.7±1.5/7.4	n.d.	n.d.	n.d.	-0.8±0.1	31±2/3.0 > 200/5.0 > 200/7.4
13f	-6.5±0.0/5.0 -6.5±0.1/6.2 -6.3±0.1/7.4	0.9±0.7	18.1±0.6	19.7	1.7±0.0	22±2/3.0 24±1/5.0 23±1/7.4
14f	-8.5±1.7/5.0 -7.3±0.3/6.2 -7.8±1.5/7.4	n.d.	n.d.	n.d.	< -1.5	35±11/3.0 > 200/5.0 > 200/7.4
19a	-4.9±0.0/5.0 -4.9±0.0/6.2 -4.9±0.1/7.4	4.4±0.1	18.8±1.7	4.3	1.9±0.1	103±8/3/0 100±6/5.0 95±5/7.4
6	-8.6±1.6/5.0 -9.3±1.4/6.2 -8.7±1.5/7.4	n.d.	n.d.	n.d.	< -1.5	> 130/3.0 > 130/5.0 > 130/7.4
19b	-5.3±0.1/5.0 -5.6±0.1/6.2 -5.1±0.2/7.4	n.d.	n.d.	n.d.	2.4±0.1	30±0/3.0 29±1/5.0 31±1/7.4
20	-8.6±1.6/5.0 -9.3±1.4/6.2 -10/7.4	n.d.	n.d.	n.d.	-1.2±0.2	> 130/3.0 > 130/5.0 > 130/7.4

Table 3. (Continued)

Compd	PAMPA $\log P_e$ [$\log 10^{-6} \text{ cm s}^{-1}$]/pH ^[a]	Caco-2 P_{app} [$10^{-6} \text{ cm s}^{-1}$] ^[b]			$\log D_{7.4}$ ^[c]	Solubility [$\mu\text{g mL}^{-1}$]/pH ^[d]
		a→b	b→a	(b→a)/(a→b)		
22	-5.1 ± 0.0/5.0	n.d.	n.d.	n.d.	1.7 ± 0.1	> 130/3.0
	-5.1 ± 0.0/6.2					> 130/5.0
	-5.1 ± 0.0/7.4					> 130/7.4
23	-7.3 ± 1.8/5.0	n.d.	n.d.	n.d.	< -1.5	> 130/3.0
	-8.1 ± 2.2/6.2					> 130/5.0
	-10/7.4					> 130/7.4
30	-5.5 ± 0.0/5.0	n.d.	n.d.	n.d.	1.6 ± 0.1	> 130/3.0
	-5.5 ± 0.0/6.2					> 130/5.0
	-5.4 ± 0.1/7.4					> 130/7.4
31	-7.7 ± 1.6/5.0	n.d.	n.d.	n.d.	< -1.5	> 130/3.0
	-8.1 ± 1.3/6.2					> 130/5.0
	-10/7.4					> 130/7.4
34	-5.3 ± 0.1/5.0	n.d.	n.d.	n.d.	2.2 ± 0.1	> 130/3.0
	-5.6 ± 0.0/6.2					> 130/5.0
	-5.3 ± 0.2/7.4					> 130/7.4
35	-8.0 ± 1.3/5.0	n.d.	n.d.	n.d.	n.d.	63 ± 8/3.0
	-8.6 ± 1.6/6.2					> 130/5.0
	-10/7.4					> 130/7.4

[a] P_e = effective permeation: passive permeation through an artificial membrane was determined by parallel artificial membrane permeation assay (PAMPA); values represent the mean ± SD of quadruplicate measurements taken at three pH values (pH 5.0, 6.2, and 7.4).^[33] [b] P_{app} = apparent permeability: permeation through cell monolayers was assessed by a Caco-2 assay in the absorptive (a→b) and secretory (b→a) directions in triplicate;^[42] n.p. = no permeation, n.d. = not determined. [c] Distribution coefficients ($\log D$) were measured by a miniaturized shake-flask procedure at pH 7.4. [d] Kinetic solubility was measured in a 96-well format using the μSOL Explorer solubility analyzer at three pH values (pH 3.0, 5.0, and 7.4) in triplicate.

PAMPA could not be confirmed by the colorectal adenocarcinoma (Caco-2) cell permeation assay. In contrast, the methyl esters (**3**, **4a**, **5a**, **13a–f**, **19a–b**, **22**, **30**, and **34**) showed $\log D_{7.4}$ values > 1.5, that is, they are more lipophilic and hence more permeable than the corresponding acids, as shown by the PAMPA and Caco-2 permeation assay. Despite this high absorption potential, the ratios between the apparent permeability coefficients (P_{app}) in the basolateral-to-apical (b→a, secretory) and apical-to-basolateral (a→b, absorptive) directions revealed active efflux processes as an additional issue of all the assessed compounds. Moreover, the methyl esters must be readily hydrolyzed after absorption to become more polar and to be renally eliminated. Rapid metabolic turnover by the enzyme carboxylesterase was previously shown for the methyl esters **4a** and **5a**.^[10e]

The different substituents at the *ortho* position of ring A (**5a**, **5b**, **13a–f**, **14a–f**; Table 3) only have a minor influence on the physicochemical properties. The addition of chloro, fluoro, methyl, trifluoromethyl, or cyclopropyl substituents slightly increases the lipophilicity of the respective acids and methyl esters, whereas methoxy and cyano substituents render the compounds more hydrophilic and less permeable. Moreover, the substituents at the *ortho* position have negligible effects on the low aqueous solubility, which is a major drawback of all methyl esters.^[35] In contrast, the modifications with increased spacer length between carbohydrate and aglycone (**6**, **19a–b**, **20**, **22**, and **23**; Table 3) show higher aqueous solubility. Extending the spacer and linking it at the *ortho* or *meta* positions of the biaryl moiety disrupts the symmetry of the molecular structure, leading to increased solubility.^[15,36] However, an additional chloro substituent at the 4-position (**19b**, **20**; Table 3) restores the symmetrical character of the structure, which in turn

lowers the solubility of the compound. Disrupted structural symmetry might also hold true for the enhanced solubility of the biphenyls with an elongated carboxylate-bearing *para* substituent (**30**, **31**, **34**, and **35**; Table 3). The introduction of a methylene or cyclopropylene group between the biphenyl and the carboxylate moiety markedly improved the aqueous solubility of the methyl esters, whereas the absorption potential was only slightly decreased.

Summary and Conclusions

In this study, we investigated the structure–affinity relationship for *ortho* substituents on ring A of the biphenyl aglycone of the FimH antagonists **13** and **14**. The correlation between vdW volumes of these substituents and the enthalpy term clearly indicates the importance of shape complementarity. This interpretation is further supported by the fact that the electronic character of the substituent [Cl in **5a** (Table 2), CF_3 in **14c** versus CH_3 in **14b**] is less important. The correlation of enthalpic improvements ($\Delta\Delta H$) with vdW volumes offers a potent tool for guiding further structural optimization.

The successful oral application using a prodrug approach was recently demonstrated with the ester **5a**.^[10e] A major drawback of the biphenyl methyl esters is their insufficient solubility, which is mostly in the range of 15–35 $\mu\text{g mL}^{-1}$. As expected,^[15] solubility could be substantially improved when the symmetry of the aglycone was disrupted. Thus, the solubility of **3** (> 150 $\mu\text{g mL}^{-1}$; Table 3), **19a** (100 $\mu\text{g mL}^{-1}$), and **22** (> 130 $\mu\text{g mL}^{-1}$) was improved by a factor of ~10. However, for these more flexible derivatives, the expected optimized fit leading to improved affinities in the in-docking mode could not be observed. In fact, the affinities for the members of this

family of compounds are drastically decreased, for example, compounds **20** or **23** (Table 1).

Finally, the elongation of the ester-bearing *para* substituent (Table 1; compounds **31** and **35**) did not lead to the expected additional polar interaction with Arg98. Instead, a five- to sevenfold decrease in affinity was observed. Clearly, the desolvation penalty for the guanidinium group could not be matched by the geometrically possible salt bridge with the carboxylate of the antagonists **31** and **35**.

In summary, our study confirms the earlier selection of the FimH antagonists **5a** for oral and **5b** for intravenous application. However, the methoxy derivative **13d** (Table 1) shows slightly improved pharmacokinetic properties and therefore represents an additional candidate for future in vivo studies.

Experimental Section

General methods: NMR spectra were recorded on a Bruker Avance DMX-500 (500.1 MHz) spectrometer. Assignment of ^1H and ^{13}C NMR spectra was achieved using 2D methods (COSY, HSQC, HMBC). Chemical shifts are expressed in ppm using residual CHCl_3 , CHD_2OD , or H_2O as references. Optical rotations were measured with a PerkinElmer Polarimeter 341. Electrospray ionization mass spectrometry (ESI-MS) data were obtained on a Waters Micromass ZQ instrument. LC-HRMS analyses were carried out using an Agilent 1100 LC equipped with a photodiode array detector and a Micromass QTOF I equipped with a 4 GHz digital time converter. Microwave-assisted reactions were carried out with a CEM Discover and Explorer. Reactions were monitored by TLC using glass plates coated with silica gel 60 F_{254} (Merck) and visualized by UV light and/or by charring with a molybdate solution (0.02 M solution of ammonium cerium sulfate dihydrate and ammonium molybdate tetrahydrate in aqueous 10% H_2SO_4). MPLC separations were carried out on a CombiFlash Companion or R_f from Teledyne Isco equipped with RediSep normal-phase or RP-18 reversed-phase flash columns. LC-MS separations were carried out on a Waters system equipped with sample manager 2767, pump 2525, PDA 2525, and Micromass ZQ. Size-exclusion chromatography was performed on Bio-Gel P-2 Gel (45–90 mm) from Bio-Rad (Reinach, Switzerland). All compounds used for biological assays are at least of 98% purity based on analytical HPLC results. Commercially available reagents were purchased from Fluka, Aldrich, Alfa Aesar or Iris Biotech (Germany). Solvents were purchased from Sigma-Aldrich (Buchs, Switzerland) or Acros Organics (Geel, Belgium) and were dried prior to use where indicated. MeOH was dried by reflux with sodium methoxide and distilled immediately before use. CH_2Cl_2 was dried by filtration over Al_2O_3 (Fluka, type 5016 A basic). Molecular sieves (4 Å) were activated in vacuo at 500 °C for 1 h immediately before use.

General procedure A for the synthesis of mannosides 10a–f and 17a–c: To an ice-cold suspension of **8**^[12] (200 mg, 0.57 mmol, 1.1 equiv), phenol **9a–f** or benzyl alcohol **16a–c** (0.52 mmol, 1.0 equiv), and molecular sieves (4 Å, 600 mg) in dry CH_2Cl_2 (5 mL), $\text{BF}_3\cdot\text{Et}_2\text{O}$ (0.3 mL, 2.44 mmol, 4.7 equiv) was added dropwise under argon. The mixture was stirred at 0 °C for 3 h, and then at RT overnight. The reaction mixture was filtered over Celite, and the filtrate was diluted with CH_2Cl_2 (50 mL), extracted with 0.5 N $\text{NaOH}_{(\text{aq})}$ (50 mL), H_2O (50 mL), and brine (50 mL). The organic layer was dried over Na_2SO_4 and concentrated in vacuo. The residue was purified by MPLC on silica gel (petroleum ether (PE)/EtOAc) to yield **10a–f** or **17a–c**.

General procedure B for the synthesis of mannosylated biphenyls: A Schlenk tube was charged with aryl bromide (1.0 equiv), boronic acid or boronate (1.1 equiv), $\text{Pd}(\text{dppf})\text{Cl}_2\cdot\text{CH}_2\text{Cl}_2$ (0.03 equiv), K_3PO_4 (1.5 equiv) and a stirring bar. The tube was closed with a rubber septum and was evacuated and flushed with argon. This procedure was repeated once, then anhydrous DMF (2 mL) was added under a stream of argon. The mixture was degassed in an ultrasonic bath and flushed with argon for 5 min, and then stirred at 80 °C overnight. The reaction mixture was cooled to RT, diluted with EtOAc (50 mL), and washed with H_2O (50 mL) and brine (50 mL). The organic layer was dried over Na_2SO_4 and concentrated in vacuo. The residue was purified by MPLC on silica gel (PE/EtOAc) to afford biphenyls **12a–f**, **18a,b**, **21**, **29** or **33**.

General procedure C for deacetylation: To a solution of **12a–f**, **18a,b**, **21**, **29** or **33** (1.0 equiv) in dry MeOH (5 mL) was added freshly prepared 1 M NaOMe/MeOH (0.1 equiv) under argon. The mixture was stirred at RT until the reaction was complete (monitored by TLC), then neutralized with Amberlyst-15 (H^+) ion-exchange resin, filtered and concentrated in vacuo. The residue was purified by MPLC on silica gel ($\text{CH}_2\text{Cl}_2/\text{MeOH}$, 10:1–8:1) to afford **13a–f**, **19a,b**, **22**, **30** or **34** as white solids.

General procedure D for saponification: To a solution of **12a–e**, **18a,b**, **21**, **29** or **33** (1.0 equiv) in MeOH (5 mL) was added 1 M NaOMe/MeOH (0.1 equiv) at RT. The reaction mixture was stirred at RT for 4 h and concentrated. The residue was treated with 0.5 M $\text{NaOH}_{(\text{aq})}$ (1 mL) for 24 h at RT. The solution was then adjusted to pH 3–4 with Amberlyst-15 (H^+), and the mixture was filtered and concentrated. The crude product was transformed into the sodium salt by passing through a small column of Dowex 50X8 (Na^+ form) ion-exchange resin. After concentration, the residue was purified by MPLC (RP-18, $\text{H}_2\text{O}/\text{MeOH}$, 1:0–2:1) followed by size-exclusion chromatography (P-2 gel, H_2O) to give **14a–e**, **6**, **20**, **23**, **31** or **35** as white solids after final lyophilization from H_2O .

4-Bromo-2-fluorophenyl 2,3,4,6-tetra-O-acetyl- α -D-mannopyranoside (10a): Prepared according to general procedure A from **8**^[12] and 4-bromo-2-fluorophenol (**9a**). Yield: 220 mg (74%) as white solid. $R_f=0.48$ (PE/EtOAc, 2:1); $[\alpha]_D^{20}+83.0$ ($c=0.70$, EtOAc); ^1H NMR (500 MHz, CDCl_3): $\delta=7.30$ (dd, $J=2.3$, 10.1 Hz, 1H, Ar-H), 7.21 (dt, $J=1.7$, 8.8 Hz, 1H, Ar-H), 7.08 (t, $J=8.6$ Hz, 1H, Ar-H), 5.54 (dd, $J=3.5$, 10.0 Hz, 1H, H-3), 5.50 (dd, $J=1.8$, 3.4 Hz, 1H, H-2), 5.46 (d, $J=1.5$ Hz, 1H, H-1), 5.36 (t, $J=10.0$ Hz, 1H, H-4), 4.26 (dd, $J=5.5$, 12.2 Hz, 1H, H-6a), 4.17 (ddd, $J=2.1$, 5.5, 10.0 Hz, 1H, H-5), 4.10 (dd, $J=2.2$, 12.2 Hz, 1H, H-6b), 2.20, 2.07, 2.05, 2.04 ppm (4 s, 12H, 4 OAc); ^{13}C NMR (125 MHz, CDCl_3): $\delta=170.51$, 169.95, 169.82, 169.76 (4 CO), 153.28 (d, $J=251.4$ Hz, Ar-C), 142.64 (d, $J=11.1$ Hz, Ar-C), 127.58 (d, $J=4.0$ Hz, Ar-C), 120.4 (d, $J=21.5$ Hz, Ar-C), 120.28 (d, $J=0.9$ Hz, Ar-C), 115.73 (d, $J=8.1$ Hz, Ar-C), 97.49 (C-1), 69.76 (C-5), 69.15 (C-2), 68.60 (C-3), 65.76 (C-4), 62.09 (C-6), 20.87, 20.71, 20.69, 20.67 ppm (4 COCH_3); elemental analysis calcd (%) for $\text{C}_{20}\text{H}_{22}\text{BrFO}_{10}$: C 46.08, H 4.25, found: C 46.11, H 4.26.

4-Bromo-2-methylphenyl 2,3,4,6-tetra-O-acetyl- α -D-mannopyranoside (10b): Prepared according to general procedure A from **8**^[12] and 4-bromo-2-methylphenol (**9b**). Yield: 254 mg (86%) as white solid. $R_f=0.60$ (PE/EtOAc, 2:1); $[\alpha]_D^{20}+61.8$ ($c=1.00$, EtOAc); ^1H NMR (500 MHz, CDCl_3): $\delta=7.31$ (d, $J=1.9$ Hz, 1H, Ar-H), 7.24 (dd, $J=2.3$, 8.7 Hz, 1H, Ar-H), 6.97 (d, $J=8.8$ Hz, 1H, Ar-H), 5.53 (dd, $J=3.4$, 10.0 Hz, 1H, H-3), 5.47 (d, $J=1.7$ Hz, 1H, H-1), 5.45 (dd, $J=2.0$, 3.4 Hz, 1H, H-2), 5.37 (t, $J=10.0$ Hz, 1H, H-4), 4.28 (dd, $J=5.6$, 12.3 Hz, 1H, H-6a), 4.10–4.03 (m, 2H, H-5, H-6b), 2.27 (s, 3H, CH_3), 2.20, 2.06, 2.05, 2.04 ppm (4 s, 12H, 4 OAc); ^{13}C NMR (125 MHz, CDCl_3): $\delta=170.53$, 170.04, 169.96, 169.73 (4 CO), 152.96, 133.78,

20.66 ppm (4C, 4 COCH₃); HRMS: *m/z*: calcd for C₂₉H₂₉F₃NaO₁₂ [M + Na]⁺: 649.1503, found: 649.1503.

Methyl 4'-(2,3,4,6-tetra-O-acetyl- α -D-mannopyranosyloxy)-3'-methoxybiphenyl-4-carboxylate (12 d): Prepared according to general procedure B from **10 d** (100 mg, 0.188 mmol), **11** (37.1 mg, 0.206 mmol), Pd(dppf)Cl₂·CH₂Cl₂ (4.6 mg, 5.6 μ mol) and K₃PO₄ (59.9 mg, 0.282 mmol). Yield: 91 mg (83%) as white solid. *R*_f = 0.25 (PE/EtOAc, 1:0.9); [α]_D²⁰ + 50.7 (*c* = 1.40, EtOAc); ¹H NMR (500 MHz, CDCl₃): δ = 8.10–8.08 (m, 2H, Ar-H), 7.62–7.60 (m, 2H, Ar-H), 7.19–7.13 (m, 3H, Ar-H), 5.64 (dd, *J* = 3.5, 10.0 Hz, 1H, H-3), 5.58 (dd, *J* = 1.8, 3.5 Hz, 1H, H-2), 5.53 (d, *J* = 1.7 Hz, 1H, H-1), 5.38 (t, *J* = 10.0 Hz, 1H, H-4), 4.34–4.28 (m, 2H, H-5, H-6a), 4.12 (m, 1H, H-6b), 3.94 (2 s, 6H, 2 OCH₃), 2.21, 2.08, 2.05, 2.04 ppm (4 s, 12H, 4 OAc); ¹³C NMR (125 MHz, CDCl₃): δ = 170.61, 170.02, 169.92, 169.83, 166.94 (5 CO), 151.01, 145.06, 144.92, 136.51, 130.13, 128.86, 126.87, 119.72, 119.32, 111.60 (12C, Ar-C), 97.50 (C-1), 69.48 (C-5), 69.43 (C-2), 68.91 (C-3), 66.12 (C-4), 62.29 (C-6), 56.01 (OCH₃), 52.18 (CO₂CH₃), 20.95, 20.76, 20.74, 20.72 ppm (4 COCH₃); HRMS: *m/z*: calcd for C₂₉H₃₂NaO₁₃ [M + Na]⁺: 611.1735, found: 611.1736.

Methyl 4'-(2,3,4,6-tetra-O-acetyl- α -D-mannopyranosyloxy)-3'-cyclopropylbiphenyl-4-carboxylate (12 e): Prepared according to general procedure B from **10 e** (100 mg, 0.184 mmol), **11** (36.4 mg, 0.202 mmol), Pd(dppf)Cl₂·CH₂Cl₂ (4.5 mg, 5.5 μ mol) and K₃PO₄ (58.6 mg, 0.276 mmol). Yield: 60 mg (55%) as white solid. *R*_f = 0.48 (PE/EtOAc, 2:1); [α]_D²⁰ + 53.0 (*c* = 0.70, EtOAc); ¹H NMR (500 MHz, CDCl₃): δ = 8.08–8.07 (m, 2H, Ar-H), 7.59–7.57 (m, 2H, Ar-H), 7.37 (dd, *J* = 2.4, 8.5 Hz, 1H, Ar-H), 7.19–7.17 (m, 2H, Ar-H), 5.64 (dd, *J* = 3.5, 10.1 Hz, 1H, H-3), 5.61 (d, *J* = 1.6 Hz, 1H, H-1), 5.54 (dd, *J* = 1.9, 3.4 Hz, 1H, H-2), 5.42 (t, *J* = 10.1 Hz, 1H, H-4), 4.31 (dd, *J* = 5.3, 12.2 Hz, 1H, H-6a), 4.19–4.10 (m, 2H, H-5, H-6b), 3.94 (s, 3H, OCH₃), 2.22 (s, 3H, OAc), 2.17 (m, 1H, H-cPr), 2.08–2.05 (m, 9H, 3 OAc), 1.06–1.05 (m, 2H, CH₂-cPr), 0.74–0.73 ppm (m, 2H, CH₂-cPr); ¹³C NMR (125 MHz, CDCl₃): δ = 170.55, 170.06, 170.02, 169.75, 166.98 (5 CO), 154.76, 145.12, 134.83, 133.56, 130.08, 128.58, 126.71, 125.33, 125.06, 114.84 (12C, Ar-C), 96.04 (C-1), 69.49 (C-5), 69.42 (C-2), 69.02 (C-3), 65.81 (C-4), 62.15 (C-6), 52.12 (OCH₃), 20.91, 20.71 (4C, 4 COCH₃), 9.78, 7.58 ppm (3C, cPr); elemental analysis calcd (%) for C₂₉H₃₂O₁₂: C 62.20, H 5.72, found: C 62.00, H 5.86.

Methyl 4'-(2,3,4,6-tetra-O-acetyl- α -D-mannopyranosyloxy)-3'-cyanobiphenyl-4-carboxylate (12 f): Prepared according to general procedure B from **10 f** (100 mg, 0.189 mmol), **11** (37.5 mg, 0.208 mmol), Pd(dppf)Cl₂·CH₂Cl₂ (4.6 mg, 5.7 μ mol) and K₃PO₄ (60.2 mg, 0.284 mmol). Yield: 92 mg (84%) as white solid. *R*_f = 0.18 (PE/EtOAc, 2:1); [α]_D²⁰ + 61.4 (*c* = 0.80, EtOAc); ¹H NMR (500 MHz, CDCl₃): δ = 8.06–8.05 (m, 2H, Ar-H), 7.80 (d, *J* = 2.3 Hz, 1H, Ar-H), 7.72 (dd, *J* = 2.3, 8.8 Hz, 1H, Ar-H), 7.53–7.51 (m, 2H, Ar-H), 7.28 (d, *J* = 8.8 Hz, 1H, Ar-H), 5.64 (d, *J* = 1.7 Hz, 1H, H-1), 5.55 (dd, *J* = 3.5, 10.0 Hz, 1H, H-3), 5.49 (dd, *J* = 1.9, 3.4 Hz, 1H, H-2), 5.37 (t, *J* = 10.0 Hz, 1H, H-4), 4.24 (dd, *J* = 5.0, 12.4 Hz, 1H, H-6a), 4.12 (ddd, *J* = 2.2, 4.9, 10.0 Hz, 1H, H-5), 4.05 (dd, *J* = 2.2, 12.4 Hz, 1H, H-6b), 3.88 (s, 3H, OCH₃), 2.16, 2.01, 1.99, 1.98 ppm (4 s, 12H, 4 OAc); ¹³C NMR (125 MHz, CDCl₃): δ = 170.45, 170.01, 169.78, 169.54, 166.65 (5 CO), 156.84, 142.44, 135.67, 132.36, 129.77, 126.76, 115.99, 115.18, 104.47 (13C, Ar-C, CN), 96.63 (C-1), 70.24 (C-5), 69.17 (C-2), 68.49 (C-3), 65.48 (C-4), 60.85 (C-6), 20.88, 20.73, 20.71, 20.64 ppm (4 COCH₃); HRMS: *m/z*: calcd for C₂₉H₂₉NNaO₁₂ [M + Na]⁺: 606.1582, found: 606.1583.

Methyl 3'-fluoro-4'-(α -D-mannopyranosyloxy)biphenyl-4-carboxylate (13 a): Prepared according to general procedure C from **12 a** (33 mg, 0.057 mmol). Yield: 15 mg (65%). [α]_D²⁰ + 114.3 (*c* = 0.30, MeOH); ¹H NMR (500 MHz, CD₃OD): δ = 7.98–7.97 (m, 2H, Ar-H),

7.63–7.61 (m, 2H, Ar-H), 7.42–7.36 (m, 3H, Ar-H), 5.45 (d, *J* = 1.7 Hz, 1H, H-1), 3.99 (dd, *J* = 1.9, 3.4 Hz, 1H, H-2), 3.82–3.84 (m, 4H, H-3, OCH₃), 3.71–3.56 ppm (m, 4H, H-4, H-5, H-6); ¹³C NMR (125 MHz, CD₃OD): δ = 168.34 (CO), 154.75 (d, *J* = 243.8 Hz, Ar-C), 145.6 (2C, Ar-C), 136.37 (d, *J* = 6.9 Hz, Ar-C), 130.20, 129.20, 127.80, 124.33, 120.33 (7C, Ar-C), 116.00 (d, *J* = 20.0 Hz, Ar-C), 101.40 (C-1), 75.97 (C-5), 72.31 (C-3), 71.82 (C-2), 68.18 (C-4), 62.65 (C-6), 52.65 ppm (OCH₃); HRMS: *m/z*: calcd for C₂₀H₂₁FNaO₈ [M + Na]⁺: 431.1113, found: 431.1112.

Methyl 4'-(α -D-mannopyranosyloxy)-3'-methylbiphenyl-4-carboxylate (13 b): Prepared according to general procedure C from **12 b** (31 mg, 0.054 mmol). Yield: 16 mg (73%). [α]_D²⁰ + 110.5 (*c* = 0.35, MeOH); ¹H NMR (500 MHz, CD₃OD): δ = 7.96–7.94 (m, 2H, Ar-H), 7.60–7.58 (m, 2H, Ar-H), 7.40–7.37 (m, 2H, Ar-H), 7.22 (d, *J* = 8.5 Hz, 1H, Ar-H), 5.47 (d, *J* = 1.6 Hz, 1H, H-1), 3.97 (dd, *J* = 1.9, 3.4 Hz, 1H, H-2), 3.87 (dd, *J* = 3.4, 9.5 Hz, 1H, H-3), 3.82 (s, 3H, OMe), 3.67–3.52 (m, 3H, H-4, H-6), 3.46 (m, 1H, H-5), 2.21 ppm (s, 3H, Me); ¹³C NMR (125 MHz, CD₃OD): δ = 168.56 (CO), 156.20, 146.86, 134.70, 131.07, 130.07, 130.54, 129.45, 128.92, 127.63, 126.85, 115.83 (12C, Ar-C), 99.76 (C-1), 75.55 (C-5), 72.64 (C-3), 72.11 (C-2), 68.31 (C-4), 62.68 (C-6), 52.59 ppm (OCH₃), 16.54 (CH₃); HRMS: *m/z*: calcd for C₂₁H₂₄NaO₈ [M + Na]⁺: 427.1363, found: 427.1370.

Methyl 3'-trifluoromethyl-4'-(α -D-mannopyranosyloxy)biphenyl-4-carboxylate (13 c): Prepared according to general procedure C from **12 c** (30 mg, 0.048 mmol). Yield: 14 mg (64%). [α]_D²⁰ + 113.1 (*c* = 0.40, MeOH); ¹H NMR (500 MHz, CD₃OD): δ = 8.11–8.10 (m, 2H, Ar-H), 7.92–7.90 (m, 2H, Ar-H), 7.75–7.73 (m, 2H, Ar-H), 7.63 (d, *J* = 8.4 Hz, 1H, Ar-H), 5.69 (d, *J* = 1.5 Hz, 1H, H-1), 4.09 (dd, *J* = 1.8, 3.3 Hz, 1H, H-2), 3.98–3.94 (m, 4H, H-3, OMe), 3.79–3.73 (m, 3H, H-4, H-6), 3.61 ppm (ddd, *J* = 2.3, 5.7, 9.6 Hz, 1H, H-5); ¹³C NMR (125 MHz, CD₃OD): δ = 168.29 (CO), 155.54, 145.13, 134.74, 133.45, 131.36, 131.29, 130.32, 127.91, 127.85, 126.44, 117.80 (Ar-C), 100.27 (C-1), 76.13 (C-5), 72.24 (C-3), 71.74 (C-2), 68.09 (C-4), 62.67 ppm (C-6), 52.69 (OMe); HRMS: *m/z*: calcd for C₂₁H₂₁F₃NaO₈ [M + Na]⁺: 481.1081, found: 481.1082.

Methyl 4'-(α -D-mannopyranosyloxy)-3'-methoxybiphenyl-4-carboxylate (13 d): Prepared according to general procedure C from **12 d** (32 mg, 0.055 mmol). Yield: 12 mg (52%). [α]_D²⁰ + 133.1 (*c* = 0.20, MeOH); ¹H NMR (500 MHz, CD₃OD): δ = 7.97–7.96 (m, 2H, Ar-H), 7.63–7.61 (m, 2H, Ar-H), 7.21–7.11 (m, 3H, Ar-H), 5.37 (d, *J* = 1.7 Hz, 1H, H-1), 4.00 (dd, *J* = 1.8, 3.4 Hz, 1H, H-2), 3.86 (dd, *J* = 3.5, 8.8 Hz, 1H, H-3), 3.82 (s, 6H, 2 CH₃), 3.70–3.63 ppm (m, 4H, H-4, H-5, H-6); ¹³C NMR (125 MHz, CD₃OD): δ = 168.50 (CO), 152.33, 147.40, 146.83, 136.56, 131.08, 129.76, 127.87, 120.86, 120.10, 112.54 (Ar-C), 101.51 (C-1), 75.66 (C-5), 72.40 (C-2), 72.00 (C-3), 68.34 (C-4), 62.70 (C-6), 56.61 (OMe), 52.63 ppm (OMe); HRMS: *m/z*: calcd for C₂₁H₂₄NaO₉ [M + Na]⁺: 443.1313, found: 443.1315.

Methyl 3'-cyclopropyl-4'-(α -D-mannopyranosyloxy)biphenyl-4-carboxylate (13 e): Prepared according to general procedure C from **12 e** (21 mg, 0.035 mmol). Yield: 10 mg (67%). [α]_D²⁰ + 101.6 (*c* = 0.24, MeOH); ¹H NMR (500 MHz, CD₃OD): δ = 8.07–8.05 (m, 2H, Ar-H), 7.68–7.67 (m, 2H, Ar-H), 7.46 (dd, *J* = 2.4, 8.5 Hz, 1H, Ar-H), 7.33 (d, *J* = 8.5 Hz, 1H, Ar-H), 7.21 (d, *J* = 2.4 Hz, 1H, Ar-H), 5.60 (d, *J* = 1.7 Hz, 1H, H-1), 4.13 (dd, *J* = 1.9, 3.3 Hz, 1H, H-2), 4.02 (dd, *J* = 3.4, 9.5 Hz, 1H, H-3), 3.93 (s, 3H, OMe), 3.81–3.74 (m, 3H, H-4, H-6), 3.69 (m, 1H, H-5), 2.19 (m, 1H, H-cPr), 1.01–0.99 (m, 2H, CH₂-cPr), 0.76–0.74 ppm (m, 2H, CH₂-cPr); ¹³C NMR (125 MHz, CD₃OD): δ = 168.54 (CO), 156.92, 146.98, 135.00, 134.59, 131.07, 127.34, 127.67, 126.39, 125.34, 116.29 (12C, Ar-C), 100.14 (C-1), 75.61 (C-5), 72.64 (C-3), 72.14 (C-2), 68.33 (C-4), 62.71 (C-6), 52.60 (OCH₃), 10.93,

8.06 ppm (3C, cPr); HRMS: *m/z*: calcd for C₂₃H₂₆NaO₈ [M+Na]⁺: 453.1520, found: 453.1519.

Methyl 3'-cyano-4'-(α -D-mannopyranosyloxy)biphenyl-4-carboxylate (13 f): Prepared according to general procedure C from **12 f** (37 mg, 0.063 mmol). Yield: 19 mg (73%). [α]_D²⁰ + 101.1 (*c* = 0.30, MeOH); ¹H NMR (500 MHz, CD₃OD): δ = 8.00–7.99 (m, 2H, Ar-H), 7.90–7.85 (m, 2H, Ar-H), 7.65–7.63 (m, 2H, Ar-H), 7.50 (d, *J* = 8.8 Hz, 1H, Ar-H), 5.63 (s, 1H, H-1), 4.03 (m, 1H, H-2), 3.91 (dd, *J* = 2.8, 9.4 Hz, 1H, H-3), 3.83 (s, 3H, OMe), 3.69–3.60 (m, 3H, H-4, H-6), 3.50 ppm (m, 1H, H-5); ¹³C NMR (125 MHz, CD₃OD): δ = 168.22 (CO), 159.29, 144.38, 135.61, 134.50, 133.08, 131.31, 130.56, 127.87, 117.36, 116.75, 104.35 (13C, Ar-C, CN), 100.62 (C-1), 76.39 (C-5), 72.27 (C-2), 71.62 (C-3), 68.07 (C-4), 62.64 (C-6), 52.71 ppm (OMe); HRMS: *m/z*: calcd for C₂₁H₂₁NNaO₈ [M+Na]⁺: 438.1159, found: 438.1162.

Sodium 3'-fluoro-4'-(α -D-mannopyranosyloxy)biphenyl-4-carboxylate (14 a): Prepared according to general procedure D from **12 a** (50 mg, 0.087 mmol). Yield: 21 mg (58%). [α]_D²⁰ + 112.7 (*c* = 0.40, MeOH); ¹H NMR (500 MHz, D₂O): δ = 7.78–7.77 (m, 2H, Ar-H), 7.46–7.45 (m, 2H, Ar-H), 7.30–7.15 (m, 3H, Ar-H), 5.43 (s, 1H, H-1), 4.07 (s, 1H, H-2), 3.93 (d, *J* = 3.3 Hz, 1H, H-3), 3.68–3.62 ppm (m, 4H, H-4, H-5, H-6); ¹³C NMR (125 MHz, D₂O): δ = 175.19 (CO), 153.02 (d, *J* = 242.6 Hz, Ar-C), 142.52 (d, *J* = 10.8 Hz, Ar-C), 141.23 (Ar-C), 135.53 (d, *J* = 6.4 Hz, Ar-C), 135.07, 129.43, 126.25, 126.01, 122.96, 119.13 (Ar-C), 114.83 (d, *J* = 19.4 Hz, Ar-C), 99.32 (C-1), 73.65 (C-5), 70.23 (C-3), 69.67 (C-2), 66.35 (C-4), 60.52 ppm (C-6); HRMS: *m/z*: calcd for C₁₉H₁₉FN₂O₈ [M+Na]⁺: 417.0956, found: 417.0957.

Sodium 4'-(α -D-mannopyranosyloxy)-3'-methylbiphenyl-4-carboxylate (14 b): Prepared according to general procedure D from **12 b** (46 mg, 0.081 mmol). Yield: 5 mg (15%). [α]_D²⁰ + 85.7 (*c* = 0.20, MeOH); ¹H NMR (500 MHz, D₂O): δ = 7.78–7.76 (m, 2H, Ar-H), 7.53–7.52 (m, 2H, Ar-H), 7.43–7.37 (m, 2H, Ar-H), 7.10 (d, *J* = 8.6 Hz, 1H, Ar-H), 5.52 (d, *J* = 1.6 Hz, 1H, H-1), 4.07 (dd, *J* = 1.9, 3.4 Hz, 1H, H-2), 3.95 (dd, *J* = 3.5, 9.6 Hz, 1H, H-3), 3.63–3.50 (m, 4H, H-4, H-5, H-6), 2.14 ppm (s, 3H, CH₃); ¹³C NMR (125 MHz, D₂O): δ = 153.33, 142.57, 134.59, 133.97, 129.47, 128.42, 126.25, 125.43, 114.99 (12C, Ar-C), 97.46 (C-1), 73.39 (C-5), 70.54 (C-3), 69.88 (C-2), 66.53 (C-4), 60.60 (C-6), 15.31 ppm (CH₃); HRMS: *m/z*: calcd for C₂₀H₂₂NaO₈ [M+Na]⁺: 413.1207, found: 413.1209.

Sodium 3'-trifluoromethyl-4'-(α -D-mannopyranosyloxy)biphenyl-4-carboxylate (14 c): Prepared according to general procedure D from **12 c** (45 mg, 0.072 mmol). Yield: 25 mg (74%). [α]_D²⁰ + 94.2 (*c* = 0.30, MeOH); ¹H NMR (500 MHz, D₂O): δ = 7.83–7.81 (m, 3H, Ar-H), 7.75 (d, *J* = 8.7 Hz, 1H, Ar-H), 7.57–7.55 (m, 2H, Ar-H), 7.31 (d, *J* = 8.8 Hz, 1H, Ar-H), 5.64 (s, 1H, H-1), 4.09 (d, *J* = 1.5 Hz, 1H, H-2), 3.94 (dd, *J* = 3.4, 9.7 Hz, 1H, H-3), 3.67–3.60 (m, 3H, H-4, H-6), 3.54 ppm (m, 1H, H-5); ¹³C NMR (125 MHz, D₂O): δ = 175.25 (CO), 152.40, 141.31, 135.09, 133.53, 131.93, 129.46, 126.34, 125.59, 115.86 (12C, Ar-C), 97.20 (C-1), 73.68 (C-5), 70.19 (C-3), 69.58 (C-2), 66.36 (C-4), 60.55 ppm (C-6); HRMS: *m/z*: calcd for C₂₀H₁₉F₃NaO₈ [M+Na]⁺: 467.0924, found: 467.0923.

Sodium 4'-(α -D-mannopyranosyloxy)-3'-methoxybiphenyl-4-carboxylate (14 d): Prepared according to general procedure D from **12 d** (47 mg, 0.080 mmol). Yield: 10 mg (29%). [α]_D²⁰ + 115.1 (*c* = 0.30, MeOH); ¹H NMR (500 MHz, D₂O): δ = 7.81–7.79 (m, 2H, Ar-H), 7.54–7.53 (m, 2H, Ar-H), 7.19–7.11 (m, 3H, Ar-H), 5.43 (d, *J* = 1.6 Hz, 1H, H-1), 4.10 (dd, *J* = 1.8, 3.5 Hz, 1H, H-2), 3.96 (dd, *J* = 3.5, 9.0 Hz, 1H, H-3), 3.78 (s, 3H, OCH₃), 3.70–3.62 ppm (m, 4H, H-4, H-5, H-6); ¹³C NMR (125 MHz, D₂O): δ = 175.24 (CO), 149.53, 144.24, 142.42, 135.59, 134.75, 129.40, 126.41, 119.86, 118.03, 111.44 (12C, Ar-C), 99.23 (C-1), 73.53 (C-5), 70.32 (C-3), 69.78 (C-2), 66.40 (C-4), 60.54

(C-6), 55.81 ppm (OCH₃); HRMS: *m/z*: calcd for C₂₀H₂₂NaO₉ [M+Na]⁺: 429.1156, found: 429.1154.

Sodium 3'-cyclopropyl-4'-(α -D-mannopyranosyloxy)biphenyl-4-carboxylate (14 e): Prepared according to general procedure D from **12 e** (28 mg, 0.047 mmol). Yield: 6 mg (26%). [α]_D²⁰ + 149.8 (*c* = 0.20, MeOH); ¹H NMR (500 MHz, D₂O): δ = 7.79–7.77 (m, 2H, Ar-H), 7.48–7.46 (m, 2H, Ar-H), 7.30 (d, *J* = 7.8 Hz, 1H, Ar-H), 7.07–7.05 (m, 2H, Ar-H), 5.52 (s, 1H, H-1), 4.10 (m, 1H, H-2), 3.98 (dd, *J* = 3.4, 9.5 Hz, 1H, H-3), 3.69–3.62 (m, 4H, H-4, H-5, H-6), 1.99 (m, 1H, H-cPr), 0.86–0.84 (m, 2H, CH₂-cPr), 0.58–0.56 ppm (m, 2H, CH₂-cPr); ¹³C NMR (125 MHz, D₂O): δ = 175.34 (CO), 153.82, 142.58, 134.57, 134.34, 133.74, 129.38, 126.26, 125.01, 124.01, 115.47 (12C, Ar-C), 97.88 (C-1), 73.47 (C-5), 70.55 (C-3), 69.93 (C-2), 66.46 (C-4), 60.57 (C-6), 9.16, 7.26, 7.06 ppm (cPr); HRMS: *m/z*: calcd for C₂₂H₂₄ONaO₈ [M+Na]⁺: 439.1363, found: 439.1363.

Sodium 3'-cyano-4'-(α -D-mannopyranosyloxy)biphenyl-4-carboxylate (14 f): A two-neck flask was charged with **10 f** (150 mg, 0.28 mmol), 4-carboxybenzene boronic acid pinacol ester (**15**) (77 mg, 0.31 mmol), Pd(dppf)Cl₂·CH₂Cl₂ (7 mg, 0.008 mmol), K₃PO₄ (89 mg, 0.42 mmol) and a stirring bar. The flask was evacuated and flushed with argon, then anhydrous DMF (2 mL) was added under a stream of argon. The mixture was degassed in an ultrasonic bath and flushed with argon for 5 min, and then stirred at 80 °C overnight. The reaction mixture was cooled to RT, diluted with EtOAc (50 mL), and washed with H₂O (50 mL) and brine (50 mL). The organic layer was dried over Na₂SO₄ and concentrated in vacuo. The residue was purified by MPLC on silica gel (CH₂Cl₂/MeOH, 10:1–8:1) to afford the biphenyl intermediate (162 mg). The intermediate was dissolved in dry MeOH (4 mL) and treated with freshly prepared 1 M NaOMe/MeOH (28 μ L) for 4 h at RT. The reaction mixture was neutralized with Amberlyst-15 (H⁺), filtered and concentrated. The crude product was transformed into the sodium salt by passing through a small column of Dowex 50X8 (Na⁺ form) ion-exchange resin. After concentration the residue was purified by MPLC (RP-18, H₂O) followed by size-exclusion chromatography (P-2 gel, H₂O) to give **14 f** (19 mg, 17%) as a white solid after final lyophilization from H₂O. [α]_D²⁰ + 75.3 (*c* = 0.20, MeOH); ¹H NMR (500 MHz, D₂O): δ = 7.86–7.79 (m, 4H, Ar-H), 7.53–7.52 (m, 2H, Ar-H), 7.31 (d, *J* = 8.9 Hz, 1H, Ar-H), 5.64 (d, *J* = 1.9 Hz, 1H, H-1), 4.11 (dd, *J* = 1.9, 3.4 Hz, 1H, H-2), 4.00 (dd, *J* = 3.5, 9.7 Hz, 1H, H-3), 3.73–3.65 (m, 3H, H-4, H-6), 3.58 ppm (ddd, *J* = 2.4, 5.5, 9.9 Hz, 1H, H-5); ¹³C NMR (125 MHz, D₂O): δ = 175.12 (CO), 156.82, 140.37, 134.39, 133.56, 131.83, 129.58, 126.25, 116.82, 115.78, 102.08 (13C, Ar-C, CN), 98.09 (C-1), 73.97 (C-5), 70.29 (C-3), 69.54 (C-2), 66.36 (C-4), 60.56 ppm (C-6); HRMS: *m/z*: calcd for C₂₁H₂₁NNaO₈ [M+Na]⁺: 424.1003, found: 424.1003.

3-Bromobenzyl 2,3,4,6-tetra-O-acetyl- α -D-mannopyranoside (17 a): Prepared according to general procedure A from **8**^[12] and 3-bromobenzyl alcohol (**16 a**). Yield: 100 mg (34%) as colorless oil. *R*_f = 0.43 (PE/EtOAc, 2:1); [α]_D²⁰ + 42.0 (*c* = 1.40, EtOAc); ¹H NMR (500 MHz, CDCl₃): δ = 7.48–7.46, 7.30–7.24 (m, 4H, Ar-H), 5.37 (dd, 1H, *J* = 3.4, 10.1 Hz, H-3), 5.33–5.29 (m, 2H, H-2, H-4), 4.88 (d, 1H, *J* = 1.3 Hz, H-1), 4.68, 4.54 (A, B of AB, *J* = 12.1 Hz, 2H, CH₂Ar), 4.29 (dd, 1H, *J* = 5.2, 12.3 Hz, H-6a), 4.07 (dd, 1H, *J* = 2.3, 12.3 Hz, H-6b), 3.99 (ddd, 1H, *J* = 2.4, 5.2, 9.9 Hz, H-5), 2.15, 2.13, 2.05, 2.00 ppm (4 s, 12H, 4 OAc); ¹³C NMR (125 MHz, CDCl₃): δ = 170.59, 169.98, 169.87, 169.69 (4 CO), 138.49, 131.34, 131.09, 130.24, 126.66, 122.57 (Ar-C), 96.83 (C-1), 69.43, 69.02, 68.90, 68.78 (C-2, C-3, C-5, CH₂Ar), 66.03 (C-4), 62.36 (C-6), 20.86, 20.76, 20.68 ppm (4C, COCH₃); ESI-MS: *m/z*: calcd for C₂₁H₂₅BrNaO₁₀ [M+Na]⁺: 539.05, found: 539.14.

5-Bromo-2-chlorobenzyl 2,3,4,6-tetra-O-acetyl- α -D-mannopyranoside (17b): Prepared according to general procedure A from **8**^[12] and 5-bromo-2-chlorobenzyl alcohol (**16b**). Yield: 152 mg (48%) as a white solid. $R_f=0.56$ (PE/EtOAc, 2:1); $[\alpha]_D^{20} + 48.0$ ($c=1.50$, EtOAc); ¹H NMR (500 MHz, CDCl₃): $\delta=7.48$ (t, $J=1.8$ Hz, 1H, Ar-H), 7.38 (s, 1H, Ar-H), 7.35 (d, $J=1.8$ Hz, 1H, Ar), 5.33 (m, 3H, H-2, H-3, H-4), 4.88 (d, $J=1.5$ Hz, 1H, H-1), 4.65, 4.51 (A, B of AB, $J=12.3$ Hz, 2H, CH₂Ar), 4.30 (dd, $J=5.3, 12.3$ Hz, 1H, H-6a), 4.09 (dd, $J=2.4, 12.3$ Hz, 1H, H-6b), 3.98 (ddd, $J=2.4, 5.2, 9.7$ Hz, 1H, H-5), 2.16, 2.13, 2.05, 2.01 ppm (4 s, 12H, 4 OAc); ¹³C NMR (125 MHz, CDCl₃): $\delta=170.58, 169.98, 169.89, 169.69$ (4 CO), 139.77, 135.35, 129.25, 126.85, 122.91 (6C, Ar-C), 96.96 (C-1), 69.33, 68.93, 68.24 (4C, C-2, C-3, C-5, CH₂Ar), 65.98 (C-4), 62.38 (C-6), 20.86, 20.77, 20.68 ppm (4C, 4COCH₃); ESI-MS: m/z : calcd for C₂₁H₂₄BrClNaO₁₀ [M+Na]⁺: 573.01, found: 573.06.

2-Bromobenzyl 2,3,4,6-tetra-O-acetyl- α -D-mannopyranoside (17c): Prepared according to general procedure A from **8**^[12] and 2-bromobenzyl alcohol (**16c**). Yield: 140 mg (47%) as a white solid. $R_f=0.55$ (petrol ether/EtOAc, 2:1); $[\alpha]_D^{20} + 44.6$ ($c=2.10$, EtOAc); ¹H NMR (500 MHz, CDCl₃): $\delta=7.57$ (dd, $J=1.0, 8.0$ Hz, 1H, Ar-H), 7.47 (dd, $J=1.4, 7.6$ Hz, 1H, Ar-H), 7.35 (td, $J=1.1, 7.5$ Hz, 1H, Ar-H), 7.20 (td, $J=1.7, 7.9$ Hz, 1H, Ar-H), 5.41 (dd, $J=3.5, 10.0$ Hz, 1H, H-3), 5.35 (dd, $J=1.8, 3.5$ Hz, 1H, H-2), 5.31 (t, $J=9.9$ Hz, 1H, H-4), 4.98 (d, $J=1.6$ Hz, 1H, H-1), 4.83, 4.61 (A, B of AB, $J=12.7$ Hz, 2H, CH₂Ar), 4.29 (dd, $J=5.8, 12.6$ Hz, 1H, H-6a), 4.10–4.06 (m, 2H, H-6b, H-5), 2.17, 2.12, 2.04, 2.00 ppm (4 s, 12H, 4 OAc); ¹³C NMR (125 MHz, CDCl₃): $\delta=170.64, 170.02, 169.88, 169.72$ (4 CO), 135.77, 132.69, 129.58, 129.49, 127.64, 122.96 (Ar-C), 97.33 (C-1), 69.48, 69.30, 69.10, 68.84 (C-2, C-3, C-5, CH₂Ar), 66.05 (C-4), 62.35 (C-6), 20.88, 20.76, 20.69 ppm (4C, 4COCH₃); ESI-MS: m/z : calcd for C₂₁H₂₅BrNaO₁₀ [M+Na]⁺: 539.05, found: 539.14.

Methyl 3'-[(2,3,4,6-tetra-O-acetyl- α -D-mannopyranosyloxy)methyl]biphenyl-4-carboxylate (18a): Prepared according to general procedure B from **17a** (87.0 mg, 0.167 mmol), **11** (33.1 mg, 0.184 mmol), Pd(dppf)Cl₂·CH₂Cl₂ (4.1 mg, 5.0 μ mol) and K₃PO₄ (53.2 mg, 0.251 mmol). Yield: 70 mg (73%) as colorless oil. $R_f=0.30$ (PE/EtOAc, 2:1); $[\alpha]_D^{20} + 41.2$ ($c=1.00$, EtOAc); ¹H NMR (500 MHz, CDCl₃): $\delta=8.13$ –8.11 (m, 2H, Ar-H), 7.68–7.67 (m, 2H, Ar-H), 7.60–7.58 (m, 2H, Ar-H), 7.48 (t, $J=4.7$ Hz, 1H, Ar-H), 7.39 (d, $J=7.7$ Hz, 1H, Ar-H), 5.41 (dd, $J=3.4, 10.0$ Hz, 1H, H-3), 5.33–5.30 (m, 2H, H-2, H-4), 4.94 (d, $J=1.5$ Hz, 1H, H-1), 4.79, 4.64 (A, B of AB, $J=12.0$ Hz, 2H, CH₂Ar), 4.30 (dd, $J=5.0, 12.1$ Hz, 1H, H-6a), 4.09–4.03 (m, 2H, H-6b, H-5), 3.94 (s, 3H, OMe), 2.15, 2.11, 2.04, 2.00 ppm (4 s, 12H, 4 OAc); ¹³C NMR (125 MHz, CDCl₃): $\delta=170.64, 170.03, 169.91, 169.73, 166.94$ (5 CO), 145.11, 140.41, 136.97, 130.15, 129.27, 129.09, 127.94, 127.22, 127.11 (12C, Ar-C), 96.76 (C-1), 69.57, 69.09, 68.94, 66.12 (C-2, C-3, C-5, CH₂Ar), 62.40 (C-4), 60.38 (C-6), 52.15 (OMe), 20.89, 20.77, 20.69 ppm (4C, 4COCH₃); ESI-MS: m/z : calcd for C₂₉H₃₂NaO₁₂ [M+Na]⁺: 595.18, found: 595.21.

Methyl 3'-[(2,3,4,6-tetra-O-acetyl- α -D-mannopyranosyloxy)methyl]-4'-chlorobiphenyl-4-carboxylate (18b): Prepared according to general procedure B from **17b** (143 mg, 0.260 mmol), **11** (51.5 mg, 0.286 mmol), Pd(dppf)Cl₂·CH₂Cl₂ (6.4 mg, 7.8 μ mol) and K₃PO₄ (82.8 mg, 0.390 mmol). Yield: 133 mg (84%) as colorless oil. $R_f=0.30$ (PE/EtOAc, 2:1); $[\alpha]_D^{20} + 45.9$ ($c=1.20$, EtOAc); ¹H NMR (500 MHz, CDCl₃): $\delta=8.13$ –8.11 (m, 2H, Ar-H), 7.65–7.64 (m, 2H, Ar-H), 7.57 (t, $J=1.8$ Hz, 1H, Ar-H), 7.47 (s, 1H, Ar-H), 7.37 (s, 1H, Ar-H), 5.40 (dd, $J=3.4, 10.1$ Hz, 1H, H-3), 5.33–5.29 (m, 2H, H-2, H-4), 4.93 (d, $J=1.4$ Hz, 1H, H-1), 4.76, 4.61 (A, B of AB, $J=12.1$ Hz, 2H, CH₂Ar), 4.31 (dd, $J=5.2, 12.3$ Hz, 1H, H-6a), 4.11 (dd, $J=2.3, 12.3$ Hz, 1H, H-6b), 4.03 (ddd, $J=2.4, 5.2, 9.9$ Hz, 1H, H-5), 3.95 (s, 3H, OMe), 2.16, 2.12, 2.05, 2.00 ppm (4 s, 12H, 4OAc); ¹³C NMR

(125 MHz, CDCl₃): $\delta=170.61, 170.02, 169.90, 169.72, 166.75$ (5 CO), 143.68, 142.16, 138.79, 135.11, 130.26, 129.68, 127.14, 125.14 (12C, Ar-C), 96.85 (C-1), 68.99, 68.89, 68.85, 66.07 (C-2, C-3, C-5, CH₂Ar), 62.42 (C-4), 60.39 (C-6), 52.23 (OMe), 20.89, 20.78, 20.71, 20.69 ppm (4COCH₃); ESI-MS: m/z : calcd for C₂₉H₃₁ClNaO₁₂ [M+Na]⁺: 629.14, found: 629.10.

Methyl 2'-[(2,3,4,6-tetra-O-acetyl- α -D-mannopyranosyloxy)methyl]biphenyl-4-carboxylate (21): Prepared according to general procedure B from **17c** (115 mg, 0.223 mmol), **11** (44.1 mg, 0.245 mmol), Pd(dppf)Cl₂·CH₂Cl₂ (5.5 mg, 6.7 μ mol) and K₃PO₄ (71.0 mg, 0.335 mmol). Yield: 120 mg (94%) as colorless oil. $R_f=0.41$ (PE/EtOAc, 2:1); $[\alpha]_D^{20} + 38.3$ ($c=2.00$, EtOAc); ¹H NMR (500 MHz, CDCl₃): $\delta=8.11$ –8.10 (m, 2H, Ar-H), 7.51–7.48 (m, 1H, Ar-H), 7.45–7.41 (m, 4H, Ar-H), 7.29 (m, 1H, Ar-H), 5.27–5.21 (m, 2H, H-3, H-4), 5.19 (dd, $J=1.9, 3.3$ Hz, 1H, H-2), 4.77 (d, $J=1.4$ Hz, 1H, H-1), 4.67, 4.34 (A, B of AB, $J=11.3$ Hz, 2H, CH₂Ar), 4.13 (dd, $J=5.2, 12.5$ Hz, 1H, H-6a), 3.94 (s, 3H, OMe), 3.90 (dd, $J=2.2, 12.3$ Hz, 1H, H-6a), 3.52 (ddd, $J=2.2, 5.1, 9.3$ Hz, 1H, H-5), 2.13, 2.05, 2.04, 1.99 ppm (4 s, 12H, 4 OAc); ¹³C NMR (125 MHz, CDCl₃): $\delta=170.52, 169.95, 169.82, 169.74, 166.77$ (5 CO), 145.48, 141.44, 133.46, 129.99, 129.91, 129.58, 129.22, 128.52, 128.21 (12C, Ar-C), 97.20 (C-1), 69.47 (C-2), 68.98 (C-3), 68.48 (C-5), 68.13 (CH₂Ar), 65.88 (C-4), 62.15 (C-6), 52.18 (OMe), 20.85, 20.66, 20.62 ppm (4C, 4COCH₃); ESI-MS: m/z : calcd for C₂₉H₃₂NaO₁₂ [M+Na]⁺: 595.18, found: 595.21.

Methyl 3'-[(α -D-mannopyranosyloxy)methyl]biphenyl-4-carboxylate (19a): Prepared according to general procedure C from **18a** (24 mg, 0.042 mmol). Yield: 11 mg (65%). $R_f=0.40$ (CH₂Cl₂/MeOH, 8:1); $[\alpha]_D^{20} + 68.0$ ($c=0.34$, MeOH); ¹H NMR (500 MHz, CD₃OD): $\delta=8.11$ –8.09 (m, 2H, Ar-H), 7.77–7.75 (m, 2H, Ar-H), 7.70 (s, 1H, Ar-H), 7.63 (d, $J=7.6$ Hz, 1H, Ar-H), 7.49 (t, $J=7.6$ Hz, 1H, Ar-H), 7.45 (d, $J=7.6$ Hz, 1H, Ar-H), 4.90 (d, $J=1.8$ Hz, 1H, H-1), 4.86, 4.63 (A, B of AB, $J=12.0$ Hz, 2H, CH₂Ar), 3.94 (s, 3H, OMe), 3.89–3.87 (m, 2H, H-2, H-3), 3.79–3.73 (m, 2H, H-4, H-6a), 3.68–3.64 ppm (m, 2H, H-5, H-6b); ¹³C NMR (125 MHz, CD₃OD): $\delta=168.42$ (CO), 146.91, 141.31, 139.97, 131.13, 130.20, 129.07, 128.17, 127.91, 127.67 (12C, Ar-C), 100.76 (C-1), 75.02 (C-5), 72.65 (C-3), 72.22 (C-2), 69.73 (CH₂Ar), 68.65 (C-4), 62.98 (C-6), 52.66 ppm (OMe); HRMS: m/z : calcd for C₂₁H₂₄NaO₈ [M+Na]⁺: 427.1363, found: 427.1361.

Methyl 4'-chloro-3'-[(α -D-mannopyranosyloxy)methyl]biphenyl-4-carboxylate (19b): Prepared according to general procedure C from **18b** (40 mg, 0.066 mmol). Yield: 26 mg (90%). $R_f=0.19$ (CH₂Cl₂/MeOH, 8:1); $[\alpha]_D^{20} + 101.8$ ($c=0.50$, MeOH); ¹H NMR (500 MHz, CD₃OD): $\delta=8.06$ (d, $J=8.4$ Hz, 2H, Ar-H), 7.69 (d, $J=8.4$ Hz, 2H, Ar-H), 7.57–7.56 (m, 2H, Ar-H), 7.41 (s, 1H, Ar-H), 4.87 (s, 1H, H-1), 4.80, 4.58 (A, B of AB, $J=12.3$ Hz, 2H, CH₂Ar), 3.91 (s, 3H, OMe), 3.87–3.83 (m, 2H, H-2, H-3), 3.74–3.57 ppm (m, 4H, H-4, H-5, H-6); ¹³C NMR (125 MHz, CD₃OD): $\delta=168.74$ (CO), 145.78, 143.68, 142.71, 136.55, 131.75, 131.31, 129.02, 128.77, 127.95, 126.63 (12C, Ar-C), 101.47 (C-1), 75.65 (C-5), 73.16 (C-3), 72.65 (C-2), 69.49 (CH₂Ar), 69.13 (C-4), 63.49 (C-6), 53.26 ppm (OMe); HRMS: m/z : calcd for C₂₁H₂₃ClNaO₈ [M+Na]⁺: 461.0974, found: 461.0975.

Methyl 2'-[(α -D-mannopyranosyloxy)methyl]biphenyl-4-carboxylate (22): Prepared according to general procedure C from **21** (48 mg, 0.084 mmol). Yield: 16 mg (47%). $R_f=0.42$ (CH₂Cl₂/MeOH, 8:1); $[\alpha]_D^{20} + 61.9$ ($c=0.90$, MeOH); ¹H NMR (500 MHz, CD₃OD): $\delta=8.11$ –8.09 (m, 2H, Ar-H), 7.57 (m, 1H, Ar-H), 7.51–7.49 (m, 2H, Ar-H), 7.43–7.40 (m, 2H, Ar-H), 7.31 (m, 1H, Ar-H), 4.71 (A of AB, $J=11.4$ Hz, 1H, CH₂Ar), 4.70 (d, $J=1.5$ Hz, 1H, H-1), 4.38 (B of AB, $J=11.4$ Hz, 1H, CH₂Ar), 3.75–3.60 (m, 5H, H-2, H-3, H-4, H-6), 3.95 (s, 3H, OMe), 3.40 ppm (ddd, $J=3.0, 5.6, 6.8$ Hz, 1H, H-5); ¹³C NMR

(125 MHz, CD₃OD): δ = 168.42 (CO), 147.33, 142.66, 136.03, 130.83, 130.53, 130.47, 129.26, 129.15 (12C, Ar-C), 101.14 (C-1), 74.78 (C-5), 72.60 (C-3), 72.18 (C-2), 68.37 (2C, C-4, CH₂Ar), 62.71 ppm (C-6), 52.69 (OMe); HRMS: m/z : calcd for C₂₁H₂₄NaO₈Na [M + Na]⁺: 427.1363, found: 427.1367.

Sodium 3'-[(α -D-mannopyranosyloxy)methyl]biphenyl-4-carboxylate (6): Prepared according to general procedure D from **18a** (35 mg, 0.061 mmol). Yield: 24 mg (96%). [α]_D²⁰ + 64.5 (c = 0.30, MeOH/H₂O 1:1); ¹H NMR (500 MHz, D₂O): δ = 7.80–7.78 (m, 2H, Ar-H), 7.50–7.43 (m, 4H, Ar-H), 7.31–7.24 (m, 2H, Ar-H), 4.82 (s, 1H, H-1), 4.58, 4.40 (A, B of AB, J = 11.5 Hz, 2H, CH₂Ar), 3.82 (m, 1H, H-2), 3.75–3.50 ppm (m, 5H, H-3, H-4, H-5, H-6); ¹³C NMR (125 MHz, D₂O): δ = 175.14 (CO), 142.69, 140.05, 137.34, 135.01, 129.46, 129.28, 127.92, 126.87, 126.64 (12C, Ar-C), 99.40 (C-1), 72.84 (C-5), 70.51 (C-3), 70.01 (C-2), 69.29 (CH₂Ar), 66.61 (C-4), 60.71 ppm (C-6); HRMS: m/z : calcd for C₂₀H₂₂NaO₈ [M + Na]⁺: 413.1207, found: 413.1211.

Sodium 4'-chloro-3'-[(α -D-mannopyranosyloxy)methyl]biphenyl-4-carboxylate (20): Prepared according to general procedure D from **18b** (54 mg, 0.089 mmol). Yield: 4 mg (10%). [α]_D²⁰ + 44.7 (c = 0.30, MeOH); ¹H NMR (500 MHz, D₂O): δ = 7.86 (d, J = 7.8 Hz, 2H, Ar-H), 7.58–7.56 (m, 3H, Ar-H), 7.46, 7.34 (2 s, 2H, Ar-H), 4.90 (s, 1H, H-1), 4.58, 4.50 (A, B of AB, J = 12.3 Hz, 2H, CH₂Ar), 3.91 (s, 1H, H-2), 3.78–3.75 (m, 2H, H-3, H-4), 3.71–3.59 ppm (m, 3H, H-5, H-6); ¹³C NMR (125 MHz, D₂O): δ = 174.76 (CO), 141.82, 141.55, 139.40, 134.37, 129.56, 127.34, 126.74, 126.62, 125.15 (12C, Ar-C), 99.99 (C-1), 72.96 (C-5), 70.55 (C-3), 70.04 (C-2), 68.72 (CH₂Ar), 66.66 (C-4), 60.77 ppm (C-6); HRMS: m/z : calcd for C₂₀H₂₁ClNaO₈ [M + Na]⁺: 447.0817, found: 447.0816.

Sodium 2'-[(α -D-mannopyranosyloxy)methyl]biphenyl-4-carboxylate (23): Prepared according to general procedure D from **21** (78 mg, 0.137 mmol). Yield: 26 mg (46%). [α]_D²⁰ + 53.2 (c = 0.40, MeOH); ¹H NMR (500 MHz, D₂O): δ = 7.91–7.89 (m, 2H, Ar-H), 7.43–7.34 (m, 5H, Ar-H), 7.26 (m, 1H, Ar-H), 4.68 (s, 1H, H-1), 4.57, 4.31 (A, B of AB, J = 10.8 Hz, 2H, CH₂Ar), 3.57 (m, 1H, H-2), 3.46–3.39 (m, 4H, H-3, H-4, H-6), 2.83 ppm (m, 1H, H-5); ¹³C NMR (125 MHz, D₂O): δ = 173.20 (CO), 144.48, 141.80, 133.47, 132.43, 130.69, 129.95, 129.27, 128.96, 128.32 (12C, Ar-C), 99.90 (C-1), 72.44 (C-5), 70.33 (C-3), 69.82 (C-2), 68.14 (CH₂Ar), 65.99 (C-4), 60.25 ppm (C-6); HRMS: m/z : calcd for C₂₀H₂₂NaO₈ [M + Na]⁺: 413.1207, found: 413.1208.

4-(4,4,5,5-Tetramethyl)-1,3,2-dioxaborolan-2-yl)phenyl 2,3,4,6-tetra-O-acetyl- α -D-mannopyranoside (27): A microwave tube was charged with **26**^[37] (240 mg, 0.55 mmol), KOAc (161 mg, 1.65 mmol), bis(pinacolato)diboron (152 mg, 0.60 mmol) and Pd(dppf)Cl₂·CH₂Cl₂ (13 mg, 0.017 mmol). The tube was closed, evacuated and flushed with argon. Then anhydrous DMF (1 mL) was added under a stream of argon. The mixture was degassed in an ultrasonic bath and flushed with argon for 5 min, and then heated by microwave irradiation at 120 °C for 2 h. The reaction mixture was cooled to RT and diluted with CH₂Cl₂/H₂O (100 mL, 1:1). The organic layer was washed with H₂O (50 mL) and brine (50 mL), dried over Na₂SO₄ and concentrated. The residue was purified by MPLC (toluene/EtOAc, 4:1) to afford **27** (120 mg, 50%) as colorless oil. [α]_D²⁰ + 58.1 (c = 0.60, EtOAc); ¹H NMR (500 MHz, CDCl₃): δ = 7.76 (d, J = 8.6 Hz, 2H, Ar-H), 7.08 (d, J = 8.6 Hz, 2H, Ar-H), 5.58–5.55 (m, 2H, H-1, H-3), 5.45 (dd, J = 1.9, 3.4 Hz, 1H, H-2), 5.37 (t, J = 10.0 Hz, 1H, H-4), 4.28 (dd, J = 5.0, 12.0 Hz, 1H, H-6a), 4.05–4.02 (m, 2H, H-6b, H-5), 2.20, 2.05, 2.03 (3 s, 12H, 4 OAc), 1.33 ppm (s, 12H, 4 CH₃); ¹³C NMR (125 MHz, CDCl₃): δ = 170.55, 169.91, 169.74 (4C, 4 CO), 157.98, 136.62, 136.58, 115.67 (5C, Ar-C), 95.44 (C-1), 83.77 (Ar-C), 69.37 (C-2), 69.21 (C-5), 68.87 (C-3), 65.92 (C-4), 62.06 (C-6),

24.86, 24.58 (4C, 4 CH₃), 20.87, 20.69 ppm (4C, 4 COCH₃); ESI-MS: m/z : calcd for C₂₆H₃₅BNaO₁₂ [M + Na]⁺: 573.21, found: 573.32.

Methyl 2-[4'-(2,3,4,6-tetra-O-acetyl- α -D-mannopyranosyloxy)biphenyl-4-yl]acetate (29): Prepared according to general procedure B from methyl 2-(4-bromophenyl)acetate (**28**, 41.2 mg, 0.180 mmol), **27** (109 mg, 0.198 mmol), Pd(dppf)Cl₂·CH₂Cl₂ (4.4 mg, 5.4 μ mol) and K₃PO₄ (57.3 mg, 0.270 mmol). Yield: 35 mg (34%) as yellow oil. R_f = 0.25 (petrol ether/EtOAc 2:1); [α]_D²⁰ + 75.09 (c = 0.8, EtOAc); ¹H NMR (500 MHz, CDCl₃): δ = 7.52–7.49 (m, 4H, Ar-H), 7.35–7.33 (m, 2H, Ar-H), 7.17–7.14 (m, 2H, Ar-H), 5.60–5.56 (m, 2H, H-1, H-3), 5.47 (dd, J = 1.8, 3.5 Hz, 1H, H-2), 5.38 (t, J = 10.0 Hz, 1H, H-4), 4.29 (dd, J = 5.0, 11.9 Hz, 1H, H-6a), 4.15–4.08 (m, 2H, H-6b, H-5), 3.71 (s, 3H, OMe), 3.66 (s, 2H, ArCH₂), 2.21, 2.06, 2.05, 2.03 ppm (4 s, 12H, 4 OAc); ¹³C NMR (125 MHz, CDCl₃): δ = 171.99, 170.53, 169.99, 169.95, 169.76 (5 CO), 155.09, 139.26, 135.72, 132.83, 129.73, 128.21, 127.03, 116.82 (12C, Ar-C), 95.87 (C-1), 69.43 (C-2), 69.23 (C-5), 68.91 (C-3), 65.99 (C-4), 62.15 (C-6), 52.11 (OMe), 40.78 (ArCH₂), 20.88, 20.71, 20.70, 20.67 ppm (4 COCH₃); ESI-MS: m/z : calcd for C₂₉H₃₂NaO₁₂ [M + Na]⁺: 595.18, found: 595.21.

Methyl 2-[4'-(2,3,4,6-tetra-O-acetyl- α -D-mannopyranosyloxy)biphenyl-4-yl]cyclopropanecarboxylate (33): Prepared according to general procedure B from methyl 1-(4-bromophenyl)cyclopropanecarboxylate (**32**, 42.6 mg, 0.167 mmol), **27** (101 mg, 0.184 mmol), Pd(dppf)Cl₂·CH₂Cl₂ (4.1 mg, 5.0 μ mol) and K₃PO₄ (53.2 mg, 0.251 mmol). Yield: 60 mg (56%) as colorless oil. R_f = 0.31 (PE/EtOAc, 2:1); [α]_D²⁰ + 70.2 (c = 1.00, EtOAc); ¹H NMR (500 MHz, CDCl₃): δ = 7.54–7.48 (m, 4H, Ar-H), 7.40–7.39 (m, 2H, Ar-H), 7.17–7.14 (m, 2H, Ar-H), 5.59 (dd, J = 3.55, 10.1 Hz, 1H, H-3), 5.56 (d, J = 1.6 Hz, 1H, H-1), 5.46 (dd, J = 1.9, 3.5 Hz, 1H, H-2), 5.38 (t, J = 10.0 Hz, 1H, H-4), 4.29 (dd, J = 5.1, 12.0 Hz, 1H, H-6a), 4.15–4.09 (m, 2H, H-6b, H-5), 3.65 (s, 3H, OMe), 2.21, 2.06, 2.05, 2.03 (4 s, 12H, 4 OAc), 1.64–1.62 (m, 2H, cPr), 1.27–1.16 ppm (m, 2H, cPr); ¹³C NMR (125 MHz, CDCl₃): δ = 175.04, 170.53, 169.98, 169.95, 169.75 (5 CO), 155.10, 139.25, 138.43, 135.76, 130.94, 128.24, 126.61, 116.80 (12C, Ar-C), 95.89 (C-1), 69.44 (C-5), 69.23 (C-2), 68.90 (C-3), 66.00 (C-4), 62.15 (C-6), 52.42 (OMe), 28.67 (cPr), 20.71, 20.68 (4C, 4 COCH₃), 16.75 ppm (cPr); ESI-MS: m/z : calcd for C₃₁H₃₄NaO₁₂ [M + Na]⁺: 621.19, found: 621.26.

Methyl 2-[4'-(α -D-mannopyranosyloxy)biphenyl-4-yl]acetate (30): Prepared according to general procedure C from **29** (30 mg, 0.052 mmol). Yield: 20 mg (95%). R_f = 0.25 (CH₂Cl₂/MeOH, 8:1); [α]_D²⁰ + 116.0 (c = 0.50, MeOH); ¹H NMR (500 MHz, CD₃OD): δ = 7.57–7.53 (m, 4H, Ar-H), 7.34–7.33 (m, 2H, Ar-H), 7.22–7.20 (m, 2H, Ar-H), 5.54 (d, J = 1.5 Hz, 1H, H-1), 4.05 (dd, J = 1.8, 3.3 Hz, 1H, H-2), 3.95 (dd, J = 3.4, 9.5 Hz, 1H, H-3), 3.82–3.74 (m, 3H, H-4, H-6), 3.71 (s, 3H, OMe), 3.66 (s, 2H, ArCH₂), 3.65 ppm (ddd, J = 2.5, 5.2, 9.7 Hz, 1H, H-5); ¹³C NMR (125 MHz, CD₃OD): δ = 174.02 (CO), 157.50, 140.77, 136.22, 134.29, 130.81, 129.00, 127.77, 118.13 (12C, Ar-C), 100.23 (C-1), 75.42 (C-5), 72.45 (C-3), 72.03 (C-2), 68.38 (C-4), 62.70 (C-6), 52.49 (OMe), 41.34 ppm (ArCH₂); HRMS: m/z : calcd for C₂₁H₂₄NaO₈ [M + Na]⁺: 427.1363, found: 427.1363.

Methyl 2-[4'-(α -D-mannopyranosyloxy)biphenyl-4-yl]cyclopropanecarboxylate (34): Prepared according to general procedure C from **33** (38 mg, 0.063 mmol). Yield: 9 mg (33%). R_f = 0.33 (CH₂Cl₂/MeOH, 8:1); [α]_D²⁰ + 108.0 (c = 0.30, MeOH); ¹H NMR (500 MHz, CD₃OD): δ = 7.46–7.39 (m, 4H, Ar-H), 7.28–7.26 (m, 2H, Ar-H), 7.10–7.07 (m, 2H, Ar-H), 5.42 (d, J = 1.7 Hz, 1H, H-1), 3.93 (dd, J = 1.9, 3.4 Hz, 1H, H-2), 3.82 (dd, J = 3.4, 9.4 Hz, 1H, H-3), 3.69–3.61 (m, 3H, H-4, H-6), 3.53 (m, 4H, OMe, H-5), 1.49–1.47 (m, 2H, cPr), 1.14–1.11 ppm (m, 2H, cPr); ¹³C NMR (125 MHz, CD₃OD): δ = 157.50, 140.87, 139.51, 136.26, 132.03, 129.04, 127.43, 118.11 (12C, Ar-C),

100.20 (C-1), 75.43 (C-5), 72.42 (C-3), 72.02 (C-2), 68.34 (C-4), 62.68 (C-6), 52.81 (OMe), 17.20 ppm (2C, cPr); HRMS: m/z : calcd for $C_{23}H_{26}NaO_8 [M+Na]^+$: 453.1520, found: 453.1523.

Sodium 2-[4'-(α -D-mannopyranosyloxy)biphenyl-4-yl]acetate (31): Prepared according to general procedure D from **29** (59 mg, 0.103 mmol). Yield: 17 mg (40%). $[\alpha]_D^{20} + 94.0$ ($c = 0.20$, MeOH/H₂O 1:1); 1H NMR (500 MHz, D₂O): $\delta = 7.61$ (d, $J = 8.6$ Hz, 2H, Ar-H), 7.55 (d, $J = 8.0$ Hz, 2H, Ar-H), 7.31 (d, $J = 8.0$ Hz, 2H, Ar-H), 7.19 (d, $J = 8.6$ Hz, 2H, Ar-H), 5.60 (s, 1H, H-1), 4.13 (m, 1H, H-2), 4.00 (dd, $J = 3.2, 8.5$ Hz, 1H, H-3), 3.75–3.67 (m, 4H, H-4, H-5, H-6), 3.51 ppm (s, 2H, ArCH₂); ^{13}C NMR (125 MHz, D₂O): $\delta = 154.94, 137.93, 136.29, 135.08, 129.76, 128.07, 126.72, 117.49$ (12C, Ar-C), 98.20 (C-1), 73.37 (C-5), 70.40 (C-3), 69.89 (C-2), 66.58 (C-4), 60.65 (C-6), 43.89 ppm (ArCH₂); HRMS: m/z : calcd for $C_{20}H_{22}NaO_8 [M+Na]^+$: 413.1207, found: 413.1208.

Sodium 2-[4'-(α -D-mannopyranosyloxy)biphenyl-4-yl]cyclopropanecarboxylate (35): Prepared according to general procedure D from **33** (59 mg, 0.099 mmol). Yield: 10 mg (23%). $[\alpha]_D^{20} + 95.0$ ($c = 0.20$, dioxane/H₂O 1:1); 1H NMR (500 MHz, D₂O): $\delta = 7.62$ –7.60 (m, 2H, Ar-H), 7.54–7.53 (m, 2H, Ar-H), 7.38–7.19 (m, 4H, Ar-H), 5.60 (s, 1H, H-1), 4.13 (m, 1H, H-2), 4.00 (m, 1H, H-3), 3.75–3.67 (4H, H-4, H-5, H-6), 1.33 (s, 2H, cPr), 1.01 ppm (s, 2H, cPr); ^{13}C NMR (125 MHz, D₂O): $\delta = 128.67, 126.10, 124.37, 115.47$ (12C, Ar-C), 96.18 (C-1), 71.35 (C-5), 68.38 (C-3), 67.87 (C-2), 64.56 (C-4), 58.62 (C-6), 12.66 ppm (2C, cPr); HRMS: m/z : calcd for $C_{22}H_{24}NaO_8 [M+Na]^+$: 439.1363, found: 439.1363.

Competitive binding assay

A recombinant protein consisting of the CRD of FimH linked with a thrombin cleavage site (Th) to a His₆-tag (FimH-CRD-Th-His₆) was expressed in *E. coli* strain HM125 and purified by affinity chromatography.^[16] To determine the affinity of the various FimH antagonists, a competitive binding assay described previously^[16] was applied. Microtiter plates (F96 MaxiSorp, Nunc) were coated with a $10 \mu\text{g mL}^{-1}$ solution of FimH-CRD-Th-His₆ in 20 mM HEPES, 150 mM NaCl, and 1 mM CaCl₂, pH 7.4 (assay buffer), 100 μL per well, overnight at 4 °C. The coating solution was discarded, and the wells were blocked with 3% BSA in assay buffer (150 μL per well) for 2 h at 4 °C. After three washing steps with assay buffer (150 μL per well), a fourfold serial dilution of the test compound (50 μL per well) in assay buffer containing 5% DMSO and streptavidin-peroxidase coupled Man- α (1–3)[Man- α (1–6)]-Man- β (1–4)-GlcNAc- β (1–4)-GlcNAc β polyacrylamide (TM-PAA) polymer (50 μL per well of a $0.5 \mu\text{g mL}^{-1}$ solution) were added. On each individual microtiter plate, *n*-heptyl α -D-mannopyranoside (**1**) was tested in parallel. The plates were incubated for 3 h at 25 °C and 350 rpm and then carefully washed four times with 150 μL per well assay buffer. After the addition of 100 μL per well of 2,2'-azino-di-(3-ethylbenzthiazoline-6-sulfonic acid) (ABTS) substrate, the colorimetric reaction was allowed to develop for 4 min and then was stopped by the addition of 2% aqueous oxalic acid before the optical density (OD) was measured at 415 nm on a microplate reader (Spectramax 190, Molecular Devices, CA, USA). The IC₅₀ values of the compounds tested in duplicate were calculated with Prism software (GraphPad Software Inc., La Jolla, CA, USA). The IC₅₀ defines the molar concentration of the test compound that decreases the maximal specific binding of TM-PAA polymer to FimH-CRD by 50%. The relative IC₅₀ (rIC₅₀) is the ratio of the IC₅₀ of the test compound to the IC₅₀ of *n*-heptyl α -D-mannopyranoside (**1**).

Cell-based flow cytometry assay

The assay was performed as described previously.^[17] Briefly, 5637 cells (DSMZ, Braunschweig, Germany) were grown to confluence in 24-well plates. Before infection, a serial dilution of test compound in 5% DMSO, PBS (Sigma–Aldrich) was prepared. GFP-labeled UTI89 bacteria (200 μL) in RPMI 1640 medium (Invitrogen, Basel, Switzerland) were pre-incubated with test compound (25 μL) for 10 min at RT. The bacteria–antagonist mixtures were then added to the monolayers of 5637 cells. The multiplicity of infection (MOI) was 1:50 (cell/bacteria). To homogenize the infection, plates were centrifuged at RT for 3 min at 600 *g*. After an incubation time of 1.5 h at 37 °C, infected cells were washed four times with RPMI 1640 medium and suspended in ice-cold PBS for 5–20 min (treatment with ice-cold PBS results in the detachment of the infected cells). Cells were then kept in the dark until analysis. Samples were measured with a CyAn ADP flow cytometer (Beckman–Coulter, Brea, CA, USA) and analyzed by gating on the eukaryotic cells based on forward (FSC) and side scatter (SSC), which excludes unbound labeled bacteria and debris from analysis. A total of 10⁴ cells were measured per sample. Data were acquired in a linear mode for the SSC and logarithmic mode for FSC and the green fluorescent channel FL1-H (GFP). The mean fluorescence intensity (MFI) of GFP was counted as a surrogate marker for the adherence of bacteria. Quantification of adhesion was evaluated with the FlowJo software 9.0.1 (Tree Star Inc., Ashland, OR, USA). IC₅₀ values were determined by plotting the concentration of the antagonist in a logarithmic mode versus the MFI and by fitting the curve with Prism software (GraphPad, inhibition curve, variable slope), ($n = 2-3$, in duplicate/triplicate).

Isothermal titration calorimetry (ITC)

For the ITC experiments, the His tag in FimH-CRD-Th-His₆ was cleaved.^[16] Briefly, the protein (1 mg) was incubated with 10 U thrombin (T-6884, Sigma–Aldrich) in 20 mM Tris-HCl, pH 8.4, 150 mM NaCl and 2.5 mM CaCl₂ (cleavage buffer) at 20 °C for 16 h. The mixture was then applied to a gel filtration column (Bio-Prep SE100/17, Bio-Rad) attached to an FPLC system. The chromatography was run with assay buffer and analyzed by SDS-PAGE. The fractions containing FimH-CRD were pooled and concentrated by ultrafiltration (MWCO10, Sartorius AG, Tagelswangen, Switzerland). The ITC experiments were performed using a VP-ITC instrument from MicroCal Inc. (GE Healthcare, Northampton, MA, USA). The measurements were performed at 25 °C. Prior to measurements, the protein was dialyzed in assay buffer (10 mM HEPES, 150 mM NaCl, 1 mM CaCl₂, pH 7.4 (HBS-Ca)). Injections of 3–5 μL ligand solutions (150 μM) were added at an interval of 10 min into the sample cell solution containing FimH-CRD (8–22 μM , sample cell volume 1.4523 mL) with stirring at 307 rpm. Protein concentration was determined by HPLC-UV against a BSA standard.^[38] The quantity $c = Mt(0) K_D^{-1}$, where $Mt(0)$ is the initial macromolecule concentration, is of importance in titration microcalorimetry. The c values ranged between 300 and 3200. Because the smallest reliable volumes were injected, sigmoidal curves were obtained. Control experiments injecting ligand solution into buffer without protein showed that the heat of dilution was small and constant. Baseline correction and peak integration were accomplished using Origin 7 as described by the manufacturer (OriginLab, Northampton, MA, USA). The first injection was always excluded from data analysis because it usually suffers from sample loss during the mounting of the syringe and the equilibration preceding the actual titration. A three-parameter (N (stoichiometry), K_D (dissociation constant) and ΔH° (change in enthalpy) nonlinear least-square data fitting was per-

formed in a Microsoft Excel spreadsheet using the Solver add-in (Frontline System)^[39,40] according to binding isotherms published by Ziegler and Seelig.^[41]

Thermodynamics parameters were calculated from Equation (4).

$$\Delta G = \Delta H - T\Delta S = RT \ln K_D = -RT \ln K_A \quad (4)$$

where ΔG , ΔH , and ΔS are the changes in free energy, enthalpy, and entropy of binding, respectively, T is the absolute temperature, and R is the universal gas constant ($8.314 \text{ J mol}^{-1} \text{ K}^{-1}$).

Determination of pharmacokinetic parameters

Materials: Dimethyl sulfoxide (DMSO), 1-octanol, Dulbecco's modified Eagle's medium (DMEM) high glucose, L-glutamine solution, penicillin–streptomycin solution, Dulbecco's phosphate-buffered saline (DPBS), and trypsin–EDTA solution were purchased from Sigma–Aldrich. MEM nonessential amino acid (MEM-NEAA) solution, fetal bovine serum (FBS), and DMEM without sodium pyruvate and phenol red were bought from Invitrogen. PAMPA System Solution, GIT-0 Lipid Solution, and Acceptor Sink Buffer were ordered from plon (Woburn, MA, USA). Acetonitrile (MeCN) was bought from Acros Organics. The Caco-2 cells were kindly provided by Prof. G. Imanidis, FHNW, Muttenz, Switzerland and originated from the American Type Culture Collection (Rockville, MD, USA).

Parallel artificial membrane permeation assay (PAMPA)

Values of $\log P_e$ were determined in a 96-well format with the PAMPA^[33] permeation assay. For each compound, measurements were performed at three pH values (5.0, 6.2, 7.4) in quadruplicate. For this purpose, 12 wells of a deep-well plate, i.e., four wells per pH value, were filled with 650 μL System Solution. Samples (150 μL) were withdrawn from each well to determine the blank spectra by UV spectroscopy (SpectraMax 190). Then, analyte dissolved in DMSO was added to the remaining System Solution to yield 50 μM solutions. To exclude precipitation, the optical density was measured at 650 nm, with 0.01 being the threshold value. Solutions exceeding this threshold were filtered. Afterward, samples (150 μL) were withdrawn to determine the reference spectra. Further 200 μL were transferred to each well of the donor plate of the PAMPA sandwich P/N 110 163 (plon, Woburn MA, USA). The filter membranes at the bottom of the acceptor plate were impregnated with 5 μL of GIT-0 Lipid Solution, and 200 μL of Acceptor Sink Buffer were filled into each acceptor well. The sandwich was assembled, placed in the GutBox, and left undisturbed for 16 h. It was then disassembled, and samples (150 μL) were transferred from each donor and acceptor well to UV plates. Quantification was performed by both UV spectroscopy and LC–MS; $\log P_e$ values were calculated with the aid of the PAMPA Explorer Software (plon, version 3.5).

Colorectal adenocarcinoma (Caco-2) cell permeation assay

Caco-2 cells were cultivated in tissue culture flasks (BD Biosciences, Franklin Lakes, NJ, USA) with DMEM high-glucose medium containing L-glutamine (2 mM), nonessential amino acids (0.1 mM), penicillin (100 U mL⁻¹), streptomycin (100 $\mu\text{g mL}^{-1}$), and FBS (10%). The cells were kept at 37 °C in humidified air containing 5% CO₂, and the medium was changed every second day. When ~90% confluence was reached, the cells were split in a 1:10 ratio and distributed to new tissue culture flasks. At passage numbers between 60

and 65, they were seeded at a density of 5.3×10^5 cells per well to Transwell 6-well plates (Corning Inc., Corning, NY, USA) with 2.5 mL culture medium in the basolateral and 1.8 mL in the apical compartment. The medium was renewed on alternate days. Permeation experiments were performed between days 19 and 21 post-seeding. Prior to the experiment, the integrity of the Caco-2 monolayers was evaluated by measuring the transepithelial electrical resistance (TEER) with an Endohm tissue resistance instrument (World Precision Instruments Inc., Sarasota, FL, USA). Only wells with TEER values > 300 Ωcm^2 were used. Experiments were performed in the apical-to-basolateral (absorptive) and basolateral-to-apical (secretory) directions in triplicate. Transport medium (DMEM without sodium pyruvate and phenol red) was withdrawn from the donor compartments of three wells and replaced by the same volume of compound stock solutions to reach an initial sample concentration of 62.5 μM . The Transwell plate was then shaken (250 rpm) in the incubator. Samples (40 μL) were withdrawn after 15, 30, and 60 min from the donor and acceptor compartments, and their concentrations were determined by LC–MS. Apparent permeability coefficients (P_{app}) were calculated according to the equation

$$P_{app} = \frac{dQ}{dt} \times \frac{1}{A \times c_0} \quad (5)$$

where dQ/dt is the permeability rate, A the surface area of the monolayer, and c_0 the initial concentration in the donor compartment.^[42] After the experiment, TEER values were assessed again for each well and results from wells with values < 300 Ωcm^2 were discarded.

log D_{7,4} determination

The *in silico* prediction tool ALOGPS^[43] was used to estimate the $\log P$ values of the compounds. Depending on these values, the compounds were classified into three categories: hydrophilic compounds ($\log P < 0$), moderately lipophilic compounds ($0 \leq \log P \leq 1$) and lipophilic compounds ($\log P > 1$). For each category, two different ratios (volume of 1-octanol to volume of buffer) were defined as experimental parameters (Table 4).

Table 4. Compound classification based on estimated $\log P$ values. ^[43]		
Compound type	$\log P$	Ratio (1-octanol)/(buffer)
hydrophilic	< 0	30:140, 40:130
moderately lipophilic	0–1	70:110, 110:70
lipophilic	> 1	3:180, 4:180

Equal amounts of phosphate buffer (0.1 M, pH 7.4) and 1-octanol were mixed and shaken vigorously for 5 min to saturate the phases. The mixture was left until separation of the two phases occurred, and the buffer was retrieved. Stock solutions of the test compounds were diluted with buffer to a concentration of 1 μM . For each compound, six determinations, i.e., three determinations per 1-octanol/buffer ratio, were performed in different wells of a 96-well plate. The respective volumes of buffer containing analyte (1 μM) were pipetted to the wells and covered by saturated 1-octanol according to the chosen volume ratio. The plate was sealed with aluminum foil, shaken (1350 rpm, 25 °C, 2 h) on a Heidolph Titramax 1000 plate shaker (Heidolph Instruments GmbH & Co. KG, Schwabach, Germany) and centrifuged (2000 rpm, 25 °C,

5 min, 5804 R Eppendorf centrifuge, Hamburg, Germany). The aqueous phase was transferred to a 96-well plate for analysis by LC-MS.

$\log D_{7,4}$ was calculated from the 1-octanol/buffer ratio (o/b), the initial concentration of the analyte in buffer ($1 \mu\text{M}$), and the concentration of the analyte in the aqueous phase (c_b) with equation:

$$\log D_{7,4} = \log \left(\frac{1 \mu\text{M} - c_b}{c_b} \times \frac{1}{o : b} \right) \quad (6)$$

Solubility

Solubility was determined in a 96-well format using the μSOL Explorer solubility analyzer (plon, version 3.4.0.5). For each compound, measurements were performed at three pH values (3.0, 5.0, 7.4) in triplicates. For this purpose, nine wells of a deep-well plate, that is, three wells per pH value, were filled with $300 \mu\text{L}$ of an aqueous universal buffer solution. Aliquots ($3 \mu\text{L}$) of a compound stock solution ($10\text{--}50 \text{ mM}$ in DMSO) were added and thoroughly mixed. The final sample concentration was $0.1\text{--}0.5 \text{ mM}$, the residual DMSO concentration was 1.0% (v/v) in the buffer solutions. After 15 h, the solutions were filtered ($0.2 \mu\text{m}$ 96-well filter plates) using a vacuum to collect manifold (Whatman Ltd., Maidstone, UK) to remove any precipitates. Equal amounts of filtrate and *n*-propanol were mixed and transferred to a 96-well plate for UV detection ($190\text{--}500 \text{ nm}$). The amount of material dissolved was calculated by comparison with UV spectra obtained from reference samples, which were prepared by dissolving compound stock solution in a 1:1 mixture of buffer and *n*-propanol (final concentrations $0.017\text{--}0.083 \text{ mM}$).

LC-MS measurements

Analyses were performed using an 1100/1200 Series HPLC System coupled to a 6410 Triple Quadrupole mass detector (Agilent Technologies, Inc., Santa Clara, CA, USA) equipped with electrospray ionization. The system was controlled with the Agilent MassHunter Workstation Data Acquisition software (version B.01.04). The column used was an Atlantis T3 C_{18} column ($2.1 \times 50 \text{ mm}$) with a $3 \mu\text{m}$ particle size (Waters Corp., Milford, MA, USA). The mobile phase consisted of two eluents: solvent A (H_2O , containing 0.1% formic acid, v/v) and solvent B (MeCN, containing 0.1% formic acid, v/v), both delivered at 0.6 mL min^{-1} . The gradient was ramped from $95\% \text{ A}/5\% \text{ B}$ to $5\% \text{ A}/95\% \text{ B}$ over 1 min, and then held at $5\% \text{ A}/95\% \text{ B}$ for 0.1 min. The system was then brought back to $95\% \text{ A}/5\% \text{ B}$, resulting in a total duration of 4 min. MS parameters such as fragmentor voltage, collision energy, and polarity were optimized individually for each analyte, and the molecular ion was followed for each compound in the multiple reaction monitoring mode. The concentrations of the analytes were quantified by the Agilent Mass Hunter Quantitative Analysis software (version B.01.04).

Abbreviations

Caco-2 cells, colorectal adenocarcinoma cells; CRD, carbohydrate recognition domain; D , distribution coefficient octanol/ H_2O ; GFP, green fluorescent protein; HPLC, high-performance liquid chromatography; IC_{50} , half-maximal inhibitory concentration; ITC, isothermal titration calorimetry; MFI, mean fluorescence intensity; PAMPA, parallel artificial membrane permeability assay; P_{app} , apparent per-

meability coefficient; P_e , effective permeation value; SAR, structure-activity relationship; SPR, structure-property relationship; UPEC, uropathogenic *E. coli*; UTI, urinary tract infection.

Acknowledgement

Financial support from the Swiss National Science Foundation (SNF interdisciplinary grant K-32K1-120904) is gratefully acknowledged.

Keywords: bacterial adhesion · FimH antagonists · flow cytometry · isothermal titration calorimetry · urinary tract infections

- [1] a) T. M. Hooton, W. E. Stamm, *Infect. Dis. Clin. North Am.* **1997**, *11*, 551–581; b) T. J. Wiles, R. R. Kulesus, M. A. Mulvey, *Exp. Mol. Pathol.* **2008**, *85*, 11–19; c) S. D. Fihn, *N. Engl. J. Med.* **2003**, *349*, 259–266.
- [2] C. Svanborg, G. Godaly, *Infect. Dis. Clin. North Am.* **1997**, *11*, 513–529.
- [3] a) J. D. Schilling, S. J. Hultgren, *Int. J. Antimicro. Ag.* **2002**, *19*, 457–460; b) M. G. Blango, M. A. Mulvey, *Antimicrob. Agents Chemother.* **2010**, *54*, 1855–1863.
- [4] G. Capitani, O. Eidam, R. Glockshuber, M. G. Grutter, *Microbes Infect.* **2006**, *8*, 2284–2290.
- [5] a) M. A. Mulvey, *Cell Microbiol.* **2002**, *4*, 257–271; b) S. G. Gouin, A. Wellens, J. Bouckaert, J. Kovensky, *ChemMedChem* **2009**, *4*, 749–755.
- [6] N. Sharon, *Biochim. Biophys. Acta.* **2006**, *1760*, 527–537.
- [7] a) N. Firon, I. Ofek, N. Sharon, *Biochem. Biophys. Res. Commun.* **1982**, *105*, 1426–1432; b) N. Firon, I. Ofek, N. Sharon, *Carbohydr. Res.* **1983**, *120*, 235–249; c) N. Sharon, *FEBS Lett.* **1987**, *217*, 145–157.
- [8] D. Choudhury, A. Thompson, V. Stojanoff, S. Langermann, J. Pinkner, S. J. Hultgren, S. D. Knight, *Science* **1999**, *285*, 1061–1066.
- [9] a) C. S. Hung, J. Bouckaert, D. Hung, J. Pinkner, C. Widberg, A. DeFusco, C. G. Auguste, R. Strouse, S. Langermann, G. Waksman, S. J. Hultgren, *Mol. Microbiol.* **2002**, *44*, 903–915; b) J. Bouckaert, J. Berglund, M. Schembri, E. D. Genst, L. Cools, M. Wuhrer, C. S. Hung, J. Pinkner, R. Slättergard, A. Zavialov, D. Choudhury, S. Langermann, S. J. Hultgren, L. Wyns, P. Klemm, S. Oscarson, S. D. Knight, H. De Greve, *Mol. Microbiol.* **2005**, *55*, 441–455; c) A. Wellens, C. Garofalo, H. Nguyen, N. Van Gerven, R. Slättergard, J.-P. Hernalsteens, L. Wyns, S. Oscarson, H. De Greve, S. Hultgren, J. Bouckaert, *PLoS ONE* **2008**, *3*, e2040.
- [10] a) N. Firon, S. Ashkenazi, D. Mirelman, I. Ofek, N. Sharon, *Infect. Immun.* **1987**, *55*, 472–476; b) T. K. Lindhorst, S. Kötter, J. Kubisch, U. Krallmann-Wenzel, S. Ehlers, V. Kren, *Eur. J. Org. Chem.* **1998**, 1669–1674; c) O. Sperling, A. Fuchs, T. K. Lindhorst, *Org. Biomol. Chem.* **2006**, *4*, 3913–3922; d) Z. Han, J. S. Pinker, B. Ford, R. Obermann, W. Nolan, S. A. Wildman, D. Hobbs, T. Ellenberger, C. K. Cusumano, S. J. Hultgren, J. W. Janetka, *J. Med. Chem.* **2010**, *53*, 4779–4792; e) T. Klein, D. Abgottspon, M. Wittwer, S. Rabbani, J. Herold, X. Jiang, S. Kleeb, C. Lüthi, M. Scharenberg, J. Bezençon, E. Gubler, L. Pang, M. Smieško, B. Cutting, O. Schwardt, B. Ernst, *J. Med. Chem.* **2010**, *53*, 8627–8641; f) O. Schwardt, S. Rabbani, M. Hartmann, D. Abgottspon, M. Wittwer, S. Kleeb, A. Zalewski, M. Smieško, B. Cutting, B. Ernst, *Bioorg. Med. Chem.* **2011**, *19*, 6454–6473; g) C. K. Cusumano, J. S. Pinkner, Z. Han, S. E. Greene, B. A. Ford, J. R. Crowley, J. P. Henderson, J. W. Janetka, S. J. Hultgren, *Sci. Transl. Med.* **2011**, *3*, 109ra115; h) J. Berglund, J. Bouckaert, H. De Greve, S. Knight, *Anti-Adhesive Compounds to Prevent and Treat Bacterial Infections*, Intl. Pat. PCT/US 2005/089733, **2005**.
- [11] Glide, version 5.7, Schrödinger, LLC, New York, NY (USA), **2011**.
- [12] I. L. Scott, R. V. Market, R. J. DeOrazio, H. Meckler, T. P. Kogan, *Carbohydr. Res.* **1999**, *317*, 210–216.
- [13] C. A. Ocasio, T. S. Scanlan, *Bioorg. Med. Chem.* **2008**, *16*, 762–770.
- [14] M. Prieto, E. Zurita, E. Rosa, L. Muñoz, P. Lloyd-Williams, E. Giralt, *J. Org. Chem.* **2004**, *69*, 6812–6820.
- [15] M. Ishikawa, Y. Hashimoto, *J. Med. Chem.* **2011**, *54*, 1539–1554.
- [16] S. Rabbani, X. Jiang, O. Schwardt, B. Ernst, *Anal. Biochem.* **2010**, *407*, 188–195.

- [17] M. Scharenberg, D. Abgottspon, E. Cicek, X. Jiang, O. Schwardt, S. Rabani, B. Ernst, *Assay Drug Dev. Technol.* **2011**, *9*, 455–464.
- [18] J. Bouckaert, J. Mackenzie, J. L. de Paz, B. Chipwaza, D. Choudhury, A. Zavalov, K. Mannerstedt, J. Anderson, D. Pierard, L. Wyns, P. H. Seeberger, S. Oscarson, H. De Greve, S. D. Knight, *Mol. Microbiol.* **2006**, *61*, 1556–1568.
- [19] G. Zhou, W. J. Mo, P. Sebbel, G. W. Min, T. A. Neubert, R. Glockshuber, *J. Cell Sci.* **2001**, *114*, 4095–4103.
- [20] P. Aprikian, V. Tchesnokova, B. Kidd, O. Yakovenko, V. Yarov-Yarovoy, E. Trinchina, V. Vogel, W. Thomas, E. Sokurenko, *J. Biol. Chem.* **2007**, *282*, 23437–23446.
- [21] I. Le Trong, P. Aprikian, B. A. Kidd, M. Forero-Shelton, V. Tchesnokova, P. Rajagopal, V. Rodriguez, G. Interlandi, R. Klevit, V. Vogel, R. E. Stenkamp, E. V. Sokurenko, W. E. Thomas, *Cell* **2010**, *141*, 645–655.
- [22] D. Abgottspon, G. Rölli, L. Hosch, A. Steinhuber, X. Jiang, O. Schwardt, B. Cutting, M. Smieško, U. Jenal, B. Ernst, A. Trampuz, *J. Microbiol. Methods* **2010**, *82*, 249–255.
- [23] a) J. E. Ladbury, *Biochem. Soc. Trans.* **2010**, *38*, 888–893; b) G. A. Holdgate, W. H. Ward, *Drug Discovery Today* **2005**, *10*, 1543–1550; c) R. Perozoz, G. Folkers, L. Scapozza, *J. Recept. Signal Transduction Res.* **2004**, *24*, 1–52; d) J. E. Ladbury, G. Klebe, E. Freire, *Nat. Rev. Drug Discovery* **2010**, *9*, 23–27; e) K. P. Murphy, D. Xie, K. S. Thompson, L. M. Amzel, E. Freire, *Proteins* **1994**, *18*, 63–67.
- [24] a) B. Baum, L. Muley, M. Smolinski, A. Heine, D. Hangauer, G. Klebe, *J. Mol. Biol.* **2010**, *397*, 1042–1054; b) M. C. Chervenak, E. J. Toone, *J. Am. Chem. Soc.* **1994**, *116*, 10533–10539; c) J. E. DeLorbe, J. H. Clements, M. G. Teresk, A. P. Benfield, H. R. Plake, L. E. Millsbaugh, S. F. Martin, *J. Am. Chem. Soc.* **2009**, *131*, 16758–16770.
- [25] S. Cabani, P. Gianni, V. Mollica, L. Lepori, *J. Solution Chem.* **1981**, *10*, 563–595.
- [26] A. V. Finkelstein, J. Janin, *Protein Eng.* **1989**, *3*, 1–3.
- [27] K. P. Murphy, *Biophys. Chem.* **1994**, *51*, 311–326.
- [28] E. Freire, *Drug Discovery Today* **2008**, *13*, 869–874.
- [29] a) T. S. G. Olsson, M. A. Williams, W. R. Pitt, J. E. Ladbury, *J. Mol. Biol.* **2008**, *384*, 1002–1017; b) C. Diehl, O. Engstrom, T. Delaine, M. Hakansson, S. Genheden, K. Modig, H. Leffler, U. Ryde, U. J. Nilsson, M. Akke, *J. Am. Chem. Soc.* **2010**, *132*, 14577–14589.
- [30] Phase, version 3.3, Schrödinger, LLC, New York, NY (USA), **2011**.
- [31] a) B. A. Williams, M. C. Chervenak, E. J. Toone, *J. Biol. Chem.* **1992**, *267*, 22907–22911; b) E. J. Toone, *Curr. Opin. Struc. Biol.* **1994**, *4*, 719–728; c) T. K. Dam, C. F. Brewer, *Chem. Rev.* **2002**, *102*, 387–429; d) M. Ambrosi, N. R. Cameron, B. G. Davis, *Org. Biomol. Chem.* **2005**, *3*, 1593–1608; e) E. Garcia-Hernandez, R. A. Zubillaga, E. A. Chavelas-Adame, E. Vazquez-Contreras, A. Rojo-Dominguez, M. Costas, *Protein Sci.* **2003**, *12*, 135–142.
- [32] H. Van de Waterbeemd, D. A. Smith, K. Beaumont, D. K. Walker, *J. Med. Chem.* **2001**, *44*, 1313–1333.
- [33] M. Kansy, F. Sennar, K. Gubernator, *J. Med. Chem.* **1998**, *41*, 1007–1010.
- [34] A. Avdeef, S. Bendels, L. Di, B. Faller, M. Kansy, K. Sugano, Y. Yamauchi, *J. Pharm. Sci.* **2007**, *96*, 2893–2909.
- [35] C. A. Lipinski, *J. Pharmacol. Toxicol. Methods* **2000**, *44*, 235–249.
- [36] J. Kasuga, M. Ishikawa, M. Yonehara, M. Makishima, Y. Hashimoto, H. Miyachi, *Bioorg. Med. Chem.* **2010**, *18*, 7164–7173.
- [37] R. Roy, S. K. Das, F. Santoyo-González, F. Hernández-Mateo, T. K. Dam, C. F. Brewer, *Chem. Eur. J.* **2000**, *6*, 1757–1762.
- [38] a) F. Bitsch, R. Aichholz, J. Kallen, S. Geisse, B. Fournier, J. M. Schlaeppli, *Anal. Biochem.* **2003**, *323*, 139–149; b) S. Mesch, K. Lemme, H. Koliwer-Brandl, D. S. Strasser, O. Schwardt, S. Kelm, B. Ernst, *Carbohydr. Res.* **2010**, *345*, 1348–1359.
- [39] G. Kemmer, S. Keller, *Nat. Protoc.* **2010**, *5*, 267–281.
- [40] O. O. Krylova, N. Jahnke, S. Keller, *Biophys. Chem.* **2010**, *150*, 105–111.
- [41] A. Ziegler, J. Seelig, *Biophys. J.* **2004**, *86*, 254–263.
- [42] P. Artursson, J. Karlsson, *Biochem. Biophys. Res. Commun.* **1991**, *175*, 880–885.
- [43] a) VCCLAB, Virtual Computational Chemistry Laboratory, 2005, <http://www.vcclab.org> (accessed May 3, 2012); b) I. V. Tetko, J. Gasteiger, R. Todeschini, A. Mauri, D. Livingstone, P. Ertl, V. A. Palyulin, E. V. Radchenko, N. S. Zefirov, A. S. Makarenko, V. Y. Tanchuk, V. V. Prokopenko, *J. Comput. Aid. Mol. Des.* **2005**, *19*, 453–463.

Received: March 6, 2012

Revised: April 27, 2012

Published online on May 29, 2012

2.6 **Manuscript 5: Urinary tract infection – which FimH conformation is therapeutically relevant?**

This manuscript describes a *Topliss*-guided SAR study starting from the biphenyl α -D-mannopyranoside lead structure. The affinity of the antagonists to a stable full-length FimH variant as well as to the isolated FimH lectin domain, which mimics the high-affinity state, was evaluated. Moreover, the determination of physicochemical parameters predictive for oral bioavailability and renal excretion (aqueous solubility, lipophilicity, membrane permeability) completes this study.

Contribution to the project:

Simon Kleeb performed all experiments regarding the physicochemical characterization of the diverse biphenyl α -D-mannopyranosides and discussed the resulting experimental data.

This manuscript is in preparation for *ChemMedChem*.

Urinary Tract Infection - Which FimH Conformation Is Therapeutically Relevant?

Katharina Mayer, Deniz Eris, Simon Kleeb, Said Rabbani, Oliver Schwardt, and Beat Ernst*

Institute of Molecular Pharmacy, Pharmacenter, University of Basel, Klingelbergstrasse 50, CH-4056 Basel, Switzerland

* Corresponding author: Prof. Beat Ernst, Institute of Molecular Pharmacy, Pharmacenter, University of Basel, Klingelbergstrasse 50, CH-4056 Basel, Tel: +41 61 267 15 51, Fax: +41 61 267 15 52; e-mail: beat.ernst@unibas.ch

Keywords: Bacterial adhesion · uropathogenic *E. coli* · affinity state · FimH antagonists · biphenyl mannosides · *Topliss* · SAR · urinary tract infections

Abbreviations: CRD, carbohydrate recognition domain; D , octanol/water distribution coefficient; *E. coli*, *Escherichia coli*; FimH-L, FimH lectin domain; FimH-P, FimH pilin domain; FP, fluorescence polarization; K_D , dissociation constant; PAMPA, parallel artificial membrane permeability assay; PD, pharmacodynamics; P_e , effective permeability; PK, pharmacokinetics; SAR, structure-activity relationship; UPEC, uropathogenic *E. coli*; UTI, urinary tract infection.

Abstract

Urinary tract infections (UTIs) caused by uropathogenic *Escherichia coli* (UPEC) are among the most prevalent infectious diseases worldwide requiring antibiotic treatment. Since recurrent antibiotic exposure can lead to resistance against antimicrobials, efficient new prevention and treatment strategies are urgently needed. The attachment of UPEC to urothelial host cells is mediated by the mannose-binding adhesin FimH located at the tip of bacterial type 1 pili. FimH can exhibit two structural conformations: A *low-affinity* state and a *high-affinity* state, which is induced only upon ligand binding and under shear stress. In order to investigate the suitability of the different conformations of FimH as targets for the development of antagonists we conducted a Topliss-guided SAR study starting from biphenyl α -D-mannoside **2** to identify potent ligands for a stable full-length FimH variant as a model for the native conformation. The affinity of the antagonists to the full-length FimH as well as to the isolated FimH lectin domain, which mimics the high-affinity state, was evaluated. In addition, the relevant pharmacokinetic parameters (solubility, permeability, renal excretion) were determined. With the *m*- & *p*-cyano substituted biphenyls **4p** & **4q** and the *m*-nitro derivative **4r** three promising candidates for *in vivo* experiments with a UTI mouse model could be identified.

Introduction

Urinary tract infection (UTI) is among the most prevalent infectious diseases worldwide and affects millions of people every year.^[1,2] In the vast majority of the reported cases, uropathogenic strains of *Escherichia coli* (UPEC) are the causal pathogen.^[3,4] To date, acute, uncomplicated lower urinary tract infection (cystitis) is mainly treated with antibiotics for symptom relief (*i.e.* reduction of dysuria, frequent and urgent urination, bacteriuria, pyuria) and for prevention of more devastating or even life threatening complications like pyelonephritis and urosepsis.^[5,6] However, the repeated use of antibacterial chemotherapeutics leads to increasing antimicrobial resistance resulting in treatment failure.^[7-9] Therefore, new strategies for the prevention and treatment of UTI with orally applicable therapeutics are urgently needed.^[10]

The key step in the establishment of the infection is the bacterial adhesion to urinary epithelial cells,^[11,12] which prevents the clearance of UPEC by the bulk flow of urine and enables the bacteria to colonize the epithelial cells. The adherence to the urothelial surface is mediated by the mannose-specific lectin FimH located at the tip of bacterial type 1 pili.^[4,13-17]

Hence, the virulence factor FimH was identified as an attractive target for the development of anti-adhesive drugs for the treatment of UTI.^[18,19] Mannose-based FimH antagonists compete with the cellular target of FimH, the mannosylated glycoprotein uroplakin Ia present on urothelial cells.^[20] As a result, the bacterial adhesion is prevented and hence the infection. A substantial advantage of this anti-adhesion therapy of UTI over treatment with antibiotics is the reduced risk of resistance formation, because no direct selection pressure is exerted on the pathogen.^[18,21]

FimH is composed of two domains: the N-terminal lectin domain (FimH-L) and, connected by a short linker, the C-terminal pilin domain (FimH-P).^[22] The lectin domain encloses the carbohydrate recognition domain (CRD) that binds to oligomannosides of the glycoprotein uroplakin Ia on the epithelial cell surface,^[19] while the pilin domain anchors the adhesin to the pilus.^[23] FimH-P exhibits an incomplete immunoglobulin-like fold that is completed by insertion of an N-terminal donor strand of FimG, the preceding subunit in pilus assembly.^[23] Due to this two-domain architecture, FimH can exhibit two experimentally observed structural states:^[22] A "compressed" FimH-L conformation (*low-affinity state*) that was observed in the crystal structure of the entire fimbrial tip in absence of ligands,^[22] and an "elongated" conformation (*high-affinity state*), which was found in several X-ray structures of the isolated lectin domain FimH-L in its ligand-bound state^[24-29] as well as in the complex between FimH and the pilus assembly chaperone FimC.^[30] The switch between these conformations is regulated by the pilin domain and can be triggered by applying mechanical forces along the molecule that occur, for example, during excretion of urine. This behavior is characteristic for the "catch-bond" phenomenon^[31-35] found for the FimH-ligand interaction.^[22] It is responsible for the remarkable ability of FimH to increase its apparent affinity to target glycans and enables the bacteria to attach tightly to oligomannosides on bladder epithelial cells, even under the harsh conditions of the urinary tract (*i.e.* flow of urine). Whereas in the *low-affinity state* the ligand binding site of FimH-L is open, the *high-affinity* conformation is characterized by a deep and narrow CRD, which is caused by structural rearrangements in the swing (amino acids 27-33), linker (residues 154-160) and insertion (residues 112-118) loops.^[22] As a result, the hydrophilic side chains of amino acids lining the FimH binding pocket establish a perfect network of hydrogen bonds with the hydroxy groups of α -D-mannopyranosides.^[36]

Interestingly, the isolated FimH-L was found to exhibit an about two orders of magnitude higher binding affinity to methyl α -D-mannopyranoside^[22] and BSA-labeled mannose^[22,37]

than the full-length FimH in the fimbrial tip. In addition, mutagenesis experiments to disrupt the inter-domain interface^[38] and the observation that crystals of the fimbrial tip broke upon carbohydrate addition further supported the opinion that binding of ligands is connected to domain separation in FimH and that mechanical force shifts the ligand binding equilibrium towards that of the isolated lectin domain.^[22]

About three decades ago, Sharon *et al.* investigated various oligomannosides and aryl α -D-mannosides as potential antagonists of the FimH-mediated bacterial adhesion^[39,40] and reported on a protective effect of methyl α -D-mannoside in a UTI mouse model.^[41] Since then, various monovalent α -D-mannosides bearing a wide range of aglycones including *n*-alkyl,^[24] phenyl,^[42] dioxocyclobutenylaminophenyl,^[43] umbelliferyl,^[42] biphenyl,^[25,44-47] indol(in)ylphenyl,^[48] triazolyl^[49] and thiazolylamino^[26] have been described as high-affinity ligands for the FimH lectin domain. In part, these modifications were the result of rational drug design based on X-ray crystal structures of FimH-L bound to α -D-mannosides.^[24,36] Additionally, different multivalent presentations of the mannose have been reported^[50-56] and a heptavalent presentation of β -cyclodextrin-tethered *n*-heptyl α -D-mannoside (**1**) (Figure 1) was shown to be highly effective when applied into the bladder of C3H/HeN mice together with the UTI89 bacterial strain.^[56] Importantly, adverse side effects resulting from non-selective binding of mannose-based FimH antagonists to human mannose receptors could be ruled out.^[57]

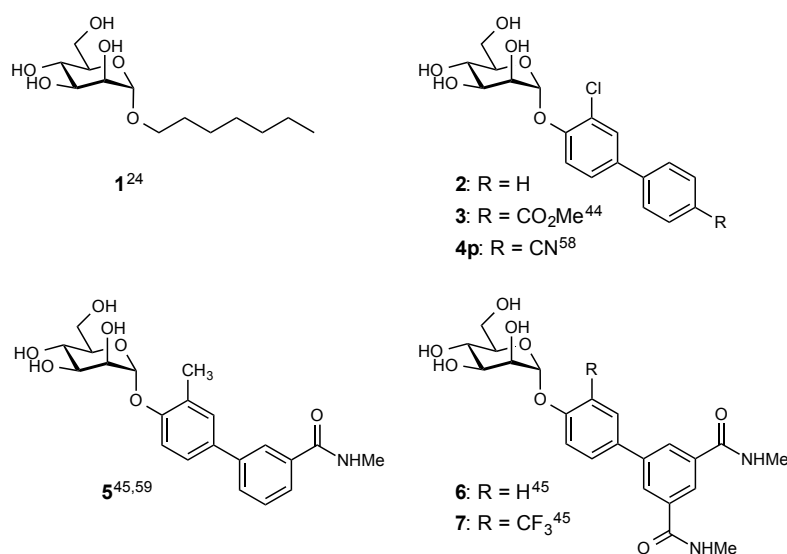


Figure 1. Monovalent FimH antagonists: *n*-Heptyl α -D-mannopyranoside (**1**) and biphenyl mannoside **2** served as reference compounds; the biphenyl derivatives **3-7** have been orally explored in *in vivo* disease models.

The high affinities of α -D-mannopyranosides towards the FimH lectin domain in the high-affinity conformation are resulting from optimal interactions with the main structural features of the CRD:^[27,28,30,36] First, the mannose binding pocket accommodates the mannose moiety by means of a perfect hydrogen bond network and, second, the entrance to the binding site, the so-called 'tyrosine gate', consisting of Tyr48, Tyr137 and Ile52, hosts hydrophobic aglycones. Aromatic groups, such as present in the biphenyl derivatives **2-7** (Figure 1), can undergo strong π - π -stacking interactions with the tyrosine gate, which are further favored by the addition of electron withdrawing substituents on the terminal ring of the biaryl moiety.^[25,44]

In the last years, the high potential of the biphenyl α -D-mannosides **3** & **5-7** for an oral treatment was proven in several *in vivo* PK studies in mice.^[44-46] However, due to the insufficient pharmacokinetic properties of the antagonists, *i.e.* modest bioavailability and short duration of the therapeutic effect in the bladder, high doses (≥ 50 mg/kg) at short intervals were necessary to achieve anti-adhesive effects over an extended period of time. Recently, we identified *para*-cyano derivative **4p**, a bioisostere of **3**, as FimH antagonist with an optimal *in vitro* PK/PD profile.^[58] Biphenyl **4p** not only showed sub-nanomolar affinity to the isolated FimH lectin domain, but also significantly improved pharmacokinetic parameters (solubility, permeability, renal excretion). The *para*-cyano substituent mediated lipophilicity as well as high plasma protein binding, which slowed down the rate of renal excretion. The beneficial PK profile of **4p** was confirmed by *in vivo* experiments in mice with steady renal excretion over more than 8 h following oral application, which allows for a long-lasting anti-adhesive effect. Furthermore, orally applied **4p** proved to be effective in a UTI mouse model in low dosage (10 mg/kg) leading to a reduction of the bacterial load in the bladder by more than 1000-fold.

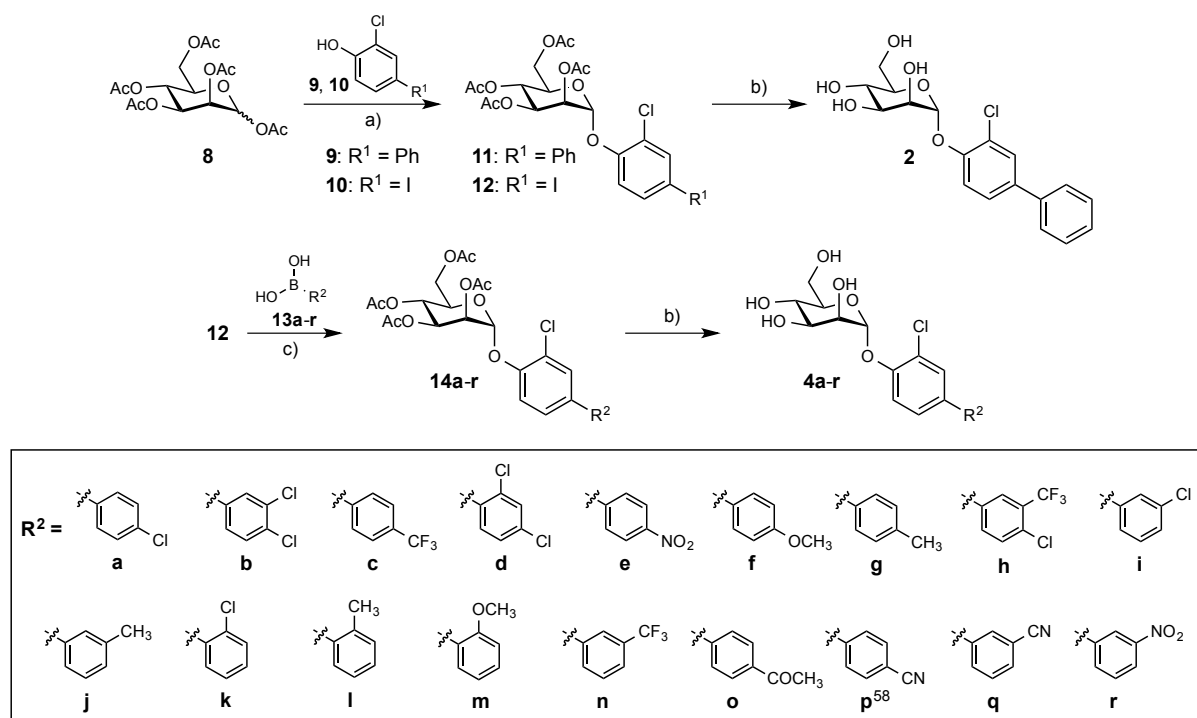
However, most previous *in vitro* ligand binding studies on FimH have been performed with the isolated FimH lectin domain where the CRD is locked in the *high-affinity* state.^[22] But in the majority of virulent UPEC strains, *e.g.* UTI89,^[60] CFT073,^[61] and J96^[62] this conformation is induced *in vivo* only after ligand binding and the onset of shear stress. Therefore it remains questionable if the isolated FimH-L is the relevant target for the development of anti-adhesive drugs. Since the compressed (*low-affinity*) conformation of FimH with its open binding site represents the state in UPEC under non-flow conditions, the binding of ligands to this FimH conformation should be investigated as well.

To address this issue, in a structure-affinity relationship (SAR) study we synthesized a series of novel derivatives of biphenyl α -D-mannoside **2** (Figure 1) as FimH antagonists and determined their binding affinity to a stable and soluble full-length FimH variant, which mimics FimH in the assembled fimbrial tip. For comparison with previous results,^[44,47,58] their affinity to the isolated FimH lectin domain was evaluated as well. In addition, the *in vitro* pharmacokinetic properties of the antagonists, which are predictive for oral bioavailability and renal excretion, were also quantified.

Results and Discussion

The aim of the present study was to identify high-affinity antagonists for the full-length FimH by introducing various substituents on the terminal aromatic ring of biphenyl α -D-mannoside **2**, which represents the parent compound of the highly active derivatives **3**^[44] and **4p**.^[58] However, finding the optimal substitution pattern on an aromatic ring in a lead compound (e.g. **2**) in order to maximize its potency is a very common problem in drug design. Since there are many possible substitutions and several different ring positions, the number of potential compounds to be considered is very large. The Topliss operational scheme,^[63,64] a manual and non-mathematical application of the Hansch method for treatment of structure activity correlations,^[65,66] presents a valuable tool in drug design to approach this problem rationally by guiding towards the most active analogue of a lead compound with the least synthetic investment. It allows for selecting a limited group of substituents that provide good discrimination between π (hydrophobic effects), σ (electronic effects) and E_S (steric effects).

Synthesis of FimH Antagonists. The biphenyl mannosides were synthesized in analogy to previously described routes (Scheme 1).^[44,47] Lewis acid promoted glycosylation of 2-chloro-4-phenylphenol (**9**) with peracetylated D-mannose **8** (\rightarrow **11**) and subsequent deprotection under Zemplén conditions afforded biphenyl α -D-mannoside **2**. For the synthesis of the substituted biphenyl derivatives **4a-r**, phenol **10** was mannosylated with **8** to give iodide **12**. In a palladium-catalyzed Suzuki coupling of **12** with aryl boronates **13a-r**, the biphenyls **14a-r** were obtained. Finally, deprotection of the mannose moiety yielded the test compounds **4a-r**.



Scheme 1. a) $\text{BF}_3 \cdot \text{Et}_2\text{O}$, 40 °C, 1 d (**11**: 77%, **12**: 76%); b) NaOMe, MeOH, 5-12 h (34-95%); c) $\text{Pd}(\text{dppf})_2 \cdot \text{CH}_2\text{Cl}_2$, K_3PO_4 , DMF, 80 °C, 5-12 h (45-90%).

Binding Affinities. The binding affinity of the biphenyl mannosides **2** and **4a-r** was determined in a competitive fluorescence polarization assay (FP-assay) to a stable variant of the full-length FimH (see below), as well as to the isolated FimH lectin domain in the form of a previously described^[67] protein construct consisting of the CRD with a C-terminal His-tag with a thrombin cleavage site (FimH-CRD-Th-His₆). In both cases, *n*-heptyl mannoside (**1**) was used as a reference compound.

Construction of a soluble full-length FimH. Since isolated FimH with a non-complemented pilin domain is only marginally stable and shows aggregation tendency under physiological conditions,^[68] a recently described^[69] soluble and stable full-length FimH variant was used in this study. For this, a FimH-FimC complex was produced by periplasmic co-expression and subsequent extraction by chemical lysis of the bacterial outer membrane. The FimH-FimC complex was purified using conventional purification methods and stable full-length FimH was obtained by replacing FimC with a synthetic peptide corresponding to the sequence of the natural FimG donor strand (FimG residues 1-14; termed DsG) that completes the Ig-like fold of the FimH pilin domain. This FimH-DsG complex represents a minimal and yet comprehensive analogue of the native FimH structure as first published by Le Trong *et al.*^[22]

Competitive Fluorescence Polarization Assay.^[58] For the rapid determination of binding affinity, a recently developed competitive binding assay based on fluorescence polarization (FP) was used with both, the full-length FimH and the isolated FimH lectin domain. The antagonist of interest displaces the fluorescent-labeled competitor **15**^[58] from the binding site, thereby reducing fluorescence polarization.^[70] Initially, the affinity of **15** to either FimH protein was evaluated in a direct binding assay. Whereas for the isolated lectin domain a dissociation constant (K_D) of 1.7 nM has been reported,^[58] for the full-length FimH a K_D of 137 nM was determined (Table 1), which represents a decrease in affinity by almost two orders of magnitude compared to FimH-L. After having established the K_D of **15** to both FimH proteins, competitive FP experiments were performed with unlabeled FimH antagonists as competitors. Before measuring FP, the test compounds were incubated for at least 1 h with full-length FimH or for at least 24 h with the isolated lectin domain. These incubation periods were empirically determined to be necessary for the reaction to reach equilibrium. Resulting competition binding curves (Figure 2) were fitted to an equilibrium competition binding model^[71] to obtain the corresponding K_D s.

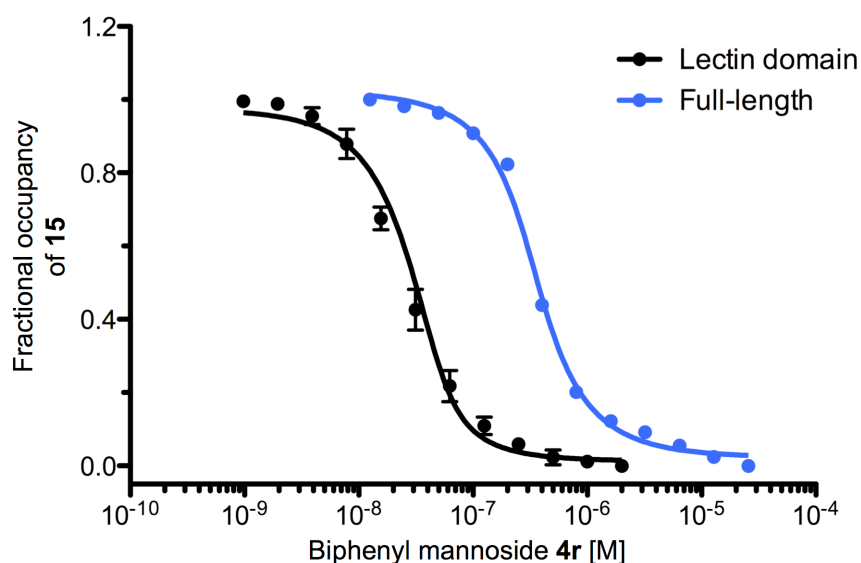


Figure 2. Inhibition curves of biphenyl mannoside **4r** from the competitive FP assay with the full-length FimH (blue) and the isolated lectin domain (black). The K_D values were determined by nonlinear least-squares fitting to a competition binding equation^[71] [K_D (full-length FimH) = 39.1 nM; K_D (lectin domain) = 0.2 nM].

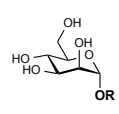
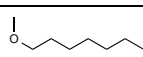
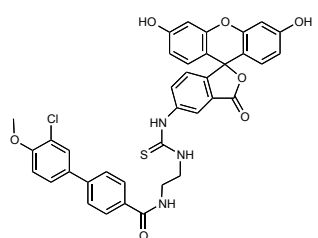
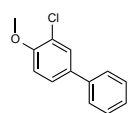
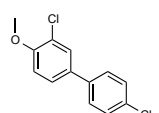
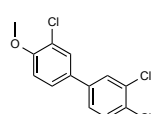
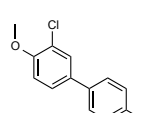
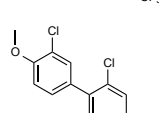
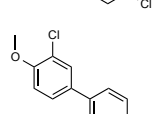
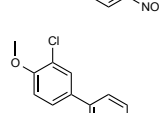
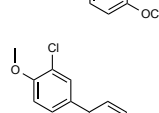
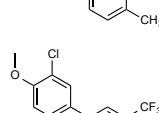
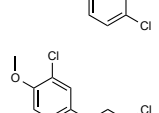
For the unsubstituted biphenyl mannoside **2** a K_D of 458 nM to the full-length FimH was measured (Table 1), which is an eightfold improvement of affinity compared to the reference compound *n*-heptyl mannoside (**1**). According to the Topliss scheme, the *p*-chloride **4a** is the

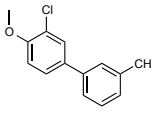
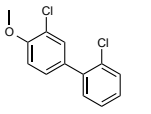
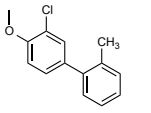
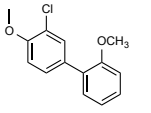
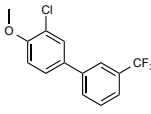
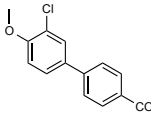
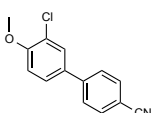
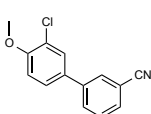
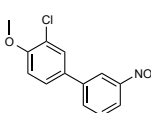
first derivative to be examined. It was found to have an about two-fold higher affinity to the FimH·DsG complex than parent compound **2** (K_D 251 nM), which most probably can be attributed to a $+\pi$ -effect, a $+\sigma$ -effect or to a combination of both. The *m,p*-dichloro derivative **4b** was synthesized next, because of the increase in both π - and σ -values when summed up for the two substituents. Since the affinity of **4b** was lower than that of the precursor **4a**, compounds **4c-e** were the next synthetic targets leading to the *p*-nitro derivative **4e**, which showed a significantly improved affinity compared to **4a** (K_D 140 nM vs 251 nM). This might be attributed to the lower lipophilicity ($-\pi$ -effect) and higher electron-withdrawing capacity ($+\sigma$ -effect) of the *p*-nitro substituent.

To cross check, the derivatives **4f-h** were also synthesized. Interestingly, the *p*-methyl biphenyl **4g** was found to be nearly as active as the *p*-chloro compound **4a** (K_D 297 nM vs 251 nM). Therefore, the middle branch of the Topliss operational scheme was investigated as well. However, all of the derivatives **4i-n** showed decreased affinities, which might be ascribed to either an unfavorable steric effect of the *ortho*-substitution in **4k-m** leading to a conformational change of the biphenyl moiety, or to the exceedance of the optimal lipophilicity and the low electron-withdrawing potential of the substituents.

If an improvement in affinity is achieved with a *p*-nitro group as in **4e**, the Topliss scheme suggests investigating substituents exhibiting a similar electron-withdrawing potential but a lower π -effect in order to find the optimal σ/π -balance.^[63,64] Therefore, the *p*-acetyl (\rightarrow **4o**) and *p*-cyano (\rightarrow **4p**) derivatives were examined next. Indeed, both compounds showed an increased affinity to the full-length FimH with $K_{DS} < 100$ nM. Finally, the beneficial nitro- and cyano-substituents were moved to the 3-position since the *meta*-substituents show a stronger $-\pi$ -effect than their *para*-counterparts while maintaining a comparable $+\sigma$ -effect. However, while 3-substitution with CN in **4q** did not improve the activity compared to **4p**, a *meta*-nitro group (\rightarrow **4r**, Figure 2) led to a 3.5-fold gain in affinity compared to the *para*-derivative **4e** (K_D 39.1 nM vs 140 nM) making compound **4r** the most active ligand to the full-length FimH identified by this approach. Apparently, the *m*-nitro substitution in **4r** provides the optimal balance between lipophilicity and electron-withdrawing effect.

Table 1. Pharmacodynamic and pharmacokinetic parameters of FimH antagonists.

	Compound 	Full-length FimH K_D [nM] ^a	FimH lectin domain K_D [nM] ^a	Solubility [$\mu\text{g/mL}$] ^b	logD_{7.4} ^c	PAMPA logP _e [cm/s] ^d
1		3600	16.7	> 3000	1.7	n.d.
15 ^[58]		137	1.7	n.d.	n.d.	n.d.
2		458	3.8	5.5 ± 0.2	2.6 ± 0.1	n.d.
4a		251	4.9	3.5 ± 0.3	3.3 ± 0.1	n.d.
4b		692	5.8	2.3 ± 0.2	n.d.	n.d.
4c		415	5.8	22 ± 0	3.4 ± 0.1	n.d.
4d		465	4.1	8.0 ± 0.8	n.d.	n.d.
4e		140	0.6	117 ± 7	2.3 ± 0.0	-5.0 ± 0.1
4f		344	2.2	3.8 ± 0.4	2.7 ± 0.1	n.d.
4g		297	3.6	7.4 ± 0.2	3.3 ± 0.0	n.d.
4h		377	7.5	1.0 ± 0.2	n.d.	n.d.
4i		353	3.2	5.7 ± 0.7	3.2 ± 0.0	n.d.

4j		380	2.2	7.1 ± 0.6	3.0 ± 0.0	n.d.
4k		434	3.1	28 ± 1	3.1 ± 0.1	-4.4 ± 0.1
4l		436	2.9	135 ± 24	2.9 ± 0.0	-4.6 ± 0.2
4m		391	2.7	> 280	2.4 ± 0.0	-4.6 ± 0.1
4n		575	5.1	36 ± 1	3.3 ± 0.1	n.d.
4o		98.6	0.3	16 ± 0	2.1 ± 0.1	n.d.
4p ^[58]		83.8	0.6	192 ± 5	2.1 ± 0.0	-5.2 ± 0.0
4q		85.9	0.4	227 ± 5	2.1 ± 0.0	-5.1 ± 0.0
4r		39.1	0.2	23 ± 2	2.4 ± 0.1	-4.9 ± 0.1

[a] Affinities (dissociation constants, K_D) to the full-length FimH (FimH·DsG) and the isolated FimH lectin domain (FimH-CRD-Th-His₆) were determined in a competitive fluorescence polarization assay.^[58] [b] Kinetic solubility was measured in a 96-well format in triplicate using the μ SOL Explorer solubility analyzer.^[72] [c] Octanol-water partition coefficients ($\log D_{7.4}$) were determined by a miniaturized shake flask procedure. The values are indicated as mean \pm SD of sextuplicate determinations.^[73] [d] Permeation through an artificial membrane ($\log P_e$, effective permeability) was determined by PAMPA (parallel artificial membrane permeability assay) in quadruplicate.^[74]

When tested with the isolated FimH CRD in the FP assay all the antagonists **2** and **4a-r** exhibited low nanomolar affinities. Compared to the full-length FimH this corresponds to an increase in affinity of about two orders of magnitude. Obviously, for FimH in the *high-affinity* state with its deep and narrow mannose binding pocket the influence of the hydrophobic and electronic effects of different substituents is not as pronounced as in the

case of the full-length FimH in the *low-affinity* conformation with an open ligand binding site. However, the antagonists bearing substituents with high $+\sigma$ -effect like *p*- and *m*-nitro (\rightarrow **4e** & **4r**, Figure 2), *p*- and *m*-cyano (\rightarrow **4p** & **4q**), and *p*-acetyl (\rightarrow **4o**) showed even sub-nanomolar affinities to the FimH lectin domain, which is in good agreement with previous findings that a high electron-withdrawing potential of substituents on the biphenyl aglycone is essential for an enhanced π - π stacking interaction with the tyrosine gate lining the entrance to the mannose binding pocket.^[44,47,58]

Physicochemical Properties. For assessing the potential of the antagonists for intestinal absorption and renal clearance, lipophilicity ($\log D_{7.4}$),^[73] aqueous solubility, and permeability through an artificial membrane (PAMPA, $\log P_e$)^[74] were determined (Table 1). According to the maximum absorbable dose (MAD) concept,^[75,76] an aqueous solubility of at least 50 $\mu\text{g/mL}$ is required to achieve quantitative absorption of a 1 mg/kg dose of compound with medium permeability. However, whereas for *n*-heptyl α -mannopyranoside (**1**), excellent aqueous solubility ($> 3000 \mu\text{g/mL}$) was determined, the unsubstituted parent compound **2** as well as the disubstituted derivatives and antagonists bearing apolar substituents in the *meta*- or *para*-position (compounds **4a-4d**, **4f-j**, **4n** and **4o**) were found to be scarcely soluble. By contrast, the polar cyano moiety (\rightarrow **4p**, **4q**) and the *para*-nitro substituent present in **4e** enhanced solubility to 117-227 $\mu\text{g/mL}$, while a nitro group in the *meta*-position (\rightarrow **4r**) led to a substantial drop in solubility below the critical limit of 50 $\mu\text{g/mL}$. Moving apolar substituents to the *ortho*-position (\rightarrow **4k-m**) also markedly improved aqueous solubility, which is in agreement with an increased distortion angle of the two phenyl moieties resulting in the disruption of the molecular planarity.

All biphenyl derivatives showed moderate to high lipophilicity with $\log D_{7.4}$ values ranging from 2.1 to 3.4, which is beneficial for oral absorption by passive diffusion. Indeed, permeability data derived from PAMPA^[74] ($\log P_e$ -4.4 to -5.2, P_e : effective permeation) suggested high permeation through the intestinal membranes for all tested antagonists. In addition, $\log D_{7.4}$ was described as a key parameter for tubular reabsorption.^[77-79] Hence, lipophilic compounds are predominantly reabsorbed from the renal filtrate. Considering that renal clearance is the major route of elimination, this will lead to a slow but steady excretion into the bladder. In contrast, hydrophilic compounds are poorly reabsorbed and therefore quickly renally eliminated, which results in high initial drug levels in the urine but limits the time range where the minimal anti-adhesive concentration is maintained. As a consequence, a

$\log D_{7.4} > 2$ as determined for the biphenyl mannosides in this study is optimal for tubular reabsorption from the glomerular filtrate and thus for slow renal clearance.

Summary and Conclusion

Recently, a panel of monovalent alkyl and aryl α -D-mannopyranosides has been reported as potent FimH antagonists. However, in most previous *in vitro* ligand binding studies the isolated FimH lectin domain, in which the CRD is locked in the *high-affinity* conformation, was used as target. Yet, in virulent UPEC strains this state is induced only after ligand binding and when shear stress is applied, while the *low-affinity* conformation of FimH represents the native state under non-flow conditions.^[22] As a consequence, it remained doubtful if the isolated FimH CRD is the relevant target for the development of FimH antagonists. Therefore, the aim of the present study was to find potent ligands for a stable full-length FimH variant (FimH·DsG), which mimics FimH in the assembled fimbrial tip. In a Topliss-guided SAR study starting from biphenyl α -D-mannoside **2** we identified a series of antagonists with electron-withdrawing substituents in the *meta*- or *para*-position of the terminal aromatic ring (\rightarrow **4o-4r**) that exhibited affinities to the full-length FimH below 100 nM. With the most potent compound, the *meta*-nitro derivative **4r**, a more than tenfold improvement of affinity was achieved compared to **2** (K_D 39.1 nM vs 458 nM). By contrast, when tested with the isolated FimH lectin domain, all biphenyl mannosides were found to be about two orders of magnitude more potent, with a very narrow affinity span in the low nanomolar range. This indicates a less distinct influence of the substituent properties (hydrophobicity and electronic effects) on FimH in the *high-affinity* conformation with a deep and narrow mannose binding pocket compared to the full-length FimH in the *low-affinity* state with its open binding site.

Besides the pharmacodynamics, the relevant pharmacokinetic parameters (solubility, lipophilicity, permeability) for oral bioavailability and renal excretion, were also investigated. However, only a few biphenyl derivatives (*o*-methyl, *o*-methoxy, *m*- & *p*-cyano, and *p*-nitro) showed aqueous solubility above the critical limit of 50 $\mu\text{g/mL}$ leading to sufficient antagonist concentration in the intestinal fluids. Nevertheless, all of these compounds exhibited substantial permeability, which, in combination with high aqueous solubility, suggests high systemic availability after oral dosing. Furthermore, due to their favorable lipophilicity, the biphenyls are susceptible to tubular reabsorption. Unless they are eliminated

via concurring hepatic pathways, this results in sustained availability of the antagonist in the urinary bladder.

In summary, the *m*-nitro substituted biphenyl α -D-mannoside **4r** was identified as a candidate for *in vivo* experiments in mice because of its high affinity to the full-length FimH. However, the low aqueous solubility of **4r** might be a drawback for an oral application. Therefore, the cyano derivatives **4p**^[58] and **4q**, although twofold less potent, should be considered as well due to their more beneficial *in vitro* PK/PD profile. In future investigations, the biphenyls **4p**-**4r** will be tested in a UTI disease model with different UPEC strains like UTI89,^[60] CFT073,^[61] and J96^[62] to further evaluate the suitability of the different conformations of FimH as targets for the development of drugs for an anti-adhesion therapy of UTI.

Experimental section

Synthesis

General Methods. NMR spectra were recorded on a Bruker Avance DMX-500 (500 MHz) spectrometer. Assignment of ¹H and ¹³C NMR spectra was achieved using 2D methods (COSY, HSQC, HMBC, TOCSY). Chemical shifts are expressed in ppm in relation to the residual solvent signals (CHCl₃ and CHD₂OD) on the δ -scale. Coupling constants *J* are given in Hertz (Hz). Multiplicities were specified as follows: s (singlet), d (doublet), dd (doublet of a doublet), t (triplet), q (quartet), m (multiplet). Commercially available reagents were purchased from Fluka, Aldrich, Acros, and Abcr. Dichloromethane (DCM) was dried by filtration over Al₂O₃ (Fluka, type 5016 A basic). *N,N*-dimethylformamide (DMF) was dried by distillation from calcium hydride. Methanol (MeOH) was dried by refluxing with sodium methoxide and distilled immediately before use. Molecular sieves were activated under vacuum at 500 °C for 1 h immediately before use. Reactions were monitored by TLC using glass plates coated with silica gel 60 F₂₅₄ (Merck) and visualized by using UV light and/or by charring with a molybdate solution (a 0.02 M solution of ammonium cerium sulfate dihydrate and ammonium molybdate tetrahydrate in 10% aq. H₂SO₄). Column chromatography was performed on a CombiFlash Companion (Teledyne-ISCO, Inc.) using RediSep normal phase disposable flash columns (silica gel, 40-63 μ m). Reversed phase chromatography was performed on LiChroprepRP-18 (Merck, 40-63 μ m). LC-MS separations were carried out using Sunfire C₁₈ columns (19 x 150 mm, 5.0 μ m) on a Waters 2525 LC, equipped with Waters 2996 photodiode array and Waters micromass ZQ MS for detection. Electron spray ionization mass spectra (ESI-MS) were obtained on a Waters micromass ZQ. HR-MS analysis were carried out using a Agilent 1100 LC equipped with a photodiode array detector and a Micromass QTOF I equipped with a 4 GHz digital-time converter. Optical rotations were measured using Perkin-Elmer polarimeter 341.

General procedure A for the synthesis of biphenyl compounds. A two-neck flask was charged with **12** (100 mg, 1.0 eq), arylboronic acid or boronate **13a-r** (1.1 eq), Pd(Cl₂)dppf·CH₂Cl₂ (0.03 eq), K₃PO₄ (2 eq), and a stirring bar under argon. Then anhydrous DMF (2 mL) was added. The mixture was flushed with argon and degassed for 5 min, then heated to 80 °C and stirred for 5-12 h. The reaction mixture was cooled to rt, diluted with EtOAc (50 mL), washed with H₂O (50 mL) and brine (50 mL), dried over Na₂SO₄, concentrated and purified by chromatography on silica (petroleum ether/EtOAc) to afford biphenyl compounds **14a-r**.

General procedure B for deacetylation. To a solution of **11** or **14a-r** (1.0 eq) in dry MeOH (2 mL) was added freshly prepared methanolic NaOMe solution (1 M, 0.1 eq) under argon. The mixture was stirred at rt until the reaction was complete (2-8 h, monitored by TLC), then neutralized with acetic acid, filtered and concentrated in vacuo. The residue was purified by chromatography on silica (DCM/MeOH, 10:1 to 8:1) to afford **2** and **4a-r** as white solids. Further purification for biological testing was performed using preparative LC-MS.

3-Chloro-biphenyl-4-yl 2,3,4,6-tetra-O-acetyl- α -D-mannopyranoside (11). To a suspension of activated MS 4Å (150 mg), α -D-mannose pentaacetate (**8**, 156 mg, 0.40 mmol) and 2-chloro-4-phenylphenol (**9**, 98 mg, 0.48 mmol) in dry DCM (1.5 mL) was added dropwise freshly distilled BF₃·Et₂O (148 μ L, 1.2 mmol) under argon. The mixture was stirred for 24 h at 40 °C. After cooling to rt the mixture was diluted with DCM (50 mL), filtered through celite, and washed with satd. aq. NaHCO₃ (50 mL), water (50 mL) and brine (50 mL). The organic phase was dried over Na₂SO₄ and concentrated under reduced pressure. The crude product was purified by chromatography on silica (petroleum ether/EtOAc, 1:0 to 1:1) to yield **11** (166 mg, 77%). [α]_D²⁰ +72.0 (*c* 0.47, CHCl₃); ¹H NMR (500 MHz, CDCl₃): δ = 7.56 (d, *J* = 1.6 Hz, 1H, Ar-H), 7.45 (d, *J* = 7.4 Hz, 2H, Ar-H), 7.32 (m, 4H, Ar-H), 7.17 (m, 1H, Ar-H), 5.63-5.42 (m, 3H, H-1, H-2, H-3), 5.33 (t, *J* = 10.1 Hz, 1H, H-4), 4.22 (dd, *J* = 12.2, 5.3 Hz, 1H, H-6a), 4.14 (m, 1H, H-5), 4.04 (d, *J* = 12.2 Hz, 1H, H-6b), 2.14 (s, 3H, COCH₃), 2.06-1.88 (m, 9H, 3 COCH₃); ¹³C NMR (126 MHz, CDCl₃): δ = 170.61, 170.08, 169.91, 169.90 (4 CO), 150.64, 139.28, 137.64, 129.25, 129.06, 127.78, 126.97, 126.40, 124.82, 117.43 (12C, Ar-C), 96.86 (C-1), 69.90 (C-5), 69.50 (C-2), 68.93 (C-3), 66.01 (C-4), 62.26 (C-6), 21.01, 20.85, 20.82, 20.80 (4 COCH₃); ESI-MS: *m/z*: Calcd for C₂₆H₂₇ClNaO₁₀ [M+Na]⁺: 557.1, found: 557.2.

2-Chloro-4-iodo-phenyl 2,3,4,6-tetra-O-acetyl- α -D-mannopyranoside (12).^[80] According to the procedure for **11**, compound **8** (390 mg, 0.77 mmol) was reacted with 2-chloro-4-iodophenol (**10**, 235 mg, 0.9 mmol) and BF₃·Et₂O (290 μ L, 2.3 mmol) in DCM (3 mL) containing MS 4Å (300 mg) for 20 h at 40 °C. Yield: 345 mg, 76%. Spectroscopic data were in accordance with reported values.^[80]

3,4'-Dichloro-biphenyl-4-yl 2,3,4,6-tetra-O-acetyl- α -D-mannopyranoside (14a). Prepared according to general procedure A from **12** (30 mg, 0.052 mmol), 4-chloro-phenylboronic acid (**13a**, 9.0 mg, 0.57 mmol), Pd(dppf)Cl₂·CH₂Cl₂ (1.3 mg, 1.6 μ mol) and K₃PO₄ (22 mg, 0.1 mmol). Yield: 16

mg (54%) as a white solid. $[\alpha]_{\text{D}}^{20} +97.8$ (*c* 0.54, CHCl₃); ¹H NMR (500 MHz, CD₃OD): δ = 7.66-7.23 (m, 7H, Ar-H), 5.67 (s, 1H, H-1), 5.49-5.43 (m, 2H, H-2, H-3), 5.25 (t, *J* = 10.0 Hz, 1H, H-4), 4.13 (dd, *J* = 12.1, 5.4 Hz, 1H, H-6a), 4.05 (ddd, *J* = 10.1, 5.4, 2.1 Hz, 1H, H-5), 3.98 (dd, *J* = 12.2, 2.2 Hz, 1H, H-6b), 2.14-1.80 (m, 12H, 4 COCH₃); ¹³C NMR (126 MHz, CD₃OD): δ = 172.17, 171.51, 171.48 (4C, 4 CO), 151.81, 139.07, 137.34, 134.80, 130.12, 129.73, 129.31, 127.49, 125.65, 118.86 (12C, Ar-C), 97.67 (C-1), 71.23 (C-5), 70.50, 70.24 (C-2, C-3), 66.97 (C-4), 63.29 (C-6), 20.58, 20.55 (4C, 4 COCH₃); ESI-MS: *m/z*: Calcd for C₂₆H₂₆Cl₂NaO₁₀ [M+Na]⁺: 591.1, found: 591.1.

3,3',4'-Trichloro-biphenyl-4-yl 2,3,4,6-tetra-*O*-acetyl- α -D-mannopyranoside (14b). Prepared according to general procedure A from **12** (79 mg, 0.135 mmol), 3,4-dichloro-phenylboronic acid (**13b**, 228 mg, 0.15 mmol), Pd(dppf)Cl₂·CH₂Cl₂ (3.3 mg, 4 μ mol) and K₃PO₄ (57 mg, 0.27 mmol). Yield: 52 mg (64%) as a white solid. $[\alpha]_{\text{D}}^{20} +66.5$ (*c* 0.23, CHCl₃); ¹H NMR (500 MHz, CDCl₃): δ = 7.59 (dt, *J* = 8.9, 4.4 Hz, 2H, Ar-H), 7.50 (d, *J* = 8.3 Hz, 1H, Ar-H), 7.41-7.31 (m, 2H, Ar-H), 7.24 (d, *J* = 8.6 Hz, 1H, Ar-H), (5.66-5.58 (m, 2H, H-2, H-3), 5.55 (d, *J* = 1.9 Hz, 1H, H-1), 5.41 (t, *J* = 10.1 Hz, 1H, H-4), 4.29 (dd, *J* = 12.3, 5.2 Hz, 1H, H-6a), 4.18 (ddd, *J* = 10.1, 5.1, 2.1 Hz, 1H, H-5), 4.10 (m, 1H, H-6b), 2.21 (s, 3H, COCH₃), 2.15-1.97 (m, 9H, 3 COCH₃); ¹³C NMR (126 MHz, CDCl₃): δ = 170.60, 170.11, 169.92, 169.89 (4 CO), 151.29, 139.26, 135.03, 133.24, 132.06, 131.01, 129.15, 128.81, 126.32, 126.18, 125.12, 117.41 (12C, Ar-C), 96.80 (C-1), 69.99 (C-5), 69.45 (C-3), 68.88 (C-2), 65.93 (C-4), 62.22 (C-6), 21.01, 20.85, 20.83 (4C, 4 COCH₃); ESI-MS: *m/z*: Calcd for C₂₆H₂₆Cl₃NaO₁₀ [M+Na]⁺: 625.0, found: 625.0.

3-Chloro-4'-(trifluoromethyl)-biphenyl-4-yl 2,3,4,6-tetra-*O*-acetyl- α -D-mannopyranoside (14c). Prepared according to general procedure A from **12** (79 mg, 0.135 mmol), 4-trifluoromethyl-phenylboronic acid (**13c**, 28 mg, 0.15 mmol), Pd(dppf)Cl₂·CH₂Cl₂ (3.3 mg, 4 μ mol) and K₃PO₄ (57 mg, 0.27 mmol). Yield: 46 mg (57%) as a white solid. $[\alpha]_{\text{D}}^{20} +63.8$ (*c* 0.31, CHCl₃); ¹H NMR (500 MHz, CD₃OD): δ = 7.84-7.77 (m, 3H, Ar-H), 7.74 (d, *J* = 8.3 Hz, 2H, Ar-H), 7.64 (dd, *J* = 8.6, 2.3 Hz, 1H, Ar-H), 7.43 (d, *J* = 8.6 Hz, 1H, Ar-H), 5.81 (s, 1H, H-1), 5.60-5.54 (m, 2H, H-2, H-3), 5.36 (t, *J* = 10.0 Hz, 1H, H-4), 4.24 (dd, *J* = 12.2, 5.4 Hz, 1H, H-6a), 4.14 (ddd, *J* = 10.0, 5.4, 2.2 Hz, 1H, H-5), 4.09 (dd, *J* = 12.2, 2.2 Hz, 1H, H-6b), 2.20, 2.07, 2.01, 1.95 (4 s, 12H, 4 COCH₃); ¹³C NMR (126 MHz, CD₃OD): δ = 172.18, 171.52, 171.50, 171.48 (4 CO), 152.30, 144.19, 136.90, 130.12, 128.39, 127.89, 126.94, 126.91, 125.75, 118.82 (13C, Ar-C, CF₃), 97.62 (C-1), 71.26 (C-5), 70.49, 70.21 (C-2, C-3), 66.95 (C-4), 63.28 (C-6), 20.59, 20.58, 20.55 (4C, 4 COCH₃); ESI-MS: *m/z*: Calcd for C₂₇H₂₆ClF₃NaO₁₀ [M+Na]⁺: 625.1, found: 625.0.

2',3,4'-Trichloro-biphenyl-4-yl 2,3,4,6-tetra-*O*-acetyl- α -D-mannopyranoside (14d). Prepared according to general procedure A from **12** (79 mg, 0.14 mmol), 2,4-dichloro-phenylboronic acid (**13d**, 28 mg, 0.15 mmol), Pd(dppf)Cl₂·CH₂Cl₂ (3.3 mg, 4 μ mol) and K₃PO₄ (57 mg, 0.27 mmol). Yield: 48 mg (59%) as a white solid. $[\alpha]_{\text{D}}^{20} +58.8$ (*c* 0.56, CHCl₃); ¹H NMR (500 MHz, CD₃OD): δ = 7.60-7.30

(m, 6H, Ar-H), 5.79 (s, 1H, H-1), 5.61-5.53 (m, 2H, H-2, H-3), 5.35 (m, 1H, H-4), 4.24 (dt, $J = 11.9$, 5.9 Hz, 1H, H-6a), 4.18-4.06 (m, 2H, H-5, H-6b), 2.19, 2.08, 2.01, 1.96 (4 s, 12H, 4 COCH₃); ¹³C NMR (126 MHz, CD₃OD): $\delta = 172.18, 171.51, 171.48$ (4C, 4 CO), 152.01, 138.68, 135.51, 135.36, 134.29, 133.49, 132.33, 130.72, 130.24, 128.66, 124.79, 118.03 (12C, Ar-C), 97.63 (C-1), 71.27 (C-5), 70.49 (C-3), 70.23 (C-2), 66.96 (C-4), 63.30 (C-6), 20.60, 20.56 (4C, 4 COCH₃); ESI-MS: m/z : Calcd for C₂₆H₂₅Cl₃NaO₁₀ [M+Na]⁺: 625.0, found: 625.0.

3-Chloro-4'-nitro-biphenyl-4-yl 2,3,4,6-tetra-*O*-acetyl- α -D-mannopyranoside (14e). Prepared according to general procedure A from **12** (41 mg, 0.07 mmol), 4-nitro-phenylboronic acid (**13e**, 13 mg, 0.08 mmol), Pd(dppf)Cl₂·CH₂Cl₂ (1.7 mg, 2 μ mol) and K₃PO₄ (30 mg, 0.14 mmol). Yield: 31 mg (76%) as a light-yellow solid. $[\alpha]_D^{20} +77.1$ (c 0.58, CHCl₃); ¹H NMR (500 MHz, CD₃OD): $\delta = 8.34$ -8.26 (m, 2H, Ar-H), 7.89-7.77 (m, 3H, Ar-H), 7.67 (dd, $J = 8.6, 2.3$ Hz, 1H, Ar-H), 7.43 (d, $J = 8.7$ Hz, 1H, Ar-H), 5.81 (s, 1H, H-1), 5.60-5.52 (m, 2H, H-2, H-3), 5.36 (m, 1H, H-4), 4.23 (dd, $J = 12.1, 5.3$ Hz, 1H, H-6a), 4.18-4.04 (m, 2H, H-5, H-6b), 2.20, 2.07, 2.02, 1.95 (4 s, 12H, 4COCH₃); ¹³C NMR (126 MHz, CD₃OD): $\delta = 172.14, 171.49, 171.48, 171.45$ (4 CO), 152.73, 148.64, 146.63, 135.95, 130.32, 128.73, 128.11, 125.84, 125.18, 118.76 (12C, Ar-C), 97.59 (C-1), 71.28 (C-5), 70.45, 70.17 (C-2, C-3), 66.91 (C-4), 63.26 (C-6), 20.59, 20.58, 20.56 (4C, 4 COCH₃); ESI-MS: m/z : Calcd for C₂₆H₂₆ClNNaO₁₂ [M+Na]⁺: 602.1, found: 602.1.

3-Chloro-4'-methoxy-biphenyl-4-yl 2,3,4,6-tetra-*O*-acetyl- α -D-mannopyranoside (14f). Prepared according to general procedure A from **12** (59.6 mg, 0.1 mmol), 4-methoxyphenylboronic acid (**13f**, 17 mg, 0.112 mmol), Pd(dppf)Cl₂·CH₂Cl₂ (2.5 mg, 3 μ mol) and K₃PO₄ (43 mg, 0.2 mmol). Yield: 52 mg (90 %) as a white solid. $[\alpha]_D^{20} +73.7$ (c 0.53, CHCl₃); ¹H NMR (500 MHz, CD₃OD): $\delta = 7.64$ (d, $J = 2.2$ Hz, 1H, Ar-H), 7.56-7.46 (m, 3H, Ar-H), 7.33 (d, $J = 8.6$ Hz, 1H, Ar-H), 7.05-6.95 (m, 2H, Ar-H), 5.73 (s, 1H, H-1), 5.56 (dd, $J = 8.1, 3.4$ Hz, 2H, H-2, H-3), 5.35 (t, $J = 10.1$ Hz, 1H, H-4), 4.23 (dd, $J = 12.1, 5.5$ Hz, 1H, H-6a), 4.17 (ddd, $J = 10.0, 5.6, 2.1$ Hz, 1H, H-5), 4.09 (dd, $J = 12.1, 2.1$ Hz, 1H, H-6b), 3.83 (s, 3H, OCH₃), 2.19 (s, 3H, COCH₃), 2.09-1.92 (m, 9H, 3 COCH₃); ¹³C NMR (126 MHz, CD₃OD): $\delta = 172.19, 171.52, 171.48$ (4C, 4 CO), 161.04, 151.01, 138.58, 132.80, 129.26, 128.85, 127.01, 125.50, 118.93, 115.43 (12C, Ar-C), 97.76 (C-1), 71.18 (C-5), 70.52, 70.30 (C-2, C-3), 67.01 (C-4), 63.32 (C-6), 55.77 (OCH₃), 20.59, 20.58, 20.56 (4C, 4 COCH₃); ESI-MS: m/z : Calcd for C₂₇H₂₉ClKO₁₁ [M+K]⁺: 603.1, found: 603.0.

3-Chloro-4'-methyl-biphenyl-4-yl 2,3,4,6-tetra-*O*-acetyl- α -D-mannopyranoside (14g). Prepared according to general procedure A from **12** (79 mg, 0.135 mmol), 4-methyl-phenylboronic acid (**13g**, 20 mg, 0.15 mmol), Pd(dppf)Cl₂·CH₂Cl₂ (3.3 mg, 4 μ mol) and K₃PO₄ (57 mg, 0.27 mmol). Yield: 50 mg (67%) as a white solid. $[\alpha]_D^{20} +71.9$ (c 0.43, CHCl₃); ¹H NMR (500 MHz, CD₃OD): $\delta = 7.67$ (d, $J = 2.2$ Hz, 1H, Ar-H), 7.52 (dd, $J = 8.6, 2.2$ Hz, 1H, Ar-H), 7.47 (t, $J = 7.3$ Hz, 2H, Ar-H), 7.35 (d, $J = 8.6$ Hz, 1H, Ar-H), 7.25 (d, $J = 7.9$ Hz, 2H, Ar-H), 5.75 (s, 1H, H-1), 5.59-5.52 (m, 2H, H-2, H-3),

5.34 (t, $J = 10.0$ Hz, 1H, H-4), 4.23 (dd, $J = 12.1, 5.5$ Hz, 1H, H-6a), 4.17 (m, 1H, H-5), 4.09 (dd, $J = 12.1, 2.1$ Hz, 1H, H-6b), 2.37 (s, 3H, PhCH₃), 2.20 (s, 3H, COCH₃), 2.12-1.92 (m, 9H, 3 COCH₃); ¹³C NMR (126 MHz, CDCl₃): $\delta = 170.64, 170.10, 169.94, 169.91$ (4 CO), 150.42, 137.66, 137.63, 136.41, 129.78, 129.03, 126.81, 126.18, 124.80, 117.47 (12C, Ar-C), 96.90 (C-1), 69.89, 69.53, 68.95 (C-5, C-3, C-2), 66.04 (C-4), 62.29 (C-6), 21.23, 21.02, 20.86, 20.83, 20.82 (5 CH₃); ESI-MS: m/z : Calcd for C₂₇H₂₉ClNaO₁₀ [M+Na]⁺: 571.1, found: 571.1.

3,4'-Dichloro-3'-(trifluoromethyl)-biphenyl-4-yl 2,3,4,6-tetra-*O*-acetyl- α -D-mannopyranoside (14h). Prepared according to general procedure A from **12** (80 mg, 0.137 mmol), 3-trifluoro-4-chlorophenylboronic acid (**13h**, 34 mg, 0.151 mmol), Pd(dppf)Cl₂·CH₂Cl₂ (3.4 mg, 4 μ mol) and K₃PO₄ (58 mg, 0.27 mmol). Yield: 70 mg (80%) as a white solid. $[\alpha]_D^{20} +60.7$ (c 0.27, CHCl₃); ¹H NMR (500 MHz, CD₃OD): $\delta = 7.95$ (d, $J = 1.9$ Hz, 1H, Ar-H), 7.84 (dd, $J = 8.3, 2.0$ Hz, 1H, Ar-H), 7.79 (d, $J = 2.3$ Hz, 1H, Ar-H), 7.72-7.58 (m, 2H, Ar-H), 7.44 (m, 1H, Ar-H), 5.80 (s, 1H, H-1), 5.60-5.51 (m, 2H, H-2, H-3), 5.36 (t, $J = 10.0$ Hz, 1H, H-4), 4.24 (dd, $J = 12.2, 5.3$ Hz, 1H, H-6a), 4.18-4.05 (m, 2H, H-5, H-6b), 2.20, 2.08, 2.02, 1.96 (4s, 12H, 4 COCH₃); ¹³C NMR (126 MHz, CD₃OD): $\delta = 172.17, 171.49, 171.47$ (4C, 4 CO), 152.43, 139.86, 135.79, 133.40, 132.76, 130.00, 127.78, 126.84, 125.87, 118.88 (12C, Ar-C), 97.65 (C-1), 71.28 (C-5), 70.49, 70.21 (C-2, C-3), 66.94 (C-4), 63.28 (C-5), 20.59, 20.56 (4C, 4 COCH₃); ESI-MS: m/z : Calcd for C₂₇H₂₅Cl₂F₃NaO₁₀ [M+Na]⁺: 659.1, found: 659.0.

3,3'-Dichloro-biphenyl-4-yl 2,3,4,6-tetra-*O*-acetyl- α -D-mannopyranoside (14i). Prepared according to general procedure A from **12** (81 mg, 0.138 mmol), 3-chloro-phenylboronic acid (**13i**, 24 mg, 0.15 mmol), Pd(dppf)Cl₂·CH₂Cl₂ (3.4 mg, 4 μ mol) and K₃PO₄ (59 mg, 0.28 mmol). Yield: 57 mg (75%) as a white solid. $[\alpha]_D^{20} +67.3$ (c 0.27, CHCl₃); ¹H NMR (500 MHz, CD₃OD): $\delta = 7.71$ (t, $J = 7.8$ Hz, 1H, Ar-H), 7.66-7.31 (m, 6H, Ar-H), 5.78 (s, 1H, H-1), 5.61-5.51 (m, 2H, H-2, H-3), 5.35 (t, $J = 10.1$ Hz, 1H, H-4), 4.23 (dd, $J = 12.2, 5.4$ Hz, 1H, H-6a), 4.19-4.02 (m, 2H, H-5, H-6b), 2.19 (s, 3H, COCH₃), 2.11-1.92 (m, 9H, 3 COCH₃); ¹³C NMR (126 MHz, CD₃OD): $\delta = 172.18, 171.50, 171.48$ (4C, 4 CO), 152.04, 142.44, 137.09, 135.96, 131.56, 129.89, 128.65, 127.75, 127.67, 126.23, 125.67, 118.82 (12C, Ar-C) 97.66 (C-1), 71.23, 70.49, 70.23 (C-2, C-3, C-5), 66.95 (C-4), 63.28 (C-6), 20.59, 20.58, 20.55 (4C, 4 COCH₃); ESI-MS: m/z : Calcd for C₂₆H₂₆Cl₂NaO₁₀ [M+Na]⁺: 591.1, found: 591.0.

3-Chloro-3'-methyl-biphenyl-4-yl 2,3,4,6-tetra-*O*-acetyl- α -D-mannopyranoside (14j). Prepared according to general procedure A from **12** (79 mg, 0.135 mmol), 3-methyl-phenylboronic acid (**13j**, 20 mg, 0.15 mmol), Pd(dppf)Cl₂·CH₂Cl₂ (3.3 mg, 4 μ mol) and K₃PO₄ (57 mg, 0.27 mmol). Yield: 51 mg (69%) as a white solid. $[\alpha]_D^{20} +78.2$ (c 0.36, CHCl₃); ¹H NMR (500 MHz, CD₃OD): $\delta = 7.68$ (d, $J = 2.1$ Hz, 1H, Ar-H), 7.53 (dd, $J = 8.6, 2.1$ Hz, 1H, Ar-H), 7.34 (m, 4H, Ar-H), 7.17 (d, $J = 7.4$ Hz, 1H, Ar-H), 5.76 (s, 1H, H-1), 5.59-5.52 (m, 2H, H-2, H-3), 5.35 (t, $J = 9.9$ Hz, 1H, H-4), 4.24 (dd, $J = 12.1, 5.5$ Hz, 1H, H-6a), 4.17 (m, 1H, H-5), 4.09 (dd, $J = 12.1, 2.1$ Hz, 1H, H-6b), 2.40 (s, 3H,

PhCH₃), 2.19 (s, 3H, COCH₃), 2.09-1.94 (m, 9H, 3 COCH₃); ¹³C NMR (126 MHz, CD₃OD): δ = 172.20, 171.53, 171.49 (4C, 4 CO), 151.44, 140.37, 139.83, 138.93, 129.93, 129.75, 129.40, 128.41, 127.52, 125.47, 124.90, 118.82 (12 Ar-C), 97.71 (C-1), 71.19 (C-5), 70.51, 70.28 (C-2, C-3), 66.99 (C-4), 63.31 (C-6), 21.52 (PhCH₃), 20.60, 20.59, 20.56 (4C, 4 COCH₃); ESI-MS: *m/z*: Calcd for C₂₇H₂₉ClNaO₁₀ [M+Na]⁺: 571.1, found: 571.1.

2',3-Dichloro-biphenyl-4-yl 2,3,4,6-tetra-O-acetyl-α-D-mannopyranoside (14k). Prepared according to general procedure A from **12** (81 mg, 0.138 mmol), 2-chloro-phenylboronic acid (**13k**, 24 mg, 0.15 mmol), Pd(dppf)Cl₂·CH₂Cl₂ (3.4 mg, 4 μmol) and K₃PO₄ (59 mg, 0.28 mmol). Yield: 52 mg (66%) as a white solid. [α]_D²⁰ +64.7 (*c* 0.42, CHCl₃); ¹H NMR (500 MHz, CD₃OD): δ = 7.48 (dd, *J* = 8.9, 1.7 Hz, 2H, Ar-H), 7.39-7.30 (m, 5H, Ar-H), 5.77 (s, 1H, H-1), 5.64-5.52 (m, 2H, H-2, H-3), 5.35 (m, 1H, H-4), 4.24 (dd, *J* = 12.1, 5.6 Hz, 1H, H-6a), 4.17 (ddd, *J* = 10.0, 5.6, 2.0 Hz, 1H, H-5), 4.08 (m, 1H, H-6b), 2.19, 2.07, 2.01, 1.96 (4 s, 12H, 4 COCH₃); ¹³C NMR (126 MHz, CD₃OD): δ = 172.16, 171.50, 171.45 (4C, 4 CO), 151.72, 139.84, 136.70, 133.35, 132.42, 132.34, 131.10, 130.31, 130.24, 128.37, 124.63, 117.98 (12 Ar-C), 97.64 (C-1), 71.22 (C-5), 70.47, 70.24 (C-2, C-3), 66.96 (C-4), 63.29 (C-6), 20.62, 20.61, 20.60, 20.57 (4 COCH₃); ESI-MS: *m/z*: Calcd for C₂₆H₂₆Cl₂NaO₁₀ [M+Na]⁺: 591.1, found: 591.0.

3-Chloro-2'-methyl-biphenyl-4-yl 2,3,4,6-tetra-O-acetyl-α-D-mannopyranoside (14l). Prepared according to general procedure A from **12** (79 mg, 0.14 mmol), 2-methyl-phenylboronic acid (**13l**, 20 mg, 0.15 mmol), Pd(dppf)Cl₂·CH₂Cl₂ (3.3 mg, 4 μmol) and K₃PO₄ (57 mg, 0.27 mmol). Yield: 39 mg (53%) as a white solid. [α]_D²⁰ +62.9 (*c* 0.42, CHCl₃); ¹H NMR (500 MHz, CD₃OD): δ = 7.37 (dd, *J* = 12.9, 5.2 Hz, 2H, Ar-H), 7.29-7.19 (m, 4H, Ar-H), 7.16 (d, *J* = 6.9 Hz, 1H, Ar-H), 5.76 (s, 1H, H-1), 5.59-5.54 (m, 2H, H-2, H-3), 5.35 (m, 1H, H-4), 4.28-4.03 (m, 3H, H-5, H-6), 2.25 (s, 3H, PhCH₃), 2.19, 2.08, 2.02, 1.98 (4 s, 12H, 4 COCH₃); ¹³C NMR (126 MHz, CD₃OD): δ = 172.19, 171.54, 171.50 (4C, 4 CO), 151.24, 141.25, 139.60, 136.36, 132.01, 131.48, 130.60, 129.93, 128.82, 127.04, 124.80, 118.24 (12 Ar-C), 97.81 (C-1), 71.21 (C-5), 70.52, 70.31 (2C, C-2, C-3), 67.02 (C-4), 63.35 (C-6), 20.60, 20.56, 20.52 (5C, 5 CH₃); ESI-MS: *m/z*: Calcd for C₂₇H₂₉ClNaO₁₀ [M+Na]⁺: 571.1, found: 571.1.

3-Chloro-2'-methoxy-biphenyl-4-yl 2,3,4,6-tetra-O-acetyl-α-D-mannopyranoside (14m). Prepared according to general procedure A from **12** (79 mg, 0.135 mmol), 2-methoxy-phenylboronic acid (**13m**, 23 mg, 0.15 mmol), Pd(dppf)Cl₂·CH₂Cl₂ (3.3 mg, 4 μmol) and K₃PO₄ (57 mg, 0.27 mmol). Yield: 34 mg (45%) as a white solid. [α]_D²⁰ +75.0 (*c* 0.52, CHCl₃); ¹H NMR (500 MHz, CD₃OD): δ = 7.58 (d, *J* = 2.1 Hz, 1H, Ar-H), 7.42 (dd, *J* = 8.6, 2.1 Hz, 1H, Ar-H), 7.38-7.25 (m, 3H, Ar-H), 7.08 (d, *J* = 8.2 Hz, 1H, Ar-H), 7.02 (m, 1H, Ar-H), 5.76 (s, 1H, H-1), 5.58 (dd, *J* = 8.5, 3.2 Hz, 2H, H-2, H-3), 5.37 (t, *J* = 10.0 Hz, 1H, H-4), 4.26 (dd, *J* = 12.1, 5.6 Hz, 1H, H-6a), 4.19 (ddd, *J* = 10.0, 5.7, 2.0 Hz, 1H, H-5), 4.12 (dt, *J* = 8.5, 5.3 Hz, 1H, H-6b), 3.82 (s, 3H, OCH₃), 2.21, 2.10, 2.04, 1.98 (4 s,

12H, 4 COCH₃); ¹³C NMR (126 MHz, CD₃OD): δ = 172.23, 171.54, 171.49 (4C, 4 CO), 157.81, 150.91, 136.27, 132.31, 131.42, 130.27, 130.11, 129.80, 124.42, 122.00, 118.00, 112.60 (12 Ar-C), 97.63 (C-1), 71.16, 70.53, 70.30 (C-2, C-3, C-5), 67.02 (C-4), 63.31 (C-6), 55.99 (OCH₃), 20.60, 20.59, 20.57 (4C, 4 COCH₃); ESI-MS: *m/z*: Calcd for C₂₇H₂₉ClNaO₁₁ [M+Na]⁺: 587.1, found: 587.2.

3-Chloro-3'-(trifluoromethyl)-biphenyl-4-yl 2,3,4,6-tetra-*O*-acetyl- α -D-mannopyranoside (14n).

Prepared according to general procedure A from **12** (80 mg, 0.137 mmol), 3-trifluoromethylphenylboronic acid (**13n**, 29 mg, 0.15 mmol), Pd(dppf)Cl₂·CH₂Cl₂ (3.4 mg, 4 μmol) and K₃PO₄ (58 mg, 0.27 mmol). Yield: 69 mg (83%) as a white solid. [α]_D²⁰ +62 (*c* 0.49, CHCl₃); ¹H NMR (500 MHz, CD₃OD): δ = 7.86 (m, 2H, Ar-H), 7.77 (d, *J* = 2.2 Hz, 1H, Ar-H), 7.71-7.59 (m, 3H, Ar-H), 7.43 (d, *J* = 8.6 Hz, 1H, Ar-H), 5.80 (s, 1H, H-1), 5.66-5.53 (m, 2H, H-2, H-3), 5.38 (t, *J* = 10.1 Hz, 1H, H-4), 4.31-4.06 (m, 3H, H-5, H-6), 2.28-1.93 (m, 12H, 4 COCH₃); ¹³C NMR (126 MHz, CD₃OD): δ = 172.15, 171.49, 171.47, 171.46 (4 CO), 152.19, 141.43, 136.92, 132.36 (q, *J* = 32 Hz), 131.56, 130.93, 128.9 (q, *J* = 279 Hz), 126.69, 125.77, 125.29 (q, *J* = 3.8 Hz), 124.53, 124.35 (q, *J* = 3.9 Hz), 118.88 (13C, 12 Ar-C, CF₃), 97.66 (C-1), 71.24 (C-5), 70.47 (C-3), 70.22 (C-2), 66.94 (C-4), 63.27 (C-6), 20.59, 20.58, 20.56, 20.55 (4 COCH₃); ESI-MS: *m/z*: Calcd for C₂₇H₂₆ClF₃NaO₁₀ [M+Na]⁺: 641.1, found: 641.1.

4'-Acetyl-3-chloro-biphenyl-4-yl 2,3,4,6-tetra-*O*-acetyl- α -D-mannopyranoside (14o).

Prepared according to general procedure A from **12** (64.3 mg, 0.11 mmol), 4-acetylphenylboronic acid (**13o**, 27 mg, 0.12 mmol), Pd(dppf)Cl₂·CH₂Cl₂ (2.7 mg, 3 μmol) and K₃PO₄ (47 mg, 0.22 mmol). Yield: 52 mg (82%) as a white solid. [α]_D²⁰ +76.9 (*c* 0.62, CHCl₃); ¹H NMR (500 MHz, CD₃OD): δ = 8.04 (d, *J* = 8.4 Hz, 2H, Ar-H), 7.77 (d, *J* = 2.2 Hz, 1H, Ar-H), 7.71 (d, *J* = 8.4 Hz, 2H, Ar-H), 7.61 (dd, *J* = 8.6, 2.2 Hz, 1H, Ar-H), 7.38 (d, *J* = 8.7 Hz, 1H, Ar-H), 5.78 (s, 1H, H-1), 5.60-5.51 (m, 2H, H-2, H-3), 5.35 (t, *J* = 10.0 Hz, 1H, H-4), 4.23 (dd, *J* = 12.2, 5.4 Hz, 1H, H-6a), 4.17-4.01 (m, 2H, H-5, H-6b), 2.62 (s, 3H, PhCOCH₃), 2.20, 2.10, 2.04, 1.98 (4 s, 12H, 4 COCH₃); ¹³C NMR (126 MHz, CD₃OD): δ = 199.93 (PhCOCH₃), 172.14, 171.49, 171.46, 171.45 (4 CO), 152.26, 144.91, 137.30, 137.07, 130.24, 130.03, 127.92, 127.82, 125.70, 118.78 (12 C, Ar-C), 97.62 (C-1), 71.23 (C-5), 70.46, 70.21 (C-2, C-3), 66.93 (C-4), 63.27 (C-6), 26.73 (PhCOCH₃), 20.61, 20.59, 20.57 (4C, 4 COCH₃); ESI-MS: *m/z*: Calcd for C₂₈H₂₉ClNaO₁₁ [M+Na]⁺: 599.1, found 599.1.

4'-(2,3,4,6-Tetra-*O*-acetyl- α -D-mannopyranosyloxy)-3'-chloro-biphenyl-4-carbonitril (14p).^[58]

Prepared according to general procedure A from **12** (79 mg, 0.135 mmol), 4-cyano-phenylboronic acid (**13p**, 22 mg, 0.15 mmol), Pd(dppf)Cl₂·CH₂Cl₂ (3.3 mg, 4 μmol) and K₃PO₄ (57 mg, 0.27 mmol). Yield: 57 mg (75%) as a white solid. [α]_D²⁰ +77.7 (*c* 0.5, CHCl₃); ¹H NMR (500 MHz, CDCl₃): δ = 7.72 (d, *J* = 8.3 Hz, 2H, Ar-H), 7.63 (m, 3H, Ar-H), 7.43 (dd, *J* = 8.6, 2.2 Hz, 1H, Ar-H), 7.27 (d, *J* = 8.6 Hz, 1H, Ar-H), 5.64-5.59 (m, 2H, H-1, H-3), 5.54 (dd, *J* = 3.2, 1.9 Hz, 1H, H-2), 5.41 (t, *J* = 10.1 Hz, 1H, H-4), 4.28 (dd, *J* = 12.3, 5.2 Hz, 1H, H-6a), 4.17 (ddd, *J* = 10.0, 5.1, 2.1 Hz, 1H, H-5), 4.10

(dd, $J = 12.3, 2.2$ Hz, 1H, H-6b), 2.21 (s, 3H, COCH₃), 2.12-2.00 (m, 9H, 3 COCH₃); ¹³C NMR (126 MHz, CDCl₃): $\delta = 170.54, 170.08, 169.90, 169.84, (4 \text{ CO}) 151.67, 143.61, 135.29, 132.87, 129.41, 127.53, 126.60, 125.20, 118.79, 117.36, 111.47 (13\text{C, Ar-C, CN}), 96.72 (C-1), 70.00 (C-5), 69.39 (C-3), 68.82 (C-2), 65.86 (C-4), 62.16 (C-6), 20.98, 20.81, 20.79, 20.78 (4 \text{ COCH}_3)$; ESI-MS: m/z : Calcd for C₂₇H₂₆ClNNaO₁₀[M+Na]⁺: 582.1, found: 582.1.

4'-(2,3,4,6-Tetra-*O*-acetyl- α -D-mannopyranosyloxy)-3'-chloro-biphenyl-3-carbonitril (14q).

Prepared according to general procedure A from **12** (80 mg, 0.137 mmol), 3-cyanophenylboronic acid pinacol ester (**13q**, 35 mg, 0.151 mmol), Pd(dppf)Cl₂·CH₂Cl₂ (3.4 mg, 4 μ mol) and K₃PO₄ (58 mg, 0.27 mmol). Yield: 57 mg (74%) as a white solid. $[\alpha]_{\text{D}}^{20} +66.2$ (c 0.6, CHCl₃); ¹H NMR (500 MHz, CDCl₃): $\delta = 7.83-7.73$ (m, 2H, Ar-H), 7.62 (dd, $J = 10.4, 5.0$ Hz, 2H, Ar-H), 7.55 (t, $J = 7.8$ Hz, 1H, Ar-H), 7.41 (dd, $J = 8.6, 2.2$ Hz, 1H, Ar-H), 7.33-7.23 (m, 2H, Ar-H), 5.61 (m, 2H, H-1, H-3), 5.54 (dd, $J = 3.3, 1.9$ Hz, 1H, H-2), 5.39 (t, $J = 10.1$ Hz, 1H, H-4), 4.27 (dd, $J = 12.3, 5.2$ Hz, 1H, H-6a), 4.22-4.05 (m, 2H, H-5, H-6b), 2.21 (s, 3H, COCH₃), 2.14-1.99 (m, 9H, 3 COCH₃); ¹³C NMR (126 MHz, CDCl₃): $\delta = 170.83, 170.23, 170.12, 170.04 (4 \text{ CO}), 151.35, 140.43, 134.98, 131.29, 131.11, 130.39, 129.89, 129.18, 126.39, 125.07, 118.60, 117.37, 113.04 (13\text{C, 12 Ar-C, CN}), 96.60 (C-1), 69.83 (C-5), 69.29 (C-3), 68.85 (C-2), 65.80 (C-4), 62.14 (C-6), 24.54, 20.78, 20.64, 20.62 (4 \text{ COCH}_3)$; ESI-MS: m/z : Calcd for C₂₇H₂₆ClNNaO₁₀[M+Na]⁺: 582.1, found: 582.1.

3-Chloro-3'-nitro-biphenyl-4-yl 2,3,4,6-tetra-*O*-acetyl- α -D-mannopyranoside (14r).

Prepared according to general procedure A from **12** (80 mg, 0.137 mmol), 3-nitro-phenylboronic acid (**13r**, 25 mg, 0.151 mmol), Pd(dppf)Cl₂·CH₂Cl₂ (3.4 mg, 4 μ mol) and K₃PO₄ (58 mg, 0.27 mmol). Yield: 55 mg (69%) as a white solid. $[\alpha]_{\text{D}}^{20} +70.6$ (c 0.23, CHCl₃); ¹H NMR (500 MHz, CD₃OD): $\delta = 8.44$ (t, $J = 1.9$ Hz, 1H, Ar-H), 8.23 (m, 1H, Ar-H), 8.02 (dd, $J = 7.8, 0.6$ Hz, 1H, Ar-H), 7.82 (d, $J = 2.3$ Hz, 1H, Ar-H), 7.77-7.61 (m, 2H, Ar-H), 7.44 (d, $J = 8.7$ Hz, 1H, Ar-H), 5.81 (s, 1H, H-1), 5.63-5.54 (m, 2H, H-2, H-3), 5.38 (t, $J = 10.0$ Hz, 1H, H-4), 4.26 (dd, $J = 12.2, 5.3$ Hz, 1H, H-6a), 4.16 (ddd, $J = 10.1, 5.3, 2.2$ Hz, 1H, H-5), 4.10 (m, 1H, H-6a), 2.22 (s, 3H, COCH₃), 2.10-1.92 (m, 9H, 3 COCH₃); ¹³C NMR (126 MHz, CD₃OD): $\delta = 172.16, 171.49, 171.47, 171.46 (4 \text{ CO}), 152.47, 150.23, 142.04, 136.00, 133.90, 131.33, 130.07, 127.85, 125.86, 123.29, 122.34, 118.88 (12 \text{ Ar-C}), 97.66 (C-1), 71.26 (C-5), 70.45, 70.21 (C-2, C-3), 66.92 (C-4), 63.26 (C-6), 20.60, 20.59, 20.56 (4\text{C, 4 COCH}_3)$; ESI-MS: m/z : Calcd for C₂₆H₂₆ClNNaO₁₂[M+Na]⁺: 602.1, found: 602.1.

3-Chloro-biphenyl-4-yl α -D-mannopyranoside (2).

Prepared according to general procedure B from **11** (101 mg, 0.19 mmol). Yield: 65 mg (93%) as a white solid. $[\alpha]_{\text{D}}^{20} +87.5$ (c 0.067, MeOH/CHCl₃, 1:1); ¹H NMR (500 MHz, CD₃OD): $\delta = 7.63$ (d, $J = 2.2$ Hz, 1H, Ar-H), 7.59-7.48 (m, 3H, Ar-H), 7.42 (dd, $J = 12.3, 5.0$ Hz, 3H, Ar-H), 7.32 (t, $J = 7.4$ Hz, 1H, Ar-H), 5.58 (d, $J = 1.5$ Hz, 1H, H-1), 4.12 (dd, $J = 3.3, 1.8$ Hz, 1H, H-2), 4.01 (dd, $J = 9.5, 3.4$ Hz, 1H, H-3), 3.83-3.64 (m, 4H, H-4, H-5, H-6); ¹³C NMR (126 MHz, CD₃OD): $\delta = 152.67, 140.68, 137.91, 129.99, 129.49, 128.52, 127.72, 127.50,$

125.24, 118.73 (12C, Ar-C), 100.86 (C-1), 75.97 (C-5), 72.43 (C-3), 71.90 (C-2), 68.26 (C-4), 62.69 (C-6); HR-MS: m/z : Calcd for $C_{18}H_{19}ClNaO_6 [M+Na]^+$: 389.0762, found 389.0764.

3,4'-Dichloro-biphenyl-4-yl α -D-mannopyranoside (4a). Prepared according to general procedure B from **14a** (45.6 mg, 0.08 mmol). Yield: 20 mg (62%) as a white solid. $[\alpha]_D^{20} +69.9$ (c 0.42, MeOH); 1H NMR (500 MHz, CD_3OD): δ = 7.66 (d, J = 2.2 Hz, 1H, Ar-H), 7.59-7.54 (m, 2H, Ar-H), 7.51 (dd, J = 8.6, 2.3 Hz, 1H, Ar-H), 7.46-7.40 (m, 3H, Ar-H), 5.58 (d, J = 1.6 Hz, 1H, H-1), 4.11 (dd, J = 3.3, 1.8 Hz, 1H, H-2), 3.99 (dd, J = 9.5, 3.4 Hz, 1H, H-3), 3.81-3.69 (m, 3H, H-4, H-6), 3.65 (ddd, J = 9.8, 5.5, 2.4 Hz, 1H, H-5); ^{13}C NMR (126 MHz, CD_3OD): δ = 152.92, 139.33, 136.43, 134.57, 130.05, 129.44, 129.23, 127.44, 125.32, 118.70 (12C, Ar-C), 100.79 (C-1), 75.99 (C-5), 72.40 (C-3), 71.86 (C-2), 68.23 (C-4), 62.66 (C-6); HR-MS: m/z : Calcd for $C_{18}H_{18}Cl_2NaO_6 [M+Na]^+$: 423.0373, found 423.0378.

3,3',4'-Trichloro-biphenyl-4-yl α -D-mannopyranoside (4b). Prepared according to general procedure B from **14b** (45.3 mg, 0.08 mmol). Yield: 26 mg (80%) as a white solid. $[\alpha]_D^{20} +92.8$ (c 0.24, MeOH); 1H NMR (500 MHz, CD_3OD): δ = 7.70 (d, J = 2.1 Hz, 1H, Ar-H), 7.63 (d, J = 2.2 Hz, 1H, Ar-H), 7.56-7.41 (m, 4H, Ar-H), 5.60 (d, J = 1.6 Hz, 1H, H-1), 4.12 (dd, J = 3.3, 1.8 Hz, 1H, H-2), 4.00 (dd, J = 9.5, 3.4 Hz, 1H, H-3), 3.81-3.69 (m, 3H, H-4, H-6), 3.64 (ddd, J = 9.7, 5.4, 2.4 Hz, 1H, H-5); ^{13}C NMR (126 MHz, CD_3OD): δ = 153.28, 140.97, 134.91, 133.84, 132.38, 131.98, 129.50, 129.49, 127.51, 127.42, 125.38, 118.60 (12 Ar-C), 100.68 (C-1), 75.99 (C-5), 72.38 (C-3), 71.81 (C-2), 68.19 (C-4), 62.63 (C-6); HR-MS: m/z : Calcd for $C_{18}H_{17}Cl_3NaO_6 [M+Na]^+$: 456.9983, found 456.9984.

3-Chloro-4'-(trifluoromethyl)-biphenyl-4-yl α -D-mannopyranoside (4c). Prepared according to general procedure B from **14c** (36.2 mg, 0.06 mmol). Yield: 25 mg (95%) as a white solid. $[\alpha]_D^{20} +83.0$ (c 0.24, MeOH); 1H NMR (500 MHz, CD_3OD): δ = 7.84-7.40 (m, 7H, Ar-H), 5.62 (d, J = 1.2 Hz, 1H, H-1), 4.13 (m, 1H, H-2), 4.01 (dd, J = 9.5, 3.4 Hz, 1H, H-3), 3.84-3.71 (m, 3H, H-4, H-6), 3.65 (m, 1H, H-5); ^{13}C NMR (126 MHz, CD_3OD): δ = 153.33, 144.34, 135.92, 130.42 (q, J = 32 Hz), 128.3 (q, J = 246 Hz), 128.28, 126.90 (q, J = 3.7 Hz), 125.38, 124.69, 118.62 (13C, 12 Ar-C, CF_3), 100.65 (C-1), 75.96 (C-5), 72.38 (C-3), 71.80 (C-2), 68.16 (C-4), 62.57 (C-6); HR-MS: m/z : Calcd for $C_{19}H_{18}ClF_3NaO_6 [M+Na]^+$: 457.0636, found 457.0641.

2',3,4'-Trichloro-biphenyl-4-yl α -D-mannopyranoside (4d). Prepared according to general procedure B from **14d** (28.4 mg, 0.05 mmol). Yield: 15 mg (73%) as a white solid. $[\alpha]_D^{20} +82.2$ (c 0.22, MeOH); 1H NMR (500 MHz, CD_3OD): δ = 7.59-7.28 (m, 6H, Ar-H), 5.60 (d, J = 1.4 Hz, 1H, H-1), 4.12 (dd, J = 3.3, 1.8 Hz, 1H, H-2), 4.00 (dd, J = 9.4, 3.4 Hz, 1H, H-3), 3.83-3.61 (m, 4H, H-4, H-5, H-6); ^{13}C NMR (126 MHz, CD_3OD): δ = 153.12, 138.93, 135.19, 134.62, 134.33, 133.51, 132.03, 130.68, 130.18, 128.60, 124.47, 117.95, (12 Ar-C), 100.82 (C-1), 76.05 (C-5), 72.41 (C-3),

71.86 (C-2), 68.25 (C-4), 62.69 (C-6); HR-MS: m/z : Calcd for $C_{18}H_{17}Cl_3NaO_6 [M+Na]^+$: 456.9983, found 456.9989.

3-Chloro-4'-nitro-biphenyl-4-yl α -D-mannopyranoside (4e). Prepared according to general procedure B from **14e** (27.3 mg, 0.05 mmol). Yield: 16 mg (83%) as a white solid. $[\alpha]_D^{20} +100.2$ (c 0.20, MeOH); 1H NMR (500 MHz, CD_3OD): δ = 8.32 (d, J = 8.8 Hz, 2H, Ar-H), 8.00 (s, 1H, Ar-H), 7.86 (d, J = 8.8 Hz, 2H, Ar-H), 7.82 (d, J = 2.2 Hz, 1H, Ar-H), 7.67 (dd, J = 8.6, 2.2 Hz, 1H, Ar-H), 7.52 (d, J = 8.7 Hz, 1H, Ar-H), 5.66 (d, J = 1.3 Hz, 1H, H-1), 4.14 (dd, J = 3.2, 1.8 Hz, 1H, H-2), 4.02 (dd, J = 9.5, 3.4 Hz, 1H, H-3), 3.85-3.71 (m, 3H, H-4, H-6), 3.65 (ddd, J = 9.6, 5.4, 2.3 Hz, 1H, H-5); ^{13}C NMR (126 MHz, CD_3OD): δ = 153.86, 148.53, 146.97, 135.06, 130.04, 128.64, 128.10, 125.53, 125.16, 118.60 (12C, Ar-C), 100.68 (C-1), 76.09 (C-5), 72.41 (C-3), 71.82 (C-2), 68.22 (C-4), 62.67 (C-6); HR-MS: m/z : Calcd for $C_{18}H_{18}ClNaO_8 [M+Na]^+$: 434.0613, found 434.0614.

3-Chloro-4'-methoxy-biphenyl-4-yl α -D-mannopyranoside (4f). Prepared according to general procedure B from **14f** (25 mg, 0.05 mmol). Yield: 13 mg (73%) as a white solid. $[\alpha]_D^{20} +84.5$ (c 0.16, $CHCl_3/MeOH$, 1:1); 1H NMR (500 MHz, CD_3OD): δ = 7.58 (d, J = 2.2 Hz, 1H, Ar-H), 7.53-7.43 (m, 3H, Ar-H), 7.39 (d, J = 8.6 Hz, 1H, Ar-H), 6.98 (d, J = 8.8 Hz, 2H, Ar-H), 5.55 (d, J = 1.4 Hz, 1H, H-1), 4.11 (dd, J = 3.3, 1.8 Hz, 1H, H-2), 3.99 (m, 1H, H-3), 3.82 (s, 3H, OCH_3), 3.81-3.62 (m, 4H, H-4, H-5, H-6); ^{13}C NMR (126 MHz, CD_3OD): δ = 160.88, 152.14, 137.70, 133.08, 129.00, 128.77, 126.97, 125.20, 118.81, 115.38 (12C, Ar-C), 100.92 (C-1), 75.91 (C-5), 72.41 (C-3), 71.90 (C-2), 68.26 (C-4), 62.68 (C-6), 55.76 (OCH_3); HR-MS: m/z : Calcd for $C_{19}H_{21}ClNaO_7 [M+Na]^+$: 419.0868, found 419.0865.

3-Chloro-4'-methyl-biphenyl-4-yl α -D-mannopyranoside (4g). Prepared according to general procedure B from **14g** (38 mg, 0.07 mmol). Yield: 14 mg (53%) as a white solid. $[\alpha]_D^{20} +95.1$ (c 0.22, MeOH); 1H NMR (500 MHz, CD_3OD): δ = 7.60 (d, J = 2.2 Hz, 1H, Ar-H), 7.51-7.37 (m, 4H, Ar-H), 7.23 (d, J = 8.0 Hz, 2H, Ar-H), 5.56 (d, J = 1.4 Hz, 1H, H-1), 4.11 (dd, J = 3.2, 1.8 Hz, 1H, H-2), 4.00 (dd, J = 9.5, 3.4 Hz, 1H, H-3), 3.82-3.64 (m, 4H, H-4, H-5, H-6), 2.36 (s, 3H, CH_3); ^{13}C NMR (126 MHz, CD_3OD): δ = 152.40, 138.43, 137.87, 137.74, 130.59, 129.23, 127.53, 127.21, 125.18, 118.73 (12C, Ar-C), 100.86 (C-1), 75.91 (C-5), 72.41 (C-3), 71.89 (C-2), 68.24 (C-4), 62.66 (C-6), 21.08 (CH_3); HR-MS: m/z : Calcd for $C_{19}H_{21}ClNaO_6 [M+Na]^+$: 403.0919, found 403.0924.

3,4'-Dichloro-3'-(trifluoromethyl)-biphenyl-4-yl α -D-mannopyranoside (4h). Prepared according to general procedure B from **14h** (76 mg, 0.12 mmol). Yield: 18 mg (36%) as a white solid. $[\alpha]_D^{20} +83.0$ (c 0.34, MeOH); 1H NMR (500 MHz, CD_3OD): δ = 7.95-7.44 (m, 6H, Ar-H), 5.61 (d, J = 1.4 Hz, 1H, H-1), 4.11 (dd, J = 3.3, 1.8 Hz, 1H, H-2), 4.00 (dd, J = 9.5, 3.4 Hz, 1H, H-3), 3.83-3.68 (m, 3H, H-4, H-6), 3.63 (ddd, J = 9.6, 5.4, 2.3 Hz, 1H, H-5); ^{13}C NMR (126 MHz, CD_3OD): δ = 153.48, 140.08, 134.83, 133.32, 132.64, 132.04, 129.79, 128.7 (q, J = 246 Hz), 126.71, 126.67, 125.51,

123.27, 118.69 (12 Ar-C, CF₃), 100.70 (C-1), 76.05 (C-5), 72.39 (C-3), 71.82 (C-2), 68.21 (C-4), 62.66 (C-6); HR-MS: *m/z*: Calcd for C₁₉H₁₇Cl₂F₃NaO₆ [M+Na]⁺: 491.0246, found 491.0250.

3,3'-Dichloro-biphenyl-4-yl α -D-mannopyranoside (4i). Prepared according to general procedure B from **14i** (34 mg, 0.06 mmol). Yield: 15 mg (62%) as a white solid. $[\alpha]_D^{20} +96.1$ (*c* 0.21, MeOH); ¹H NMR (500 MHz, CD₃OD): $\delta = 7.64$ (d, *J* = 1.9 Hz, 1H, Ar-H), 7.57 (s, 1H, Ar-H), 7.55-7.29 (m, 5H, Ar-H), 5.59 (s, 1H, H-1), 4.12 (s, 1H, H-2), 4.00 (dd, *J* = 9.5, 3.3 Hz, 1H, H-3), 3.83-3.69 (m, 3H, H-4, H-6), 3.64 (m, 1H, H-5); ¹³C NMR (126 MHz, CD₃OD): $\delta = 153.12, 142.67, 136.15, 135.88, 131.47, 129.57, 128.42, 127.66, 127.59, 126.13, 125.32, 118.64$ (12 Ar-C), 100.74 (C-1), 75.98 (C-5), 72.39 (C-3), 71.84 (C-2), 68.21 (C-4), 62.65 (C-6); HR-MS: *m/z*: Calcd for C₁₈H₁₈Cl₂NaO₆ [M+Na]⁺: 423.0373, found 423.0378.

3-Chloro-3'-methyl-biphenyl-4-yl α -D-mannopyranoside (4j). Prepared according to general procedure B from **14j** (40.6 mg, 0.07 mmol). Yield: 26 mg (92%) as a white solid. $[\alpha]_D^{20} +98.5$ (*c* 0.30, MeOH); ¹H NMR (500 MHz, CD₃OD): $\delta = 7.61$ (d, *J* = 2.2 Hz, 1H, Ar-H), 7.39 (m, 5H, Ar-H), 7.15 (d, *J* = 7.3 Hz, 1H, Ar-H), 5.56 (d, *J* = 1.5 Hz, 1H, H-1), 4.11 (dd, *J* = 3.3, 1.8 Hz, 1H, H-2), 3.99 (dd, *J* = 9.5, 3.4 Hz, 1H, H-3), 3.84-3.62 (m, 4H, H-4, H-5, H-6), 2.39 (s, 3H, CH₃); ¹³C NMR (126 MHz, CD₃OD): $\delta = 152.59, 140.64, 139.76, 138.07, 129.88, 129.48, 129.21, 128.37, 127.48, 125.18, 124.85, 118.71$ (12 Ar-C) 100.87 (C-1), 75.95 (C-5), 72.43 (C-3), 71.91 (C-2), 68.27 (C-4), 62.68 (C-6), 21.53 (CH₃); HR-MS: *m/z*: Calcd for C₁₉H₂₁ClNaO₆ [M+Na]⁺: 403.0919, found 403.0925.

2',3-Dichloro-biphenyl-4-yl α -D-mannopyranoside (4k). Prepared according to general procedure B from **14k** (38.7 mg, 0.07 mmol). Yield: 20 mg (73%) as a white solid. $[\alpha]_D^{20} +85.6$ (*c* 0.3, MeOH); ¹H NMR (500 MHz, CD₃OD): $\delta = 7.53-7.24$ (m, 7H, Ar-H), 5.60 (d, *J* = 1.3 Hz, 1H, H-1), 4.13 (dd, *J* = 3.2, 1.8 Hz, 1H, H-2), 4.01 (dd, *J* = 9.5, 3.4 Hz, 1H, H-3), 3.86-3.64 (m, 4H, H-4, H-5, H-6); ¹³C NMR (126 MHz, CD₃OD): $\delta = 152.84, 140.11, 135.85, 133.40, 132.43, 132.05, 131.05, 130.18, 130.15, 128.30, 124.32, 117.89$ (12 Ar-C), 100.83 (C-1), 75.98 (C-5), 72.39, 71.86, (C-3, C-2), 68.23 (C-4), 62.66 (C-6); HR-MS: *m/z*: Calcd for C₁₈H₁₈Cl₂NaO₆ [M+Na]⁺: 423.0373, found 423.0378.

3-Chloro-2'-methyl-biphenyl-4-yl α -D-mannopyranoside (4l). Prepared according to general procedure B from **14l** (26 mg, 0.05 mmol). Yield: 17 mg (95%) as a white solid. $[\alpha]_D^{20} +88.0$ (*c* 0.22, MeOH); ¹H NMR (500 MHz, CD₃OD): $\delta = 7.40-6.93$ (m, 7H, Ar-H), 5.47 (d, *J* = 1.5 Hz, 1H, H-1), 4.02 (dd, *J* = 3.3, 1.8 Hz, 1H, H-2), 3.90 (dd, *J* = 9.4, 3.4 Hz, 1H, H-3), 3.74-3.55 (m, 4H, H-4, H-5, H-6), 2.14 (s, 3H, CH₃); ¹³C NMR (126 MHz, CD₃OD): $\delta = 152.30, 141.49, 138.70, 136.37, 131.70, 131.42, 130.62, 129.84, 128.67, 126.97, 124.50, 118.20$ (12 Ar-C), 100.97 (C-1), 75.97 (C-5), 72.42 (C-3), 71.91 (C-2), 68.28 (C-4), 62.70 (C-6), 20.52 (CH₃); HR-MS: *m/z*: Calcd for C₁₉H₂₁ClNaO₆ [M+Na]⁺: 403.0919, found 403.0922.

3-Chloro-2'-methoxy-biphenyl-4-yl α -D-mannopyranoside (4m). Prepared according to general procedure B from **14m** (26.6 mg, 0.05 mmol). Yield: 15 mg (80%) as a white solid. $[\alpha]_D^{20} +81.2$ (*c*

0.12, MeOH); ^1H NMR (500 MHz, CD_3OD): δ = 7.51 (s, 1H, Ar-H), 7.41-6.93 (m, 6H, Ar-H), 5.56 (d, J = 1.4 Hz, 1H, H-1), 4.11 (dd, J = 3.3, 1.8 Hz, 1H, H2), 4.00 (dd, J = 9.4, 3.4 Hz, 1H, H-3), 3.81 (s, 3H, OCH_3), 3.79-3.66 (m, 4H, H-4, H-5, H-6); ^{13}C NMR (126 MHz, CD_3OD): δ = 157.83, 152.11, 135.39, 132.06, 131.40, 130.08, 130.05, 124.14, 121.98, 117.93, 112.62 (12C, Ar-C), 100.87 (C-1), 75.89 (C-5), 72.41 (C-3), 71.91 (C-2), 68.26 (C-4), 62.67 (C-6), 56.01 (OCH_3); HR-MS: m/z : Calcd for $\text{C}_{19}\text{H}_{21}\text{ClNaO}_7$ $[\text{M}+\text{Na}]^+$: 419.0868, found 419.0871.

3-Chloro-3'-(trifluoromethyl)-biphenyl-4-yl α -D-mannopyranoside (4n). Prepared according to general procedure B from **14n** (60 mg, 0.1 mmol). Yield: 39 mg (91%) as a white solid. $[\alpha]_{\text{D}}^{20}$ +84.3 (c 0.42, MeOH); ^1H NMR (500 MHz, CD_3OD): δ = 7.87-7.78 (m, 2H, Ar-H), 7.70-7.44 (m, 5H, Ar-H), 5.61 (d, J = 1.1 Hz, 1H, H-1), 4.13 (dd, J = 3.0, 1.7 Hz, 1H, H-2), 4.01 (dd, J = 9.5, 3.4 Hz, 1H, H-3), 3.84-3.60 (m, 4H, H-4, H-5, H-6); ^{13}C NMR (126 MHz, CD_3OD): δ = 153.25, 141.66, 135.98, 132.30 (q, J = 246 Hz), 131.45, 130.85, 128.68 (q, J = 32 Hz), 126.71, 125.42, 125.05 (q, J = 3.8 Hz), 124.55, 124.23 (q, J = 3.8 Hz), 118.68 (12 Ar-C, CF_3), 100.71 (C-1), 75.99 (C-5), 72.39 (C-3), 71.82 (C-2), 68.20 (C-4), 62.64 (C-6); HR-MS: m/z : Calcd for $\text{C}_{19}\text{H}_{18}\text{ClF}_3\text{NaO}_6$ $[\text{M}+\text{Na}]^+$: 457.0636, found 457.0640.

4'-Acetyl-3-chloro-biphenyl-4-yl α -D-mannopyranoside (4o). Prepared according to general procedure B from **14o** (32 mg, 0.06 mmol). Yield: 21 mg (93%) as a white solid. $[\alpha]_{\text{D}}^{20}$ +103.2 (c 0.27, MeOH); ^1H NMR (500 MHz, CD_3OD): δ = 8.06 (d, J = 8.4 Hz, 2H, Ar-H), 7.74 (dd, J = 8.6, 5.3 Hz, 3H, Ar-H), 7.61 (dd, J = 8.6, 2.2 Hz, 1H, Ar-H), 7.48 (d, J = 8.7 Hz, 1H, Ar-H), 5.61 (d, J = 1.3 Hz, 1H, H-1), 4.12 (dd, J = 3.3, 1.8 Hz, 1H, H-2), 4.00 (dd, J = 9.5, 3.4 Hz, 1H, H-3), 3.83-3.59 (m, 4H, H-4, H-5, H-6), 2.63 (s, 3H, COCH_3); ^{13}C NMR (126 MHz, CD_3OD): δ = 200.02 (CO), 153.40, 145.29, 137.16, 136.20, 130.22, 129.76, 127.86, 127.80, 125.39, 118.61 (12C, Ar-C), 100.72 (C-1), 76.03 (C-5), 72.40 (C-3), 71.83 (C-2), 68.22 (C-4), 62.66 (C-6), 26.71 (COCH_3); HR-MS: m/z : Calcd for $\text{C}_{20}\text{H}_{21}\text{ClNaO}_7$ $[\text{M}+\text{Na}]^+$: 431.0868, found 431.0869.

3'-Chloro-4'-(α -D-mannopyranosyloxy)-biphenyl-4-carbonitril (4p).^[58] Prepared according to general procedure B from **14p** (36 mg, 0.06 mmol). Yield: 12 mg (48%) as a white solid. $[\alpha]_{\text{D}}^{20}$ +109.4 (c 0.23, MeOH); ^1H NMR (500 MHz, CD_3OD): δ = 7.80-7.72 (m, 5H, Ar-H), 7.59 (dd, J = 8.6, 2.2 Hz, 1H, Ar-H), 7.48 (d, J = 8.7 Hz, 1H, Ar-H), 5.62 (d, J = 1.4 Hz, 1H, H-1), 4.12 (dd, J = 3.3, 1.8 Hz, 1H, H-2), 4.00 (dd, J = 9.5, 3.4 Hz, 1H, H-3), 3.83-3.68 (m, 3H, H-4, H-6), 3.63 (ddd, J = 9.6, 5.4, 2.3 Hz, 1H, H-5); ^{13}C NMR (126 MHz, CD_3OD): δ = 153.65, 145.15, 135.42, 133.86, 129.82, 128.53, 127.87, 125.47, 119.70, 118.59, 111.97 (13C, 12 Ar-C, CN), 100.66 (C-1), 76.05 (C-5), 72.39 (C-3), 71.80 (C-2), 68.20 (C-4), 62.65 (C-6); IR (KBr): ν = 3400 (O-H), 2227 ($\text{C}\equiv\text{N}$), 1606, 1487 (Ar-C=C) cm^{-1} ; HR-MS: m/z : Calcd for $\text{C}_{19}\text{H}_{18}\text{ClNNaO}_6$ $[\text{M}+\text{Na}]^+$: 414.0715, found 414.0721.

3'-Chloro-4'-(α -D-mannopyranosyloxy)-biphenyl-3-carbonitril (4q). Prepared according to general procedure B from **14q** (84 mg, 0.15 mmol). Yield: 14 mg (34%) as a white solid. $[\alpha]_{\text{D}}^{20}$ +96.3

(*c* 0.23, MeOH); ^1H NMR (500 MHz, CD_3OD): δ = 8.03-7.88 (m, 2H, Ar-H), 7.71 (m, 2H, Ar-H), 7.65-7.54 (m, 2H, Ar-H), 7.48 (d, J = 8.6 Hz, 1H, Ar-H), 5.61 (d, J = 1.4 Hz, 1H, H-1), 4.12 (dd, J = 3.3, 1.8 Hz, 1H, H-2), 4.00 (dd, J = 9.5, 3.4 Hz, 1H, H-3), 3.85-3.56 (m, 4H, H-4, H-5, H-6); ^{13}C NMR (126 MHz, CD_3OD): δ = 153.45, 142.02, 135.30, 132.39, 132.00, 131.28, 131.15, 129.71, 127.74, 125.49, 119.62, 118.68, 114.15 (12 Ar-C, CN), 100.72 (C-1), 76.04 (C-5), 72.40 (C-3), 71.83 (C-2), 68.21 (C-4), 62.66 (C-6); HR-MS: m/z : Calcd for $\text{C}_{19}\text{H}_{18}\text{ClNNaO}_6$ $[\text{M}+\text{Na}]^+$: 414.0715, found 414.0715.

3-Chloro-3'-nitro-biphenyl-4-yl α -D-mannopyranoside (4r). Prepared according to general procedure B from **14r** (48 mg, 0.08 mmol). Yield: 32 mg (94%) as a white solid. $[\alpha]_{\text{D}}^{20}$ +93.2 (*c* 0.52, MeOH); ^1H NMR (500 MHz, CD_3OD): δ = 8.47-7.97 (m, 3H, Ar-H), 7.80-7.48 (m, 4H, Ar-H), 5.63 (s, 1H, H-1), 4.11 (m, 1H, H-2), 4.00 (dd, J = 9.5, 3.4 Hz, 1H, H-3), 3.82-3.58 (m, 4H, H-4, H-5, H-6); ^{13}C NMR (126 MHz, CD_3OD): δ = 153.56, 150.26, 142.38, 135.13, 133.86, 131.29, 129.78, 127.82, 125.53, 123.09, 122.28, 118.70 (12 Ar-C), 100.71 (C-1), 76.06 (C-5), 72.40 (C-3), 71.82 (C-2), 68.21 (C-4), 62.66 (C-6); HR-MS: m/z : Calcd for $\text{C}_{18}\text{H}_{18}\text{ClNNaO}_8$ $[\text{M}+\text{Na}]^+$: 434.0613, found 434.0612.

Biological Evaluation

Expression and purification of the FimH lectin domain (FimH-L). A recombinant protein consisting of the CRD of FimH linked to a 6His-tag via a thrombin cleavage site (FimH-CRD-Th-His₆) was expressed in *E. coli* strain HM125^[81] and purified by affinity chromatography as previously described.^[67]

Expression and purification of full-length FimH (FimH·DsG). Full-length FimH was purified for the most part as previously described.^[69] Briefly, FimH and FimC were co-expressed in *E. coli* HM125^[81] harboring pFimH-FimC. Cells were grown at 30 °C in LB medium containing ampicillin (100 $\mu\text{g}/\text{mL}$) to an OD_{600} of 1.5, whereupon co-expression of FimH and FimC was induced by adding isopropyl- β -D-thiogalactoside (IPTG) to a final concentration of 1 mM. Expression was continued for 12-16 h before cells were harvested by centrifugation and resuspended in 50 mM Tris (pH 7.5), 150 mM NaCl, 5 mM EDTA and 1 mg/mL polymyxin B sulfate (13 mL per liter of culture). After stirring the suspension at 4 °C for 1.5 h, cells and cell debris were pelleted and the supernatant (periplasmic extract) was dialyzed against 20 mM Tris (pH 8.0). All following purification steps were performed at 4 °C. The supernatant was loaded onto an Uno Q column (Bio-Rad, USA), which was equilibrated with the same buffer. The flow-through, which contained the FimH-FimC complex, was dialyzed against 10 mM MOPS (pH 7.0) and loaded onto a Mono S column (GE Healthcare, UK) equilibrated with the same buffer. The complex was eluted with a linear gradient from 0 to 300 mM NaCl. Fractions containing the FimH-FimC complex were pooled and dialyzed against a buffer containing 20 mM NaH_2PO_4 (pH 7.4) and 50 mM NaCl. Concentrated to 40 μM , FimH-FimC was incubated for

48 h at 37 °C with a 3-fold molar excess of a synthetic peptide (DsG) corresponding to the N-terminal sequence of the FimG donor strand with an additional arginine at the C-term to improve peptide solubility.^[82] After incubation, the excess of DsG displaced FimC from FimH, thereby forming a stable full-length FimH construct. The mixture was dialyzed against 20 mM acetic acid (pH 4.5) and loaded onto a Mono S column, which was equilibrated with the same buffer. Full-length FimH was eluted with a linear gradient from 0 to 400 mM, separating it from isolated FimC, unreacted FimH-FimC complex and excess DsG. Fractions containing full-length FimH were pooled, dialyzed against 20 mM acetic acid (pH 4.5), analyzed by SDS-PAGE and ESI-mass spectrometry (m/z : Calcd: 30635.3 Da, found: 30635.0 Da), and stored at -80 °C.

Competitive fluorescence polarization assay (FP assay). FP assays were essentially performed as previously described.^[58] The affinity (dissociation constant K_D) of **15** to either FimH protein was determined in a direct binding assay. The K_D of **15** to the isolated FimH lectin domain (FimH-L) has been reported as 1.7 nM.^[58] In the case of the full-length FimH (FimH·DsG), the K_D was determined by mixing a serial dilution of FimH from 1 nM to 5 μ M with a constant concentration of **15**, which was fixed at either 5, 10 or 20 nM. All solutions were dialyzed against or prepared in a buffer containing 20 mM HEPES (pH 7.4), 150 mM NaCl and 50 μ g/mL BSA. The mixture was incubated at rt for at least 1 h in black, flat bottom, NBS-treated 96-well microtiter plates (Corning, USA) and in a final volume of 100 μ L per well. The K_D was determined by monitoring the binding of **15** to full-length FimH and measuring the associated increase in FP using a Synergy H1 Hybrid microplate reader (BioTek, USA). FP was measured at 528 nm through polarizing filters that were oriented parallel and perpendicular to the incident polarizing light at 485 nm. The resulting binding isotherm was fitted to a single-site binding model, which accounts for ligand depletion^[83] to determine the K_D .

K_D determination of FimH antagonists. The fluorescently labeled ligand **15**^[58] was used for the competitive fluorescence polarization assay. In these competition assays, a serial dilution of competitor was titrated into fixed concentrations of FimH protein and **15**. For the determination of competitor K_{DS} to FimH-L, equimolar concentrations of protein and **15** were used (50 nM). By comparison, 10 nM **15** and 300 nM FimH were used in competition assays with FimH·DsG. FP was measured as described above and incubation times were varied for either FimH protein. The mixture with the labeled FimH antagonist and the unlabeled competing antagonist was incubated for at least 24 h with the isolated lectin domain, while with full-length FimH the incubation period could be reduced to a minimum of 1 h. These time periods were determined empirically to be necessary for the reaction to equilibrate and are inherently tied to diverging binding kinetics of these FimH proteins. Data were fit to an equilibrium competition function^[71] and analyzed with Prism (GraphPad Software, USA).

Physicochemical and *in vitro* Pharmacokinetic Studies

Materials. DMSO, 1-propanol and 1-octanol were purchased from Sigma-Aldrich. PAMPA System Solution, GIT-0 Lipid Solution, and Acceptor Sink Buffer were ordered from pIon (Woburn, MA, USA). Acetonitrile (MeCN) was purchased from Acros Organics (Geel, Belgium).

log $D_{7.4}$ determination. The *in silico* prediction tool ALOGPS^[84] was used to estimate the log P values of the compounds. Depending on these values, the compounds were classified into three categories: hydrophilic compounds (log P below zero), moderately lipophilic compounds (log P between zero and one) and lipophilic compounds (log P above one). For each category, two different ratios (volume of 1-octanol to volume of buffer) were defined as experimental parameters (Table 2).

Table 2. Compound classification based on estimated log P values.

Compound type	log P	ratio (1-octanol / buffer)
hydrophilic	< 0	30:140, 40:130
moderately lipophilic	0 - 1	70:110, 110:70
lipophilic	> 1	3:180, 4:180

Equal amounts of phosphate buffer (0.1 M, pH 7.4) and 1-octanol were mixed and shaken vigorously for 5 min to saturate the phases. The mixture was left until separation of the two phases occurred, and the buffer was retrieved. Stock solutions of the test compounds were diluted with buffer to a concentration of 1 μ M. For each compound, six determinations, *i.e.* three determinations per 1-octanol:buffer ratio, were performed in different wells of a 96-well plate. The respective volumes of buffer containing analyte (1 μ M) were pipetted to the wells and covered by saturated 1-octanol according to the chosen volume ratio. The plate was sealed with aluminum foil, shaken (1350 rpm, 25 °C, 2 h) on a Heidolph Titramax 1000 plate-shaker (Heidolph Instruments GmbH & Co. KG, Schwabach, Germany) and centrifuged (2000 rpm, 25 °C, 5 min, 5804 R Eppendorf centrifuge, Hamburg, Germany). The aqueous phase was transferred to a 96-well plate for analysis by LC-MS. The log $D_{7.4}$ was calculated from the 1-octanol:buffer ratio (o/b), the initial concentration of the analyte in buffer (1 μ M), and the concentration of the analyte in buffer (c_B) with equation (2):

$$\log D_{7.4} = \log \left(\frac{1\mu M - c_B}{c_B} \times \frac{1}{o:b} \right) \quad (2)$$

LC-MS measurements. Analyses were performed using an 1100/1200 Series HPLC System coupled to a 6410 Triple Quadrupole mass detector (Agilent Technologies, Inc., Santa Clara, CA, USA) equipped with electrospray ionization. The system was controlled with the Agilent MassHunter Workstation Data Acquisition software (version B.01.04). The column used was an Atlantis® T3 C18 column (2.1 x 50 mm) with a 3 μ m particle size (Waters Corp., Milford, MA, USA). The mobile phase consisted of two eluents: eluent A (H₂O, containing 0.1% formic acid, v/v) and eluent B

(acetonitrile, containing 0.1% formic acid, v/v), both delivered at 0.6 mL/min. The gradient was ramped from 95% A/5% B to 5% A/95% B over 1 min, and then hold at 5% A/95% B for 0.1 min. The system was then brought back to 95% A/5% B, resulting in a total duration of 4 min. MS parameters such as fragmentor voltage, collision energy, polarity were optimized individually for each analyte, and the molecular ion was followed for each compound in the multiple reaction monitoring mode. The concentrations of the analytes were quantified by the Agilent Mass Hunter Quantitative Analysis software (version B.01.04).

Solubility. Solubility was determined in a 96-well format using the μ SOL Explorer solubility analyzer (pIon, version 3.4.0.5). Measurements were performed at pH 7.4 in triplicates. Three wells of a deep well plate were filled with 300 μ L of aqueous universal buffer solution. Aliquots (3 μ L) of compound stock solution (100 mM in DMSO) were added and thoroughly mixed. The final sample concentration was 1 mM, the residual DMSO concentration was 1.0% (v/v) in the buffer solutions. After 15 h, the solutions were filtrated (0.2 μ m 96-well filter plates) using a vacuum to collect manifold (Whatman Ltd., Maidstone, UK) to remove any precipitates. Equal amounts of filtrate and 1-propanol were mixed and transferred to a 96-well plate for UV detection (190 to 500 nm, SpectraMax 190, Molecular Devices, Sunnyvale, CA, USA). The amount of material dissolved was calculated by comparison with UV spectra obtained from reference samples, which were prepared by dissolving compound stock solution in a 1:1 mixture of buffer and 1-propanol (final concentrations 0.167 mM).

Parallel Artificial Membrane Permeation Assay (PAMPA). Values of $\log P_e$ were determined in a 96-well format with the PAMPA^[74] permeation assay. Measurements were performed at pH 7.4 in quadruplicates. Four wells of a deep well plate were filled with 650 μ L System Solution. Samples (150 μ L) were withdrawn from each well to determine the blank spectra by UV-spectroscopy (SpectraMax 190). Then, analyte dissolved in DMSO was added to the remaining System Solution to yield 50 μ M solutions. To exclude precipitation, the optical density was measured at 650 nm, with 0.01 being the threshold value. Solutions exceeding this threshold were filtrated. Afterwards, samples (150 μ L) were withdrawn to determine the reference spectra. Further 200 μ L were transferred to each well of the donor plate of the PAMPA sandwich (pIon, P/N 110 163). The filter membranes at the bottom of the acceptor plate were infused with 5 μ L of GIT-0 Lipid Solution, and 200 μ L of Acceptor Sink Buffer were filled into each acceptor well. The sandwich was assembled, placed in the GutBoxTM, and left undisturbed for 16 h. Then, it was disassembled and samples (150 μ L) were transferred from each donor and acceptor well to UV-plates. Quantification was performed by UV spectroscopy. The $\log P_e$ -values were calculated with the aid of the PAMPA Explorer Software (pIon, version 3.5).

Acknowledgements

The authors gratefully acknowledge the financial support by the Swiss National Science Foundation (grant no. 200020_129935).

References

- [1] Foxman, B.; Barlow, R.; D'Arcy, H.; Gillespie, B.; Sobel, J. D. Urinary tract infection: Self-reported incidence and associated costs. *Ann. Epidemiol.* **2000**, *10*, 509-515.
- [2] Foxman, B. Epidemiology of urinary tract infections: incidence, morbidity, and economic costs. *Am. J. Med.* **2002**, *113 Suppl. 1A*, 5S-13S.
- [3] Ronald, A. The etiology of urinary tract infection: traditional and emerging pathogens. *Am. J. Med.* **2002**, *113 Suppl. 1A*, 14S-19S.
- [4] Wiles, T. J.; Kulesus, R. R.; Mulvey, M. A. Origins and virulence mechanisms of uropathogenic *Escherichia coli*. *Exp. Mol. Pathol.* **2008**, *85*, 11-19.
- [5] Fihn, S. D. Acute uncomplicated urinary tract infection in women. *N. Engl. J. Med.* **2003**, *349*, 259-266.
- [6] Hooton, T. M.; Besser, R.; Foxman, B.; Fritsche, T. R.; Nicolle, L. E. Acute uncomplicated cystitis in an era of increasing antibiotic resistance: a proposed approach to empirical therapy. *Clin. Infect. Dis.* **2004**, *39*, 75-80.
- [7] Sanchez, G. V.; Master, R. N.; Karlowsky, J. A.; Bordon, J. M. In vitro antimicrobial resistance of urinary *Escherichia coli* isolates among U. S. outpatients from 2000 to 2010. *Antimicrob. Agents Chemother.* **2012**, *56*, 2181-2183.
- [8] Schito, G. C.; Naber, K. G.; Botto, H.; Palou, J.; Mazzei, T.; Gualco, L.; Marchese, A. The ARESC study: an international survey on the antimicrobial resistance of pathogens involved in uncomplicated urinary tract infections. *Int. J. Antimicrob. Agents* **2009**, *34*, 407-413.
- [9] Zhanel, G. G.; Hisanaga, T. L.; Laing, N. M.; DeCorby, M. R.; Nichol, K. A.; Weshnoweski, B.; Johnson, J.; Noreddin, A.; Low, D. E.; Karlowsky, J. A.; Group, N.; Hoban, D. J. Antibiotic resistance in *Escherichia coli* outpatient urinary isolates: final results from the North American Urinary Tract Infection Collaborative Alliance (NAUTICA). *Int. J. Antimicrob. Agents* **2006**, *27*, 468-475.
- [10] Clatworthy, A. E.; Pierson, E.; Hung, D. T. Targeting virulence: a new paradigm for antimicrobial therapy. *Nature Chem. Biol.* **2007**, *3*, 541-548.
- [11] Mulvey, M. A.; Schilling, J. D.; Martinez, J. J.; Hultgren, S. J. Bad bugs and beleaguered bladders: interplay between uropathogenic *Escherichia coli* and innate host defenses. *Proc. Natl. Acad. Sci. USA* **2000**, *97*, 8829-8835.
- [12] Schilling, J. D.; Mulvey, M. A.; Hultgren, S. J. Structure and function of *Escherichia coli* type 1 pili: new insight into the pathogenesis of urinary tract infections. *J. Infect. Dis.* **2001**, *183 Suppl. 1*, S36-40.
- [13] Jones, C. H.; Pinkner, J. S.; Roth, R.; Heuser, J.; Nicholes, A. V.; Abraham, S. N.; Hultgren, S. J. FimH adhesin of type 1 pili is assembled into a fibrillar tip structure in the Enterobacteriaceae. *Proc. Natl. Acad. Sci. USA* **1995**, *92*, 2081-2085.
- [14] Hahn, E.; Wild, P.; Hermanns, U.; Sebbel, P.; Glockshuber, R.; Haner, M.; Taschner, N.; Burkhard, P.; Aebi U.; Muller, S. A. Exploring the 3D molecular architecture of *Escherichia coli* type 1 pili. *J. Mol. Biol.* **2002**, *323*, 845-857.
- [15] Sokurenko, E. V.; Chesnokova, V.; Doyle, R. J.; Hasty, D. L. Diversity of the *Escherichia coli* Type 1 Fimbrial Lectin. *J. Biol. Chem.* **1997**, *272*, 17880-17886.
- [16] Sharon, N. Bacterial lectins, cell-cell recognition and infectious disease. *FEBS Lett.* **1987**, *217*, 145-157.

- [17] Capitani, G.; Eidam, O.; Glockshuber, R.; Grütter, M. G. Structural and functional insights into the assembly of type 1 pili from *Escherichia coli*. *Microbes Infect.* **2006**, *8*, 2284-2290.
- [18] Ofek, I.; Hasty, D. L.; Sharon, N. Anti-adhesion therapy of bacterial diseases: prospects and problems. *FEMS Immunol. Med. Microbiol.* **2003**, *38*, 181-191.
- [19] Sharon, N. Carbohydrates as future anti-adhesion drugs for infectious diseases. *Biochim. Biophys. Acta.* **2006**, *1760*, 527-537.
- [20] Zhou, G.; Mo, W. J.; Sebbel, P.; Min, G.; Neubert, T. A.; Glockshuber, R.; Wu, X. R.; Sun, T. T.; Kong, X. P. Uroplakin Ia is the urothelial receptor for uropathogenic *Escherichia coli*: evidence from in vitro FimH binding. *J. Cell Sci.* **2001**, *114*, 4095-4103.
- [21] Pieters, R. J. Intervention with bacterial adhesion by multivalent carbohydrates. *Med. Res. Rev.* **2007**, *27*, 796-816.
- [22] Le Trong, I.; Aprikian, P.; Kidd, B. A.; Forero-Shelton, M.; Tchesnokova, V.; Rajagopal, P.; Rodriguez, V.; Interlandi, G.; Klevit, R.; Vogel, V.; Stenkamp, R. E.; Sokurenko, E. V.; Thomas, W. E. Structural basis for mechanical force regulation of the adhesin FimH via finger trap-like β sheet twisting. *Cell* **2010**, *141*, 645-655.
- [23] Waksman, G.; Hultgren, S. J. Structural biology of the chaperone-usher pathway of pilus biogenesis. *Nat. Rev. Microbiol.* **2009**, *7*, 765-774.
- [24] Bouckaert, J.; Berglund, J.; Schembri, M.; De Genst, E.; Cools, L.; Wuhler, M.; Hung, C.-S.; Pinkner, J.; Slättegård, R.; Zavialov, A.; Choudhury, D.; Langermann, S.; Hultgren, S. J.; Wyns, L.; Klemm, P.; Oscarson, S.; Knight, S. D.; De Greve, H. Receptor binding studies disclose a novel class of high-affinity inhibitors of the *Escherichia coli* FimH adhesin. *Mol. Microbiol.* **2005**, *55*, 441-455.
- [25] Han, Z.; Pinkner, J. S.; Ford, B.; Obermann, R.; Nolan, W.; Wildman, S. A.; Hobbs, D.; Ellenberger, T.; Cusumano, C. K.; Hultgren, S. J.; Janetka, J. W. Structure-based drug design and optimization of mannoside bacterial FimH antagonists. *J. Med. Chem.* **2010**, *53*, 4779-4792.
- [26] Brument, S.; Sivignon, A.; Dumych, T. I.; Moreau, N.; Roos, G.; Guérardel, Y.; Chalopin, T.; Deniaud, D.; Bilyy, R. O.; Darfeuille-Michaud, A.; Bouckaert, J.; Gouin, S. G. Thiazolylaminomannosides as potent antiadhesives of type 1 piliated *Escherichia coli* isolated from Crohn's disease patients. *J. Med. Chem.* **2013**, *56*, 5395-5406.
- [27] Wellens, A.; Garofalo, C.; Nguyen, H.; Van Gerven, N.; Slättegård, R.; Henalsteens, J.-P.; Wyns, L.; Oscarson, S.; De Greve, H.; Hultgren, S. J.; Bouckaert, J. Intervening with urinary tract infections using anti-adhesives based on the crystal structure of the FimH-oligomannose-3 complex. *PLoS One* **2008**, *3*, e2040.
- [28] Wellens, A.; Lahmann, M.; Touaibia, M.; Vaucher, J.; Oscarson, S.; Roy, R.; Remaut, H.; Bouckaert, J. The tyrosine gate as a potential entropic lever in the receptor-binding site of the bacterial adhesin FimH. *Biochemistry* **2012**, *51*, 4790-4799.
- [29] Vanwetswinkel, S.; Volkov, A. N.; Sterckx, Y. G.; Garcia-Pino, A.; Buts, L.; Vranken, W. F.; Bouckaert, J.; Roy, R.; Wyns, L.; van Nuland, N. A. Study of the structural and dynamic effects in the FimH adhesin upon alpha-D-heptyl mannose binding. *J. Med. Chem.* **2014**, *57*, 1416-1427.
- [30] Choudhury, D.; Thompson, A.; Stojanoff, V.; Langermann, S.; Pinkner, J.; Hultgren, S. J.; Knight, S. D. X-ray structure of the FimC-FimH chaperone-adhesin complex from uropathogenic *Escherichia coli*. *Science* **1999**, *285*, 1061-1066.
- [31] Buckley, C. D.; Tan, J.; Anderson, K. L.; Hanein, D.; Volkmann, N.; Weis, W. I.; Nelson, W. J.; Dunn, A. R. Cell adhesion. The minimal cadherin-catenin complex binds to actin filaments under force. *Science* **2014**, *346*, 1254211.
- [32] Evans, E.; Leung, A.; Heinrich, V.; Zhu, C. Mechanical switching and coupling between two dissociation pathways in a P-selectin adhesion bond. *Proc. Natl. Acad. Sci. U S A* **2004**, *101*, 11281-11286.
- [33] Guo, B.; Guilford, W. H. Mechanics of actomyosin bonds in different nucleotide states are

- tuned to muscle contraction. *Proc. Natl. Acad. Sci. U S A* **2006**, *103*, 9844-9849.
- [34] Liu, B.; Chen, W.; Evavold, B. D.; Zhu, C. Accumulation of dynamic catch bonds between TCR and agonist peptide-MHC triggers T cell signaling. *Cell* **2014**, *157*, 357-368.
- [35] Marshall, B. T.; Long, M.; Piper, J. W.; Yago, T.; McEver, R. P.; Zhu, C. Direct observation of catch bonds involving cell-adhesion molecules. *Nature* **2003**, *423*, 190-193.
- [36] Hung, C.-S.; Bouckaert, J.; Hung, D.; Pinkner, J.; Widberg, C.; DeFusco, A.; Auguste, C. G.; Strouse, R.; Langermann, S.; Waksman, G.; Hultgren, S. J. Structural basis of tropism of *Escherichia coli* to the bladder drug in urinary tract infection. *Mol. Microbiol.* **2002**, *44*, 903-915.
- [37] Schwartz, D. J.; Kalas, V.; Pinkner, J. S.; Chen, S. L.; Spaulding, C. N.; Dodson, K. W.; Hultgren, S. J. Positively selected FimH residues enhance virulence during urinary tract infection by altering FimH conformation. *Proc. Natl. Acad. Sci. U S A* **2013**, *110*, 15530-15537.
- [38] Yakovenko, O.; Sharma, S.; Forero, M.; Tchesnokova, V.; Aprikian, P.; Kidd, B.; Mach, A.; Vogel, V.; Sokurenko, E.; Thomas, W. E. FimH forms catch bonds that are enhanced by mechanical force due to allosteric regulation. *J. Biol. Chem.* **2008**, *283*, 11596-11605.
- [39] Firon, N.; Itzhak, O.; Sharon, N. Interaction of mannose-containing oligosaccharides with the fimbrial lectin of *Escherichia coli*. *Biochem. Biophys. Res. Commun.* **1982**, *105*, 1426-1432.
- [40] Firon, N.; Ofek, I.; Sharon, N. Carbohydrate specificity of the surface lectins of *Escherichia coli*, *Klebsiella pneumoniae*, and *Salmonella typhimurium*. *Carbohydr. Res.* **1983**, *120*, 235-249.
- [41] Aronson, M.; Medalia, O.; Schori, L.; Mirelman, D.; Sharon, N.; Ofek, I. Prevention of Colonization of the Urinary Tract of Mice with *Escherichia coli* by Blocking of Bacterial Adherence with Methyl α -D-Mannopyranoside. *J. Infect Dis.* **1979**, *139*, 329-332.
- [42] Firon, N.; Ashkenazi, S.; Mirelman, D.; Ofek, I.; Sharon, N. Aromatic alpha-glycosides of mannose are powerful inhibitors of the adherence of type 1 fimbriated *Escherichia coli* to yeast and intestinal epithelial cells. *Infect. Immun.* **1987**, *55*, 472-476.
- [43] Sperling, O.; Fuchs, A.; Lindhorst, T. K. Evaluation of the carbohydrate recognition domain of the bacterial adhesin FimH. Design, synthesis and binding properties of mannoside ligands. *Org. Biomol. Chem.* **2006**, *4*, 3913-3922.
- [44] Klein, T.; Abgottspon, D.; Wittwer, M.; Rabbani, S.; Herold, J.; Jiang, X.; Kleeb, S.; Lüthi, C.; Scharenberg, M.; Bezençon, J.; Gubler, E.; Pang, L.; Smiesko, M.; Cutting, B.; Schwardt, O.; Ernst, B. FimH antagonists for the oral treatment of urinary tract infections: from design and synthesis to in vitro and in vivo evaluation. *J. Med. Chem.* **2010**, *53*, 8627-8641.
- [45] Cusumano, C. K.; Pinkner, J. S.; Han, Z.; Greene, S. E.; Ford, B. A.; Crowley, J. R.; Henderson, J. P.; Janetka, J. W.; Hultgren, S. J. Treatment and prevention of urinary tract infection with orally active FimH inhibitors. *Sci. Transl. Med.* **2011**, *3*, 109ra115.
- [46] Han, Z.; Pinkner, J. S.; Ford, B.; Chorell, E.; Crowley, J. M.; Cusumano, C. K.; Campbell, S.; Henderson, J. P.; Hultgren, S. J.; Janetka, J. W. Lead optimization studies on FimH antagonists: discovery of potent and orally bioavailable *ortho*-substituted biphenyl mannosides. *J. Med. Chem.* **2012**, *55*, 3945-3959.
- [47] Pang, L.; Kleeb, S.; Lemme, K.; Rabbani, S.; Scharenberg, M.; Zalewski, A.; Schädler, F.; Schwardt, O.; Ernst, B. FimH antagonists: structure-activity and structure-property relationships for biphenyl α -D-mannopyranosides. *ChemMedChem.* **2012**, *7*, 1404-1422.
- [48] Jiang, X.; Abgottspon, D.; Kleeb, S.; Rabbani, S.; Scharenberg, M.; Wittwer, M.; Haug, M.; Schwardt, O.; Ernst, B. Anti-adhesion therapy for urinary tract infections – a balanced PK/PD profile proved to be key for success. *J. Med. Chem.* **2012**, *55*, 4700-4713.
- [49] Schwardt, O.; Rabbani, S.; Hartmann, M.; Abgottspon, D.; Wittwer, M.; Kleeb, S.; Zalewski, A.; Smiesko, M.; Cutting, B.; Ernst, B. Design, synthesis and biological evaluation of mannosyl triazoles as FimH antagonists. *Bioorg. Med. Chem.* **2011**, *19*, 6454-6473.

- [50] Lindhorst, T. K.; Kieburg, C.; Krallmann-Wenzel, U. Inhibition of the type 1 fimbriae-mediated adhesion of *Escherichia coli* to erythrocytes by multiantennary D-mannosyl clusters: The effect of multivalency. *Glycoconj. J.* **1998**, *15*, 605-613.
- [51] Nagahori, N.; Lee, R. T.; Nishimura, S.-L.; Pagé, S.; Roy, R.; Lee, Y. C. Inhibition of adhesion of type 1 fimbriated *Escherichia coli* to highly mannosylated ligands. *ChemBioChem* **2002**, *3*, 836-844.
- [52] Appeldoorn, C. C. M.; Joosten, J. A. F.; Maate, F. A.; Dobrindt, U.; Hacker, J.; Liskamp, R. M. J.; Khan, A. S.; Pieters, R. J. Novel multivalent mannose compounds and their inhibition of the adhesion of type 1 fimbriated uropathogenic *E. coli*. *Tetrahedron Asym.* **2005**, *16*, 361-372.
- [53] Patel, A.; Lindhorst, T. K. A modular approach for the synthesis of oligosaccharide mimetics. *Carbohydr. Res.* **2006**, *341*, 1657-1668.
- [54] Touaibia, M.; Wellens, A.; Shiao, T. C.; Wang, Q.; Sirois, S.; Bouckaert, J.; Roy, R. Mannosylated G(0) dendrimers with nanomolar affinities to *Escherichia coli* FimH. *ChemMedChem* **2007**, *2*, 1190-1201.
- [55] Durka, M.; Buffet, K.; Iehl, J.; Holler, M.; Nierengarten, J.-F.; Taganna, J.; Bouckaert, J.; Vincent, S. P. The functional valency of dodecamannosylated fullerenes with *Escherichia coli* FimH - towards novel bacterial antiadhesives. *Chem. Commun.* **2011**, *47*, 1321-1323.
- [56] Bouckaert, J.; Li, Z.; Xavier, C.; Almant, M.; Caveliers, V.; Lahoutte, T.; Weeks, S. D.; Kovensky, J.; Gouin, S. G. Heptyl α -D-mannosides grafted on a β -cyclodextrin core to interfere with *Escherichia coli* adhesion: An *in vivo* multivalent effect. *Chem. Eur. J.* **2013**, *19*, 7847-7855.
- [57] Scharenberg, M.; Schwardt, O.; Rabbani, S.; Ernst, B. Target selectivity of FimH antagonists. *J. Med. Chem.* **2012**, *55*, 9810-9816.
- [58] Kleeb, S.; Pang, L.; Mayer, K.; Eris, D.; Sigl, A.; Preston, R. C.; Zihlmann, P.; Sharpe, T.; Jakob, R. P.; Abgottspon, D.; Hutter, A. S.; Scharenberg, M.; Jiang, X.; Navarra, G.; Rabbani, S.; Smiesko, M.; Lüdin, N.; Bezençon, J.; Schwardt, O.; Maier, T.; Ernst, B. FimH antagonists: bioisosteres to improve the *in vitro* and *in vivo* PK/PD profile. *J. Med. Chem.* **2015**, *58*, 2221-2239.
- [59] Totsika, M.; Kostakioti, M.; Hannan, T. J.; Upton, M.; Beatson, S. A.; Janetka, J. W.; Hultgren, S. J.; Schembri, M. A. A FimH inhibitor prevents acute bladder infection and treats chronic cystitis caused by multidrug-resistant uropathogenic *Escherichia coli* ST131. *J. Infect. Dis.* **2013**, *208*, 921-928.
- [60] Chen, S. L.; Hung, C.-S.; Xu, J.; Reigstad, C. S.; Magrini, V.; Sabo, A.; Blasiar, D.; Bieri, T.; Meyer, R. R.; Ozersky, P.; Armstrong, J. R.; Fulton, R. S.; Latreille, J. P.; Spieth, J.; Hooton, T. M.; Mardis, E. R.; Hultgren, S. J.; Gordon, J. I. Identification of genes subject to positive selection in uropathogenic strains of *Escherichia coli*: A comparative genomics approach. *Proc. Natl. Acad. Sci. U S A* **2006**, *103*, 5977-5982.
- [61] Mobley, H. L. T.; Green, D. M.; Trifillis, A. L.; Johnson, D. E.; Chippendale, G. R.; Lockatell, C. V.; Jones, B. D.; Warren, J. W. Pyelonephritogenic *E. coli* and killing of cultured human renal proximal tubular epithelial cells: Role of alpha hemolysin in some strains. *Infect. Immun.* **1990**, *58*, 1281-1289.
- [62] Hull, R.A.; Gill, R. E.; Hsu, P.; Minshew, B. H.; Falkow, S. Construction and expression of recombinant plasmids encoding type 1 or D-mannose-resistant pili from a urinary tract infection *Escherichia coli* isolate. *Infect. Immun.* **1981**, *33*, 933-938.
- [63] Topliss, J. G. Utilization of operational schemes for analog synthesis in drug design. *J. Med. Chem.* **1972**, *15*, 1006-1011.
- [64] Topliss, J. G. A manual method for applying the Hansch approach to drug design. *J. Med. Chem.* **1977**, *20*, 463-469.
- [65] Hansch, C.; Fujita, T. p - σ - π Analysis. A Method for the Correlation of Biological Activity and Chemical Structure *J. Am. Chem. Soc.* **1964**, *86*, 1616-1626.
- [66] Hansch, C. In *Drug Design*; E. J. Ariens, Ed.; Academic Press: New York, **1971**; Vol. 1, p 271.

- [67] Rabbani, S.; Jiang, X.; Schwardt, O.; Ernst, B. Expression of the carbohydrate recognition domain of FimH and development of a competitive binding assay. *Anal. Biochem.* **2010**, *407*, 188-195.
- [68] Vetsch, M.; Sebbel, P.; Glockshuber, R. Chaperone-independent folding of type 1 pilus domains. *J. Mol. Biol.* **2002**, *322*, 827-840.
- [69] Sauer, M. M.; Jakob, R. P.; Eras, J.; Baday, S.; Eriş , D.; Navarra, G.; Bernèche, S.; Ernst, B.; Maier, T.; Glockshuber R. Catch-bond mechanism of the bacterial adhesin FimH. Submitted.
- [70] Nikolovska-Coleska, Z.; Wang, R.; Fang, X.; Pan, H.; Tomita, Y.; Li, P.; Roller, P.; Krajewski, K.; Saito, N.; Stuckey, J.; Wang, S. Development and optimization of a binding assay for the XIAP BIR3 domain using fluorescence polarization. *Anal. Biochem.* **2004**, *332*, 261-273.
- [71] Wang, Z.X. An exact mathematical expression for describing competitive binding of two different ligands to a proteinmolecule. *FEBS Lett.* **1995**, *360*, 111-114.
- [72] Avdeef, A. High-througput measurements of solubility profiles. In *Pharmacokinetic Optimization in Drug Research; Biological, Physicochemical and Computational Strategies* (Eds.: Testa, B.; van de Waterbeemd, H.; Folkers, G.; Guy, R.), Verlag Helvetica Chimica Acta, Zurich, **2001**, pp 305-326.
- [73] Dearden, J. C.; Bresnen, G. M. The measurement of partition coefficients. *Quant. Struct.-Act. Rel.* **1988**, *7*, 133-144.
- [74] Kansy, M.; Senner, F.; Gubernator, K. Physicochemical high throughput screening: Parallel artificial membrane permeation assay in the description of passive absorption processes. *J. Med. Chem.* **1998**, *41*, 1007-1010.
- [75] Johnson, K. C.; Swindell, A. C. Guidance in the setting of drug particle size specifications to minimize variability in absorption. *Pharm. Res.* **1996**, *13*, 1795-1798.
- [76] Lipinski, C. A. Drug-like properties and the causes of poor solubility and poor permeability. *J. Pharmacol. Toxicol. Methods* **2000**, *44*, 235-249.
- [77] Smith, D. A.; Jones, B. C.; Walker, D. K. Design of drugs involving the concepts and theories of drug metabolism and pharmacokinetics. *Med. Res. Rev.* **1996**, *16*, 243-266.
- [78] Van de Waterbeemd, H.; Smith, D. A.; Beaumont, K.; Walker, D. K. Property-based design: optimization of drug absorption and pharmacokinetics. *J. Med. Chem.* **2001**, *44*, 1313-1333.
- [79] Varma, M. V. S.; Feng, B.; Obach, R. S.; Troutman, M. D.; Chupka, J.; Miller, H. R.; El-Kattan, A. Physicochemical determinants of human renal clearance. *J. Med. Chem.* **2009**, *52*, 4844-4852.
- [80] Ernst, B.; Herold, J. Mannose Derivatives as Antagonists of Bacterial Adhesion, EP2010/069436 (University of Basel), WO2011073112 A3, **2011**.
- [81] Meerman, H. J.; Georgiou, G. Construction and characterization of a set of *E. coli* strains deficient in all known loci affecting the proteolytic stability of secreted recombinant proteins. *Nature Biotech.* **1994**, *12*, 1107-1110.
- [82] Vetsch, M.; Puorger, C.; Spirig, T.; Grauschkopf, U.; Weber-Ban, E. U.; Glockshuber, R. Pilus chaperones represent a new type of protein-folding catalyst. *Nature* **2004**, *431*, 329-333.
- [83] Cooper, A. *Biophysical Chemistry*, 2nd ed., RSC Publishing: Cambridge, U.K. **2011**, p 122-123.
- [84] (a) VCCLAB, Virtual Computational Chemistry Laboratory, **2005**, www.vcclab.org (accessed September 13, 2012); (b) Tetko, I. V.; Gasteiger, J.; Todeschini, R.; Mauri, A.; Livingstone, D.; Ertl, P.; Palyulin V. A.; Radchenko, E. V.; Zefirov, N. S.; Makarenko, A. S.; Tanchuk, V. Y.; Prokopenko, V. V. Virtual computational chemistry laboratory – design and description. *J. Comput. Aided Mol. Des.* **2005**, *19*, 453-463.

2.7 **Paper 6: FimH antagonists: bioisosteres to improve the *in vitro* and *in vivo* PK/PD profile**

The following paper explores various bioisosteres of the *para*-carboxylate moiety on the terminal ring of the biphenyl mannoside. For assessing the binding affinity of the antagonists to the FimH-CRD, a competitive fluorescence polarization assay and isothermal titration calorimetry were implemented. Moreover, the binding poses of two bioisosteres were determined by X-ray crystallography. The assessment of the key physicochemical properties predictive for oral bioavailability and antagonist elimination as well as *in vivo* studies in a mouse model complete this thorough characterization.

Contribution to the project:

Simon Kleeb performed all assays regarding the physicochemical and *in vitro* pharmacokinetic characterization of the bioisosteres. He furthermore interpreted the resulting data and was responsible for the writing of the respective section as well as the introduction part. He furthermore contributed to the writing of the entire manuscript.

This paper was published in the *Journal of Medicinal Chemistry*:

Kleeb, S. *; Pang, L. *; Mayer, K. *; Eris, D. *; Sigl, A. *; Preston, R. C.; Zihlmann, P.; Sharpe, T.; Jakob, R. P.; Abgottspon, D.; Hutter, A. S.; Scharenberg, M.; Jiang, X.; Navarra, G.; Rabbani, S.; Smiesko, M.; Lüdin, N.; Bezençon, J.; Schwaradt, O., Maier, T.; Ernst, B. FimH antagonists: bioisosteres to improve the *in vitro* and *in vivo* PK/PD profile. *J. Med. Chem.* **2015**, *58*, 2221-2239.

* These authors contributed equally to the project.

© 2015 American Chemical Society

FimH Antagonists: Bioisosteres To Improve the in Vitro and in Vivo PK/PD Profile

Simon Kleeb,^{†,||} Lijuan Pang,^{†,||} Katharina Mayer,^{†,||} Deniz Eris,^{†,||} Anja Sigl,^{†,||} Roland C. Preston,[†] Pascal Zihlmann,[†] Timothy Sharpe,[§] Roman P. Jakob,[‡] Daniela Abgottspon,[†] Aline S. Hutter,[†] Meike Scharenberg,[†] Xiaohua Jiang,[†] Giulio Navarra,[†] Said Rabbani,[†] Martin Smiesko,[†] Nathalie Lüdin,[†] Jacqueline Bezençon,[†] Oliver Schwardt,[†] Timm Maier,[‡] and Beat Ernst^{*,†}

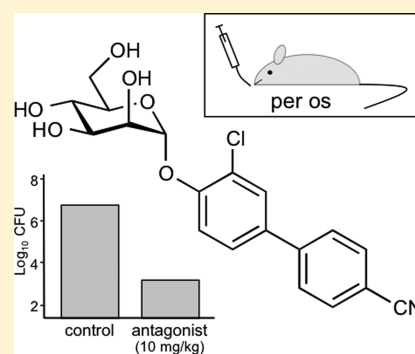
[†]Institute of Molecular Pharmacy, Pharmcenter, University of Basel, Klingelbergstrasse 50, CH-4056 Basel, Switzerland

[‡]Structural Biology, Biocenter, University of Basel, Klingelbergstrasse 70, CH-4056 Basel, Switzerland

[§]Biophysical Facility, Biocenter, University of Basel, Klingelbergstrasse 70, CH-4056 Basel, Switzerland

S Supporting Information

ABSTRACT: Urinary tract infections (UTIs), predominantly caused by uropathogenic *Escherichia coli* (UPEC), belong to the most prevalent infectious diseases worldwide. The attachment of UPEC to host cells is mediated by FimH, a mannose-binding adhesin at the tip of bacterial type 1 pili. To date, UTIs are mainly treated with antibiotics, leading to the ubiquitous problem of increasing resistance against most of the currently available antimicrobials. Therefore, new treatment strategies are urgently needed. Here, we describe the development of an orally available FimH antagonist. Starting from the carboxylate substituted biphenyl α -D-mannoside **9**, affinity and the relevant pharmacokinetic parameters (solubility, permeability, renal excretion) were substantially improved by a bioisosteric approach. With 3'-chloro-4'-(α -D-mannopyranosyloxy)biphenyl-4-carbonitrile (**10j**) a FimH antagonist with an optimal in vitro PK/PD profile was identified. Orally applied, **10j** was effective in a mouse model of UTI by reducing the bacterial load in the bladder by about 1000-fold.



INTRODUCTION

Urinary tract infection (UTI) is one of the most frequent infectious diseases worldwide and affects millions of people every year.¹ In more than 70% of the reported cases, uropathogenic *Escherichia coli* (UPEC) is the causal pathogen.² Acute, uncomplicated lower urinary tract infection, commonly referred to as cystitis, requires an antibiotic treatment for symptom relief (i.e., reduction of dysuria, frequent and urgent urination, bacteriuria, pyuria) and for prevention of more devastating or even life threatening complications like pyelonephritis and urosepsis.^{3,4} However, the repeated use of antibacterial chemotherapeutics provokes antimicrobial resistance leading to treatment failure.⁵ Hence, a new approach for the prevention and treatment of UTI with orally applicable therapeutics is urgently needed.⁶

UPEC undergo a well-defined infection cycle within the host.⁷ The key step in pathogenesis is bacterial adhesion to the epithelial cells in the lower urinary tract.⁸ This interaction prevents UPEC from clearance by the bulk flow of urine and enables the bacteria to colonize the epithelial cells. The adhesion is mediated by the virulence factor FimH located at the tip of bacterial type 1 pili.^{9,10} FimH consists of two immunoglobulin-like domains: the N-terminal lectin domain and (connected by a short linker) the C-terminal pilin domain.¹¹ The lectin domain encloses the carbohydrate recognition domain (CRD) that binds

to the oligomannosides of the glycoprotein uroplakin Ia on the epithelial cell surface.¹² The pilin domain anchors the adhesin to the pilus and regulates the switch between two conformational states of the CRD with high and low affinity for mannoses, respectively.

More than 3 decades ago, Sharon and co-workers described various oligomannosides and aryl α -D-mannosides as potential antagonists of the FimH-mediated bacterial adhesion.^{13,14} However, only weak interactions in the milli- to micromolar range were observed. In recent years, several high-affinity monovalent mannose-based FimH antagonists with various aglycones like *n*-alkyl,¹⁵ phenyl,¹⁶ dioxocyclobutenyl-aminophenyl,¹⁷ umbelliferyl,¹⁶ biphenyl,^{18–22} indol(in)-ylphenyl,²³ triazolyl,²⁴ and thiazolylamino²⁵ have been reported. In addition, different multivalent presentations of the mannose have been synthesized^{26–32} and a heptavalent presentation of *n*-heptyl α -D-mannoside (**1**) tethered to β -cyclodextrin proved to be highly effective when applied together with the UTI89 bacterial strain through a catheter into the bladder of C3H/HeN mice.³² Importantly, adverse side effects resulting from nonselective binding of FimH antagonists (they are all α -D-mannopyrano-

Received: October 3, 2014

Published: February 10, 2015

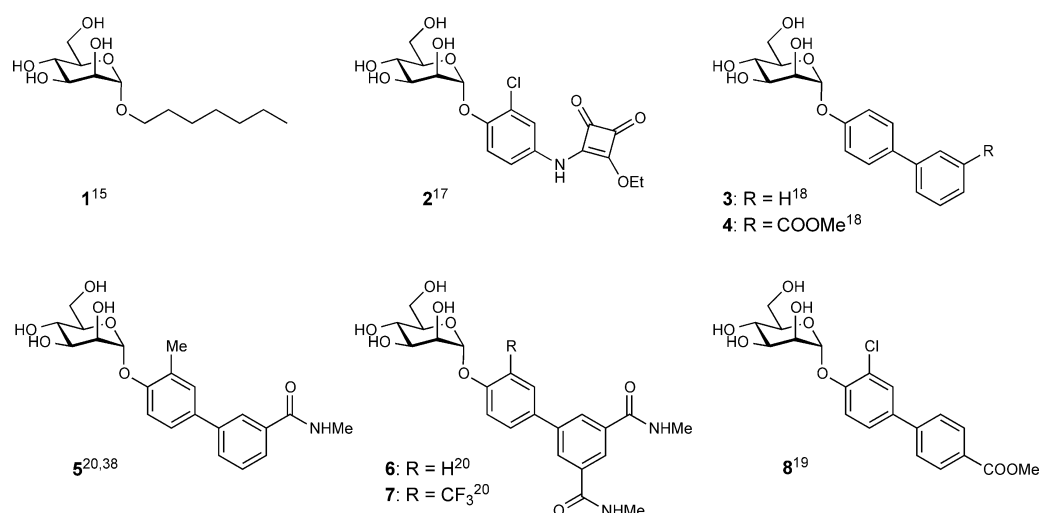


Figure 1. Monovalent FimH antagonists 1–4 acting as reference compounds and 5–8 which have been orally explored in vivo disease models.

sides) to mannose receptors of the human host system have recently been ruled out.³⁵

The high affinities of the monovalent α -D-mannopyranosides are based on optimal interactions with the main structural features of the CRD:^{34–37} first, the mannose binding pocket accommodating the mannose moiety by means of an extended hydrogen bond network and, second, the entrance to the binding site composed of three hydrophobic amino acids (Tyr48, Tyr137, and Ile52) and therefore referred to as “tyrosine gate” hosting aliphatic and aromatic aglycones. As an example, *n*-heptyl α -D-mannopyranoside (**1**) exhibits nanomolar affinity due to hydrophobic contacts of the alkyl aglycone with the hydrophobic residues of the tyrosine gate.¹⁵ Furthermore, aromatic aglycones, such as present in mannosides **2** and **3** (Figure 1), provide strong π - π stacking interactions with the tyrosine gate. This interaction is further favored by the addition of an electron withdrawing substituent on the terminal ring of the biaryl portion (\rightarrow **4**).^{18,19}

Recent in vivo PK studies in mice proved the high potential of the biphenyl α -D-mannosides **5**–**8** for an oral treatment, although high doses (≥ 50 mg/kg) were necessary to achieve the minimal concentrations required for the antiadhesive effect in the urinary bladder.^{19–21} Moreover, the therapeutic effect could only be maintained for a few hours, i.e., 4 h for a po (per os) single-dose application of **7** (50 mg/kg), because of rapid elimination by glomerular filtration and low reabsorption from the primary urine in the renal tubules.²⁰

To date, the physicochemical properties affecting the rate of renal excretion, i.e., lipophilicity and plasma protein binding (PPB), or metabolic liabilities promoting nonrenal elimination pathways have been barely investigated for FimH antagonists. The goal of the present study was to optimize the biphenyl α -D-mannoside with respect to oral bioavailability and renal excretion. Starting from antagonist **9**¹⁹ (Figure 2), we synthesized new biphenyl derivatives, characterized their affinity to the CRD, structurally investigated their binding mode, and determined physicochemical and pharmacokinetic parameters predictive for intestinal absorption and renal elimination. Furthermore, we determined in vivo PK (pharmacokinetics) of the most promising new antagonists in a mouse model. After oral administration, the compound with the best PK profile proved effective in reducing the bacterial loads upon bladder infection in a mouse model of UTI.

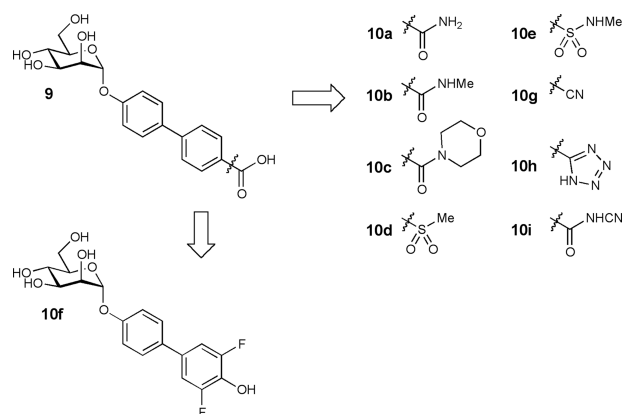


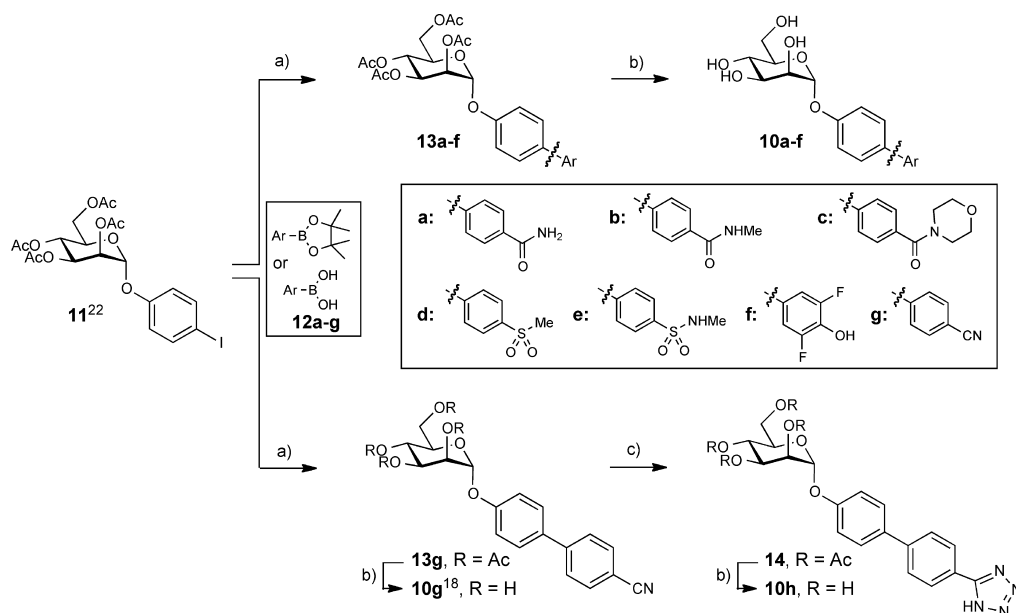
Figure 2. Bioisosteric replacement of the carboxylic acid substituent of biphenyl α -D-mannopyranoside **9**.

RESULTS AND DISCUSSION

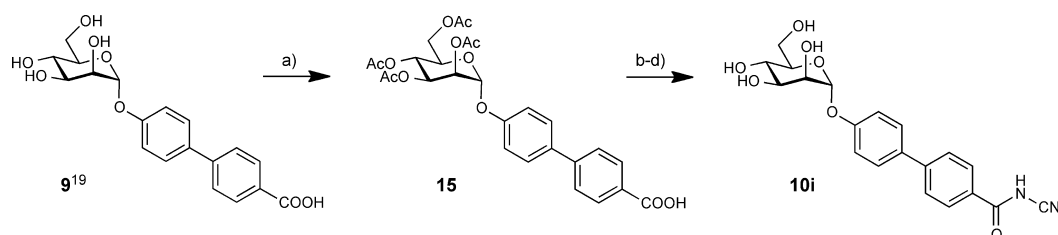
As previously reported, the carboxylate substituent present in the biphenyl mannoside **9** (its electron withdrawing potential being essential for an enhanced drug target interaction) strongly decreases the lipophilicity of the antagonist ($\log D_{7.4} < -1.5$ ¹⁹) in comparison to the *n*-heptyl (\rightarrow **1**, $\log P = 1.7$ ¹⁹) or the unsubstituted biphenyl aglycone (\rightarrow **3**, $\log P = 2.1$ ²²). Since low lipophilicity is a major reason for low intestinal absorption and rapid renal excretion of the systemically available antagonist,^{19,23} we aspired to improve oral bioavailability as well as renal excretion by replacing the carboxylate in **9** with various bioisosteric groups³⁹ (Figure 2).

Synthesis. Iodide **11** was prepared from peracetylated mannose and 4-iodophenol in the presence of $\text{BF}_3 \cdot \text{Et}_2\text{O}$.²² In a palladium-catalyzed Miyaura–Suzuki coupling⁴⁰ with the boronic acid or boronate derivatives **12a–g**, the biphenyl derivatives **13a–g** were obtained in good to excellent yields. Final deprotection yielded the test compounds **10a–g**. When microwave-assisted reaction conditions⁴¹ were utilized, the conversion of aryl nitrile **13g** to tetrazole **14** proceeded rapidly and with good yield. After deprotection of **14** using Zemplén conditions, the test compound **10h** was obtained (Scheme 1).

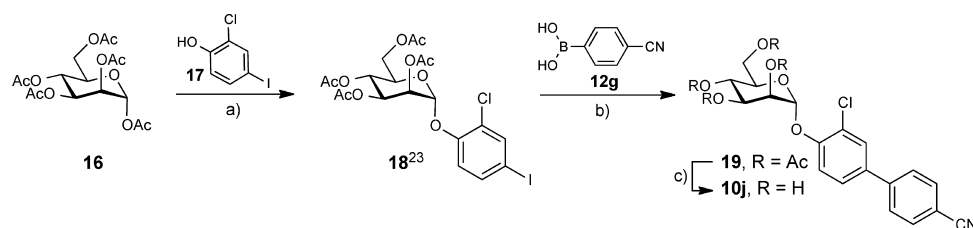
The cyanobenzamide derivative **10i** (Scheme 2) was obtained from **9** by peracetylation (\rightarrow **15**) followed by conversion of the

Scheme 1^a

^a(a) $\text{Pd}(\text{Cl}_2)\text{dppf}\cdot\text{CH}_2\text{Cl}_2$, K_3PO_4 , DMF, 80 °C, 4 h (13a–g, 44–99%); (b) NaOMe, MeOH, rt, 4 h (10a–h, 29–86%); (c) TMSN_3 , $\text{Bu}_2\text{Sn}(\text{O})$, DME, 150 °C, microwave, 10 min (81%).

Scheme 2^a

^a(a) (i) Ac_2O , DMAP, pyridine, 0 °C to rt, overnight; (ii) sat. NaHCO_3 aq, DCM, rt, 2 h (15, 53%); (b) 1-chloro-*N,N*,2-trimethyl-1-propenylamine, toluene, 0 °C to rt, 2 h; (c) NaH, NH_2CN , DMF, 0 °C to rt, overnight; (d) NaOMe, MeOH, rt, 4 h (10i, 21% for three steps).

Scheme 3^a

^a(a) $\text{BF}_3\cdot\text{Et}_2\text{O}$, CH_2Cl_2 , 40 °C (76%); (b) $\text{Pd}(\text{Cl}_2)\text{dppf}\cdot\text{CH}_2\text{Cl}_2$, K_3PO_4 , DMF, 80 °C (75%); (c) NaOMe, MeOH, rt, 4 h (48%).

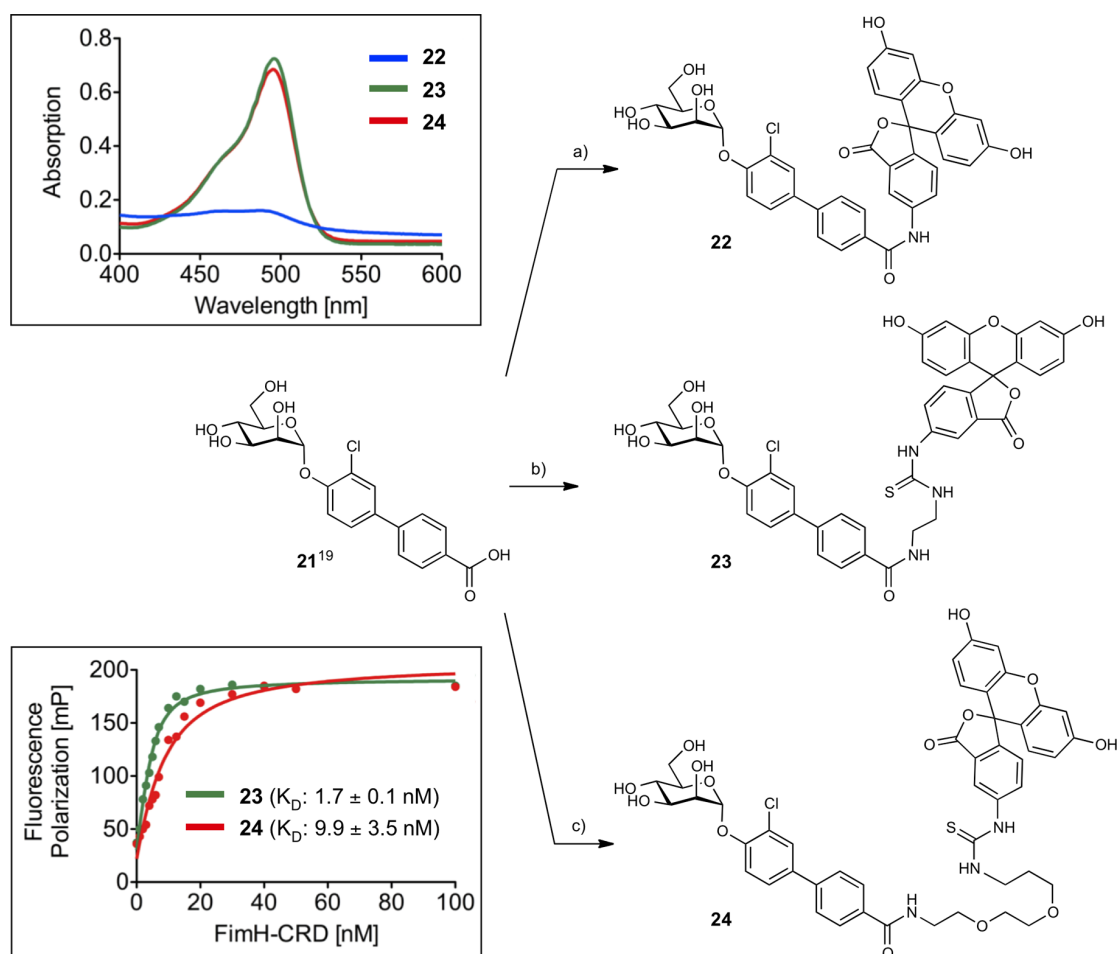
carboxylic acid into its acid chloride with 1-chloro-*N,N*,2-trimethyl-1-propenylamine.⁴² Without isolation, the acid chloride was reacted with sodium hydrogen cyanamide in DMF followed by deacetylation under Zemplén conditions to yield the test compound 10i.

Finally, to further improve the pharmacokinetic properties of mannoside 10g¹⁸ (see Table 3), a chloride substituent was introduced to the ortho-position of the aromatic ring adjacent to the anomeric oxygen. For its synthesis, peracetylated α -D-mannose (16) was coupled with 2-chloro-4-iodophenol (17) using $\text{BF}_3\cdot\text{Et}_2\text{O}$ as promoter (\rightarrow 18, 76%). After the introduction

of the second aromatic ring by Miyaura–Suzuki coupling (\rightarrow 19, 75%), deprotection yielded mannoside 10j (Scheme 3).

Binding Affinity. The binding affinity of heptyl mannoside 1, the biphenyl mannosides 3, 9, 20,¹⁸ and the bioisosteres 10a–j was determined in a competitive fluorescence polarization assay (FP assay) and with isothermal titration calorimetry (ITC). A protein construct consisting of the CRD with a C-terminal His-tag with a thrombin cleavage site (FimH-CRD-Th-His₆) was used for all experiments.⁴³

Competitive Fluorescence Polarization Assay. For the rapid evaluation of binding affinity, we established a competitive

Scheme 4^a

^a(a) 1-[(1-(Cyano-2-ethoxy-2-oxoethylideneaminoxy)dimethylaminomorpholinomethylene)]methanaminium hexafluorophosphate (COMU), NEt_3 , fluoresceinamine, DMF, rt, 7 h (**22**, 19%); b) (i) DIC, NHS, *N*-Boc-ethylenediamine, DMF, rt, 12 h; (ii) TFA, DCM, rt, 10 min (68% over two steps), (iii) fluorescein isothiocyanate (FITC), NEt_3 , DMF, rt, 3 h (**23**, 48%); c) (i) DIC, NHS, *N*-Boc-PEG2- NH_2 , DMF, rt, 14 h; (ii) TFA, DCM, rt, 30 min (62% over two steps); (iii) FITC, DMF, rt (**24**, 65%).

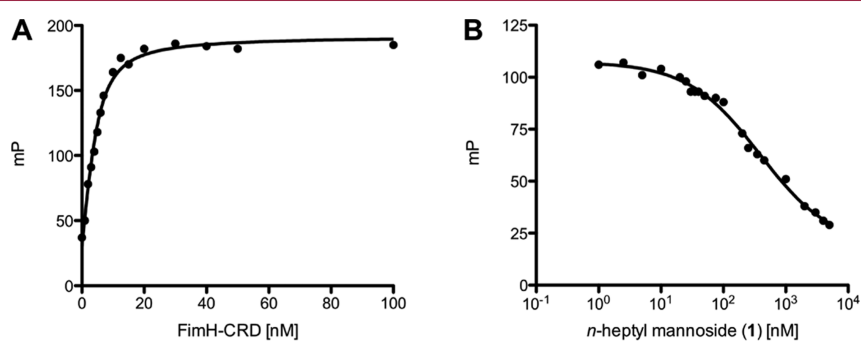


Figure 3. (A) Direct binding curve of the labeled competitor **23** obtained by adding a linear dilution of FimH-CRD (0–100 nM) and a constant concentration of competitor **23** (5 nM). The K_D was determined by fitting the experimental data to a single-site binding fit that accounts for ligand depletion. In three FP based direct binding experiments the K_D of competitor **23** was determined to be 1.7 nM. (B) Inhibition curve of *n*-heptyl mannoside (**1**) from the competitive FP assay. The IC_{50} value was determined by nonlinear least-squares fitting to a standard four-parameter equation. A modified Cheng–Prusoff equation⁴⁵ was used to calculate the corresponding K_D value ($K_D = 28.3$ nM).

binding assay based on fluorescence polarization (FP). Similar formats have been applied before for the detection of carbohydrate–lectin interactions.^{18,44} In this assay, the antagonist of interest displaces a fluorescently labeled competitor from

the binding site, thereby causing a reduction in fluorescence polarization.⁴⁵ To identify the optimal competitor, fluorescein isothiocyanate (FITC) was connected to the FimH ligand **21** by three linkers of different lengths (\rightarrow **22–24**, Scheme 4). For

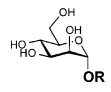
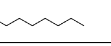
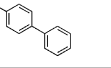
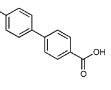
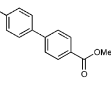
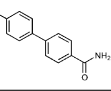
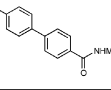
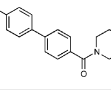
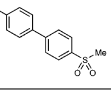
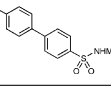
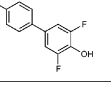
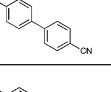
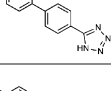
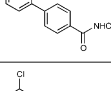
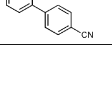
optimal sensitivity and signal-to-noise ratio, three main parameters need to be considered: (i) the affinity of the competitor should not be impaired by the fluorescent label; (ii) the conformational flexibility of the label upon binding of the competitor to the CRD should be low; (iii) the fluorescence properties of the label should not be affected by the connected ligand.^{46–48} A change in fluorescence properties was observed for reporter ligand **22** in which the label was linked to the biphenyl aglycone by an amide bond. The absorption spectrum revealed a lack of the characteristic fluorescein absorption peak at 494 nm (Scheme 4), likely due to an extension of the conjugated system to the biphenyl moiety of the ligand. The elongated saturated spacer groups in competitors **23** and **24** ensured that the expected spectral properties of the dye were retained (Scheme 4).

For the determination of their binding affinity, fixed concentrations of the reporter ligands **23** and **24** were incubated for 24 h with a linear dilution of the FimH-CRD (0–100 nM). FP was measured using a plate reader, with polarized excitation at 485 nm and emission at 528 nm measured through appropriately oriented polarizers. Fitting the single-site binding function of Cooper⁴⁹ to the observed FP data resulted for compound **23** in a dissociation constant ($K_D = 1.7$ nM, Figure 3A) similar to that of the unlabeled parent compound **21**,¹⁹ whereas **24** showed a 5-fold lower affinity (9.9 nM) (Scheme 4). Therefore, the reporter ligand **23** fulfills all characteristics as an optimal competitor and was used for the FP assay.

For the test compounds **1**, **3**, **9**, **20**, and **10a–j**, a 24 h incubation time was applied before FP was measured because of the long residence time of FimH antagonists ($t_{1/2} > 3.5$ h, Figure 3B⁵⁰). The 24 h incubation period was empirically determined to be necessary to reach equilibrium between reporter ligand and compound of interest. IC_{50} values were obtained by nonlinear least-squares regression (standard four-parameter dose–response curve) and converted to K_D values using a modified Cheng–Prusoff equation.⁴⁵ This equation accounts for the ligand depletion effect in competitive titrations involving high-affinity interaction partners present in similar concentrations. Under these conditions, the free concentration of an interacting species cannot be assumed to equal the total concentration.

The K_D values determined for the test compounds **1**, **3**, **9**, **20**, and **10a–j** are summarized in Table 1. Against our expectations, the biphenyl mannosides **3** and **9** exhibit similar affinities (Table 1), despite the presence of an electron withdrawing carboxylate substituent in antagonist **9**. According to the crystal structure of FimH cocrystallized with the sulfonamide derivative **10e** (Figure 4A), the outer aromatic ring of the biphenyl aglycone forms π – π interactions with the electron rich Tyr48, which is part of the tyrosine gate of FimH.¹⁵ A reduction of electron density of the aglycone by the electron withdrawing carboxylate was expected to enforce these π – π stacking interactions and lead to improved affinity. However, this beneficial effect might be compensated by an entropic penalty originating from the improved π – π stacking to Tyr48 that might lead to the reduced flexibility of both protein and antagonist. Furthermore, a beneficial enthalpy effect might be partially compensated by an enthalpy penalty originating from the desolvation of the charged carboxylate in **9**⁵¹ (see also Experimental Section). Although this substituent is solvent exposed, at least a partial desolvation may be necessary upon antagonist binding. To prove this assumption, we replaced the carboxylate by the corresponding methyl ester (\rightarrow **20**)¹⁸ in order to reduce the desolvation penalty and, as predicted by the Hammett constant σ_p ,⁵² to further improve the π – π stacking.

Table 1. Affinities (K_D) of FimH Antagonists to FimH-CRD-Th-His₆^b

Entry	Compd		Affinity K_D [nM]
1	1		28.3 ± 5.0
2	3		15.1 ± 2.2
3	9		17.9 ± 1.5
4	20		3.6 ± 0.9
5	10a		2.8 ± 0.3
6	10b		2.9 ± 0.5
7	10c		3.0 ± 0.1
8	10d		1.7 ± 0.2
9	10e		2.7 ± 0.4
10	10f		3.7 ± 0.2
11	10g		2.0 ± 0.6
12	10h		5.7 ± 0.1
13	10i		8.4 ± 0.3
14	10j		< 1 ^{a)}

^aThe K_D value of **10j** was approximated to be in the subnanomolar range. The IC_{50} value obtained in the competitive FP assay was equal to the lowest value that can be resolved by the assay, indicating stoichiometric titration of **10j** due to its high affinity. Consequently, its K_D must be below the K_D of competitor **23**. ^bDissociation constants (K_D) were determined in a competitive fluorescence polarization assay.

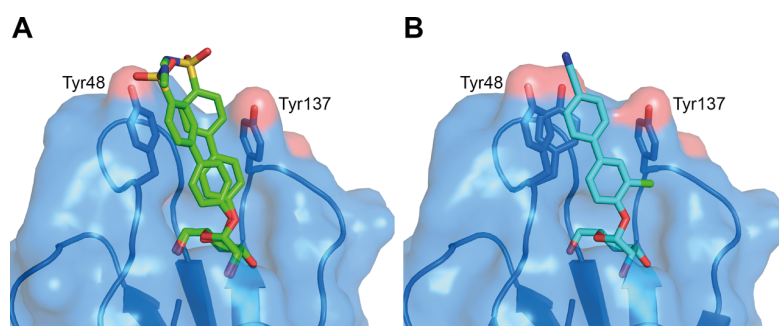


Figure 4. Ligand binding poses determined by X-ray cocrystallization with compounds **10e** resolved to 1.07 Å (A) and **10j** resolved to 1.10 Å (B). The electron density surrounding the aglycone of **10e** indicates flexibility of the aglycone and was modeled in two poses. Both compounds bind in a similar pose with a well-defined hydrogen network surrounding the mannose moiety and π - π stacking interactions between the second aromatic ring and Tyr48 side chain (A). In contrast, in the FimH-CRD/**10j** structure the amino acid side chain of Y48 can be modeled in two distinct rotamers, suggesting flexibility also of the receptor (B).

Indeed, a 6-fold improvement in affinity was achieved. However, since the methyl ester undergoes rapid enzyme-mediated hydrolysis *in vivo*,¹⁹ it will not be available at the place of action in the urinary bladder. The methyl ester was therefore replaced by metabolically stable bioisosteres³⁹ exhibiting comparable electron withdrawing properties⁵² (Table 1, entries 5–13). The most potent derivatives **10d**, **10e**, and **10g** showed affinities in the low nanomolar range.

As previously reported,²² a chloro substituent in the ortho-position of the aromatic ring adjacent to the anomeric oxygen is favorable for affinity and improves the physicochemical properties relevant for oral bioavailability. Indeed, the corresponding antagonist **10j** was the most potent compound tested in this study.

Isothermal Titration Calorimetry (ITC). To further confirm our hypothesis regarding π - π stacking and desolvation, we performed ITC experiments with the reference compound **1**, the unsubstituted biphenyl mannoside **3**, the carboxylic acid **9**, and the bioisosteres **10b–e,g,j** (Table 2). ITC allows the simultaneous determination of the stoichiometry (N), the change in enthalpy (ΔH) and the dissociation constant (K_D) for ligand–protein binding.^{53,54} The reliable determination of these three parameters requires well-defined sigmoidal titration curves characterized by the dimensionless Wiseman parameter c ($c = Mt(0) K_D^{-1}$, where $Mt(0)$ is the initial macromolecule concentration).⁵⁵ To be sure that data can be fitted with confidence, the c -value should be between 1 and 1000 (ideally between 5 and 500),⁵⁶ which could be achieved for the antagonists **3** and **9**. For titrations involving low micromolar $Mt(0)$ and interactions in the low nanomolar or picomolar range, as suggested for the bioisosteres **10b–j**, c -values above 1000 were expected. Since these conditions lead to steep titration curves that do not allow the determination of the curve slope representing $1/K_D$, we applied an alternative, competitive format referred to as displacement assay.^{57,58} First, FimH-CRD-Th-His₆ was preincubated with the low affinity antagonist *n*-heptyl 2-deoxy- α -D-mannopyranoside (**25**, for synthesis see Supporting Information). The high-affinity bioisosteres of interest were titrated into the protein–ligand complex giving well-defined sigmoidal titration curves.

The resulting K_D values (Table 2) correspond well with the data obtained from the FP assay (Table 1). A comparison of the thermodynamic fingerprints of antagonists **3** and **9** reveals that the more favorable enthalpic contribution resulting from facilitated π - π stacking leads to a net enthalpy gain ($\Delta\Delta H =$

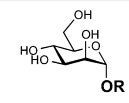
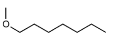
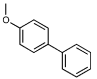
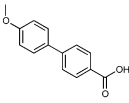
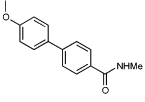
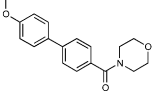
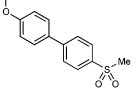
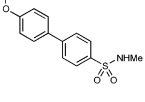
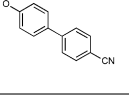
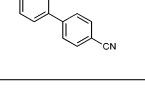
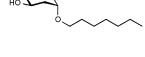
-3.7 kJ/mol). However, an even greater increase in enthalpy is likely countered by the enthalpy costs for desolvation of the electron withdrawing carboxylate.

The gain in enthalpy is in turn compensated by an unfavorable entropy ($-T\Delta\Delta S = 3.2$ kJ/mol) as a result of the reduced flexibility of both the antagonist and the Tyr48 side chain caused by the improved interaction. This is not entirely outweighed by the beneficial entropy contribution related to the partial desolvation of the carboxylate and the related release of water into the bulk. Added together, the enthalpy and entropy contributions of antagonists **3** and **9** result in similar affinities (K_D of 17.7 and 15.0 nM, respectively).

In contrast, the replacement of the carboxylate group by various neutral bioisosteres (entries 4–7) reduces the enthalpy costs for desolvation (see calculated free energies of desolvation, Experimental Section) and therefore leads to a markedly improved enthalpy ($\Delta\Delta H$ from -3.5 to -5.8 kJ/mol). As a result, an up to 5-fold improvement of the K_D values was achieved. Finally, with a cyano substituent (entries 8 and 9), the enthalpy term was further improved ($\Delta\Delta H = -3.7$ kJ/mol) because of a reduced desolvation penalty and improved π - π stacking interactions. However, this beneficial component is again partially compensated by a decrease in entropy. This can be attributed, first, to the loss of flexibility of the tightly bound ligand (Figure 4B) and, second, to the smaller surface area of the cyano substituent compared to amide, sulfonamide, and sulfone, which results in a smaller number of water molecules being released to bulk upon binding.

X-ray Crystallography. To determine the binding poses of the bioisosteres, we cocrystallized the compounds **10e** and **10j** with the FimH-CRD (Figure 4). Atomic resolution crystal structures were obtained at 1.07 Å (**10e**) and 1.10 Å (**10j**). As observed in previous mannoside cocrystal structures,^{15,18,36} the mannose moiety forms an extensive hydrogen bond network to the well-defined binding site with all of its hydroxyl groups. The biphenyl aglycone is located between the tyrosine gate residues (Tyr48/Tyr137). The π - π stacking of the second aromatic ring of the aglycone to the side chain of Tyr48 contributes most to the interaction energy of the aglycone moiety. Interactions to the Tyr137 side chain on the other hand are only limited. Whereas a previously published crystal structure of a biphenyl mannoside in complex with FimH-CRD suffers from crystal contacts of binding site residues (Tyr48 side chain to backbone oxygen of Val27) possibly causing the distortion of the binding site,¹⁸ the binding sites of our structures are mostly solvent exposed. This

Table 2. Thermodynamic Parameters from ITC for Selected FimH Antagonists Binding to FimH-CRD-Th-His₆^d

Entry	Compd		$K_D^{[a]}$ [nM]	ΔG [kJ/mol]	$\Delta H^{[a]}$ [kJ/mol]	$-T\Delta S$ [kJ/mol]	n	Type of measurement
1	1 ^[b,c]		28.9 (25.8 – 32.3)	-43.0	-50.3 (-50.2 – -50.7)	7.3	1.00	direct
2	3 ^[b]		17.7 (14.1 – 22.3)	-44.2	-45.0 (-44.5 – -45.6)	0.8	1.07	direct
3	9		15.0 (13.4 – 16.7)	-44.7	-48.7 (-48.4 – -49.0)	4.0	1.05	direct
4	10b		4.3 (3.2 – 5.6)	-47.8	-54.5 (-54.1 – -54.9)	6.7	1.02	competitive vs. 25
5	10c		5.0 (3.8 – 6.6)	-47.4	-54.5 (-54.1 – -54.8)	7.1	0.97	competitive vs. 25
6	10d		3.0 (2.1 – 4.2)	-48.7	-52.3 (-51.5 – -53.1)	3.6	0.99	competitive vs. 25
7	10e		3.5 (2.9 – 4.3)	-48.2	-52.2 (-51.6 – -52.8)	3.9	1.06	competitive vs. 25
8	10g		2.8 (2.3 – 3.3)	-48.8	-58.2 (-57.8 – -58.6)	9.4	1.00	competitive vs. 25
9	10j		1.3 (1.1 – 1.6)	-50.7	-60.9 (-60.4 – -61.4)	10.1	1.01	competitive vs. 25
10	25		9'386 (8'555 – 10'287)	-28.7	-19.5 (-19.1 – -20.0)	-9.1	1.00	direct

^a95% confidence interval from fitting in parentheses. ^bGlobal fit including two direct titration measurements. ^cITC data were previously published with an n -value of 0.82.³⁷ ^d n , stoichiometric correction factor.

revealed the flexibility of the aglycone in the FimH-CRD/**10e** structure, since the electron density toward the solvent-exposed sulfonamide indicates that there is not one single orientation. Therefore, the aglycone was modeled in two distinct poses. In contrast, in the FimH-CRD/**10j** structure the amino acid side chain of Y48 can be modeled in two distinct rotamers, suggesting flexibility also of the receptor.

Physicochemical Properties and in Vitro Pharmacokinetics. Intestinal absorption and renal excretion are prerequisites for a successful oral treatment of UTI with FimH

antagonists. Furthermore, reabsorption of antagonist from the renal ultrafiltrate is desirable for maintaining the minimal antiadhesive concentration in the target organ, namely, the bladder, over an extended period of time. To estimate the influence of the bioisostere approach on oral bioavailability and the rate of renal excretion, we determined lipophilicity by means of the octanol–water distribution coefficient ($\log D_{7.4}$),⁵⁹ aqueous solubility, and membrane permeability in the artificial membrane permeability assay (PAMPA)⁶⁰ and the colorectal adenocarcinoma (Caco-2) cell monolayer model.⁶¹

Table 3. Physicochemical and in Vitro Pharmacokinetic Parameters^h

compd	pK _a ^a	log D _{7.4} ^b	solubility [μg/mL]/pH ^c	PAMPA log P _e ^d [cm/s]/pH ^d	Caco-2 P _{app} [10 ⁻⁶ cm/s] ^e		PPB f _b [%] ^f	metabolic stability t _{1/2} [min] ^g
					a → b	b → a		
1		1.65	>3000	-4.89	7.0 ± 0.6	9.4 ± 0.2	81	13
3		2.1 ± 0.1	21 ± 1/7.4	-4.7 ± 0.1/7.4	10.0 ± 0.9	19.0 ± 1.2	93 ± 1	nd
20		2.14	33.8/6.51	-4.7	4.23	nd	93	1.0
9	3.88	<-1.5	>3000/6.61	no permeation	nd	nd	73	>60
10a		0.5 ± 0.1	12 ± 1/7.4	-6.8 ± 0.3/7.4	0.12 ± 0.01	0.61 ± 0.03	nd	nd
10b		0.8 ± 0.0	122 ± 13/7.4	-9.2 ± 1.4/7.4	1.10 ± 0.82	0.87 ± 0.15	nd	nd
10c		0.2 ± 0.1	>250/7.4	-7.8 ± 0.3/7.4	0.18 ± 0.07	1.30 ± 0.03	48 ± 2	>60
10d		0.4 ± 0.0	246 ± 17/7.4	-7.2 ± 0.0/7.4	0.36 ± 0.01	1.76 ± 0.12	99 ± 1	>60
10e		0.7 ± 0.1	>250/7.4	-8.6 ± 0.2/7.4	0.28 ± 0.23	1.82 ± 0.14	>99	>60
10f	6.5	1.1 ± 0.0	>150/3.0	-7.7 ± 0.8/5.0	0.40 ± 0.02	1.90 ± 0.17	nd	nd
			>150/7.4	-8.8 ± 0.1/7.4				
10g		1.4 ± 0.0	186 ± 4/7.6	-5.7 ± 0.0/7.4	2.0 ± 0.1	13.2 ± 2.1	99 ± 0	>60
10h	3.7	-1.4 ± 0.1	11 ± 0/3.0	-9.3 ± 1.4/5.0	0.17 ± 0.00	0.22 ± 0.01	nd	nd
			273 ± 2/7.4	-8.8 ± 1.4/7.4				
10i	2.5	-1.1 ± 0.1	>150/3.0	-6.8 ± 0.2/5.0	0.22 ± 0.14	0.29 ± 0.03	nd	nd
			>150/7.4	-7.0 ± 0.1/7.4				
10j		2.1 ± 0.0	192 ± 5/7.4	-5.2 ± 0.0/7.4	2.2 ± 0.4	22.1 ± 1.5	89 ± 1	>60

^apK_a values were determined by NMR spectroscopy. ^bOctanol–water distribution coefficients (log D_{7.4}) were determined by a miniaturized shake-flask procedure at pH 7.4. Values represent the mean ± SD of sextuplicate measurements.⁵⁹ ^cKinetic solubility was measured in a 96-well format using the μSOL Explorer solubility analyzer at the indicated pH in triplicate. ^dP_e = effective permeability. Passive permeation through an artificial membrane was determined by the parallel artificial membrane permeation assay (PAMPA). Values represent the mean ± SD of quadruplicate measurements performed at the indicated pH.⁶⁰ ^eP_{app} = apparent permeability. Permeation through a Caco-2 cell monolayer was assessed in the absorptive (a → b) and secretory (b → a) directions in triplicate.⁶¹ ^fPlasma protein binding (PPB) was determined by equilibrium dialysis in triplicate.⁶² ^gMetabolic stability was determined by incubating the compounds (2 μM) with pooled rat liver microsomes (RLM, 0.5 mg/mL) in the presence of NADPH (1 mM, compounds 1, 9, 10c–e,g,j) or without NADPH (compound 20).⁶³ ^hnd = not determined.

Oral Bioavailability. Oral bioavailability of a compound relies on solubility, permeation through the membranes lining the intestine, and stability against first pass metabolism.^{64,65} As discussed by Lipinski⁶⁶ and Curatolo,⁶⁷ dose and permeability define the minimum aqueous solubility required for oral administration. Thus, a dose of 1 mg/kg of a moderately permeable compound requires a solubility of at least 52 μg/mL. Whereas sufficient aqueous solubility (>3000 μg/mL) was reported for *n*-heptyl α-mannopyranoside (1),¹⁹ the unsubstituted biphenyl α-D-mannopyranoside 3 and the antagonists bearing a methylcarboxylate, carboxamide, or tetrazole substituent (compounds 20, 10a, and 10h) were found to be scarcely soluble.²² As proposed by Ishikawa,⁶⁸ a possible reason is the apolar and planar aglycone. By contrast, the polar carboxylic acid moiety present in antagonist 9 or the substituents in the bioisosteres 10b–j enhance solubility to 122–273 μg/mL, a level sufficient for in vivo PK studies. For in vivo disease studies, however, dosages of up to 10 mg/kg were foreseen (see below), requiring a solubility of 520 μg/mL.^{66,67} For this reason, surfactant Tween 80 (1%) had to be added.

Furthermore, permeability data derived from PAMPA⁶⁹ and the Caco-2 model⁷⁰ suggest moderate to high permeation of the moderately lipophilic antagonists 1, 3, and 20 (log D_{7.4} > 1.6) through the intestinal membranes. The bioisosteres 10a–f,h,i, although slightly more permeable than the strongly hydrophilic carboxylic acid derivative 9, show only low values of permeability compared to *n*-heptyl α-D-mannopyranoside (1) or the unsubstituted biphenyl mannoside 3. However, the *p*-cyanobiphenyl derivatives 10g and 10j display elevated log D_{7.4} and effective permeability (log P_e) in the range for successful intestinal absorption. Regarding both sufficient aqueous solubility and elevated membrane permeability, the *p*-cyano substituted bioisosteres 10g and 10j are thus the most promising

candidates for oral absorption. Moreover, combining the bioisosteric replacement with the addition of a chloro substituent in the ortho-position of the aromatic ring adjacent to the anomeric oxygen (→10j)²² resulted in the most advantageous physicochemical profile for oral bioavailability.

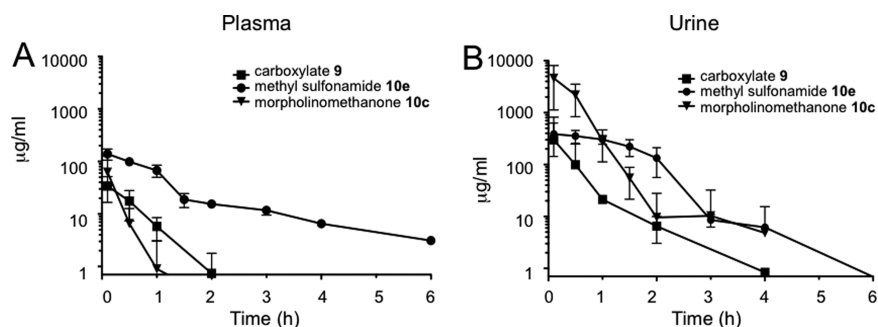
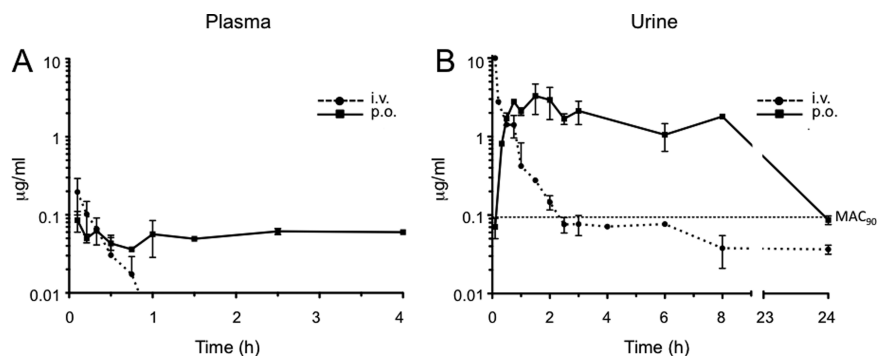
Renal Excretion. The rate of renal excretion depends on the rate of glomerular filtration and the propensity to tubular secretion and reabsorption of an antagonist.⁷¹ Only the fraction that is not bound to plasma proteins is expected to enter the glomerular filtrate.⁷² Plasma protein binding (PPB) data indicating the fraction bound (f_b) are listed in Table 2.⁶² The biphenyls 9 and 10c were identified as moderate binders to plasma proteins (f_b ≤ 65%), which suggests a low impact of PPB on antagonist filtration. The f_b values of the antagonists 1, 3, 20, and 10j were between 80% and 93%, whereas the bioisosteres 10d,e,g showed particularly high protein binding (f_b ≥ 99%) implying slow compound entry into the primary urine. However, the kinetic aspects of PPB, that is, association and dissociation rate constants, remain to be determined to quantify precisely the influence of PPB on filtration.⁷³

Furthermore, log D_{7.4} was identified as key determinant of tubular reabsorption.^{74–76} Accordingly, lipophilic compounds are predominantly reabsorbed from the renal filtrate. Given that renal clearance is the major route of elimination, this will result in a slow but steady excretion into the bladder. In contrast, hydrophilic compounds are poorly reabsorbed and thus quickly renally eliminated, which leads to high initial compound levels in the urine but narrows the time range where the minimal antiadhesive concentration is maintained. Consequently, low log D_{7.4} as shown for the antagonists 9, 10h, and 10i implies low tubular reabsorption and rapid elimination of the filtered molecules by the urine. Otherwise, log D_{7.4} between 0.2 and 0.7, such as determined for the bioisosteres 10a–e, suggests

Table 4. Pharmacokinetic Parameters Determined after a Single iv Application of Compounds **9**, **10c**, **10e**, and **10j** in Female C3H/HeN Mice^a

compd	plasma							urine, C_{max} ($\mu\text{g/mL}$)
	C_0 ($\mu\text{g/mL}$)	dose (mg/kg)	V_z (mL)	$t_{1/2}$ (h)	$AUC_{0-\text{inf}}$ ($\mu\text{g}\cdot\text{h/mL}$)	CL_{tot} (mL/h)		
9	40	50	25.2	0.33	23.5	53.1	300	
10c	109.7	50	28.3	0.4	25.3	49.4	4611	
10e	151.6	50	19.5	1.9	175.1	7.1	387	
10j	0.36	0.625	52.8	0.17	0.07	218	10	

^aValues were calculated using PKSolver.⁷⁸ C_0 , initial concentration; V_z , volume of distribution in terminal phase; AUC, area under the curve; CL_{tot} , total clearance; C_{max} , maximal concentration.

**Figure 5.** Antagonist concentrations in (A) plasma and (B) urine after a single iv application of **9**, **10c**, and **10e** (50 mg/kg).**Figure 6.** Antagonist concentrations in (A) plasma and (B) urine after a single iv and po application of compound **10j** (iv, 0.625 mg/kg; po, 1.25 mg/kg). MAC_{90} is the minimal antiadhesive concentration to inhibit 90% adhesion (0.094 $\mu\text{g/mL}$).

increasing propensity to tubular reuptake, whereas $\log D_{7.4} > 1$ as shown for heptyl mannoside **1** and the biphenyl mannosides **3**, **20**, **10g**, **10f**, and **10j** is optimal for tubular reabsorption from the glomerular filtrate and thus for slow renal clearance.

Metabolic Stability. Increasing lipophilicity is usually paralleled by increasing susceptibility to metabolism.⁷⁷ Liabilities toward metabolic clearance pathways that prevent the intact antagonist from reaching the target in the bladder were therefore of interest. To assess their propensity to cytochrome P450 (CYP450) mediated metabolism, heptyl mannoside **1**, the carboxylic acid derivative **9**, and the bioisosteres **10c–e,g,j** were incubated with rat liver microsomes (RLM, 0.5 mg/mL) in the presence of the cofactor β -nicotinamide adenine dinucleotide phosphate (NADPH).⁶³ To confirm the high propensity of the methyl ester present in antagonist **20** to carboxylesterase (CES) mediated hydrolysis, this antagonist was incubated with RLM only. The profiles of unchanged compound versus time revealed high susceptibility of heptyl mannoside **1** to CYP450-mediated metabolism ($t_{1/2} = 13$ min) and rapid hydrolysis of the ester **20** by the hepatic CES ($t_{1/2} = 1.0$ min). Otherwise, the bioisosteres **10c–e,g,j** were stable against enzyme-mediated bioconversion

($t_{1/2} > 60$ min), suggesting lower propensity to metabolic, nonrenal elimination pathways.

Considering PPB, lipophilicity, and metabolic stability data, we therefore expected (i) a steady release of compounds **10d,e,g,j** into the bladder because of high PPB decelerating glomerular filtration (**10d,e,g**) and/or high $\log D_{7.4}$ supporting tubular reabsorption (**10g,j**), (ii) a fast excretion of antagonists **9** and **10c** via the urine due to low PPB and low $\log D_{7.4}$, and (iii) a rapid clearance of heptyl mannoside **1** from the body by renal and metabolic pathways. Compounds featuring high propensity to renal excretion as major route of elimination (**10c**, **10e** and **10j**) were selected for in vivo PK studies in a mouse model.

Pharmacokinetic Studies in C3H/HeN Mice. This first part of our study explored the predicted effects of lipophilicity, PPB, and metabolic stability on antagonist disposition and elimination upon a single dose iv application (50 mg/kg) of compounds **10c** and **10e**. The PK parameters of these applications and those of the previously published carboxylate **9** are summarized in Table 4. The table also contains the results of the iv administration of compound **10j** (0.625 mg/kg).

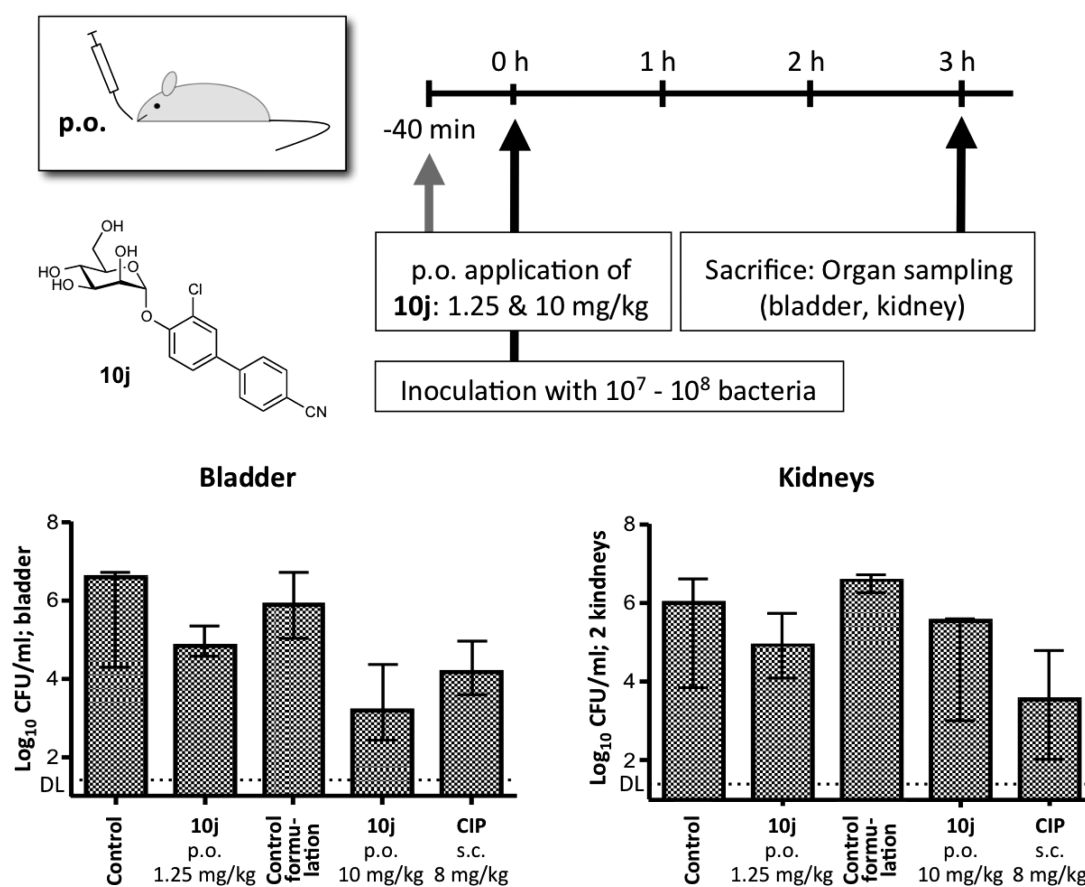


Figure 7. Preventive efficacy of **10j** in the UTI mouse model 3 h after infection. The bars depict the median bacterial load with the interquartile range in the different study groups. Shown are the results of the control group (PBS), control group formulation (5% DMSO in PBS containing 1% Tween 80), and the intervention groups with the preventive applications of either 1.25 or 10 mg/kg **10j** po or 8 mg/kg CIP sc (representing the murine dose equivalent to a human standard dose).⁸¹ DL, detection limit. CFU, colony forming units.

In contrast to the fast plasma clearance of antagonists **9** and **10c** (Figure 5A), the methylsulfonamide bioisostere **10e** attained higher initial concentration in plasma (C_0) and lower total clearance (CL_{tot}). Therefore, it could be detected until 6 h after application, resulting in markedly higher plasma AUC. The observed high C_0 of compound **10e** may be attributed to a small volume of distribution (V_z) resulting from the high PPB ($f_b \geq 99\%$).⁷² In urine (Figure 5B), the carboxylic acid **9** and the morpholinomethanone **10c** displayed high levels immediately following administration and a rapid concentration decrease within the first 2 h, reflecting the rapid elimination from plasma. Fast renal excretion as major route of elimination can be rationalized by the physicochemical properties of the antagonists **9** and **10c**, that is, moderate PPB and $\log D_{7.4}$, as well as high metabolic stability. Otherwise, the methylsulfonamide bioisostere **10e** showed sustained compound levels in urine over a period of 2 h and subsequent slow decrease until 6 h after administration. This sustained renal excretion is a result of the interplay of the antagonist's elevated PPB and $\log D_{7.4}$.

In a second study, the *p*-cyano bioisostere **10j**, characterized by a high oral absorption potential, was administered as a single dose iv (0.625 mg/kg) and po (1.25 mg/kg). The plasma concentration curve upon iv dosing displays a steep decline within the first hour after application, while the po curve shows a prolonged period where absorption and elimination are in equilibrium (Figure 6A). The urine concentration profiles

(Figure 6B) parallel the plasma curves obtained by the two modes of application; i.e., high plasma clearance upon iv bolus injection led to high initial antagonist levels in urine and a rapid concentration decline. By contrast, sustained plasma concentrations upon po administration resulted in prolonged urine levels.

As a result, urine concentrations exceed the minimum level required for the antiadhesive effect as estimated from the in vitro cell infection model⁷⁹ (minimal antiadhesion concentration,²³ $MAC_{90} = 0.094 \mu\text{g/mL}$) for more than 8 h upon oral single-dose administration (Figure 6B).

Infection Study in C3H/HeN Mice. In a preventive study, six mice were inoculated with UTI89 following an oral application of **10j** (1.25 mg/kg) 40 min prior to infection. Three hours after inoculation, the animals were sacrificed and bladder and kidneys were removed. Organs were homogenized and analyzed for bacterial counts. The effect of the FimH antagonist was compared to a 8 mg/kg dose of ciprofloxacin (CIP), applied subcutaneously (sc) 10 min before infection. CIP is used as standard antibiotic therapy in humans for the treatment of UTI.⁸⁰ In mice, the dose of 8 mg/kg sc was shown to mimic the standard human dose regarding peak levels and the AUC_{24} in serum.⁸¹ The median reductions in bacterial counts in mice treated with **10j** and CIP compared to the control group 3 h after infection are displayed in Figure 7.

The median value in the untreated control group showed bacterial counts of $6.6 \log_{10}$ colony forming units (CFU) in the bladder and $6 \log_{10}$ CFU in the kidneys. After oral application of 1.25 mg/kg **10j**, bacterial loads in the bladder decreased by $1.78 \log_{10}$ CFU and $1.07 \log_{10}$ CFU in the kidneys. The lower reduction in the kidneys is most likely due to the differing adhesion mechanisms between bladder and kidneys (type 1 pili vs P-pili), which is not targeted by **10j**.⁸² With CIP (8 mg/kg sc) a substantial reduction in both bladder and kidneys (median reductions of $2.44 \log_{10}$ and $2.47 \log_{10}$, respectively) was observed. Despite the low oral dose of **10j** (1.25 mg/kg), the approximately 100-fold reduction of CFU in the bladder promised an even higher effect upon dose increase to 10 mg/kg. Since the solubility of **10j** for this increased dose is too low ($192 \mu\text{g/mL}$), we used 5% DMSO and surfactant Tween 80 (1%) as solubilizer. To effectively compare the effect of a higher dose of **10j**, a control group receiving the formulation only (5% DMSO in PBS containing 1% Tween 80, termed control group formulation) was tested in parallel. When 10 mg/kg **10j** was applied, bacterial loads in the bladder decreased by $2.68 \log_{10}$ CFU/mL compared to the control group formulation, clearly exceeding the effect of CIP with a reduction of $2.44 \log_{10}$ CFU/mL. However, only a moderate reduction of $1.04 \log_{10}$ CFU was achieved in the kidneys.

SUMMARY AND CONCLUSION

Recently, numerous monovalent alkyl and aryl α -D-mannopyranosides have been described as potent FimH antagonists. However, most of them suffer from insufficient pharmacokinetic properties, i.e., modest bioavailability and short duration of the therapeutic effect in the bladder, their site of action. As a consequence, high doses at short intervals are required to achieve antiadhesive effects over an extended period of time. Therefore, the goal of the present study was an appropriate optimization of the pharmacokinetic profile of biphenyl α -D-mannopyranosides while keeping their high affinity to the CRD of FimH. The starting point was the biphenylcarboxylate **9** where the critical carboxylate was replaced by bioisosteres.^{39,83}

With a series of bioisosteres, a 3- to 5-fold improvement of affinity was achieved compared to **9**. Although binding necessitates only partial desolvation of the carboxylate and its bioisosteric replacements, a reduction of the enthalpy penalty for desolvation⁵¹ was identified as the source of the improved affinity exhibited by the bioisosteres. Thermodynamic evaluation of antagonists **10b–e** revealed almost identical enthalpy contribution to binding. However, for antagonists with the *p*-cyano substituent (**10g** and **10j**) an enhancement of up to -8.7 kJ/mol was observed, indicating a reduced desolvation penalty and an improved stacking as derived from the crystal structure of **10j** cocrystallized with the CRD of FimH (Figure 4B). On the other hand, higher affinity originating from a reduction of conformational flexibility of ligand and protein resulted in a concomitant entropy penalty of up to 6.5 kJ/mol .

In addition to the improved pharmacodynamics, the relevant pharmacokinetic parameters (solubility, permeability, renal excretion) were substantially improved. With 3'-chloro-4'-(α -D-mannopyranosyloxy)biphenyl-4-carbonitrile (**10j**), a FimH antagonist with an optimal in vitro PK/PD profile was identified. The *p*-cyano substituent conferred lipophilicity and high binding to plasma proteins, which slowed the rate of renal excretion. Despite higher lipophilicity, antagonist **10j** was insensitive to CYP450-mediated metabolism and therefore predominantly eliminated via the renal pathway. In vivo experiments confirmed

the excellent PK profile of **10j** with steady renal excretion for more than 8 h after oral application (1.25 mg/kg), suggesting a long-lasting antiadhesive effect. Finally, the preventive oral application of **10j** (10 mg/kg) reduced the bacterial load in the bladder by almost 1000-fold 3 h after infection. Although the first 3 h of the infection do not represent the complete infection cycle, they represent the time span of bacteria adhering and invading urothelial cells.^{84,85} Nevertheless, the effect of FimH antagonist **10j** within a longer infection time and at higher dosing will be the subject of future investigations.

EXPERIMENTAL SECTION

Synthesis. The synthesis of compounds **10a–d**, **10f**, **10g**, **10i**, **13a–d**, **13f**, **13g**, **15**, **18**, and **25**, including compound characterization data, can be found in the Supporting Information.

General Methods. NMR spectra were recorded on a Bruker Avance DMX-500 (500.1 MHz) spectrometer. Assignment of ¹H and ¹³C NMR spectra was achieved using 2D methods (COSY, HSQC, HMB). Chemical shifts are expressed in ppm using residual CHCl₃, CHD₂OD, or HDO as references. Optical rotations were measured using PerkinElmer polarimeter 341. Electron spray ionization mass spectra were obtained on a Waters micromass ZQ. The LC/HRMS analyses were carried out using an Agilent 1100 LC equipped with a photodiode array detector and a Micromass QTOF I equipped with a 4 GHz digital time converter. Microwave-assisted reactions were carried out with a CEM Discover and Explorer. Reactions were monitored by TLC using glass plates coated with silica gel 60 F₂₅₄ (Merck) and visualized by using UV light and/or by charring with a molybdate solution (a 0.02 M solution of ammonium cerium sulfate dihydrate and ammonium molybdate tetrahydrate in aqueous 10% H₂SO₄). MPLC separations were carried out on a CombiFlash Companion or Rf (Teledyne Isco) equipped with RediSep normal-phase or RP-18 reversed-phase flash columns. LC–MS separations were done on a Waters system equipped with sample manager 2767, pump 2525, PDA 2525, and Micromass ZQ. All compounds used for biological assays are at least of 95% purity based on HPLC analytical results. Commercially available reagents were purchased from Fluka, Aldrich, Alfa Aesar, or abcr GmbH & Co. KG (Germany). Solvents were purchased from Sigma-Aldrich or Acros and were dried prior to use where indicated. Methanol (MeOH) was dried by refluxing with sodium methoxide and distilled immediately before use. Dimethoxyethane (DME) was dried by filtration over Al₂O₃ (Fluka, type 5016 A basic).

4'-(2,3,4,6-Tetra-O-acetyl- α -D-mannopyranosyloxy)-N-methylbiphenyl-4-sulfonamide (13e). A Schlenk tube was charged with aryl iodide **11**²² (116 mg, 0.21 mmol), 4-(N-methylsulfamoyl)-phenylboronic acid (**12e**, 50 mg, 0.23 mmol), Pd(dppf)Cl₂·CH₂Cl₂ (5 mg, 0.006 mmol), K₃PO₄ (67 mg, 0.32 mmol), and a stirring bar. The tube was closed with a rubber septum and was evacuated and flushed with argon. This procedure was repeated once, and then anhydrous DMF (1 mL) was added under a stream of argon. The mixture was degassed in an ultrasonic bath and flushed with argon for 5 min and then stirred at 80 °C overnight. The reaction mixture was cooled to rt, diluted with EtOAc (50 mL), and washed with water (50 mL) and brine (50 mL). The organic layer was dried over Na₂SO₄ and concentrated in vacuo. The residue was purified by MPLC on silica gel (petroleum ether/EtOAc) to afford **13e** (105 mg, 84%) as a white solid. [α]_D²⁰ +56.4 (c 0.50, MeOH). ¹H NMR (500 MHz, CDCl₃): δ = 7.92–7.90 (m, 2H, Ar–H), 7.70–7.68 (m, 2H, Ar–H), 7.57–7.55 (m, 2H, Ar–H), 7.21–7.19 (m, 2H, Ar–H), 5.60–5.57 (m, 2H, H-1, H-3), 5.48 (dd, *J* = 1.8, 3.4 Hz, 1H, H-2), 5.40 (t, *J* = 10.0 Hz, 1H, H-4), 4.38 (dd, *J* = 5.4, 10.8 Hz, 1H, NH), 4.30 (dd, *J* = 4.9, 12.3 Hz, 1H, H-6a), 4.13–4.08 (m, 2H, H-5, H-6b), 2.72 (d, *J* = 5.4 Hz, 3H, NCH₃), 2.22, 2.07, 2.05, 2.04 (4 s, 12H, 4 COCH₃). ¹³C NMR (126 MHz, CDCl₃): δ = 170.55, 170.06, 170.03, 169.75 (4 CO), 155.97, 144.81, 137.16, 134.09, 128.62, 127.85, 127.39, 117.01 (Ar–C), 95.78 (C-1), 69.34 (C-5), 69.31 (C-2), 68.81 (C-3), 65.86 (C-4), 62.07 (C-6), 29.44 (NHCH₃), 20.92, 20.74, 20.72 (4C, 4 COCH₃). ESI-MS *m/z*, calcd for C₂₇H₃₁NNaO₁₂S [M + Na]⁺: 616.1. Found: 616.1.

4'-(α -D-Mannopyranosyloxy)-N-methylbiphenyl-4-sulfonamide (10e). To a solution of **13e** (40 mg, 0.07 mmol) in dry MeOH (5 mL) was added freshly prepared 1 M NaOMe/MeOH (0.1 equiv) under argon. The mixture was stirred at rt until the reaction was complete (monitored by TLC), then neutralized with Amberlyst-15 (H⁺) ion-exchange resin, filtered, and concentrated in vacuo. The residue was purified by MPLC on silica gel (DCM/MeOH, 10:1 to 7:1) to afford **10e** (22 mg, 76%) as white solid. $[\alpha]_{\text{D}}^{20} +105.7$ (c 0.30, MeOH). ¹H NMR (500 MHz, CD₃OD): δ = 7.90–7.88 (m, 2H, Ar–H), 7.80–7.79 (m, 2H, Ar–H), 7.66–7.64 (m, 2H, Ar–H), 7.26–7.25 (m, 2H, Ar–H), 5.58 (d, J = 1.7 Hz, 1H, H-1), 4.06 (dd, J = 1.8, 3.3 Hz, 1H, H-2), 3.96 (dd, J = 3.4, 9.5 Hz, 1H, H-3), 3.79–3.74 (m, 3H, H-4, H-6a, H-6b), 3.63 (ddd, J = 2.5, 5.2, 9.7 Hz, 1H, H-5), 2.57 (s, 3H, NHCH₃). ¹³C NMR (126 MHz, CD₃OD): δ = 158.34, 146.13, 138.67, 134.55, 129.53, 128.82, 128.21, 118.29 (Ar–C), 100.09 (C-1), 75.53 (C-5), 72.42 (C-3), 71.96 (C-2), 68.32 (C-4), 62.68 (C-6), 29.31 (NHCH₃). HRMS m/z , calcd for C₁₉H₂₃NNaO₈S [M + Na]⁺: 448.1037. Found: 448.1038.

5-(4'-(2,3,4,6-Tetra-O-acetyl- α -D-mannopyranosyloxy)-biphenyl-4-yl)-1H-tetrazole (14). A Schlenk tube was charged with **13g** (30 mg, 0.06 mmol), trimethylsilyl azide (16 μ L, 0.12 mmol), dibutyltin oxide (2 mg, 0.006 mmol), DME (1 mL), and a stirring bar. The mixture was heated to 150 °C for 10 min by microwave irradiation. The reaction mixture was cooled to rt and then concentrated in vacuo. The residue was purified by MPLC on silica gel (DCM/MeOH, 9:1 to 8:1) to afford **14** (26 mg, 81%) as a colorless oil. $[\alpha]_{\text{D}}^{20} +56.1$ (c 0.3, MeOH). ¹H NMR (500 MHz, CDCl₃): δ = 8.25–8.15 (m, 2H, Ar–H), 7.75–7.65 (m, 2H, Ar–H), 7.60–7.55 (m, 2H, Ar–H), 7.20–7.17 (m, 2H, Ar–H), 5.64–5.55 (m, 2H, H-1, H-3), 5.49 (dd, J = 1.7, 3.3 Hz, 1H, H-2), 5.40 (t, J = 10.1 Hz, 1H, H-4), 4.31 (dd, J = 5.3, 12.4 Hz, 1H, H-6a), 4.17–4.06 (m, 2H, H-5, H-6b), 2.22, 2.07, 2.06, 2.05 (4 s, 12H, 4 COCH₃). ¹³C NMR (126 MHz, CDCl₃): δ = 170.67, 170.14, 170.11, 169.81 (4 CO), 155.61, 128.36, 127.84, 127.49, 116.93 (Ar–C), 95.78 (C-1), 69.36 (C-5), 69.26 (C-2), 68.90 (C-3), 65.89 (C-4), 62.12 (C-6), 20.92, 20.76, 20.73 (4 COCH₃). ESI-MS m/z , calcd for C₂₇H₂₈N₄NaO₁₀ [M + Na]⁺: 591.2. Found: 591.1.

5-(4'-(α -D-Mannopyranosyloxy)biphenyl-4-yl)-1H-tetrazole (10h). Prepared according to the procedure described for **10e** from **14** (26 mg, 0.03 mmol). Yield: 18 mg (quant) as a white solid. $[\alpha]_{\text{D}}^{20} +112.1$ (c 0.1, MeOH/H₂O, 2:1). ¹H NMR (500 MHz, CD₃OD): δ = 7.98–7.96 (m, 2H, Ar–H), 7.72–7.71 (m, 2H, Ar–H), 7.58–7.54 (m, 2H, Ar–H), 7.16–7.13 (m, 2H, Ar–H), 5.46 (d, J = 1.7 Hz, 1H, H-1), 3.94 (dd, J = 1.9, 3.5 Hz, 1H, H-2), 3.83 (dd, J = 3.4, 9.5 Hz, 1H, H-3), 3.68–3.61 (m, 3H, H-4, H-6a, H-6b), 3.52 (ddd, J = 2.5, 5.4, 9.7 Hz, 1H, H-5). ¹³C NMR (126 MHz, CD₃OD): δ = 158.19, 145.07, 134.97, 129.29, 128.74, 128.55, 118.26 (Ar–C), 100.13 (C-1), 75.52 (C-5), 72.42 (C-3), 71.98 (C-2), 68.33 (C-4), 62.69 (C-6). HRMS m/z , calcd for C₁₉H₂₁N₄O₆ [M + H]⁺: 401.1456. Found: 401.1450.

4-(2,3,4,6-Tetra-O-acetyl- α -D-mannopyranosyloxy)-3'-chlorobiphenyl-4-carbonitrile (19). Prepared according to the procedure described for **13e** from aryl iodide **18**²⁵ (79 mg, 0.135 mmol), **12g** (22 mg, 0.15 mmol), Pd(dppf)Cl₂·CH₂Cl₂ (3.3 mg, 4 μ mol), and K₃PO₄ (57 mg, 0.27 mmol). Yield: 57 mg (75%) as a white solid. $[\alpha]_{\text{D}}^{20} +77.7$ (c 0.5, CHCl₃). ¹H NMR (500 MHz, CDCl₃): δ = 7.72 (d, J = 8.3 Hz, 2H, Ar–H), 7.63 (m, 3H, Ar–H), 7.43 (dd, J = 2.2, 8.6 Hz, 1H, Ar–H), 7.27 (d, J = 8.6 Hz, 1H, Ar–H), 5.64–5.59 (m, 2H, H-1, H-2), 5.54 (dd, J = 1.9, 3.2 Hz, 1H, H-3), 5.41 (t, J = 10.1 Hz, 1H, H-4), 4.28 (dd, J = 5.2, 12.3 Hz, 1H, H-6a), 4.17 (ddd, J = 2.1, 5.1, 10.0 Hz, 1H, H-5), 4.10 (dd, J = 2.2, 12.3 Hz, 1H, H-6b), 2.21 (s, 3H, COCH₃), 2.12–2.00 (m, 9H, 3 COCH₃). ¹³C NMR (126 MHz, CDCl₃): δ = 170.54, 170.08, 169.90, 169.84, (4C, CO) 151.67, 143.61, 135.29, 132.87, 129.41, 127.53, 126.60, 125.20, 118.79, 117.36, 111.47 (Ar–C, CN), 96.72 (C-1), 70.00 (C-5), 69.39 (C-3), 68.82 (C-2), 65.86 (C-4), 62.16 (C-6), 20.98, 20.81, 20.79, 20.78 (4 COCH₃). ESI-MS m/z , calcd for C₂₇H₂₆ClN₃NaO₁₀ [M + Na]⁺: 582.1. Found: 582.1.

3'-Chloro-4'-(α -D-mannopyranosyloxy)biphenyl-4-carbonitrile (10j). Prepared according to the procedure described for **10e** from **19** (36 mg, 0.06 mmol). Yield: 12 mg (48%) as a white solid. $[\alpha]_{\text{D}}^{20} +109.4$ (c 0.23, MeOH). ¹H NMR (500 MHz, CD₃OD): δ = 7.80–7.72 (m, 5H, Ar–H), 7.59 (dd, J = 2.2, 8.6 Hz, 1H, Ar–H), 7.48 (d, J = 8.7 Hz, 1H, Ar–H), 5.62 (d, J = 1.4 Hz, 1H, H-1), 4.12 (dd, J = 1.8, 3.3 Hz, 1H,

H-2), 4.00 (dd, J = 3.4, 9.5 Hz, 1H, H-3), 3.83–3.68 (m, 3H, H-4, H-6a, H-6b), 3.63 (ddd, J = 2.3, 5.4, 9.6 Hz, 1H, H-5). ¹³C NMR (126 MHz, CD₃OD): δ = 153.65, 145.15, 135.42, 133.86, 129.82, 128.53, 127.87, 125.47, 119.70, 118.59 (Ar–C), 111.97 (CN), 100.66 (C-1), 76.05 (C-5), 72.39 (C-3), 71.80 (C-2), 68.20 (C-4), 62.65 (C-6). IR (KBr), ν = 3400 (OH), 2227 (C \equiv N), 1606, 1487 (Ar–C=C) cm⁻¹. HRMS m/z , calcd for C₁₉H₁₈ClN₃NaO₆ [M + Na]⁺: 414.0715. Found: 414.0721.

3'-Chloro-N-(3',6'-dihydroxy-3-oxo-3H-spiro-[isobenzofuran-1,9'-xanthen]-5-yl)-4'-(α -D-mannopyranosyloxy)biphenyl-4-carboxamide (22). Compound **21** (10.0 mg, 0.024 mmol), fluoresceinamine isomer I (12.7 mg, 0.037 mmol), and COMU (20.9 mg, 0.049 mmol) were dissolved in dry DMF (1 mL). Then NEt₃ (10 μ L, 0.073 mmol) was added and the mixture was stirred at rt for 7 h. 1 N HCl in DMF was added until acid reaction on pH paper and the mixture was concentrated. The residue was dissolved in DCM/MeOH (3:1) and loaded onto a silica gel column. The complex mixture of compounds was only partially resolved. The fractions containing the product were collected, concentrated, and purified by preparative HPLC (gradient H₂O/MeCN, +0.2% HCO₂H) to afford compound **22** (5 mg, 19%). $[\alpha]_{\text{D}}^{20} +21.1$ (c 0.10, MeOH). ¹H NMR (500 MHz, CD₃OD): δ = 8.26 (d, J = 8.4 Hz, 2H, Ar–H), 7.88–7.74 (m, 3H, Ar–H), 7.66 (dd, J = 2.2, 8.6 Hz, 1H, Ar–H), 7.51 (d, J = 8.7 Hz, 1H, Ar–H), 7.29 (dd, J = 1.9, 5.3 Hz, 2H, Ar–H), 7.19 (dd, J = 2.1, 8.3 Hz, 1H, Ar–H), 7.08–6.99 (m, 2H, Ar–H), 6.95 (d, J = 8.7 Hz, 1H, Ar–H), 6.72 (dd, J = 5.5, 10.6 Hz, 2H, Ar–H), 6.61 (dd, J = 2.3, 8.7 Hz, 1H, Ar–H), 5.65 (s, 1H, H-1), 4.15 (dd, J = 1.8, 3.2 Hz, H-2), 4.03 (dd, J = 3.4, 9.5 Hz, H-3), 3.87–3.72 (m, 3H, H-4, H-6a, H-6b), 3.65 (m, 1H, H-5). ¹³C NMR (126 MHz, CD₃OD): δ = 137.50, 136.01, 131.90, 130.24, 130.20, 129.87, 129.24, 128.03, 127.91, 125.79, 125.46, 124.73, 118.99, 118.76, 118.65 (Ar–C), 100.73 (C-1), 76.06 (C-5), 72.42 (C-3), 71.85 (C-2), 68.24 (C-4), 62.69 (C-2). ESI-MS m/z , calcd for C₃₉H₃₁ClNO₁₂ [M + H]⁺: 740.2. Found: 740.2.

3'-Chloro-N-(2-(3-(3',6'-dihydroxy-3-oxo-3H-spiro-[isobenzofuran-1,9'-xanthen]-5-yl)thioureido)ethyl)-4'-(α -D-mannopyranosyloxy)biphenyl-4-carboxamide (23). To a stirred solution of compound **21** (25 mg, 0.061 mmol) in dry DMF (1 mL), NHS (21 mg, 0.183 mmol) was added, followed by DIC (9.2 mg, 0.073 mmol). The mixture was stirred at rt for 2 h. Then *N*-Boc-ethylendiamine (10.7 mg, 0.067 mmol) was added and the reaction was stirred for 10 h. It was then cooled down to 0 °C, diluted with water, and concentrated. Chromatography on silica gel (DCM/MeOH) yielded **23** mg (0.042 mmol, 68%) of *tert*-butyl (3'-chloro-4'-(α -D-mannopyranosyloxy)biphenyl-4-yl-carboxamido)ethyl)carbamate. This product was dissolved in DCM (3 mL), and TFA (1 mL) was added. The solid dissolved during addition of TFA. After 10 min the reaction was complete. The mixture was evaporated, and excess TFA was removed in high vacuum. The intermediate *N*-(2-aminoethyl)-3'-chloro-4'-(α -D-mannopyranosyloxy)biphenyl-4-carboxamide TFA salt (**23** mg, 0.042 mmol, quant) was used directly in the next step. It was dissolved in dry DMF (0.5 mL), and NEt₃ (12.8 mg, 0.127 mmol) was added. The mixture was cooled to 0 °C. Then FITC (14.8 mg, 0.038 mmol) was added and the mixture was stirred for 3 h in the dark. The mixture was then coevaporated with water, taken up in MeOH/10% aq acetic acid and evaporated. Chromatography on silica gel (DCM/MeOH) yielded compound **23**, contaminated with triethylammonium acetate. The compound was then redissolved in MeOH, and 0.5 N HCl in MeOH was added. The mixture was evaporated and chromatographed on silica gel to yield pure **23** (15 mg, 47%). $[\alpha]_{\text{D}}^{20} +12.1$ (c 0.30, MeOH). ¹H NMR (500 MHz, CD₃OD): δ = 8.12 (s, 1H), 7.92 (d, J = 8.3 Hz, 2H, Ar–H), 7.70 (dd, J = 5.0, 13.1 Hz, 2H, Ar–H), 7.64 (d, J = 8.3 Hz, 2H, Ar–H), 7.54 (dd, J = 2.2, 8.6 Hz, 1H, Ar–H), 7.46 (d, J = 8.7 Hz, 1H, Ar–H), 7.09 (d, J = 8.2 Hz, 1H, Ar–H), 6.74 (s, 2H), 6.69 (d, J = 1.4 Hz, 2H, Ar–H), 6.55 (d, J = 8.4 Hz, 2H, Ar–H), 5.63 (d, J = 1.3 Hz, H-1), 4.15 (dd, J = 1.8, 3.1 Hz, H-2), 4.03 (dd, J = 3.4, 9.5 Hz, H-3), 3.94 (s, 2H, CH₂), 3.86–3.64 (m, 6H, H-4, H-5, H-6, CH₂). ¹³C NMR (126 MHz, CD₃OD): δ = 153.21, 143.84, 136.41, 129.66, 129.18, 127.76, 127.70, 125.37, 118.64, 103.62 (Ar–C), 100.75 (C-1), 76.00 (C-5), 72.41 (C-3), 71.86 (C-2), 68.24 (C-4), 62.69 (C-6), 40.76 (CH₂). ESI-MS m/z , calcd for C₄₂H₃₇ClN₃O₁₂S [M + H]⁺: 842.2. Found: 842.2.

3'-Chloro-N-(2-(2-(3-(3',6'-dihydroxy-3-oxo-3H-spiro[isobenzofuran-1,9'-xanthen]-5-yl)thioureido)ethoxy)ethoxy)ethyl)-4'-(α -D-mannopyranosyloxy)biphenyl-4-carboxamide (24). Compound **21** (280 mg, 0.68 mmol) was dissolved in dry DMF (5 mL) under argon. Then NHS (235 mg, 2.04 mmol) was added, followed by DIC (0.12 mL, 0.78 mmol) and the mixture was stirred at rt for 4 h. Then Boc-PEG2-NH₂ (186 mg, 0.75 mmol) was added, and the mixture was stirred at rt under argon for 10 h. It was then slowly diluted with water and concentrated. The residue was purified by chromatography on silica gel (DCM/MeOH) to give *tert*-butyl (2-(2-(2-(3'-chloro-4'-(α -D-mannopyranosyloxy)biphenyl-4-ylcarboxamido)ethoxy)ethoxy)ethyl)-carbamate (300 mg, 0.468 mmol, 69%). Then the carbamate was suspended in DCM (3 mL), and TFA (1 mL) was added dropwise at rt. After 30 min, the solvents were evaporated and the crude mixture was dissolved in CHCl₃/MeOH (6:4, +0.5% conc NH₄OH) and transferred to a silica gel column, eluting with the same solvent mixture, to yield *N*-(2-(2-(2-aminoethoxy)ethoxy)ethyl)-3'-chloro-4'-(α -D-mannopyranosyloxy)biphenyl-4-carboxamide (228 mg, 90%). A fraction of the amine (10 mg, 0.018 mmol) was dissolved in dry DMF (0.5 mL) and cooled to 0 °C. FITC (6.5 mg, 0.017 mmol) was added, and the mixture was stirred for 1 h. The mixture was concentrated and the residue was purified by chromatography on silica (DCM/MeOH) to yield **24** (10 mg, 65%). ¹H NMR (500 MHz, CD₃OD): δ = 8.21 (d, *J* = 1.4 Hz, 1H, Ar-H), 7.88 (d, *J* = 8.3 Hz, 2H, Ar-H), 7.68 (d, *J* = 2.2 Hz, 2H, Ar-H), 7.63 (d, *J* = 8.3 Hz, 2H, Ar-H), 7.53 (dd, *J* = 2.2, 8.6 Hz, 1H, Ar-H), 7.43 (d, *J* = 8.7 Hz, 1H, Ar-H), 7.09 (d, *J* = 8.2 Hz, 1H, Ar-H), 6.68 (d, *J* = 2.3 Hz, 2H, Ar-H), 6.65 (dd, *J* = 2.6, 8.6 Hz, 2H, Ar-H), 6.53 (dd, *J* = 1.6, 8.7 Hz, 2H, Ar-H), 5.61 (d, *J* = 1.3 Hz, 1H, H-1), 4.14 (dd, *J* = 1.8, 3.2, Hz, 1H, H-2), 4.03 (dd, *J* = 3.4, 9.5 Hz, 1H, H-3), 3.93–3.53 (m, 16H), 3.37 (s, 2H, NCH₂), 1.30 (s, 2H, CH₂). ¹³C NMR (126 MHz, CD₃OD): δ = 170.01 (CO), 153.17, 143.72, 136.37, 134.37, 130.39, 129.69, 129.04, 127.78, 127.73, 125.35, 118.60, 103.60 (Ar-C), 100.72 (C-1), 75.97 (C-5), 72.41 (C-3), 71.86, 71.40, 70.59 (SC, C-2, OCH₂), 68.23 (C-4), 62.64 (C-6), 49.88, 45.49, 40.97 (CH₂). ESI-MS *m/z*, calcd for C₄₆H₄₅ClN₃O₁₄S [M + H]⁺: 930.2. Found: 930.4.

Competitive Fluorescence Polarization Assay. *Expression and Purification of CRD of FimH.* A recombinant protein consisting of the CRD of FimH linked to a 6His-tag via a thrombin cleavage site (FimH-CRD-Th-His₆) was expressed in *E. coli* strain HM125 and purified by affinity chromatography as previously described.⁴³

K_D Determination of FITC-Labeled Ligands. The functionalized ligands (**23**, **24**) were prepared as a 10 mM stock solution in pure DMSO (Sigma-Aldrich, Buchs, Switzerland). All further dilutions of compounds and FimH-CRD-Th-His₆ protein were prepared in assay buffer (20 mM HEPES, 150 mM NaCl, 50 μ g/mL BSA, pH 7.4). BSA was added to the assay buffer to prevent nonspecific binding of protein to the plastic surface. Binding isotherms for the fluorescent ligands were obtained in direct binding studies by adding a constant concentration of ligand (final concentration 5 nM) and a linear dilution of protein (final concentration 0–100 nM) to a final volume of 200 μ L in 96-well, black, flat bottom NBS plates (Corning Inc., Corning, NY, USA). After incubation of the plate for 24 h at rt with gentle shaking, the fluorescence polarization was measured with the Synergy H1 hybrid multimode microplate reader (BioTek Instruments Inc., Winooski, VT, USA) with polarized excitation at 485 nm and emission measured at 528 nm through polarizing filters parallel and perpendicularly oriented to the incident polarized light. *K_D* values were determined by plotting the FP readout as a function of the protein concentration and applying the following single-site binding equation (eq 1) that accounts for ligand depletion:

$$S_{\text{obs}} = S_{\text{F}} + (S_{\text{B}} - S_{\text{F}}) \times \left(\frac{C_{\text{P}} + C_{\text{L}} + K_{\text{D}} - \sqrt{(C_{\text{P}} + C_{\text{L}} + K_{\text{D}})^2 - 4C_{\text{P}}C_{\text{L}}}}{2C_{\text{L}}} \right) \quad (1)$$

where *S_{obs}* is the observed signal from the ligand, *S_F* is the signal from free ligand, *S_B* is the signal from bound ligand, *C_P* is the total concentration of protein, and *C_L* is the total concentration of ligand.⁴⁹

K_D Determination of FimH Antagonists. The fluorescently labeled ligand **23** was used for the competitive fluorescence polarization assay. A linear dilution of nonlabeled FimH antagonist with final concentrations ranging from 0 to 10 μ M was titrated into 96-well, black, flat-bottom NBS plates (Corning Inc.) to a final volume of 200 μ L containing a constant concentration of protein (final concentration 25 nM) and FITC-labeled ligand which was fixed at a higher concentration in competitive binding assays than in direct binding experiments to obtain higher fluorescence intensities (final concentration 20 nM). Prior to measuring the fluorescence polarization, the plates were incubated on a shaker for 24 h at rt until the reaction reached equilibrium. The *IC*₅₀ value was determined with Prism (GraphPad Software Inc., La Jolla, CA, USA) by applying a standard four-parameter *IC*₅₀ function. The obtained *IC*₅₀ values were converted into their corresponding *K_D* values using the derivation of the Cheng–Prusoff equation.⁴⁵ This variation of the Cheng–Prusoff equation is applied to competition assays with tight-binding inhibitors and includes terms to correct for ligand depletion effects. However, the *K_D* for antagonists having a higher affinity toward FimH than the labeled ligand could not be accurately determined.⁴⁵

Isothermal Titration Calorimetry (ITC). All ITC experiments were performed with the FimH-CRD-Th-His₆ protein using a VP-ITC instrument from MicroCal, Inc. (Malvern Instruments, Worcestershire, U.K.) with a sample cell volume of 1.4523 mL. The measurements were performed with 0–5% DMSO at 25 °C, a stirring speed of 307 rpm, and 10 μ cal s⁻¹ reference power. The protein samples were dialyzed in assay buffer prior to all experiments. Because of the high protein consumption of ITC, only the experiments for the reference compounds (**1**, **3**, and **25**) were measured in duplicates. Compounds **1**, **3**, **9**, and **25** were measured in a direct fashion by titration of ligand (100–2,000 μ M) into protein (8.6–55 μ M) with injections of 3–8 μ L at intervals of 10 min to ensure nonoverlapping peaks. The quantity *c* = Mt(0) *K_D*⁻¹, where Mt(0) is the initial macromolecule concentration, is of importance in titration microcalorimetry. The *c*-values of the direct titrations were below 1000 and thus within the reliable range. For the compounds **10b–e**, **10g**, and **10j** additional competitive ITC experiments were performed because of their high affinity resulting in *c*-values above 1000 for direct titrations. These ligands (600 μ M) were titrated into protein (30 μ M), which was preincubated with compound **25** (300 μ M) resulting in sigmoidal titration curves. Because of slow reaction kinetics, titration intervals of 20 min were used.

Baseline correction and peak integration were performed using the Origin 7 software (OriginLab, Northampton, MA, USA). An initial 2 μ L injection was excluded from data analysis. Baseline subtraction and curve-fitting with the three variables *N* (concentration correction factor), *K_D* (dissociation constant), and ΔH° (change in enthalpy) were performed with the SEDPHAT software, version 10.40 (National Institutes of Health).⁸⁶ A global fitting analysis was performed for the competition titration (**10b–e**, **10g**, or **10j** competing for the protein binding site with compound **25**) and the direct titration of the competitor (compound **25** binding to protein) to fit for *K_D*, ΔH° and *N* were fitted from direct titrations of **10b–e**, **10g**, or **10j** into protein. For the compounds **3**, **9**, and **25** binding to protein all variables could be determined from a global analysis of the direct titration.

The thermodynamic parameters were calculated with the following equation (eq 2):

$$\Delta G^{\circ} = \Delta H^{\circ} - T\Delta S^{\circ} = RT \ln K_{\text{D}} = -RT \ln K_{\text{A}} \quad (2)$$

where ΔG° , ΔH° , and ΔS° are the changes in free energy, enthalpy, and entropy of binding, respectively, *T* is the absolute temperature, and *R* is the universal gas constant (8.314 J mol⁻¹ K⁻¹). The 95% confidence intervals of the measurements were calculated for the two variables *K_D* and ΔH° with the one-dimensional error surface projection within the SEDPHAT software.

Calculation of the Free Energy of Desolvation. The three-dimensional representation for each of the aglycons (4-methoxybiphenyl scaffold, Figure 8) was built in the Maestro⁸⁷ modeling environment, and the global minimum conformation was identified by performing 500 iterations of the mixed torsional/low-mode conformational sampling in combination with the OPLS-2005 force-field and the implicit solvent model (water) as implemented in the MacroModel

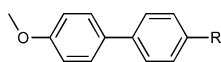


Figure 8. 4-Methoxybiphenyl scaffold of aglycons.

9.9.⁸⁸ The global minimum structures were used as input for the AMSOL 7.1 program⁸⁹ to obtain the free energy of desolvation ΔG_{des} (Table 5) with the SMS.4A solvation model⁹⁰ and the AM1⁹¹ level of theory (used keywords “AM1 SMS.4A SOLVNT=WATER TRUES”).

Table 5. Aqueous Free Energy of Desolvation

R	ΔG_{des} [kJ/mol]
neutral	
H	15.6
CONHCH ₃	39.9
COOCH ₃	23.0
SO ₂ NHCH ₃	65.5
SO ₂ CH ₃	56.4
4-morpholineamide	45.3
CN	22.0
deprotonated	
COO ⁻	298.2
SO ₂ -N ⁻ -Me	342.0

Determination of the MAC₉₀ by Flow Cytometry. The MAC₉₀ was determined in principle as in the previously published flow cytometry assay⁷⁹ but with some modifications. The human epithelial bladder carcinoma cell line 5637 (DSMZ, Braunschweig, Germany) was grown in RPMI 1640 medium, supplemented with 10% fetal calf serum (FCS), 100 U/mL penicillin, and 100 $\mu\text{g}/\text{mL}$ streptomycin at 37 °C, 5% CO₂. All solutions were purchased from Invitrogen (Basel, Switzerland). The cells were subcultured 1:6 twice per week [using trypsin/EDTA (Sigma-Aldrich) for the detachment]. Two days before infection, 1.8×10^5 cells were seeded in each well of a 24-well plate in RPMI 1640 containing 10% FCS without antibiotics. The cell density was approximately $(3-5) \times 10^5$ cells/well at the assay day.

For infection, the GFP-expressing clinical *E. coli* isolate UTI89⁹² (UTI89 wt) and the GFP-expressing FimA-H knockout strain UTI89 $\Delta\text{fimA-H}$ were used (strains were provided by Prof. Urs Jenal, Biocenter, University of Basel, Switzerland).⁹³ Bacteria were cultivated at 37 °C in 10 mL Luria–Bertani (LB) broth (Becton, Dickinson and Company) overnight, harvested by centrifugation (3800 rpm, 10 min), and washed three times in phosphate buffered saline (PBS, Sigma-Aldrich), and a bacterial solution of OD₆₀₀ of 0.75 in RPMI + 10% FCS was prepared. For the determination of the MAC₉₀ value, the IC₉₀, linear dilutions of the FimH antagonist were prepared in 5% DMSO and PBS. Bacteria and antagonists were preincubated for 10 min at 37 °C, before cells were infected with either only 200 μL of bacterial solution of UTI89 or UTI89 $\Delta\text{fimA-H}$ (positive and negative controls), or 225 μL of the preincubated bacteria–antagonist mixture. Infection lasted for 1.5 h. During this time infected cells were incubated at 37 °C. Then, cells were washed with PBS and detached from wells by the addition of 150 μL of trypsin and incubation at 37 °C for 10 min, before flushing from wells PBS containing 2% FCS and transferred to tubes. To dilute the trypsin, cells were centrifuged at 13 000 rpm, 1 min, 600 μL of the supernatant was discarded, and the pellet was resuspended in the remaining 300 μL of PBS containing 2% FCS. Samples were stored on ice until measurement. Before analysis with the flow cytometer (Becton Dickinson, FACSCanto II), the samples were gently mixed and filtered using a 35 μm nylon mesh (Corning Life Sciences) to prevent cellular aggregation. Cells were gated with linear scaling for side scatter (SSC) and forward scatter (FSC) and GFP intensity of live cells was evaluated. IC₉₀ values were determined by plotting the concentration of the antagonist in a logarithmic mode versus the mean fluorescence intensity (MFI) of living cells and by fitting a dose–response curve (variable slope, four parameters) with the Prism software (GraphPad Prism).

X-ray Analysis of the Antagonists 10e and 10j Cocrystallized with FimH-CRD.

FimH-CRD/10e Cocrystallization. Initial FimH-CRD (18 mg/mL in 20 mM HEPES, pH 7.4) crystals were obtained in complex with 4-(5-nitroindolin-1-yl)phenyl α -D-mannopyranoside (5 mM).²³ Crystals were grown in sitting-drop vapor diffusion at 20 °C with 200 nL of protein–antagonist mixture together with 200 nL of precipitant solution in well D3 (0.2 M sodium phosphate monobasic monohydrate, 20% w/v PEG 3,350) of the PEG/Ion HT screen (Hampton Research, CA, USA). Cubic crystals appeared within 1 week, which served as cross-seeding crystals. A solution of FimH-CRD (20 mg/mL) and 10e (5 mM) was mixed with 0.2 M sodium phosphate monobasic monohydrate, 20% w/v PEG 400 with 0.5 μL of each solution. Streak-seeding was performed after 1 day of incubation. Cubic FimH-CRD/10e crystals formed within 24 h. Crystals were flash cooled to 100 K with perfluoropolyether cryo oil (Hampton Research, CA, USA) as cryoprotectant. Data were collected with synchrotron radiation ($\lambda = 0.99999 \text{ \AA}$) at the PXIII beamline, Swiss Light Source, Switzerland.

FimH-CRD/10j Cocrystallization. Cocrystals were initially grown in sitting-drop vapor diffusion at 20 °C with 0.5 μL of a mixture of FimH-CRD (20 mg/mL) and 10j (5 mM) together with 0.5 μL of 0.1 M HEPES, pH 7.5, 2 M ammonium sulfate. Platelike crystals formed within 2 weeks and were used as seeds for subsequent crystallization. Diffraction quality crystals were grown by streak-seeding in 0.5 μL of FimH-CRD (10 mg/mL) with 10j (2.5 mM) and 0.5 μL of 0.1 M HEPES, pH 7.5, 1.25 M ammonium sulfate. The drops were covered with perfluoropolyether cryo oil prior to flash cooling to 100 K. Data were collected with synchrotron radiation ($\lambda = 1.00003 \text{ \AA}$) at the PXIII beamline, Swiss Light Source, Switzerland.

Structure Determination and Refinement. Data were indexed and integrated with the XDS package⁹³ for the FimH-CRD/10e cocrystal structure, and with mosflm⁹⁴ for the FimH-CRD/10j cocrystal structure (Table 6). Scaling was performed with XDS and SCALA included in the CCP4 suite, respectively.⁹⁵ Structures were solved by molecular

Table 6. Data Collection and Refinement Statistics for FimH-CRD/10e and FimH-CRD/10j Cocrystals

	FimH-CRD/10e	FimH-CRD/10j
PDB code	4CSS	4CST
space group	<i>P</i> ₂ ₁ ₂ ₁	<i>P</i> ₂ ₁ ₂ ₁
no. of molecules in the asymmetric unit	1	1
Cell Dimensions		
<i>a</i> , <i>b</i> , <i>c</i> (Å)	48.38, 56.23, 61.59	48.84, 55.89, 61.00
α , β , γ (deg)	90, 90, 90	90, 90, 90
Data Collection		
beamline	Swiss Light Source PXIII	Swiss Light Source PXIII
resolution range (Å) ^a	30.0–1.07 (1.13–1.07)	23.5–1.10 (1.12–1.10)
unique observations ^a	72000 (9354)	66470 (2500)
average multiplicity ^a	10.9 (3.7)	5.4 (2.4)
completeness (%)	96.1 (78.0)	97.2 (76.5)
<i>R</i> _{merge} ^a	0.056 (0.57)	0.051 (0.305)
mean <i>I</i> / σ (<i>I</i>) ^a	21.5 (2.22)	15.5 (2.9)
Refinement		
resolution range (Å)	15.7–1.07	23.5–1.10
<i>R</i> , <i>R</i> _{free}	11.2, 13.2	11.4, 13.0
rms deviation from ideal bond length (Å)	0.010	0.010
rms deviation from ideal bond angle (deg)	1.170	1.420

^aValues in parentheses are for highest-resolution shell.

replacement with PHASER⁹⁶ using the FimH-CRD-butyl α -D-mannopyranoside complex (PDB code 1UWF) as search model. The structures were iteratively built using the COOT software⁹⁷ and refined with the PHENIX software.⁹⁸ Geometric restraints for **10e** and **10j** were generated with PRODRG.⁹⁹ The models were validated using molprobity.¹⁰⁰ Residues 113–115 were not modeled in the **10e** structure because of disorder. Furthermore, the ligand was modeled in two possible conformations. For both ligands, electron density is reduced on the second aromatic ring because of flexibility of the ligand.

Physicochemical and in Vitro Pharmacokinetic Studies.

Materials. Dimethyl sulfoxide (DMSO), 1-propanol, 1-octanol, Dulbecco's modified Eagle medium (DMEM)–high glucose, L-glutamine solution, penicillin–streptomycin solution, Dulbecco's phosphate buffered saline (DPBS), trypsin–EDTA solution, magnesium chloride hexahydrate, and reduced nicotinamide adenine dinucleotide phosphate (NADPH) were purchased from Sigma-Aldrich. MEM nonessential amino acid (MEM-NEAA) solution, fetal bovine serum (FBS), and DMEM without sodium pyruvate and phenol red were bought from Invitrogen (Carlsbad, CA, USA). PRISMA HT universal buffer, GIT-0 Lipid Solution, and Acceptor Sink Buffer were ordered from pIon (Woburn, MA, USA). Human plasma was bought from Biopredic (Rennes, France), and acetonitrile (MeCN) and methanol (MeOH) were from Acros Organics (Geel, Belgium). Pooled male rat liver microsomes were purchased from BD Bioscience (Franklin Lakes, NJ, USA). Tris(hydroxymethyl)aminomethane (TRIS) was obtained from AppliChem (Darmstadt, Germany). The Caco-2 cells were kindly provided by Prof. G. Imanidis, FHNW, Muttentz, and originated from the American Type Culture Collection (Rockville, MD, USA).

pK_a . The pK_a values were determined as described elsewhere.¹⁰¹ In brief, the pH of a sample solution was gradually changed and the chemical shift of protons adjacent to ionizable centers was monitored by ¹H nuclear magnetic resonance (NMR) spectroscopy. The shift was plotted against the pH of the respective sample, and the pK_a was read out from the inflection point of the resulting sigmoidal curve.

$\log D_{7.4}$. The in silico prediction tool ALOGPS¹⁰² was used to estimate $\log P$ values of the compounds. Depending on these values, the compounds were classified into three categories: hydrophilic compounds ($\log P$ below zero), moderately lipophilic compounds ($\log P$ between zero and one), and lipophilic compounds ($\log P$ above one). For each category, two different ratios (volume of 1-octanol to volume of buffer) were defined as experimental parameters (Table 7).

Table 7. Compound Classification Based on Estimated $\log P$ Values

compd type	$\log P$	ratio (1-octanol/buffer)
hydrophilic	<0	30:140, 40:130
moderately lipophilic	0–1	70:110, 110:70
lipophilic	>1	3:180, 4:180

Equal amounts of phosphate buffer (0.1 M, pH 7.4) and 1-octanol were mixed and shaken vigorously for 5 min to saturate the phases. The mixture was left until separation of the two phases occurred, and the buffer was retrieved. Stock solutions of the test compounds were diluted with buffer to a concentration of 1 μ M. For each compound, six determinations, that is, three determinations per 1-octanol/buffer ratio, were performed in different wells of a 96-well plate. The respective volumes of buffer containing analyte (1 μ M) were pipetted to the wells and covered by saturated 1-octanol according to the chosen volume ratio. The plate was sealed with aluminum foil, shaken (1350 rpm, 25 °C, 2 h) on a Heidolph Titramax 1000 plate-shaker (Heidolph Instruments GmbH & Co. KG, Schwabach, Germany), and centrifuged (2000 rpm, 25 °C, 5 min, 5804 R Eppendorf centrifuge, Hamburg, Germany). The aqueous phase was transferred to a 96-well plate for analysis by LC–MS.

The $\log D_{7.4}$ coefficient was calculated from the 1-octanol/buffer ratio (o/b), the initial concentration of the analyte in buffer (1 μ M), and the concentration of the analyte in buffer (c_B) with eq 3:

$$\log D_{7.4} = \log \left(\frac{1 \mu\text{M} - c_B}{c_B} \frac{1}{o/b} \right) \quad (3)$$

Aqueous Solubility. Solubility was determined in a 96-well format using the μ SOL Explorer solubility analyzer (pIon, version 3.4.0.5). For each compound, measurements were performed at pH 3.0 and 7.4 in triplicate. For this purpose, six wells of a deep well plate, that is, three wells per pH value, were filled with 300 μ L of PRISMA HT universal buffer, adjusted to pH 3.0 or 7.4 by adding the requested amount of NaOH (0.5 M). Aliquots (3 μ L) of a compound stock solution (10–50 mM in DMSO) were added and thoroughly mixed. The final sample concentration was 0.1–0.5 mM, and the residual DMSO concentration was 1.0% (v/v) in the buffer solutions. After 15 h, the solutions were filtered (0.2 μ m 96-well filter plates) using a vacuum to collect manifold (Whatman Ltd, Maidstone, U.K.) to remove the precipitates. Equal amounts of filtrate and 1-propanol were mixed and transferred to a 96-well plate for UV/vis detection (190–500 nm, SpectraMax 190). The amount of material dissolved was calculated by comparison with UV/vis spectra obtained from reference samples, which were prepared by dissolving compound stock solution in a 1:1 mixture of buffer and 1-propanol (final concentrations 0.017–0.083 mM).

Parallel Artificial Membrane Permeation Assay (PAMPA). Effective permeability ($\log P_e$) was determined in a 96-well format with the PAMPA.⁶⁰ For each compound, measurements were performed at pH 5.0 and 7.4 in quadruplicates. Eight wells of a deep well plate, that is, four wells per pH value, were filled with 650 μ L of PRISMA HT universal buffer adjusted to pH 5.0 or 7.4 by adding the requested amount of NaOH (0.5 M). Samples (150 μ L) were withdrawn from each well to determine the blank spectra by UV/vis spectroscopy (190–500 nm, SpectraMax 190). Then analyte dissolved in DMSO was added to the remaining buffer to yield 50 μ M solutions. To exclude precipitation, the optical density was measured at 650 nm, with 0.01 being the threshold value. Solutions exceeding this threshold were filtered. Afterward, samples (150 μ L) were withdrawn to determine the reference spectra. Further 200 μ L was transferred to each well of the donor plate of the PAMPA sandwich (pIon, P/N 110163). The filter membranes at the bottom of the acceptor plate were infused with 5 μ L of GIT-0 lipid solution, and 200 μ L of Acceptor Sink Buffer was filled into each acceptor well. The sandwich was assembled, placed in the GutBox, and left undisturbed for 16 h. Then it was disassembled and samples (150 μ L) were transferred from each donor and acceptor well to UV plates for determination of the UV/vis spectra. Effective permeability ($\log P_e$) was calculated from the compound flux deduced from the spectra, the filter area, and the initial sample concentration in the donor well with the aid of the PAMPA Explorer software (pIon, version 3.5).

Colorectal Adenocarcinoma (Caco-2) Cell Permeation Assay. Caco-2 cells were cultivated in tissue culture flasks (BD Biosciences) with DMEM high glucose medium, containing L-glutamine (2 mM), nonessential amino acids (0.1 mM), penicillin (100 U/mL), streptomycin (100 μ g/mL), and fetal bovine serum (10%). The cells were kept at 37 °C in humidified air containing 5% CO₂, and the medium was changed every second day. When approximately 90% confluence was reached, the cells were split in a 1:10 ratio and distributed to new tissue culture flasks. At passage numbers between 60 and 65, they were seeded at a density of 5.3×10^5 cells per well to Transwell six-well plates (Corning Inc.) with 2.5 mL of culture medium in the basolateral and 1.8 mL in the apical compartment. The medium was renewed on alternate days. Permeation experiments were performed between days 19 and 21 after seeding. Prior to the experiment, the integrity of the Caco-2 monolayers was evaluated by measuring the transepithelial electrical resistance (TEER) with an Endohm tissue resistance instrument (World Precision Instruments Inc., Sarasota, FL, USA). Only wells with TEER values higher than 250 Ω cm² were used. Experiments were performed in the apical-to-basolateral (absorptive) and basolateral-to-apical (secretory) directions in triplicate. Transport medium (DMEM without sodium pyruvate and phenol red) was withdrawn from the donor compartments of three wells and replaced by the same volume of compound stock solution (10 mM in DMSO) to reach an initial sample concentration of 62.5 μ M. The Transwell plate was then shaken (600 rpm, 37 °C) on a Heidolph

Titramax 1000 plate-shaker. Samples (40 μL) were withdrawn from the donor and acceptor compartments 30 min after initiation of the experiment, and the compound concentrations were determined by LC–MS (see below). Apparent permeability (P_{app}) was calculated according to eq 4:

$$P_{\text{app}} = \frac{dQ}{dt} \frac{1}{Ac_0} \quad (4)$$

where dQ/dt is the compound flux (mol s^{-1}), A is the surface area of the monolayer (cm^2), and c_0 is the initial concentration in the donor compartment (mol cm^{-3}).⁶⁰ After the experiment, TEER values were assessed again for each well and results from wells with values below 250 $\Omega \text{ cm}^2$ were discarded.

Plasma Protein Binding (PPB). PPB was determined in a 96-well format using a high throughput dialysis block (HTD96b; HTDialysis LCC, Gales Ferry, CT, USA). For each compound, measurements were performed in triplicate. Dialysis membranes (MWCO 12–14 K; HTDialysis LCC) were hydrated according to the instructions of the manufacturer and placed into the dialysis block. Human plasma was centrifuged (5800 rpm, 5 $^{\circ}\text{C}$, 10 min), the pH of the supernatant (without floating plasma lipids) was adjusted to 7.4 by adding the requested amount of HCl (4 M), and analyte was added to yield a final concentration of 10 μM . Equal volumes (150 μL) of plasma containing the analyte or TRIS-HCl buffer (0.1 M, pH 7.4) were transferred to the compartments separated by the dialysis membrane. The block was covered with a sealing film and left undisturbed (5 h, 37 $^{\circ}\text{C}$). Afterward, samples (90 μL) were withdrawn from the buffer compartments and diluted with plasma (10 μL). From the plasma compartments, samples (10 μL) were withdrawn and diluted with TRIS-HCl buffer (90 μL). The solutions were further diluted with ice-cooled MeCN (300 μL) to precipitate the proteins and centrifuged (3600 rpm, 4 $^{\circ}\text{C}$, 10 min). The supernatants (50 μL) were retrieved, and the analyte concentrations were determined by LC–MS (see below). The fraction bound (f_b) was calculated as follows (eq 5):

$$f_b = 1 - \frac{c_b}{c_p} \quad (5)$$

where c_b is the concentration of the analyte withdrawn from the buffer compartment before dilution and c_p is the concentration in the plasma compartment. The values were accepted if the recovery of analyte was between 80% and 120% of the initial amount.

Cytochrome P450 Mediated Metabolism. Incubations consisted of pooled male rat liver microsomes (0.5 mg microsomal protein/mL), test compound (2 μM), MgCl_2 (2 mM), and NADPH (1 mM) in a total volume of 300 μL TRIS-HCl buffer (0.1 M, pH 7.4) and were performed in a 96-well plate on a Thermomixer Comfort (Eppendorf). Compounds and microsomes were preincubated (37 $^{\circ}\text{C}$, 700 rpm, 10 min) before NADPH was added. Samples (50 μL) at $t = 0$ min and after an incubation time of 5, 10, 20, and 30 min were quenched with 150 μL of ice-cooled MeOH, centrifuged (3600 rpm, 4 $^{\circ}\text{C}$, 10 min), and 80 μL of supernatant was transferred to a 96-well plate for LC–MS analysis (see below). The metabolic half-life ($t_{1/2}$) was calculated from the slope of the linear regression from the log percentage remaining compound versus incubation time relationship. Control experiments without NADPH were performed in parallel.

LC–MS Measurements. Analyses were performed using an 1100/1200 series HPLC system coupled to a 6410 triple quadrupole mass detector (Agilent Technologies, Inc., Santa Clara, CA, USA) equipped with electrospray ionization. The system was controlled with the Agilent MassHunter Workstation Data Acquisition software (version B.01.04). The column used was an Atlantis T3 C18 column (2.1 mm \times 50 mm) with a 3 μm particle size (Waters Corp., Milford, MA, USA). The mobile phase consisted of eluent A (H_2O containing 0.1% formic acid (for 10a–f, h, i), or 10 mM ammonium acetate, pH 5.0 in 95:5, $\text{H}_2\text{O}/\text{MeCN}$ (for 10g, j)) and eluent B (MeCN containing 0.1% formic acid). The flow rate was maintained at 0.6 mL/min. The gradient was ramped from 95% A/5% B to 5% A/95% B over 1 min and then held at 5% A/95% B for 0.1 min. The system was then brought back to 95% A/5% B, resulting in a total duration of 4 min. MS parameters such as fragmentor voltage,

collision energy, polarity were optimized individually for each analyte, and the molecular ion was followed for each compound in the multiple reaction monitoring mode. The concentrations of the analytes were quantified by the Agilent Mass Hunter Quantitative Analysis software (version B.01.04).

In Vivo Studies. Animals. Female C3H/HeN mice weighing between 19 and 25 g were obtained from Charles River Laboratories (Sulzfeld, Germany) or Harlan (Venray, The Netherlands) and were housed three or four per cage. The mice were kept under specific pathogen-free conditions in the Animal House of the Department of Biomedicine, University Hospital of Basel, and animal experimentation guidelines according to the regulations of the Swiss veterinary law were followed. After 7 days of acclimatization, 9- to 10-week-old mice were used for the studies. Animals had free access to chow and water at any time and were kept in a 12 h/12 h light/dark cycle. For administration volumes and sampling the good practice guidelines were followed.¹⁰³

Pharmacokinetic Studies. The single-dose studies for the first experiment set were performed by intravenous application of FimH antagonists at a dosage of 50 mg/kg body weight, followed by plasma and urine sampling. Antagonists were diluted in PBS (Sigma-Aldrich) for injection into the tail vein. Blood and urine samples (10 μL) were taken at 6 and 30 min and at 1, 2, 4, 6, and 8 h after injection. For the PK studies with 10j, the antagonist was dissolved in PBS with 5% DMSO (Sigma-Aldrich) and injected into the tail vein (0.625 mg/kg) or given orally (1.25 mg/kg) using a gavage (syringes from BD Micro Fine, U-100 Insuline, 30 G with BD Microlance 3, 25 G needles, Becton Dickinson and Soft-Ject, 1 mL syringes from Henke Sass Wolf; gavage from Fine Science Tools). Blood and urine were sampled (10 μL) after 7, 13, 20, 30, 45 min and after 1, 1.5, 2, 2.5, 3, 4, 6, 8, and 24 h. Both blood and urine samples were directly diluted after sampling with MeOH (Acros Organics) to precipitate the proteins and centrifuged for 11 min at 13 000 rpm. The supernatants were transferred to a 96-well plate (Agilent Technologies, 0.5 mL, polypropylene), and the analyte concentrations were determined by LC–MS (see above).

Infection Study. For all infection studies, the drinking water of the mice was replaced by water containing 5% glucose (monohydrate from AppliChem, BioChemica), 3 days before the start of the experiment. 10j was dosed at 1.25 mg/kg (in 5% DMSO and PBS) and 10 mg/kg (in 5% DMSO in PBS containing 1% Tween 80, all purchased from Sigma-Aldrich) and applied orally via gavage to six and four mice, respectively, as described in the section Pharmacokinetic Studies, 40 min prior to infection. Ciprofloxacin (Ciproxin solution, 2 mg/mL, Bayer) was dosed with 8 mg/kg, which would correspond to a human dose of 500 mg,⁸¹ subcutaneously 10 min prior to infection with UTI89 to 4 mice. The values for the control group (PBS, po) resulted from the infection of 11 mice. Four mice were orally treated with the formulation vehicle for 10j (5% DMSO in PBS containing 1% Tween 80) and termed controls formulation. Before infection, remaining urine in the bladder was expelled by gentle pressure on the abdomen. Mice were anesthetized in 2.5 vol % isoflurane/oxygen mixture (Attane, Minrad Inc., USA) and placed on their back. Infection was performed transurethrally using a polyethylene catheter (Intramedic polyethylene tubing, inner diameter 0.28 mm, outer diameter 0.61 mm, Becton Dickinson), on a syringe (Hamilton Gastight Syringe 50 μL , removable 30G needle, BGB Analytik AG, Switzerland). After gentle insertion of the catheter into the bladder, 50 μL of bacterial suspension of UTI89 (5.5×10^9 to 2.25×10^{10} CFU/mL) was slowly injected. This corresponded to approximately 10^7 – 10^8 CFU per mouse. Mice were killed by CO_2 3 h after inoculation, and bladder and kidneys were aseptically removed. Organs were homogenized in 1 mL of PBS using a tissue lyser (Retsch, Germany). Serial dilutions of bladder and kidneys were plated on Levine Eosin Methylene Blue Agar plates (Becton Dickinson), and CFUs were counted after overnight incubation at 37 $^{\circ}\text{C}$.

■ ASSOCIATED CONTENT

Supporting Information

HPLC data and chromatograms of target compounds and ¹H NMR spectra of the synthetic compounds. This material is available free of charge via the Internet at <http://pubs.acs.org>.

AUTHOR INFORMATION

Corresponding Author

*Phone: +41 61 267 15 51. Fax: +41 61 267 15 52. E-mail: beat.ernst@unibas.ch.

Author Contributions

[†]S.K., L.P., K.M., D.E., and A.S. contributed equally to the project.

Notes

The authors declare no competing financial interest.

ACKNOWLEDGMENTS

The authors thank Prof. Dr. med. Radek Skoda, Department of Biomedicine, University Hospital Basel, Switzerland, for giving us access to the animal facility. The financial support by the Swiss National Science Foundation (SNF Interdisciplinary Grant K-32K1-120904) is gratefully acknowledged.

ABBREVIATIONS USED

ΔH , change in enthalpy; ΔS , change in entropy; AUC, area under the curve; BSA, bovine serum albumin; C_{max} , maximal concentration; Caco-2, colorectal adenocarcinoma; CFU, colony forming unit; CL_{tot} , total clearance; CRD, carbohydrate recognition domain; C_0 , initial concentration; DL, detection limit; FITC, fluorescein isothiocyanate; FP, fluorescence polarization; ITC, isothermal titration calorimetry; iv, intravenous; K_D , dissociation constant; MAC_{90} , minimal antiadhesion concentration to inhibit 90% adhesion; PAMPA, parallel artificial membrane permeation assay; P_{app} , apparent permeability; PD, pharmacodynamics; P_e , effective permeability; PK, pharmacokinetics; po, per os; sc, subcutaneous; UPEC, uropathogenic *Escherichia coli*; UTI, urinary tract infection; V_d , volume of distribution in terminal phase

REFERENCES

- (1) Foxman, B.; Barlow, R.; D'Arcy, H.; Gillespie, B.; Sobel, J. D. Urinary tract infection: self-reported incidence and associated costs. *Ann. Epidemiol.* **2000**, *10*, 509–515.
- (2) Ronald, A. The etiology of urinary tract infection: traditional and emerging pathogens. *Am. J. Med.* **2002**, *113* (Suppl. 1A), 14S–19S.
- (3) Fihn, S. D. Acute uncomplicated urinary tract infection in women. *N. Engl. J. Med.* **2003**, *349*, 259–266.
- (4) Hooton, T. M.; Besser, R.; Foxman, B.; Fritsche, T. R.; Nicolle, L. E. Acute uncomplicated cystitis in an era of increasing antibiotic resistance: a proposed approach to empirical therapy. *Clin. Infect. Dis.* **2004**, *39*, 75–80.
- (5) Sanchez, G. V.; Master, R. N.; Karlowsky, J. A.; Bordon, J. M. In vitro antimicrobial resistance of urinary *Escherichia coli* isolates among U.S. outpatients from 2000 to 2010. *Antimicrob. Agents Chemother.* **2012**, *56*, 2181–2183.
- (6) Clatworthy, A. E.; Pierson, E.; Hung, D. T. Targeting virulence: a new paradigm for antimicrobial therapy. *Nat. Chem. Biol.* **2007**, *3*, 541–548.
- (7) Mulvey, M. A.; Schilling, J. D.; Martinez, J. J.; Hultgren, S. J. Bad bugs and beleaguered bladders: interplay between uropathogenic *Escherichia coli* and innate host defenses. *Proc. Natl. Acad. Sci. U.S.A.* **2000**, *97*, 8829–8835.
- (8) Schilling, J. D.; Mulvey, M. A.; Hultgren, S. J. Structure and function of *Escherichia coli* type 1 pili: new insight into the pathogenesis of urinary tract infections. *J. Infect. Dis.* **2001**, *183* (Suppl. 1), S36–S40.
- (9) Wiles, T. J.; Kulesus, R. R.; Mulvey, M. A. Origins and virulence mechanisms of uropathogenic *Escherichia coli*. *Exp. Mol. Pathol.* **2008**, *85*, 11–19.
- (10) Capitani, G.; Eidam, O.; Glockshuber, R.; Grütter, M. G. Structural and functional insights into the assembly of type 1 pili from *Escherichia coli*. *Microbes Infect.* **2006**, *8*, 2284–2290.
- (11) Le Trong, I.; Aprikian, P.; Kidd, B. A.; Forero-Shelton, M.; Tchesnokova, V.; Rajagopal, P.; Rodriguez, V.; Interlandi, G.; Klevit, R.; Vogel, V.; Stenkamp, R. E.; Sokurenko, E. V.; Thomas, W. E. Structural basis for mechanical force regulation of the adhesin FimH via finger trap-like β sheet twisting. *Cell* **2010**, *141*, 645–655.
- (12) Sharon, N. Carbohydrates as future anti-adhesion drugs for infectious diseases. *Biochim. Biophys. Acta* **2006**, *1760*, 527–537.
- (13) Firon, N.; Itzhak, O.; Sharon, N. Interaction of mannose-containing oligosaccharides with the fimbrial lectin of *Escherichia coli*. *Biochem. Biophys. Res. Commun.* **1982**, *105*, 1426–1432.
- (14) Firon, N.; Ofek, I.; Sharon, N. Carbohydrate specificity of the surface lectins of *Escherichia coli*, *Klebsiella pneumoniae*, and *Salmonella typhimurium*. *Carbohydr. Res.* **1983**, *120*, 235–249.
- (15) Bouckaert, J.; Berglund, J.; Schembri, M.; De Genst, E.; Cools, L.; Wührer, M.; Hung, C.-S.; Pinkner, J.; Slättegård, R.; Zavalov, A.; Choudhury, D.; Langermann, S.; Hultgren, S. J.; Wyns, L.; Klemm, P.; Oscarson, S.; Knight, S. D.; De Greve, H. Receptor binding studies disclose a novel class of high-affinity inhibitors of the *Escherichia coli* FimH adhesin. *Mol. Microbiol.* **2005**, *55*, 441–455.
- (16) Firon, N.; Ashkenazi, S.; Mirelman, D.; Ofek, I.; Sharon, N. Aromatic alpha-glycosides of mannose are powerful inhibitors of the adherence of type 1 fimbriated *Escherichia coli* to yeast and intestinal epithelial cells. *Infect. Immun.* **1987**, *55*, 472–476.
- (17) Sperl, O.; Fuchs, A.; Lindhorst, T. K. Evaluation of the carbohydrate recognition domain of the bacterial adhesin FimH. Design, synthesis and binding properties of mannoside ligands. *Org. Biomol. Chem.* **2006**, *4*, 3913–3922.
- (18) Han, Z.; Pinkner, J. S.; Ford, B.; Obermann, R.; Nolan, W.; Wildman, S. A.; Hobbs, D.; Ellenberger, T.; Cusumano, C. K.; Hultgren, S. J.; Janetka, J. W. Structure-based drug design and optimization of mannoside bacterial FimH antagonists. *J. Med. Chem.* **2010**, *53*, 4779–4792.
- (19) Klein, T.; Abgottspon, D.; Wittwer, M.; Rabbani, S.; Herold, J.; Jiang, X.; Kleeb, S.; Lüthi, C.; Scharenberg, M.; Bezençon, J.; Gubler, E.; Pang, L.; Smiesko, M.; Cutting, B.; Schwardt, O.; Ernst, B. FimH antagonists for the oral treatment of urinary tract infections: from design and synthesis to in vitro and in vivo evaluation. *J. Med. Chem.* **2010**, *53*, 8627–8641.
- (20) Cusumano, C. K.; Pinkner, J. S.; Han, Z.; Greene, S. E.; Ford, B. A.; Crowley, J. R.; Henderson, J. P.; Janetka, J. W.; Hultgren, S. J. Treatment and prevention of urinary tract infection with orally active FimH inhibitors. *Sci. Transl. Med.* **2011**, *3*, 109ra115.
- (21) Han, Z.; Pinkner, J. S.; Ford, B.; Chorem, E.; Crowley, J. M.; Cusumano, C. K.; Campbell, S.; Henderson, J. P.; Hultgren, S. J.; Janetka, J. W. Lead optimization studies on FimH antagonists: discovery of potent and orally bioavailable ortho-substituted biphenyl mannosides. *J. Med. Chem.* **2012**, *55*, 3945–3959.
- (22) Pang, L.; Kleeb, S.; Lemme, K.; Rabbani, S.; Scharenberg, M.; Zalewski, A.; Schädler, F.; Schwardt, O.; Ernst, B. FimH antagonists: structure–activity and structure–property relationships for biphenyl α -D-mannopyranosides. *ChemMedChem* **2012**, *7*, 1404–1422.
- (23) Jiang, X.; Abgottspon, D.; Kleeb, S.; Rabbani, S.; Scharenberg, M.; Wittwer, M.; Haug, M.; Schwardt, O.; Ernst, B. Anti-adhesion therapy for urinary tract infections—a balanced PK/PD profile proved to be key for success. *J. Med. Chem.* **2012**, *55*, 4700–4713.
- (24) Schwardt, O.; Rabbani, S.; Hartmann, M.; Abgottspon, D.; Wittwer, M.; Kleeb, S.; Zalewski, A.; Smiesko, M.; Cutting, B.; Ernst, B. Design, synthesis and biological evaluation of mannosyl triazoles as FimH antagonists. *Bioorg. Med. Chem.* **2011**, *19*, 6454–6473.
- (25) Brument, S.; Sivignon, A.; Dumych, T. I.; Moreau, N.; Roos, G.; Guéardel, Y.; Chalopin, T.; Deniaud, D.; Bilyy, R. O.; Darfeuille-Michaud, A.; Bouckaert, J.; Gouin, S. G. Thiazolylaminomannosides as potent antiadhesives of type 1 pilated *Escherichia coli* isolated from Crohn's disease patients. *J. Med. Chem.* **2013**, *56*, 5395–5406.
- (26) Lindhorst, T. K.; Kieburg, C.; Krallmann-Wenzel, U. Inhibition of the type 1 fimbriae-mediated adhesion of *Escherichia coli* to erythrocytes by multiantennary D-mannosyl clusters: the effect of multivalency. *Glycoconjugate J.* **1998**, *15*, 605–613.

- (27) Nagahori, N.; Lee, R. T.; Nishimura, S.-L.; Pagé, S.; Roy, R.; Lee, Y. C. Inhibition of adhesion of type 1 fimbriated *Escherichia coli* to highly mannosylated ligands. *ChemBioChem* **2002**, *3*, 836–844.
- (28) Appeldoorn, C. C. M.; Joosten, J. A. F.; Maate, F. A.; Dobrindt, U.; Hacker, J.; Liskamp, R. M. J.; Khan, A. S.; Pieters, R. J. Novel multivalent mannose compounds and their inhibition of the adhesion of type 1 fimbriated uropathogenic *E. coli*. *Tetrahedron: Asymmetry* **2005**, *16*, 361–372.
- (29) Patel, A.; Lindhorst, T. K. A modular approach for the synthesis of oligosaccharide mimetics. *Carbohydr. Res.* **2006**, *341*, 1657–1668.
- (30) Touaibia, M.; Wellens, A.; Shiao, T. C.; Wang, Q.; Sirois, S.; Bouckaert, J.; Roy, R. Mannosylated G(0) dendrimers with nanomolar affinities to *Escherichia coli* FimH. *ChemMedChem* **2007**, *2*, 1190–1201.
- (31) Durka, M.; Buffet, K.; Iehl, J.; Holler, M.; Nierengarten, J.-F.; Taganna, J.; Bouckaert, J.; Vincent, S. P. The functional valency of dodecamannosylated fullerenes with *Escherichia coli* FimH—towards novel bacterial antiadhesives. *Chem. Commun.* **2011**, *47*, 1321–1323.
- (32) Bouckaert, J.; Li, Z.; Xavier, C.; Almant, M.; Caveliers, V.; Lahoutte, T.; Weeks, S. D.; Kovensky, J.; Gouin, S. G. Heptyl α -D-mannosides grafted on a β -cyclodextrin core to interfere with *Escherichia coli* adhesion: an in vivo multivalent effect. *Chem.—Eur. J.* **2013**, *19*, 7847–7855.
- (33) Scharenberg, M.; Schwardt, O.; Rabbani, S.; Ernst, B. Target selectivity of FimH antagonists. *J. Med. Chem.* **2012**, *55*, 9810–9816.
- (34) Choudhury, D.; Thompson, A.; Stojanoff, V.; Langermann, S.; Pinkner, J.; Hultgren, S. J.; Knight, S. D. X-ray structure of the FimC-FimH chaperone-adhesin complex from uropathogenic *Escherichia coli*. *Science* **1999**, *285*, 1061–1066.
- (35) Hung, C.-S.; Bouckaert, J.; Hung, D.; Pinkner, J.; Widberg, C.; DeFusco, A.; Auguste, C. G.; Strouse, R.; Langermann, S.; Waksman, G.; Hultgren, S. J. Structural basis of tropism of *Escherichia coli* to the bladder drug in urinary tract infection. *Mol. Microbiol.* **2002**, *44*, 903–915.
- (36) Wellens, A.; Garofalo, C.; Nguyen, H.; Van Gerven, N.; Slättegård, R.; Henalsteens, J.-P.; Wyns, L.; Oscarson, S.; De Greve, H.; Hultgren, S. J.; Bouckaert, J. Intervening with urinary tract infections using anti-adhesives based on the crystal structure of the FimH-oligomannose-3 complex. *PLoS One* **2008**, *3*, e2040.
- (37) Wellens, A.; Lahmann, M.; Touaibia, M.; Vaucher, J.; Oscarson, S.; Roy, R.; Remaut, H.; Bouckaert, J. The tyrosine gate as a potential entropic lever in the receptor-binding site of the bacterial adhesin FimH. *Biochemistry* **2012**, *51*, 4790–4799.
- (38) Totsika, M.; Kostakioti, M.; Hannan, T. J.; Upton, M.; Beatson, S. A.; Janetka, J. W.; Hultgren, S. J.; Schembri, M. A. A FimH inhibitor prevents acute bladder infection and treats chronic cystitis caused by multidrug-resistant uropathogenic *Escherichia coli* ST131. *J. Infect. Dis.* **2013**, *208*, 921–928.
- (39) Meanwell, M. A. Synopsis of some recent tactical application of bioisosteres in drug design. *J. Med. Chem.* **2011**, *54*, 2529–2591.
- (40) Prieto, M.; Zurita, E.; Rosa, E.; Luño, L.; Lloyd-Williams, P.; Giral, E. Arylboronic acids and arylpinacolboronate esters in Suzuki coupling reactions involving indoles. Partner role swapping and heterocycle protection. *J. Org. Chem.* **2004**, *69*, 6812–6820.
- (41) Schulz, M. J.; Coats, S. J.; Hlasta, D. J. Microwave-assisted preparation of aryltetrazoleboronate esters. *Org. Lett.* **2004**, *6*, 3265–3268.
- (42) Devos, A.; Remion, J.; Frisque-Hesbain, A. M.; Colens, A.; Ghosez, L. Synthesis of acyl halides under very mild conditions. *J. Chem. Soc., Chem. Commun.* **1979**, 1180–1181.
- (43) Rabbani, S.; Jiang, X.; Schwardt, O.; Ernst, B. Expression of the carbohydrate recognition domain of FimH and development of a competitive binding assay. *Anal. Biochem.* **2010**, *407*, 188–195.
- (44) Waetherman, R. V.; Kiessling, L. L. Fluorescence anisotropy assay reveals affinities of C- and O-glycosides for concanavalin A. *J. Org. Chem.* **1996**, *61*, 534–538.
- (45) Cer, R. Z.; Mudunuri, U.; Stephens, R.; Lebeda, F. J. IC50-to-Ki: a web-based tool for converting IC50 to Ki values for inhibitors of enzyme activity and ligand binding. *Nucleic Acids Res.* **2009**, *37*, W441–W445.
- (46) Lynch, B. A.; Loiacono, K. A.; Tiong, C. L.; Adams, S. E.; MacNeil, I. A. A fluorescence polarization based Src-SH2 binding assay. *Anal. Biochem.* **1997**, *247*, 77–82.
- (47) Wu, P.; Brasseur, M.; Schindler, U. A high-throughput STAT binding assay using fluorescence polarization. *Anal. Biochem.* **1997**, *249*, 29–36.
- (48) Huang, X. Fluorescence polarization competition assay: the range of resolvable inhibitor potency is limited by the affinity of the fluorescent ligand. *J. Biomol. Screening* **2003**, *8*, 34–38.
- (49) Cooper, A. *Biophysical Chemistry*, 2nd ed.; RSC Publishing: Cambridge, U.K., 2011; pp 122–123.
- (50) Scharenberg, M.; Jiang, X.; Pang, L.; Navarra, G.; Rabbani, S.; Binder, F.; Schwardt, O.; Ernst, B. Kinetic properties of carbohydrate-lectin interactions: FimH antagonists. *ChemMedChem* **2014**, *9*, 78–83.
- (51) Cabani, S.; Gianni, P.; Mollica, V.; Lepori, L. Group contribution to the thermodynamic properties of non-ionic solutes in dilute aqueous solution. *J. Solution Chem.* **1981**, *10*, 563–595.
- (52) Hansch, C.; Leo, A.; Taft, R. W. A survey of Hammett substituent constants and resonance and field parameters. *Chem. Rev.* **1991**, *91*, 165–195.
- (53) Chen, A.; Wadso, I. Simultaneous determination of delta G, delta H and delta S by an automatic microcalorimetric titration technique: application to protein ligand binding. *J. Biochem Biophys Methods* **1982**, *6*, 307–316.
- (54) Freire, E.; Mayorga, O. L.; Straume, M. Isothermal titration calorimetry. *Anal. Chem.* **1990**, *62*, 950A–959A.
- (55) Wiseman, T.; Williston, S.; Brandts, J. F.; Lin, L.-N. Rapid measurement of binding constants and heats of binding using a new titration calorimeter. *Anal. Biochem.* **1989**, *179*, 131–137.
- (56) Turnbull, W. B.; Daranas, A. H. On the value of c: can low affinity systems be studied by isothermal titration calorimetry? *J. Am. Chem. Soc.* **2003**, *125*, 14859–14866.
- (57) Sigurskjold, B. W. Exact analysis of competition ligand binding by displacement isothermal titration calorimetry. *Anal. Biochem.* **2000**, *277*, 260–266.
- (58) Velazquez-Campoy, A.; Freire, E. Isothermal titration calorimetry to determine association constants for high-affinity ligands. *Nat. Protoc.* **2006**, *1*, 186–191.
- (59) Dearden, J. C.; Bresnen, G. M. The measurement of partition coefficients. *QSAR Comb. Sci.* **1988**, *7*, 133–144.
- (60) Kansy, M.; Senner, F.; Gubernator, K. Physicochemical high throughput screening: parallel artificial membrane permeation assay in the description of passive absorption processes. *J. Med. Chem.* **1998**, *41*, 1007–1010.
- (61) Hubatsch, I.; Ragnarsson, E. G. E.; Artursson, P. Determination of drug permeability and prediction of drug absorption in Caco-2 monolayers. *Nat. Protoc.* **2007**, *2*, 2111–2119.
- (62) Banker, M. J.; Clark, T. H.; Williams, J. A. Development and validation of a 96-well equilibrium dialysis apparatus for measuring plasma protein binding. *J. Pharm. Sci.* **2003**, *92*, 967–974.
- (63) Obach, R. S. Prediction of human clearance of twenty-nine drugs from hepatic microsomal intrinsic clearance data: an examination of in vitro half-life approach and nonspecific binding to microsomes. *Drug Metab. Dispos.* **1999**, *27*, 1350–1359.
- (64) Chaturvedi, P. R.; Decker, C. J.; Odinec, A. Prediction of pharmacokinetic properties using experimental approaches during early drug discovery. *Curr. Opin. Chem. Biol.* **2001**, *5*, 452–463.
- (65) Di, L.; Kerns, E. H. Profiling drug-like properties in discovery research. *Curr. Opin. Chem. Biol.* **2003**, *7*, 402–408.
- (66) Lipinski, C. A. Drug-like properties and the causes of poor solubility and poor permeability. *J. Pharmacol. Toxicol. Methods* **2000**, *44*, 235–249.
- (67) Curatolo, W. Physical chemical properties of oral drug candidates in the discovery and exploratory development settings. *Pharm. Sci. Technol. Today* **1998**, *1*, 387–393.
- (68) Ishikawa, M.; Hashimoto, Y. Improvement in aqueous solubility in small molecule drug discovery programs by disruption of molecular planarity and symmetry. *J. Med. Chem.* **2011**, *54*, 1539–1554.

- (69) Avdeef, A.; Bendels, S.; Di, L.; Faller, B.; Kansy, M.; Sugano, K.; Yamauchi, Y. PAMPA – critical factors for better predictions of absorption. *J. Pharm. Sci.* **2007**, *96*, 2893–2909.
- (70) Artursson, P.; Karlsson, J. Correlation between oral drug absorption in humans and apparent drug permeability coefficients in human intestinal epithelial (Caco-2) cells. *Biochem. Biophys. Res. Commun.* **1991**, *175*, 880–885.
- (71) Feng, B.; LaPerle, J. L.; Chang, G.; Varma, M. V. S. Renal clearance in drug discovery and development: molecular descriptors, drug transporters and disease state. *Expert Opin. Drug. Metab. Toxicol.* **2010**, *6*, 939–952.
- (72) Schmidt, S.; Gonzalez, D.; Derendorf, H. Significance of protein binding in pharmacokinetics and pharmacodynamics. *J. Pharm. Sci.* **2010**, *99*, 1107–1122.
- (73) Weisiger, R. A. Dissociation from albumin: A potentially rate-limiting step in the clearance of substances by the liver. *Proc. Natl. Acad. Sci. U.S.A.* **1985**, *82*, 1563–1567.
- (74) Smith, D. A.; Jones, B. C.; Walker, D. K. Design of drugs involving the concepts and theories of drug metabolism and pharmacokinetics. *Med. Res. Rev.* **1996**, *16*, 243–266.
- (75) Van de Waterbeemd, H.; Smith, D. A.; Beaumont, K.; Walker, D. K. Property-based design: optimization of drug absorption and pharmacokinetics. *J. Med. Chem.* **2001**, *44*, 1313–1333.
- (76) Varma, M. V. S.; Feng, B.; Obach, R. S.; Troutman, M. D.; Chupka, J.; Miller, H. R.; El-Kattan, A. Physicochemical determinants of human renal clearance. *J. Med. Chem.* **2009**, *52*, 4844–4852.
- (77) Waring, M. J. Lipophilicity in drug discovery. *Expert Opin. Drug Discovery* **2010**, *5*, 235–248.
- (78) Zhang, Y.; Huo, M.; Solver, P. K. An add-in program for pharmacokinetic and pharmacodynamic data analysis in Microsoft Excel. *Comput. Methods Programs Biomed.* **2010**, *99*, 306–314.
- (79) Scharenberg, M.; Abgottspon, D.; Cicek, E.; Jiang, X.; Schwarzt, O.; Rabbani, S.; Ernst, B. Cytometry-based assay for screening FimH antagonists. *Assay Drug Dev. Technol.* **2011**, *9*, 455–464.
- (80) Hooton, T. M. Fluoroquinolones and resistance in the treatment of uncomplicated urinary tract infection. *Int. J. Antimicrob. Agents* **2003**, *22*, 65–72.
- (81) Jakobsen, L.; Cattoir, V.; Jensen, K. S.; Hammerum, A. M.; Nordmann, P.; Frimodt-Møller, N. Impact of low-level fluoroquinolone resistance genes *qnrA1*, *qnrB19*, and *qnrS1* on ciprofloxacin treatment of isogenic *Escherichia coli* strains in a murine urinary tract infection model. *J. Antimicrob. Chemother.* **2012**, *67*, 2438–2444.
- (82) Mulvey, M. A. Adhesion and entry of uropathogenic *Escherichia coli*. *Cell. Microbiol.* **2002**, *4*, 257–271.
- (83) Ballatore, C.; Huryn, D. M.; Smith, A. B. Carboxylic acid (bio)isosteres in drug design. *ChemMedChem* **2013**, *8*, 385–395.
- (84) Justice, S. S.; Hung, C.; Theriot, J. A.; Fletcher, D. A.; Anderson, G. G.; Footer, M. J.; Hultgren, S. J. Differentiation and developmental pathways of uropathogenic *Escherichia coli* in urinary tract pathogenesis. *Proc. Natl. Acad. Sci. U.S.A.* **2004**, *101*, 1333–1338.
- (85) Mulvey, M. A.; Schilling, J. D.; Hultgren, S. J. Establishment of a persistent *Escherichia coli* reservoir during the acute phase of a bladder infection. *Infect. Immun.* **2001**, *69*, 4572–9.
- (86) Houtman, J. C.; Brown, P. C.; Bowden, B.; Yamaguchi, H.; Appella, E.; Samelson, L. E.; Schuck, P. Studying multisite binary and ternary protein interactions by global analysis of isothermal titration calorimetry data in SEDPHAT: application to adaptor protein complexes in cell signaling. *Protein Sci.* **2007**, *16*, 30–42.
- (87) *Maestro*, version 9.3; Schrödinger, LLC: New York, NY, 2012.
- (88) *MacroModel*, version 9.9; Schrödinger, LLC: New York, NY, 2012.
- (89) Hawkins, G. D.; Giesen, D. J.; Lynch, G. C.; Chambers, C. C.; Rossi, I.; Storer, J. W.; Li, J.; Thompson, J. D.; Winget, P.; Lynch, B. J.; Rinaldi, D.; Liotard, D. A.; Cramer, C. J.; Truhlar, D. G. *AMSOL*, version 7.1; University of Minnesota: Minneapolis, MN, 2003; based in part on the following: Liotard, D. A.; Healy, E. F.; Ruiz, J. M.; Dewar, M. J. S. *AMPAC*, version 2.1; Semichem, Inc.: Shawnee, KS.
- (90) Chambers, C. C.; Hawkins, G. D.; Cramer, C. J.; Truhlar, D. G. Model for aqueous solvation based on class IV atomic charges and first solvation shell effects. *J. Phys. Chem.* **1996**, *100*, 16385–16398.
- (91) Dewar, M. J. S.; Zoebisch, E. G.; Healy, E. F.; Stewart, J. J. P. AM1: a new general purpose quantum mechanical molecular model. *J. Am. Chem. Soc.* **1993**, *115*, 5348–5348 [Erratum to *J. Am. Chem. Soc.* **1985**, *107*, 3902–3909].
- (92) Mulvey, M. A.; Schilling, J. D.; Hultgren, S. J. Establishment of a persistent *Escherichia coli* reservoir during the acute phase of a bladder infection. *Infect. Immun.* **2001**, *69*, 4572–4579.
- (93) Kabsch, W. Automatic processing of rotation diffraction data from crystals of initially unknown symmetry and cell constants. *J. Appl. Crystallogr.* **1993**, *26*, 795–800.
- (94) Leslie, A. G. W. The integration of macromolecular diffraction data. *Acta Crystallogr. D* **2006**, *62*, 48–57.
- (95) Winn, M. D.; Ballard, C. C.; Cowtan, K. D.; Dodson, E. J.; Emsley, P.; Evans, P. R.; Keegan, R. M.; Krissinel, E. B.; Leslie, A. G. W.; McCoy, A.; McNicholas, S. J.; Murshudov, G. N.; Pannu, N. S.; Potterton, E. A.; Powell, H. R.; Read, R. J.; Vagin, A.; Wilson, K. S. Overview of the CCP4 suite and current developments. *Acta Crystallogr. D* **2011**, *67*, 235–242.
- (96) McCoy, A. J. Solving structures of protein complexes by molecular replacement with Phaser. *Acta Crystallogr. D* **2007**, *63*, 32–41.
- (97) Emsley, P.; Cowtan, K. Coot: model-building tools for molecular graphics. *Acta Crystallogr. D* **2004**, *60*, 2126–2132.
- (98) Adams, P. D.; Grosse-Kunstleve, R. W.; Hung, L.-W.; Ioerger, T. R.; McCoy, A. J.; Moriarty, N. W.; Read, R. J.; Sacchettini, J. C.; Sauter, N. K.; Terwilliger, T. C. PHENIX: building new software for automated crystallographic structure determination. *Acta Crystallogr., Sect. D: Biol. Crystallogr.* **2002**, *58*, 1948–1954.
- (99) van Aalten, D. M. F.; Bywater, R.; Findlay, J. B. C.; Hendlich, M.; Hoof, R. W. W.; Vriend, G. PRODRG, a program for generating molecular topologies and unique molecular descriptors from coordinates of small molecules. *J. Comput.-Aided Mol. Des.* **1996**, *10*, 255–262.
- (100) Chen, V. B.; Arendall, W. B.; Headd, J. J.; Keedy, D. A.; Immormino, R. M.; Kapral, G. J.; Murray, L. W.; Richardson, J. S.; Richardson, D. C. MolProbity: all-atom structure validation for macromolecular crystallography. *Acta Crystallogr. D* **2010**, *66*, 12–21.
- (101) Bezençon, J.; Wittwer, M. B.; Cutting, B.; Smiesko, M.; Wagner, B.; Kansy, M.; Ernst, B. pK_a determination by 1H NMR spectroscopy—an old methodology revisited. *J. Pharm. Biomed. Anal.* **2014**, *93*, 147–155.
- (102) (a) VCCLAB, Virtual Computational Chemistry Laboratory, 2005. <http://www.vcclab.org> (accessed August 14, 2012). (b) Tetko, I. V.; Gasteiger, J.; Todeschini, R.; Mauri, A.; Livingstone, D.; Ertl, P.; Palyulin, V. A.; Radchenko, E. V.; Zefirov, N. S.; Makarenko, A. S.; Tanchuk, V. Y.; Prokopenko, V. V. Virtual computational chemistry laboratory—design and description. *J. Comput.-Aided Mol. Des.* **2005**, *19*, 453–463.
- (103) Diehl, K.-H.; Hull, R. A. Good practice guide to the administration of substances and removal of blood, including routes and volumes. *J. Appl. Toxicol.* **2001**, *21*, 15–23.

2.8 Chapter 7: Prodrugability of Carbohydrates – Investigations on FimH Antagonists

The following chapter specifically addresses the low membrane permeability of the *para*-(methylsulfonyl)biphenyl α -D-mannopyranoside. By introducing short-chain acyl promoieties at the C-6 position of biphenyl α -D-mannopyranoside, prodrugs with an excellent absorption potential were obtained. The human carboxylesterase 2 was identified as a main enzyme mediating rapid bioconversion to the active principle. Despite their propensity to hydrolysis within the enterocytes during absorption, these ester prodrugs present a considerable progress in the development of orally available FimH antagonists.

Contribution to the project:

Simon Kleeb performed all experiment regarding the physicochemical and *in vitro* pharmacokinetic characterization of the various ester prodrugs. He established and performed the assays for exploring the enzyme-mediated transformation of the prodrugs to the pharmacologically active parent compound and interpreted the resulting data. He was responsible for the writing of the chapter with exception of the synthesis section.

Wojciech Schönemann and Philipp Dätwyler synthesized all the tested compounds and were responsible for the writing of the synthesis section. Furthermore, Wojciech Schönemann revised the manuscript.

Abbreviations:

BNPP, bis(4-nitrophenyl) phosphate; Caco-2 cells, colorectal adenocarcinoma cells; CES, carboxylesterase; CRD, carbohydrate recognition domain; hCE1, human carboxylesterase isotype 1; hCE2, human carboxylesterase isotype 2; HLM, human liver microsomes; P , octanol-water partition coefficient; P_{app} , apparent permeability; P_e , effective permeability; PAMPA, parallel artificial membrane permeability assay; PPB, plasma protein binding; RLM, rat liver microsomes; UPEC, uropathogenic *Escherichia coli*; UTI, urinary tract infection.

Introduction

Urinary tract infection primarily caused by uropathogenic *Escherichia coli* (UPEC) is among the most prevalent infectious diseases, requiring an antibiotic treatment.^[1] Frequent and repeated use of antibiotics can lead to antimicrobial resistance and treatment failure, which manifests the need for alternative therapeutic strategies.^[2] Bacterial adhesion to the bladder cell surface is crucial for the infection cycle, because it prevents the bacteria from being washed out by the bulk flow of urine and enables UPEC to colonize urothelial cells.^[3] This initial interaction is mediated by the mannose-specific lectin FimH localized at the tip of the bacterial type 1 pili.^[4] FimH encloses a carbohydrate recognition domain (CRD) which specifically targets the mannosylated glycoprotein uroplakin Ia on the urothelial cell surface and a pilin domain regulating the switch between the low and high affinity states of the CRD.^[5]

For more than three decades, FimH antagonists have been explored as novel therapeutics for the prevention and treatment of UTI.^[6] In recent years, several alkyl and aryl α -D-mannopyranosides were reported, showing nanomolar affinities towards the FimH-CRD.^[7] *In vivo* pharmacokinetic studies supporting oral bioavailability of biphenyl α -D-mannopyranosides in a mouse model were first performed in 2010,^[7d] and since then, further reports describing orally active FimH antagonists have been published.^[7f, 7g] In either case, high oral dosages (≥ 50 mg/kg) were necessary to achieve the minimal concentrations required for antiadhesive effects in the bladder. The antagonists were furthermore rapidly eliminated from circulation, such that the therapeutic effect – upon a single dose – could be maintained only for few hours.

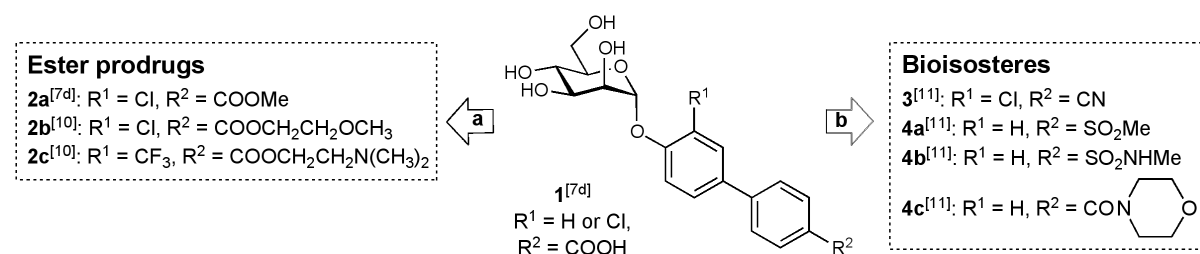


Figure 1. Pharmacokinetic optimization of biphenyl α -D-mannopyranosides by (a) an ester prodrug approach^[7d, 10] and (b) bioisosteric modifications.^[11] Compared to the parent carboxylate **1**, the ester prodrugs **2a-c** exhibit oral availability; with bioisosteres of the carboxylate **1** (\rightarrow **3** & **4a-c**) a prolonged renal excretion could be achieved.

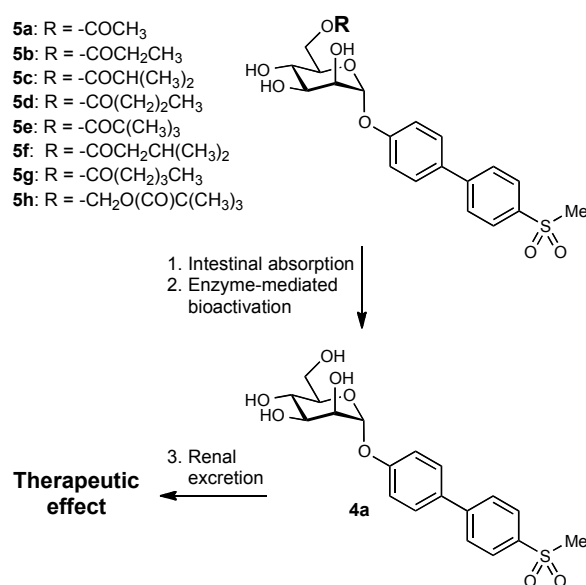
Low antagonist availability in the urine despite high oral dosages might be a consequence of low intestinal absorption (*i.e.* low aqueous solubility or low membrane permeability) or extensive non-renal elimination.^[8] Moreover, undesirably fast renal excretion of the systemically available fraction is due to high glomerular filtration, *i.e.* low plasma protein binding (PPB), or poor reabsorption of polar molecules from the ultrafiltrate in the renal tubules.^[9] We recently described ester prodrugs of antagonist **1** (Figure 1) which mask the carboxylic acid moiety on the terminal ring of the biphenyl aglycone and consequently increase the intestinal absorption.^[7d, 10] In a further publication, we introduced bioisosteres that confer moderate lipophilicity and high PPB leading to prolonged excretion of the systemically available antagonist into the urinary bladder.^[11] Only in the case of the cyanide **3**, the physicochemical profile allowed for oral absorption and sustained renal excretion, whereas further bioisosteres, *e.g.* the methylsulfonyl-biphenyl mannoside **4a**, were too polar for absorption.

A common feature of most carbohydrate derivatives is their high polarity, resulting from the many hydroxyl groups of the sugar moiety. In order to enhance absorption of such species, the hydrophilic character should be reduced. Peracylation of saccharides can markedly increase their cellular uptake, an effect that was observed in the case of peracetylated monosaccharides and disaccharides containing one peracetylated subunit.^[12a, 12b] Moreover, a similar strategy was applied for oligoribonucleotides,^[12c-12g] leading to enhanced cellular uptake as well as to improved nuclease stability.^[12d] However, polyacylated carbohydrate derivatives may have certain disadvantages, *i.e.* very low solubility and/or complicated *in vivo* pharmacokinetic profile due to different rates for deacylation leading to numerous metabolic intermediates.

Here we describe the optimization of the PK parameters relevant for oral absorption for methylsulfonyl bioisostere **4a** following an ester prodrug strategy. As opposed to peracylation, we acylated only one of the hydroxyl groups. For the adjustment of lipophilicity, the aliphatic esters were elongated or branched, thereby paving the way for orally available prodrugs with sustained excretion of the pharmacologically active principle **4a** into the bladder (Scheme 1).

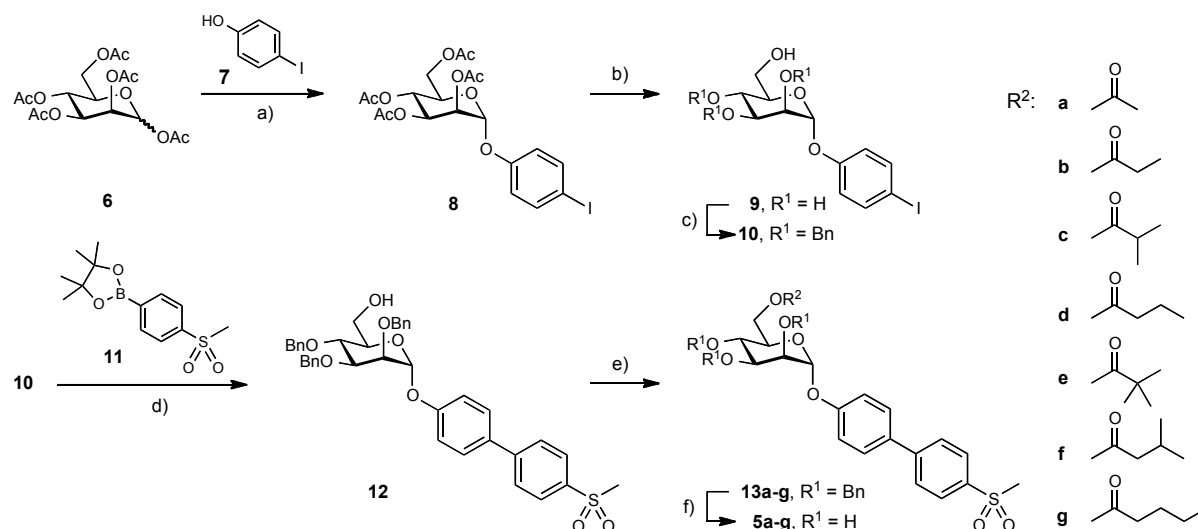
Results and Discussion

A series of acyl promoieties were introduced at the C-6 hydroxyl group of the mannose moiety of antagonist **4a**. A common feature of the prodrugs **5a-g** is the direct acylation of the C-6 hydroxy group. In the case of prodrug **5h**, an additional acetal linker was introduced for improving the steric accessibility of the metabolic cleavage site. Upon hydrolysis of the ester, the resulting hemiacetal intermediate is expected to break down spontaneously, releasing the active principal as well as formaldehyde.



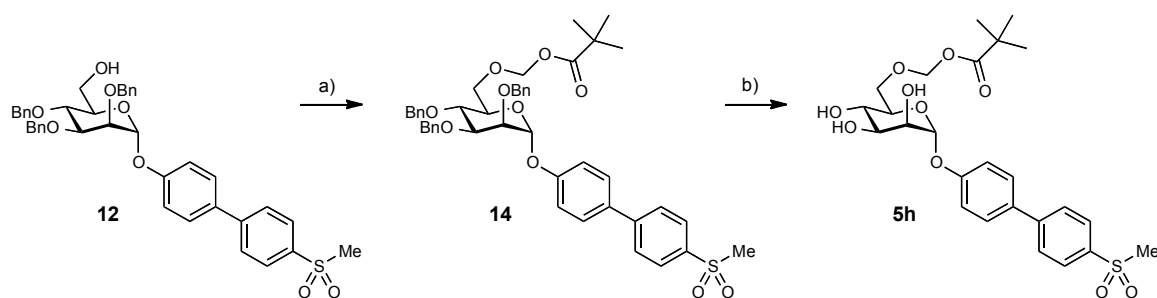
Scheme 1. Ester prodrugs of the biphenyl α -D-mannopyranoside (**4a**). Carboxylic acids of different chain length were esterified with the C-6 hydroxyl group of the mannose moiety.

Compounds **5a-g** were obtained according to the synthetic route depicted in Scheme 2. $\text{BF}_3 \cdot \text{Et}_2\text{O}$ -promoted mannosylation of phenol **7** followed by deacetylation under standard Zemplén conditions gave mannoside **9**. Intermediate **10** was obtained by selectively protecting the primary alcohol in **9** with *tert*-butyldimethylsilyl chloride, benzylation of remaining three hydroxyl groups and finally removal of TBDMS group under acidic conditions. The Suzuki cross-coupling reaction with 4-(methanesulfonyl)phenylboronic acid pinacol ester (**11**) afforded mannoside **12**. Esterification of 6-OH was performed with acetic anhydride (\rightarrow **13a**) or corresponding acid chlorides (\rightarrow **13b-g**). Final compounds were obtained after hydrogenolysis with palladium hydroxide on carbon in hydrogen atmosphere.



Scheme 2. a) $\text{BF}_3 \cdot \text{Et}_2\text{O}$, CH_2Cl_2 , 4Å MS, 40 °C, 30 h, 67%; b) MeONa/MeOH , rt, 27 h, 61%; c) i. TBDMSCl , imidazole, DMF, 0°C → rt, 18 h; ii. BnBr , NaH, TBAI, DMF, 0 °C → rt, 5 h; iii. H_2SO_4 (1 M), MeOH, 0 °C, 18 h, 58% (for 3 steps); d) $\text{PdCl}_2(\text{dppf}) \cdot \text{CH}_2\text{Cl}_2$, K_3PO_4 , DMF, 80 °C, 19 h, 86%; e) Ac_2O or $\text{R}^2\text{-Cl}$, DMAP, pyridine, 60 °C, 3-24 h, 58-91%; f) $\text{Pd}(\text{OH})_2/\text{C}$, H_2 (g), EtOH, rt, 1-16 h, 55-75%.

For synthesizing **5h**, the final acylation step was modified. Starting from **12**, methylthiomethyl ether was introduced into the structure via Pummerer rearrangement. After removal of the main impurities by flash column chromatography the obtained intermediate was coupled with pivalic acid in presence of *N*-iodosuccinimide yielding the pivaloyloxymethyl ester **14**.^[13] Final debenzylation by hydrogenolysis using palladium hydroxide on carbon as a catalyst yielded **5h**.



Scheme 3. a) i. Ac_2O , AcOH, DMSO, 4Å MS, rt, 23 h; ii. PivOH, NIS, 0 °C → rt, 15 h, 33%; b) $\text{Pd}(\text{OH})_2/\text{C}$, H_2 (g), EtOH, rt, 16 h, 24%.

Table 1 summarizes the physicochemical properties of the ester prodrugs **5a-h**, *i.e.* aqueous solubility,^[14] lipophilicity as quantified by the octanol-water partition coefficient ($\log P$),^[15] and permeability determined in permeation experiments through an artificial membrane (PAMPA)^[16] as well as a colorectal adenocarcinoma (Caco-2) cell monolayer.^[17] The table

further includes metabolic stability data, describing the susceptibility of the esters to hydrolysis by rat or human liver associated esterases.^[18]

Table 1. Physicochemical and pharmacokinetic parameters of different ester prodrugs **5a-h**

Compd	log P ^[a]	Solubility ^[b] [$\mu\text{g/mL}$]	PAMPA ^[c] log P_e [cm/s]	Caco-2 P_{app} ^[d] [10^{-6} cm/s]			RLM ^[e] $t_{1/2}$ [min]	HLM $t_{1/2}$ [min]
				a-b	b-a	b-a/a-b		
4a ^[11]	0.4 \pm 0.0	246 \pm 17	-7.2 \pm 0.0	0.4 \pm 0.0	1.8 \pm 0.1	5.0	---	---
5a	0.9 \pm 0.1	146 \pm 6	-5.4 \pm 0.1	1.8 \pm 0.7	17.7 \pm 1.1	10	33	n.d.
5b	1.5 \pm 0.1	253 \pm 10	-5.0 \pm 0.0	4.0 \pm 0.6	15.2 \pm 0.7	3.8	6.5	3.0
5c	1.8 \pm 0.1	61 \pm 1	-4.6 \pm 0.0	10.5 \pm 0.9	19.5 \pm 0.1	1.9	3.7	n.d.
5d	1.8 \pm 0.0	145 \pm 9	-4.7 \pm 0.1	17.3 \pm 1.9	23.5 \pm 1.2	1.4	1.8	1.1
5e	2.3 \pm 0.1	58 \pm 7	-4.6 \pm 0.1	14.1 \pm 1.2	19.8 \pm 3.3	1.4	15	n.d.
5f	2.1 \pm 0.1	65 \pm 4	-4.4 \pm 0.0	17.8 \pm 2.4	24.3 \pm 3.0	1.4	2.0	n.d.
5g	2.2 \pm 0.1	149 \pm 5	-4.5 \pm 0.1	18.1 \pm 0.2	29.4 \pm 4.0	1.6	< 1	< 1
5h	2.1 \pm 0.1	154 \pm 12	-4.5 \pm 0.1	9.4 \pm 1.3	30.3 \pm 3.2	3.2	44	n.d.

The indicated values represent the mean \pm standard deviation (SD) of replicate determinations.

^[a] Octanol-water partition coefficients (log P) were determined by a miniaturized shake-flask procedure in sextuplicate.^[15]

^[b] Kinetic aqueous solubility was measured in triplicate.^[14]

^[c] P_e = effective permeability: diffusion through an artificial membrane was determined by the parallel artificial membrane permeability assay (PAMPA) in quadruplicate.^[16]

^[d] P_{app} = apparent permeability: permeation through a Caco-2 cell monolayer was assessed in the absorptive (a \rightarrow b) and secretory (b \rightarrow a) direction in triplicate. The initial compound concentration (c_0) in the donor chamber was 62.5 μM .^[17]

^[e] Microsomal stability was determined with pooled male rat liver microsomes (0.125 mg/mL) and pooled human liver microsomes (0.125 mg/mL) at pH 7.4 and 37 °C. The initial compound concentration was 2 μM . The concentration of the prodrug in the incubation was monitored by LC-MS and $t_{1/2}$ was calculated from the slope of the linear regression from the log percentage compound remaining versus incubation time relationship.^[18]

The primary goal of this ester prodrug approach, that is, to increase lipophilicity and permeability of the biphenyl mannoside **4a**, could clearly be achieved. The log P coefficients increased in parallel with the number of carbons of the acyl moiety. The acetate **5a** was only a little more lipophilic than the parent compound, whereas the propionate **5b**, the isobutyrate **5c**, and the butyrate **5d** exhibited markedly elevated lipophilicity. Log P values above 2 were observed in the case of the pivalate **5e**, the pivaloyloxymethyl **5h**, the isovalerate **5f**, and the valerate **5g**. Furthermore, the effective permeability (log P_e) deduced from the artificial membrane permeability assay (PAMPA) rose proportionally to log P . Log P_e values above -5.7 are a strong indicator of oral availability. The PAMPA results for the prodrugs **5a** and **5b** (log P_e -5.4 & -5.0) indicate a relevant improvement in membrane

permeability compared to the parent compound **4a** ($\log P_e$ -7.2) and optimal permeability for the more lipophilic esters **5c-h** ($\log P_e$ -4.7 \cdot / \cdot -4.4).^[19]

In addition to PAMPA, bi-directional permeation studies through Caco-2 cell monolayers were performed in order to reveal carrier-mediated transport through the membranes lining the intestine.^[17] Since Caco-2 cells express esterases, the system was treated with the esterase inhibitor bis(4-nitrophenyl) phosphate (BNPP).^[18] This step enabled us to study membrane permeation independently from enzyme-mediated hydrolysis. Apparent permeability (P_{app}) derived from the experiments in the absorptive direction (apical \rightarrow basal) complied with the increasing trend observed in lipophilicity and PAMPA. The first two compounds in the series (**5a**, **5b**) showed low permeability ($P_{app} < 5 \cdot 10^{-6}$ cm/s) whereas for the remaining prodrugs, high permeability ($P_{app} > 9 \cdot 10^{-6}$ cm/s) was observed. For the most polar prodrugs **5a** & **5b**, high P_{app} in the secretory direction (basal \rightarrow apical) is leading to unfavorable efflux ratios (b \rightarrow a/a \rightarrow b). In these cases, strong efflux carrier activity probably outbalanced the slow diffusion in the absorptive direction.^[21] Otherwise, the more lipophilic compounds **5c-g** diffused more rapidly and therefore appeared as weak efflux transporter substrates. The pivaloyloxymethyl **5h** is the only exception to the described tendency showing a smaller P_{app} in the absorptive direction compared to the other lipophilic prodrugs. Although the performance of **5h** remains in the high-permeability range, its overall evaluation becomes worse when efflux ratio of 3.2 is taken into account. This extraordinary result might be attributed to a much different structure of the promoiety.

For achieving oral bioavailability, quantitative dissolution of the orally administered prodrug in the intestine is an additional requirement.^[22] Regarding aqueous solubility, the compounds listed in Table 1 can be divided into two categories: The esters with branched acyl promoieties (isobutyrate **5c**, pivalate **5e**, and isovalerate **5f**) were sparsely soluble in aqueous medium (around 60 μ g/mL), whereas the linear esters (acetate **5a**, propionate **5b**, butyrate **5d**, valerate **5g**) and heteroatom-containing promoiety (pivaloyloxymethyl **5h**) showed solubility values of at least 145 μ g/mL. Provided that the prodrugs are applied at a therapeutic dose of at most 1 mg/kg body weight, aqueous solubility of 52 μ g/mL should be aspired,^[22] which could barely be achieved with the branched-chain derivatives. By contrast, the prodrugs **5a**, **5b**, **5d**, **5g**, and **5h** markedly exceeded this minimum solubility criterion for quantitative intestinal absorption.

Considering the two pivotal criteria for oral absorption – aqueous solubility and membrane permeability – the prodrug **5b** (high solubility, moderate permeability) as well as the derivatives **5d** and **5g** (moderate solubility, high permeability) showed the most balanced profiles for successful absorption.

Another prerequisites for developing orally available prodrugs are chemical stability under the conditions encountered in stomach and intestine as well as resistance to hydrolysis during the absorption phase.^[23] In order to assess the stability of the esters against hydrolysis under acidic and slightly basic conditions, the butyrate prodrug **5d** was dissolved in phosphate buffer (20 mM, pH 2.5 and 7.4), acetate buffer (20 mM, pH 5.0), and borate buffer (20 mM, pH 9.5) and kept at 37 °C for three hours.^[24] At acidic or physiological pH, **5d** proved to be stable, whereas 29% were hydrolyzed at pH 9.5. We, therefore, expect only marginal prodrug loss in the strongly acidic environment of the stomach and the slightly acidic environment of the proximal small bowel.^[25]

Furthermore, the ester fulfilling stability requirements prior to absorption, should be rapidly cleaved once in circulation.^[23] Enzymatic ester hydrolysis, which is basically undesirable during absorption but necessary once the prodrug has reached the bloodstream, can be mediated by plasma-borne esterases or, as in case of many ester prodrugs, by the carboxylesterase (CES) localized in the endoplasmic reticulum of different tissues.^[26] The CES superfamily encloses various isozymes classified into five subfamilies. The isozymes hCE1, highly expressed in the liver but scarcely observed in the gastrointestinal tract, and hCE2, present in both, liver and small intestine, have been identified as major human CES.^[18,27] In order to estimate the prodrugs' propensity to CES-mediated hydrolysis irrespective of the type of isozyme involved, we incubated the compounds **5a-h** (initial conc. = 2 µM) with rat liver microsomes (RLM; 0.125 mg/mL in TRIS-HCl 0.1 M, pH 7.4). In a further step, we assessed the most promising esters **5b**, **5d**, and **5g** using human liver microsomes (HLM; 0.125 mg/mL). The metabolic half-lives ($t_{1/2}$) derived from the microsomal incubations revealed two major trends: First, the increasing susceptibility to hydrolysis along with the lipophilicity of the linear esters and, second, sterically hindered acyl moieties, such as present in the pivalate **5e** and pivaloyloxymethyl **5h**, hampering the enzymatic turnover. Moreover, exposing the pivalate ester by an acetal linker (\rightarrow **5h**) actually did not increase the rate of enzyme-mediated hydrolysis.

Rapid hydrolysis as detected for the propionate, butyrate, and valerate esters is basically essential to yield the pharmacologically active principle. However, the prodrug approach

might only be successful if the cleavage takes place in the liver and not in the intestine during absorption or, more precisely, if the hydrolysis is mediated by the isozyme hCE1 rather than by hCE2.^[23] Since liver microsomes prepared by differential centrifugation from a crude liver homogenate contain both carboxylesterases, selective inhibition of only one would reveal which isozyme is mainly involved in the hydrolysis of the esters. Therefore, loperamide (a specific inhibitor of hCE2) was added to the incubation of **5b**, **5d**, and **5g** with HLM.^[28] Figure 2 summarizes the hydrolytic activity in presence of the hCE2 specific inhibitor at ascending concentrations (1 μ M, 10 μ M, and 100 μ M). The metabolic turnover of the esters **5b**, **5d**, and **5g** was in fact inhibited by loperamide, which attributes the hydrolysis to the hCE2 isozyme.^[28] High recognition of our promoieties by isotype 2 complies with the distinct substrate specificity of the two isozymes. Accordingly, hCE2 prefers esters with a relatively small acyl moiety and a large alcohol group, whereas hCE1 primarily catalyzes the hydrolysis of esters with a large acyl but small alcohol moiety.^[18] Isotype 2 mediated bioconversion might interfere with the intestinal absorption, even in the case of the well soluble and permeable prodrugs **5b**, **5d**, and **5g**. Hydrolysis within the enterocytes yields the polar active principle **4a**, which is as likely to be effluxed back into the gut lumen as it is to proceed into the portal blood.^[23]

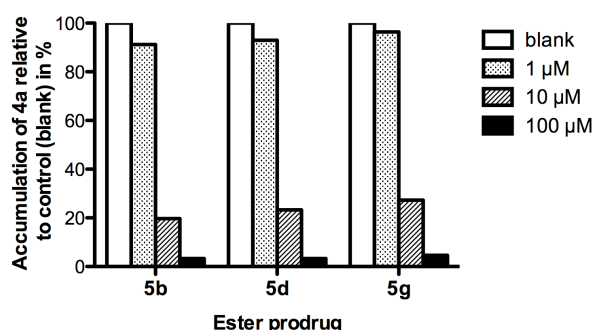


Figure 2. Human liver microsome (HLM) mediated hydrolysis of ester prodrugs **5b**, **5d**, and **5g** in presence of loperamide (0 μ M, 1 μ M, 10 μ M, 100 μ M), a specific inhibitor of the human carboxylesterase isotype 2 (hCE2). The bars represent the accumulation of the parent compound **4a** in the incubation with inhibitor (1 μ M, 10 μ M, 100 μ M) relative to the accumulation in the control experiment without Loperamide (blank).

Conclusions

In summary, we have identified several short-chain fatty acids (propionic acid, butyric acid, and valeric acid) as useful acyl promoieties for optimizing the intestinal absorption potential of the biphenyl mannoside **4a**. We showed that acylation of only one hydroxyl group on the sugar moiety was sufficient to move $\log P$ into the range preferred for good absorption.

Nonetheless, other carbohydrates containing less lipophilic reducing-end moiety (e.g. disaccharide) may require acylation of additional hydroxyl groups. Moreover, introducing the ester promoiety to the sugar may be advantageous for the stability towards other enzymes, *i.e.* glycosidases. All sugar-based drug candidates, if prone to glycosidic bond cleavage, may become more resistant to glycosidases located in saliva and gastrointestinal tract, since they probably would no longer fit to the active site.

The downside of this approach is possible premature cleavage of the promoiety by hCE2 located in the enterocytes. Therefore, choosing the best prodrug should be supported by enzymatic stability studies and the half-life should be long enough to enable the majority of the prodrug to be absorbed in unchanged form.

For proving the benefits of the prodrug approach on oral bioavailability and for assessing whether the intestinal uptake is affected by concomitant hydrolysis, *in vivo* pharmacokinetic studies of our compounds in a mouse model shall be performed in a next step.

Experimental Section

Chemistry

General methods: NMR spectra were recorded on a Bruker Avance DMX-500 (500 MHz) spectrometer. Assignment of ^1H and ^{13}C NMR spectra was achieved using 2D methods (COSY, HSQC, HMBC). Chemical shifts are expressed in ppm using residual CHCl_3 , CHD_2OD or HDO as references. Optical rotations were measured using Perkin-Elmer Polarimeter 341. Electron spray ionization mass spectra (ESI-MS) were obtained on a Waters micromass ZQ Mass Spectrometer. The LC-HRMS analysis were carried out using a Agilent 1100 LC equipped with a photodiode array detector and a Micromass QTOF I equipped with a 4 GHz digital-time converter. Reactions were monitored by TLC using glass plates coated with silica gel 60 F₂₅₄ (Merck) and visualized by using UV light and/or by charring with a molybdate solution (a 0.02 M solution of ammonium cerium sulfate dihydrate and ammonium molybdate tetrahydrate in aqueous 10% H_2SO_4). MPLC separations were carried out on a CombiFlash Companion or Rf from Teledyne Isco equipped with RediSep normal-phase. All compounds used for biological assays are at least of 97% purity based on HPLC analytical results. Commercially available reagents were purchased from Aldrich, Alfa Aesar, ABCR or Acros Organics. Solvents were purchased from Sigma-Aldrich or Acros and were dried prior to use where indicated. Methanol (MeOH), pyridine and DMSO were dried by storing with activated molecular sieves 3Å or 4Å for at least one day. Dichloromethane (DCM) was dried by filtration over Al_2O_3 (Fluka, type 5016 A basic). Molecular sieves 4Å were activated in vacuo at 500 °C for 1 h immediately before use.

General procedure A for esterification. To a solution of **12** in dry pyridine (2 mL) was added Ac₂O or the corresponding acyl chloride and a catalytic amount of DMAP. The mixture was stirred at rt under argon until the reaction was complete (monitored by TLC), then diluted with EtOAc and washed with H₂O and brine. The organic layer was dried over Na₂SO₄, concentrated in vacuo and co-evaporated with xylene. The residue was purified by MPLC on silica gel (petroleum ether/EtOAc, 7:3) to afford **13a-g**.

General procedure B for hydrogenolysis. A solution of **13a-g** or **14** in EtOH was stirred under hydrogen in the presence of Pd(OH)₂/C (E101 NE/W, 20% Pd). The mixture was stirred at rt until the reaction was complete (monitored by TLC), then filtered through Celite, washed with MeOH and concentrated in vacuo. The residue was purified by MPLC on silica gel (DCM/MeOH) to give **5a-h**.

4-Iodophenyl 2,3,4,6-tetra-O-acetyl- α -D-mannopyranoside (8). 1,2,3,4,6-O-pentaacetyl-D-mannopyranoside (15.0 g, 45.4 mmol), 4-iodophenol (11.2 g, 50.0 mmol, 1.1 eq) and activated molecular sieves 4 Å (2.00 g) were stirred in dry DCM (60 mL) under argon. After 1 h of mixing, first portion of BF₃·Et₂O (10 mL, 81 mmol, 1.8 eq) was added dropwise followed by the addition of second portion (6.8 mL, 55.2 mmol, 1.2 eq) 4 h later. The reaction was carried out at 40 °C for 30 h. The reaction mixture was filtered through Celite and the filtrate was diluted with EtOAc (250 mL), washed with satd aq NaHCO₃ (3 x 100 mL) and brine (100 mL). The organic layer was dried over Na₂SO₄ and concentrated in vacuo. The residue was crystallized from Et₂O/hexan (1:1) to give **8**. The mother liquor was concentrated and **8** was crystallized again from Et₂O/hexan (2:1). The filtrate was concentrated and purified by MPLC on silica gel (petroleum ether/EtOAc, 9:1). The compound **8** was obtained in an overall yield of 67% (16.8 g). Analytical data are with accordance with the literature data.^[29]

4-Iodophenyl α -D-mannopyranoside (9). To a solution of **8** (16.8 g, 30.5 mmol) in dry MeOH (100 mL) was added freshly prepared 1 M MeONa/MeOH (2 mL) under argon. The reaction mixture was stirred overnight at rt, then neutralized with Amberlyst-15 (H⁺) ion-exchange resin, filtered and concentrated in vacuo. Recrystallization from ethanol (250 mL) afforded white crystals of **9**. The mother liquor was concentrated and purified by MPLC on silica gel (DCM/MeOH, 9:1). The compound **9** was obtained in an overall yield of 61% (7.10 g). [α]_D²⁰ +106.5 (*c* 1.00, MeOH); ¹H NMR (500 MHz, CD₃OD): δ = 7.61 (d, *J* = 8.9 Hz, 2H, Ar-H), 6.96 (d, *J* = 8.9 Hz, 2H, Ar-H), 5.48 (d, *J* = 1.4 Hz, 1H, H-1), 4.01 (dd, *J* = 1.8, 3.2 Hz, 1H, H-2), 3.89 (dd, *J* = 3.4, 9.4 Hz, 1H, H-3), 3.80-3.69 (m, 3H, H-4, H-6a, H-6b), 3.57 ppm (ddd, *J* = 2.4, 5.4, 9.7 Hz, 1H, H-5); ¹³C NMR (125 MHz, CD₃OD): δ = 157.84, 139.52, 120.15 (5C, Ar-C), 100.13 (C-1), 85.31 (Ar-C), 75.52 (C-5), 72.32 (C-3), 71.84 (C-2), 68.28 (C-4), 62.65 ppm (C-6); HRMS: *m/z*: Calcd for C₁₂H₁₅INaO₆ [M+Na]⁺: 404.9811, found: 404.9808.

4-Iodophenyl 2,3,4-tri-*O*-benzyl- α -D-mannopyranoside (10). To a stirred solution of **9** (6.61 g, 17.3 mmol) in dry DMF (17 mL) were added TBDMSCl (2.61 g, 17.3 mmol, 1.0 eq) and imidazole (2.35 g, 34.6 mmol, 2.0 eq) under argon at 0 °C. After 1 h, the reaction mixture was removed from the ice bath and allowed to reach rt. Another portion of TBDMSCl (0.26 g, 1.73 mmol, 0.1 eq) was added after 15 h. The reaction was carried out for next 3 h until **9** was completely consumed. The reaction mixture was diluted with DCM (200 mL), washed with satd aq NaHCO₃ (2 x 150 mL) and brine (150 mL). The organic layer was dried over Na₂SO₄, concentrated in vacuo and co-evaporated with toluene (2 x 100 mL) to afford 9.60 g of crude product. The obtained compound (6.01 g) was dissolved in dry DMF (28 mL) under argon. Sodium hydride (1.75 g, 43.6 mmol, 60% in mineral oil) was added to the stirred solution together with an additional portion of DMF (16 mL) at 0 °C followed by the addition of BnBr (6.47 mL, 54.5 mmol). The reaction mixture was removed from the ice bath and allowed to reach rt. Bu₄NI (0.88 g, 2.42 mmol) was added after 2 h. When the reaction was complete after another 2 h, the mixture was diluted with EtOAc (250 mL) and washed with satd aq NaHCO₃ (150 mL), H₂O (150 mL) and brine (100 mL). The organic layer was dried over Na₂SO₄, concentrated in vacuo and co-evaporated with toluene (75 mL) to afford 10.8 g of yellowish product. The crude compound (10.8 g) was then dissolved in MeOH (70 mL) under argon and a solution of H₂SO₄ in MeOH (1 M, 560 μ L) was added dropwise. The reaction was stirred at 0 °C until completion (18 h, monitored by TLC), then the mixture was diluted with EtOAc (100 mL) and washed with satd aq NaHCO₃ (100 mL), H₂O (100 mL) and brine (100 mL). The aqueous layer was extracted with EtOAc (100 mL). The combined organic layers were dried over Na₂SO₄, concentrated in vacuo and pre-purified by MPLC on silica gel (petroleum ether/EtOAc, 85:15). The crude **10** was crystallized from petroleum ether/EtOAc (3:1). The mother liquor was concentrated and the residue was recrystallized from MeOH (20 mL). The compound **10** was obtained in an overall yield of 58% (4.32 g) over three steps. $[\alpha]_D^{20} +55.9$ (*c* 1.00, EtOAc); ¹H NMR (500 MHz, CDCl₃): δ = 7.48 (d, *J* = 8.7 Hz, 2H, Ar-H), 7.35-7.24 (m, 15H, Ar-H), 6.67 (d, *J* = 8.7 Hz, 2H, Ar-H), 5.49 (d, *J* = 1.7 Hz, 1H, H-1), 4.90 (d, *J* = 10.9 Hz, 1H, PhCH₂O), 4.78 (d, *J* = 12.2 Hz, 1H, PhCH₂O), 4.70-4.62 (m, 4H, PhCH₂O), 4.07-4.02 (m, 2H, H-4, H-3), 3.89 (br s, 1H, H-2), 3.70-3.69 (m, 2H, H-6a, H-6b), 3.62 (m, 1H, H-5), 1.81 ppm (s, 1H, OH); ¹³C NMR (125 MHz, CDCl₃): δ = 155.93, 138.53, 138.42, 138.35, 138.09, 128.61, 128.58, 128.19, 128.03, 127.95, 127.86, 127.80, 118.73 (23C, Ar-C), 96.66 (C-1), 85.12 (Ar-C), 79.88 (C-3 or C-4), 75.40 (PhCH₂O), 74.74 (C-2), 74.43 (C-3 or C-4), 73.38 (PhCH₂O), 73.28 (C-5), 72.69 (PhCH₂O), 62.06 ppm (C-6); ESI-MS: *m/z*: Calcd for C₃₃H₃₃INaO₆ [M+Na]⁺: 675.12, found: 675.18.

4'-(Methylsulfonyl)-biphenyl-4-yl 2,3,4-tri-*O*-benzyl- α -D-mannopyranoside (12). The compounds **10** (2.50 g, 3.83 mmol) and **11** (843 mg, 4.21 mmol) were dissolved in dry DMF (20 mL) under argon. The mixture was degassed in an ultrasonic bath and flushed with argon for 5 min followed by the addition of K₃PO₄ (2.44 g, 11.5 mmol, 3.0 eq) and Pd(dppf)Cl₂·CH₂Cl₂ (156 mg, 0.19 mmol, 0.05

eq). The mixture was stirred at 80 °C for 19 h. The reaction mixture was diluted with EtOAc (200 mL), washed with H₂O (2 x 120 mL) and brine (120 mL), dried over Na₂SO₄ and concentrated in vacuo. The residue was purified by MPLC on silica gel (petroleum ether/EtOAc, 1:1) to give **12** (2.24 g, 86%) as a white solid. $[\alpha]_D^{20} +70.8$ (*c* 1.01, EtOAc); ¹H NMR (500 MHz, CDCl₃): δ = 7.99-7.97 (m, 2H, Ar-H), 7.72-7.70 (m, 2H, Ar-H), 7.53-7.52 (m, 2H, Ar-H), 7.42-7.29 (m, 15H, Ar-H), 7.08-7.06 (m, 2H, Ar-H), 5.58 (d, *J* = 1.9 Hz, 1H, H-1), 4.97 (d, *J* = 10.9 Hz, 1H, PhCH₂O), 4.87 (d, *J* = 12.3 Hz, 1H, PhCH₂O), 4.78-4.69 (m, 4H, PhCH₂O), 4.16-4.09 (m, 2H, H-3, H-4), 4.00 (d, *J* = 2.2 Hz, 1H, H-2), 3.79-3.73 (m, 3H, H-5, H-6a, H-6b), 3.09 ppm (s, 3H, SO₂CH₃); ¹³C NMR (125 MHz, CDCl₃): δ = 156.68, 146.14, 138.87, 138.46, 138.35, 138.15, 133.34, 128.78, 128.65, 128.63, 128.24, 128.09, 128.06, 128.02, 127.91, 127.84, 127.67, 116.99 (30C, Ar-C), 96.67 (C-1), 80.00 (C-3 or C-4), 75.46 (PhCH₂O), 74.79 (C-2), 74.59 (C-3 or C-4), 73.41 (PhCH₂O), 73.31 (C-5), 72.74 (PhCH₂O), 62.25 (C-6), 44.79 ppm (SO₂CH₃); ESI-MS: *m/z*: Calcd for C₄₀H₄₀NaO₈S [M+Na]⁺: 703.23, found: 703.26.

4'-(Methylsulfonyl)-biphenyl-4-yl 6-O-acetyl-2,3,4-tri-O-benzyl-α-D-mannopyranoside (13a).

Prepared according to the general procedure A from **12** (100 mg, 0.147 mmol), Ac₂O (27 μL, 0.294 mmol, 2.0 eq) and DMAP (1 mg, 0.008 mmol, 0.05 eq). The reaction was started at 0 °C and allowed to warm up to rt. Yield: 104 mg (96%) as colorless oil. $[\alpha]_D^{20} +70.0$ (*c* 1.00, CHCl₃); ¹H NMR (500 MHz, CDCl₃): δ = 7.90 (d, *J* = 8.5 Hz, 2H, Ar-H), 7.63 (d, *J* = 8.4 Hz, 2H, Ar-H), 7.46 (d, *J* = 8.8 Hz, 2H, Ar-H), 7.33-7.17 (m, 15H, Ar-H), 7.03 (d, *J* = 8.7 Hz, 2H, Ar-H), 5.52 (d, *J* = 1.7 Hz, 1H, H-1), 4.88 (d, *J* = 10.8 Hz, 1H, PhCH₂O), 4.77-4.63 (m, 4H, PhCH₂O), 4.54 (d, *J* = 10.8 Hz, 1H, PhCH₂O), 4.26-4.18 (m, 2H, H-6a, H-6b), 4.07 (dd, *J* = 3.0, 9.2 Hz, 1H, H-3), 3.98-3.92 (m, 2H, H-2, H-4), 3.81 (m, 1H, H-5), 2.99 (s, 3H, SO₂CH₃), 1.92 ppm (s, 3H, COCH₃); ¹³C NMR (125 MHz, CDCl₃): δ = 170.83 (CO), 156.71, 146.07, 138.84, 138.29, 138.10, 138.09, 133.31, 128.64, 128.59, 128.57, 128.55, 128.24, 128.05, 127.99, 127.95, 127.93, 127.90, 127.84, 127.61, 117.12 (30C, Ar-C), 96.43 (C-1), 79.97 (C-3), 75.34 (PhCH₂O), 74.48 (C-2), 74.32 (C-4), 73.05, 72.56 (2 PhCH₂O), 71.01 (C-5), 63.21 (C-6), 44.74 (SO₂CH₃), 20.95 ppm (COCH₃); ESI-MS: *m/z*: Calcd for C₄₂H₄₂NaO₉S [M+Na]⁺: 745.24, found: 745.31.

4'-(Methylsulfonyl)-biphenyl-4-yl 2,3,4-tri-O-benzyl-6-O-propionyl-α-D-mannopyranoside (13b).

Prepared according to the general procedure A from **12** (70 mg, 0.103 mmol), propionyl chloride (33 μL, 0.309 mmol, 3.0 eq) and DMAP (1 mg, 0.008 mmol, 0.08 eq). The reaction was started at rt and then warmed up to 60 °C. Yield: 38 mg (58%) as colorless oil. $[\alpha]_D^{20} +63.0$ (*c* 1.84, CHCl₃); ¹H NMR (500 MHz, CDCl₃): δ = 7.97 (d, *J* = 8.4 Hz, 2H, Ar-H), 7.70 (d, *J* = 8.4 Hz, 2H, Ar-H), 7.51 (d, *J* = 8.7 Hz, 2H, Ar-H), 7.41-7.27 (m, 15H, Ar-H), 7.10 (d, *J* = 8.7 Hz, 2H, Ar-H), 5.58 (d, *J* = 1.5 Hz, 1H, H-1), 4.95 (d, *J* = 10.7 Hz, 1H, PhCH₂O), 4.83 (d, *J* = 12.3 Hz, 1H, PhCH₂O), 4.77-4.72 (m, 3H, PhCH₂O), 4.60 (d, *J* = 10.7 Hz, 1H, PhCH₂O), 4.34-4.28 (m, 2H, H-6a, H-6b), 4.14 (dd, *J* = 3.0, 9.2 Hz, 1H, H-3), 4.03 (t, *J* = 9.5 Hz, 1H, H-4), 3.99 (m, 1H, H-2), 3.88 (ddd, *J* = 2.4, 4.4, 9.8

Hz, 1H, H-5), 3.08 (s, 3H, SO₂CH₃), 2.27 (q, $J = 7.5$ Hz, 2H, CH₂COO), 1.07 ppm (t, $J = 7.6$ Hz, 3H, CH₃); ¹³C NMR (125 MHz, CDCl₃): $\delta = 174.29$ (CO), 156.77, 146.18, 138.89, 138.36, 138.17, 138.15, 137.46, 137.16, 133.37, 128.70, 128.65, 128.63, 128.61, 128.29, 128.12, 128.01, 127.99, 127.97, 127.92, 127.68, 118.42, 117.18 (30C, Ar-C), 96.44 (C-1), 80.02 (C-3), 75.44 (PhCH₂O), 74.61 (C-2), 74.50 (C-4), 73.15, 72.65 (2 PhCH₂O), 71.19 (C-5), 63.14 (C-6), 44.80 (SO₂CH₃), 27.66 (CH₂COO), 9.21 ppm (CH₃); ESI-MS: m/z : Calcd for C₄₃H₄₄NaO₉S [M+Na]⁺: 759.26, found: 759.13.

4'-(Methylsulfonyl)-biphenyl-4-yl 2,3,4-tri-*O*-benzyl-6-*O*-isobutyryl- α -D-mannopyranoside (13c). Prepared according to the general procedure A from **12** (70 mg, 0.103 mmol), isobutyryl chloride (33 μ L, 0.309 mmol, 3.0 eq) and DMAP (2 mg, 0.016 mmol, 0.16 eq). The reaction was started at rt and then warmed up to 60 °C. Yield: 63 mg (82%) as colorless oil. $[\alpha]_D^{20} +60.0$ (c 3.17, CHCl₃); ¹H NMR (500 MHz, CDCl₃): $\delta = 7.96$ (d, $J = 8.4$ Hz, 2H, Ar-H), 7.68 (d, $J = 8.4$ Hz, 2H, Ar-H), 7.49 (d, $J = 8.7$ Hz, 2H, Ar-H), 7.39-7.26 (m, 15H, Ar-H), 7.09 (d, $J = 8.7$ Hz, 2H, Ar-H), 5.57 (d, $J = 1.6$ Hz, 1H, H-1), 4.94 (d, $J = 10.6$ Hz, 1H, PhCH₂O), 4.81 (d, $J = 12.2$ Hz, 1H, PhCH₂O), 4.74-4.71 (m, 3H, PhCH₂O), 4.58 (d, $J = 10.6$ Hz, 1H, PhCH₂O), 4.35 (dd, $J = 1.7, 11.9$ Hz, 1H, H-6a), 4.25 (dd, $J = 5.2, 11.9$ Hz, 1H, H-6b), 4.12 (dd, $J = 3.0, 9.2$ Hz, 1H, H-3), 4.00 (t, $J = 9.5$ Hz, 1H, H-4), 3.97 (m, 1H, H-2), 3.86 (ddd, $J = 1.6, 5.0, 9.8$ Hz, 1H, H-5), 3.06 (s, 3H, SO₂CH₃), 2.49 (hept, $J = 7.0$ Hz, 1H, CH(CH₃)₂), 1.09 (d, $J = 7.0$ Hz, 3H, CH₃), 1.06 ppm (d, $J = 7.0$ Hz, 3H, CH₃); ¹³C NMR (125 MHz, CDCl₃): $\delta = 176.85$ (CO), 156.73, 146.17, 138.85, 138.33, 138.14, 133.31, 128.67, 128.62, 128.56, 128.22, 128.06, 128.01, 127.95, 127.90, 127.64, 117.14 (30C, Ar-C), 96.34 (C-1), 79.96 (C-3), 75.48 (PhCH₂O), 74.67 (C-2), 74.61 (C-4), 73.16, 72.63 (2 PhCH₂O), 71.32 (C-5), 62.98 (C-6), 44.77 (SO₂CH₃), 34.10 (CH), 19.12, 18.92 ppm (2 CH₃); ESI-MS: m/z : Calcd for C₄₄H₄₆NaO₉S [M+Na]⁺: 773.28, found: 773.28.

4'-(Methylsulfonyl)-biphenyl-4-yl 2,3,4-tri-*O*-benzyl-6-*O*-butyryl- α -D-mannopyranoside (13d). Prepared according to the general procedure A from **12** (54 mg, 0.080 mmol), butyryl chloride (10 μ L, 0.094 mmol, 1.2 eq) and DMAP (1 mg, 0.008 mmol, 0.1 eq). The reaction mixture was stirred at rt. Yield: 45 mg (75%) as colorless oil. $[\alpha]_D^{20} +68.6$ (c 1.13, CHCl₃); ¹H NMR (500 MHz, CDCl₃): $\delta = 8.02$ (d, $J = 8.4$ Hz, 2H, Ar-H), 7.75 (d, $J = 8.5$ Hz, 2H, Ar-H), 7.56 (d, $J = 8.8$ Hz, 2H, Ar-H), 7.45-7.32 (m, 15H, Ar-H), 7.15 (d, $J = 8.8$ Hz, 2H, Ar-H), 5.64 (d, $J = 1.7$ Hz, 1H, H-1), 5.00 (d, $J = 10.7$ Hz, 1H, PhCH₂O), 4.87 (d, $J = 12.3$ Hz, 1H, PhCH₂O), 4.81-4.77 (m, 3H, PhCH₂O), 4.65 (d, $J = 10.7$ Hz, 1H, PhCH₂O), 4.40-4.33 (m, 2H, H-6a, H-6b), 4.19 (dd, $J = 3.0, 9.2$ Hz, 1H, H-3), 4.07 (t, $J = 9.5$ Hz, 1H, H-4), 4.04 (m, 1H, H-2), 3.92 (ddd, $J = 2.2, 4.6, 9.8$ Hz, 1H, H-5), 3.12 (s, 3H, SO₂CH₃), 2.29 (t, $J = 7.5$ Hz, 2H, CH₂COO), 1.67-1.59 (m, 2H, CH₂), 0.91 ppm (t, $J = 7.4$ Hz, 3H, CH₃); ¹³C NMR (125 MHz, CDCl₃): $\delta = 173.42$ (CO), 156.72, 146.10, 138.83, 138.31, 138.12, 138.10, 133.27, 128.64, 128.59, 128.57, 128.55, 128.21, 128.05, 127.98, 127.95, 127.93, 127.91, 127.86, 127.60, 117.10 (30C, Ar-C), 96.37 (C-1), 79.95 (C-3), 75.40 (PhCH₂O), 74.58, 74.49 (C-2, C-4), 73.10, 72.59 (2

PhCH₂O), 71.17 (C-5), 62.94 (C-6), 44.73 (SO₂CH₃), 36.23 (CH₂COO), 18.47 (CH₂), 13.80 ppm (CH₃); ESI-MS: *m/z*: Calcd for C₄₄H₄₆NaO₉S [M+Na]⁺: 773.28, found: 773.44.

4'-(Methylsulfonyl)-biphenyl-4-yl 2,3,4-tri-*O*-benzyl-6-*O*-pivaloyl- α -D-mannopyranoside (13e).

Prepared according to the general procedure A from **12** (100 mg, 0.147 mmol), pivaloyl chloride (36 μ L, 0.294 mmol, 2.0 eq) and DMAP (1 mg, 0.008 mmol, 0.05 eq). The reaction was started at rt and then warmed up to 60 °C. Yield: 101 mg (90%) as colorless oil. $[\alpha]_D^{20}$ +88.7 (*c* 1.02, CHCl₃); ¹H NMR (500 MHz, CDCl₃): δ = 7.90 (d, *J* = 8.4 Hz, 2H, Ar-H), 7.62 (d, *J* = 8.4 Hz, 2H, Ar-H), 7.44 (d, *J* = 8.7 Hz, 2H, Ar-H), 7.35-7.20 (m, 15H, Ar-H), 7.05 (d, *J* = 8.7 Hz, 2H, Ar-H), 5.53 (d, *J* = 1.6 Hz, 1H, H-1), 4.90 (d, *J* = 10.6 Hz, 1H, PhCH₂O), 4.77 (d, *J* = 12.2 Hz, 1H, PhCH₂O), 4.68-4.65 (m, 3H, PhCH₂O), 4.55 (d, *J* = 10.7 Hz, 1H, PhCH₂O), 4.36 (dd, *J* = 1.5, 11.8 Hz, 1H, H-6a), 4.15-4.08 (m, 2H, H-3, H-6b), 3.98-3.93 (m, 2H, H-2, H-4), 3.82 (ddd, *J* = 1.3, 5.3, 9.8 Hz, 1H, H-5), 2.99 (s, 3H, SO₂CH₃), 1.05 ppm (s, 9H, CH₃); ¹³C NMR (125 MHz, CDCl₃): δ = 178.19 (CO), 156.61, 146.05, 138.75, 138.25, 138.07, 133.16, 128.59, 128.52, 128.46, 128.11, 127.97, 127.91, 127.84, 127.83, 127.52, 127.59, 117.08 (30C, Ar-C), 96.13 (C-1), 79.84 (C-3), 75.40 (PhCH₂O), 74.71, 74.64 (C-2, C-4), 73.11, 72.50 (2 PhCH₂O), 71.33 (C-5), 63.07 (C-6), 44.62 (SO₂CH₃), 38.82 (C(CH₃)₃), 27.17 ppm (3 CH₃); ESI-MS: *m/z*: Calcd for C₄₅H₄₈NaO₉S [M+Na]⁺: 787.29, found: 787.36.

4'-(Methylsulfonyl)-biphenyl-4-yl 2,3,4-tri-*O*-benzyl-6-*O*-isovaleryl- α -D-mannopyranoside (13f).

Prepared according to the general procedure A from **12** (38 mg, 0.056 mmol), isovaleryl chloride (27 μ L, 0.223 mmol, 4.0 eq) and DMAP (1 mg, 0.008 mmol, 0.14 eq). The reaction mixture was stirred at rt. Yield: 35 mg (81%) as colorless oil. $[\alpha]_D^{20}$ +59.0 (*c* 0.93, CHCl₃); ¹H NMR (500 MHz, CDCl₃): δ = 7.99 (d, *J* = 8.4 Hz, 2H, Ar-H), 7.72 (d, *J* = 8.4 Hz, 2H, Ar-H), 7.53 (d, *J* = 8.7 Hz, 2H, Ar-H), 7.42-7.29 (m, 15H, Ar-H), 7.11 (d, *J* = 8.7 Hz, 2H, Ar-H), 5.59 (d, *J* = 1.6 Hz, 1H, H-1), 4.97 (d, *J* = 10.7 Hz, 1H, PhCH₂O), 4.84 (d, *J* = 12.3 Hz, 1H, PhCH₂O), 4.77-4.74 (m, 3H, PhCH₂O), 4.62 (d, *J* = 10.7 Hz, 1H, PhCH₂O), 4.38 (dd, *J* = 1.9, 11.9 Hz, 1H, H-6a), 4.29 (dd, *J* = 4.9, 12.0 Hz, 1H, H-6b), 4.15 (dd, *J* = 3.0, 9.2 Hz, 1H, H-3), 4.04 (t, *J* = 9.5 Hz, 1H, H-4), 4.00 (m, 1H, H-2), 3.88 (ddd, *J* = 1.8, 4.8, 9.8 Hz, 1H, H-5), 3.09 (s, 3H, SO₂CH₃), 2.16 (d, *J* = 7.1 Hz, 2H, CH₂COO), 2.04 (m, 1H, CH(CH₃)₂), 0.89 (d, *J* = 3.0 Hz, 3H, CH₃), 0.88 ppm (d, *J* = 3.0 Hz, 3H, CH₃); ¹³C NMR (125 MHz, CDCl₃): δ = 172.93 (CO), 156.76, 146.14, 138.85, 138.33, 138.15, 138.13, 133.29, 128.66, 128.62, 128.60, 128.58, 128.22, 128.09, 127.98, 127.96, 127.94, 127.89, 127.62, 117.11 (30C, Ar-C), 96.39 (C-1), 79.97 (C-3), 75.45 (PhCH₂O), 74.61, 74.57 (C-2, C-4), 73.13, 72.62 (2 PhCH₂O), 71.22 (C-5), 62.89 (C-6), 44.77 (SO₂CH₃), 43.48 (CH₂COO), 25.70 (CH(CH₃)₂), 22.56 ppm (2 CH₃); ESI-MS: *m/z*: Calcd for C₄₅H₄₈NaO₉S [M+Na]⁺: 787.29, found: 787.46.

4'-(Methylsulfonyl)-biphenyl-4-yl 2,3,4-tri-*O*-benzyl-6-*O*-valeryl- α -D-mannopyranoside (13g).

Prepared according to the general procedure A from **12** (69 mg, 0.101 mmol), valeryl chloride (49 μ L, 0.404 mmol, 4.0 eq) and DMAP (1 mg, 0.008 mmol, 0.08 eq). The reaction was started at rt and then

wormed up 60 °C. Yield: 70 mg (91%) as yellowish oil. $[\alpha]_D^{20} +63.9$ (*c* 1.00, CHCl₃); ¹H NMR (500 MHz, CDCl₃): $\delta = 7.90$ (d, *J* = 8.4 Hz, 2H, Ar-H), 7.64 (d, *J* = 8.4 Hz, 2H, Ar-H), 7.45 (d, *J* = 8.7 Hz, 2H, Ar-H), 7.33-7.20 (m, 15H, Ar-H), 7.03 (d, *J* = 8.7 Hz, 2H, Ar-H), 5.52 (d, *J* = 1.5 Hz, 1H, H-1), 4.88 (d, *J* = 10.7 Hz, 1H, PhCH₂O), 4.76 (d, *J* = 12.3 Hz, 1H, PhCH₂O), 4.70-4.63 (m, 3H, PhCH₂O), 4.53 (d, *J* = 10.7 Hz, 1H, PhCH₂O), 4.28-4.21 (m, 2H, H-6a, H-6b), 4.07 (dd, *J* = 3.0, 9.2 Hz, 1H, H-3), 3.95 (t, *J* = 9.5 Hz, 1H, H-4), 3.92 (m, 1H, H-2), 3.81 (ddd, *J* = 2.3, 4.4, 9.8 Hz, 1H, H-5), 3.01 (s, 3H, SO₂CH₃), 2.19 (t, *J* = 9.5 Hz, 2H, CH₂COO), 1.50-1.44 (m, 2H, CH₂), 1.24-1.17 (m, 2H, CH₂), 0.77 ppm (t, *J* = 7.4 Hz, 3H, CH₃); ¹³C NMR (125 MHz, CDCl₃): $\delta = 173.63$ (CO), 156.76, 146.12, 138.84, 138.32, 138.14, 138.12, 133.29, 128.65, 128.60, 128.59, 128.57, 128.22, 128.06, 127.99, 127.97, 127.94, 127.92, 127.88, 127.61, 117.12 (30C, Ar-C), 96.43 (C-1), 79.97 (C-3), 75.21 (PhCH₂O), 74.59, 74.52 (C-2, C-4), 73.11, 72.60 (2 PhCH₂O), 71.17 (C-5), 63.01 (C-6), 44.75 (SO₂CH₃), 34.04 (CH₂COO), 27.00, 22.35 (2 CH₂), 13.78 ppm (CH₃); ESI-MS: *m/z*: Calcd for C₄₅H₄₈NaO₉S [M+Na]⁺: 787.29, found: 787.56.

4'-(Methylsulfonyl)-biphenyl-4-yl 2,3,4-tri-*O*-benzyl-6-*O*-pivaloyloxymethyl- α -D-mannopyranoside (14). The compound **12** (250 mg, 0.367 mmol) was dissolved in dry DMSO under argon followed by the addition of Ac₂O (2 mL) and AcOH (0.2 mL). The reaction was stirred at rt for 19 h. The mixture was diluted with EtOAc (50 mL) and washed with satd aq NaHCO₃ (2 x 50 mL) and brine (50 mL). The organic layer was dried over Na₂SO₄, concentrated in vacuo and pre-purified by MPLC on silica gel (petroleum ether/EtOAc, 7:3) to afford 153 mg of the intermediate. The obtained compound (113 mg) was dissolved in dry DMF (2 mL) under argon and PivOH (47 mg, 0.460 mmol) and NIS (52 mg, 0.230 mmol) were added. The reaction was quenched after 17 h with Et₃N (0.100 mL). Then, the mixture was diluted with EtOAc (50 mL) and washed with satd aq NaHCO₃ (50 mL), H₂O (50 mL) and brine (50 mL). The organic layer was dried over Na₂SO₄, concentrated in vacuo and purified by MPLC on silica gel (petroleum ether/EtOAc, 7:3). The compound **14** was obtained in overall yield of 33% (72 mg) over two steps. $[\alpha]_D^{20} +64.3$ (*c* 0.58, CHCl₃); ¹H NMR (500 MHz, CDCl₃): $\delta = 7.84$ (d, *J* = 8.4 Hz, 2H, Ar-H), 7.63 (d, *J* = 8.4 Hz, 2H, Ar-H), 7.45 (d, *J* = 8.7 Hz, 2H, Ar-H), 7.32-7.21 (m, 15H, Ar-H), 7.02 (d, *J* = 8.7 Hz, 2H, Ar-H), 5.50 (d, *J* = 1.6 Hz, 1H, H-1), 5.22 (s, 2H, OCH₂O), 4.88 (d, *J* = 10.9 Hz, 1H, PhCH₂O), 4.75 (d, *J* = 12.4 Hz, 1H, PhCH₂O), 4.70 (d, *J* = 12.4 Hz, 1H, PhCH₂O), 4.65-4.62 (m, 2H, PhCH₂O), 4.59 (d, *J* = 11.0 Hz, 1H, PhCH₂O), 4.05-3.97 (m, 2H, H-3, H-4), 3.90 (m, 1H, H-2), 3.83 (dd, *J* = 4.4, 10.7 Hz, 1H, H-6a), 3.78-3.72 (m, 2H, H-5, H-6b), 2.99 (s, 3H, SO₂CH₃), 1.08 ppm (s, 9H, CH₃); ¹³C NMR (125 MHz, CDCl₃): $\delta = 178.10$ (CO), 156.90, 146.19, 138.83, 138.47, 138.19, 133.28, 128.74, 128.60, 128.59, 128.55, 128.08, 128.00, 127.98, 127.86, 127.83, 127.67, 117.16 (30C, Ar-C), 96.74 (C-1), 89.94 (OCH₂O), 80.00 (C-3), 75.25 (PhCH₂O), 74.55, 74.50 (C-2, C-4), 73.16, 72.62 (2 PhCH₂O), 72.38 (C-5), 69.04 (C-6), 44.78 (SO₂CH₃), 39.04 (C(CH₃)₃), 27.17 ppm (3 CH₃); ESI-MS: *m/z*: Calcd for C₄₆H₅₀NaO₁₀S [M+Na]⁺: 817.30, found: 817.39.

4'-(Methylsulfonyl)-biphenyl-4-yl 6-O-acetyl- α -D-mannopyranoside (5a). Prepared according to the general procedure B from **13a** (50 mg, 0.069 mmol) with 15 mg of Pd(OH)₂/C (E101 NE/W, 20% Pd) in EtOH (5 mL). Purified using DCM/MeOH (9:1) solvent system. Yield: 24 mg (75%) as white solid. $[\alpha]_D^{20}$ +101.2 (*c* 0.19, MeOH); ¹H NMR (500 MHz, CD₃OD): δ = 8.02 (d, *J* = 8.5 Hz, 2H, Ar-H), 7.88 (d, *J* = 8.5 Hz, 2H, Ar-H), 7.71 (d, *J* = 8.8 Hz, 2H, Ar-H), 7.26 (d, *J* = 8.6 Hz, 2H, Ar-H), 5.57 (d, *J* = 1.5 Hz, 1H, H-1), 4.39 (dd, *J* = 1.9, 11.8 Hz, 1H, H-6a), 4.24 (dd, *J* = 6.4, 11.8 Hz, 1H, H-6b), 4.08 (dd, *J* = 1.8, 3.4 Hz, 1H, H-2), 3.94 (dd, *J* = 3.4, 9.0 Hz, 1H, H-3), 3.82-3.73 (m, 2H, H-4, H-5), 3.18 (s, 3H, SO₂CH₃), 1.93 ppm (s, 3H, CH₃); ¹³C NMR (125 MHz, CD₃OD): δ = 172.68 (CO), 158.24, 147.29, 140.20, 134.42, 129.59, 129.03, 128.47, 118.37 (12C, Ar-C), 99.90 (C-1), 73.02 (C-5), 72.39 (C-3), 71.77 (C-2), 68.52 (C-4), 64.81 (C-6), 44.48 (SO₂CH₃), 20.69 ppm (CH₃); HRMS: *m/z*: Calcd for C₂₁H₂₄NaO₉S [M+Na]⁺: 475.1039, found: 475.1037.

4'-(Methylsulfonyl)-biphenyl-4-yl 6-O-propionyl- α -D-mannopyranoside (5b). Prepared according to the general procedure B from **13b** (28 mg, 0.038 mmol) with 20 mg of Pd(OH)₂/C (E101 NE/W, 20% Pd) in EtOH (5 mL). Purified using DCM/MeOH (1:0-9:1) solvent system. Yield: 11 mg (59%) as white oil. $[\alpha]_D^{20}$ +93.8 (*c* 0.50, MeOH); ¹H NMR (500 MHz, CD₃OD): δ = 8.02 (d, *J* = 8.4 Hz, 2H, Ar-H), 7.87 (d, *J* = 8.4 Hz, 2H, Ar-H), 7.70 (d, *J* = 8.7 Hz, 2H, Ar-H), 7.25 (d, *J* = 8.7 Hz, 2H, Ar-H), 5.58 (d, *J* = 1.0 Hz, 1H, H-1), 4.42 (dd, *J* = 1.6, 11.7 Hz, 1H, H-6a), 4.23 (dd, *J* = 6.7, 11.7 Hz, 1H, H-6b), 4.09 (d, *J* = 1.6 Hz, 1H, H-2), 3.95 (dd, *J* = 3.4, 9.1 Hz, 1H, H-3), 3.82-3.73 (m, 2H, H-4, H-5), 3.18 (s, 3H, SO₂CH₃), 2.25 (dq, *J* = 2.8, 7.6 Hz, 2H, CH₂COO), 1.02 ppm (t, *J* = 7.6 Hz, 3H, CH₃); ¹³C NMR (125 MHz, CD₃OD): δ = 175.92 (CO), 158.18, 147.26, 140.19, 134.37, 129.57, 129.03, 128.45, 118.34 (12C, Ar-C), 99.75 (C-1), 73.11 (C-5), 72.39 (C-3), 71.74 (C-2), 68.57 (C-4), 64.75 (C-6), 44.48 (SO₂CH₃), 28.20 (CH₂COO), 9.31 ppm (CH₃); HRMS: *m/z*: Calcd for C₂₂H₂₆NaO₉S [M+Na]⁺: 489.1195, found: 489.1192.

4'-(Methylsulfonyl)-biphenyl-4-yl 6-O-isobutyryl- α -D-mannopyranoside (5c). Prepared according to the general procedure B from **13c** (40 mg, 0.053 mmol) with 25 mg of Pd(OH)₂/C (E101 NE/W, 20% Pd) in EtOH (4 mL). Purified using DCM/MeOH (1:0-9:1) solvent system. Yield: 18 mg (70%) as white oil. $[\alpha]_D^{20}$ +109.8 (*c* 0.85, MeOH); ¹H NMR (500 MHz, CD₃OD): δ = 8.02 (d, *J* = 8.4 Hz, 2H, Ar-H), 7.86 (d, *J* = 8.5 Hz, 2H, Ar-H), 7.68 (d, *J* = 8.7 Hz, 2H, Ar-H), 7.25 (d, *J* = 8.7 Hz, 2H, Ar-H), 5.60 (d, *J* = 1.1 Hz, 1H, H-1), 4.45 (dd, *J* = 1.6, 11.7 Hz, 1H, H-6a), 4.20 (dd, *J* = 7.0, 11.7 Hz, 1H, H-6b), 4.09 (dd, *J* = 1.7, 3.2 Hz, 1H, H-2), 3.95 (dd, *J* = 3.4, 9.1 Hz, 1H, H-3), 3.82-3.72 (m, 2H, H-4, H-5), 3.18 (s, 3H, SO₂CH₃), 2.45 (hept, *J* = 7.0 Hz, 1H, CH(CH₃)₂), 1.06 (d, *J* = 7.0 Hz, 3H, CH₃), 1.02 ppm (d, *J* = 7.0 Hz, 3H, CH₃); ¹³C NMR (125 MHz, CD₃OD): δ = 178.50 (CO), 158.14, 147.26, 140.17, 134.34, 129.60, 129.02, 128.43, 118.29 (12C, Ar-C), 99.61 (C-1), 73.27 (C-5), 72.37 (C-3), 71.71 (C-2), 68.57 (C-4), 64.84 (C-6), 44.48 (SO₂CH₃), 35.12 (CH), 19.23, 19.14 ppm (2 CH₃); HRMS: *m/z*: Calcd for C₂₃H₂₈NaO₉S [M+Na]⁺: 503.1352, found: 503.1353.

4'-(Methylsulfonyl)-biphenyl-4-yl 6-O-butyryl- α -D-mannopyranoside (5d). Prepared according to the general procedure B from **13d** (45 mg, 0.060 mmol) with 40 mg of Pd(OH)₂/C (E101 NE/W, 20% Pd) in EtOH (5 mL). Purified using DCM/MeOH (9:1) solvent system. Yield: 21 mg (72%) as colorless oil. $[\alpha]_D^{20} +97.3$ (*c* 1.05, MeOH); ¹H NMR (500 MHz, CD₃OD): δ = 8.01 (d, *J* = 8.5 Hz, 2H, Ar-H), 7.87 (d, *J* = 8.5 Hz, 2H, Ar-H), 7.69 (d, *J* = 8.8 Hz, 2H, Ar-H), 7.24 (d, *J* = 8.8 Hz, 2H, Ar-H), 5.58 (d, *J* = 1.4 Hz, 1H, H-1), 4.43 (dd, *J* = 1.8, 11.7 Hz, 1H, H-6a), 4.20 (dd, *J* = 6.9, 11.7 Hz, 1H, H-6b), 4.08 (dd, *J* = 1.7, 3.3 Hz, 1H, H-2), 3.93 (dd, *J* = 3.4, 9.1 Hz, 1H, H-3), 3.79 (m, 1H, H-5), 3.73 (m, 1H, H-4), 3.17 (s, 3H, SO₂CH₃), 2.21-2.17 (m, 2H, CH₂COO), 1.55-1.47 (m, 2H, CH₂), 0.83 ppm (t, *J* = 7.4 Hz, 3H, CH₃); ¹³C NMR (125 MHz, CD₃OD): δ = 175.09 (CO), 158.18, 147.24, 140.19, 134.31, 129.56, 129.03, 128.43, 118.31 (12C, Ar-C), 99.70 (C-1), 73.17 (C-5), 72.39 (C-3), 71.74 (C-2), 68.59 (C-4), 64.72 (C-6), 44.47 (SO₂CH₃), 36.88 (CH₂COO), 19.29 (CH₂), 13.92 ppm (CH₃); HRMS: *m/z*: Calcd for C₂₃H₂₈NaO₉S [M+Na]⁺: 503.1352, found: 503.1350.

4'-(Methylsulfonyl)-biphenyl-4-yl 6-O-pivaloyl- α -D-mannopyranoside (5e). Prepared according to the general procedure B from **13e** (50 mg, 0.065 mmol) with 15 mg of Pd(OH)₂/C (E101 NE/W, 20% Pd) in EtOH (5 mL). Purified using DCM/MeOH (9:1) solvent system. Yield: 24 mg (73%) as white oil. $[\alpha]_D^{20} +96.0$ (*c* 1.18, MeOH); ¹H NMR (500 MHz, CD₃OD): δ = 8.02 (d, *J* = 8.5 Hz, 2H, Ar-H), 7.85 (d, *J* = 8.6 Hz, 2H, Ar-H), 7.68 (d, *J* = 8.7 Hz, 2H, Ar-H), 7.26 (d, *J* = 8.9 Hz, 2H, Ar-H), 5.62 (d, *J* = 1.5 Hz, 1H, H-1), 4.45 (dd, *J* = 1.7, 11.7 Hz, 1H, H-6a), 4.15 (dd, *J* = 7.4, 11.7 Hz, 1H, H-6b), 4.09 (dd, *J* = 1.8, 3.4 Hz, 1H, H-2), 3.96 (dd, *J* = 3.4, 9.2 Hz, 1H, H-3), 3.81 (ddd, *J* = 1.6, 7.4, 9.2 Hz, 1H, H-5), 3.73 (t, *J* = 9.6 Hz, 1H, H-4), 3.18 (s, 3H, SO₂CH₃), 1.07 ppm (s, 9H, CH₃); ¹³C NMR (125 MHz, CD₃OD): δ = 179.92 (CO), 158.09, 147.28, 140.16, 134.31, 129.65, 129.03, 128.43, 118.26 (12C, Ar-C), 99.43 (C-1), 73.38 (C-5), 72.35 (C-3), 71.68 (C-2), 68.59 (C-4), 65.14 (C-6), 44.48 (SO₂CH₃), 39.72 (C(CH₃)₃), 27.43 ppm (CH₃); HRMS: *m/z*: Calcd for C₂₄H₃₀NaO₉S [M+Na]⁺: 517.1508, found: 517.1507.

4'-(Methylsulfonyl)-biphenyl-4-yl 6-O-isovaleryl- α -D-mannopyranoside (5f). Prepared according to the general procedure B from **13f** (34 mg, 0.044 mmol) with 40 mg of Pd(OH)₂/C (E101 NE/W, 20% Pd) in EtOH (7 mL). Purified using DCM/MeOH (9:1) solvent system. Yield: 12 mg (55%) as colorless oil. $[\alpha]_D^{20} +120.3$ (*c* 0.60, MeOH); ¹H NMR (500 MHz, CD₃OD): δ = 8.02 (d, *J* = 8.5 Hz, 2H, Ar-H), 7.88 (d, *J* = 8.5 Hz, 2H, Ar-H), 7.70 (d, *J* = 8.8 Hz, 2H, Ar-H), 7.25 (d, *J* = 8.8 Hz, 2H, Ar-H), 5.58 (d, *J* = 1.3 Hz, 1H, H-1), 4.45 (dd, *J* = 1.6, 11.7 Hz, 1H, H-6a), 4.18 (dd, *J* = 7.0, 11.7 Hz, 1H, H-6b), 4.07 (dd, *J* = 1.7, 3.3 Hz, 1H, H-2), 3.94 (dd, *J* = 3.4, 9.2 Hz, 1H, H-3), 3.79 (m, 1H, H-5), 3.72 (m, 1H, H-4), 3.17 (s, 3H, SO₂CH₃), 2.09 (dd, *J* = 3.0, 7.2 Hz, 2H, CH₂COO), 1.95 (m, 1H, CH(CH₃)₂), 0.83 ppm (app-t, *J* = 6.3 Hz, 6H, 2 CH₃); ¹³C NMR (125 MHz, CD₃OD): δ = 174.55 (CO), 158.20, 147.24, 140.19, 134.28, 129.57, 129.03, 128.42, 118.30 (12C, Ar-C), 99.69 (C-1), 73.25 (C-5), 72.39 (C-3), 71.74 (C-2), 68.60 (C-4), 64.72 (C-6), 44.47 (SO₂CH₃), 44.16 (CH₂COO),

26.67 (CH(CH₃)₂), 22.68, 22.66 ppm (2 CH₃); HRMS: *m/z*: Calcd for C₂₄H₃₀NaO₉S [M+Na]⁺: 517.1508, found: 517.1499.

4'-(Methylsulfonyl)-biphenyl-4-yl 6-O-valeryl- α -D-mannopyranoside (5g). Prepared according to the general procedure B from **13g** (51 mg, 0.067 mmol) with 40 mg of Pd(OH)₂/C (E101 NE/W, 20% Pd) in EtOH (15 mL). Purified using DCM/MeOH (95:5) solvent system. Yield: 25 mg (76%) as white solid. $[\alpha]_D^{20}$ +111.4 (*c* 1.00, MeOH); ¹H NMR (500 MHz, CD₃OD): δ = 7.99 (d, *J* = 8.5 Hz, 2H, Ar-H), 7.85 (d, *J* = 8.5 Hz, 2H, Ar-H), 7.68 (d, *J* = 8.8 Hz, 2H, Ar-H), 7.23 (d, *J* = 8.8 Hz, 2H, Ar-H), 5.56 (d, *J* = 1.4 Hz, 1H, H-1), 4.41 (dd, *J* = 1.8, 11.7 Hz, 1H, H-6a), 4.18 (dd, *J* = 7.0, 11.7 Hz, 1H, H-6b), 4.05 (dd, *J* = 1.7, 3.3 Hz, 1H, H-2), 3.91 (dd, *J* = 3.4, 9.1 Hz, 1H, H-3), 3.77 (m, 1H, H-5), 3.70 (t, *J* = 9.6 Hz, 1H, H-4), 3.15 (s, 3H, SO₂CH₃), 2.21-2.17 (m, 2H, CH₂COO), 1.48-1.42 (m, 2H, CH₂), 1.24-1.17 (m, 2H, CH₂), 0.79 ppm (t, *J* = 7.4 Hz, 3H, CH₃); ¹³C NMR (125 MHz, CD₃OD): δ = 175.26 (CO), 163.63, 158.20, 147.22, 140.20, 134.28, 129.56, 129.02, 128.41, 118.31 (12C, Ar-C), 99.73 (C-1), 73.18 (C-5), 72.40 (C-3), 71.74 (C-2), 68.60 (C-4), 64.75 (C-6), 44.48 (SO₂CH₃), 34.71 (CH₂COO), 27.96, 23.20 (2 CH₂), 13.99 ppm (CH₃); HRMS: *m/z*: Calcd for C₂₄H₃₀NaO₉S [M+Na]⁺: 517.1508, found: 517.1499.

4'-(Methylsulfonyl)-biphenyl-4-yl 6-O-pivaloyloxymethyl- α -D-mannopyranoside (5h). Prepared according to the general procedure B from **14** (36 mg, 0.045 mmol) with 30 mg of Pd(OH)₂/C (E101 NE/W, 20% Pd) in EtOH (5 mL). Purified using DCM/MeOH (95:5) solvent system. Yield: 10 mg (24%) as white solid. $[\alpha]_D^{20}$ +111.4 (*c* 1.00, MeOH); ¹H NMR (500 MHz, CD₃OD): δ = 7.99 (d, *J* = 8.5 Hz, 2H, Ar-H), 7.86 (d, *J* = 8.5 Hz, 2H, Ar-H), 7.67 (d, *J* = 8.8 Hz, 2H, Ar-H), 7.23 (d, *J* = 8.8 Hz, 2H, Ar-H), 5.52 (d, *J* = 1.6 Hz, 1H, H-1), 5.26 (s, 2H, OCH₂O), 4.03 (dd, *J* = 1.8, 3.3 Hz, 1H, H-2), 3.91-3.90 (m, 2H, H-3, H-6a), 3.85 (m, 1H, H-6b), 3.75-3.71 (m, 2H, H-4, H-5), 3.15 (s, 3H, SO₂CH₃), 1.19 ppm (s, 9H, CH₃); ¹³C NMR (125 MHz, CD₃OD): δ = 179.44 (CO), 158.49, 147.36, 140.16, 134.45, 129.65, 129.01, 128.50, 118.44 (12C, Ar-C), 100.20 (C-1), 90.45 (OCH₂O), 74.36 (C-5), 72.42 (C-2), 71.83 (C-3), 70.53 (C-6), 68.32 (C-4), 44.48 (SO₂CH₃), 39.92 (C(CH₃)₃), 27.39 ppm (3 CH₃); HRMS: *m/z*: Calcd for C₂₅H₃₂NaO₁₀S [M+Na]⁺: 547.1614, found: 547.1607.

Pharmacokinetic Assays

Materials: Dimethyl sulfoxide (DMSO), 1-propanol, 1-octanol, Dulbecco's Modified Eagle's Medium (DMEM) high glucose, penicillin-streptomycin (solution stabilized, with 10'000 units penicillin and 10 mg streptomycin/mL), L-glutamine solution (200 mM), magnesium chloride, ammonium acetate, bis(4-nitrophenyl) phosphate (BNPP), and loperamide hydrochloride were purchased from Sigma-Aldrich (St. Louis, MI, USA). PRISMA HT universal buffer, GIT-0 Lipid Solution, and Acceptor Sink Buffer were ordered from pIon (Woburn, MA, USA). MEM non-essential amino acids solution 10 mM (100X), fetal bovine serum (FBS), and DMEM without sodium pyruvate and phenol red were bought from Invitrogen (Carlsbad, CA, USA). Acetonitrile (MeCN) and

methanol (MeOH) were ordered from Acros Organics (Geel, Belgium). Pooled male rat liver microsomes (Sprague Dawley), and pooled human liver microsomes were ordered from BD Bioscience (Franklin Lakes, NJ, USA). The Caco-2 cells were kindly provided by Prof G. Imanidis, FHNW, Muttenz, Switzerland and originated from the American Type Culture Collection (Rockville, MD, USA).

log *P* determination. The in silico prediction tool ALOGPS^[30] was used to estimate the octanol-water partition coefficients (log *P*) of the compounds. Depending on these values, the compounds were classified into three categories: hydrophilic compounds (log *P* below zero), moderately lipophilic compounds (log *P* between zero and one) and lipophilic compounds (log *P* above one). For each category, two different ratios (volume of 1-octanol to volume of buffer) were defined as experimental parameters (Table 2).

Table 2. Compound classification based on estimated log *P* values.

Compound type	log <i>P</i>	ratios (1-octanol: buffer)
hydrophilic	< 0	30:140, 40:130
moderately lipophilic	0 - 1	70:110, 110:70
lipophilic	> 1	3:180, 4:180

Equal amounts of phosphate buffer (0.1 M, pH 7.4) and 1-octanol were mixed and shaken vigorously for 5 min to saturate the phases. The mixture was left until separation of the two phases occurred, and the buffer was retrieved. Stock solutions of the test compounds were diluted with buffer to a concentration of 1 μM. For each compound, six determinations, *i.e.* three determinations per 1-octanol:buffer ratio, were performed in different wells of a 96-well plate. The respective volumes of buffer containing analyte (1 μM) were pipetted to the wells and covered by saturated 1-octanol according to the chosen volume ratio. The plate was sealed with aluminium foil, shaken (1350 rpm, 25 °C, 2 h) on a Heidolph Titramax 1000 plate-shaker (Heidolph Instruments GmbH & Co. KG, Schwabach, Germany) and centrifuged (2000 rpm, 25 °C, 5 min, 5804 R Eppendorf centrifuge, Hamburg, Germany). The aqueous phase was transferred to a 96-well plate for analysis by liquid chromatography-mass spectrometry (LC-MS, see below).

The log *P* coefficients were calculated from the 1-octanol:buffer ratio (o:b), the initial concentration of the analyte in buffer (1 μM), and the concentration of the analyte in buffer (*c_B*) with Equation 1:

$$\log P = \log \left(\frac{1\mu M - c_B}{c_B} \times \frac{1}{o:b} \right) \quad (1)$$

The average of the three log *P* values per 1-octanol:buffer ratio was calculated. If the two means obtained for a compound did not differ by more than 0.1 units, the results were accepted.

Parallel artificial membrane permeability assay (PAMPA). Effective permeability ($\log P_e$) was determined in a 96-well format with PAMPA.^[31] For each compound, measurements were performed at pH 7.4 in quadruplicate. Four wells of a deep well plate were filled with 650 μL of PRISMA HT universal buffer, adjusted to pH 7.4 by adding the requested amount of NaOH (0.5 M). Samples (150 μL) were withdrawn from each well to determine the blank spectra by UV/Vis-spectroscopy (190 to 500 nm, SpectraMax 190, Molecular Devices, Silicon Valley, CA, USA). Then, analyte dissolved in DMSO (10 mM) was added to the remaining buffer to yield 50 μM solutions. To exclude precipitation, the optical density (OD) was measured at 650 nm, and solutions exceeding OD 0.01 were filtrated. Afterwards, samples (150 μL) were withdrawn to determine the reference spectra. Further 200 μL was transferred to each well of the donor plate of the PAMPA sandwich (pIon, P/N 110 163). The filter membranes at the bottom of the acceptor plate were infused with 5 μL of GIT-0 Lipid Solution and 200 μL of Acceptor Sink Buffer was filled into each acceptor well. The sandwich was assembled, placed in the GutBoxTM, and left undisturbed for 16 h. Then, it was disassembled and samples (150 μL) were transferred from each donor and acceptor well to UV-plates for determination of the UV/Vis spectra. Effective permeability ($\log P_e$) was calculated from the compound flux deduced from the spectra, the filter area, and the initial sample concentration in the donor well with the aid of the PAMPA Explorer Software (pIon, version 3.5).

Colorectal adenocarcinoma (Caco-2) cell permeation assay. Caco-2 cells were cultivated in tissue culture flasks (BD Biosciences, Franklin Lakes, NJ, USA) with DMEM high glucose medium, containing L-Glutamine (2 mM), nonessential amino acids (0.1 mM), Penicillin (100 U/mL), Streptomycin (100 $\mu\text{g/mL}$), and fetal bovine serum (10%). The cells were kept at 37 °C in humidified air containing 5% CO₂, and the medium was changed every second day. When approximately 90% confluence was reached, the cells were split in a 1:10 ratio and distributed to new tissue culture flasks. At passage numbers between 60 and 65, they were seeded at a density of 5.3×10^5 cells per well to Transwell 6-well plates (Corning Inc., Corning, NY, USA) with 2.5 mL of culture medium in the basolateral and 2 mL in the apical compartment. The medium was renewed on alternate days. Permeation experiments were performed between days 19 and 21 post seeding. Previously to the experiment, the integrity of the Caco-2 monolayers was evaluated by measuring the transepithelial electrical resistance (TEER) with an Endohm tissue resistance instrument (World Precision Instruments Inc., Sarasota, FL, USA). Only wells with TEER values higher than 250 $\Omega \text{ cm}^2$ were used. To inhibit carboxylesterase activity, the Caco-2 cell monolayers were pre-incubated with bis(4-nitrophenyl) phosphate (BNPP, 200 μM) dissolved in transport medium (DMEM without sodium pyruvate and phenol red) for 40 min.^[32] Experiments were performed in the apical-to-basolateral (absorptive) and basolateral-to-apical (secretory) directions in triplicates. Transport medium was withdrawn from the donor compartments and replaced by the same volume of compound stock solution (10 mM in DMSO) to reach an initial sample concentration of 62.5 μM . The Transwell plate

was shaken (600 rpm, 37 °C) on a Heidolph Titramax 1000 plate-shaker. Samples (40 µL) were withdrawn from the donor and acceptor compartments 30 min after initiation of the experiment and the concentrations were determined by LC-MS (see below). Apparent permeability (P_{app}) was calculated according to Equation 2:

$$P_{app} = \frac{dQ}{dt} \times \frac{1}{A \times c_0} \quad (2)$$

where dQ/dt is the compound flux (mol s^{-1}), A the surface area of the monolayer (cm^2), and c_0 the initial concentration in the donor compartment (mol cm^{-3}).^[33] After the experiment, TEER values were measured again and results from wells with values below $250 \Omega \text{ cm}^2$ were discarded.

Aqueous solubility. Solubility was determined in a 96-well format using the µSOL Explorer solubility analyzer (pIon, version 3.4.0.5). For each compound, measurements were performed in triplicate. Three wells of a deep well plate were filled with 300 µL of PRISMA HT universal buffer, adjusted to pH 7.4 by adding the requested amount of NaOH (0.5 M). Aliquots (3 µL) of a compound stock solution (40-100 mM in DMSO) were added and thoroughly mixed. The final sample concentration was 0.4-1.0 mM, the residual DMSO concentration was 1.0% (v/v). Fifteen hours after initiation of the experiment, the solutions were filtrated (0.2 µm 96-well filter plates) using a vacuum to collect manifold (Whatman Ltd., Maidstone, UK) to remove any precipitates. Equal amounts of filtrate and 1-propanol were mixed and transferred to a 96-well plate for UV detection (190 to 500 nm). The amount of material dissolved was calculated by comparison with UV spectra obtained from reference samples, which were prepared by dissolving compound stock solution in a 1:1 mixture of buffer and 1-propanol (final concentrations 0.067-0.167 mM).

Enzymatic hydrolysis by liver microsome associated carboxylesterase. Incubations were performed in triplicate in a 96-well format on an Eppendorf Thermomixer Comfort. The reaction mixture (270 µL) consisting of liver microsomes (0.139 µg/mL), TRIS-HCl buffer (0.1 M, pH 7.4) and MgCl_2 (2 mM) was preheated (37 °C, 500 rpm, 10 min), and the incubation was initiated by adding 30 µL of compound solution (20 µM) in TRIS-HCl buffer. The final concentration of the compound was 2 µM, and the microsomal concentration was 0.125 mg/mL. At the beginning of the experiment ($t = 0$ min) and after an incubation time of 2, 5, 10, 20, and 30 min, samples (40 µL) were transferred to 120 µL of ice-cooled MeOH and centrifuged (3600 rpm, 4 °C, 10 min). Then, 80 µL of supernatant was transferred to a 96-well plate for analysis by LC-MS (see below). The metabolic half-life ($t_{1/2}$) was calculated from the slope of the linear regression from the log percentage remaining compound versus incubation time relationship. Control experiments were performed in parallel by preincubating the microsomes with the specific carboxylesterase inhibitor BNPP (1 mM) for 5 min before addition of the compound solution.^[34]

Isozyme specific inhibition of carboxylesterase mediated hydrolysis. Test compounds were dissolved in DMSO to 1 mM and then diluted with TRIS-HCl buffer (0.1 M, pH 7.4) containing MgCl₂ (2 mM) to a concentration of 6 μM. Loperamide hydrochloride was dissolved in DMSO to 20 mM, 2 mM, and 0.2 mM and then diluted with TRIS-HCl buffer containing MgCl₂ to a concentration of 750 μM, 75 μM, and 7.5 μM. Human liver microsomes were suspended in TRIS-HCl buffer containing MgCl₂ to a concentration of 30 μg/mL. Compound solution (100 μL) and microsomal suspension (200 μL) mixed with loperamide solution or blank buffer (50 μL) were preheated (37 °C, 500 rpm, 15 min) in separate wells of a 96-well plate. The incubation was initiated by transferring 200 μL of microsome suspension containing loperamide to the compound solution. The final compound concentration was 2 μM, the microsomal concentration was 0.02 mg/mL, and the loperamide concentration was 100 μM, 10 μM, 1 μM, and 0 μM (blank). At the beginning of the experiment (t = 0 min) and after an incubation time of 10, 20, 30, 45, and 60 min, samples (20 μL) were transferred to 60 μL of ice-cooled MeOH and analysed by LC-MS (see below). The metabolic turnover was assessed as accumulation of product **4a** versus incubation time.^[35]

LC-MS measurements. Analyses were performed using a 1100/1200 Series HPLC System coupled to a 6410 Triple Quadrupole mass detector (Agilent Technologies, Inc., Santa Clara, CA, USA) equipped with electrospray ionization. The system was controlled with the Agilent MassHunter Workstation Data Acquisition software (version B.01.04). The column used was an Atlantis[®] T3 C18 column (2.1 x 50 mm) with a 3 μm-particle size (Waters Corp., Milford, MA, USA). The mobile phase consisted of eluent A: 10 mM ammonium acetate, pH 5.0 in 95:5, H₂O:MeCN; and eluent B: MeCN containing 0.1% formic acid. The flow rate was maintained at 0.6 mL/min. The gradient was ramped from 95% A/5% B to 5% A/95% B over 1 min, and then hold at 5% A/95% B for 0.1 min. The system was then brought back to 95% A/5% B, resulting in a total duration of 4 min. MS parameters such as fragmentor voltage, collision energy, polarity were optimized individually for each drug, and the molecular ion was followed for each compound in the multiple reaction monitoring mode. The concentrations of the analytes were quantified by the Agilent Mass Hunter Quantitative Analysis software (version B.01.04).

References

- [1] (a) Fihn, S. D. *N. Engl. J. Med.* **2003**, *349*, 259-266; (b) Hooton, T. M.; Besser, R.; Foxman, B.; Fritsche, T. R.; Nicolle, L. E. *Clin. Infect. Dis.* **2004**, *39*, 75-80.
- [2] Sanchez, G. V.; Master, R. N.; Karlowsky, J. A.; Bordon, J. M. *Antimicrob. Agents Chemother.* **2012**, *56*, 2181-2183.
- [3] Schilling, J. D.; Mulvey, M. A.; Hultgren, S. J. *J. Infect. Dis.* **2001**, *183 Suppl. 1*, S36-40.
- [4] Capitani, G.; Eidam, O.; Glockshuber, R.; Grütter, M. G. *Microbes Infect.* **2006**, *8*, 2284-2290.
- [5] (a) Sharon, N. *Biochim. Biophys. Acta* **2006**, *1760*, 527-537; (b) Le Trong, I.; Aprikian, P.; Kidd, B. A.; Forero-Shelton, M.; Tchesnokova, V.; Rajagopal, P.; Rodriguez, V.; Interlandi, G.; Klevit, R.; Vogel, V.; Stenkamp, R. E.; Sokurenko, E. V.; Thomas, W. E. *Cell* **2010**, *141*, 645-655.

- [6] (a) Firon, N.; Ofek, I.; Sharon, N. *Biochem. Biophys. Res. Commun.* **1982**, *105*, 1426-1432; (b) Firon, N.; Ofek, I.; Sharon, N. *Carbohydr. Res.* **1983**, *120*, 235-249; (c) Firon, N.; Ashkenazi, S.; Mirelman, D.; Ofek, I.; Sharon, N. *Infect. Immun.* **1987**, *55*, 472-476.
- [7] (a) Bouckaert, J.; Berglund, J.; Schembri, M.; Genst, E. D.; Cools, L.; Wuhrer, M.; Hung, C. S.; Pinkner, J.; Slättergard, R.; Zavialov, A.; Choudhury, D.; Langermann, S.; Hultgren, S. J.; Wyns, L.; Klemm, P.; Oscarson, S.; Knight, S. D.; Greve, H. D. *Mol. Microbiol.* **2005**, *55*, 441– 455; (b) Sperling, O.; Fuchs, A.; Lindhorst, T. K. *Org. Biomol. Chem.* **2006**, *4*, 3913-3922; (c) Han, Z.; Pinkner, J. S.; Ford, B.; Obermann, R.; Nolan, W.; Wildman, S. A.; Hobbs, D.; Ellenberger, T.; Cusumano, C. K.; Hultgren, S. J.; Janetka, J. W. *J. Med. Chem.* **2010**, *53*, 4779-4792; (d) Klein, T.; Abgottspon, D.; Wittwer, M.; Rabbani, S.; Herold, J.; Jiang, X.; Kleeb, S.; Lüthi, C.; Scharenberg, M.; Bezençon, J.; Gubler, E.; Pang, L.; Smiesko, M.; Cutting, B.; Schwardt, O.; Ernst, B. *J. Med. Chem.* **2010**, *53*, 8627 – 8641; (e) Schwardt, O.; Rabbani, S.; Hartmann, M.; Abgottspon, D.; Wittwer, M.; Kleeb, S.; Zalewski, A.; Smiesko, M.; Cutting, B.; Ernst, B. *Bioorg. Med. Chem.* **2011**, *19*, 6454-6473; (f) Cusumano, C. K.; Pinkner, J. S.; Han, Z.; Greene, S. E.; Ford, B. A.; Crowley, J. R.; Henderson, J. P.; Janetka, J. W.; Hultgren, S. J. *Sci. Transl. Med.* **2011**, *3*, 109ra115; (g) Han, Z.; Pinkner, J. S.; Ford, B.; Chorell, E.; Crowley, J. M.; Cusumano, C. K.; Campbell, S.; Henderson, J. P.; Hultgren, S. J.; Janetka, J. W. *J. Med. Chem.* **2012**, *55*, 3945-3959; (h) Jiang, X.; Abgottspon, D.; Kleeb, S.; Rabbani, S.; Scharenberg, M.; Wittwer, M.; Haug, M.; Schwardt, O.; Ernst, B. *J. Med. Chem.* **2012**, *55*, 4700-4713; (i) Pang, L.; Kleeb, S.; Lemme, K.; Rabbani, S.; Scharenberg, M.; Zalewski, A.; Schädler, F.; Schwardt, O.; Ernst, B. *ChemMedChem.* **2012**, *7*, 1404-1422.
- [8] (a) Smith, D. A.; Jones, B. C.; Walker, D. K. *Med. Res. Rev.* **1996**, *16*, 243-266; (b) van de Waterbeemd, H.; Smith, D. A.; Beaumont, K.; Walker, D. K. *J. Med. Chem.* **2001**, *44*, 1313-1333.
- [9] Feng, B.; LaPerle, J. L.; Chang, G.; Varma, M. V. *Expert Opin. Drug Metab. Toxicol.* **2010**, *6*, 939-952.
- [10] Kleeb, S.; Schönemann, W.; Dätwyler, P.; Ernst, B. *In preparation*.
- [11] Kleeb, S.; Pang, L.; Mayer, K.; Eris, D.; Sigl, A.; Preston, R. C.; Zihlmann, P.; Sharpe, T.; Jakob, R. P.; Abgottspon, D.; Hutter, A. S.; Scharenberg, M.; Jiang, X.; Navarra, G.; Rabbani, S.; Smiesko, M.; Lüdin, N.; Bezençon, J.; Schwardt, O.; Maier, T.; Ernst, B. *J. Med. Chem.* **2015**, *58*, 2221-2239.
- [12] (a) Saxon, E.; Bertozzi, C. R. *Science*, **2000**, *287*, 2007-2010; (b) Sarkar, A. K.; Fritz, T. A.; Taylor, W. H.; Esko, J. D. *Proc. Natl. Acad. Sci. U.S.A.*, **1995**, *92*, 3323-3327; (c) Lavergne, T.; Baraguey, C.; Dupouy, C.; Parey, N.; Wuensche, W.; Sczakiel, G.; Vasseur, J.-J.; Debart, F. *J. Org. Chem.*, **2011**, *76*, 5719–5731; (d) Parey, N.; Baraguey, C.; Vasseur, J.-J.; Debart, F. *Org. Lett.*, **2006**, *8*, 3869–3872; (e) Martin, A. R.; Lavergne, T.; Vasseur, J.-J.; Debart, F. *Bioorg. Med. Chem. Lett.*, **2009**, *19*, 4046-4049; (f) Ochi, Y.; Nakagawa, O.; Sakaguchi, K.; Wada, S.-i.; Uarata, H. *Chem. Commun.*, **2013**, *49*, 7620-7622; (g) Thillier, Y.; Stevens, S. K.; Moy, C.; Taylor, J.; Vasseur, J.-J.; Beigelman, L.; Debart, F. *Bioorg. Med. Chem.*, **2013**, *21*, 5461–5469.
- [13] Ali, A.; van den Berg, R. J. B. H. N.; Overkleeft, H. S.; van der Marel, G. A.; Codee, J. D. C. *Tetrahedron* **2010**, *32*, 6121-6132.
- [14] Avdeef, A. In *Pharmacokinetic Optimization in Drug Research; Biological, Physicochemical and Computational Strategies*; Testa, B., van de Waterbeemd, H., Folkers, G., Guy, R., Eds.; Helvetica Chimica Acta: Zurich, 2001; pp 305-326.
- [15] Dearden, J. C.; Bresnen, G. M. *QSAR Comb. Sci.* **1988**, *7*, 133-144.
- [16] Kansy, M.; Senner, F.; Gubernator, K. *J. Med. Chem.* **1998**, *41*, 1007-1010.
- [17] Artursson, P.; Karlsson, J. *Biochem. Biophys. Res. Commun.* **1991**, *175*, 880-885.
- [18] (a) Imai, T.; Taketani, M.; Shii, M.; Hosokawa, M.; Chiba, K. *Drug Metab. Dispos.* **2006**, *34*, 1734-1741; (b) Taketani, M.; Shii, M.; Ohura, K.; Ninomiya, S.; Imai, T. *Life Sci.* **2007**, *81*, 924-932.
- [19] Avdeef, A.; Bendels, S.; Di, L.; Faller, B.; Kansy, M.; Sugano, K.; Yamauchi, Y. *J. Pharm. Sci.* **2007**, *96*, 2893-2909.

- [20] (a) Imai, T.; Imoto, M.; Sakamoto, H.; Hashimoto, M. *Drug Metab. Dispos.* **2005**, *33*, 1185-1190; (b) Ohura, K.; Sakamoto, H.; Ninomiya, S.; Imai, T. *Drug Metab. Dispos.* **2010**, *38*, 323-331.
- [21] Seelig, A.; Gerebtzoff, G. *Expert Opin. Drug. Metab. Toxicol.* **2006**, *2*, 733-752.
- [22] Lipinski, C. A. *J. Pharmacol. Toxicol. Methods* **2000**, *44*, 235-249.
- [23] (a) Beaumont, K.; Webster, R.; Gardner, I.; Dack, K. *Curr. Drug Metab.* **2003**, *4*, 461-485; (b) Ettmayer, P.; Amidon, G. L.; Clement, B.; Testa, B. *J. Med. Chem.* **2004**, *47*, 2393-2404.
- [24] Nielsen, A. B.; Buur, A.; Larsen, C. *Eur. J. Pharm. Sci.* **2005**, *24*, 433-440.
- [25] Evans, D. F.; Pye, G.; Bramley, R.; Clark, A. G.; Dyson, T. J.; Hardcastel, J. D. *Gut*, **1988**, *29*, 1035-1041.
- [26] (a) Li, B.; Sedlacek, M.; Manoharan, I.; Boopathy, R.; Duysen, E. G.; Masson, P.; Lockridge, O. *Biochem. Pharmacol.* **2005**, *70*, 1673-1684. (b) Liederer, B. M.; Borchardt, R. T. *J. Pharm. Sci.* **2006**, *95*, 1177-1195.
- [27] Satoh, T.; Hosokawa, M. *Chem. Biol. Interact.* **2006**, *162*, 195-211.
- [28] (a) Quinney, S. K.; Sanghani, S. P.; Davis, W. I.; Hurley, T. D.; Sun, Z.; Murry, D. J.; Bosron, W. F. *J. Pharmacol. Exp. Ther.* **2005**, *313*, 1011-1016; (b) Wang, J.; Williams, E. T.; Bourgea, J.; Wong, Y. N.; Patten, C. J. *Drug Metab. Dispos.* **2011**, *39*, 1329-1333.
- [29] Roy, R.; Das, S. K.; Santoyo-González, F.; Hernández-Mateo, F.; Dam, T. K.; Brewer, C. F. *Chem. Eur. J.* **2000**, *6*, 1757-1762.
- [30] a) VCCLAB, Virtual Computational Chemistry Laboratory, 2005, <http://www.vcclab.org> (accessed November 19, 2012); b) Tetko, I. V.; Gasteiger, J.; Todeschini, R.; Mauri, A.; Livingstone, D.; Ertl, P.; Palyulin, V. A.; Radchenko, E. V.; Zefirov, N. S.; Makarenko, A. S.; Tanchuk, V. Y.; Prokopenko, V. V. *J. Comput. Aided Mol. Des.* **2005**, *19*, 453-463.
- [31] Kansy, M.; Senner, F.; Gubernator, K. *J. Med. Chem.* **1998**, *41*, 1007-1010.
- [32] Ohura, K.; Sakamoto, H.; Ninomiya, S.; Imai, T. *Drug Metab. Dispos.* **2010**, *38*, 323-331.
- [33] Hubatsch, I.; Ragnarsson, E. G. E.; Artursson, P. *Nat. Protoc.* **2007**, *2*, 2111-2119.
- [34] (a) Imai, T.; Taketani, M.; Shii, M.; Hosokawa, M.; Chiba, K. *Drug Metab. Dispos.* **2006**, *34*, 1734-1741; (b) Taketani, M.; Shii, M.; Ohura, K.; Ninomiya, S.; Imai, T. *Life Sci.* **2007**, *81*, 924-932.
- [35] (a) Quinney, S. K.; Sanghani, S. P.; Davis, W. I.; Hurley, T. D.; Sun, Z.; Murry, D. J.; Bosron, W. F. *J. Pharmacol. Exp. Ther.* **2005**, *313*, 1011-1016; (b) Wang, J.; Williams, E. T.; Bourgea, J.; Wong, Y. N.; Patten, C. J. *Drug Metab. Dispos.* **2011**, *39*, 1329-1333.

2.9 **Paper 8: Antiadhesion therapy for urinary tract infections – a balanced PK/PD profile proved to be key for success**

This publication presents the identification of the indolinyphenyl α -D-mannopyranosides as highly potent FimH antagonists. The assessment of the physicochemical profile and a single-dose pharmacokinetic study complete the characterization of this promising new antagonist category.

Contribution to the project:

Simon Kleeb contributed to the *in vitro* pharmacokinetic characterization of the antagonist molecules. He was responsible for the collection and interpretation of the data presented in this section and edited the description of the experimental procedure. He furthermore contributed to the writing of the manuscript.

This paper was published in the *Journal of Medicinal Chemistry*:

Jiang, X.*; Abgottspon, D.*; Kleeb, S.*; Rabbani, S.; Scharenberg, M.; Wittwer, M.; Haug, M.; Schwardt, O.; Ernst, B. Antiadhesion therapy for urinary tract infections – a balanced PK/PD profile proved to be key for success. *J. Med. Chem.* **2012**, *55*, 4700-4713.

* These authors contributed equally to the project.

© 2012 American Chemical Society

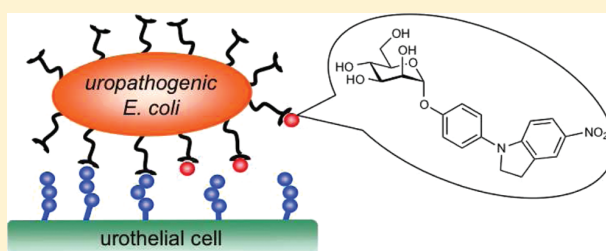
Antiadhesion Therapy for Urinary Tract Infections—A Balanced PK/PD Profile Proved To Be Key for Success

Xiaohua Jiang,[†] Daniela Abgottspon,[†] Simon Kleeb,[†] Said Rabbani, Meike Scharenberg, Matthias Wittwer, Martina Haug, Oliver Schwardt, and Beat Ernst*

Institute of Molecular Pharmacy, University of Basel, Klingelbergstrasse 50, 4056 Basel, Switzerland

Supporting Information

ABSTRACT: The initial step for the successful establishment of urinary tract infections (UTIs), predominantly caused by uropathogenic *Escherichia coli*, is the adhesion of bacteria to urothelial cells. This attachment is mediated by FimH, a mannose-binding adhesin, which is expressed on the bacterial surface. To date, UTIs are mainly treated with antibiotics, leading to the ubiquitous problem of increasing resistance against most of the currently available antimicrobials. Therefore, new treatment strategies are urgently needed, avoiding selection pressure and thereby implying a reduced risk of resistance. Here, we present a new class of highly active antimicrobials, targeting the virulence factor FimH. When the most potent representative, an indolylphenyl mannoside, was administered in a mouse model at the low dosage of 1 mg/kg (corresponding to approximately 25 $\mu\text{g}/\text{mouse}$), the minimal therapeutic concentration to prevent UTI was maintained for more than 8 h. In a treatment study, the colony-forming units in the bladder could be reduced by almost 4 orders of magnitude, comparable to the standard antibiotic treatment with ciprofloxacin (8 mg/kg, sc).



INTRODUCTION

Adhesion to target cells enables microorganisms to evade the natural clearing mechanisms and to ensure survival in the host environment. In urinary tract infections (UTIs), which are predominantly caused by uropathogenic *Escherichia coli* (UPEC), adhesion is accomplished by bacterial lectins, recognizing carbohydrate ligands located on the endothelial cells of the urinary tract.¹ For example, UPEC expressing P-pili cause pyelonephritis by binding to galabiose-containing ligands on the kidney epithelium, while mannose-binding type 1 piliated UPEC promote cystitis by targeting the glycoprotein uroplakin Ia (UPIa) on the mucosal surface of the urinary bladder. This initial step of the infection, the adhesion to the bacterial surface, prevents the rapid clearance of UPECs from the urinary tract by the bulk flow of urine and, at the same time, enables the invasion of host cells.^{2,3} The most prevalent fimbriae encoded by UPEC consist of four subunits, FimA, FimF, FimG, and FimH.⁴ The FimH lectin caps the fimbriae of type 1 pili and contains the carbohydrate recognition domain (CRD), mediating the crucial bacteria–cell interaction.³

UTIs affect a large proportion of the world population and account for significant morbidity and high medical costs.² Symptomatic UTIs should be treated with antibiotics to prevent potential devastating complications, like pyelonephritis and urosepsis. However, recurrent infections with subsequent antibiotic exposure can lead to emergence of antimicrobial resistance, which often results in treatment failure and reduces the range of therapeutic options. Hence, it is an urgent need for public health to develop an efficient, cost-effective, and

nonantibiotic therapy to both prevent and treat UTIs without facilitating antimicrobial resistance.⁵

More than two decades ago, Sharon and co-workers have investigated various mannosides as antagonists for type 1 fimbriae-mediated bacterial adhesion.⁶ For the further improvement of these FimH antagonists, two different approaches were explored. First, multivalent mannosides were investigated,^{7,8} and second, monovalent high-affinity antagonists were designed (for representative examples, see Figure 1)⁸ based on structural information obtained from crystal structures of the carbohydrate-recognition domain (CRD) of FimH cocrystallized with FimH antagonists.⁹

In this article, we present a new class of FimH antagonists. The binding affinities of these indolylphenyl and indolylphenyl α -D-mannosides were determined in several target- and function-based assays. In addition, their in vitro pharmacokinetic properties were assigned, before the potential of selected compounds for in vivo application in a UTI mouse model was explored.

RESULTS AND DISCUSSION

Rational Design of FimH Antagonists. Crystal structures of FimH cocrystallized with various mannosides⁹ disclosed a carbohydrate binding pocket with a hydrophobic entrance, the so-called tyrosine gate. The latter is formed by two tyrosines (Tyr48 and Tyr137) and an isoleucine (Ile52). Whereas *n*-butyl

Received: February 12, 2012

Published: April 23, 2012

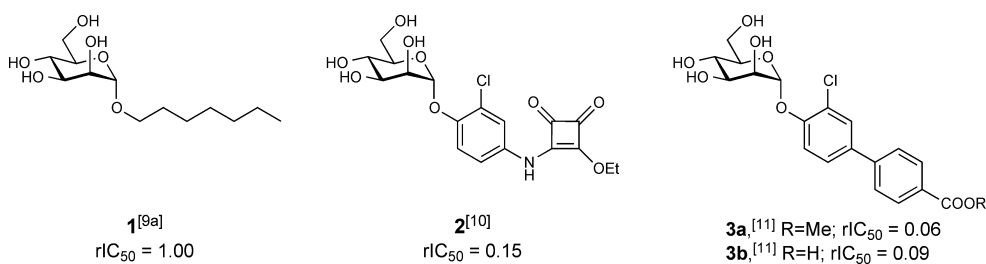


Figure 1. Alkyl (**1**) and aryl (**2** and **3**) α -D-mannopyranosides with nanomolar affinities. *n*-Heptyl α -D-mannoside (**1**) serves as a reference compound throughout our studies. Mannosides **2** and **3** exhibit low nanomolar affinities. Compound **3a** is the first reported orally available FimH antagonist that is hydrolyzed to the renally excretable acid **3b**. The IC_{50} values were determined with a cell-free binding assay.¹² Relative IC_{50} values (rIC_{50}) were calculated by dividing the IC_{50} of the substance of interest by the IC_{50} of the reference compound **1**.

α -D-mannoside populates the tyrosine gate and interacts with both tyrosines (in-docking mode),^{9b,c} biphenyl α -D-mannosides, probably due to insufficient flexibility, adopt an out-docking mode, leading to an optimal π - π stacking of their outer aromatic ring with Tyr48.^{9d} In several recent publications, biphenyl α -D-mannosides with excellent affinities were reported.^{9d,11,13}

Here, antagonists with (aza)indolylphenyl and indolylphenyl aglycones (see Table 1) are explored. According to our docking studies, the increased volume of the outer aromatic ring (indolyl/indolyl vs phenyl) leads to an improved fit. Details are given in the Supporting Information.

Synthesis of FimH Antagonists. Starting from trichloroacetimidate **5**, which was obtained from D-mannose (**4**) as reported earlier,¹⁴ Lewis acid-promoted mannosylation of the phenols **6a–d** yielded the phenyl α -D-mannosides **7–10** (Scheme 1). In the subsequent copper-catalyzed Ullmann type coupling reaction¹⁵ with the indoles **11e–j**, a partial deacetylation of the mannose moiety was observed due to the use of K_2CO_3 or K_3PO_4 as a base. Therefore, the crude products were reacylated to give the substituted 4-(indol-1-yl)phenyl α -D-mannopyranosides **12–20** and **30**. Saponification afforded the test compounds **21–29**, **31**, and **32** (Table 1).

Careful reduction of the nitro group in **13** by catalytic hydrogenation with PtO_2 in the presence of catalytic amounts of morpholine¹⁶ quantitatively yielded the corresponding amine **33** (Scheme 2). Acylation with 4-chlorobenzoyl chloride or methanesulfonyl chloride (\rightarrow **34** and **35**) and subsequent deacetylation under Zemplén conditions gave the amides **36** and **37** (Table 1).

Starting from phenyl mannoside **7**, 7-azaindole derivatives **39** and **40** (Scheme 3) were obtained by an Ullmann type coupling reaction as well. Final deprotection yielded the test compounds **41** and **42** (Table 1).

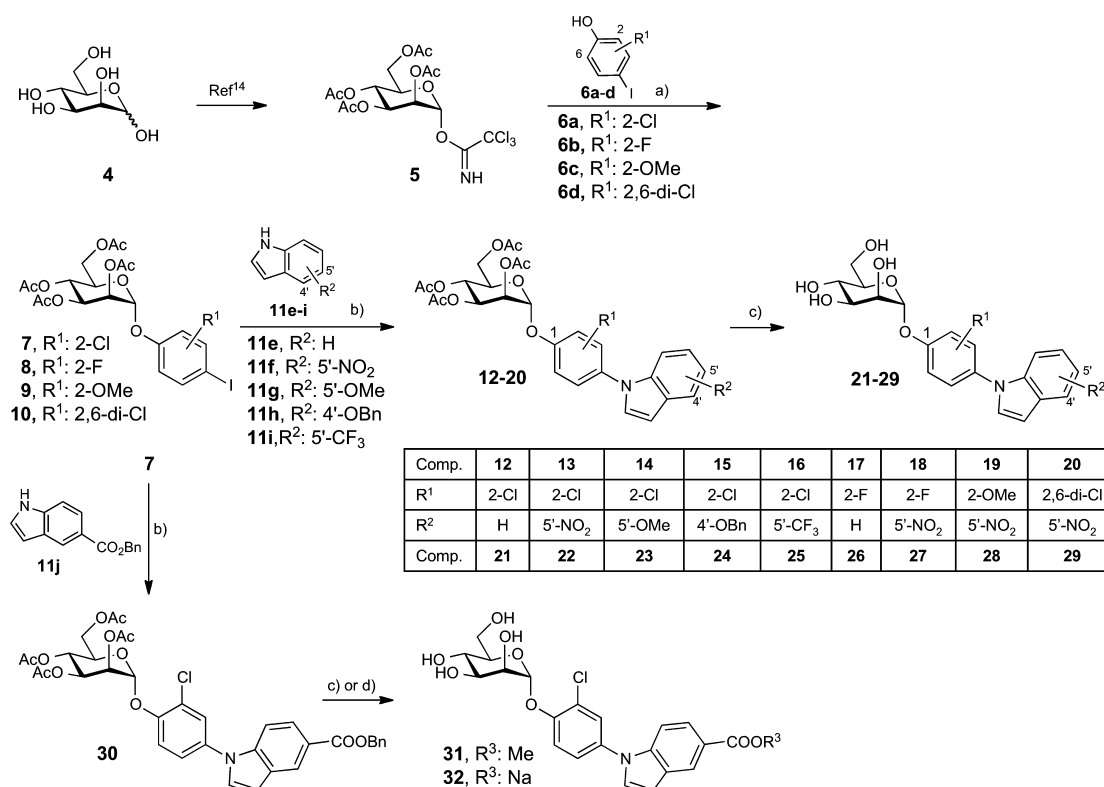
To further explore the contribution of the indole aglycone to binding, it was replaced by indoline moieties (\rightarrow **48a–d** and **52**, Scheme 4). The phenyl mannosides **44** and **50** were synthesized using the procedure as described for **7**. In a palladium-catalyzed Buchwald–Hartwig coupling¹⁷ with 5-nitro-indoline (**45**) or indoline (**46**), the protected mannosides **47a–d** and **51** were obtained in 43–80% yield. Final deacetylation under Zemplén conditions gave the indoline derivatives **48a–d** and **52** (Table 1).

Finally, the synthesis of the 5-linked 7-aza-indole **57** and the imidazo-pyridine derivative **58** is outlined in Scheme 5. Palladium-catalyzed Suzuki–Miyaura coupling¹⁸ of **7** with boronic esters **53** or **54** (\rightarrow **55** and **56**) and subsequent deprotection afforded the test compounds **57** and **58** (Table 1).

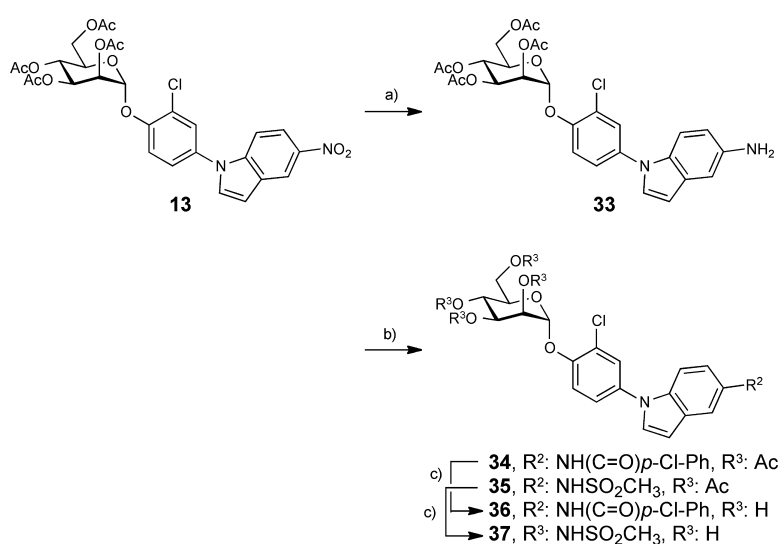
In Vitro Binding Affinities. To evaluate the potential of indolylphenyl and indolylphenyl mannosides to prevent FimH-dependent adhesion of UPECs to urothelial cell surfaces, two different assay formats were applied. First, in the cell-free binding assay,¹² which is based on the interaction of a biotinylated polyacrylamide glycopolymer with the CRD of FimH, the inhibitory potency of FimH antagonists was measured. Second, in the cell-based aggregation assay,¹⁹ the disaggregation of guinea pig erythrocytes (GPE) incubated with UPEC, strain UTI89 was determined as a function of various concentrations of FimH antagonists.

In the two assay formats, different affinities were expected. Whereas in the cell-free binding assay only the CRD of FimH is used, the complete pili are present in the cell-based aggregation assay. Furthermore, both formats are competitive assays, that is, the analyzed antagonists compete with mannosides for the binding site. In the cell-free binding assay, the competitor is a polymer-bound trimannoside, whereas in the aggregation assay, the antagonist competes with more potent oligo- and polysaccharide chains²⁰ present on the surface of erythrocytes.²¹ The interaction is further complicated by the existence of a high- and a low-affinity state of the CRD of FimH. Aprikan et al. experimentally demonstrated that in full-length fimbriae the pilin domain stabilizes the CRD domain in the low-affinity state, whereas the CRD domain alone adopts the high-affinity state.²² Furthermore, it was recently shown that shear stress can induce a conformational switch (twist in the β -sandwich fold of the CRD domain) resulting in improved affinity.²³ Despite these differences, the ranking of the half maximal inhibitory concentration (IC_{50}) values within the two assay formats is expected to be in a similar order.

According to molecular dynamics (MD) simulations, a cavity between the *ortho*-hydrogen of the phenyl ring adjacent to the anomeric center and the binding pocket offers the opportunity to improve binding with a substituent of appropriate size, leading to refined van der Waals interactions. We therefore replaced the *ortho*-hydrogen by a chloro (entries 3–7 and 12–17), fluoro (entries 8 and 9), or methoxy substituent (entry 10). The *ortho*-chloro substituted antagonist showed the best binding affinities in both assays (Table 1). When a second chloro substituent was introduced to the *ortho*-position (**29**, entry 11), the binding affinity unexpectedly decreased in both assays, indicating that the entropic gain expected by symmetrization of the antagonist could not be realized, probably because of rotational constraints. Therefore, an *ortho*-chloro substituent in the first aromatic ring was retained when the indole/indoline moiety was further optimized (**48a–d**, entries 18–21). As compared to the reference compound **1**, the indoline derivative **48c** (entry 20) exhibited an

Scheme 1^a

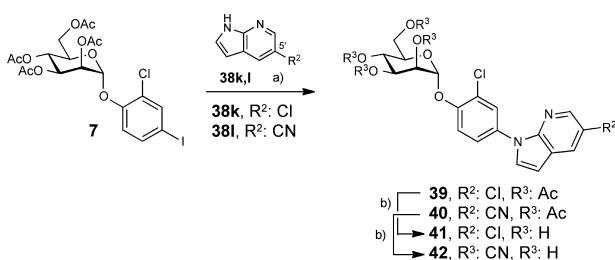
^aReagents and conditions: (a) 4 Å MS, TMSOTf, toluene, rt, 2 h (37–94%). (b) (i) CuI, K₂CO₃, L-proline, DMSO, 90°C, overnight or CuI, K₃PO₄, *trans*-1,2-cyclohexanediamine, dioxane, 105°C, overnight; (ii) Ac₂O/pyr, DMAP, 2–4 h. (c) 0.5 M NaOMe/MeOH, rt. (d) 2N NaOH, THF/MeOH/H₂O (5:5:2), 40 °C (→ 32).

Scheme 2^a

^aReagents and conditions: (a) H₂ (1 atm), PtO₂, cat. morpholine, MeOH/EtOAc (quant). (b) 4-Cl-BzCl or MeSO₂Cl, Et₃N, DCM, rt, 1 h (34, 94%; 35, 82%). (c) 0.5 M NaOMe/MeOH, rt (36, 85%; 37, 82%).

up to 30-fold improved affinity in the cell-free binding assay and the aggregometry assay. Finally, when the indolyl substituent was introduced in the *meta*-position (→ 52, entry 22) or aza-indolyl

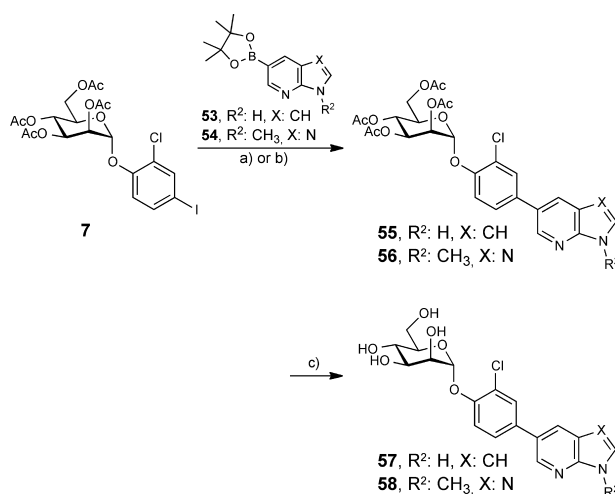
(→ 57, entry 23) and imidazo-pyridyl substituents (→ 58, entry 24) were introduced in the *para*-position of the first aromatic ring, a substantial reduction in affinity was observed.

Scheme 3^a

^aReagents and conditions: (a) (i) CuI, K₂CO₃, L-proline, DMSO, 90 °C, overnight or CuI, K₃PO₄, *trans*-1,2-cyclohexanediamine, dioxane, 105 °C, overnight; (ii) Ac₂O/pyr, DMAP, 2–4 h (**39**, 82%; **40**, 80%). (b) 0.5 M NaOMe/MeOH, rt (**41**, 63%; **42**, 91%).

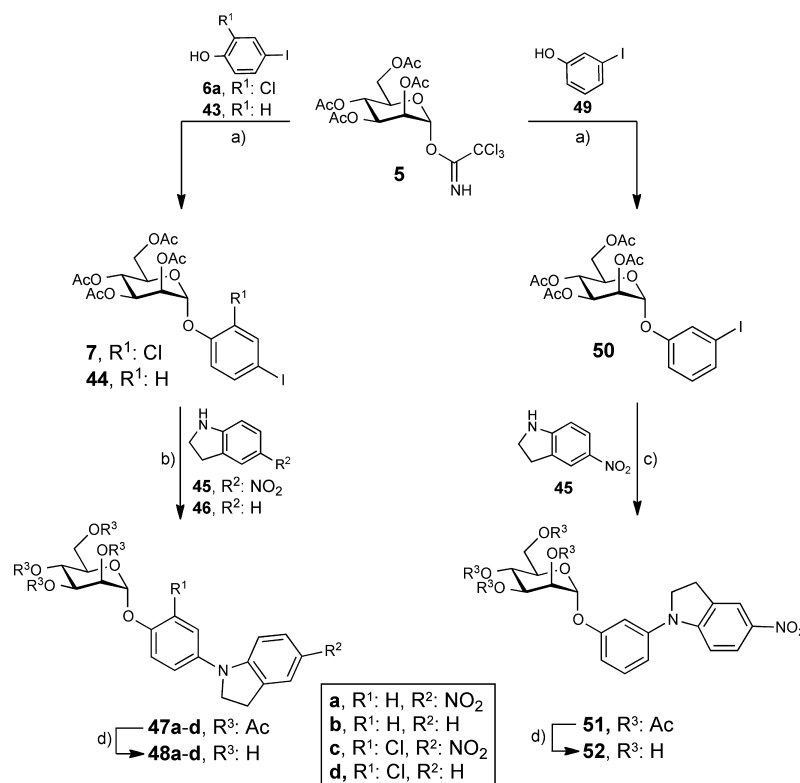
In Vitro Pharmacokinetic Characterization. To reach their therapeutic target, orally applied FimH antagonists should be gastrointestinal absorbed and renally eliminated; that is, an optimal balance between solubility, permeability, and lipophilicity is required. To identify the most promising candidates among the high-affinity FimH antagonists for the in vivo validation, membrane permeability, thermodynamic solubility, octanol–water partition, and plasma protein binding (PPB) were therefore determined.

The parallel artificial membrane permeability assay (PAMPA) predicts a medium to high oral absorption potential

Scheme 5^a

^aReagents and conditions: (a) K₃PO₄, Pd(Ph₃P)₄, dioxane, 100 °C, overnight (**55**, 56%). (b) K₃PO₄, PdCl₂(dppf), DMF, 100 °C, overnight (**56**, 96%). (c) 0.5 M NaOMe/MeOH, rt, 2–2.5 h (**57**, 42%; **58**, 37%).

for compounds with an effective permeability (log *P_e*) above –6.3,²⁴ a property fulfilled by most of the listed indole and indoline derivatives (Table 2). Apparently, elevated lipophilicity of most antagonists, that is, log *D*_{7,4} > 2, facilitates permeation

Scheme 4^a

^aReagents and conditions: (a) 4 Å MS, TMSOTf, toluene or DCM, rt, 2 h (**7**, 73%; **44**, quant; **50**, 93%). (b) Cs₂CO₃, Pd₂(dba)₃, X-Phos, toluene, 80 °C, 140 h or microwave, 80 °C, 8 h (**47a-d**, 43–75%). (c) Cs₂CO₃, Pd₂(dba)₃, X-Phos, dioxane, Ac₂O, pyr, 80 °C, 53 h (80%). (d) NaOMe/MeOH, rt, 20–23 h, (**48a-d**, 37–77%; **52**, 60%).

Table 1. In Vitro Pharmacodynamic Parameters of FimH Antagonists^a

Entry	Comp. No.	R ¹	R ²	X	Cell-free binding assay		Aggregometry assay	
					IC ₅₀ [nM]	rIC ₅₀	IC ₅₀ [μM]	rIC ₅₀
1	1 ^[9a,11]	<i>n</i> -Heptyl α-D-mannopyranoside			73	1	77.1	1
2	3b ^[11]	Sodium 3'-chloro-4'-(α-D-mannopyranosyloxy)-biphenyl-4-carboxylate			6.7	0.09	10.0	0.13
3	21	2-Cl	H	CH	14.9	0.2	8.3	0.11
4	22	2-Cl	5'-NO ₂	CH	7.7	0.1	1.3	0.01
5	23	2-Cl	5'-OMe	CH	59.0	0.81	n.d.	-
6	24	2-Cl	4'-OBn	CH	48.6	0.66	n.a.	-
7	25	2-Cl	5'-CF ₃	CH	18.8	0.26	6.4	0.08
8	26	2-F	H	CH	35.3	0.48	29.5	0.38
9	27	2-F	5'-NO ₂	CH	52.8	0.72	5	0.06
10	28	2-OMe	5'-NO ₂	CH	18.7	0.26	4.1	0.05
11	29	2,6-di-Cl	5'-NO ₂	CH	28.1	0.38	7.1	0.09
12	31	2-Cl	5'-COOMe	CH	8.0	0.11	n.d.	-
13	32	2-Cl	5'-COOH	CH	20.3	0.28	3.1	0.04
14	36	2-Cl	5'-NH(C=O) <i>p</i> Cl-Ph	CH	40.1	0.55	n.a.	-
15	37	2-Cl	5'-NHS(=O) ₂ Me	CH	20.7	0.28	5.6	0.07
16	41	2-Cl	5'-Cl	N	20.0	0.26	23.1	0.3
17	42	2-Cl	5'-CN	N	12.8	0.17	8.2	0.11
18	48a	H	NO ₂	-	20	0.27	26.9	0.35
19	48b	H	H	-	14.5	0.20	n.d.	-
20	48c	Cl	NO ₂	-	2.4	0.03	3.4	0.04
21	48d	Cl	H	-	27.8	0.43	n.d.	-
22	52	-			15.1	0.32	19.2	0.25
23	57	-	H	CH	40.1	0.55	35.9	0.47
24	58	-	Me	N	15.1	0.21	25.3	0.33

^aThe IC₅₀ values were determined with the cell-free binding assay¹² and the aggregometry assay.¹⁹ The rIC₅₀ values were calculated by dividing the IC₅₀ of the compound of interest by the IC₅₀ of the reference compound **1**. This leads to rIC₅₀ values below 1 for derivatives binding better than **1** and rIC₅₀ values above 1.00 for compounds with a lower affinity than **1**. n.a., not active; n.d., not determined.

across the artificial membrane. In contrast to the promising PAMPA results, thermodynamic solubility strongly limited the dosages, which could be applied for the in vivo pharmacokinetic (PK) studies (see below).^{25,26}

Regarding their renal elimination, lipophilic FimH antagonists (log *D*_{7,4} > 2) are expected to undergo considerable reabsorption in the renal tubules, leading overall only to a slow excretion into the bladder. On the contrary, hydrophilic

Table 2. Distribution Coefficients (log $D_{7.4}$ Values) Were Measured by a Miniaturized Shake Flask Procedure^{29a}

entry	compd no.	log $D_{7.4}$	solubility/pH ($\mu\text{g/mL}$)	PAMPA log P_e (log 10^{-6} cm/s)	PPB (%)
25	3b ¹¹	-0.8	>3000	NP	89
26	21	1.8	31.5/6.5	-4.7	98
27	22	1.8	1.4/6.5	-4.9	99
28	23	3.0	9.6/6.6	-4.6	96
29	24	2.7	<0.1/6.5	NP	ND
30	25	ND	0.1/6.5	-4.6	>99
31	26	2.4	67/6.5	-4.7	98
32	27	1.9	4.0/6.5	-5.4	95
33	31	2.8	2.1/6.5	-4.4	99
34	32	1.1	1050/5.6	-6.4	93
35	36	ND	<0.001/6.5	-6	>99
36	37	1.8	279/6.3	NP	94
37	41	3.4	3.8/6.5	-5.0	96
38	42	1.6	8.5/6.3	-6.3	95
39	48a	1.9	24/6.5	-5.5	95
40	48b	2.3	31/6.5	-4.7	97
41	48c	1.9	3.6/6.5	-5.7	99
42	48d	2.8	21/6.5	-4.6	99
43	57	3.2	5.5/6.4	NP	90
44	58	1.3	2.4/6.3	-8.0	<30

^aThermodynamic solubility (S) was measured by an equilibrium shake flask approach.³⁰ Passive permeation through an artificial membrane and retention therein was determined by PAMPA.^{24a} PPB was assessed following a miniaturized equilibrium dialysis protocol.³¹ P_e , effective permeation; ND, not determined; NP, no permeation.

compounds (log $D_{7.4} < 0$) are poorly reabsorbed and thus rapidly renally cleared, which leads to high initial compound levels in the urine but narrows the time range where a therapeutic concentration ($T > \text{MIC}_{\text{adhesion}}$, see below) is maintained.²⁷ Consequently, moderate lipophilicity, that is, log $D_{7.4}$ in the range of 1–2, is beneficial to maintain the drug concentration in the bladder over an extended time period. Most of the FimH antagonists listed in Table 2 show moderate to high lipophilicity and are therefore potentially affected by renal reabsorption. Moreover, PPB values $\geq 90\%$ as found for most of the antagonists in Table 2 attenuate fast renal clearance, because, in line with the free drug hypothesis, molecules bound to plasma proteins evade excretion.²⁸ Compounds for the further evaluation were selected according to affinity (22 and 48c, Table 1) or their PK properties (21 and 48a, Table 2).

Determination of the Minimal Inhibitory Concentration of Adhesion ($\text{MIC}_{\text{adhesion}}$). Whereas in antimicrobial chemotherapy the MIC is defined as the lowest concentration of a drug that inhibits visible growth of an organism,³² we defined a modified MIC for FimH antagonists because of their different mode of action (they neither kill nor inhibit the growth of bacteria). The $\text{MIC}_{\text{adhesion}}$ can be used for the determination of the therapeutic dosage in vivo and is defined as the concentration of antagonist leading to 90% inhibition of adhesion of the pathogen to the target cells (IC_{90}). To determine the $\text{MIC}_{\text{adhesion}}$, human bladder cells are infected with green fluorescent protein (GFP) labeled UPEC (strain UTI89) in the presence of different concentrations of FimH antagonists and analyzed by flow cytometry.³³ The half-maximal inhibitory concentration (IC_{50}) was calculated by plotting the mean fluorescent intensity (MFI) of the cells versus the concentration of the antagonist. From this plot, the concentration where 90% bacterial adhesion to human bladder cells is inhibited (IC_{90}) can

Entry	Comp. No.	IC_{50} [μM]	IC_{90} [μM]	$\text{MIC}_{\text{adhesion}}$ [$\mu\text{g/mL}$]
45	3b	0.33 \pm 0.05	1.4	0.61
46	21	20.14 \pm 7.6	~350	~140
47	22	0.5 \pm 0.29	2.9	1.32
48	48a	0.14 \pm 0.05	1.16	0.49
49	48c	0.04 \pm 0.02	0.3	0.14

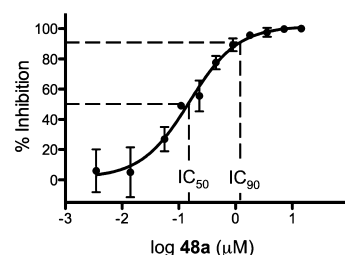


Figure 2. Determination of the $\text{MIC}_{\text{adhesion}}$. The table lists the half-maximal inhibitory concentration (IC_{50}), the 90% inhibitory concentration of adhesion [IC_{90} (μM)] and the $\text{MIC}_{\text{adhesion}}$ ($\mu\text{g/mL}$) of selected indolylphenyl (21 and 22) and indolylphenyl (48a and 48c) mannosides as well as the previously reported biphenyl derivative 3b.¹¹ IC_{50} values were determined using the cell-based flow cytometry infection assay³³ (see the graph, representing results for 48a). The $\text{MIC}_{\text{adhesion}}$ is the concentration in $\mu\text{g/mL}$ of antagonist that inhibits adhesion of the pathogen to host cells by 90% (IC_{90}).

be deduced. The corresponding concentration in $\mu\text{g/mL}$ was defined as $\text{MIC}_{\text{adhesion}}$. IC_{50} , IC_{90} , and $\text{MIC}_{\text{adhesion}}$ values of the four selected FimH antagonists and of the previously reported biphenyl derivative 3b¹¹ are listed in Figure 2.

Pharmacokinetic Studies in C3H/HeN Mice with a Single iv Dose. In our previously reported study,¹¹ FimH antagonist 3b was applied at a dosage of 50 mg/kg. For the in vivo characterization of the compounds of the new series, the dosage was adjusted according to their maximal solubility [in 5% aqueous dimethyl sulfoxide (DMSO)]. Plasma and urine concentrations of the selected FimH antagonists 3b,¹¹ 21, 22, 48a, and 48c after single iv application are summarized in Figure 3. The $\text{MIC}_{\text{adhesion}}$ values are indicated in the individual graphs with a dotted line. An important parameter for the prediction of the therapeutic outcome in the UTI mouse model is the time period for which the antagonist concentration in the urine is above the $\text{MIC}_{\text{adhesion}}$ ($T > \text{MIC}_{\text{adhesion}}$), representing the therapeutic time range.

As a consequence of fast renal excretion, the $\text{MIC}_{\text{adhesion}}$ value for reference compound 3b applied at a dosage of 50 mg/kg could be maintained for approximately 4 h (Figure 3A). When 21 and 22 were applied at dosages of 25 and 5 mg/kg, respectively, substantially lower urine concentrations were observed, for 21 below the $\text{MIC}_{\text{adhesion}}$ value and for 22 only marginally above (Figure 3B,C). Although compound 48a was applied with a single dose of 1 mg/kg (50-fold reduced dosage as compared to 3b), it exhibited the highest availability in the urine [area under the curve (AUC_{0-24})] with a $T > \text{MIC}_{\text{adhesion}}$ of >8 h (Figure 3D). Finally, antagonist 48c was applied at 0.05 mg/kg, which is a 1000-fold reduced dosage as compared to 3b. Nevertheless, it still showed an improved therapeutic time range of 8 h ($T > \text{MIC}_{\text{adhesion}}$, Figure 3E).

Treatment Study in C3H/HeN Mice. For the in vivo UTI treatment study, antagonist 48a was selected for iv application (1 mg/kg) into the tail vein, followed by infection with UPEC (UTI89). The animals were sacrificed 3 h after inoculation, and

Antagonist Dosage	Compartment	AUC ₀₋₂₄ [$\mu\text{g} \times \text{h/mL}$]	T > MIC _{Adhesion} [h]
3b 50 mg/kg	Plasma	20.8 \pm 7.3	-
	Urine	209.6 \pm 72.3	4
21 25 mg/kg	Plasma	8.2 \pm 3.2	-
	Urine	19.3 \pm 3.9	0
22 5 mg/kg	Plasma	2.3 \pm 1.1	-
	Urine	13.2 \pm 4.2	3
48a 1 mg/kg	Plasma	2.2 \pm 0.8	-
	Urine	586.4 \pm 251.6	> 8
48c 0.05 mg/kg	Plasma	3.5 \pm 1.2	-
	Urine	33.4 \pm 11	8

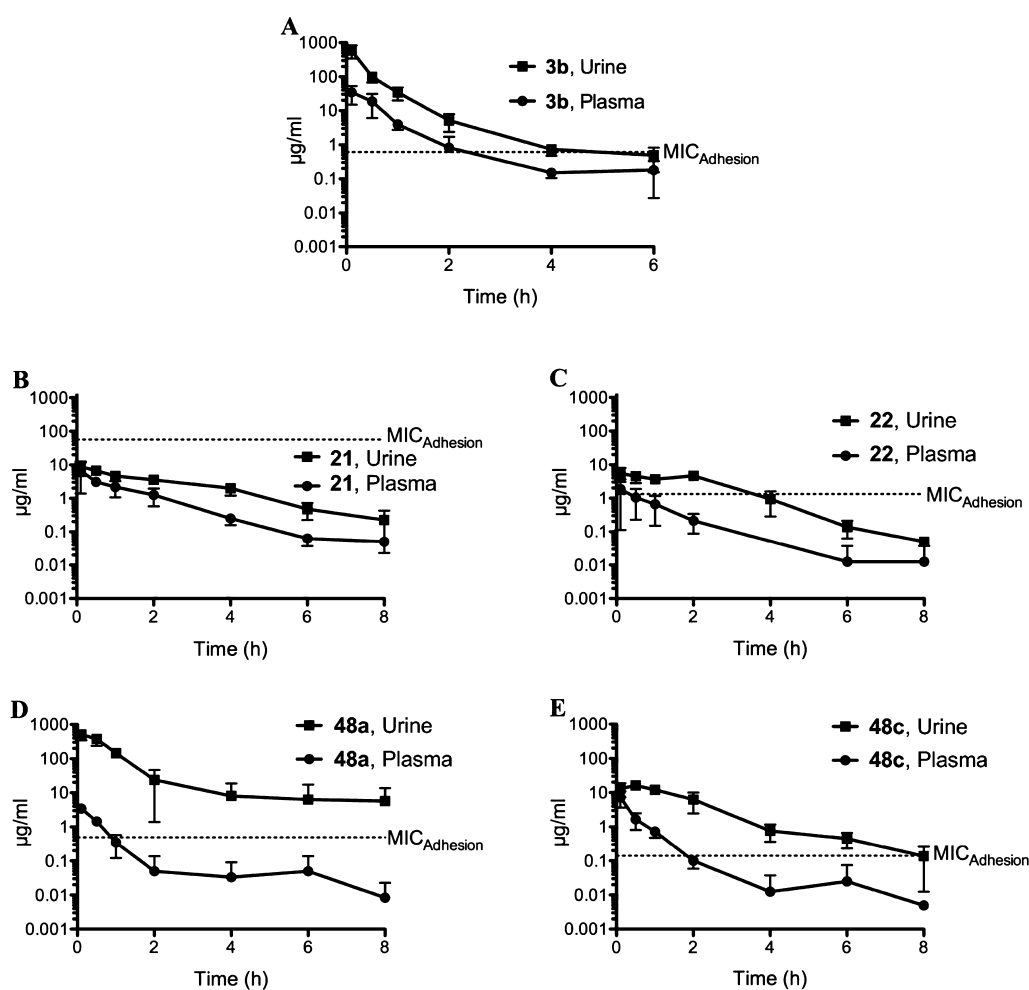


Figure 3. Determination of antagonist concentration in urine and plasma after a single iv application ($n = 4$). The data (table and graphs) show time-dependent urine and plasma concentrations and the MIC_{adhesion} values as dotted lines for **3b** (reference compound¹¹), **21**, **22**, **48a**, and **48c**. AUC₀₋₂₄ is the AUC over 24 h; MIC_{adhesion} is the minimal inhibitory concentration of adhesion.

homogenized organs (bladder and kidneys) were examined for bacterial counts. The results were compared to ciprofloxacin (CIP), used as standard antibiotic therapy against UTI.³⁴

The mean value in the untreated control group showed bacterial counts of 1.4×10^8 colony-forming units (CFU) in the bladder and 9.7×10^6 CFU in the kidneys. The bar diagram in Figure 4 summarizes the bacterial counts after treatment. The baseline represents the values obtained for the control group, which was used as reference for CFU reductions. After iv application of **48a**, a substantial decrease of the bacterial counts

by $3.7 \log_{10}$ CFU was observed in the bladder. Results were compared to the previously presented antagonist **3b**,¹¹ which was tested using the same protocol. With **3b**, a 50-fold higher dosage (50 mg/kg) had to be applied to obtain a comparable reduction of $4 \log_{10}$ CFU for bladder counts. Mice treated with CIP (8 mg, sc) showed an almost identical reduction of bacterial counts in the bladder as the tested FimH antagonists **3b** (50 mg/kg) and **48a** (1 mg/kg). Furthermore, antagonist **48a** prevented bacteria from ascending into the kidneys ($-1.3 \log_{10}$ CFU) twice as efficiently as **3b** ($-0.7 \log_{10}$ CFU).

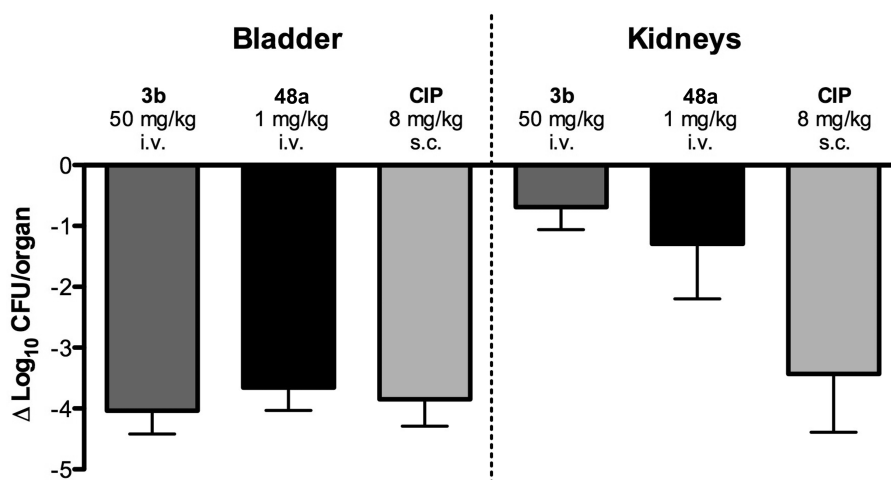


Figure 4. Treatment efficacy in the UTI mouse model 3 h after infection ($n = 6$). The bar diagram shows the reduction of bacterial counts of the indolylphenyl mannoside **48a** at an iv dosage of 1 mg/kg, the biphenyl derivative **3b** at an iv dosage of 50 mg/kg, and ciprofloxacin (CIP) at an sc dosage of 8 mg/kg (representing the murine dose equivalent to a human standard dose).³⁵ The baseline represents the mean counts of the untreated control group; that is, the values of the control group were subtracted from the results of the tested antagonists.

As previously addressed,¹¹ urine samples show in general higher bacterial counts as compared to the bladder. A possible explanation is the varying urine volumes, leading to either a concentration or a dilution of bacteria in the urine samples. Therefore, results were limited to the evaluation of bladder and kidney counts. Furthermore, as compared to bladder counts, the bacterial counts in the kidneys were reduced to a smaller extent, probably due to different bacterial adhesion mechanisms in bladder and kidney (type 1 pili- vs P pili-dependent interactions).³ Therefore, the considerable reduction of the bacterial counts in the kidney as observed for antagonist **48a** may originate from the inability of UPECs blocked by **48a** to adhere to bladder cells and their subsequent removal from the bladder by the urine flow. As a result, only a reduced population for ascending into the kidneys is available.

CONCLUSIONS

The FimH antagonists presented in this article exhibit an alternative mode of action as compared to antibiotics as they neither kill nor inhibit growth of bacteria. By blocking FimH, a lectin located at the tip of the bacterial fimbriae, they interfere with the adhesion of UPEC to the endothelial cells of the urinary tract and therewith the initial step of the infection. To select the most promising candidates for in vivo studies,³⁶ a thorough investigation of the in vitro potency and the physicochemical/PK properties of these FimH antagonists (Tables 1 and 2) was performed.

Starting from the known FimH antagonist biphenyl α -D-mannopyranoside (**3b**), we designed antagonists with spatially more demanding aglycones and therefore a better fit in the out-docking mode.^{9d,13,37} Thus, a series of indolylphenyl and indolylphenyl α -D-mannopyranosides were synthesized. For the initial evaluation of their affinities, a target-based, cell-free binding assay¹² and a cell-based aggregometry assay¹⁹ were applied. In both series, an *ortho*-chloro substituent on the phenyl ring adjacent to the anomeric oxygen and an electron-withdrawing substituent on the indole/indoline moiety yielded the antagonists with the highest affinities/activities (see Table 1), presumably by favoring the π - π stacking with the electron rich Tyr48.

The most important requirement for a successful treatment in the UTI mouse model is the maintenance of a $\text{MIC}_{\text{adhesion}}$ of the antagonist in the urine. To avoid a fast renal clearance as experienced with the biphenyl mannoside **3b**¹¹ ($\log D_{7.4}$ of -0.8 , PPB 89%) (Figure 3A), the indole derivatives **21** and **22** and the indoline derivatives **48a** and **48c** exhibiting higher lipophilicity ($\log D_{7.4}$ values of 1.8 and 1.9) and PPB (>95%) were selected as candidates for the in vivo PK study. Whereas for the indole derivatives **21** and **22** only insufficient urine concentrations (Figure 3B,C) were obtained, **48a** and **48c** exhibited a substantially improved renal elimination profile with $T > \text{MIC}_{\text{adhesion}}$ of >8 and 8 h, respectively, although 50–1000-fold lower dosages were applied (Figure 3D,E).

On the basis of these results, **48a** was selected for the treatment study in the UTI mouse model (dosage of 1 mg/kg). It reduced the CFUs in the bladder by 3.7 orders of magnitude, which is almost comparable to **3b**, applied at a 50-fold higher dosage (50 mg/kg, $-4 \log_{10}$ CFU). Furthermore, **48a** led to a considerably better reduction of bacterial counts in the kidneys ($-1.3 \log_{10}$ CFU vs $-0.7 \log_{10}$ CFU for **3b**). Of additional interest is the fact that the FimH antagonist **48a** was able to reduce bacterial infection in the bladder comparably well as the standard antibiotic treatment with ciprofloxacin (CIP),³⁴ indicating a promising profile for the alternative treatment of UTIs with FimH antagonists. Overall, the indoline derivative **48a** is the most active antagonist tested in vivo to date.^{11,13} Because the experimental setup used in this study is a prophylactic approach, an adopted protocol for the treatment of an established infection is currently developed.

According to the PAMPA values, most representatives of the indole and indoline series are expected to be orally available (Table 2). However, a major drawback is their low solubility, limiting, for example, the dosage of **48a** to 1 mg/kg and **48c** to 0.05 mg/kg. To evaluate the dosage dependence, that is, whether higher dosages will further reduce the bacterial counts in bladder and kidney, the physicochemical issue of solubility will be addressed by appropriate formulations and structural modifications (e.g., by disruption of the molecular planarity of the aromatic aglycone²⁶).

Overall, these results clearly indicate the high therapeutic potential of this new series of FimH antagonists. Because of optimized PK properties, a substantial reduction of the dosage could be achieved. Thus, with the most promising representative to date, the indolinylphenyl α -D-mannoside **48a**, the infection can be successfully treated with a low dosage of 1 mg/kg (approximately 25 μ g/mouse) without any additional administration of antibiotics.

EXPERIMENTAL SECTION

Synthesis. The synthesis of compounds **7–10**, **14–20**, **23–37**, **39–42**, **44**, **47b,d**, **48b,d**, **50–52**, and **55–58**, including compound characterization data, can be found in the Supporting Information.

General Methods. Commercially available reagents were purchased from Fluka, Aldrich, Merck, AKSci, ASDI, or Alfa Aesar. Methanol (MeOH) was dried by distillation from sodium methoxide. Toluene and dioxane were dried by distillation from sodium/benzophenone. Optical rotations were measured at 20 °C on a Perkin-Elmer 341 polarimeter. Nuclear magnetic resonance (NMR) spectra were obtained on a Bruker Avance 500 UltraShield spectrometer at 500.13 MHz (^1H) or 125.76 MHz (^{13}C). Chemical shifts are given in ppm and were calibrated on residual solvent peaks or to tetramethylsilane as an internal standard. Multiplicities are specified as s (singlet), d (doublet), dd (doublet of a doublet), t (triplet), q (quartet), or m (multiplet). Assignment of the ^1H and ^{13}C NMR spectra was achieved using 2D methods (COSY, HSQC). ESI mass spectra were recorded on a Waters micromass ZQ instrument. High-resolution mass spectra were obtained on an ESI Bruker Daltonics micrOTOF spectrometer equipped with a TOF hexapole detector. Microwave-assisted reactions were carried out with CEM Discover and Explorer. Reactions were monitored by TLC using glass plates coated with silica gel 60 F_{254} and visualized by using UV light and/or by charring with a molybdate solution (a 0.02 M solution of ammonium cerium sulfate dihydrate and ammonium molybdate tetrahydrate in aqueous 10% H_2SO_4) with heating to 150 °C for 5 min. Column chromatography was performed on a CombiFlash Companion (ISCO, Inc.) using RediSep normal phase disposable flash columns (silica gel). Reversed phase chromatography was performed on LiChroPrepRP-18 (Merck, 40–63 μm).

Compound Purity. Each test compound was purified by chromatography on silica (dichloromethane (DCM)/MeOH, 10:1) or reversed-phase chromatography (RP-18 column, $\text{H}_2\text{O}/\text{MeOH}$, gradient from 0 to 20% MeOH), followed by Bio-Gel P2 (exclusion limit 1800 Da, Bio-Rad Laboratories) size exclusion chromatography (elution with water containing up to 20% MeOH at 0.25 mL/min) prior to HPLC, HRMS, NMR, and activity testing. The purity of all test compounds was determined by NMR and HPLC [Beckman Coulter Gold, consisting of pump 126, DAD 168 (190–410 nm), and autosampler 508. Column: Waters Atlantis T3, 3 μm , 2.1 mm \times 100 mm. A, H_2O + 0.1% TFA; B, MeCN + 0.1% TFA. Detection, 270 nm. Gradient, 5 \rightarrow 95% B (22 min); flow rate, 0.5 mL/min] to be $\geq 95\%$ (for ^1H NMR spectra and HPLC traces, see the Supporting Information).

2-Chloro-4-(indol-1-yl)phenyl α -D-Mannopyranoside (21). A resealable Schlenk tube, which was equipped with a magnetic stirring bar, was charged with **7** (146 mg, 0.25 mmol), CuI (10 mg, 0.05 mmol), indole (**11e**, 35.0 mg, 0.30 mmol), K_2CO_3 (86 mg, 0.63 mmol), and L-proline (11.5 mg, 0.10 mmol). The vessel was sealed with a rubber septum, evacuated, and backfilled with argon (this process was repeated twice). Then, DMSO (1 mL) was added under a stream of argon, the reaction tube was quickly sealed, and the suspension was stirred at 90 °C overnight. The reaction mixture was cooled to rt, diluted with EtOAc (5 mL), and filtered through a plug of Celite. The filtrate was concentrated in vacuo, and the residue was treated for 2 h with Ac_2O /pyridine (3 mL, 1:2) and a catalytic amount of DMAP. The reaction was quenched by the addition of MeOH and concentrated, and the residue was purified by chromatography on silica (petroleum ether/EtOAc, 4:1 to 1:1) to give slightly impure **12** (40 mg, 28%). Compound **12** (40 mg, 0.07 mmol) was dissolved in MeOH (1 mL) and treated at rt with

0.5 M NaOMe/MeOH (14 μL) until completion of the reaction. The reaction mixture was neutralized with amberlyst-15 (H^+) ion-exchange resin and filtered. The filtrate was concentrated, and the residue was purified by chromatography on silica (DCM/MeOH, 10:1) and P2 size exclusion chromatography to afford **21** (20 mg, 70%) as a white solid after a final lyophilization from water/dioxane. $[\alpha]_{\text{D}}^{20}$ +171.6 (*c* 0.18, MeOH). ^1H NMR (500 MHz, CD_3OD): δ 7.62–7.54 (m, 3H, Ar–H), 7.45–7.38 (m, 3H, Ar–H), 7.18 (t, J = 7.0 Hz, 1H, Ar–H), 7.11 (t, J = 7.0 Hz, 1H, Ar–H), 6.65 (s, 1H, Ar–H), 5.61 (s, 1H, H-1), 4.14 (m, 1H, H-2), 4.01 (dd, J = 9.0, 2.5 Hz, 1H, H-3), 3.81–3.69 (m, 4H, H-6a, H-4, H-6b, H-5). ^{13}C NMR (125 MHz, CD_3OD): δ 151.81, 137.30, 136.22, 130.81, 128.98, 127.04, 125.58, 124.98, 123.49, 122.06, 121.42, 119.23, 111.00, 104.71 (Ar–C), 101.03 (C-1), 76.11 (C-5), 72.38 (C-3), 71.84 (C-2), 68.22 (C-4), 62.70 (C-6). HRMS (ESI) m/z calcd for $\text{C}_{20}\text{H}_{20}\text{ClNNaO}_6$ $[\text{M} + \text{Na}]^+$, 428.0877; found, 428.0875.

2-Chloro-4-(5-nitroindol-1-yl)phenyl α -D-Mannopyranoside (22). According to the procedure described for **21**, compound **22** was prepared from **7** (117 mg, 0.20 mmol) and 5-nitroindole (**11f**, 39 mg, 0.24 mmol) via the acetylated intermediate **13**. After workup, the residue was purified by chromatography on silica (DCM/MeOH, 10:1) and P2 size exclusion chromatography to yield **22** (54 mg, 60%) as a yellow solid after a final lyophilization from water/dioxane. $[\alpha]_{\text{D}}^{20}$ +85.7 (*c* 0.25, MeOH). ^1H NMR (500 MHz, CD_3OD): δ 8.63 (d, J = 2.0 Hz, 1H, Ar–H), 8.11 (dd, J = 9.0, 2.0 Hz, 1H, Ar–H), 7.65–7.55 (m, 4H, Ar–H), 7.48 (dd, J = 8.5, 2.5 Hz, 1H, Ar–H), 6.91 (d, J = 3.0 Hz, 1H, Ar–H), 5.65 (s, 1H, H-1), 4.14 (m, 1H, H-2), 4.01 (dd, J = 9.5, 3.5 Hz, 1H, H-3), 3.83–3.72 (m, 3H, H-6a, H-4, H-6b), 3.66 (m, 1H, H-5). ^{13}C NMR (125 MHz, CD_3OD): δ 152.73, 143.52, 140.14, 134.75, 132.99, 130.01, 127.65, 125.75, 125.57, 119.11, 118.95, 118.79, 111.51, 106.68 (Ar–C), 100.90 (C-1), 76.19 (C-5), 72.37 (C-3), 71.78 (C-2), 68.18 (C-4), 62.69 (C-6). HRMS (ESI) m/z calcd for $\text{C}_{20}\text{H}_{19}\text{ClN}_2\text{NaO}_8$ $[\text{M} + \text{Na}]^+$, 473.0728; found, 473.0728.

4-(5-Nitroindolin-1-yl)phenyl 2,3,4,6-Tetra-O-acetyl- α -D-mannopyranoside (47a). In a Schlenk tube, a mixture of 2-dicyclohexylphosphino-2',4',6'-triisopropylbiphenyl (X-Phos) (9.1 mg, 0.019 mmol) and $\text{Pd}_2(\text{dba})_3$ (3.85 mg, 0.0037 mmol) in dry toluene (3.5 mL) was stirred for 15 min at 40 °C under argon. Then, **44** (200 mg, 0.37 mmol), Cs_2CO_3 (364 mg 1.12 mmol), and 5-nitroindoline (**45**, 91.6 mg, 0.56 mmol) were added. The reaction mixture was degassed in an ultrasonic bath and stirred for 140 h at 80 °C. The reaction mixture was diluted with EtOAc (10 mL) and washed with aqueous saturated NaHCO_3 and brine. The aqueous layers were extracted with EtOAc (3 \times 10 mL), and the combined organic layers were dried over Na_2SO_4 , filtered, and concentrated under reduced pressure. The residue was purified by chromatography on silica (5–40% gradient of EtOAc in petrol ether) to give **47a** (163 mg, 75%) as an orange solid. $[\alpha]_{\text{D}}^{20}$ +55.0 (*c* 1.00, CHCl_3). ^1H NMR (500 MHz, CDCl_3): δ 7.98 (dd, J = 2.3 Hz, 8.9 Hz, 1H, Ar–H), 7.95 (s, 1H, Ar–H), 7.21 (m, 1H, Ar–H), 7.13 (m, 3H, Ar–H), 6.73 (d, J = 8.9 Hz, 1H, Ar–H), 5.55 (dd, J = 10.1, 3.5 Hz, 1H, H-3), 5.50 (d, J = 1.6 Hz, 1H, H-1), 5.44 (dd, J = 3.5, 1.8 Hz, 1H, H-2), 5.38 (t, J = 10.1 Hz, 1H, H-4), 4.28 (dd, J = 12.5, 5.2 Hz, 1H, H-6a), 4.08 (m, 4H, CH_2 , H-6b, H-5), 3.19 (t, J = 8.6 Hz, 2H, CH_2), 2.20, 2.18, 2.04, 2.02 (4s, 12H, OAc). ^{13}C NMR (125 MHz, CDCl_3): δ 170.70, 170.23, 170.19, 169.90 (4 CO), 137.21, 128.40, 126.27, 122.03, 121.32, 117.92, 117.81, 105.52 (Ar–C), 96.36 (C-1), 69.53 (C-5), 69.40 (C-2), 68.98 (C-3), 66.03 (C-4), 62.28 (C-6), 53.85 (CH_2), 27.27 (CH_2), 21.65, 21.09, 20.92, 20.90 (4 COCH₃). MS (ESI) m/z calcd for $\text{C}_{28}\text{H}_{31}\text{N}_2\text{O}_{12}$ $[\text{M} + \text{H}]^+$, 587.19; found, 587.29.

2-Chloro-4-(5-nitroindolin-1-yl)phenyl 2,3,4,6-Tetra-O-acetyl- α -D-mannopyranoside (47c). According to the procedure described for **47a**, compound **7** (60 mg, 0.10 mmol) was microwave irradiated with Cs_2CO_3 (100 mg 0.30 mmol), X-Phos (4.9 mg, 0.010 mmol), $\text{Pd}_2(\text{dba})_3$ (2.21 mg, 0.0020 mmol), and 5-nitroindoline (**45**, 50.5 mg, 0.30 mmol) in toluene (1 mL) to yield **47c** (36 mg, 56%) as an orange solid. $[\alpha]_{\text{D}}^{20}$ +99.6 (*c* 0.08, CHCl_3). ^1H NMR (500 MHz, CDCl_3): δ 8.03 (dd, J = 8.8, 2.3 Hz, 1H, Ar–H), 7.99 (m, 1H, Ar–H), 7.30 (d, J = 2.7 Hz, 1H, Ar–H), 7.26–7.08 (m, 2H, Ar–H), 6.82 (d, J = 8.9 Hz, 1H, Ar–H), 5.59 (dd, J = 10.1, 3.4 Hz, 1H, H-3), 5.54–5.46 (m, 2H, H-2, H-1), 5.39 (t, J = 10.1 Hz, 1H, H-4), 4.28 (dd, J = 12.2, 5.1 Hz, 1H, H-6a), 4.21 (m, 1H, H-5), 4.10 (dd, J = 12.3, 2.2 Hz,

1H, H-6b), 4.06 (t, $J = 9.0$ Hz, 2H, CH₂), 3.20 (t, $J = 8.6$ Hz, 2H, CH₂), 2.19, 2.06, 2.05, 2.03 (4s, 12H, OAc). ¹³C NMR (125 MHz, CDCl₃): δ 170.69, 170.21, 170.04, 169.94 (4 CO), 152.91, 147.91, 138.24, 131.61, 129.24, 128.43, 125.72, 122.33, 121.42, 119.52, 118.45, 106.00 (Ar-C), 97.42 (C-1), 70.00 (C-3), 69.53 (C-2), 68.90 (C-5), 65.99 (C-4), 62.31 (C-6), 53.70 (CH₂), 27.31 (CH₂), 21.11, 20.94, 20.92 (4C, 4 COCH₃). MS (ESI) m/z calcd for C₂₈H₂₉ClN₂NaO₁₂ [M + Na]⁺, 643.13; found, 643.19.

4-(5-Nitroindolin-1-yl)phenyl α -D-Mannopyranoside (48a). Compound 47a (218 mg, 0.37 mmol) was dissolved in MeOH (2 mL) and treated at rt with 0.5 M NaOMe/MeOH (1 mL) for 20 h. The reaction mixture was neutralized with amberlyst-15 (H⁺) ion-exchange resin and filtered. The filtrate was concentrated, and the residue was purified by RP-18 chromatography (H₂O/MeOH, gradient from 0 to 20% MeOH), followed by P2 size exclusion chromatography to yield 48a (77.7 mg, 50%) as a colorless solid after a final lyophilization from water/dioxane. [α]_D²⁰ +57.0 (c 0.10, MeOH). ¹H NMR (500 MHz, CD₃OD): δ 8.00 (m, 2H, Ar-H), 7.31 (m, 2H, Ar-H), 7.21 (m, 2H, Ar-H), 6.78 (d, $J = 8.5$ Hz, 1H, Ar-H), 5.47 (d, $J = 2.0$ Hz, 1H, H-1), 4.12 (m, 2H, NCH₂), 4.02 (dd, $J = 3.3, 1.8$ Hz, 1H, H-2), 3.90 (dd, $J = 9.4, 3.4$ Hz, 1H, H-3), 3.79 (dd, $J = 12.0, 6.4$ Hz, 1H, H-6a), 3.73 (m, 2H, H-6b, H-4), 3.62 (ddd, $J = 9.7, 5.3, 2.3$ Hz, 1H, H-5), 3.21 (t, $J = 8.5$ Hz, 2H, CH₂). ¹³C NMR (125 MHz, CD₃OD): δ 154.98, 137.95, 127.14, 123.52, 122.02, 119.08, 106.41 (Ar-C), 100.69 (C-1), 75.62 (C-5), 72.54 (C-3), 72.13 (C-2), 68.50 (C-4), 62.86 (C-6), 55.07 (CH₂), 28.03 (CH₂). HRMS (ESI) m/z calcd for C₂₀H₂₃N₂O₈ [M + H]⁺, 419.1449; found, 419.1453.

2-Chloro-4-(5-nitroindolin-1-yl)phenyl α -D-Mannopyranoside (48c). According to the procedure described for 48a, compound 47c (36 mg, 0.058 mmol) was treated with 0.5 M NaOMe/MeOH (0.5 mL) in MeOH (1 mL) for 21 h. After workup, the residue was purified by RP-18 chromatography (H₂O/MeOH, gradient from 0 to 20% MeOH) and P2 size exclusion chromatography to yield 48c (16.5 mg, 63%) as a colorless solid after a final lyophilization from water/dioxane. [α]_D²⁰ +53.8 (c 0.21, MeOH/CHCl₃). ¹H NMR (500 MHz, CD₃OD): δ 8.05–8.01 (m, 2H, Ar-H), 7.42 (m, 2H, Ar-H), 7.28 (dd, $J = 9.0, 2.5$ Hz, 1H, Ar-H), 6.86 (d, $J = 8.5$ Hz, 1H, Ar-H), 5.51 (d, $J = 1.5$ Hz, 1H, H-1), 4.11 (m, 3H, NCH₂, H-2), 3.97 (dd, $J = 9.3, 3.4$ Hz, 1H, H-3), 3.81 (dd, $J = 11.7, 2.2$ Hz, 1H, H-6a), 3.64 (ddd, $J = 9.7, 5.6, 2.2$ Hz, 1H, H-5), 3.23 (t, $J = 8.6$ Hz, 2H, CH₂). ¹³C NMR (125 MHz, CD₃OD): δ 134.69, 133.05, 132.87, 130.67, 129.03, 126.83, 123.31, 121.97, 121.31, 119.65, 106.72 (Ar-C), 101.25 (C-1), 76.04 (C-5), 72.40 (C-3), 71.88 (C-2), 68.27 (C-4), 62.73 (C-6), 54.74 (CH₂), 27.93 (CH₂). HRMS (ESI) m/z calcd for C₂₀H₂₁ClN₂NaO₈ [M + Na]⁺, 475.0879; found, 475.0875.

In Vitro Activity. Cell-Free Binding Assay. To determine the affinity of the various FimH antagonists, a cell-free binding assay described previously¹² was applied. A recombinant protein consisting of the CRD of FimH linked with a thrombin cleavage site to a 6His-tag (FimH-CRD-Th-6His) was expressed in *E. coli* strain HM125 and purified by affinity chromatography. Microtiter plates (F96 MaxiSorp, Nunc) were coated with 100 μ L/well of a 10 μ g/mL solution of FimH-CRD-Th-6His in 20 mM HEPES, 150 mM NaCl, and 1 mM CaCl₂, pH 7.4 (assay buffer), overnight at 4 °C. The coating solution was discarded, and the wells were blocked with 150 μ L/well of 3% BSA in assay buffer for 2 h at 4 °C. After three washing steps with assay buffer (150 μ L/well), a 4-fold serial dilution of the test compound (50 μ L/well) in assay buffer containing 5% DMSO and streptavidin-peroxidase coupled biotinylated polyacrylamide (PAA) glycopolymers [Man α 1–3(Man α 1–6)Man β 1–4GlcNAc β 1–4GlcNAc β -PAA-biotin, TM-PAA] (50 μ L/well of a 0.5 μ g/mL solution), was added. On each individual microtiter plate, *n*-heptyl α -D-mannopyranoside (1) was tested as a reference compound. The plates were incubated for 3 h at 25 °C and 350 rpm and then carefully washed four times with 150 μ L/well assay buffer. After the addition of 100 μ L/well of the horseradish peroxidase substrate 2,2'-azino-di(3-ethylbenzothiazoline-6-sulfonic acid) (ABTS), the colorimetric reaction was allowed to develop for 4 min, then stopped by the addition

of 2% aqueous oxalic acid before the optical density (OD) was measured at 415 nm on a microplate-reader (Spectramax 190, Molecular Devices, CA). The IC₅₀ values of the compounds tested in duplicates were calculated with the prism software (GraphPad Software, Inc., La Jolla, CA). The IC₅₀ defines the molar concentration of the test compound that reduces the maximal specific binding of TM-PAA polymer to FimH-CRD by 50%. The relative IC₅₀ (rIC₅₀) is the ratio of the IC₅₀ of the test compound to the IC₅₀ of *n*-heptyl α -D-mannopyranoside (1).

Bacteria and Growth. The clinical *E. coli* isolate UTI89³⁸ (UTI89wt) was kindly provided by the group of Prof. Urs Jenal, Biocenter, University of Basel, Switzerland. Microorganisms were stored at –70 °C and incubated for 24 h before the experiments under static conditions at 37 °C in 10 mL of Luria–Bertani broth (Becton, Dickinson and Company, Le Pont de Claix, France) using 50 mL tubes. Prior to each experiment, the microorganisms were washed twice and resuspended in phosphate-buffered saline (PBS, Sigma-Aldrich, Buchs, Switzerland). Bacterial concentrations were determined by plating serial 1:10 dilutions on blood agar, followed by colony counting with 20–200 colonies after overnight incubation at 37 °C.

Aggregometry Assay. The aggregometry assay was carried out as previously described.¹⁹ In short, the percentage of aggregation of *E. coli* UTI89 with GPEs was quantitatively determined by measuring the optical density at 740 nm and 37 °C under stirring at 1000 rpm using an APACT 4004 aggregometer (Endotell AG, Allschwil, Switzerland). Bacteria were cultivated as described above. GPEs were separated from guinea pig blood (Charles River Laboratories, Sulzfeld, Germany) using Histopaque (density of 1.077 g/mL at 24 °C, Sigma-Aldrich). Prior to the measurements, the cell densities of *E. coli* and GPE were adjusted to an OD₆₀₀ of 4, corresponding to 1.9 \times 10⁸ CFU/mL and 2.2 \times 10⁶ cells/mL, respectively. For the calibration of the instrument, the aggregation of platelet poor plasma (PPP) using PBS alone was set as 100%, and the aggregation of platelet rich plasma (PRP) using GPE was set as 0%. After calibration, measurements were performed with 250 μ L of GPE and 50 μ L of bacterial suspension, and the aggregation was monitored over 600 s. After the aggregation phase of 600 s, 25 μ L of antagonist in PBS was added to each cuvette, and disaggregation was monitored for 1400 s.

Cultivation of 5637 Cells. The human epithelial bladder carcinoma cell line 5637 was obtained from the German Collection of Microorganisms and Cell Cultures (DSMZ, Braunschweig, Germany). The cells were grown in RPMI 1640 medium, supplemented with 10% fetal calf serum (FCS), 100 U/mL penicillin, and 100 μ g/mL streptomycin at 37 °C, 5% CO₂. All solutions were purchased from Invitrogen (Basel, Switzerland). The cells were subcultured 1:5 twice per week for six passages before using them in the infection assay. Two days before infection, 1.8 \times 10⁵ cells were seeded in each well of a 24-well plate in RPMI 1640 containing 10% FCS without antibiotics. The cell density was approximately (3–5) \times 10⁵ cells/well prior the infection.

Flow Cytometry Infection Assay. The infection assay was carried out as previously described.³³ Briefly, to evaluate FimH antagonists, a serial dilution of the antagonists in 5% DMSO was prepared. Before infection, a suspension of green fluorescently labeled (GFP) bacteria (UTI89, 200 μ L) and 25 μ L of the test compound were preincubated for 10 min at room temperature. The bacteria–antagonist mixture was then added to the monolayer of 5637 cells (grown in 24-well plates, as described above) at a multiplicity of infection (MOI) of 1:50 (cell:bacteria). To homogenize the infection, plates were centrifuged at room temperature for 3 min at 600g. After an incubation of 1.5 h at 37 °C, infected cells were washed four times with RPMI 1640 medium and suspended in ice-cold PBS for 5–20 min. Cells were then kept in the dark until analysis. All measurements were made within 1 h after the termination of the infection. Samples were acquired in a CyAn ADP flow cytometer (Becton, Dickinson and Company) and analyzed by gating on the eukaryotic cells based on forward (FSC) and side scatter (SSC), which excludes unbound GFP-labeled bacteria and debris from analysis. A total of 10⁴ cells were measured per sample. Data were acquired in a linear mode for the side scatter (SSC) and in a logarithmic mode for the forward scatter (FSC) and the green

fluorescent channel FL1-H (e.g., GFP). The MFI of FL1-H was counted as a surrogate marker for the adherence of bacteria. Quantification of adhesion was evaluated with the FlowJo software 9.0.1 (Tree Star, Inc., Ashland, OR). IC_{50} values were determined by plotting the concentration of the antagonist in logarithmic mode versus the MFI and by fitting the curve with the prism software (GraphPad, inhibition curve, nonlinear regression, variable slope, $n = 4$). The IC_{90} ($F = 90$) was calculated from the determined IC_{50} value and the hill slope (H) as follows:

$$IC_F = \left(\frac{F}{100 - F} \right)^{1/H} \times IC_{50}$$

In Vitro Pharmacokinetic Parameters. *Materials.* DMSO and 1-octanol were purchased from Sigma-Aldrich. PAMPA System Solution, GIT-0 Lipid solution, and Acceptor Sink Buffer were ordered from pIon (Woburn, MA). Human plasma was bought from Biopredic (Rennes, France), and acetonitrile (MeCN) was from Acros Organics (Geel, Belgium).

Log $D_{7,4}$ Determination. The in silico prediction tool ALOGPS³⁹ was used to estimate the log P values of the compounds. Depending on these values, the compounds were classified into three categories: hydrophilic compounds (log P below zero), moderately lipophilic compounds (log P between zero and one), and lipophilic compounds (log P above one). For each category, two different ratios (volume of 1-octanol to volume of buffer) were defined as experimental parameters (Table 3).

Table 3

compd type	log P	ratios (1-octanol:buffer)
hydrophilic	<0	30:140, 40:130
moderately lipophilic	0–1	70:110, 110:70
lipophilic	>1	3:180, 4:180

Equal amounts of phosphate buffer (0.1 M, pH 7.4) and 1-octanol were mixed and shaken vigorously for 5 min to saturate the phases. The mixture was left until separation of the two phases occurred, and the buffer was retrieved. Stock solutions of the test compounds were diluted with buffer to a concentration of 1 μ M. For each compound, six determinations, that is, three determinations per 1-octanol:buffer ratio, were performed in different wells of a 96-well plate. The respective volumes of buffer containing analyte (1 μ M) were pipetted to the wells and covered by saturated 1-octanol according to the chosen volume ratio. The plate was sealed with aluminum foil, shaken (1350 rpm, 25 °C, 2 h) on a Heidolph Titramax 1000 plate-shaker (Heidolph Instruments GmbH & Co. KG, Schwabach, Germany), and centrifuged (2000 rpm, 25 °C, 5 min, 5804 R Eppendorf centrifuge, Hamburg, Germany). The aqueous phase was transferred to a 96-well plate for analysis by LC-MS (see below).

log $D_{7,4}$ was calculated from the 1-octanol:buffer ratio (o:b), the initial concentration of the analyte in buffer (1 μ M), and the concentration of the analyte in the aqueous phase (c_B) with equation:

$$\log D_{7,4} = \log \left(\frac{1 \mu\text{M} - c_B}{c_B} \times \frac{1}{\text{o: b}} \right)$$

The average of the three log $D_{7,4}$ values per 1-octanol:buffer ratio was calculated. If the two means obtained for a compound did not differ by more than 0.1 unit, the results were accepted.

PAMPA. Log P_e was determined in a 96-well format with the PAMPA^{24a} permeation assay. For each compound, measurements were performed at three pH values (5.0, 6.2, and 7.4) in quadruplicates. For this purpose, 12 wells of a deep well plate, that is, four wells per pH value, were filled with 650 μ L of System Solution. Samples (150 μ L) were withdrawn from each well to determine the blank spectra by UV spectroscopy (SpectraMax 190, Molecular Devices). Then, analyte dissolved in DMSO was added to the remaining System Solution to yield 50 μ M solutions. To exclude

precipitation, the optical density was measured at 650 nm, with 0.01 being the threshold value. Solutions exceeding this threshold were filtrated. Afterward, samples (150 μ L) were withdrawn to determine the reference spectra. Further samples (200 μ L) were transferred to each well of the donor plate of the PAMPA sandwich (pIon, Woburn, MA, P/N 110 163). The filter membranes at the bottom of the acceptor plate were impregnated with 5 μ L of GIT-0 Lipid Solution, and 200 μ L of Acceptor Sink Buffer was filled into each acceptor well. The sandwich was assembled, placed in the GutBox, and left undisturbed for 16 h. Then, it was disassembled, and samples (150 μ L) were transferred from each donor and acceptor well to UV plates. Quantification was performed by both UV spectroscopy and LC-MS (see below). log P_e values were calculated with the aid of the PAMPA Explorer Software (pIon, version 3.5).

Thermodynamic Solubility. Microanalysis tubes (LaboTech J. Stofer LTS AG, Muttens, Switzerland) were charged with 1 mg of solid substance and 250 μ L of phosphate buffer (50 mM, pH 6.5). The tubes were briefly shaken by hand, sonicated for 15 min, and vigorously shaken (600 rpm, 25 °C, 2 h) on an Eppendorf Thermomixer Comfort. Afterward, they were left undisturbed for 24 h. After the pH was measured, the compound solutions were filtered (MultiScreen HTS 96-well Filtration System, Millipore, Billerica, MA) by centrifugation (1500 rpm, 25 °C, 3 min). The filtrates were diluted (1:2, 1:10, and 1:100 or, if the results were outside of the calibration range, 1:1000 and 1:10000), and the concentrations were determined by LC-MS (see below). The calibration was based on six values ranging from 0.1 to 10 μ g/mL.

PPB. The dialysis membranes (MWCO 12–14 K; HTDialysis LCC, Gales Ferry, CT) were prepared according to the instructions of the manufacturer. The human plasma was centrifuged (5800 rpm, 25 °C, 10 min), the pH of the supernatant (without floating plasma lipids) was adjusted to 7.5, and the analyte was added to yield 10 μ M solutions. PPB determinations were performed in triplicate. Equal volumes (150 μ L) of phosphate buffer (0.1 M, pH 7.4) and plasma containing the analyte were transferred to the separated compartments of the 96-well high throughput dialysis block (HTDialysis LCC). The plate was covered with a sealing film and incubated (5 h, 37 °C). Afterward, samples (90 μ L) were withdrawn from the buffer compartments and diluted with plasma (10 μ L). From the plasma compartments, samples (10 μ L) were withdrawn and diluted with phosphate buffer (90 μ L). The solutions were further diluted with ice-cooled MeCN (300 μ L) to precipitate the proteins and centrifuged (3600 rpm, 4 °C, 11 min). The supernatants (50 μ L) were retrieved, and the analyte concentrations were determined by LC-MS (see below). The fraction bound (f_b) was calculated as follows:

$$f_b = 1 - \frac{c_b}{c_p}$$

where c_b is the concentration of the analyte in the buffer compartment and c_p is the concentration in the plasma compartment. The values were accepted if the recovery of analyte was between 80 and 120% of the initial amount.

LC-MS Measurements. Analyses were performed using a 1100/1200 Series HPLC System coupled to a 6410 Triple Quadrupole mass detector (Agilent Technologies, Inc., Santa Clara, CA) equipped with electrospray ionization. The system was controlled with the Agilent MassHunter Workstation Data Acquisition software (version B.01.04). The column used was an Atlantis T3 C18 column (2.1 mm \times 50 mm) with a 3 μ m particle size (Waters Corp., Milford, MA). The mobile phase consisted of two eluents: solvent A (H₂O, containing 0.1% formic acid, v/v) and solvent B (acetonitrile, containing 0.1% formic acid, v/v), both delivered at a flow rate of 0.6 mL/min. The gradient was ramped from 95% A/5% B to 5% A/95% B over 1 min and then held at 5% A/95% B for 0.1 min. The system was then brought back to 95% A/5% B, resulting in a total duration of 4 min. MS parameters such as fragmentor voltage, collision energy, and polarity were optimized individually for each compound, and the molecular ion was followed for each compound in the multiple reaction monitoring

mode. The concentration of each analyte was quantified by the Agilent Mass Hunter Quantitative Analysis software (version B.01.04).

In Vivo Pharmacokinetic and Treatment Studies. *Animals.* Female C3H/HeN mice weighing between 19 and 25 g were obtained from Charles River Laboratories and were housed three or four to a cage. Mice were kept under specific pathogen-free conditions in the Animal House of the Department of Biomedicine, University Hospital Basel, and animal experimentation guidelines according to the regulations of Swiss veterinary law were followed. After 7 days of acclimatization, 9–10 week old mice were used for the PK and infection study. During the studies, animals were allowed free access to chow and water. Three days before infection studies and during infection, 5% D-(+)-glucose (AppliChem, Baden-Dättwil, Switzerland) was added to the drinking water, to increase the number of bacterial counts in the urine and kidneys.⁴⁰

Pharmacokinetic Studies. Single-dose PK studies were performed by iv application of the FimH antagonist at the designated dosages followed by urine and plasma sampling. For iv application, the antagonists were diluted in 100 μ L of PBS and injected into the tail vein. Blood and urine were sampled (10 μ L) after 6 and 30 min and 1, 2, 4, 6, and 8 h. Before analysis, proteins in blood and urine samples were precipitated using methanol (Acros Organics) and centrifuged for 11 min at 13000 rpm. The supernatant was transferred into a 96-well plate (0.5 mL, polypropylene, Agilent Technologies) and analyzed by LC-MS as described above.

UTI Mouse Model. Mice were infected as previously described.⁴⁰ In brief, before infection, all remaining urine was depleted from the bladder by gentle pressure on the abdomen. Mice were anesthetized with 1.1 vol% isoflurane/oxygen mixture (Attane, Minrad Inc., Buffalo, NY) and placed on their backs. Anesthetized mice were inoculated transurethrally with the bacterial suspension by use of a 2 cm polyethylene catheter (Intramedic polyethylene tubing; inner diameter, 0.28 mm; outer diameter, 0.61 mm; Beckton, Dickinson and Company), which was placed on a syringe (Hamilton Gastight Syringe 50 μ L, removable 30G needle, BGB Analytik AG, Boeckten, Switzerland). The catheter was gently inserted through the urethra until it reached the top of the bladder, followed by slow injection of 50 μ L of bacterial suspension at a concentration of approximately 5×10^7 to 5×10^8 CFU.

Antagonist Treatment Studies. The FimH antagonists were applied iv in 100 μ L of PBS into the tail vein 10 min before infection. Three hours after the onset of infection, mice were sacrificed with CO₂. Organs were removed aseptically and homogenized in 1 mL of PBS by using a tissue lyser (Retsch, Haan, Germany). Serial dilutions of bladder and kidneys were plated on Levine Eosin Methylene Blue Agar plates (Beckton, Dickinson and Company). CFU counts were determined after overnight incubation at 37 °C and expressed as CFU/organ, corresponding to CFU/bladder and CFU/2 kidneys.

■ ASSOCIATED CONTENT

🔗 Supporting Information

Synthesis of compounds 7–10, 14–20, 23–37, 39–42, 44, 47b,d, 48b,d, 50–52, and 55–58; HRMS data, HPLC traces, and ¹H NMR spectra for the target compounds 21–29, 31, 32, 36, 37, 41, 42, 48a–d, 52, 57, and 58. This material is available free of charge via the Internet at <http://pubs.acs.org>.

■ AUTHOR INFORMATION

Corresponding Author

*Tel: +41 61 267 15 51. Fax: +41 61 267 15 52. E-mail: beat.ernst@unibas.ch.

Author Contributions

[†]These authors contributed equally to the project.

Notes

The authors declare no competing financial interest.

■ ACKNOWLEDGMENTS

We thank Prof. Urs Jenal, Biocenter of the University of Basel, Switzerland, for the clinical *E. coli* isolate UTI89. We further appreciate the support by Prof. Dr. med. Radek Skoda, Department of Biomedicine, University Hospital Basel, Switzerland, for giving us access to the animal facility. The financial support by the Swiss National Science Foundation (SNF interdisciplinary grant K-32K1-120904) is gratefully acknowledged.

■ ABBREVIATIONS USED

ABTS, 2,2'-azino-di(3-ethylbenzthiazoline-6-sulfonic acid); AUC, area under the curve; CFU, colony-forming units; CRD, carbohydrate recognition domain; log *D*_{7.4}, distribution coefficient at pH 7.4; DCM, dichloromethane; dba, dibenzylideneacetone; DMSO, dimethyl sulfoxide; GFP, green fluorescent protein; GPE, guinea pig erythrocytes; IC₅₀, half maximal inhibitory concentration; IC₉₀, concentration where 90% of the maximal observed effect is obtained; iv, intravenous; MIC_{adhesion}, minimal inhibitory concentration of adhesion; Man, D-mannose; MD, molecular dynamics; MFI, mean fluorescent intensity; NMR, nuclear magnetic resonance; PAMPA, parallel artificial membrane permeation assay; *P*_{eff}, effective permeation; PPB, plasma protein binding; PK, pharmacokinetic; PPP, platelet poor plasma; PRP, platelet rich plasma; rIC₅₀, relative inhibitory concentration; S, solubility; SAR, structure–activity relationship; sc, subcutaneous; *T* > MIC_{adhesion}, time over the minimal inhibitory concentration of adhesion; TM-PAA, Man α 1–3(Man α 1–6)Man β 1–4GlcNAc β 1–4GlcNAc β -polyacrylamide-biotin; TMSOTf, trimethylsilyl trifluoromethanesulfonate; UPEC, uropathogenic *Escherichia coli*; UPIa, uroplakin Ia; UTI, urinary tract infection; X-Phos, 2-dicyclohexylphosphino-2',4',6'-triisopropylbiphenyl

■ REFERENCES

- (1) (a) Berglund, J.; Knight, S. D. Structural basis for bacterial adhesion in the urinary tract. *Adv. Exp. Med. Biol.* **2003**, *535*, 33–52. (b) Westerlund-Wikström, B.; Korhonen, T. K. Molecular structure of adhesin domains in *Escherichia coli* fimbriae. *Int. J. Med. Microbiol.* **2005**, *295*, 479–486.
- (2) Wiles, T. J.; Kulesus, R. R.; Mulvey, M. A. Origins and virulence mechanisms of uropathogenic *Escherichia coli*. *Exp. Mol. Pathol.* **2008**, *85*, 11–19.
- (3) Mulvey, M. A. Adhesion and entry of uropathogenic *Escherichia coli*. *Cell Microbiol.* **2002**, *4*, 257–271.
- (4) Capitani, G.; Eidam, O.; Glockshuber, R.; Grutter, M. G. Structural and functional insights into the assembly of type 1 pili from *Escherichia coli*. *Microbes Infect.* **2006**, *8*, 2284–2290.
- (5) Sharon, N. Carbohydrates as future anti-adhesin drugs for infectious diseases. *Biochim. Biophys. Acta* **2006**, *1760*, 527–537.
- (6) (a) Firon, N.; Ofek, I.; Sharon, N. Interaction of mannose-containing oligosaccharides with the fimbrial lectin of *Escherichia coli*. *Biochem. Biophys. Res. Commun.* **1982**, *105*, 1426–1432. (b) Firon, N.; Ofek, I.; Sharon, N. Carbohydrate specificity of the surface lectins of *Escherichia coli*, *Klebsiella pneumoniae* and *Salmonella typhimurium*. *Carbohydr. Res.* **1983**, *120*, 235–249. (c) Sharon, N. Bacterial lectins, cell-cell recognition and infectious disease. *FEBS Lett.* **1987**, *217*, 145–157.
- (7) (a) Pieters, R. J. Maximising multivalency effects in protein-carbohydrate interactions. *Org. Biomol. Chem.* **2009**, *7*, 2013–2025. (b) Imberty, A.; Chabre, Y. M.; Roy, R. Glycomimetics and glycodendrimers as high affinity microbial anti-adhesins. *Chem.—Eur. J.* **2008**, *14*, 7490–7499.

- (8) Hartmann, M.; Lindhorst, T. K. The bacterial lectin FimH, a target for drug discovery-carbohydrate inhibitors of type 1 fimbriae-mediated bacterial adhesion. *Eur. J. Org. Chem.* **2011**, 3583–3609.
- (9) (a) Choudhury, D.; Thompson, A.; Stojanoff, V.; Langermann, S.; Pinkner, J.; Hultgren, S. J.; Knight, S. D. X-ray structure of the FimC-FimH chaperone-adhesin complex from uropathogenic *Escherichia coli*. *Science* **1999**, *285*, 1061–1066. (b) Bouckaert, J.; Berglund, J.; Schembri, M.; Genst, E. D.; Cools, L.; Wuhler, M.; Hung, C. S.; Pinkner, J.; Slättergard, R.; Zavalov, A.; Choudhury, D.; Langermann, S.; Hultgren, S. J.; Wyns, L.; Klemm, P.; Oscarson, S.; Knight, S. D.; Greve, H. D. Receptor binding studies disclose a novel class of high-affinity inhibitors of the *Escherichia coli* FimH adhesin. *Mol. Microbiol.* **2005**, *55*, 441–455. (c) Wellens, A.; Garofalo, C.; Nguyen, H.; Van Gerven, N.; Slättergård, R.; Hernalsteens, J.-P.; Wyns, L.; Oscarson, S.; De Greve, H.; Hultgren, S.; Bouckaert, J. Intervening with urinary tract infections using anti-adhesives based on the crystal structure of the FimH-oligomannose-3 complex. *PLoS One* **2008**, *3*, 4–13. (d) Han, Z.; Pinker, J. S.; Ford, B.; Obermann, R.; Nolan, W.; Wildman, S. A.; Hobbs, D.; Ellenberger, T.; Cusumano, C. K.; Hultgren, S. J.; Janetka, J. W. Structure-based drug design and optimization of mannoside bacterial FimH antagonists. *J. Med. Chem.* **2010**, *53*, 4779–4792.
- (10) (a) Sperling, O.; Fuchs, A.; Lindhorst, T. K. Evaluation of the carbohydrate recognition domain of the bacterial adhesin FimH: design, synthesis and binding properties of mannoside ligands. *Org. Biomol. Chem.* **2006**, *4*, 3913–3922. (b) Grabosch, C.; Hartmann, M.; Schmidt-Lassen, J.; Lindhorst, T. K. Squaric acid monoamide mannosides as ligands for the bacterial lectin FimH: Covalent inhibition or not? *ChemBioChem* **2011**, *12*, 1066–1074.
- (11) Klein, T.; Abgottspon, D.; Wittwer, M.; Rabbani, S.; Herold, J.; Jiang, X.; Kleeb, S.; Lüthi, C.; Scharenberg, M.; Bezençon, J.; Gubler, E.; Pang, L.; Smiesko, M.; Cutting, B.; Schwardt, O.; Ernst, B. FimH antagonist for the oral treatment of urinary tract infections: From design and synthesis to in vitro and in vivo evaluation. *J. Med. Chem.* **2010**, *53*, 8627–8641.
- (12) Rabbani, S.; Jiang, X.; Schwardt, O.; Ernst, B. Expression of the carbohydrate recognition domain of FimH and development of a competitive binding assay. *Anal. Biochem.* **2010**, *407*, 188–195.
- (13) Cusumano, C. K.; Pinkner, J. S.; Han, Z.; Greene, S. E.; Ford, B. A.; Crowley, J. R.; Henderson, J. P.; Janetka, J. W.; Hultgren, S. J. Treatment and prevention of urinary tract infection with orally active FimH inhibitors. *Sci. Transl. Med.* **2011**, *3*, 1–10.
- (14) Kerékgyártó, J.; Kamerling, J. P.; Bouwstra, J. B.; Vliegentshrst, J. F. G.; Liptak, A. Synthesis of four structural elements of xylose-containing carbohydrate chains from N-glycoproteins. *Carbohydr. Res.* **1989**, *186*, 51–62.
- (15) (a) Ma, D.; Cai, Q. L-Proline promoted Ullmann type coupling reactions of aryl iodides with indoles, pyrroles, imidazoles or pyrazoles. *Synlett* **2004**, 128–130. (b) Ma, D.; Cai, Q. Copper/Amino acid catalyzed cross-couplings of aryl and vinyl halides with nucleophiles. *Acc. Chem. Res.* **2008**, *41*, 1450–1460. and the references thereof (c) Ley, S. V.; Thomas, A. W. Modern Synthetic methods for copper-mediated C(aryl)-O, C(aryl)-N, and C(aryl)-S bond formation. *Angew. Chem., Int. Ed.* **2003**, *42*, 5400–5449. (d) Antilla, J. C.; Klapars, A.; Buchwald, S. L. The copper-catalyzed N-arylation of indoles. *J. Am. Chem. Soc.* **2002**, *124*, 11684–11688.
- (16) Kosak, J. R. Catalytic hydrogenation of aromatic halonitro compounds. *Ann. N.Y. Acad. Sci.* **1970**, *172*, 175–185.
- (17) Wolfe, J. P.; Wagaw, S.; Marcoux, J.-F.; Buchwald, S. L. Rational development of practical catalysts for aromatic carbon-nitrogen bond formation. *Acc. Chem. Res.* **1998**, *31*, 805–818.
- (18) Prieto, M.; Zurita, E.; Rosa, E.; Muñoz, L.; Lloyd-Williams, P.; Giral, E. Arylboronic acids and arylpinacolboronate esters in Suzuki-coupling reactions involving indoles. Partner role swapping and heterocycle protection. *J. Org. Chem.* **2004**, *69*, 6812–6820.
- (19) Abgottspon, D.; Rölli, G.; Hosch, L.; Steinhuber, A.; Jiang, X.; Schwardt, O.; Cutting, B.; Smiesko, M.; Jenal, U.; Ernst, B.; Trampuz, A. Development of an aggregation assay to screen FimH antagonists. *J. Microbiol. Methods* **2010**, *82*, 249–255.
- (20) Bouckaert, J.; Mackenzie, J.; de Paz, J. L.; Chipwaza, B.; Choudhury, D.; Zavalov, A.; Mannerstedt, K.; Anderson, J.; Pierard, D.; Wyns, L.; Seeberger, P. H.; Oscarson, S.; De Greve, H.; Knight, S. D. The affinity of the FimH fimbrial adhesin is receptor-driven and quasi-independent of *Escherichia coli* pathotypes. *Mol. Microbiol.* **2006**, *61*, 1556–1568.
- (21) Giampapa, C. S.; Abraham, S. N.; Chiang, T. M.; Beachey, E. H. Isolation and characterization of a receptor for type 1 fimbriae of *Escherichia coli* from guinea pig erythrocytes. *J. Biol. Chem.* **1988**, *263*, 5362–5367.
- (22) Aprikian, P.; Tchesnokova, V.; Kidd, B.; Yakovenko, O.; Yarov-Yarovoy, V.; Trinchina, E.; Vogel, V.; Thomas, W.; Sokurenko, E. Interdomain interaction in the FimH adhesin of *Escherichia coli* regulates the affinity to mannose. *J. Biol. Chem.* **2007**, *282*, 23437–23446.
- (23) Trong, I. L.; Aprikian, P.; Kidd, B. A.; Forero-Shelton, M.; Tchesnokova, V.; Rajagopal, P.; Rodriguez, V.; Interlandi, G.; Klevit, R.; Vogel, V.; Stenkamp, R. E.; Sokurenko, E. V.; Thomas, W. E. Structural basis for mechanical force regulation of the adhesin FimH via finger trap-like beta sheet twisting. *Cell* **2010**, *141*, 645–655.
- (24) (a) Kansy, M.; Senner, F.; Gubernator, K. Physicochemical high throughput screening: Parallel artificial membrane permeation assay in the description of passive absorption processes. *J. Med. Chem.* **1998**, *41*, 1007–1010. (b) Avdeef, A.; Bendels, S.; Di, L.; Faller, B.; Kansy, M.; Sugano, K.; Yamauchi, Y. Parallel artificial membrane permeability assay (PAMPA)-critical factors for better predictions of absorption. *J. Pharm. Sci.* **2007**, *96*, 2893–2909.
- (25) Lipinski, C. A. Drug-like properties and the causes of poor solubility and poor permeability. *J. Pharmacol. Toxicol. Methods* **2000**, *44*, 235–249.
- (26) Lovering, F.; Bikker, J.; Humblet, C. Escape from flatland: increasing saturation as an approach to improving clinical success. *J. Med. Chem.* **2009**, *52*, 6752–6756.
- (27) van de Waterbeemd, H.; Smith, D. A.; Beaumont, K.; Walker, D. K. Property-based design: optimization of drug absorption and pharmacokinetics. *J. Med. Chem.* **2001**, *44*, 1313–1333.
- (28) (a) Schmidt, S.; Gonzalez, D.; Derendorf, H. Significance of protein binding in pharmacokinetics and pharmacodynamics. *J. Pharm. Sci.* **2010**, *99*, 1107–1122. (b) Trainor, G. L. The importance of plasma protein binding in drug discovery. *Expert Opin. Drug Discovery* **2007**, *2*, 51–64. (c) Weisiger, R. A. Dissociation from albumin: a potentially rate-limiting step in the clearance of substances by the liver. *Proc. Natl. Acad. Sci. U.S.A.* **1985**, *82*, 1563–1567.
- (29) Dearden, J. C.; Bresnen, J. G. M. The measurement of partition coefficients. *QSAR Comb. Sci.* **1988**, *7*, 133–144.
- (30) Kerns, E. H. High throughput physicochemical profiling for drug discovery. *J. Pharm. Sci.* **2001**, *90*, 1838–1858.
- (31) Banker, M. J.; Clark, T. H.; Williams, J. A. Development and validation of a 96-well equilibrium dialysis apparatus for measuring plasma protein binding. *J. Pharm. Sci.* **2003**, *92*, 967–974.
- (32) Andrews, J. M. Determination of minimum inhibitory concentrations. *J. Antimicrob. Chemother.* **2001**, *48* (Suppl1), 5–16.
- (33) Scharenberg, M.; Abgottspon, D.; Ciceck, E.; Jiang, X.; Schwardt, O.; Rabbani, S.; Ernst, B. Flow cytometry-based assay for screening FimH antagonists. *Assay Drug Dev. Technol.* **2011**, *9*, 455–464.
- (34) Hooton, T. M. Fluoroquinolones and resistance in the treatment of uncomplicated urinary tract infection. *Int. J. Antimicrob. Agents* **2003**, *22*, 65–72.
- (35) Jakobsen, L.; Cattoir, V.; Hammerum, A. M.; Nordmann, P.; Frimodt-Møller, N. Impact of low-level fluoroquinolone resistance genes qnrA1, qnrB19, and qnrS1 on ciprofloxacin treatment of *Escherichia coli* urinary tract infection in murine model. Poster presented at ICAAC 2010. 50th Interscience Conference on Antimicrobial Agents and Chemotherapy, 2010, Sep 12–15, Boston, MA.
- (36) (a) Russell, W. M. S.; Burch, R. L. *The Principles of Humane Experimental Technique*; Methuen: London, 1959; reprinted: Universities Federation for Animal Welfare, Wheathampstead, United

Kingdom, 1992. (b) Demers, G.; Griffin, G.; De Vroey, G.; Haywood, J. R.; Zurlo, J.; Bédard, M. Harmonization of animal care and use guidance. *Science* **2006**, *312*, 700–701.

(37) Schwardt, O.; Rabbani, S.; Hartmann, M.; Abgottspon, D.; Wittwer, M.; Kleeb, S.; Zalewski, A.; Smiesko, M.; Cutting, B.; Ernst, B. Design, Synthesis and biological evaluation of mannosyl triazoles as FimH antagonists. *Bioorg. Med. Chem.* **2011**, *19*, 6454–6473.

(38) Mulvey, M. A.; Schilling, J. D.; Hultgren, S. J. Establishment of a persistent *Escherichia coli* reservoir during the acute phase of a bladder infection. *Infect. Immun.* **2001**, *69*, 4572–4579.

(39) (a) VCCLAB, Virtual Computational Chemistry Laboratory; <http://www.vcclab.org>, 2005. (b) Tetko, I. V.; Gasteiger, J.; Todeschini, R.; Mauri, A.; Livingstone, D.; Ertl, P.; Palyulin, V. A.; Radchenko, E. V.; Zefirov, N. S.; Makarenko, A. S.; Tanchuk, V. Y.; Prokopenko, V. V. Virtual computational chemistry laboratory—Design and description. *J. Comput.-Aided Mol. Des.* **2005**, *19*, 453–463.

(40) Kern, M. B.; Frimodt-Møller, N.; Espersen, F. Effects of sulfamethizole and amdinocillin against *Escherichia coli* strains (with various susceptibilities) in an ascending urinary tract infection model. *Antimicrob. Agents Chemother.* **2003**, *47*, 1002–1009.

2.10 **Manuscript 9: FimH antagonists – phosphate prodrugs improve oral bioavailability**

The following manuscript addresses the low aqueous solubility of the biphenyl and indolinyphenyl mannosides by a phosphate ester prodrug approach. A Caco-2 cell model was implemented to characterize the enzyme-mediated cleavage of the phosphate promoiety and the subsequent permeation of the pharmacologically active parent compound through the confluent cell monolayer. Preliminary observations *in vitro* were completed by an *in vivo* pharmacokinetic study. As a result, phosphate prodrugs showing high oral availability and leading to prolonged high concentrations of FimH antagonist in the urine were identified.

Contribution to the project:

Simon Kleeb implemented all *in vitro* assays regarding the phosphatase-mediated release of the parent compound from the prodrug as well as the *in vitro* absorption studies. He furthermore interpreted the resulting data and was responsible for the writing of the manuscript except for the sections about synthesis and the *in vivo* pharmacokinetic study.

This manuscript is in preparation for *J. Med. Chem.*

FimH Antagonists - Phosphate Prodrugs Improve Oral Bioavailability

Simon Kleeb,[#] Xiaohua Jiang,[#] Priska Frei,[#] Anja Sigl, Jacqueline Bezençon, Karen Bamberger, Oliver Schwardt, and Beat Ernst*

Institute of Molecular Pharmacy, Pharmacenter, University of Basel, Klingelbergstrasse 50, 4056 Basel (Switzerland)

* To whom correspondence should be addressed: Prof. Dr. B. Ernst, Institute of Molecular Pharmacy, Pharmacenter, University of Basel, Klingelbergstrasse 50, 4056 Basel, Switzerland; Tel: +41 61 267 15 51, Fax: +41 61 267 15 52; E-mail: beat.ernst@unibas.ch

[#] Contributed equally.

Keywords: aqueous solubility, FimH antagonists, oral bioavailability, phosphate prodrugs.

Abbreviations: ALP, alkaline phosphatase; C_{\max} , maximum concentration; Caco-2 cells, colorectal adenocarcinoma cells; cpd, compound; CRD, carbohydrate recognition domain; DCM, dichloromethane; DMF, *N,N*-dimethylformamide; LC-MS, liquid chromatography-mass spectrometry; MPLC, medium pressure liquid chromatography; P , octanol-water partition coefficient; P_{app} , apparent permeability; P_e , effective permeability; PAMPA, parallel artificial membrane permeability assay; PK, pharmacokinetic; $t_{1/2}$, half life; T_{\max} , time when maximum concentration is observed; UPEC, uropathogenic *Escherichia coli*; UTI, urinary tract infection.

Abstract

Urinary tract infections by uropathogenic *Escherichia coli* belong to the most common infectious diseases and frequently require antibiotic treatment. Since frequent exposure to antibiotics leads to the emergence of antimicrobial resistance, alternative prevention and treatment strategies are urgently needed. In the initial step of the host cell colonization, FimH a lectin located at the tip of bacterial type 1 pili interacts with mannosylated glycoproteins on the urinary bladder mucosa. Although this initial pathogen/host interaction can be efficiently antagonized by biaryl α -D-mannopyranosides, their physicochemical profile, namely low aqueous solubility, however, is unfavorable for an oral treatment.

Here we report the syntheses and the pharmacokinetic evaluation of phosphate prodrugs of biaryl α -D-mannopyranosides, which are characterized by strongly increased aqueous solubility. In a Caco-2 cell model, hydrolysis of the phosphate esters by brush border-associated enzymes created a supersaturated solution of the active principal and thus a high concentration gradient across the cell monolayer. As a result, an up to tenfold increase in the absorptive flux could be observed. Compared to the same molecular dose of the active principle, a substantial increase of the FimH antagonists in the urine was achieved with phosphate prodrugs. An oral availability of up to 95% of the administered dose marks a milestone in the development of FimH antagonists.

Introduction

Urinary tract infection (UTI) are the most common bacterial infections in humans and affect millions of people.^[1] UTI remains one of the most common indications for prescribing antimicrobials to tackle the symptoms (dysuria, frequent and urgent urination, bacteriuria, and pyuria) and to prevent complications (pyelonephritis and urosepsis).^[2] However, frequent and repeated use of antibiotics can lead to the emergence of antimicrobial resistance. Alternative prevention and treatment strategies are therefore urgently needed.^[3]

Uropathogenic *Escherichia coli* (UPEC) strains are the causative agents of more than 70% of all UTI episodes.^[4,5] Bacterial adherence to the bladder cell surface is the initial step of the pathogenesis, preventing UPEC from being cleared by the bulk flow of urine and enabling the bacteria to colonize the urothelial cells.^[6] Among the different adhesins expressed on the bacterial surface, mannose-binding type 1 pili are the most prevalent. They consist of a helical rod formed by 500 to 3000 copies of the main structural subunit FimA and of a linear

tip fibrillum formed by the subunits FimG, FimF, and FimH.^[7] The latter subunit is expressed on the tip of the pili and encloses the carbohydrate recognition domain (CRD), which targets the mannosylated glycoprotein uroplakin 1a on the mucosal surface of the bladder.^[8]

More than three decades ago, Sharon and co-workers described various oligomannosides and aryl α -D-mannosides as potential antagonists of the FimH-mediated bacterial adhesion.^[9,10] Later on, several high-affinity monovalent mannose-based FimH antagonists with various aglycones like *n*-alkyl,^[11] phenyl,^[12] dioxocyclobutenylaminophenyl,^[13] umbelliferyl,^[12] biphenyl,^[14-18] indol(in)ylphenyl,^[19] triazolyl^[20] and thiazolylamino^[21] have been reported. In addition, different multivalent presentations of mannose have been synthesized.^[22-28] Most importantly, adverse side effects resulting from non-selective binding of FimH antagonists - they are all α -D-mannopyranosides - to mannose receptors of the human host system could recently be ruled out.^[29]

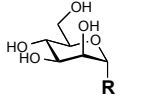
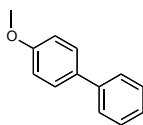
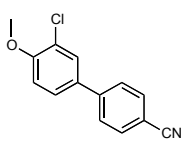
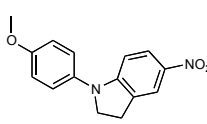
In vivo studies in mice impressively proved the therapeutic potential of biaryl mannosides for an oral treatment of UTI.^[15-17] However, since only low oral bioavailability could be achieved, basic determinants such as aqueous solubility and membrane permeability should be further optimized.^[30] A possible solution is offered by a phosphate prodrug approach which is either applied when the active principal exhibits high membrane permeability but suffers from low aqueous solubility^[31] or when the therapeutic dose exceeds the maximum amount of drug dissolvable in the intestinal fluids.^[32] Successful applications led to various marketed drugs, *e.g.* to the antiretroviral drug fosamprenavir,^[33,34] the anesthetic propofol,^[35] or the chemotherapeutic drug fludarabine phosphate.^[36]

The goal of the present study was to optimize the physicochemical profile of the biaryl mannosides **3-5** by a phosphate prodrug approach, enhancing aqueous solubility and, consequently, oral availability.

Results and Discussion

The potent FimH antagonists **3-5**^[14,18,19,37] are perfect candidates for a phosphate approach due to their low aqueous solubility and elevated membrane permeability. Table 1 summarizes their (previously published) binding affinity (IC_{50})^[14,18,19,37] and their physicochemical properties (solubility, lipophilicity, and permeability).

Table 1. Binding affinity and physicochemical parameters of the biaryl α -D-mannopyranosides **3-5**^[14,18,37]. IC₅₀ values, aqueous solubility, log *P*, and PAMPA data were adopted from references^[18,19,37], the IC₅₀ of antagonist **4** and Caco-2 *P*_{app} values of antagonist **5** were obtained according to the procedure described in^[18].

Cpd.		IC ₅₀ ^[a] [nM]	Solubility ^[b] ¹ [μg/ml]	log <i>P</i> ^[c]	PAMPA log <i>P</i> _e ^[d] [cm/s]	Caco-2 <i>P</i> _{app} ^[e] [10 ⁻⁶ cm/s]	
						a→b	b→a
3 ^[14,18]		84.9	21	2.1	-4.7	10.0 ± 0.9	19.0 ± 1.2
4 ^[37]		10.1	192	2.1	-5.2	2.2 ± 0.4	22.1 ± 1.5
5 ^[19]		20	24	1.9	-5.5	2.9 ± 0.6	39.3 ± 5.8

[a] IC₅₀ values were determined in a cell-free competitive binding assay,^[38] [b] **3** and **5**: Thermodynamic solubility, **4**: Kinetic solubility,^[39] [c] Octanol-water partition coefficients (log *P*) were determined by a miniaturized shake-flask procedure,^[40] [d] *P*_e = effective permeability: passive permeation through an artificial membrane was determined by the parallel artificial membrane permeability assay (PAMPA);^[41,42] [e] *P*_{app} = apparent permeability: permeation through a Caco-2 cell monolayer was assessed in the absorptive (a→b) and secretory (b→a) directions in triplicate.^[43,44]

For identifying the optimal position of the phosphate promoiety within the biaryl mannoside **3-5**, a series of phosphate esters was synthesized (Figure 1) and subjected to alkaline phosphatase (ALP)-mediated hydrolysis. In the prodrugs **6a-d** and **7a-d**, the phosphate ester bond was directly linked to the various hydroxyl groups of the mannose moiety. Alternatively, an acetal linker was used in the prodrugs **6e** and **8** in order to increase the distance between the enzymatic cleavage site and the derivatized hydroxyl group of the active principal to enhance accessibility of the phosphate ester and increase the dephosphorylation rate. The hemiacetal formed as intermediate is expected to collapse spontaneously releasing the active principle as well as formaldehyde.^[45]

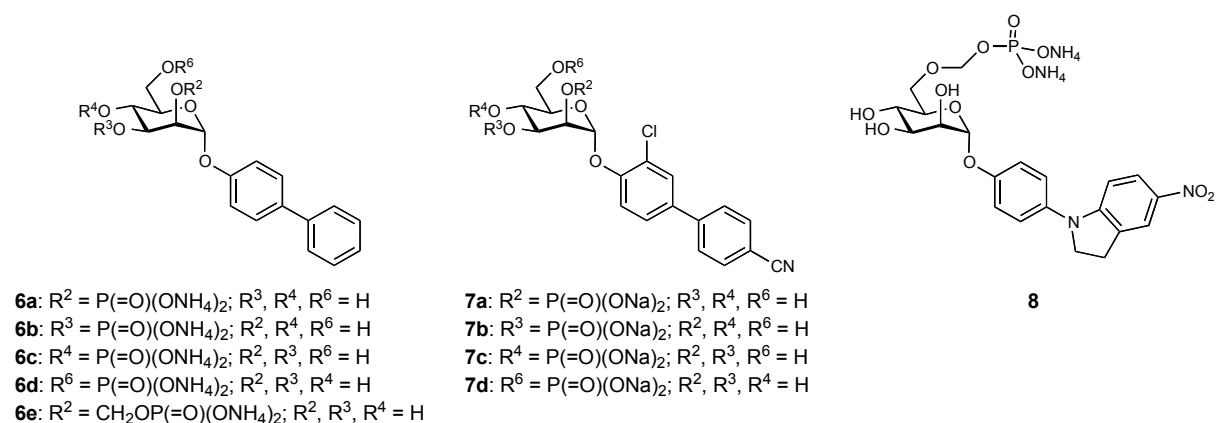
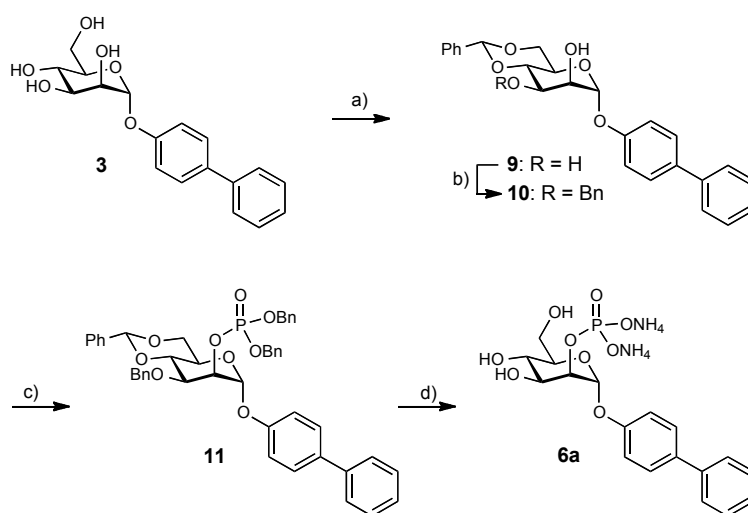


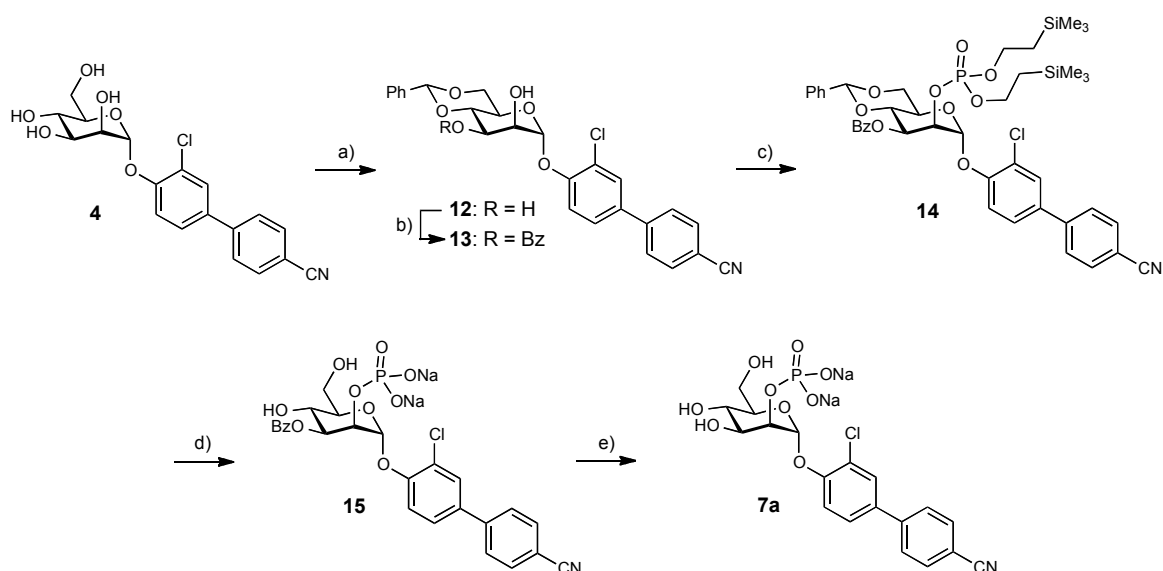
Figure 1. Phosphate monoester **6a-e** of biphenyl α -D-mannopyranoside **3**, **7a-d** of the substituted biphenyl α -D-mannopyranoside **4** and **8** of the indolinyphenyl α -D-mannopyranoside **5**.

Synthesis of phosphates 6a-d. The 2-phosphate **6a** of biphenyl α -D-mannopyranoside (**3**) was synthesized according to the procedure depicted in Scheme 1. Starting from **3**,^[14,18] a benzylidene acetal (\rightarrow **9**) was used to protect the 4- and 6-OH of the mannose moiety. Then, the 3-position was protected by a selective dibutyltin oxide-mediated benzylation (\rightarrow **10**). By phosphorylation using dibenzyl *N,N*-diisopropyl-phosphoramidite in the presence of 1,2,4-triazole and subsequent oxidation with *tert*-butylhydroperoxide the protected intermediate **11** was obtained. The final deprotection of the phosphate and the mannose moiety by catalytic hydrogenation yielded the 2-phosphate **6a**. The 3-, 4- and 6-phosphates **6b-d** were obtained in analogous procedures from suitably protected precursors (for the synthesis see the Supporting Information).



Scheme 1. Reagents and conditions: a) PhCH(OMe)_2 , *p*-TsOH, DMF, 50 °C, overnight (70%); b) i. Bu_2SnO , toluene, 135 °C, 3 h; ii. BnBr, toluene, 115 °C, overnight (80%); c) dibenzyl *N,N*-diisopropylphosphoramidite, 1,2,4-triazole, MeCN, 0 °C to rt, overnight; then 70% aq. *tert*-BuOOH, rt, 1 h (62%); d) i. H_2 (4 bar), $\text{Pd(OH)}_2/\text{C}$, EtOAc, cat. HOAc, overnight; ii. 25% aq. NH_3/MeOH (4:1), rt, overnight (45%).

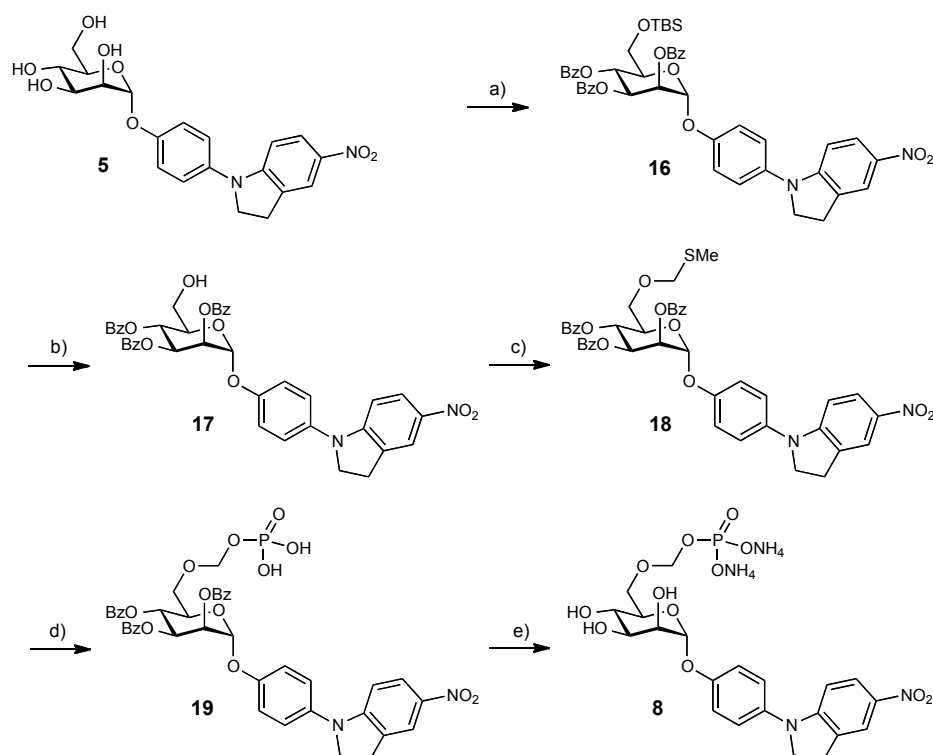
Synthesis of Phosphates 7a-d. Due to the labile chloro- and cyano-substituents present in biphenyl α -D-mannopyranoside **4**^[37], the 2-phosphate **7a** was obtained by a modified strategy (Scheme 2), because synthetic steps affording hydrogenation had to be omitted. After protecting the 4- and 6-OH of **4** with a benzylidene acetal (\rightarrow **12**), selective benzylation of the 3-OH of the mannose moiety afforded **13**.^[46] The phosphorylated of the 2-OH group with bis[2-(trimethylsilyl)ethyl] *N,N*-diisopropylphosphoramidite in the presence of 1,2,4-triazole and subsequent oxidation with *tert*-butylhydroperoxid yielded intermediate **14**. When the (trimethylsilyl)ethyl esters in **14** were cleaved with TFA and the benzoate removed with NH_3/MeOH 2-phosphate **7a** was obtained. For the synthesis of the 3-, 4- and 6-phosphates **7b-d** the same phosphorylation protocol was applied (see the Supporting Information for details).



Scheme 2. Reagents and conditions: a) $\text{PhCH}(\text{OMe})_2$, *p*-TsOH, rt, 17 h (22%); b) BzCl , DCM/pyr, 0 °C to rt, 3 h (60%); c) bis[2-(trimethylsilyl)ethyl] *N,N*-diisopropylphosphoramidite, 1,2,4-triazole, MeCN, 0 °C to rt, 16 h; then 70% aq. *tert*-BuOOH, rt, 1 h (55%); d) TFA/DCM (1:4), rt, 2 h (61%); e) 25% aq. NH_3/MeOH (4:1), rt, 16 h (71%).

Synthesis of Acetal-linked Phosphates 8 & 6e. Scheme 3 describes the synthesis of the acetal-linked phosphate **8** of indolinyphenyl α -D-mannopyranoside **5**.^[19] Selective protection of the 6-OH of **5** with *tert*-butyldimethylsilyl, subsequent benzylation of the remaining hydroxy functions (\rightarrow **16**), and selective cleavage of the silyl group gave precursor **17**. The introduction of a 6-*O*-(thiomethyl)methyl group by reaction of **17** with DMSO and acetic anhydride under acidic conditions (\rightarrow **18**) followed by treatment with phosphoric acid and *N*-iodosuccinimide yielded phosphate **19**. Finally, debenzoylation with NH_3/MeOH provided

test compound **8**. The acetal-linked phosphate **6e** was prepared analogously from **3** (see Supporting Information).



Scheme 3. Reagents and conditions: a) i. TBSCl, cat. DMAP, pyr, rt, overnight, ii. BzCl, rt, 2 h, (quant.); b) 1 M H₂SO₄/MeOH, rt, 1.5 h (73%); c) DMSO/Ac₂O/HOAc, rt, overnight (74%); d) H₃PO₄/NIS/THF, 0 °C to rt, 1 h (67%); e) 25% aq. NH₃/MeOH/DCM (8:5:4), rt, overnight (41%).

Pharmacokinetic Evaluation. Thermodynamic solubilities of the phosphate prodrug were determined in phosphate buffer (50 mM, pH 6.5) and confirmed the expected raise in aqueous solubility and exceed those of the active principles **3-5** by several orders of magnitude (Table 2). For the ALP-mediated hydrolysis of the different phosphate esters Caco-2 cells were used, which express the enzyme on the apical brush border surface of the confluent cell monolayer.^[47] Prodrugs **6a-e**, **7a-d** and **8**, dissolved in Dulbecco's Modified Eagle's Medium (62.5 μM), were applied into the apical compartment of the Caco-2 cell monolayer and their concentrations were monitored by LC-MS for a period of 60 min. The experimental half-life ($t_{1/2}$) was calculated from the percentage of remaining prodrug vs. incubation time. (Table 2).

Table 2. Aqueous solubility and Caco-2 phosphatase-mediated hydrolysis ($t_{1/2}$) of the prodrugs **6a-6e**, **7a-7d**, **8**, and their active compound **3-5**, respectively.

Cpd	Solubility [$\mu\text{g/ml}$]	$t_{1/2}$ [min]	Cpd	Solubility [$\mu\text{g/ml}$]	$t_{1/2}$ [min]
3	21	---	6e	>3000	8.7
4	172	---	7a	>3000	13
5	24	---	7b	>3000	12
6a	>3000	12	7c	>3000	43
6b	>3000	13	7d	>3000	48
6c	2703	>60	8	>3000	11
6d	>3000	>60			

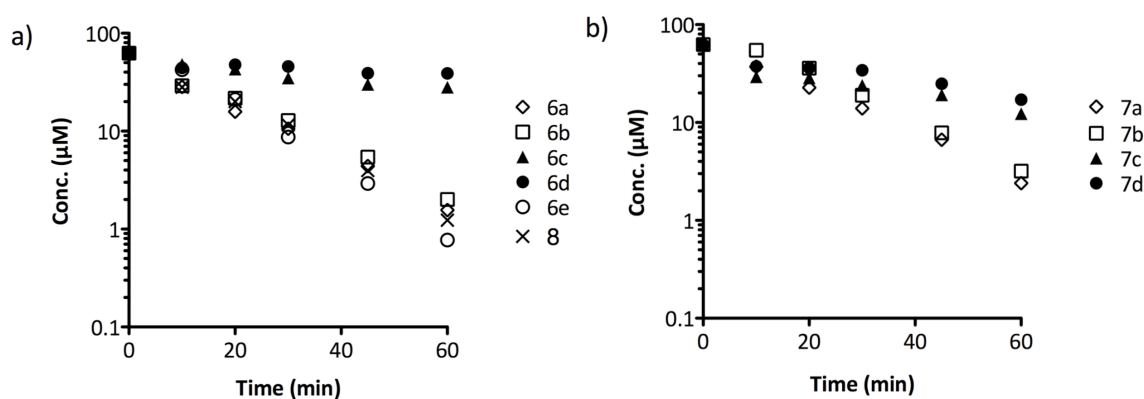


Figure 2. Decomposition of phosphomonoester and phosphonooxymethyl ether prodrugs in the apical Caco-2 cell compartment: (a) **6a-e**, **8**; (b) **7a-d**. Prodrugs dissolved in Dulbecco's Modified Eagle's Medium (62.5 μM) were given into the apical chamber and the concentrations of unchanged prodrug were monitored by LC-MS.

As visualized in Figure 2, the prodrugs showed varying propensity to dephosphorylation, depending on the position of the promoiety. The 2- and 3-phosphate esters **6a**, **6b**, **7a**, and **7b** were rapidly hydrolyzed, whereas the 4- and 6-phosphate esters **6c**, **6d**, **7c**, and **7d** were more stable and showed $t_{1/2}$ of more than 40 min. This high stability is probably due to steric reasons, *i.e.* hindered accessibility of the ester bonds in the C4 and C6-position by the nucleophile within the active site of the ALP.^[45,48,49] Actually, exposing the phosphate promoiety in C6 by introduction of an acetal linker to form a phosphonooxymethyl ether (\rightarrow **6e**, **8**) markedly increased its susceptibility to ALP-mediated cleavage ($t_{1/2}$ = 8.7 min and 11 min, respectively).

Due to their high propensity to ALP-mediated hydrolysis, the phosphate esters **6a**, **6b**, **7a**, **7b**, and **8** were almost entirely converted to parent drug within 60 min. The parent compounds on

their part slowly permeated the Caco-2 cell monolayer. As an example, Figure 3a depicts the concentrations of prodrug **7b** and active principal **4** in the apical and basal chamber 60 min after application of prodrug on the apical side. When applied to the basal chamber of the Caco-2 system, the prodrug concentrations remained at a high level, due to the lack of ALP on the basal enterocyte membrane^[47] and high chemical stability of the phosphate ester bond under the chosen assay conditions (Figure 3b). Irrespective of dosing the prodrugs on the apical or basal side, it could not be detected in the receiver compartments, which corroborates the poor membrane permeability of the polar phosphate ester.

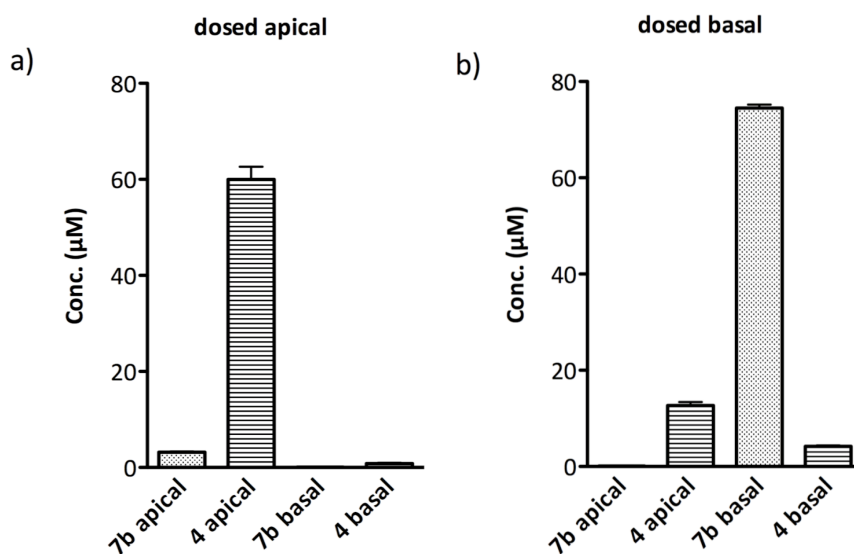


Figure 3. Conversion of prodrug **7b** to the parent compound **4** in a Caco-2 cell monolayer model within 60 min of incubation. A prodrug solution (62.5 µM) was applied either into the apical (a) or basal (b) chamber. The columns represent the concentrations of prodrug and parent compound in the apical and basal chambers 60 min after initiation of the experiment.

Chemical stability under different pH conditions and stability against degradation by digestive enzymes were furthermore assessed by incubating the prodrugs **7a**, **7c**, and **7d** with simulated gastric and intestinal fluids.^[50,51] All tested compounds proved stable under the chosen conditions (see supporting information). We therefore expect, that the phosphates should only be cleaved by the ALP in the intestine.

For proving the benefits of high solubility provided by the promoiety on parent compound absorption, we applied in a next step the most labile prodrugs **6e** and **8** into the apical chambers of the Caco-2 system at concentrations exceeding the parent drugs' equilibrium solubility and monitored the accumulation of **3** and **5** on the basal side of the cell monolayer. Figures 4a and 4b summarize the concentrations of parent compound in the basal receiver

chambers 60 min after apical application of the antagonists **3** and **5** at 62.5 μM (equivalent to their aqueous solubility) as well as the prodrugs **6e** and **8** at concentrations ranging from 100 to 400 μM . In fact, dosing the parent compounds at 62.5 μM or the respective prodrugs at 100 μM led to similar receiver concentrations – in the former case due to antagonist permeating through the cell monolayer, in the latter case as a result of ALP-mediated hydrolysis (*i.e.* conversion of the prodrug to the antagonist) and subsequent permeation. Raising the prodrug doses to 200 μM or 400 μM markedly increased the apparent flux. In the case of **6e**, the receiver concentration of **3** rose proportionally to the amount of applied prodrug and did not display saturation kinetics.^[52] Indeed, in a bi-directional Caco-2 experiments, antagonist **3** displayed a low efflux ratio ($b \rightarrow a/a \rightarrow b = 1.9$, Table 1) suggesting a major contribution of non-saturable, passive diffusion and a minor contribution of saturable, active efflux to the net absorptive flux. By contrast, prodrug **8** dosed at 400 μM induced about tenfold higher receiver concentrations of parent compound **5** than the same prodrug applied at 100 μM . Obviously, the highly concentrated, supersaturated antagonist solution upon dephosphorylation promoted the diffusion through the cell monolayer. Moreover, the high concentrations saturated the strong transporter mediated efflux of compound **5** ($b \rightarrow a/a \rightarrow b = 14$, Table 1).

For prodrug **7b**, similar results were observed even though the parent compound **4** – an efflux transporter substrate as well ($b \rightarrow a/a \rightarrow b = 10$) – is markedly more soluble than the antagonists **3** and **5** (Figure 4c). Overall, these observations predict a significant increase in intestinal uptake of the antagonists **3-5** due to the highly polar phosphate moiety.

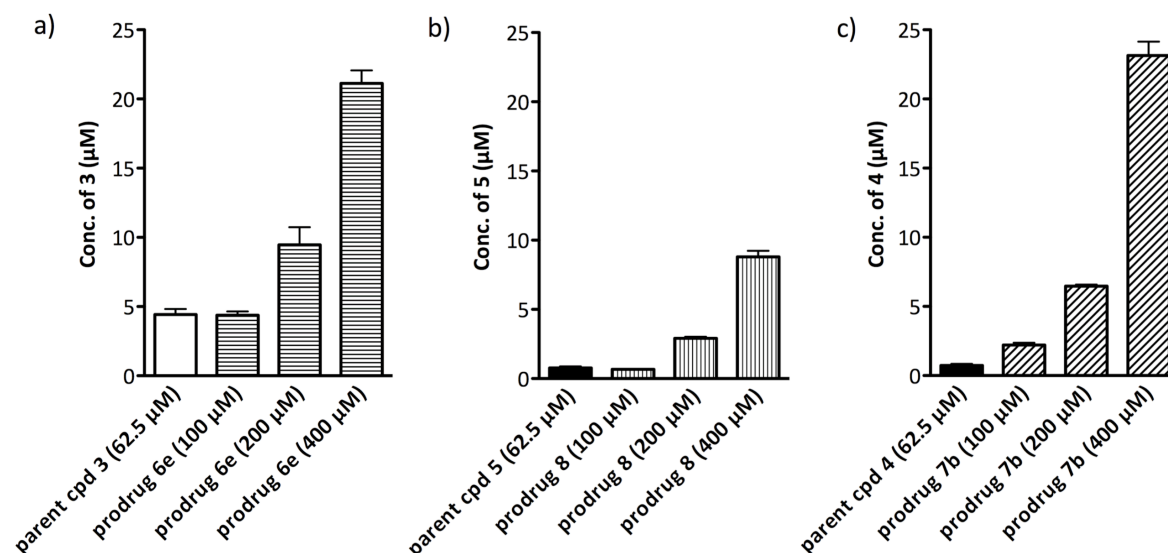


Figure 4. Accumulation of parent compound (a) **3**, (b) **5**, and (c) **4** in the basal receiver chamber of a Caco-2 cell system 60 min after applying (a) parent compound **3** or prodrug **6e**, (b) parent compound **5** or prodrug **8**, and (c) parent compound **4** or prodrug **7b** into the apical chamber. The parent compounds were dosed at a concentration of 62.5 μM , which corresponds to approx. the aqueous solubility of the **3** and **5**, the phosphate prodrugs were dosed at three different concentrations ranging from 100 μM to 400 μM .

In vivo pharmacokinetic studies. Since dissolution, hydrolysis of the phosphate pro moiety, and membrane permeation of the active principle were successfully tested *in vitro*, the prodrugs **7b**, **7c**, and **8** were selected for pharmacokinetic studies in the mouse model. All three compounds were administered per os at a dose of 10 mg/kg. As all prodrugs are highly soluble in aqueous medium ($> 3000 \mu\text{g/ml}$), they were dissolved and dosed in phosphate buffered saline (PBS). The concentrations of prodrug and active principle in plasma and urine were monitored for a period of 24 h (Figure 5). The prodrugs **7b**, **7c**, and **8** could not be detected in any of the plasma and urine samples. The concentrations of **4** and **5** in plasma were close to the detection limit of the used analytical method and are therefore not shown.

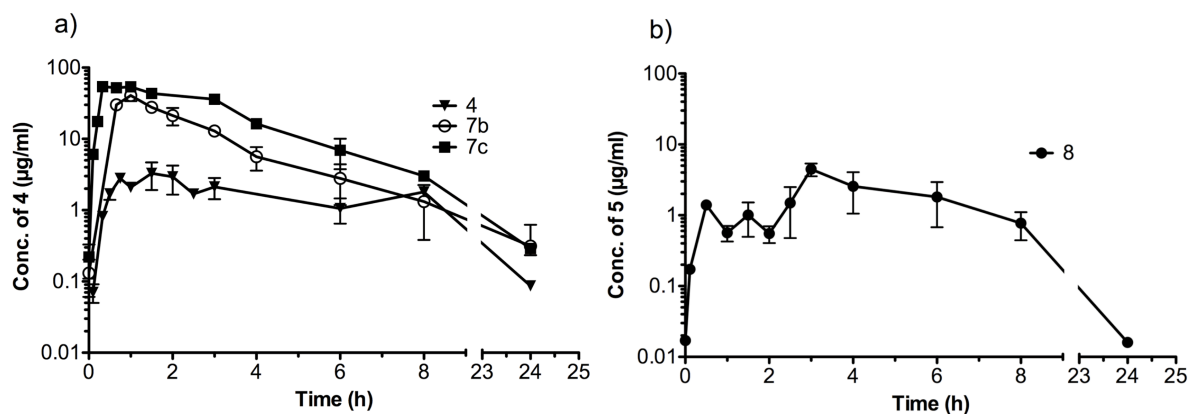


Figure 5. Urine concentration in C3H HeN mice of (a) **4** upon oral administration of **4** and the phosphate prodrugs **7b** and **7c**, (b) **5** upon oral administration of the phosphate prodrug **8**.

Although the prodrugs **7b** and **8** proved similarly prone to ALP-mediated hydrolysis *in vitro* (Table 2), the urine level vs. time profiles summarizing all biopharmaceutical processes upon oral single-dose administration (*i.e.* bioactivation, intestinal uptake, metabolic transformation, and renal excretion) differed significantly. Within the first two hours, the levels of **5** in urine (Figure 5b) rose to concentrations between 0.6 and 1.4 $\mu\text{g/mL}$ and remained at a plateau before rising again to reach maximum concentration (C_{max} , 4.5 $\mu\text{g/mL}$) 3 h post administration. Then, they dropped steadily until the end of the observation period. The overall amount of compound appearing in urine was approximately 5 % of the given dose. By contrast, urine levels of **4** after the administration of **7b** peaked 1 h post administration (40.5 $\mu\text{g/mL}$) and around 80 % of the orally applied dose appeared in the urine. Given the almost identical propensity to ALP-mediated hydrolysis and similarly high solubility of the prodrugs **7b** and **8**, the observed differences are rather a consequence of varying physicochemical properties of the parent compounds **4** and **5**. Indeed, antagonist **5** is supposed to permeate biological membranes less easily and to be a stronger substrate of efflux transporters than antagonist **4** (Table 1). Moreover, **5** is markedly less soluble in aqueous media. It therefore risks precipitating from the supersaturated solution in the intestine upon ALP-mediated dephosphorylation.

Both prodrugs **7b** and **8** being rapidly hydrolysed *in vitro*, we assessed in a further experiment the impact of slower ALP-mediated bioactivation on parent compound availability in urine. Indeed, we hypothesized that a slower conversion prolongs intestinal uptake and compound excretion into urine. This would be an advantage for UTI treatment, as the dosing interval and the therapeutic effects might be prolonged. For this purpose, we administered prodrug **7c** showing *in vitro* $t_{1/2}$ of 43 min (Table 2). Figure 5a compares the urine concentration profiles of parent compound **4** upon oral single dose administration of the prodrugs **7b** and **7c** (10 mg/kg), and upon oral administration of the parent compound itself (1.25 mg/kg).

After applying **7c**, compound **4** reached C_{max} (54 $\mu\text{g/mL}$) after only 20 min – compared to 40.5 $\mu\text{g/mL}$ after one hour for **7b** – and remained at a high level for the next 3 h. Within the observation period of 3-24 h, the compound levels upon administration of the two prodrugs dropped steadily; however, the concentrations in the experiment with prodrug **7c** were about three times higher than those reached with **7b**. As a consequence, the amount of compound appearing in urine corresponds to approx. 95% of the administered dose of **7c**, which suggests a higher absorption rate than the one of **7b**.

Against our expectations, T_{\max} (time when C_{\max} is observed) of **4** from **7c** did not occur markedly later than T_{\max} of **4** from **7b**. The observed difference in *in vitro* $t_{1/2}$ (approx. 30 min, see Table 2) was not sufficient to provoke a clear shift. Even slower ALP-mediated bioactivation would probably be required for a significant effect. Nonetheless, the higher and more constant levels of **4** after application of **7c** are advantageous for UTI treatment.

Overall, **7c** increased C_{\max} of the parent compound in urine by a factor of 16 compared to the application of the parent compound **4** itself (from 3.3 $\mu\text{g/ml}$ at 1.5h to 54 $\mu\text{g/ml}$ at 20 min). The elimination slopes of all three curves in Figure 6 parallel nicely, reflecting the intrinsic pharmacokinetic properties of the parent compound. Nevertheless, the increase in solubility using a phosphate prodrug led to a saturation of efflux-transporter in the intestine and increased the cumulative amount of parent compound appearing in the urine, which is the compartment of action. Bioavailability is exceptionally high and marks a milestone in the development of orally available FimH antagonists.

Summary and Conclusions

The phosphate prodrug approach applied to previously published FimH antagonists with low solubility led to improved *in vivo* pharmacokinetics. We analyzed the properties of the phosphate promoiety in different positions of the mannose ring. When the phosphate ester bond was directly linked to position C2 and C3 (\rightarrow **6a**, **6b**, **7a**, **7b**) of the mannose moiety or when an acetal linker at position 6 was used (\rightarrow **6e** & **8**) enzymatic cleavage was fast ($t_{1/2} < 15$ min). In contrast, a phosphate in the 4 or 6-position (\rightarrow **7c** & **7d**) showed an improved stability ($t_{1/2} > 40$ min). *In vivo* administration of prodrug **7c** exhibited an increased C_{\max} compared to a phosphate prodrug with a fast cleavage (**7b**, $t_{1/2} < 15$ min). A possible reason is related to a slower conversion to the active principle, prolonging intestinal uptake and renal excretion. Nevertheless, the observed difference of the *in vitro* $t_{1/2}$ was not sufficient to provoke a clear shift of the PK curve. Moreover, different physicochemical properties (solubility and permeability) of the active principle influence the *in vivo* PK curves. For antagonist **5** with an 8-fold lower solubility compared to **4**, the risk of precipitation from the supersaturated solution in the small intestines has to be considered. With a slower cleavage of the phosphate prodrug the oral uptake of FimH antagonist **5** could be improved. Furthermore, a high concentration gradient across the Caco-2 cell monolayer promotes the absorptive flux and apparently saturates the efflux carrier activity of **6e**, **8**, and **7b**. This observation was confirmed in the *in vivo* PK study in a mouse, where urine levels (C_{\max}) of the active

principle **4** were 16 times higher when the phosphate prodrug **7c** was administered instead of the active principle **4**. However, therapeutic dose of **4** was restricted by its low solubility and could only be applied at a dose of 1.25 mg/kg. The introduction of the polar phosphate moiety leads to a sufficient solubility for a therapeutic dose of 10 mg/kg. Availability in urine of more than 80% of the administered dose illustrates the high potential of phosphate prodrugs for optimizing the pharmacokinetic profile of low soluble FimH antagonists.

Experimental Section

Synthesis

General Methods. NMR spectra were recorded on a Bruker Avance DMX-500 (500.1 MHz) spectrometer. Assignment of ^1H and ^{13}C NMR spectra was achieved using 2D methods (COSY, HSQC). Chemical shifts are expressed in ppm using residual CHCl_3 or MeOH as references. Optical rotations were measured with a PerkinElmer Polarimeter 341. Electrospray ionization mass spectrometry (ESI-MS) data were obtained on a Waters Micromass ZQ instrument. Microwave-assisted reactions were carried out with a CEM Discover and Explorer. Reactions were monitored by TLC using glass plates coated with silica gel 60 F254 (Merck) and visualized by UV light and/or by charring with a molybdate solution (0.02 M solution of ammonium cerium sulfate dihydrate and ammonium molybdate tetrahydrate in aqueous 10% H_2SO_4). Medium pressure chromatography (MPLC) separations were carried out on a CombiFlash Companion or R_f from Teledyne Isco equipped with RediSep normal-phase or RP-18 reversed-phase flash columns. Commercially available reagents were purchased from Fluka, Aldrich, or Alfa Aesar (Germany). Solvents were purchased from Sigma–Aldrich (Buchs, Switzerland) or Acros Organics (Geel, Belgium) and were dried prior to use where indicated. MeOH was dried by reflux with sodium methoxide and distilled and stored under argon atmosphere. DCM and MeCN were dried by filtration over Al_2O_3 (Fluka, type 5016 A basic) and stored over molecular sieves under argon. Molecular sieves (4 Å) were activated *in vacuo* at 300°C for 0.5 h before use.

General procedure for phosphorylation. To an ice-cooled solution (0 °C) of protected mannoside (1 eq) and 1,2,4-triazole (4 eq) in dry MeCN was added dibenzyl *N,N*-diisopropylphosphoramidite or bis[2-(trimethylsilyl)ethyl] *N,N*-diisopropylphosphoramidite (2 eq) and the mixture was stirred for 30 min at 0 °C and then overnight at rt. Then, 70% aq. *tert*-butylhydroperoxid (4 eq) was added and the solution was stirred for 1 h. The reaction was quenched with 1 M aq. $\text{Na}_2\text{S}_2\text{O}_3$ and 1 M aq. NaHCO_3 and the mixture was extracted twice with DCM. The combined organic layers were dried over Na_2SO_4 , filtered and the solvents removed *in vacuo*. The residue was purified by MPLC on silica gel (petroleum ether/EtOAc) to yield the phosphorylated compounds.

Biphenyl 4,6-*O*-benzylidene- α -D-mannopyranoside (9). To a mixture of biphenyl α -D-mannopyranoside (**1**)^[14,18] (1.16 g, 3.51 mmol) and benzaldehyde dimethyl acetal (1.58 mL, 10.5 mmol) in dry MeCN/DMF (10 mL/1 mL) was added *p*-toluenesulfonic acid (40 mg). The reaction mixture was stirred at 80 °C overnight and then neutralized with satd. aq. NaHCO₃. Then the mixture was diluted with DCM (20 mL) and washed with water (2 × 10 mL) and brine (10 mL). The organic layer was dried over Na₂SO₄ and concentrated. The residue was purified by MPLC on silica (DCM/MeOH, 20:1-9:1) to afford **9** (1.03 g, 70%) as a white solid. $[\alpha]_{\text{D}}^{20} +163.1$ (*c* 1.09, CHCl₃/MeOH, 1:1); ¹H NMR (CDCl₃, 500 MHz): δ = 3.83 (t, *J* = 10.0 Hz, 1H, H-6a), 3.99 (td, *J* = 4.5, 9.5 Hz, 1H, H-5), 4.04 (t, *J* = 9.5 Hz, 1H, H-4), 4.22 (dd, *J* = 5.0, 10.0 Hz, 1H, H-6b), 4.28 (m, 1H, H-2), 4.33 (dd, *J* = 3.5, 9.5 Hz, 1H, H-3), 5.60 (s, 1H, PhCH), 5.66 (s, 1H, H-1), 7.13 (m, 2H, Ar-H), 7.31-7.50 (m, 8H, Ar-H), 7.55 (m, 4H, Ar-H); ¹³C NMR (CDCl₃, 126 MHz): δ = 63.8 (C-5), 68.6 (C-3), 68.7 (C-6), 70.9 (C-2), 78.7 (C-4), 98.1 (C-1), 102.3 (PhCH), 116.6, 126.3, 126.8, 127.0, 128.3, 128.4, 128.8, 129.0, 129.3, 129.7, 134.5, 135.7, 137.1, 140.5, 155.4 (18C, Ar-C); ESI-MS: *m/z*: Calcd for C₂₅H₂₄NaO₆ [M+Na]⁺: 443.15, found: 443.12.

Biphenyl 3-*O*-benzyl-4,6-*O*-benzylidene- α -D-mannopyranoside (10). A suspension of **9** (380 mg, 0.900 mmol) and dibutyl tin oxide (247 mg, 0.990 mmol) in dry toluene (6 mL) was refluxed at 135 °C for 3 h. The mixture was concentrated to dryness and tetrabutylammonium bromide (320 mg, 0.990 mmol) and benzyl bromide (0.13 mL, 1.08 mmol) in dry toluene (6 mL) were added. The reaction mixture was stirred at 115 °C overnight, the solvent was removed under reduced pressure and the residue was purified by MPLC on silica (petroleum ether/EtOAc, 6:1-4:1) to give **10** (370 mg, 80%) as a white solid. $[\alpha]_{\text{D}}^{20} +139.6$ (*c* 2.66, CHCl₃); ¹H NMR (CDCl₃, 500 MHz): δ = 3.87 (t, *J* = 10.5 Hz, 1H, H-6a), 4.01 (td, *J* = 5.0, 10.0 Hz, 1H, H-5), 4.17 (dd, *J* = 3.0, 9.5 Hz, 1H, H-3), 4.20-4.26 (m, 2H, H-6b, H-4), 4.31 (dd, *J* = 1.5, 3.0 Hz, 1H, H-2), 4.82 (d, *J* = 12.0 Hz, 1H, OCH₂Ph), 4.97 (d, *J* = 12.0 Hz, 1H, OCH₂Ph), 5.66 (s, 1H, PhCH), 5.69 (d, *J* = 1.0 Hz, 1H, H-1), 7.13 (m, 2H, Ar-H), 7.37-7.46 (m, 10H, Ar-H), 7.51-7.58 (m, 7H, Ar-H); ¹³C NMR (CDCl₃, 126 MHz): δ = 64.0 (C-5), 68.7 (C-6), 70.0 (C-2), 73.3 (OCH₂Ph), 75.4 (C-3), 78.7 (C-4), 97.9 (C-1), 101.7 (PhCH), 116.7, 126.1, 126.8, 127.8, 127.0, 127.8, 128.0, 128.2, 128.3, 128.5, 128.7, 128.8, 128.9, 129.0, 129.7, 134.5, 135.7, 137.4, 137.9, 140.5, 155.3 (24C, Ar-C); ESI-MS: *m/z*: Calcd for C₃₂H₃₀NaO₆ [M+Na]⁺: 533.19, found: 533.17.

Biphenyl 2-*O*-dibenzylphosphoryl-3-*O*-benzyl-4,6-*O*-benzylidene- α -D-mannopyranoside (11). According to the general procedure, compound **10** (194 mg, 0.250 mmol) was reacted with 1,2,4-triazole (69.5 mg, 1.00 mmol) and dibenzyl *N,N*-diisopropylphosphoramidite (90%, 187 μ L, 0.500 mmol) in MeCN (3.0 mL), followed by treatment with 70% aq. *tert*-butylhydroperoxide (150 μ L) to yield **11** (120 mg, 62%) as a white solid. $[\alpha]_{\text{D}}^{20} +55.3$ (*c* 0.38, DCM); ¹H NMR (CDCl₃, 500 MHz): δ = 3.81 (t, *J* = 10.5 Hz, 1H, H-6a), 3.99 (td, *J* = 5.0, 10.0 Hz, 1H, H-5), 4.11 (t, *J* = 10.0 Hz, 1H, H-4),

4.22 (m, 2H, H-3, H-6b), 4.85 (m, 2H, OCH₂Ph), 5.30 (m, 1H, H-2), 5.08-5.12 (m, 4H, OCH₂Ph), 5.62 (m, 2H, H-1, PhCH), 7.03 (m, 2H, Ar-H), 7.26-7.58 (m, 27H, Ar-H); ¹³C NMR (CDCl₃, 126 MHz): δ = 64.6 (C-5), 68.5 (C-6), 69.5 (d, J = 6 Hz, OCH₂Ph), 69.6 (d, J = 6 Hz, OCH₂Ph), 72.8 (OCH₂Ph), 73.9 (d, J = 5 Hz, C-3), 74.6 (d, J = 6 Hz, C-2), 78.2 (C-4), 97.2 (d, J = 3 Hz, C-1), 101.6 (PhCH), 116.8, 126.0, 126.8, 126.9, 127.0, 127.6, 127.7, 127.74, 127.85, 127.92, 128.19, 128.22, 128.3, 128.45, 128.52, 128.6, 128.7, 128.9, 135.66, 135.71, 135.76, 135.8, 135.9, 137.4, 137.5, 138.0, 140.5, 155.0 (36C, Ar-C); ESI-MS: m/z : Calcd for C₄₆H₄₄O₉P [M+H]⁺: 771.27, found: 771.37.

Biphenyl 2-*O*-phosphoryl- α -D-mannopyranoside diammonium salt (6a). Hydrogenolysis of compound **11** (100 mg, 0.129 mmol) was conducted in a Parr shaker with 10% Pd(OH)₂/C (12 mg) and a catalytic amount of HOAc in EtOAc (6.0 mL) under hydrogen (4 bar) at rt overnight. Then, the reaction suspension was filtered through celite and the filtrate was concentrated *in vacuo*. The residue was stirred in 25% aq. NH₃ (4 mL) and MeOH (1 mL) overnight. Then, the solvents were removed under reduced pressure and the residue was purified by MPLC on silica (DCM/MeOH/H₂O, 6:4:0.6) to give **6a** (26.0 mg, 45%) as a white solid. $[\alpha]_D^{20}$ +66.7 (c 0.12, H₂O); ¹H NMR (D₂O, 500 MHz): δ = 3.77-3.82 (m, 3H, H-5, H-6), 3.87 (t, J = 10.0 Hz, 1H, H-4), 4.14 (ddd, J = 2.0, 3.0, 10.0 Hz, 1H, H-3), 4.62 (ddd, J = 2.0, 3.0, 8.5 Hz, 1H, H-2), 5.89 (d, J = 1.5 Hz, 1H, H-1), 7.31 (m, 2H, Ar-H), 7.44 (m, 1H, Ar-H), 7.55 (t, J = 7.5 Hz, 2H, Ar-H), 7.71 (m, 4H, Ar-H); ¹³C NMR (D₂O, 126 MHz): δ = 60.5 (C-6), 66.6 (C-4), 70.1 (d, J = 5 Hz, C-3), 73.5 (C-5), 73.6 (d, J = 5 Hz, C-2), 97.0 (d, J = 3 Hz, C-1), 117.2, 117.6, 126.7, 127.4, 128.0, 128.2, 129.1, 135.3, 140.0, 155.0 (12C, Ar-C); ESI-MS: m/z : Calcd for C₁₈H₂₀O₉P [M-2NH₄+H]⁻: 411.08, found: 411.06.

4'-(4,6-*O*-Benzylidene- α -D-mannopyranosyloxy)-3'-chloro-biphenyl-4-carbonitrile (12). To a solution of **4**^[37] (500 mg, 1.28 mmol) in anhydrous DMF (20 mL) were added benzaldehyde dimethyl acetal (575 μ L, 3.83 mmol) and *p*-toluenesulfonic acid (20 mg). The mixture was stirred at 50 °C overnight. Then, the reaction mixture was neutralized with satd. aq. NaHCO₃ (10 mL), diluted with DCM (30 mL), and washed with water (3 \times 10 mL) and brine (10 mL). The organic layer was dried over Na₂SO₄, filtered and the solvents removed *in vacuo*. The residue was purified by MPLC on silica (DCM/MeOH, 1:0-5:1, +0.5% NEt₃) to yield **12** (132 mg, 22%). $[\alpha]_D^{20}$ +62.3 (c 0.59, CHCl₃/MeOH, 1:1); ¹H NMR (500 MHz, CDCl₃): δ = 3.76 (t, J = 10.2 Hz, 1H, H-6a), 3.91 (td, J = 4.8, 9.8 Hz, 1H, H-5), 3.99 (t, J = 9.4 Hz, 1H, H-4), 4.14 (dd, J = 4.8, 10.3 Hz, 1H, H-6a), 4.28-4.33 (m, 2H, H-2, H-3), 5.53 (s, 1H, PhCH), 5.62 (s, 1H, H-1), 7.19 (m, 1H, Ar-H), 7.29-7.31 (m, 3H, Ar-H), 7.38 (m, 1H, Ar-H), 7.40-7.44 (m, 2H, Ar-H), 7.54-7.58 (m, 3H, Ar-H), 7.63-7.67 (m, 2H, Ar-H); ¹³C NMR (126 MHz, CDCl₃): δ = 64.2 (C-5), 68.5, 70.6 (3C, C-2, C-3, C-6), 78.4 (C-4), 98.7 (C-1), 102.4 (PhCH), 111.2, 116.8, 118.7, 124.6, 126.2, 126.6, 127.4, 128.4, 132.5, 143.7, 151.8 (19 C, 18 Ar-C, CN); ESI-MS: m/z : Calcd for C₃₃H₂₆ClNNaO₇ [M+Na]⁺: 502.90, found: 502.04.

4'-(3-*O*-Benzoyl-4,6-*O*-benzylidene- α -D-mannopyranosyloxy)-3'-chloro-biphenyl-4-carbonitrile

(13). To a solution of **12** (131 mg, 0.275 μmol) in DCM/pyridine (6 mL, 5:1) was added dropwise over 30 min a 0.1 M benzoyl chloride solution in dry DCM (2.8 mL, 0.280 mmol) at 0 °C under argon. The mixture was stirred another 30 min at 0 °C, then the ice-bath was removed and stirring continued for 2 h at rt. Then, the mixture was diluted with DCM (10 mL) and washed with 0.1 M aq. HCl (5 mL) and satd. aq. NaHCO₃ (10 mL). The organic layer was dried with Na₂SO₄, filtered and concentrated. The residue was purified by MPLC on silica (petroleum ether/EtOAc, +0.5% NEt₃) to yield **13** (96.8 mg, 60%). $[\alpha]_{\text{D}}^{20} +113.8$ (*c* 1.02, DCM); ¹H NMR (500 MHz, CDCl₃): δ = 3.91 (t, *J* = 10.2 Hz, 1H, H-6a), 4.17 (td, *J* = 4.9, 9.7 Hz, 1H, H-5), 4.24 (dd, *J* = 4.8, 10.2 Hz, 1H, H-6b), 4.45 (t, *J* = 9.9 Hz, 1H, H-4), 4.65 (dd, *J* = 1.6, 3.2 Hz, 1H, H-2), 5.64 (s, 1H, PhCH), 5.70 (d, *J* = 1.2 Hz, 1H, H-1), 7.25-7.34 (m, 4H, Ar-H), 7.37-7.47 (m, 5H, Ar-H), 7.51-7.60 (m, 4H, Ar-H), 7.51-7.60 (m, 2H, Ar-H), 8.06-8.11 (m, 2H, Ar-H); ¹³C NMR (126 MHz, CDCl₃): δ = 65.1 (C-5), 68.4 (C-6), 69.1 (C-2), 71.2 (C-3), 75.6 (C-4), 99.1 (C-1), 101.8 (PhCH), 110.8, 116.9, 118.6, 124.8, 126.0, 126.3, 127.2, 128.1, 128.3, 132.6, 133.2, 136.9, 143.5, 151.6 (25C, 24 Ar-C, CN), 165.7 (CO); IR (KBr): ν = 3437 (vs, OH), 2227 (m, CN), 1721 (vs, C=O) cm⁻¹; ESI-MS: *m/z*: Calcd for C₃₃H₂₆ClNNaO₇ [M+Na]⁺: 606.13, found: 606.11.

4'-(3-O-Benzoyl-4,6-O-benzylidene-2-O-bis[2-(trimethylsilyl)ethoxy]phosphoryl- α -D-mannopyranosyloxy)-3'-chloro-biphenyl-4-carbonitrile (14). According to the general procedure, compound **13** (96.8 mg, 0.166 mmol) was reacted with 1,2,4-triazole (45.8 mg, 0.663 mmol) and bis[2-(trimethylsilyl)ethyl] *N,N*-diisopropylphosphoramidite (136 μL , 0.331 mmol) in MeCN (3.0 mL), followed by treatment with 70% aq. *tert*-butylhydroperoxide (91 μL , 0.663 mmol) to yield **14** (79.6 mg, 55%) as a 4:1-mixture of 2- and 3-phosphorylated isomers. ¹H NMR (500 MHz, CDCl₃): δ = -0.09, -0.02 (2s, 18H, 2 Si(CH₃)₃), 0.92-01.06 (m, 4H, 2 SiCH₂), 3.87 (td, *J* = 4.5, 10.1 Hz, 1H, H-6a), 4.12 (m, 6H, H-5, H-6b, 2 OCH₂), 4.36 (t, *J* = 9.9 Hz, 1H, H-4), 5.17 (ddd, *J* = 1.7, 3.1, 9.1 Hz, 1H, H-2), 5.63 (s, 1H, PhCH), 5.81 (m, 1H, H-3), 5.84 (d, *J* = 1.5 Hz, 1H, H-1), 7.22-7.33 (m, 4H, Ar-H), 7.37-7.45 (m, 4H, Ar-H), 7.46-7.56 (m, 2H, Ar-H), 7.57-7.64 (m, 3H, Ar-H), 7.66-7.71 (m, 2H, Ar-H), 8.08-8.14 (m, 2H, Ar-H); ¹³C NMR (126 MHz, CDCl₃): δ = -1.7, -1.6 (6C, Si(CH₃)₃), 19.4 (d, *J* = 5 Hz, 2C, 2 SiCH₂), 65.2 (C-5), 66.9 (t, *J* = 6 Hz, 2C, 2 OCH₂), 68.4 (C-6), 69.1 (d, *J* = 5 Hz, C-3), 73.2 (d, *J* = 5 Hz, C-2), 75.4 (C-4), 97.8 (d, *J* = 2 Hz, C-1), 101.9 (PhCH), 111.1, 117.1, 118.6, 125.0, 126.2, 126.4, 127.3, 128.2, 128.3, 128.6, 129.0, 129.7, 129.9, 130.0, 132.6, 133.2, 134.9, 136.8, 143.5, 151.5 (25C, 24 Ar-C, CN), 165.6 (CO); ESI-MS: *m/z*: Calcd for C₄₉H₆₇ClN₂O₁₀PSi₂ [M+NEt₃+H]⁺: 965.38, found: 965.53.

4'-(3-O-Benzoyl-2-O-phosphoryl- α -D-mannopyranosyloxy)-3'-chloro-biphenyl-4-carbonitrile disodium salt (15). A solution of **14** (79.6 mg, 0.275 mmol) in dry DCM (1.5 mL) was treated with TFA (150 μL) for 1 h at rt under argon. Then, a drop of water was added and stirring continued for 30 min. The solvents were removed *in vacuo*, the residue was dissolved in H₂O (1 mL) containing a drop of 1 M aq. NaOH and purified by MPLC on RP-18 (H₂O/MeOH, 95:5-4:1) to yield **15** (34.7 mg,

61%) as a 4:1-mixture of 2- and 3-phosphate. ^1H NMR (500 MHz, CD_3OD): δ = 3.78-3.90 (m, 3H, H-5, H-6), 4.20 (t, J = 9.9 Hz, 1H, H-4), 5.01 (ddd, J = 2.0, 3.1, 9.4 Hz, 1H, H-2), 5.60-5.65 (td, J = 2.6, 10.1 Hz, 1H, H-3), 5.91 (d, J = 1.6 Hz, 1H, H-1), 7.45-7.53 (m, 3H, Ar-H), 7.57-7.65 (m, 2H, Ar-H), 7.75-7.81 (m, 5H, Ar-H), 8.15-8.18 (m, 2H, Ar-H); ^{13}C NMR (126 MHz, CD_3OD): δ = 62.2 (C-6), 65.3 (C-4), 73.9 (dd, J = 5.8 Hz, 2C, C-2, C-3), 76.3 (C-5), 98.8 (d, J = 2 Hz, C-1), 112.0, 118.8, 119.7, 125.8, 127.9, 131.0, 133.9, 136.0, 145.0, 153.2 (19C, 18 Ar-C, CN), 167.8 (CO); ESI-MS: m/z : Calcd for $\text{C}_{26}\text{H}_{22}\text{ClNO}_{10}\text{P}$ [M-2Na+H] $^-$: 574.07, found: 574.21.

3'-Chloro-4'-(2-*O*-phosphoryl- α -D-mannopyranosyloxy)-biphenyl-4-carbonitrile disodium salt (7a). Compound **15** (34.7 mg, 56.0 μmol) was dissolved in MeOH (0.25 mL) and 25% aq. NH_3 (1 mL). The mixture was stirred for 16 h at rt. The solvents were removed *in vacuo*, the residue was dissolved in H_2O (0.5 mL) containing a drop of 1 M aq. NaOH and purified by MPLC on RP-18 ($\text{H}_2\text{O}/\text{MeOH}$) to yield pure 2-phosphate **7a** (20.4 mg, 71%) as the sodium salt. $[\alpha]_{\text{D}}^{20}$ +17.9 (c 0.78, H_2O); ^1H NMR (500 MHz, D_2O): δ = 3.70-3.82 (m, 3H, H-5, H-6), 3.92 (t, J = 9.8 Hz, 1H, H-4), 4.13 (dd, J = 3.0, 9.7 Hz, 1H, H-3), 4.66 (dt, J = 2.4, 8.3 Hz, 1H, H-2), 5.97 (d, J = 1.2 Hz, 1H, H-1), 7.40 (d, J = 8.7 Hz, 1H, Ar-H), 7.45-7.53 (m, 4H, Ar-H), 7.66 (d, J = 8.4 Hz, 2H, Ar-H); ^{13}C NMR (126 MHz, D_2O): δ = 62.0 (C-6), 68.6 (C-4), 72.3 (d, J = 3 Hz, C-3), 73.8 (d, J = 4 Hz, C-2), 99.2 (d, J = 5 Hz, C-1), 111.0, 118.9, 121.2, 125.5, 128.2, 128.4, 130.1, 134.4, 135.4, 144.7, 152.5 (13C, 12 Ar-C, CN); IR (KBr): ν = 3436 (vs, OH), 2230 (w, CN) cm^{-1} ; ESI-MS: m/z : Calcd for $\text{C}_{19}\text{H}_{18}\text{ClNO}_9\text{P}$ [M-2Na+H] $^-$: 470.04, found: 469.96.

4-(5-Nitroindolin-1-yl)phenyl

2,3,4-tri-*O*-benzoyl-6-*O*-(*tert*-butylsilyldimethyl)- α -D-mannopyranoside (16).

To a solution of **5**^[19] (709 mg, 1.69 mmol) in pyridine were added *tert*-butyldimethylsilyl chloride (319 mg, 2.12 mmol) and DMAP (20.6 mg) and the mixture was stirred at rt overnight. Then, a solution of benzoyl chloride (0.98 mL, 8.45 mmol) in pyridine (2.0 mL) was added and the mixture was stirred at rt for 2 h. The mixture was diluted with DCM (30 mL) and subsequently washed with 0.1 M aq. HCl (10 mL) and satd. aq. NaHCO_3 (10 mL). The organic layer was dried over Na_2SO_4 , filtered and the solvent removed *in vacuo*. The residue was purified by MPLC on silica (petroleum ether/EtOAc, 9:1-7:3) to yield crude **16** (1.43 g, quant.) as a yellow solid, which was used in the next step without further purification. ^1H NMR (CDCl_3 , 500 MHz): δ = -0.01 (s, 3H, $\text{Si}(\text{CH}_3)_2$), 0.00 (s, 3H, $\text{Si}(\text{CH}_3)_2$), 0.87 (s, 9H, $\text{C}(\text{CH}_3)_3$), 3.22 (t, J = 8.5 Hz, 2H, CH_2), 3.83 (dd, J = 2.3, 11.5 Hz, 1H, H-6a), 3.88 (dd, J = 4.7, 11.5 Hz, 1H, H-6b), 4.10 (t, J = 8.7 Hz, 2H, NCH_2), 4.43 (m, 1H, H-5), 5.77 (d, J = 1.8 Hz, 1H, H-1), 5.87 (m, 1H, H-2), 6.03-6.15 (m, 2H, H-3, H-4), 6.77 (d, J = 8.9 Hz, 1H, Ar-H), 7.22-7.31 (m, 6H, Ar-H), 7.38 (t, J = 7.8 Hz, 2H, Ar-H), 7.41-7.55 (m, 5H, Ar-H), 7.60-7.67 (m, 1H, Ar-H), 7.88 (dd, J = 1.2, 8.3 Hz, 2H, Ar-H), 7.94-8.01 (m, 3H, Ar-H), 8.03 (dd, J = 2.3, 8.9 Hz, 1H, Ar-H), 8.14 (dd, J = 1.2, 8.3 Hz, 1H, Ar-H); ^{13}C NMR (CDCl_3 , 126 MHz): δ = -5.51, -5.50 ($\text{Si}(\text{CH}_3)_2$), 25.8 (3C, $\text{C}(\text{CH}_3)_3$), 27.1 (CH_2), 53.7 (NCH_2), 62.1 (C-6), 66.6 (C-3), 70.3, 70.4 (C-2, C-4), 72.3 (C-5), 96.4 (C-1), 105.3, 118.0, 121.1, 122.0, 126.1, 128.3, 128.4, 128.43,

128.6, 129.1, 129.2, 129.3, 129.7, 129.8, 130.0, 131.0, 133.2, 133.3, 133.6, 136.8, 139.1, 152.8, 153.8 (30C, Ar-C), 165.3, 165.6, 165.7 (3 CO); ESI-MS: m/z : Calcd for $C_{47}H_{48}N_2NaO_{11}Si$ $[M+Na]^+$: 867.29, found: 867.25.

4-(5-Nitroindolin-1-yl)phenyl 2,3,4-tri-*O*-benzoyl- α -D-mannopyranoside (17). A solution of **16** (1.43 g, 1.69 mmol) in DCM/MeOH (16 mL, 1:1) was treated with 1 M H_2SO_4 in MeOH (1.6 mL) for 1.5 h at rt. The reaction mixture was neutralized with NEt_3 and the solvents were removed *in vacuo*. The residue was purified by MPLC on silica (petroleum ether/EtOAc, 3:1-3:2) to yield **17** (900 mg, 73%). 1H NMR ($CDCl_3$, 500 MHz): δ = 3.22 (t, J = 8.6 Hz, 2H, CH_2), 3.77 (dd, J = 3.3, 13.0 Hz, 1H, H-6a), 3.84 (dd, J = 1.8, 13.0 Hz, 1H, H-6b), 4.11 (t, J = 9.4 Hz, 2H, NCH_2), 4.20 (m, 1H, H-5), 5.83 (d, J = 1.6 Hz, 1H, H-1), 5.88 (dd, J = 1.9, 3.3 Hz, 1H, H-2), 5.96 (t, J = 10.1 Hz, 1H, H-4), 6.22 (dd, J = 3.4, 10.2 Hz, 1H, H-3), 6.78 (d, J = 8.9 Hz, 1H, Ar-H), 7.21-7.34 (m, 6H, Ar-H), 7.37-7.43 (m, 3H, Ar-H), 7.45 (t, J = 7.4 Hz, 1H, Ar-H), 7.50-7.57 (m, 3H, Ar-H), 7.65 (t, J = 7.5 Hz, 1H, Ar-H), 7.84-7.89 (m, 2H, Ar-H), 7.97-8.02 (m, 3H, Ar-H), 8.04 (dd, J = 2.3, 8.9 Hz, 1H, Ar-H), 8.12-8.16 (m, 2H, Ar-H); ^{13}C NMR ($CDCl_3$, 126 MHz): δ = 27.1 (CH_2), 53.7 (NCH_2), 61.1 (C-6), 67.0 (C-4), 69.3 (C-3), 70.4 (C-2), 71.8 (C-5), 96.4 (C-1), 105.4, 117.6, 121.1, 122.0, 126.1, 127.0, 128.3, 128.4, 128.5, 128.6, 128.7, 129.0, 129.03, 129.5, 129.7, 129.9, 130.0, 131.1, 133.4, 133.77, 133.8, 137.0, 139.2, 152.5, 153.6 (30C, Ar-C), 165.5, 165.6, 166.6 (3 CO); ESI-MS: m/z : Calcd for $C_{41}H_{34}N_2NaO_{11}$ $[M+Na]^+$: 753.21, found: 753.33.

4-(5-Nitroindolin-1-yl)phenyl 2,3,4-tri-*O*-benzoyl-6-*O*-(methylthio)methyl α -D-mannopyranoside (18). Degassed DMSO (2.5 mL) was added to a degassed mixture of **27** (200 mg, 0.273 mmol) in Ac_2O (1.65 mL) and HOAc (0.5 mL). The mixture was stirred at rt overnight, then diluted with EtOAc (20 mL), and subsequently washed with satd. aq. $NaHCO_3$ (2×10 mL), H_2O (2×10 mL) and brine (10 mL). The organic layer was dried over Na_2SO_4 and concentrated. The residue was purified by MPLC on silica (petroleum ether/EtOAc, 3:1-7:3) to yield **18** (160 mg, 74%). 1H NMR ($CDCl_3$, 500 MHz): δ = 2.08 (s, 3H, CH_3), 3.23 (t, J = 8.6 Hz, 2H, CH_2), 3.72 (dd, J = 2.4, 11.1 Hz, 1H, H-6a), 3.89 (dd, J = 4.5, 11.2 Hz, 1H, H-6b), 4.12 (m, 2H, NCH_2), 4.43 (m, 1H, H-5), 4.61, 4.72 (A, B of ABX, J = 11.6 Hz, 2H, CH_2), 5.79 (d, J = 1.6 Hz, 1H, H-1), 5.86 (m, 1H, H-2), 6.03-6.11 (m, 2H, H-3, H-4), 6.78 (d, J = 8.9 Hz, 1H, Ar-H), 7.22-7.33 (m, 7H, Ar-H), 7.36-7.42 (m, 2H, Ar-H), 7.46 (t, J = 7.4 Hz, 1H, Ar-H), 7.48-7.56 (m, 3H, Ar-H), 7.64 (t, J = 7.5 Hz, 1H, Ar-H), 7.85-7.91 (m, 2H, Ar-H), 7.96-8.01 (m, 3H, Ar-H), 8.04 (dd, J = 2.2, 8.8 Hz, 1H, Ar-H), 8.10-8.17 (m, 2H, Ar-H); ^{13}C NMR ($CDCl_3$, 126 MHz): δ = 13.9 (CH_3), 27.1 (CH_2), 53.7 (NCH_2), 66.3 (C-6), 67.8 (C-4), 70.1 (C-3), 70.4 (C-2), 71.7 (C-5), 75.9 (CH_2), 96.5 (C-1), 105.4, 117.9, 121.1, 122.0, 126.1, 128.4, 128.5, 128.7, 129.0, 129.2, 129.7, 129.8, 131.0, 131.1, 133.3, 133.4, 133.7, 137.0, 139.2, 152.7, 153.7 (30C, Ar-C), 165.5, 165.60, 165.62 (3 CO); ESI-MS: m/z : Calcd for $C_{43}H_{38}N_2NaO_{11}S$ $[M+Na]^+$: 813.21, found: 813.32.

4-(5-Nitroindolin-1-yl)phenyl 2,3,4-tri-*O*-benzoyl-6-*O*-(phosphonoxy)-methyl α -D-mannopyranoside (19). Compound **28** (400 mg, 0.500 mmol) was dissolved in a mixture of H₃PO₄ (366 mg, 3.73 mmol) in THF (5 mL). Then, *N*-iodosuccinimide (225 mg, 1.00 mmol) was added and the mixture was stirred for 15 min at 0 °C and for 1 h at rt. The reaction was quenched with 1 M aq. Na₂S₂O₃ and 28% aq. ammonia (2 mL), then the volatiles were removed *in vacuo* at < 30 °C. The residue was purified by MPLC on silica (DCM/[MeOH/ H₂O 10:1], 1:0-3.5:1) to yield slightly impure **19** (278 mg, 67%), which was used in the next step without further purification.

4-(5-Nitroindolin-1-yl)phenyl 6-*O*-(phosphonoxy)-methyl α -D-mannopyranoside diammonium salt (8). Compound **19** (278 mg, 0.337 mmol) was stirred in a mixture of MeOH (5 mL), DCM (4 mL) and 25% aq. NH₃ (8 mL) overnight. The solvent was removed under reduced pressure and the residue was purified by MPLC on RP-18 (H₂O/MeOH) to give **8** (78 mg, 41%). ¹H NMR (D₂O, 500 MHz): δ = 3.21 (t, *J* = 8.4 Hz, 2H, CH₂), 3.81 (dd, *J* = 1.8, 11.3 Hz, 1H, H-6a), 3.86 (m, 1H, H-5), 3.91 (t, *J* = 9.7 Hz, 2H, NCH₂), 3.96 (dd, *J* = 4.2, 11.3 Hz, 1H, H-6b), 4.04 (dd, *J* = 3.5, 9.6 Hz, 1H, H-3), 4.14 (t, *J* = 8.8 Hz, 2H, CH₂), 4.16 (dd, *J* = 1.8, 3.4 Hz, 1H, H-2), 4.89 (A of ABX, *J* = 5.6, 10.8 Hz, 1H, CH₂), 5.00 (B of ABX, *J* = 5.6, 8.1 Hz, 1H, CH₂), 5.60 (s, 1H, H-1), 6.86 (d, *J* = 8.9 Hz, 1H, Ar-H), 7.22 (d, *J* = 8.9 Hz, 2H, Ar-H), 7.39 (d, *J* = 8.8 Hz, 2H, Ar-H), 8.01 (s, 1H, Ar-H), 8.05 (d, *J* = 9.3 Hz, 1H, Ar-H); ¹³C NMR (D₂O, 126 MHz): δ = 26.3 (CH₂), 53.6 (NCH₂), 66.1, 66.3 (C-4, C-6), 69.9 (C-2), 70.2 (C-3), 72.3 (C-5), 90.1 (d, *J* = 4 Hz, CH₂), 98.7 (C-1), 105.6, 118.1, 121.2, 121.9, 122.0, 127.0, 132.5, 136.6, 137.5, 151.9, 154.6 (12C, 12 Ar-C), ESI-MS: *m/z*: Calcd for C₂₁H₂₄N₂O₁₂P [M-2NH₄+H]⁺: 527.11, found: 527.18.

Physicochemical and pharmacokinetic characterization

Materials. Dulbecco's Modified Eagle's Medium (DMEM) - high glucose, L-glutamine solution, penicillin-streptomycin solution, Dulbecco's Phosphate Buffered Saline (DPBS), and trypsin-EDTA solution were purchased from Sigma-Aldrich. MEM nonessential amino acid (MEM-NEAA) solution, fetal bovine serum (FBS), and DMEM without sodium pyruvate and phenol red were bought from Invitrogen (Carlsbad, CA, USA). Acetonitrile (MeCN) was from Acros Organics (Geel, Belgium). The Caco-2 cells were kindly provided by Prof. G. Imanidis, FHNW, Muttentz, and originated from the American Type Culture Collection (Rockville, MD, USA).

Aqueous Solubility. Microanalysis tubes (LaboTech J. Stofer LTS AG, Muttentz, Switzerland) were charged with 500 μ g of solid substance and 100 μ L of phosphate buffer (50 mM, pH 6.5). The tubes were briefly shaken by hand, sonicated for 15 min, and vigorously shaken (600 rpm, 25 °C, 2 h) on an Eppendorf Thermomixer Comfort (Eppendorf, Hamburg, Germany). Afterwards, they were left undisturbed for 24 h. Then, the compound solutions were filtered (MultiScreen HTS 96-well Filtration System, Millipore, Billerica, MA) by centrifugation (1500 rpm, 25 °C, 3 min). The filtrates

were further diluted with buffer (1:1000 and 1:10000), and the concentrations were determined by LC-MS (see below).

Colorectal adenocarcinoma (Caco-2) cell permeation assay and hydrolysis studies. Caco-2 cells were cultivated in tissue culture flasks (BD Biosciences, Franklin Lakes, NJ, USA) with DMEM high glucose medium, containing L-glutamine (2 mM), nonessential amino acids (0.1 mM), penicillin (100 U/mL), streptomycin (100 µg/mL), and fetal bovine serum (10%). The cells were kept at 37 °C in humidified air containing 5% CO₂, and the medium was changed every second day. When approximately 90% confluence was reached, the cells were split in a 1:10 ratio and distributed to new tissue culture flasks. At passage numbers between 60 and 65, they were seeded at a density of 5.3×10^5 cells per well to Transwell six-well plates (Corning Inc., Corning, NY, USA) with 2.5 mL of culture medium in the basolateral and 2.0 mL in the apical compartment. The medium was renewed on alternate days. Enzymatic hydrolysis and permeation experiments were performed between days 19 and 21 post seeding. Prior to the experiment, the integrity of the Caco-2 monolayers was evaluated by measuring the transepithelial electrical resistance (TEER) with an Endohm tissue resistance instrument (World Precision Instruments Inc., Sarasota, FL, USA). Only wells with TEER values higher than 250 Ω cm² were used. After the experiment, TEER values were assessed again for each well and results from wells with values below 250 Ω cm² were discarded.

Permeation experiments with the compounds **3-5** were performed in the apical-to-basolateral and basolateral-to-apical directions in triplicates. Transport medium (DMEM without sodium pyruvate and phenol red) was withdrawn from the donor compartments of three wells and replaced by the same volume of compound stock solution (10 mM in DMSO) to reach an initial sample concentration of 62.5 µM. The Transwell plate was shaken (600 rpm, 37 °C) on a Heidolph Titramax 1000 plate-shaker (Heidolph Instruments GmbH & Co. KG, Schwabach, Germany). Samples (40 µL) were withdrawn from the donor and acceptor compartments 30 min after initiation of the experiment and the compound concentrations were determined by LC-MS. Apparent permeability (P_{app}) was calculated according to Equation 1:

$$P_{\text{app}} = \frac{dQ}{dt} \times \frac{1}{A \times c_0} \quad (1)$$

where dQ/dt is the compound flux (mol s⁻¹), A the surface area of the monolayer (cm²), and c_0 the initial concentration in the donor compartment (mol cm⁻³).^[37]

Hydrolysis studies with the compounds **6a-e**, **7a-d** and **8** were performed in triplicates. Transport medium was withdrawn from the apical compartments of three wells and replaced by the same volume of compound stock solution (10 mM in H₂O) to reach an initial sample concentration of 62.5 µM. The Transwell plate was shaken (600 rpm, 37 °C) on a Heidolph Titramax 1000 plate-shaker. Samples (40 µL) were withdrawn from the apical compartment 10, 20, 30, 45, and 60 min after the initiation of the experiment and the concentrations of prodrug were determined by LC-MS. Metabolic

half-life ($t_{1/2}$) was calculated from the slope of the linear regression from the log percentage remaining compound versus incubation time relationship.

Studies of hydrolysis and subsequent permeation in the apical-to-basolateral and basolateral-to-apical directions were performed with compound **7b** in triplicate. Transport medium was withdrawn from the apical or basal donor compartments of three wells and replaced by the same volume of compound stock solution (10 mM in H₂O) to reach an initial sample concentration of 62.5 μ M. The Transwell plate was shaken (600 rpm, 37 °C) on a Heidolph Titramax 1000 plate-shaker. Samples (40 μ L) were withdrawn from the apical and basal compartments 60 min after the initiation of the experiment and the concentrations of prodrug **7b** and parent compound **4** were determined by LC-MS.

Studies of hydrolysis and subsequent permeation in the apical-to-basolateral direction were performed with the compounds **6e**, **7b** and **8** at different concentrations (100, 200, or 400 μ M) in duplicate. Transport medium was withdrawn from the apical compartments of two wells and replaced by the same volume of compound stock solution (16, 32, or 64 mM in H₂O) to reach initial sample concentrations of 100, 200, or 400 μ M. The Transwell plate was shaken (600 rpm, 37 °C) on a Heidolph Titramax 1000 plate-shaker. Samples (40 μ L) were withdrawn from the basal compartments 60 min after the initiation of the experiment and the concentrations of prodrug **6e**, **7b** and **8** as well as parent compound **3-5**, respectively, were determined by LC-MS.

Stability Assay. The simulated fluids were prepared according to UPS specifications and Dressman *et al.* [48,49] All fluids were preheated at 37 °C. The compounds were then added to yield 20 μ M solutions ($t = 0$ min). Incubations were performed on a Heidolph 1000 incubator (500 rpm, 37 °C). After an incubation time of 0, 10, 20, 30, 60, and 120 min, samples (30 μ L) were withdrawn, precipitated with ice-cooled methanol (120 μ L), put into the freezer (-20 °C, 10 min), and then centrifuged (13,200 rpm, 3 min). The supernatant was transferred into a 96-well plate. The concentration of analyte in the supernatant was analysed by LC-MS.

LC-MS Measurement. Analyses were performed using an 1100/1200 Series HPLC System coupled to a 6410 Triple Quadrupole mass detector (Agilent Technologies, Inc., Santa Clara, CA, USA) equipped with electrospray ionization. The system was controlled with the Agilent MassHunter Workstation Data Acquisition software (version B.01.04). The column used was an Atlantis[®] T3 C18 column (2.1 x 50 mm) with a 3 μ m particle size (Waters Corp., Milford, MA, USA). The mobile phase consisted of two eluents: Eluent A (H₂O, containing 0.1% formic acid, v/v for compounds **5**, **6a-e**, **7c**, **7d** and **8**; ammonium acetate buffer, 10 mM, pH 5 for compounds **3** and **4**; formiate buffer, 10 mM, pH 3 for compounds **7a** and **7b**) and eluent B (MeCN, containing 0.1% formic acid, v/v), delivered at 0.6 mL/min. The gradient was ramped from 95% A/5% B to 5% A/95% B over 1 min, and then held at 5% A/95% B for 0.1 min. The system was then brought back to 95% A/5% B, resulting in a total duration of 4 min. MS parameters such as fragmentor voltage, collision energy,

polarity were optimized individually for each analyte, and the molecular ion was followed for each compound in the multiple reaction monitoring mode. The concentrations of the analytes were quantified by the Agilent Mass Hunter Quantitative Analysis software (version B.01.04).

In vivo pharmacokinetics. For the PK studies, eight-week-old female C3H/HeN mice (21-27 g) from Harlan (Venray, The Netherlands) were purchased. The mice were housed in groups of three per cage and kept under specific pathogen-free conditions in the Animal House of the Department of Biomedicine, University Hospital of Basel. For experimentation, all guidelines according to the Swiss veterinary law were followed. The animals were kept in a 12h/12h light/dark cycle and had chow and water *ad libitum*. After one week of acclimatization, the mice were used in groups of three for the pharmacokinetic studies. Compounds were diluted in PBS and applied using an oral gavage (10 mg/kg). All administered solutions consisted of prodrug (min. 94%) and active principle (max. 6%). Blood and urine samples (10 µL) were taken before the experiment (0 min) and at 6, 13, 20, 40 min, 1, 1.5, 2, 3, 4, 6, 8, and 24 h after administration. Directly after sampling, the samples were diluted in methanol (1:5) to precipitate proteins. After centrifugation (11 min, 13000 rpm) the supernatant was transferred to a 96-well plate and analysed by LC-MS as described before. The samples at 0 min were used to define the detection limit in plasma and urine. The percentages of absorbed fractions in urine were calculated by the average urine concentration opposed to the sampled urine volumes and divided by the dosed amount of drug. Sampling and administration was performed following the guidelines in reference.^[53]

Acknowledgement

The authors gratefully acknowledge the financial support by the Swiss National Science Foundation.

References

- [1] Fihn, S. D. Clinical practice. Acute uncomplicated urinary tract infection in women. *N. Eng. J. Med.* **2003**, *349*, 259–266.
- [2] Wiles, T. J.; Kulesus, R. R.; Mulvey, M. A. Origins and virulence mechanisms of uropathogenic *Escherichia coli*. *Exp. Mol. Pathol.* **2008**, *85*, 11–19.
- [3] Sanchez, G. V.; Master, R. N.; Karlowsky, J. A.; Bordon, J. M. In vitro antimicrobial resistance of urinary *Escherichia coli* isolates among U.S. outpatients from 2000 to 2010. *Antimicrob. Agents Chemother.* **2012**, *56*, 2181–2183.
- [4] Hooton, T. M.; Stamm, W. E. Diagnosis and treatment of uncomplicated urinary tract infection. *Infect. Dis. Clin. North Am.* **1997**, *11*, 551-581.
- [5] Svanborg, C.; Godaly, G. Bacterial virulence in urinary tract infection. *Infect. Dis. Clin. North Am.* **1997**, *11*, 513-529.
- [6] Schilling, J. D.; Mulvey, M. A.; Hultgren, S. J. Structure and function of *Escherichia coli* type 1 pili: new insight into the pathogenesis of urinary tract infections. *J. Infect. Dis.* **2001**, *183* Suppl. 1, S36–S40.
- [7] Capitani, G.; Eidam, O.; Glockshuber, R.; Grütter, M. G. Structural and functional insights into the assembly of type 1 pili from *Escherichia coli*. *Microbes Infect.* **2006**, *8*, 2284–2290.

- [8] Sharon, N. Carbohydrates as future anti-adhesion drugs for infectious diseases. *Biochim. Biophys. Acta.* **2006**, *1760*, 527–537.
- [9] Firon, N.; Itzhak, O.; Sharon, N. Interaction of mannose-containing oligosaccharides with the fimbrial lectin of *Escherichia coli*. *Biochem. Biophys. Res. Commun.* **1982**, *105*, 1426-1432.
- [10] Firon, N.; Ofek, I.; Sharon, N. Carbohydrate specificity of the surface lectins of *Escherichia coli*, *Klebsiella pneumoniae*, and *Salmonella typhimurium*. *Carbohydr. Res.* **1983**, *120*, 235-249.
- [11] Bouckaert, J.; Berglund, J.; Schembri, M.; De Genst, E.; Cools, L.; Wuhler, M.; Hung, C.-S.; Pinkner, J.; Slättegård, R.; Zavialov, A.; Choudhury, D.; Langermann, S.; Hultgren, S. J.; Wyns, L.; Klemm, P.; Oscarson, S.; Knight, S. D.; De Greve, H. Receptor binding studies disclose a novel class of high-affinity inhibitors of the *Escherichia coli* FimH adhesin. *Mol. Microbiol.* **2005**, *55*, 441-455.
- [12] Firon, N.; Ashkenazi, S.; Mirelman, D.; Ofek, I.; Sharon, N. Aromatic alpha-glycosides of mannose are powerful inhibitors of the adherence of type 1 fimbriated *Escherichia coli* to yeast and intestinal epithelial cells. *Infect. Immun.* **1987**, *55*, 472-476.
- [13] Sperling, O.; Fuchs, A.; Lindhorst, T. K. Evaluation of the carbohydrate recognition domain of the bacterial adhesin FimH. Design, synthesis and binding properties of mannoside ligands. *Org. Biomol. Chem.* **2006**, *4*, 3913-3922.
- [14] Han, Z.; Pinkner, J. S.; Ford, B.; Obermann, R.; Nolan, W.; Wildman, S. A.; Hobbs, D.; Ellenberger, T.; Cusumano, C. K.; Hultgren, S. J.; Janetka, J. W. Structure-based drug design and optimization of mannoside bacterial FimH antagonists. *J. Med. Chem.* **2010**, *53*, 4779-4792.
- [15] Klein, T.; Abgottspon, D.; Wittwer, M.; Rabbani, S.; Herold, J.; Jiang, X.; Kleeb, S.; Lüthi, C.; Scharenberg, M.; Bezençon, J.; Gubler, E.; Pang, L.; Smiesko, M.; Cutting, B.; Schwardt, O.; Ernst, B. FimH antagonists for the oral treatment of urinary tract infections: from design and synthesis to in vitro and in vivo evaluation. *J. Med. Chem.* **2010**, *53*, 8627-8641.
- [16] Cusumano, C. K.; Pinkner, J. S.; Han, Z.; Greene, S. E.; Ford, B. A.; Crowley, J. R.; Henderson, J. P.; Janetka, J. W.; Hultgren, S. J. Treatment and prevention of urinary tract infection with orally active FimH inhibitors. *Sci. Transl. Med.* **2011**, *3*, 109ra115.
- [17] Han, Z.; Pinkner, J. S.; Ford, B.; Chorell, E.; Crowley, J. M.; Cusumano, C. K.; Campbell, S.; Henderson, J. P.; Hultgren, S. J.; Janetka, J. W. Lead optimization studies on FimH antagonists: discovery of potent and orally bioavailable *ortho*-substituted biphenyl mannosides. *J. Med. Chem.* **2012**, *55*, 3945-3959.
- [18] Pang, L.; Kleeb, S.; Lemme, K.; Rabbani, S.; Scharenberg, M.; Zalewski, A.; Schädler, F.; Schwardt, O.; Ernst, B. FimH antagonists: structure-activity and structure-property relationships for biphenyl α -D-mannopyranosides. *ChemMedChem.* **2012**, *7*, 1404-1422.
- [19] Jiang, X.; Abgottspon, D.; Kleeb, S.; Rabbani, S.; Scharenberg, M.; Wittwer, M.; Haug, M.; Schwardt, O.; Ernst, B. Anti-adhesion therapy for urinary tract infections – a balanced PK/PD profile proved to be key for success. *J. Med. Chem.* **2012**, *55*, 4700-4713.
- [20] Schwardt, O.; Rabbani, S.; Hartmann, M.; Abgottspon, D.; Wittwer, M.; Kleeb, S.; Zalewski, A.; Smiesko, M.; Cutting, B.; Ernst, B. Design, synthesis and biological evaluation of mannosyl triazoles as FimH antagonists. *Bioorg. Med. Chem.* **2011**, *19*, 6454-6473.
- [21] Brument, S.; Sivignon, A.; Dumych, T. I.; Moreau, N.; Roos, G.; Guérardel, Y.; Chalopin, T.; Deniaud, D.; Bilyy, R. O.; Darfeuille-Michaud, A.; Bouckaert, J.; Gouin, S. G. Thiazolylaminomannosides as potent antiadhesives of type 1 piliated *Escherichia coli* isolated from Crohn's disease patients. *J. Med. Chem.* **2013**, *56*, 5395-5406.
- [22] Lindhorst, T. K.; Kieburg, C.; Krallmann-Wenzel, U. Inhibition of the type 1 fimbriae-mediated adhesion of *Escherichia coli* to erythrocytes by multiantennary D-mannosyl clusters: The effect of multivalency. *Glycoconj. J.* **1998**, *15*, 605-613.

- [23] Nagahori, N.; Lee, R. T.; Nishimura, S.-L.; Pagé, S.; Roy, R.; Lee, Y. C. Inhibition of adhesion of type 1 fimbriated *Escherichia coli* to highly mannosylated ligands. *ChemBioChem* **2002**, *3*, 836-844.
- [24] Appeldoorn, C. C. M.; Joosten, J. A. F.; Maate, F. A.; Dobrindt, U.; Hacker, J.; Liskamp, R. M. J.; Khan, A. S.; Pieters, R. J. Novel multivalent mannose compounds and their inhibition of the adhesion of type 1 fimbriated uropathogenic *E. coli*. *Tetrahedron Asym.* **2005**, *16*, 361-372.
- [25] Patel, A.; Lindhorst, T. K. A modular approach for the synthesis of oligosaccharide mimetics. *Carbohydr. Res.* **2006**, *341*, 1657-1668.
- [26] Touaibia, M.; Wellens, A.; Shiao, T. C.; Wang, Q.; Sirois, S.; Bouckaert, J.; Roy, R. Mannosylated G(0) dendrimers with nanomolar affinities to *Escherichia coli* FimH. *ChemMedChem* **2007**, *2*, 1190-1201.
- [27] Durka, M.; Buffet, K.; Iehl, J.; Holler, M.; Nierengarten, J.-F.; Taganna, J.; Bouckaert, J.; Vincent, S. P. The functional valency of dodecamannosylated fullerenes with *Escherichia coli* FimH - towards novel bacterial antiadhesives. *Chem. Commun.* **2011**, *47*, 1321-1323.
- [28] Bouckaert, J.; Li, Z.; Xavier, C.; Almant, M.; Caveliers, V.; Lahoutte, T.; Weeks, S. D.; Kovensky, J.; Gouin, S. G. Heptyl α -D-mannosides grafted on a β -cyclodextrin core to interfere with *Escherichia coli* adhesion: An *in vivo* multivalent effect. *Chem. Eur. J.* **2013**, *19*, 7847-7855.
- [29] Scharenberg, M.; Schwardt, O.; Rabbani, S.; Ernst, B. Target selectivity of FimH antagonists. *J. Med. Chem.* **2012**, *55*, 9810-9816.
- [30] Van de Waterbeemd, H.; Smith, D. A.; Beaumont, K.; Walker, D. K. Property-based design: Optimization of drug absorption and pharmacokinetics. *J. Med. Chem.* **2001**, *44*, 1313-1333.
- [31] Amidon, G. L.; Lennernäs, H.; Shah, V. P.; Crison, J. R. A theoretical basis for a biopharmaceutic drug classification: the correlation of *in vitro* drug product dissolution and *in vivo* bioavailability. *Pharm. Res.* **1995**, *12*, 413-420.
- [32] Heimbach, T.; Oh, D.-M.; Li, L.Y.; Forsberg, M.; Savolainen, J.; Leppänen, J.; Matsunaga, Y.; Flynn, G.; Fleisher, D. Absorption rate limit considerations for oral phosphate prodrugs. *Pharm. Res.* **2003**, *20*, 848-856.
- [33] Stella, V. J.; Nti-Addae, K. W. Prodrug strategies to overcome poor water solubility. *Adv. Drug Deliv. Rev.* **2007**, *59*, 677-694.
- [34] Wire, M. B.; Shelton, M. J.; Studenberg, S. Fosamprenavir : clinical pharmacokinetics and drug interactions of the amprenavir prodrug. *Clin. Pharmacokinet.* **2006**, *45*, 137-168.
- [35] Rautio, J.; Kumpulainen, H.; Heimbach, T.; Oliyai, R.; Oh, D.; Järvinen, T.; Savolainen, J. Prodrugs: design and clinical applications. *Nat. Rev. Drug. Discov.* **2008**, *7*, 255-280.
- [36] Hersh, M. R.; Kuhn, J. G.; Phillips, J. L.; Clark, G.; Ludden, T. M.; Von Hoff, D. D. Pharmacokinetic study of fludarabine phosphate (NSC 312887). *Cancer Chemother. Pharmacol.* **1986**, *3*, 277-280.
- [37] S. Kleeb, L. Pang, K. Mayer, D. Eris, A. Sigl, R. C. Preston, P. Zihlmann, D. Abgottspon, A. Hutter, M. Scharenberg, X. Jiang, G. Navarra, S. Rabbani, M. Smiesko, N. Lüdin, R. P. Jakob, O. Schwardt, T. Maier, T. Sharpe, B. Ernst, FimH antagonists: bioisosteres to improve the *in vitro* and *in vivo* PK/PD profile. *J. Med. Chem.* **2015**, *58*, 2221-2239.
- [38] Rabbani, S.; Jiang, X. H.; Schwardt, O.; Ernst, B. Expression of the carbohydrate recognition domain of FimH and development of a competitive binding assay. *Anal. Biochem.* **2010**, *407*, 188-195.
- [39] Alsenz, J.; Kansy, M. High throughput solubility measurement in drug discovery and development. *Adv. Drug Deliv. Rev.* **2007**, *59*, 546-67.
- [40] Waring, M. J. Lipophilicity in drug discovery. *Expert Opin. Drug Discov.* **2010**, *5*, 235-48.

- [41] Kansy, M.; Senner, F.; Gubernator, K. Physicochemical high throughput screening: Parallel artificial membrane permeation assay in the description of passive absorption processes. *J. Med. Chem.* **1998**, *41*, 1007-1010.
- [42] Avdeef, A.; Bendels, S.; Di, L.; Faller, B.; Kansy, M.; Sugano, K.; Yamauchi, Y. PAMPA - Critical factors for better predictions of absorption. *J. Pharm. Sci.* **2007**, *96*, 2893-2909.
- [43] Artursson, P.; Karlsson, J. Correlation between oral drug absorption in humans and apparent drug permeability coefficients in human intestinal epithelial (Caco-2) cells. *Biochem. Biophys. Res. Commun.* **1991**, *175*, 880-5.
- [44] Hubatsch, I.; Ragnarsson, E. G. E.; Artursson, P. Determination of drug permeability and prediction of drug absorption in Caco-2 monolayers. *Nat. Protoc.* **2007**, *2*, 2111-2119.
- [45] DeGoey, D. A.; Grampovnik, D. J.; Flosi, W. J.; Marsh, K. C.; Wang, X. C.; Klein, L. L.; McDanile, K. F.; Liu, Y.; Long, M. A.; Kati, W. M.; Molla, A.; Kempf, D. J. Water-soluble prodrugs of the human immunodeficiency virus protease inhibitors lopinavir and ritonavir. *J. Med. Chem.* **2009**, *52*, 2964-2970.
- [46] Ma, Z.; Zhang, J.; Kong, F. Facile synthesis of arabinomannose penta- and decasaccharide fragments of the lipoarabinomannan of the equine pathogen, *Rhodococcus equi*. *Carbohydr. Res.* **2004**, *339*, 1761-1771.
- [47] Yuan, H.; Li, N.; Lai, Y. Evaluation of in vitro models for screening phosphatase-mediated bioconversion of phosphate ester prodrugs. *Drug Metab. Dispos.* **2009**, *37*, 1443-1447.
- [48] Kearny, A. S.; Stella, V.J. The in vitro enzymic labilities of chemically distinct phosphomonoester prodrugs. *Pharm. Res.* **1992**, *9*, 497-503.
- [49] Dhareshwar, S. S.; Stella, V. J. A novel prodrug strategy for beta-dicarbonyl carbon acids: syntheses and evaluation of the physicochemical characteristics of C-phosphoryloxymethyl (POM) and phosphoryloxymethyloxymethyl (POMOM) prodrug derivatives. *J. Pharm. Sci.* **2010**, *99*, 2711-2723.
- [50] "The United States Pharmacopeia (USP 28)", **2004**.
- [51] Dressman, J. B.; Thelen, K.; Jantratid, E. Towards quantitative prediction of oral drug absorption. *Clinical pharmacokinetics* **2008**, *47*, 655-667.
- [52] Stevens, R. H.; O'Neill, C. A.; Warhurst, A.; Carlson, G. L.; Rowland, M.; Warhurst, G. Kinetic profiling of P-glycoprotein-mediated drug efflux in rat and human intestinal epithelia. *J. Pharmacol. Exp. Ther.* **2001**, *296*, 584-591.
- [53] Diehl K.-H.; Hull, R.; Morton, D.; Pfister, R.; Rabemampianina, Y.; Smith, D.; Vidal, J.-M.; Van de Vorstenbosch, C. A good practice guide to the administration of substances and removal of blood, including routes and volumes. *J. Appl. Toxicol.* **2001**, *21*, 15-23.

2.11 **Paper 10: Design, synthesis, and biological evaluation of mannosyl triazoles as FimH antagonists**

The following publication explores FimH antagonists with aglycones of increased flexibility. The modes of binding to the FimH-CRD and the physicochemical properties of triazolyl-methyl and -ethyl α -D-mannopyranosides, N-linked mannosyl triazoles, and triazolyl-methyl-C-mannosides are exposed in details.

Contribution to the project:

Simon Kleeb contributed to the experimental characterization of the antagonists' physicochemical properties.

This paper was published in *Bioorganic & Medicinal Chemistry*:

Schwardt, O.; Rabbani, S.; Hartmann, M.; Abgottspon, D.; Wittwer, M.; Kleeb, S.; Zalewski, A.; Smiesko, M.; Cutting, B.; Ernst, B. Design, synthesis, and biological evaluation of mannosyl triazoles as FimH antagonists. *Bioorg. Med. Chem.* **2011**, *19*, 6454-6473.

© 2011 Elsevier Ltd.



Contents lists available at SciVerse ScienceDirect

Bioorganic & Medicinal Chemistry

journal homepage: www.elsevier.com/locate/bmc

Design, synthesis and biological evaluation of mannosyl triazoles as FimH antagonists

Oliver Schwardt, Said Rabbani, Margrit Hartmann, Daniela Abgottspon, Matthias Wittwer, Simon Kleeb, Adam Zalewski, Martin Smieško, Brian Cutting, Beat Ernst*

Institute of Molecular Pharmacy, Pharmacenter, University of Basel, Klingelbergstrasse 50, CH-4056 Basel, Switzerland

ARTICLE INFO

Article history:

Received 22 April 2011
Revised 24 August 2011
Accepted 25 August 2011
Available online 31 August 2011

Keywords:

Uropathogenic *Escherichia coli*
Urinary tract infections
Bacterial adhesin FimH
FimH antagonists
Competitive binding assay
Aggregometry assay
NMR spectroscopy

ABSTRACT

Urinary tract infection (UTI) caused by uropathogenic *Escherichia coli* (UPEC) is one of the most prevalent infectious diseases. Particularly affected are women, who have a 40–50% risk to experience at least one symptomatic UTI episode at some time during their life. In the initial step of the infection, the lectin FimH, located at the tip of bacterial pili, interacts with the high-mannosylated uroplakin Ia glycoprotein on the urinary bladder mucosa. This interaction is critical for the ability of UPEC to colonize and invade the bladder epithelium. X-ray structures of FimH co-crystallized with two different ligands, the physiological binding epitope oligomannose-3 and the antagonist biphenyl α -D-mannoside **4a** revealed different binding modes, an *in-docking-mode* and an *out-docking-mode*, respectively. To accomplish the *in-docking-mode*, that is the docking mode where the ligand is hosted by the so-called tyrosine gate, FimH antagonists with increased flexibility were designed and synthesized. All derivatives **5–8** showed nanomolar affinities, but only one representative, the 4-pyridiyl derivative **5j**, was as potent as the reference compound *n*-heptyl α -D-mannoside (**1b**). Furthermore, a loss of affinity was observed for C-glycosides and derivatives where the triazole aglycone is directly *N*-linked to the anomeric center. A conformational analysis by NMR revealed that the triazolyl-methyl-C-mannosides **8** adopt an unusual ¹C₄ chair conformation, explaining the comparably lower affinity of these compounds. Furthermore, to address the drug-likeness of this new class of FimH antagonists, selected pharmacokinetic parameters, which are critical for oral bioavailability (lipophilicity, solubility, and membrane permeation), were determined.

© 2011 Elsevier Ltd. All rights reserved.

1. Introduction

Urinary tract infections (UTIs) are among the most common infections, affecting millions of people each year. Although UTIs rarely cause severe diseases such as pyelonephritis or urosepsis, they are associated with extensive morbidity and generate considerable medical expenses.¹ Uropathogenic *Escherichia coli* (UPEC) are the primary cause of UTIs accounting for 70–95% of the

ported cases. Particularly affected are women, who have a 40–50% risk to suffer from a symptomatic UTI episode at some time during their life.^{2,3} Symptomatic UTIs require antimicrobial treatment, resulting in selection and development of bacterial resistance. Consequently, treatment of consecutive infections becomes increasingly difficult. Especially patients with diabetes, urinary tract anomaly, paraplegia and those with permanent urinary catheter experience repeated UTIs with resistant strains. Therefore, a new approach for the treatment and prevention of UTI with non-antibiotic and orally applicable therapeutics with a low potential for resistance would have a great impact on patient care, public healthcare, and medical expenses.

UPEC express a number of well-studied virulence factors for successful colonization of and survival within the host.^{1,4,5} One important virulence factor, the mannose-specific FimH adhesin, is located at the tip of bacterial type 1 pili.⁶ Type 1 pili are the most prevalent fimbriae encoded by UPEC, consisting of the four subunits FimA, FimF, FimG and FimH. The FimH lectin enables UPEC to attach to high-mannosylated uroplakin Ia glycoproteins on the urinary bladder mucosa, thus enabling adherence and invasion of host cells and at the same time preventing the rapid clearance of

Abbreviations: ABTS, 2,2'-azino-di-(3-ethylbenzthiazoline-6-sulfonic acid); AUC, area under the curve; BSA, bovine serum albumin; CRD, carbohydrate recognition domain; D, distribution coefficient; DCM, dichloromethane; DMSO, dimethyl sulfoxide; GIT, gastrointestinal tract; GPE, guinea pig erythrocytes; HEPES, 4-(2-hydroxyethyl)-piperazine-1-ethanesulfonic acid; IC₅₀, half maximal inhibitory concentration; iv, intravenous; Man, D-mannose; NMR, nuclear magnetic resonance; NOESY, nuclear Overhauser enhancement spectroscopy; PAA, polyacrylamide; PAMPA, parallel artificial membrane permeation assay; P_{app}, apparent permeability; P_e, effective permeation; po, peroral; rIC₅₀, relative inhibitory concentration; SAR, structure-activity relationship; THF, tetrahydrofuran; TM-PAA, Man α (1-3)-[Man α (1-6)]-Man β (1-4)-GlcNAc β (1-4)-GlcNAc β -PAA; UPEC, uropathogenic *E. coli*; UTI, urinary tract infection.

* Corresponding author. Tel.: +41 61 2 67 15 51; fax: +41 61 2 67 15 52.

E-mail address: beat.ernst@unibas.ch (B. Ernst).

E. coli from the UTI by the bulk flow of urine.^{1,7} As a part of the FimH subunit, a carbohydrate-recognition domain (CRD) is responsible for bacterial interactions with the host cells within the urinary tract.⁷ The crystal structure of methyl α -D-mannopyranoside bound to the FimH-CRD was solved⁸ and the structures of the corresponding complexes with *n*-butyl α -D-mannopyranoside,⁹ Man α (1-3)-[Man α (1-6)]-Man β (1-4)-GlcNAc β -(1-4)GlcNAc (oligomannose-3)¹⁰ and biphenyl α -D-mannopyranoside¹¹ recently became available.

Previous studies showed that colonization and subsequent *E. coli* infection of the human urothelium can be prevented by vaccination with FimH adhesin.^{12,13} Furthermore, adherence and invasion of host cells by *E. coli* can also be inhibited by oligomannosides representing the glycosylation of uroplakin **1a**.¹⁴ For some α -D-mannosides it was shown that they prevent type 1 pili mediated adhesion, that is, they do not act by killing or arresting the growth of the pathogen as antibiotics do. Therefore, the spread of strains resistant to such agents are expected to be significantly delayed as compared to that of strains resistant to antibiotics.¹⁵ In addition, environmental contamination is less problematic compared to antibiotics.^{15a}

More than two decades ago, various oligomannosides and aromatic α -D-mannosides that antagonize type 1 fimbriae-mediated bacterial adhesion were identified.^{15,16} However, for these mannosides only weak interactions in the milli- to micromolar range were observed. To improve their affinity, the multivalent presentation of the α -mannoside epitope,¹⁷ and the rational design of ligands guided by structural information were explored.^{9–11} Recently, various reports on high affinity monovalent FimH antagonists were published.^{11,18,19}

The CRD of the FimH protein consists of amino acids with hydrophilic side chains and can therefore establish a perfect network of hydrogen bonds with the hydroxyl groups at the 2-, 3-, 4- and 6-positions of D-mannose. The entrance to this mannose-binding pocket, the so-called 'tyrosine gate', is shaped by two tyrosines (Tyr48 and Tyr137), and one isoleucine (Ile52) which support hydrophobic contacts.²⁰ Generally, long chain alkyl and aryl mannosides (for selected examples see Fig. 1) displayed the highest affinities.^{8,9,11,16–21}

Recently, we reported the synthesis, the critical pharmacokinetic properties and affinity data of low molecular weight α -D-mannosides with the ability to block the FimH-mediated bacterial adhesion in a mouse infection model.¹⁹ The orally available, nanomolar FimH antagonist **4b** (Fig. 1) exhibited the potential to reduce the colony forming units (CFU) in the urine and in the bladder by two and four orders of magnitude, respectively, demonstrating the therapeutic potential of this new class of anti-infectives for the effective treatment of urinary tract infections.

However, a potential drawback of FimH antagonists with aglycons consisting of biphenyls directly linked to the carbohydrate moiety is their limited conformational flexibility, which could

hamper an optimal fit with the tyrosine gate.¹¹ To increase the conformational flexibility, the spacers between the mannose moiety and the first aromatic ring of the biphenyl moiety in **i** (Fig. 2) as well as between the aromatic rings was extended. Furthermore, the rotational barrier of the biphenyl²⁵ was reduced by replacing one of the rings by a triazole (for the torsion profile see Fig. 2). Overall, these modifications should lead to a reduction of the conformational restraints and therefore an optimized spatial arrangement of the aglycone in the tyrosine gate.

Oligomannose-3 is present on the high-mannosylated uroplakin Ia located on urothelial cells and is supposed to interact with UPEC. The crystal structure of the FimH-CRD¹⁰ complexed with oligomannose-3 (PDB code 2VCO, Fig. 3A) clearly shows the important role of the tyrosine gate hosting this physiological ligand in the so-called *in-docking-mode*. Interestingly, for **4a** complexed with FimH-CRD a different binding mode outside of the tyrosine gate was reported (*out-docking-mode*, see Fig. 3B).¹¹ In analogy to oligomannose-3, docking of triazole derivative **5b** to the crystal structure of the FimH lectin domain (PDB code 3MCY)¹¹ led - as a result of the increased flexibility of the aglycone - to the *in-docking-mode*. Thus, in contrast to the biphenyl aglycone present in **4a**, the phenyl-triazole **5b** is expected to be hosted by the tyrosine gate. The three-dimensional structure **5b** was generated using Glide 5.5²⁶ and the kinetic stability of the protein-ligand complex was then assessed with a 2 ns molecular-dynamics simulation using Desmond.²⁷

A comparison of the docking modes of oligomannose-3, **4a** and **5b** reveals that the interaction of the mannose moiety is highly conserved for all three compounds. However, in contrast to oligomannose-3 and **5b**, the biphenyl moiety in **4a** is not able to reach the tyrosine gate due to its rigid structure. Instead, a π - π -stacking interaction of the second aromatic ring of the biphenyl aglycone with Tyr48 outside of the tyrosine gate¹¹ (*out-docking-mode*, Fig. 3B) is achieved by induced fit, that is, a substantial move of Tyr48. In addition, a further stabilization of the protein-ligand complex by a hydrogen bond between the ester in the *meta*-position of **4a** and the side-chain of Arg98 was assumed.¹¹

Based on these evidences, a library of derivatives according to the criteria summarized in Figure 2 was designed. Here, we describe synthesis, biological evaluation, and determination of pharmacokinetic parameters of triazole derivatives.

2. Results and discussion

2.1. Synthesis of triazolyl-methyl and -ethyl α -D-mannopyranosides

In a first approach, the phenyl ring adjacent to the anomeric center (see Fig. 2) was replaced by a triazolyl-methyl moiety to increase the conformational flexibility. To avoid solubility problems as well as to take advantage of additional polar interactions, for

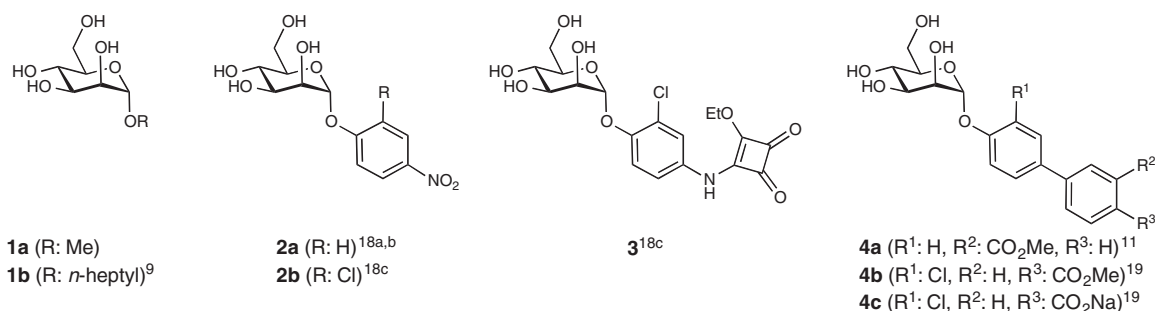


Figure 1. Known alkyl (**1**) and aryl (**2–4**) α -D-mannosides exhibiting micro- to nanomolar affinities.

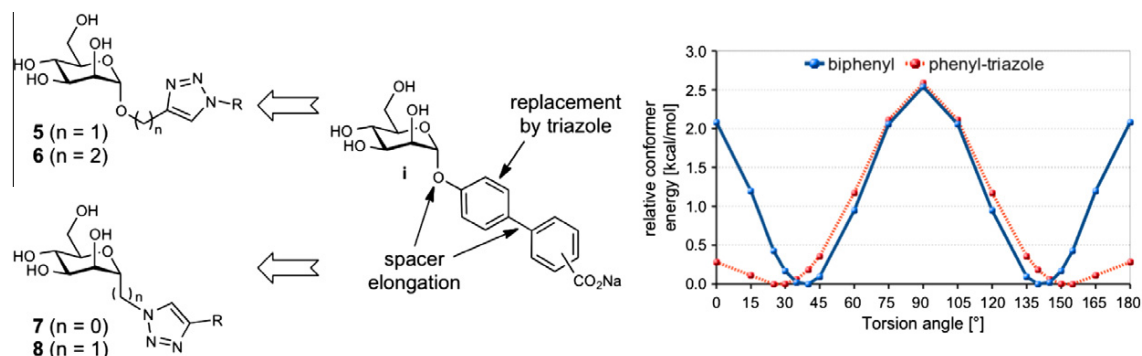


Figure 2. Design of FimH antagonists with aglycons of increased flexibility. Spacer elongations and replacement of one phenyl ring by a triazole should reduce the conformational restraints and lead to an improved fit in the tyrosine gate. The torsion profiles for biphenyl and 1-phenyl-1,2,3-triazole were calculated at the B3LYP level of theory^{22,23} with 6-31G(d,p) basis set in the gas phase using Gaussian 03.²⁴

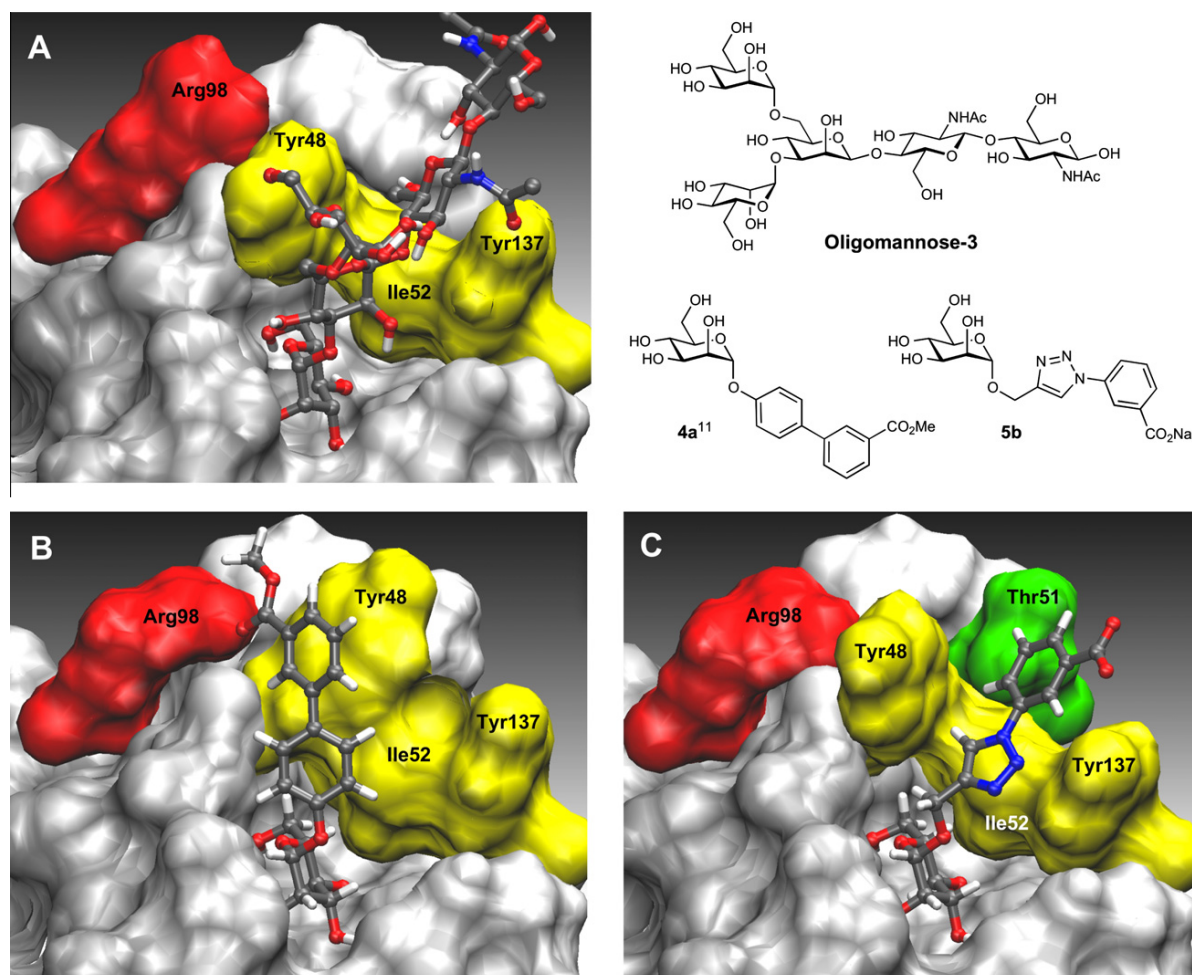
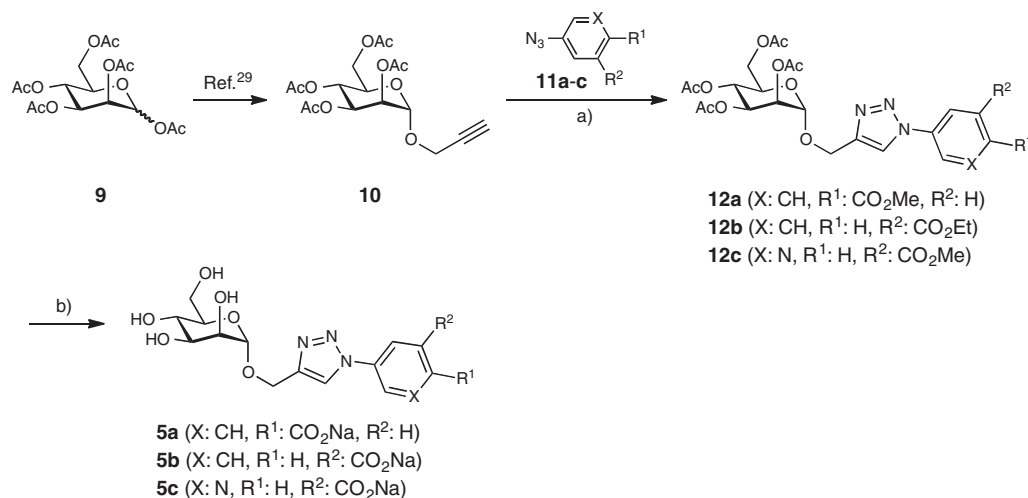


Figure 3. (A) & (B) Crystal structures of oligomannose-3 (A, PDB code 2VCO)¹⁰ and biphenyl **4a** (B, PDB code 3MCY)¹¹ bound to the FimH-CRD. (C) Automated docking of triazole **5b** into the lectin domain of FimH (PDB code 3MCY).¹¹ The images have been generated using VMD.²⁸ The ligands are depicted colored by atom (C: dark grey, H: white, O: red, N: blue); the tyrosine gate (residues Tyr48, Tyr137 and Ile52) is shown in yellow, residue Thr51 in green and residue Arg98 in red. While **4a** binds in the *out-docking-mode*, compound **5b**, like oligomannose-3, is inserted into the tyrosine gate (*in-docking-mode*).

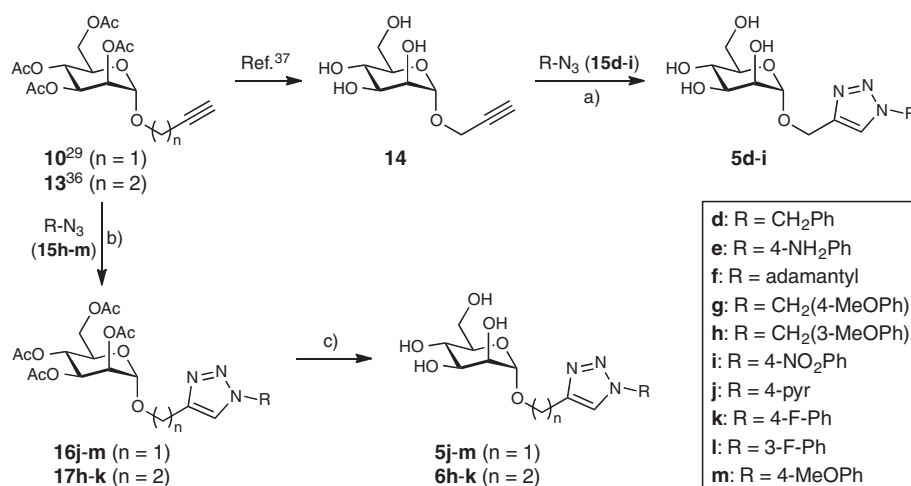
example, H-bonds with the hydroxyl-groups of Thr51 or Tyr137 (Fig. 3C), the second aromatic ring was substituted with a carboxylate in *para*- or *meta*-position (\rightarrow **5a–c**, Scheme 1).

For the synthesis of mannosyl triazoles **5a–c**, alkyne **10**²⁹ readily available from peracetylated β -mannose (**9**) was reacted with

the known aryl azides **11a**,³⁰ **11b**,³¹ and **11c**³² in a copper(I)-catalyzed Huisgen 1,3-dipolar cycloaddition^{33,34} using *tert*-butanol/water/THF (1:1:1) as solvent.³⁵ The saponification of the *anti*-substituted triazoles **12a–c** yielded the test compounds **5a–c** (Table 1).



Scheme 1. Reagents and conditions: (a) CuSO₄·5H₂O, Na-ascorbate, *t*-BuOH/H₂O/THF (1:1:1), rt, 24 h, 73–97%; (b) (i) NaOMe, MeOH, rt, 3 h; (ii) 1 M NaOH, H₂O/dioxane (1:1), 16 h, 78–91%.



Scheme 2. Reagents and conditions: (a) CuSO₄·5H₂O, Na-ascorbate, *t*-BuOH/H₂O (1:1), rt, 24 h, (**5d-i**: 27–77%); (b) CuSO₄·5H₂O, Na-ascorbate, *t*-BuOH/H₂O/THF (1:1:1), rt, 24 h (**16j-m**: 85–94%, **17h-k**: 83–96%); (c) NaOMe, MeOH, rt, 2–6 h, (**5j-m**: 75–85%, **6h-k**: 73–90%).

In a second approach, the terminal aromatic ring was replaced by various substituents like (hetero)aryl, benzyl, and adamantyl groups (\rightarrow **5d-i** & **5j-m**). Furthermore, in compounds **6h-k** the spacer between the carbohydrate moiety and the triazole ring was elongated from methyl to ethyl allowing for a higher conformational flexibility (Scheme 2).

The mannopyranosyl triazoles **5d-m** and **6h-k** were obtained by reacting the known mannopyranosyl alkynes **10**,²⁹ **13**³⁶ and **14**³⁷ with the azides **15d-m**. Whereas the azides **15d-f** are commercially available, **15g**,³⁸ **15h**,³⁹ **15i**,⁴⁰ **15j**,⁴¹ and **15m**⁴⁰ were obtained by known procedures.

The cycloaddition of alkyne **14** and azides **15d-i** under Cu(I)-catalyzed click conditions^{33,34} yielded directly the *anti*-substituted triazoles **5d-i** in 27–77% (Table 1). However, due to the cumbersome purification of the unprotected mannopyranosyl triazoles, test compounds **5j-m** were obtained by an alternative sequence starting from the protected alkyne **10** and azides **15j-m** followed by saponification of the intermediates **16j-m**. The analogous cycloaddition of butynyl mannopyranoside **13** with azides **15h-k** yielded the protected

triazoles **17h-k** in 83–96%. Final deacetylation under Zemplén conditions gave the test compounds **6h-k**, which contain a linker extended by an additional carbon between mannose and aglycone (Table 1).

2.2. Synthesis of FimH antagonists modified at the anomeric center

To avoid the low metabolic stability of *O*-mannosides like compounds **5** and **6** due to potential cleavage by mannosidases, the corresponding *N*-linked mannopyranosyl triazoles **7** and *C*-mannosides **8** were prepared (Scheme 3). Mannopyranosyl azide **18** was obtained according to published procedures.⁴² The Cu(I)-catalyzed click reaction of **18** with the commercially available acetylenes **19n-s** gave exclusively the anomerically pure *anti*-substituted α -*D*-mannopyranosyl-triazoles **20n-s** in 84–98% yield and after deacetylation the test compounds **7n-s** (Table 1).

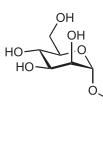
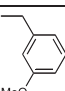
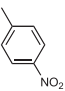
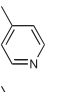
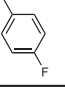
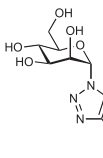
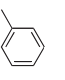
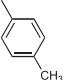
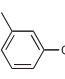
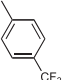
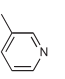
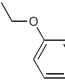
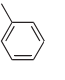
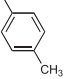
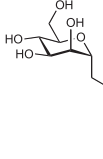
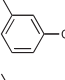
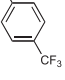
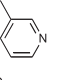
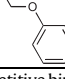
Finally, the synthesis of triazolyl-methyl-*C*-mannosides **8n-s** (Scheme 3) started from mannopyranosyl cyanide **21**, which was obtained

Table 1
Pharmacodynamic and pharmacokinetic parameters of mannosylated triazoles 5–8

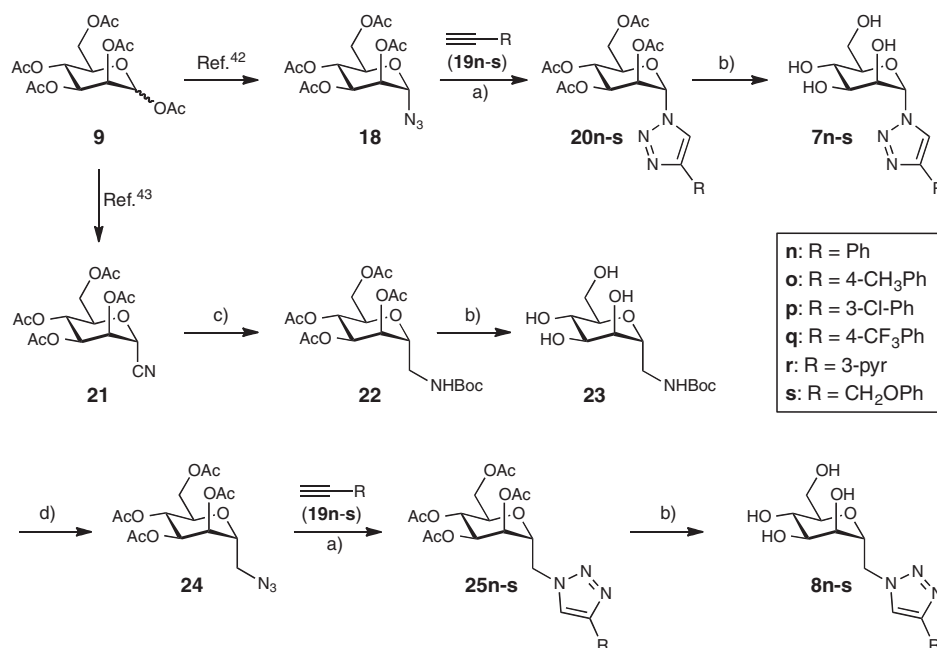
Entry	Ligand	R	Competitive binding assay		logD _{7.4}	PAMPA logP _e [log10 ⁻⁶ cm/s]/%Mm	Solubility [μg/mL]
			IC ₅₀ [μM]	rIC ₅₀			
1		1a ⁴⁵	1.9	29	n.d.	n.d./n.d.	n.d.
2		1b ⁹	0.0656	1.0	1.65	-4.89/21.0	> 3000
3		5a	0.207	3.2	n.d.	n.d./n.d.	> 3000
4		5b	0.296	4.5	n.d.	n.d./n.d.	> 3000
5		5c	0.169	2.6	n.d.	n.d./n.d.	> 3000
6		5d	0.667	10.2	-0.33	-8.60/3.0	> 3000
7		5e	0.420	6.4	0.20	-10/4.0	> 2000
8		5f	0.135	2.1	0.07	-7.42/9.8	> 3000
9		5g	0.511	7.8	-0.40	-8.21/3.1	> 3000
10		5h	0.452	6.9	-0.38	-8.18/4.0	> 3000
11		5i	0.397	6.1	-0.16	-9.40/4.9	2600
12		5j	0.070	1.1	0.24	-8.70/9.2	> 3000
13		5k	0.778	11.9	-0.15	-10/4.6	> 3000
14		5l	0.348	5.3	0.18	-8.80/5.4	> 3000
15		5m	0.161	2.5	-0.05	-8.90/7.9	2600

(continued on next page)

Table 1. (continued)

Entry	Ligand	R	Competitive binding assay		logD _{7.4}	PAMPA logP _e [log10 ⁻⁶ cm/s]/%Mm	Solubility [μg/mL]	
			IC ₅₀ [μM]	rIC ₅₀				
16		6h		0.229	3.5	< -1	-8.70/11.8	> 3000
17		6i		0.112	1.7	-0.30	-9.20/2.9	> 3000
18		6j		0.153	2.3	< -1.5	-9.10/4.3	> 3000
19	6k		0.196	3.0	-0.21	-10/4.0	> 3000	
20		7n		0.250	3.8	0.21	-8.6/6.4	> 3000
21		7o		0.248	3.8	0.91	-8.1/11.5	445
22		7p		0.331	5.1	1.22	-7.8/13.2	705
23		7q		0.144	2.2	1.45	-7.7/17.2	159
24		7r		0.216	3.3	-1.04	-10/10.3	1378
25		7s		0.493	7.5	-0.18	-9.0/5.5	> 3000
26		8n		0.560	8.5	-0.36	-9.1/7.8	> 3000
27	8o		0.565	8.6	0.23	-9.3/6.3	1489	
28		8p		0.639	9.7	0.68	-9.7/n.p.	> 3000
29		8q		0.194	3.0	1.07	-9.3/n.p.	525
30		8r		0.333	5.1	< -1.5	-10/n.p.	1877
31		8s		0.327	5.0	-0.83	-10/n.p.	n.d.

The IC₅₀s were determined with a cell-free competitive binding assay.⁴⁵ Relative IC₅₀s (rIC₅₀) were calculated by dividing the IC₅₀ of the substance of interest by the IC₅₀ of the reference compound **1b** (entry 2). Passive permeation through an artificial membrane and retention therein was determined by PAMPA (parallel artificial membrane permeation assay).⁵⁰ Distribution coefficients (logD_{7.4} values) were measured by a miniaturized shake flask procedure.⁵¹ Thermodynamic solubility was measured by an equilibrium shake flask approach.⁵² P_e effective permeation; n.p. not permeable; n.d. not determined.



Scheme 3. Reagents and conditions: (a) CuSO₄·5H₂O, Na-ascorbate, *t*-BuOH/H₂O/THF (1:1:1), rt, 1–2 d (**20n-s**: 84–98%, **25n-s**: 93–98%); (b) NaOMe, MeOH, rt, 3–6 h, (**7n-s**: 65–92%, **8n-s**: 83–87%, **23**: 95%); (c) H₂ (4 bar), cat. Pd/C, Boc₂O, EtOAc, 1 d (72%); (d) (i) concd HCl, dioxane/H₂O (2:1), 4 h; (ii) TfN₃, NaHCO₃, cat. CuSO₄·5H₂O, PhMe/H₂O/MeOH, rt, 20 h; (iii) Ac₂O, pyridine, rt, 4 h (81%).

from **9** as reported earlier.⁴³ Catalytic hydrogenation in the presence of Boc₂O (→**22**) followed by deacetylation led to the Boc-protected amine **23**. Cleavage of the Boc-group, amine-azide exchange⁴⁴ and subsequent re-acetylation yielded azide **24** in 81% over three steps. The cycloaddition of **24** and the acetylenes **19n-s** gave the *anti*-substituted triazoles **25n-s** in excellent yields. Final deprotection afforded the test compounds **8n-s** (Table 1).

2.3. Biological evaluation

For an initial biological *in vitro* characterization, a cell-free competitive binding assay⁴⁵ and later on, a cell-based aggregation assay⁴⁶ were applied. Whereas for the cell-free competitive binding assay only the CRD of the pili was expressed, the complete pili are present in the cell-based assay format. Furthermore, both formats are competitive assays, that is, the analyzed antagonists compete with mannosides for the binding site. In the cell-free competitive binding assay, the competitors are polymer-bound trimannosides, whereas in the aggregation assay the antagonist competes with more potent oligo- and polysaccharide chains¹⁴ present on the surface of erythrocytes.⁴⁷ The interaction is further complicated by the existence of a high- and a low-affinity state of the CRD of FimH. Aprikian et al. experimentally demonstrated that in full-length fimbriae the pilin domain stabilizes the CRD domain in the low-affinity state, whereas the CRD domain alone adopts the high-affinity state.⁴⁸ Furthermore, it was recently shown that shear stress can induce a conformational switch (twist in the β -sandwich fold of the CRD domain) resulting in improved affinity.⁴⁹ Therefore, different affinities are expected when – as in the cell-based aggregation assay – full-length fimbriae are present, when compared to the CRD domain alone.

2.4. Cell-free competitive binding assay

The cell-free inhibition assay is based on the interaction of a biotinylated polyacrylamide glycopolymer with the carbohydrate

recognition domain (CRD) of FimH as previously reported.⁴⁵ A soluble recombinant protein consisting of the FimH-CRD (amino acid residues 1–156), a C-terminal thrombin cleavage site and a 6His-tag (FimH-CRD-Th-6His) was expressed in *E. coli* strain HM125 and purified by affinity chromatography on a Ni-NTA column. For the determination of IC₅₀ values, a microtiter plate coated with FimH-CRD-Th-6His was incubated with biotinylated Man α (1-3)-[Man α (1-6)]-Man β (1-4)-GlcNAc β (1-4)-GlcNAc β -polyacrylamide (TM-PAA) polymer conjugated to streptavidin-horseradish peroxidase and the FimH antagonist in fourfold serial dilution (Fig. 4). The assay was performed in duplicates and repeated twice for each compound. To ensure comparability of different antagonists, the reference compound *n*-heptyl α -D-mannopyranoside (**1b**)^{9,46} was tested in parallel on each individual microtiter plate. The affinities are reported relative to **1b** as rIC₅₀ in Table 1. The relative IC₅₀ (rIC₅₀) is the ratio of the IC₅₀ of the test compound to the IC₅₀ of **1b** (entry 2).

Interestingly, all antagonists in Table 1 except methyl α -D-mannoside (**1a**) exhibit nanomolar affinities. When compared to **1a**, an up to 30-fold improvement was obtained. In the first series, containing a triazolyl-methyl moiety (**5a-m**, entries 3–15), **5j** (entry 12) exhibits the highest affinity with an IC₅₀ of 70 nM. This is in the range of *n*-heptyl α -D-mannoside (**1b**), however, compared to the biphenyl derivative **4b**¹⁹ (Fig. 1), this in fact represents a 18-fold reduction of affinity (rIC₅₀ 0.06¹⁹ for **4b** vs. rIC₅₀ 1.1 for **5j**). At this point, we should recollect that **4b** and **5j** address different docking modes (*out*- and *in*-docking-mode) and therefore also different structural environments.

Antagonists where the linker between the anomeric center and the triazole is extended by an additional carbon (→**6h-k**, entries 16–19) show affinities in the range of 200 nM and therefore – with the exception of 4-pyridyl derivative **6j** (entry 18) – two- to four-fold higher affinity compared to their counterparts with the shorter linker. When the triazole is directly linked to the anomeric center (→**7n-s**, entries 20–25) affinities are 2- to 8-fold reduced, probably as a consequence of the reduced flexibility preventing an optimal

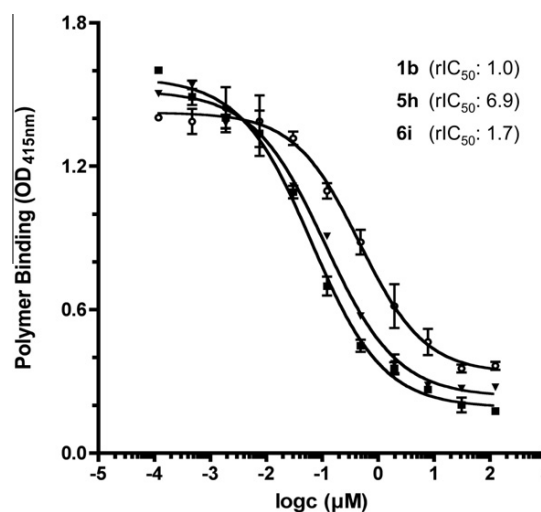


Figure 4. Examples of inhibition curves obtained from the cell-free competitive binding assay.⁴⁵ Each assay was run in duplicate and was repeated at least twice. For antagonists **5h**, **6i** and the reference compound **1b** IC₅₀ values in the nM range were obtained.

interaction of the aglycone with the tyrosine gate. Finally, the C-mannosides **8n–s** (entries 26–31), which do not exhibit the exanomeric effect of the O-mannosides and therefore can more easily adopt the optimal orientation within the tyrosine gate, surprisingly show a twofold reduction in affinity.

2.5. Aggregometry assay

The potential to disaggregate *E. coli* from guinea pig erythrocytes (GPE) was determined for a variety of the mannosylated triazoles in a function-based aggregometry assay.⁴⁶ The measurements were performed in triplicates and the corresponding IC₅₀ values were calculated by plotting the area under the curve (AUC) of disaggregation against the concentration of the antagonists. *n*-Heptyl α -D-mannopyranoside (**1b**) was again used as reference compound with an IC₅₀ of 77.1 μ M (Table 2, entry 1). While the antagonists **5e**, **6j**, **6k**, **7o** and **7q** showed IC₅₀ values in the range of 200–300 μ M, surprisingly no activities could be determined for compounds **5j**, **8q** and **8r** up to a concentration of 700 μ M. As earlier observed,⁴⁶ the activities obtained from the aggregometry assay are approximately 1000-fold lower than the affinities determined in the target-based competitive assay.

2.6. Conformational analysis of mannosyl triazoles

Compared to their counterparts **7**, where the triazole is directly linked to the anomeric center, most of the C-mannosides **8** exhibit a lower affinity. By applying NMR techniques, it was investigated whether this loss of affinity originates from distorted ring conformations. Due to signal overlap, the unprotected mannosides **7** and **8** were not suited for the conformational analysis. However, for the peracetylated derivatives **20n** and **25n** the ring conformation could be assigned based on coupling constants and NOESY experiments. First, the observed ³J coupling constants for their ring protons were strikingly different. In **20n**, they were in agreement with those expected for a regular ⁴C₁ chair conformation of an α -D-mannopyranosyl ring, with small *J*_{1,2} and *J*_{2,3} couplings and large values for *J*_{3,4} and *J*_{4,5} (Fig. 5A). In contrast, the large *J*_{1,2} coupling constant (8.4 Hz) and small to medium values for *J*_{2,3}, *J*_{3,4} and *J*_{4,5} found for **25n**, are in agreement with a ring flip of the α -D-mannopyranosyl chair from the common ⁴C₁ to the unusual ¹C₄ conformation (Fig. 5B). A similar

conformational switch has also been observed for α -CF₂-mannosides.⁵³ As a consequence, the triazolyl-methyl group now is oriented equatorially in C-mannoside **25n**, while in **20n** the triazole moiety adopts an axial position.

Subsequent 2D-NOESY measurements (Fig. 5C and D) confirmed this analysis. For both compounds a sequence of seven 2D-NOESY experiments with increasing mixing times from 0.5 s to 2.0 s in steps of 0.25 s was recorded. The intensity of the positive signals grows with increasing mixing time and indicates the relative spatial proximity of a particular proton to that of the source proton. The NOEs of the proton of interest (int_{cross}) were normalized to the intensity of the diagonal peak of the source proton (int_{diag}). Plotting these normalized intensities against the mixing time results in a straight line for each pair of protons. The distances *r*_{ij} were then calculated from the slopes σ of the linear regression according to $r_{ij} = r_{ref} (\sigma_{ref} / \sigma_{ij})^{1/6}$, where *r*_{ref} is the average distance of the geminal protons H-6a and H-6b, which was chosen as reference (*r*_{ref} = 1.78 Å).^{54,55}

Typically, in the chair conformation of carbohydrates the vicinal proton–proton distances are approx. 2.95 ± 0.15 Å for a diaxial, 2.45 ± 0.15 Å for an axial-equatorial and 2.50 ± 0.20 Å for a diequatorial orientation.⁵⁶ As shown in Figure 5A and B, the distances of the ring protons in **20n** and **25n** determined from NOE experiments correlate well with the theoretical values and support the results obtained from the analysis of the coupling constants. In summary, NMR spectroscopic data indicate that the mannopyranosyl chairs in these compounds adopt different conformations, depending on the substituent at C-1.

This conformational analysis offers an explanation for the twofold reduction of affinity found for most of the C-mannosides **8** compared to the corresponding N-linked triazoles **7**. Due to the inversion of the ring conformation in **8** (¹C₄ vs ⁴C₁), the optimal fit into the hydrophilic mannose-binding pocket of FimH is disturbed.

2.7. Pharmacokinetic properties of mannosyl triazoles

Finally, the druglikeness of this new class of FimH antagonists was addressed. For a successful po application in our UTI mouse model,¹⁹ FimH antagonists have to exhibit oral bioavailability, metabolic stability and fast renal elimination to the urinary tract, their place of action. For the evaluation of oral absorption and renal excretion of the triazoles **5–8** physicochemical parameters such as solubility, lipophilicity (distribution coefficients, log *D*_{7,4}) and permeability were determined (Table 1). The mannosides of all four compound families (**5–8**) are all highly soluble (159 μ g/mL to > 3 mg/mL) and therefore fulfill a first prerequisite for absorption in the gastrointestinal tract (GIT). All compounds showed low to moderate log *D*_{7,4} values in the range of < -1.5 to 1.45. While these parameters are beneficial for renal excretion,⁵⁷ oral absorption by passive diffusion can only be expected to a minor extent. Indeed, for none of the tested compounds a significant permeation through an artificial membrane (PAMPA,⁵⁰ log *P*_e, *P*_e: effective permeation) nor membrane retention could be detected. Whereas for a successful oral absorption a log *P*_e > -5.7 and/or a membrane retention %Mm > 80 % are required,⁵⁸ the corresponding values for all triazoles are far from being in this range. Overall, only poor absorption from the GIT can be therefore expected.

3. Conclusions

Crystal structures indicate that the natural ligand oligomannose-3¹⁰ inserts into the tyrosine gate formed by Tyr48, Tyr137 and Ile52 of the carbohydrate recognition domain of FimH (*in-docking-mode*). In contrast, the recently reported high-affinity

Table 2
IC₅₀ values of mannosylated triazoles determined in the aggregometry assay⁴⁶

Entry	Ligand	R	Aggregometry assay	
			IC ₅₀ [μM]	rIC ₅₀
1	1b ⁹		77.1	1.0
2	5e		299	3.9
3	5j		n.a.	-
5	6j		277	3.6
6	6k		216	2.8
8	7o		289	3.7
9	7q		249	3.2
10	8q		n.a.	-
11	8r		n.a.	-

The relative IC₅₀ (rIC₅₀) was calculated by dividing the IC₅₀ of the substance of interest by the IC₅₀ of the reference compound **1b**. n.a., not active.

biphenyl mannoside **4c** was shown to bind in the *out-docking-mode*, that is, it establishes a π - π -stacking interaction with Tyr48 from the outside of the tyrosine gate.¹¹ Based on docking studies, we designed a series of low molecular weight mannosyl triazoles, which exhibit an increased conformational flexibility of the aglycone and therefore should allow for binding to the tyrosine gate in the *in-docking-mode*. For their pharmacodynamical evaluation two assay formats, a target-based binding assay⁴⁵ and a function-based aggregation assay,⁴⁶ were applied. In general, all triazoles **5–8** showed nanomolar affinities, but only one representative, the 4-pyridyl derivative **5j**, was as potent as the reference compound *n*-heptyl mannoside (**1b**). Obviously, the high flexibility of the *n*-heptyl aglycone in **1b** optimally fulfills the spatial requirements of the tyrosine gate. In addition, the hydrophobic contacts established by the substituted triazole aglycone within the tyrosine gate in the *in-docking-mode* are less favorable than the π - π -stacking interaction of biphenyl derivatives^{11,19} with Tyr48 in the *out-docking-mode*.

Furthermore, the reduced affinities of the triazolyl-methyl-C-mannosides **8** can be rationalized by a disturbed interaction of the mannose moiety. A conformational analysis by ¹H NMR and NOESY NMR revealed that in contrast to the other three classes of mannosyl triazoles (compounds **5**, **6** and **7**), the C-mannosides **8** do not adopt the common ⁴C₁ but an unusual ¹C₄ chair conforma-

tion, thus preventing an optimal fit of the mannose moiety into the hydrophilic mannose-binding pocket of FimH.

Finally, for a successful therapeutic application, FimH antagonists have to exhibit appropriate pharmacokinetic properties, that is, oral bioavailability and fast renal elimination to the urinary tract, their place of action. One prerequisite for absorption in the GIT is sufficient solubility, a property, which is fulfilled by all synthesized antagonists. However, according to their lipophilicity and membrane permeation properties, the mannosyl triazoles are not expected to be orally absorbed. Possible improvements of the pharmacokinetic profiles of mannosyl triazoles are currently studied.

4. Experimental part

4.1. Chemistry

General. NMR spectra were recorded on a Bruker Avance DMX-500 (500 MHz) spectrometer. Assignment of ¹H and ¹³C NMR spectra was achieved using 2D methods (COSY, HSQC). Chemical shifts are expressed in ppm using residual CHCl₃ and CD₂HOD as references. Optical rotations were measured using a Perkin-Elmer Polarimeter 341. Electron spray ionization mass

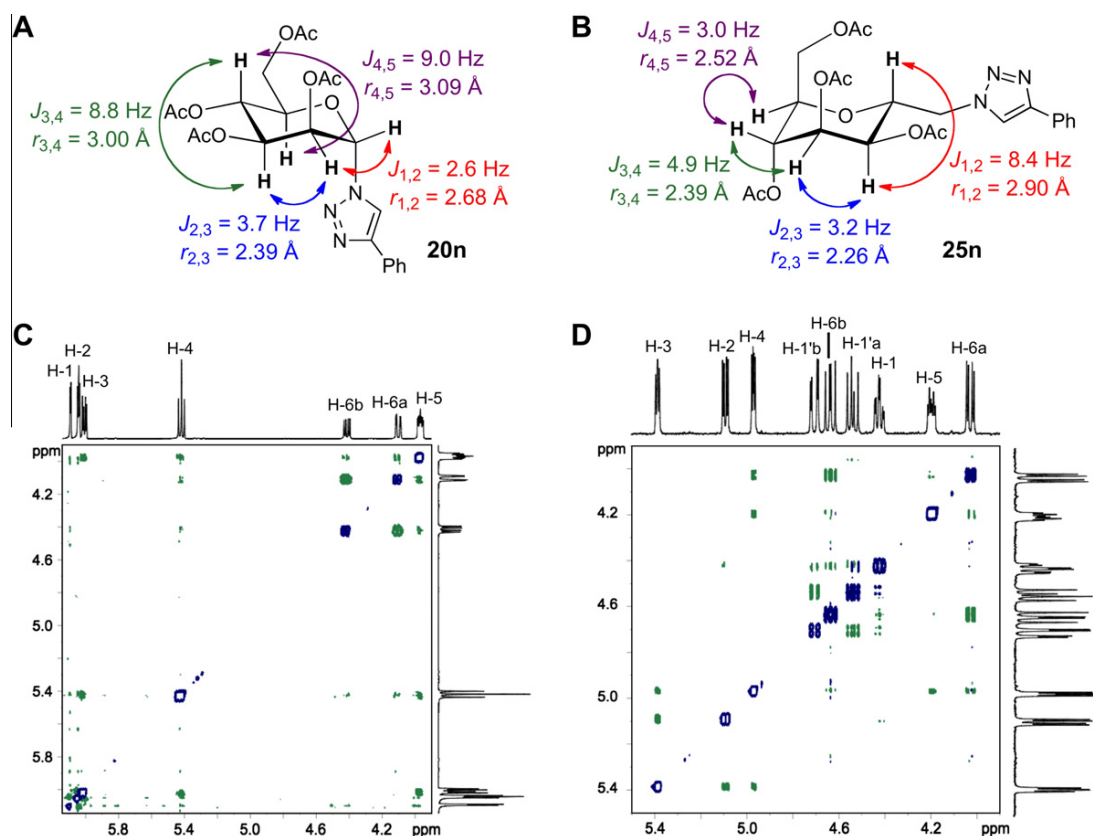


Figure 5. Coupling constants and proton-proton distances for peracetylated triazoles **20n** (A) and **25n** (B) determined by ^1H NMR and 2D-NOESY experiments; 2D-NOESY spectra of **20n** (C) and **25n** (D) in CDCl_3 with mixing times of 1.5 s (C) and 750 ms (D).

spectra (ESI-MS) were obtained on a Waters micromass ZQ. The HRMS analyses were carried out using a Bruker QTOF. Reactions were monitored by TLC using glass plates coated with silica gel 60 F₂₅₄ (Merck) and visualized by using UV light and/or by charring with a molybdate solution (a 0.02 M solution of ammonium cerium sulfate dihydrate and ammonium molybdate tetrahydrate in aqueous 10% H_2SO_4). MPLC separations were carried out on a Combi-Flash Companion from Teledyne Isco equipped with RediSep normal-phase or C₁₈ reversed-phase flash columns. Tetrahydrofuran (THF) was freshly distilled under argon over sodium and benzophenone. Methanol (MeOH) was dried by refluxing with sodium methoxide and distilled immediately before use. Dichloromethane (DCM), ethyl acetate (EtOAc), and toluene were dried by filtration over Al_2O_3 (Fluka, type 5016 A basic).

4.1.1. General procedure A for the synthesis of mannosyl triazoles **5d–i**

A mixture of acetylene **14**³⁷ (1.0 eq), azide **15d–i** (1.5 eq), $\text{CuSO}_4 \cdot 5\text{H}_2\text{O}$ (0.25 eq) and sodium ascorbate (0.5 eq) was dissolved in degassed *tert*-BuOH/ H_2O (1:1, 2 mL/0.1 mmol **14**) under argon. After stirring for 1 d the solvents were removed in vacuo and the crude product was first purified by MPLC on silica (DCM/MeOH) and then by reversed-phase chromatography (RP-18, H_2O /MeOH) to yield **5d–i** as colorless solids.

4.1.2. General procedure B for the synthesis of mannosyl triazoles **12a–c**, **16j–m** and **17h–k**

Acetylene **10**²⁹ or **13**³⁶ (1.0 eq) and azide **11a–c** or **15h–m** (1.5–2 eq) were dissolved in THF/*tert*-BuOH/ H_2O (1:1:1, 1.5 mL/0.1 mmol **10** or **11**). The mixture was degassed in an ultrasound bath under a flow of argon for 20 min. Then 0.5 M aq $\text{CuSO}_4 \cdot 5\text{H}_2\text{O}$

(0.25 eq) and 1 M aq sodium ascorbate (0.5 eq) were added under argon at rt. After stirring overnight the solvents were removed in vacuo and the crude product was purified by MPLC on silica (petrol ether/EtOAc) to yield **12a–c**, **16j–m** and **17h–k** as colorless oils.

4.1.3. General procedure C for the synthesis of mannosyl triazoles **20n–s** and **25n–s**

Azide **18**⁴² or **24** (1.0 eq) and acetylene **19n–s** (2.0 eq) were dissolved in THF/*tert*-BuOH/ H_2O (1:1:1, 3 mL/0.1 mmol **18** or **24**). The mixture was degassed in an ultrasound bath under a flow of argon for 20 min. Then 0.2 M aq $\text{CuSO}_4 \cdot 5\text{H}_2\text{O}$ (0.2 eq) and 1 M aq sodium ascorbate (0.4 eq) were added under argon at rt. After stirring for 1–2 d the solvents were removed in vacuo and the crude product was purified by MPLC on silica (petrol ether/EtOAc) to yield **20n–s** and **25n–s** as colorless oils.

4.1.4. General procedure D for deacetylation

To a solution of the acetylated compound (38–50 mg) in MeOH (3 mL) was added 1 M NaOMe/MeOH (0.3 mL). The mixture was stirred at rt for 3–6 h. The solution was concentrated and the residue was purified by MPLC on reversed phase (RP-18 column, H_2O /MeOH) and P2 size-exclusion chromatography to afford the target molecule as a colorless solid after a final lyophilization from water/dioxane.

4.1.5. Synthesis of azide **24**

4.1.5.1. (2,3,4,6-Tetra-O-acetyl- α -D-mannopyranosyl)-N-tert-butoxycarbonyl-methylamine (22**).** Cyanide **21**⁴³ (1.63 g, 4.57 mmol), Boc₂O (1.49 g, 6.86 mmol) and Pd/C (10%, 250 mg) were suspended in EtOAc (25 mL) and hydrogenated (4 bar H_2) at rt for 4 h. After filtration over Celite, fresh Pd/C (10%, 750 mg)

was added and the mixture was hydrogenated (4 bar H₂) for additional 17 h. The suspension was filtered over Celite and concentrated. The residue was purified by MPLC on silica (petrol ether/EtOAc) to give **22** (1.51 g, 72%) as a colorless solid.

¹H NMR (500 MHz, CDCl₃): δ 1.44 (s, 9H, C(CH₃)₃), 2.07, 2.10, 2.10 (3 s, 12H, 4 COCH₃), 3.38 (m, 2H, H-1'), 3.99–4.05 (m, 2H, H-1, H-5), 4.07 (dd, *J* = 3.8, 11.8 Hz, 1H, H-6a), 4.54 (dd, *J* = 6.9, 11.7 Hz, 1H, H-6b), 4.79 (m, 1H, NH), 5.07 (dd, *J* = 5.3, 6.4 Hz, 1H, H-4), 5.10 (dd, *J* = 3.3, 6.0 Hz, 1H, H-2), 5.26 (dd, *J* = 3.3, 6.5 Hz, 1H, H-3); ¹³C NMR (125 MHz, CDCl₃): δ 20.70, 20.73, 20.76, 20.81 (4 COCH₃), 28.3 (C(CH₃)₃), 39.7 (C-1'), 61.2 (C-6), 67.50, 67.51 (C-2, C-4), 68.0 (C-3), 71.1 (C-1), 72.2 (C-5), 79.7 (C(CH₃)₃), 155.8 (NCO), 169.5, 169.6, 169.9, 170.7 (4 COCH₃); ESI-MS Calcd for C₂₀H₃₁NNaO₁₁ [M+Na]⁺: 484.18, Found: 484.11.

4.1.5.2. *N*-tert-Butoxycarbonyl-(α -D-mannopyranosyl)methylamine (23**).** A solution of **22** (1.47 g, 3.19 mmol) in MeOH (20 mL) was treated with 1 M methanolic NaOMe (2 mL) under argon at rt for 3 h. The reaction mixture was neutralized with acetic acid and concentrated. The residue was purified by MPLC on silica (DCM/MeOH) to give **23** (925 mg, 99%) as a colorless solid.

¹H NMR (500 MHz, CD₃OD): δ 1.44 (s, 9H, C(CH₃)₃), 3.32 (m, 2H, H-1'), 3.54 (m, 1H, H-5), 3.63 (t, *J* = 7.6 Hz, 1H, H-4), 3.68 (dd, *J* = 3.1, 7.8 Hz, 1H, H-3), 3.74 (dd, *J* = 2.8, 11.8 Hz, 1H, H-6a), 3.77 (m, 1H, H-2), 3.79 (dd, *J* = 6.4, 11.8 Hz, 1H, H-6b), 3.86 (m, 1H, H-1), 6.72 (m, 1H, NH); ¹³C NMR (125 MHz, CD₃OD): δ 28.8 (C(CH₃)₃), 40.6 (C-1'), 62.7 (C-6), 69.6 (C-4), 70.2 (C-2), 72.7 (C-3), 76.9 (C-1), 77.4 (C-5), 80.2 (C(CH₃)₃), 158.6 (NCO); ESI-MS Calcd for C₁₂H₂₃NNaO₇ [M+Na]⁺: 316.14, Found: 316.03.

4.1.5.3. (2,3,4,6-Tetra-O-acetyl- α -D-mannopyranosyl)methylazide (24**).** *Triflyl azide stock solution preparation:*⁴⁴ Sodium azide (796 mg, 12.2 mmol) was dissolved in water (2 mL). Toluene (2 mL) was added, and the mixture was cooled to 0 °C with stirring. Then triflic anhydride (1.31 mL, 6.12 mmol) was added dropwise. The biphasic reaction mixture was stirred vigorously at 0 °C for 30 min and at 10 °C for another 2 h. The reaction mixture was neutralized with satd aq NaHCO₃. The phases were separated, and the aqueous phase extracted with toluene (2 × 2 mL). The organic layers were combined to give the triflyl azide stock solution. *Amine-azide exchange:* A solution of **23** (430 mg, 1.47 mmol) in dioxane/water (2:1, 15 mL) was treated with concentrated HCl (5 mL) under argon at rt for 4 h. The mixture was concentrated and the residue was dried in high vacuo. Then, the crude amine hydrochloride (341 mg), NaHCO₃ (492 mg, 5.86 mmol) and CuSO₄·5H₂O (14.1 mg, 61 μmol) were dissolved in water (1.91 mL). The triflyl azide stock solution (3.25 mL, 3.3 mmol) was added and the biphasic reaction mixture was made homogenous by the addition of MeOH (12.6 mL). The mixture was stirred at rt for 20 h. The solvents were removed in vacuo and the residue was taken up in dry pyridine (10 mL), and acetic anhydride (4 mL) was added. The reaction mixture was stirred at rt under argon for 4 h. The solvents were removed in vacuo and the crude product was purified by MPLC on silica (petrol ether/EtOAc) to yield **24** (459 mg, 81%) as a colorless oil.

IR (film) 2102 (vs, N₃), 1747 (vs, CO) cm⁻¹; ¹H NMR (500 MHz, CDCl₃): δ 2.04, 2.07, 2.08, 2.10 (4 s, 12H, 4 COCH₃), 3.29 (dd, *J* = 3.3, 13.4 Hz, 1H, H-1'a), 3.49 (dd, *J* = 7.3, 13.4 Hz, 1H, H-1'b), 4.05–4.09 (m, 2H, H-5, H-6a), 4.15 (dt, *J* = 3.2, 7.1 Hz, 1H, H-1), 4.60 (m, 1H, H-6b), 5.01 (dd, *J* = 4.4, 6.0 Hz, 1H, H-4), 5.14 (dd, *J* = 3.4, 6.9 Hz, 1H, H-2), 5.27 (dd, *J* = 3.4, 6.0 Hz, 1H, H-3); ¹³C NMR (125 MHz, CDCl₃): δ 20.61, 20.63, 20.65, 20.74 (4 COCH₃), 50.1 (C-1'), 60.8 (C-6), 67.0 (C-2), 67.5 (C-3), 67.6 (C-4), 70.5 (C-1), 72.9 (C-5), 169.3, 169.5, 169.6, 170.6 (4 COCH₃); ESI-MS Calcd for C₁₅H₂₁N₃NaO₉ [M+Na]⁺: 410.12, Found: 410.04.

4.1.6. Synthesis of peracetylated mannosyl triazoles

4.1.6.1. Methyl 4-[4-((2,3,4,6-tetra-O-acetyl- α -D-mannopyranosyloxy)methyl)-1H-1,2,3-triazol-1-yl]-benzoate (12a**).** Following general procedure B, **10** (40.0 mg, 0.103 mmol) was reacted with methyl 4-azidobenzoate (**11a**,³⁰ 36.5 mg, 0.206 mmol), 0.5 M CuSO₄ (52 μL, 26 μmol) and 1 M sodium ascorbate (52 μL, 52 μmol) to yield **12a** (55.8 mg, 96%).

[α]_D +45.0 (c 1.03, CHCl₃); IR (film) 1747 (vs, CO) cm⁻¹; ¹H NMR (500 MHz, CDCl₃): δ 1.99, 2.04, 2.12, 2.16 (4 s, 12H, 4 COCH₃), 3.97 (s, 3H, OMe), 4.10 (ddd, *J* = 2.2, 5.1, 9.5 Hz, 1H, H-5), 4.14 (dd, *J* = 2.3, 12.2 Hz, 1H, H-6a), 4.32 (dd, *J* = 5.2, 12.2 Hz, 1H, H-6b), 4.79, 4.95 (A, B of AB, *J* = 12.6 Hz, 2H, H-1'), 5.01 (d, *J* = 1.1 Hz, 1H, H-1), 5.28 (dd, *J* = 1.7, 3.1 Hz, 1H, H-2), 5.32 (t, *J* = 9.8 Hz, 1H, H-4), 5.36 (dd, *J* = 3.2, 10.0 Hz, 1H, H-3), 7.88 (AA' of AA'BB', *J* = 8.7 Hz, 2H, C₆H₄), 8.11 (s, 1H, C₂N₃H), 8.23 (BB' of AA'BB', *J* = 8.7 Hz, 2H, C₆H₄); ¹³C NMR (125 MHz, CDCl₃): δ 20.7, 20.8, 20.9 (4C, 4 COCH₃), 52.5 (OMe), 61.0 (C-1'), 62.4 (C-6), 66.0 (C-4), 68.8, 69.0, 69.4 (C-2, C-3, C-5), 97.0 (C-1), 120.0 (2C, C₆H₄), 121.0 (C₂N₃H-C5), 130.4 (C₆H₄-C1), 131.4 (2C, C₆H₄), 139.9 (C₆H₄-C4), 144.7 (C₂N₃H-C4), 169.7, 170.0, 170.1, 170.7 (5C, 5 CO); ESI-MS Calcd for C₂₅H₂₉N₃NaO₁₂ [M+Na]⁺: 586.02, Found: 586.16.

4.1.6.2. Ethyl 3-[4-((2,3,4,6-tetra-O-acetyl- α -D-mannopyranosyloxy)methyl)-1H-1,2,3-triazol-1-yl]-benzoate (12b**).** Following general procedure B, **10** (50.0 mg, 0.129 mmol) was reacted with ethyl 3-azidobenzoate (**11b**,³¹ 49.3 mg, 0.258 mmol), 0.5 M CuSO₄ (64 μL, 32 μmol) and 1 M sodium ascorbate (64 μL, 64 μmol) to yield **12b** (72.7 mg, 97%).

[α]_D +40.2 (c 1.04, CHCl₃); IR (film) 1749 (vs, CO) cm⁻¹; ¹H NMR (500 MHz, CDCl₃): δ 1.43 (t, *J* = 7.2 Hz, 1H, CH₃), 1.99, 2.04, 2.12, 2.16 (4 s, 12H, 4 COCH₃), 4.09–4.15 (m, 2H, H-5, H-6a), 4.32 (dd, *J* = 5.0, 12.1 Hz, 1H, H-6b), 4.44 (q, *J* = 7.2 Hz, 2H, OCH₂), 4.79, 4.95 (A, B of AB, *J* = 12.4 Hz, 2H, H-1'), 5.02 (d, *J* = 1.4 Hz, 1H, H-1), 5.28 (dd, *J* = 1.7, 3.2 Hz, 1H, H-2), 5.31 (m, 1H, H-4), 5.36 (dd, *J* = 3.3, 9.9 Hz, 1H, H-3), 7.64 (t, *J* = 8.0 Hz, 1H, C₆H₄-H5), 8.02 (ddd, *J* = 0.9, 2.1, 8.0 Hz, 1H, C₆H₄-H4), 8.11 (s, 1H, C₂N₃H), 8.14 (d, *J* = 7.9 Hz, 1H, C₆H₄-H6), 8.38 (t, *J* = 1.7 Hz, 1H, C₆H₄-H2); ¹³C NMR (125 MHz, CDCl₃): δ 14.3 (CH₃), 20.67, 20.69, 20.78, 20.88 (4 COCH₃), 60.9 (C-1'), 61.7 (OCH₂), 62.4 (C-6), 66.0 (C-4), 68.8 (C-3), 69.0 (C-5), 69.4 (C-2), 96.9 (C-1), 121.2 (C₆H₄), 121.3 (C₂N₃H-C5), 124.8, 129.9, 130.0, 132.3, 137.0 (C₆H₄), 144.5 (C₂N₃H-C4), 165.2, 169.7, 169.9, 170.1, 170.7 (5 CO); ESI-MS Calcd for C₂₆H₃₂N₃O₁₂ [M+H]⁺: 578.20, Found: 578.19.

4.1.6.3. Methyl 5-[4-((2,3,4,6-tetra-O-acetyl- α -D-mannopyranosyloxy)methyl)-1H-1,2,3-triazol-1-yl]-nicotinate (12c**).** Following general procedure B, **10** (40.0 mg, 0.103 mmol) was reacted with methyl 5-azidonicotinate (**11c**,³² 32.5 mg, 0.182 mmol), 0.5 M CuSO₄ (52 μL, 26 μmol) and 1 M sodium ascorbate (52 μL, 52 μmol). The crude product was dissolved in DCM (10 mL) and washed with 0.1 M aq EDTA (5 mL). The aqueous phase was extracted with DCM (2 × 10 mL) and the combined organic layers were dried with Na₂SO₄ and evaporated to dryness. The residue was purified by MPLC on silica (petrol ether/EtOAc) to give **12c** (42.4 mg, 73%).

[α]_D +39.7 (c 1.06, CHCl₃); IR (film) 1733 (vs, CO) cm⁻¹; ¹H NMR (500 MHz, CDCl₃): δ 1.98, 2.03, 2.11, 2.15 (4 s, 12H, 4 COCH₃), 4.01 (s, 3H, OCH₃), 4.09 (m, 1H, H-5), 4.14 (dd, *J* = 2.4, 12.2 Hz, 1H, H-6a), 4.31 (dd, *J* = 5.2, 12.3 Hz, 1H, H-6b), 4.79, 4.96 (A, B of AB, *J* = 12.5 Hz, 2H, H-1'), 5.01 (d, *J* = 1.4 Hz, 1H, H-1), 5.27 (dd, *J* = 1.7, 3.0 Hz, 1H, H-2), 5.30 (t, *J* = 9.8 Hz, 1H, H-4), 5.34 (dd, *J* = 3.3, 9.9 Hz, 1H, H-3), 8.17 (s, 1H, C₂N₃H), 8.69 (t, *J* = 2.0 Hz, 1H, C₅H₃N-H2), 9.27, 9.30 (2 s, 2H, C₅H₃N-H4, H6); ¹³C NMR (125 MHz, CDCl₃): δ 20.63, 20.65, 20.75, 20.84 (4 COCH₃), 52.9 (OMe), 60.8 (C-1'), 62.4 (C-6), 66.0 (C-4), 68.8, 68.9 (C-3, C-5), 69.3 (C-2), 97.0 (C-1), 121.2 (C₂N₃H-C5), 126.9, 128.6, 133.3

1H, H-6b), 4.24 (dt, $J = 5.1, 7.4$ Hz, 1H, H-1), 4.72–4.75 (m, 2H, H-1'), 7.24, 7.69 (AA', BB' of AA'BB', $J = 8.0$ Hz, 4H, C₆H₄), 8.40 (s, 1H, C₂N₃H); ¹³C NMR (125 MHz, CD₃OD): δ 21.3 (PhCH₃), 50.8 (C-1'), 62.0 (C-6), 69.1 (C-2), 69.9 (C-4), 72.4 (C-3), 75.0 (C-1), 78.4 (C-5), 123.0 (C₂N₃H-C5), 126.6, 128.9, 130.5, 139.3 (6C, C₆H₅), 148.9 (C₂N₃H-C4); HR-MS Calcd for C₁₆H₂₁NaN₃O₅ [M+Na]⁺: 358.1379, Found: 358.1380.

4.1.7.26. 4-(3-Chlorophenyl)-1-(α -D-mannopyranosyl)methyl-1,2,3-triazole (8p). Prepared from **25p** (40 mg, 77 μ mol) according to general procedure D. Yield: 23 mg, 83%.

$[\alpha]_D^{+31.5}$ (c 1.05, MeOH); ¹H NMR (500 MHz, CD₃OD): δ 3.73 (m, 1H, H-4), 3.74 (dd, $J = 3.0, 11.5$ Hz, 1H, H-6a), 3.79–3.82 (m, 2H, H-3, H-5), 3.83 (dd, $J = 3.4, 8.7$ Hz, 1H, H-2), 3.89 (dd, $J = 7.4, 11.6$ Hz, 1H, H-6b), 4.24 (dt, $J = 4.7, 7.9$ Hz, 1H, H-1), 4.73 (dd, $J = 8.0, 14.4$ Hz, 1H, H-1'a), 4.77 (dd, $J = 4.4, 14.5$ Hz, 1H, H-1'b), 7.33 (dd, $J = 0.9, 8.1$ Hz, 1H, C₆H₄-H6), 7.41 (t, $J = 7.9$ Hz, 1H, C₆H₄-H5), 7.74 (d, $J = 7.8$ Hz, 1H, C₆H₄-H4), 7.90 (t, $J = 1.6$ Hz, 1H, C₆H₄-H2), 8.51 (s, 1H, C₂N₃H); ¹³C NMR (125 MHz, CD₃OD): δ 50.9 (C-1'), 62.0 (C-6), 69.0 (C-2), 70.0 (C-4), 72.4 (C-3), 74.7 (C-1), 78.5 (C-5), 124.0 (C₂N₃H-C5), 124.9, 126.5, 129.1, 131.5, 133.9, 135.9 (6C, C₆H₄), 147.4 (C₂N₃H-C4); HR-MS Calcd for C₁₅H₁₈ClNaN₃O₅ [M+Na]⁺: 378.0833, Found: 378.0833.

4.1.7.27. 4-(4-Trifluoromethylphenyl)-1-(α -D-mannopyranosyl)methyl-1,2,3-triazole (8q). Prepared from **25q** (47 mg, 84 μ mol) according to general procedure D. Yield: 28 mg, 86%.

$[\alpha]_D^{+32.6}$ (c 1.03, MeOH); ¹H NMR (500 MHz, CD₃OD): δ 3.73–3.76 (m, 2H, H-4, H-6a), 3.81–3.86 (m, 3H, H-2, H-3, H-5), 3.89 (dd, $J = 7.5, 11.5$ Hz, 1H, H-6b), 4.25 (dt, $J = 4.8, 7.9$ Hz, 1H, H-1), 4.76 (dd, $J = 8.0, 14.5$ Hz, 1H, H-1'a), 4.79 (dd, $J = 4.4, 14.5$ Hz, 1H, H-1'b), 7.72, 8.01 (AA', BB' of AA'BB', $J = 8.2$ Hz, 4H, C₆H₄), 8.60 (s, 1H, C₂N₃H); ¹³C NMR (125 MHz, CD₃OD): δ 51.0 (C-1'), 62.0 (C-6), 69.0 (C-2), 70.0 (C-4), 72.4 (C-3), 74.7 (C-1), 78.6 (C-5), 124.5 (C₂N₃H-C5), 125.6 (q, $J = 271$ Hz, CF₃), 126.9 (q, $J = 3.7$ Hz, 2C, C₆H₄-C3, C5), 127.0 (2C, C₆H₄-C2, C6), 130.9 (q, $J = 32.4$ Hz, C₆H₄-C4), 135.7 (C₆H₄-C1), 147.2 (C₂N₃H-C4); HR-MS Calcd for C₁₆H₁₈F₃NaN₃O₅ [M+Na]⁺: 412.1096, Found: 412.1095.

4.1.7.28. 1-(α -D-Mannopyranosyl)methyl-4-(3-pyridyl)-1,2,3-triazole (8r). Prepared from **25r** (44 mg, 90 μ mol) according to general procedure D. Yield: 24 mg, 83%.

$[\alpha]_D^{+31.2}$ (c 0.99, MeOH); ¹H NMR (500 MHz, CD₃OD): δ 3.71–3.74 (m, 2H, H-4, H-6a), 3.80–3.83 (m, 3H, H-2, H-3, H-5), 3.89 (dd, $J = 7.7, 11.6$ Hz, 1H, H-6b), 4.23 (dt, $J = 4.6, 8.6$ Hz, 1H, H-1), 4.76 (dd, $J = 8.4, 14.4$ Hz, 1H, H-1'a), 4.80 (dd, $J = 4.2, 14.4$ Hz, 1H, H-1'b), 7.53 (dd, $J = 5.0, 7.9$ Hz, 1H, C₅H₄N-H5), 8.28 (d, $J = 8.0$ Hz, 1H, C₅H₄N-H6), 8.51 (d, $J = 4.8$ Hz, 1H, C₅H₄N-H4), 8.63 (s, 1H, C₂N₃H), 9.02 (s, 1H, C₅H₄N-H2); ¹³C NMR (125 MHz, CD₃OD): δ 48.1 (C-1'), 60.6 (C-6), 67.2 (C-2), 68.5 (C-4), 70.6 (C-3), 75.1 (C-1), 76.2 (C-5), 123.2 (C₂N₃H-C5), 124.5 (C₅H₄N-C5), 126.82 (C₅H₄N-C1), 134.3 (C₅H₄N-C6), 144.4 (C₂N₃H-C4), 145.7 (C₅H₄N-C2), 148.4 (C₅H₄N-C4); HR-MS Calcd for C₁₄H₁₈NaN₄O₅ [M+Na]⁺: 345.1175, Found: 345.1175.

4.1.7.29. 1-(α -D-Mannopyranosyl)methyl-4-phenoxyethyl-1,2,3-triazole (8s). Prepared from **25s** (41 mg, 79 μ mol) according to general procedure D. Yield: 23 mg, 83%.

$[\alpha]_D^{+22.8}$ (c 1.01, MeOH); ¹H NMR (500 MHz, CD₃OD): δ 3.69–3.76 (m, 3H, H-4, H-5, H-6a), 3.79–3.82 (m, 2H, H-2, H-3), 3.83 (dd, $J = 6.5, 11.5$ Hz, 1H, H-6b), 4.19 (dt, $J = 5.0, 7.0$ Hz, 1H, H-1), 4.69 (dd, $J = 7.5, 14.5$ Hz, 1H, H-1'a), 4.72 (dd, $J = 5.0, 14.5$ Hz, 1H, H-1'b), 5.15 (s, 2H, CH₂OPh), 6.94 (t, $J = 7.4$ Hz, 1H, C₆H₅-H4), 7.00 (d, $J = 8.1$ Hz, 2H, C₆H₅-H2, H6), 7.27 (m, 2H, C₆H₅-H3, H5), 8.17 (s, 1H, C₂N₃H); ¹³C NMR (125 MHz, CD₃OD): δ 50.9 (C-1'), 62.0 (C-6), 62.3 (CH₂OPh), 69.0 (C-2), 69.8 (C-4), 72.4 (C-3), 74.9 (C-1),

78.4 (C-5), 115.9 (2C, C₆H₅-C2, C6), 122.2 (C₆H₅-C4), 126.4 (C₂N₃H-C5), 130.5 (2C, C₆H₅-C3, C5), 145.0 (C₂N₃H-C4), 159.8 (C₆H₅-C1); HR-MS Calcd for C₁₆H₂₁N₃NaO₅ [M+Na]⁺: 374.1328, Found: 374.1328.

4.2. Biological evaluation

4.2.1. Competitive binding assay

A recombinant protein consisting of the CRD of FimH linked with a thrombin cleavage site to a 6His-tag (FimH-CRD-Th-6His) was expressed in *E. coli* strain HM125 and purified by affinity chromatography.⁴⁵ To determine the affinity of the various FimH antagonists, a competitive binding assay described previously⁴⁵ was applied. Microtiter plates (F96 MaxiSorp, Nunc) were coated with 100 μ L/well of a 10 μ g/mL solution of FimH-CRD-Th-6His in 20 mM HEPES, 150 mM NaCl and 1 mM CaCl₂, pH 7.4 (assay buffer) overnight at 4 °C. The coating solution was discarded and the wells were blocked with 150 μ L/well of 3% BSA in assay buffer for 2 h at 4 °C. After three washing steps with assay buffer (150 μ L/well), a four-fold serial dilution of the test compound (50 μ L/well) in assay buffer containing 5% DMSO and streptavidin-peroxidase coupled TM-PAA polymer (50 μ L/well of a 0.5 μ g/mL solution) were added. On each individual microtiter plate *n*-heptyl α -D-mannopyranoside (**1b**) was tested in parallel. The plates were incubated for 3 h at 25 °C and 350 rpm and then carefully washed four times with 150 μ L/well assay buffer. After the addition of 100 μ L/well of ABTS-substrate, the colorimetric reaction was allowed to develop for 4 min, then stopped by the addition of 2% aqueous oxalic acid before the optical density (OD) was measured at 415 nm on a microplate-reader (Spectramax 190, Molecular Devices, California, USA). The IC₅₀ values of the compounds tested in duplicates were calculated with prism software (GraphPad Software, Inc., La Jolla, USA). The IC₅₀ defines the molar concentration of the test compound that reduces the maximal specific binding of TM-PAA polymer to FimH-CRD by 50%. The relative IC₅₀ (rIC₅₀) is the ratio of the IC₅₀ of the test compound to the IC₅₀ of **1b**.

4.2.2. Aggregometry assay

The aggregometry assay was carried out as previously described.⁴⁶ In short, the percentage of aggregation of *E. coli* UTI89⁵⁹ (UTI89wt) with guinea pig erythrocytes (GPE) was quantitatively determined by measuring the optical density at 740 nm and 37 °C under stirring at 1000 rpm using an APACT 4004 aggregometer (Endotell AG, Allschwil, Switzerland). GPE were separated from guinea pig blood (Charles River Laboratories, Sulzfeld, Germany) using Histopaque (density of 1.077 g/mL at 24 °C, Sigma-Aldrich, Buchs, Switzerland). Prior to the measurements, the cell densities of *E. coli* and GPE were adjusted to an OD₆₀₀ of 4, corresponding to 1.9×10^8 CFU/mL and 2.2×10^6 cells/mL respectively. For the calibration of the instrument, the aggregation of protein poor plasma (PPP) using PBS alone was set as 100% and the aggregation of protein rich plasma (PRP) using GPE as 0%. After calibration, measurements were performed with 250 μ L GPE and 50 μ L bacterial suspension and the aggregation monitored over 600 s. After the aggregation phase of 600 s, 25 μ L of antagonist in PBS were added to each cuvette and disaggregation was monitored for 1400 s. UTI89 Δ *fimA-H* was used as negative control.

4.3. Determination of the pharmacokinetic parameters

4.3.1. Materials

Dimethyl sulfoxide (DMSO) and 1-octanol were purchased from Sigma-Aldrich (St. Louis MI, USA). PAMPA System Solution, GIT-0 Lipid Solution, and Acceptor Sink Buffer were ordered from plon (Woburn MA, USA). Acetonitrile (MeCN) was bought from Acros Organics (Geel, Belgium).

4.3.2. LC–MS measurements

Analyses were performed using an Agilent 1100/1200 Series HPLC System coupled to a 6410 Triple Quadrupole mass detector (Agilent Technologies, Inc., Santa Clara CA, USA) equipped with electrospray ionization. The system was controlled with the Agilent MassHunter Workstation Data Acquisition software (version B.01.04). The column used was an Atlantis[®] T3 C18 column (2.1 x 50 m) with a 3 µm particle size (Waters Corp., Milford MA, USA). The mobile phase consisted of two eluents: solvent A (H₂O, containing 0.1% formic acid, v/v) and solvent B (MeCN, containing 0.1% formic acid, v/v), both delivered at 0.6 mL/min. The gradient was ramped from 95% A/5% B to 5% A/95% B over 1 min, and then hold at 5% A/95% B for 0.1 min. The system was then brought back to 95% A/5% B, resulting in a total duration of 4 min. MS parameters such as fragmentor voltage, collision energy and polarity were optimized individually for each compound, and the molecular ion was followed for each compound in the multiple reaction monitoring mode. The concentrations of the analytes were quantified by the Agilent Mass Hunter Quantitative Analysis software (version B.01.04).

4.3.3. log *D*_{7.4} determination

The *in silico* prediction tool ALOGPS⁶⁰ was used to estimate the log *P* values. Depending on these values, the compounds were classified into three categories: hydrophilic compounds (log *P* below zero), moderately lipophilic compounds (log *P* between zero and one) and lipophilic compounds (log *P* above one). For each category, two different ratios (volume of 1-octanol to volume of buffer) were defined as experimental parameters:

Compound type	log <i>P</i>	Ratios (1-octanol:buffer)
Hydrophilic	<0	30:140, 40:130
Moderately lipophilic	0–1	70:110, 110:70
Lipophilic	>1	3:180, 4:180

Equal amounts of phosphate buffer (0.1 M, pH 7.4) and 1-octanol were mixed and shaken vigorously for 5 min to saturate the phases. The mixture was left until separation of the two phases occurred, and the buffer was retrieved. Stock solutions of the test compounds were diluted with buffer to a concentration of 1 µM. For each compound, six determinations, that is, three determinations per 1-octanol : buffer ratio, were performed in different wells of a 96-well plate. The respective volumes of buffer containing analyte (1 µM) were pipetted to the wells and covered by saturated 1-octanol according to the chosen volume ratio. The plate was sealed with aluminium foil, shaken (1350 rpm, 25 °C, 2 h) on a Heidolph Titramax 1000 plate-shaker (Heidolph Instruments GmbH & Co. KG, Schwabach, Germany) and centrifuged (2000 rpm, 25 °C, 5 min, 5804 R Eppendorf centrifuge, Hamburg, Germany). The aqueous phase was transferred to a 96-well plate for analysis by liquid chromatography-mass spectrometry (LC-MS).

log *D*_{7.4} was calculated from the 1-octanol : buffer ratio (o:b), the initial concentration of the analyte in buffer (1 µM), and the concentration of the analyte in buffer (c_B) with equilibration:

$$\log D_{7.4} = \left(\frac{1 \mu\text{M} - c_B}{c_B} \times \frac{1}{o : b} \right)$$

The average of the three log *D*_{7.4} values per 1-octanol:buffer ratio was calculated. If the two mean values obtained for a compound did not differ by more than 0.1 unit, the results were accepted.

4.3.4. Parallel artificial membrane permeation assay (PAMPA)

log *P*_e was determined in a 96-well format with the PAMPA⁵⁰ permeation assay. For each compound, measurements were

performed at three pH values (5.0, 6.2 and 7.4) in quadruplicates. For this purpose, 12 wells of a deep well plate, that is, four wells per pH-value, were filled with 650 µL PAMPA System Solution. Samples (150 µL) were withdrawn from each well to determine the blank spectra by UV-spectroscopy (SpectraMax 190, Molecular Devices, Silicon Valley Ca, USA). Then, analyte dissolved in DMSO was added to the remaining PAMPA System Solution to yield 50 µM solutions. To exclude precipitation, the optical density was measured at 650 nm, with 0.01 being the threshold value. Solutions exceeding this threshold were filtrated. Afterwards, samples (150 µL) were withdrawn to determine the reference spectra. Further 200 µL were transferred to each well of the donor plate of the PAMPA sandwich (plon, Woburn MA, USA, P/N 110 163). The filter membranes at the bottom of the acceptor plate were impregnated with 5 µL of GIT-0 Lipid Solution and 200 µL of Acceptor Sink Buffer were filled into each acceptor well. The sandwich was assembled, placed in the GutBox[™], and left undisturbed for 16 h. Then, it was disassembled and samples (150 µL) were transferred from each donor and acceptor well to UV-plates. Quantification was performed by both UV-spectroscopy and LC-MS. log *P*_e-values were calculated with the aid of the PAMPA Explorer Software (plon, version 3.5).

4.3.5. Thermodynamic solubility

Microanalysis tubes (Labo-Tech J. Stofer LTS AG, Muttensz, Switzerland) were charged with 1 mg of solid substance and 250 µL of phosphate buffer (50 mM, pH 6.5). The samples were briefly shaken by hand, then sonicated for 15 min and vigorously shaken (600 rpm, 25 °C, 2 h) on a Eppendorf Thermomixer comfort. Afterwards, the samples were left undisturbed for 24 h. After measuring the pH, the saturated solutions were filtered through a filtration plate (MultiScreen[®] HTS, Millipore, Billerica MA, USA) by centrifugation (1500 rpm, 25 °C, 3 min). Prior to concentration determination by LC-MS, the filtrates were diluted (1:1, 1:10 and 1:100 or, if the results were outside of the calibration range, 1:1000 and 1:10000). The calibration was based on six values ranging from 0.1 to 10 µg/mL.

Acknowledgement

We thank the Swiss National Science Foundation (project K-32KI-120904) for their support.

Supplementary data

Supplementary data (HRMS and HPLC data of target compounds 5–8) associated with this article can be found, in the online version, at doi:10.1016/j.bmc.2011.08.057.

References and notes

- Wiles, T. J.; Kulesus, R. R.; Mulvey, M. A. *Exp. Mol. Pathol.* **2008**, *85*, 11.
- Fihn, S. D. *N. Engl. J. Med.* **2003**, *349*, 259.
- Hooton, T. M. *Int. J. Antimicrob. Agents* **2001**, *17*, 259.
- Gouin, S. G.; Wellens, A.; Bouckaert, J.; Kovensky, J. *ChemMedChem* **2009**, *4*, 749.
- Rosen, D. A.; Hung, C. S.; Kline, K. A.; Hultgren, S. J. *Infect. Immun.* **2008**, *76*, 4290.
- Capitani, G.; Eidam, O.; Glockshuber, R.; Grutter, M. G. *Microbes Infect.* **2006**, *8*, 2284.
- Mulvey, M. A. *Cell Microbiol.* **2002**, *4*, 257.
- Choudhury, D.; Thompson, A.; Stojanoff, V.; Langermann, S.; Pinkner, J.; Hultgren, S. J.; Knight, S. D. *Science* **1999**, *285*, 1061.
- Bouckaert, J.; Berglund, J.; Schembri, M.; Genst, E. D.; Cools, L.; Wührer, M.; Hung, C. S.; Pinkner, J.; Slättergård, R.; Zavialov, A.; Choudhury, D.; Langermann, S.; Hultgren, S. J.; Wyns, L.; Klemm, P.; Oscarson, S.; Knight, S. D.; Greve, H. D. *Mol. Microbiol.* **2005**, *55*, 441.
- Wellens, A.; Garofalo, C.; Nguyen, H.; Van Gerven, N.; Slättergård, R.; Hernalsteens, J.-P.; Wyns, L.; Oscarson, S.; De Greve, H.; Hultgren, S.; Bouckaert, J. *PLoS ONE* **2008**, *3*, 4.

11. Han, Z.; Pinker, J. S.; Ford, B.; Obermann, R.; Nolan, W.; Wildman, S. A.; Hobbs, D.; Ellenberger, T.; Cusumano, C. K.; Hultgren, S. J.; Janetka, J. W. *J. Med. Chem.* **2010**, *53*, 4779.
12. Langermann, S.; Mollby, R.; Burlein, J. E.; Palaszynski, S. R.; Auguste, C. G.; DeFusco, A.; Strouse, R.; Schenerman, M. A.; Hultgren, S. J.; Pinkner, J. S.; Winberg, J.; Guldevall, L.; Soderhall, M.; Ishikawa, K.; Normark, S.; Koenig, S. *J. Infect. Dis.* **2000**, *181*, 774.
13. Langermann, S.; Palaszynski, S.; Barnhart, M.; Auguste, G.; Pinkner, J. S.; Burlein, J.; Barren, P.; Koenig, S.; Leath, S.; Jones, C. H.; Hultgren, S. *J. Science* **1997**, *276*, 607.
14. Bouckaert, J.; Mackenzie, J.; de Paz, J. L.; Chipwaza, B.; Choudhury, D.; Zavalov, A.; Mannerstedt, K.; Anderson, J.; Pierard, D.; Wyns, L.; Seeberger, P. H.; Oscarson, S.; De Greve, H.; Knight, S. D. *Mol. Microbiol.* **2006**, *61*, 1556.
15. (a) Sharon, N. *Biochim. Biophys. Acta* **2006**, *1760*, 527; (b) Ofek, I.; Hasty, D. L.; Sharon, N. *FEMS Immun. Med. Microbiol.* **2003**, *38*, 181; (c) Sharon, N.; Ofek, I. In *Protein-Carbohydrate Interactions in Infectious Diseases*; Bewley, C. A., Ed.; RSC Biomolecular Sciences: Cambridge, UK, 2006; pp 49–72.
16. (a) Firon, N.; Ofek, I.; Sharon, N. *Biochem. Biophys. Res. Commun.* **1982**, *105*, 1426; (b) Firon, N.; Ofek, I.; Sharon, N. *Carbohydr. Res.* **1983**, *120*, 235; (c) Sharon, N. *FEBS Lett.* **1987**, *217*, 145.
17. (a) Neeser, J.-R.; Koellreutter, B.; Wuersch, P. *Infect. Immun.* **1986**, *52*, 428; (b) Lindhorst, T. K. *Top. Curr. Chem.* **2002**, *218*, 201. review; (c) Patel, A.; Lindhorst, T. K. *Carbohydr. Res.* **2006**, *341*, 1657; (d) Nagahori, N.; Lee, R. T.; Nishimura, S.-L.; Pagé, S.; Roy, R.; Lee, Y. C. *ChemBioChem* **2002**, *3*, 836; (e) Appeldoorn, C. C. M.; Joosten, J. A. F.; Maate, F. A.; Dobrindt, U.; Hacker, J.; Liskamp, R. M. J.; Khan, A. S.; Pieters, R. *J. Tetrahedron: Asymmetry* **2005**, *16*, 361; (f) Touaibia, M.; Wellens, A.; Shiao, T. C.; Wang, Q.; Sirois, S.; Bouckaert, J.; Roy, R. *ChemMedChem* **2007**, *2*, 1190.
18. (a) Firon, N.; Ashkenazi, S.; Mirelman, D.; Ofek, I.; Sharon, N. *Infect. Immun.* **1987**, *55*, 472; (b) Lindhorst, T. K.; Kötter, S.; Kubisch, J.; Krallmann-Wenzel, U.; Ehlers, S.; Kren, V. *Eur. J. Org. Chem.* **1998**, 1669; (c) Sperling, O.; Fuchs, A.; Lindhorst, T. K. *Org. Biomol. Chem.* **2006**, *4*, 3913; (d) Berglund, J.; Bouckaert, J.; De Greve, H.; Knight, S. PCT/US 2005/089733, 2005.
19. Klein, T.; Abgottspon, D.; Wittwer, M.; Rabbani, S.; Herold, J.; Jiang, X.; Kleeb, S.; Lüthi, C.; Scharenberg, M.; Bezençon, J.; Gubler, E.; Pang, L.; Smiesko, M.; Cutting, B.; Schwardt, O.; Ernst, B. *J. Med. Chem.* **2010**, *53*, 8627.
20. Hung, C. S.; Bouckaert, J.; Hung, D.; Pinkner, J.; Widberg, C.; Defusco, A.; Auguste, C. G.; Strouse, R.; Langermann, S.; Waksman, G.; Hultgren, S. *J. Mol. Microbiol.* **2002**, *44*, 903.
21. Ernst, B.; Magnani, J. L. *Nat. Rev. Drug Disc.* **2009**, *8*, 661.
22. Becke, A. D. *J. Chem. Phys.* **1993**, *98*, 5648.
23. Stephens, P. J.; Devlin, F. J.; Chabalowski, C. F.; Frisch, M. J. *J. Phys. Chem.* **1994**, *98*, 11623.
24. Frisch, M. J.; Trucks, G. W.; Schlegel, H. B.; Scuseria, G. E.; Robb, M. A.; Cheeseman, J. R.; Montgomery, J., Jr.; Vreven, T.; Kudin, T. K. N.; Burant, J. C. et al. *Gaussian 2003*, Gaussian Inc: Pittsburgh, PA, 2003.
25. Sancho-García, J. C.; Cornil, J. *J. Chem. Theory Comput.* **2005**, *1*, 581.
26. *Glide*, version 5.5; Schrödinger, LLC: New York, NY, 2009.
27. *Desmond Molecular Dynamics System*, version 2.2; D. E. Shaw Research: New York, NY, 2009.
28. Humphrey, W.; Dalke, A.; Schulten, K. *J. Mol. Graphics* **1996**, *14*, 33.
29. Kaufman, R. J.; Sidhu, R. S. *J. Org. Chem.* **1982**, *47*, 4941.
30. (a) Lamara, K.; Smalley, R. K. *Tetrahedron* **1991**, *47*, 2277; (b) Li, Y.; Gao, L.-X.; Han, F.-S. *Chem. Eur. J.* **2010**, *16*, 7969.
31. Hu, M.; Li, J.; Yao, S. Q. *Org. Lett.* **2008**, *10*, 5529.
32. (a) Sawanishi, H.; Tajima, K.; Tsuchiya, T. *Chem. Pharm. Bull.* **1987**, *35*, 4101; (b) Sapountzis, I.; Ettmayer, P.; Klein, C.; Mantoulidis, A.; Steegmaier, M.; Steurer, S.; Waizenegger, I. PCT/EP2008/058432, 2008.
33. (a) Tornøe, C. W.; Meldal, M. In *Peptides: The Wave of the Future: Proceedings of the Second International and the Seventeenth American Peptide Symposium*; Lebl, M., Houghten, R. A., Eds.; Springer, 2001; p 263; (b) Tornøe, C. W.; Christensen, C.; Meldal, M. *J. Org. Chem.* **2002**, *67*, 3057.
34. Kolb, H. C.; Sharpless, K. B. *Angew. Chem., Int. Ed.* **2001**, *40*, 2004.
35. Palomo, C.; Aizpurua, J. M.; Balentová, E.; Azcune, I.; Santos, J. I.; Jiménez-Barbero, J.; Cañada, J.; Miranda, J. I. *Org. Lett.* **2008**, *10*, 2227.
36. (a) Tietze, L.; Bothe, U. *Chem. Eur. J.* **1998**, *4*, 1179; (b) Gouin, S. G.; Vanquelef, E.; García Fernández, J. M.; Ortiz Mellet, C.; Dupradeau, F.-Y.; Kovensky, J. *J. Org. Chem.* **2007**, *72*, 9032.
37. Fernández-Megía, E.; Correa, J.; Rodríguez-Meizoso, I.; Riguera, R. *Macromolecules* **2006**, *39*, 2113.
38. Buckle, D. R.; Rockell, C. J. M. *J. Chem. Soc., Perkin Trans. 1* **1982**, 627.
39. Stefely, J. A.; Palchadhuri, R.; Miller, P. A.; Peterson, R. J.; Moraski, G. C.; Hergenrother, P. J.; Miller, M. J. *J. Med. Chem.* **2010**, *53*, 3389.
40. Benati, L.; Bencivenni, G.; Leardini, R.; Minozzi, M.; Nanni, D.; Scialpi, R.; Spagnolo, P.; Zanardi, G. *J. Org. Chem.* **2006**, *71*, 5822.
41. Ito, S.; Satoh, A.; Nagatomi, Y.; Hirata, Y.; Suzuki, G.; Kimura, T.; Satow, A.; Maehara, S.; Hikichi, H.; Hata, M.; Kawamoto, H.; Ohta, H. *Bioorg. Med. Chem.* **2008**, *16*, 9817.
42. (a) Kunz, H.; Pfrengle, W.; Rück, K.; Sager, W. *Synthesis* **1991**, *103*, 1039; (b) Györgydeak, Z.; Szilágyi, L.; Paulsen, H. *J. Carbohydr. Chem.* **1993**, *12*, 139.
43. (a) Myers, R. W.; Lee, Y. C. *Carbohydr. Res.* **1986**, *154*, 145; (b) Köll, P.; Förttsch, A. *Carbohydr. Res.* **1987**, *171*, 301.
44. Titz, A.; Radic, Z.; Schwardt, O.; Ernst, B. *Tetrahedron Lett.* **2006**, *47*, 2383.
45. Rabbani, S.; Jiang, X.; Schwardt, O.; Ernst, B. *Anal. Biochem.* **2010**, *407*, 188.
46. Abgottspon, D.; Rölli, G.; Hosch, L.; Steinhuber, A.; Jiang, X.; Schwardt, O.; Cutting, B.; Smiesko, M.; Jenal, U.; Ernst, B.; Trampuz, A. *J. Microbiol. Methods* **2010**, *82*, 249.
47. Giampapa, C. S.; Abraham, S. N.; Chiang, T. M.; Beachey, E. H. *J. Biol. Chem.* **1988**, *263*, 5362.
48. Aprikian, P.; Tchesnokova, V.; Kidd, B.; Yakovenko, O.; Yarov-Yarovoy, V.; Trinchina, E.; Vogel, V.; Thomas, W.; Sokurenko, E. *J. Biol. Chem.* **2007**, *282*, 23437.
49. Trong, I. L.; Aprikian, P.; Kidd, B. A.; Forero-Shelton, M.; Tchesnokova, V.; Rajagopal, P.; Rodriguez, V.; Interlandi, G.; Klevit, R.; Vogel, V.; Stenkamp, R. E.; Sokurenko, E. V.; Thomas, W. *E. Cell* **2010**, *141*, 645.
50. Kansy, M.; Senner, F.; Gubernator, K. *J. Med. Chem.* **1998**, *41*, 1007.
51. Dearden, J. C.; Bresnen, J. G. M. *QSAR Comb. Sci.* **1988**, *7*, 133.
52. Kerns, E. H. *J. Pharm. Sci.* **2001**, *90*, 1838.
53. Poulain, F.; Serre, A.-L.; Lalot, J.; Leclerc, E.; Quirion, J.-C. *J. Org. Chem.* **2008**, *73*, 2435.
54. Kessler, H.; Gehrke, M.; Griesinger, C. *Angew. Chem.* **1988**, *100*, 507; *Angew. Chem. Int. Ed.* **1988**, *27*, 490.
55. Reid, B. R.; Banks, K.; Flynn, P.; Nerdalt, W. *Biochemistry* **1989**, *28*, 10001.
56. Szilágyi, L.; Forgó, P. *Carbohydr. Res.* **1993**, *247*, 129.
57. Varma, M. V. S.; Feng, B.; Obach, R. S.; Troutman, M. D.; Chupka, J.; Miller, H. R.; El-Kattan, A. *J. Med. Chem.* **2009**, *52*, 4844.
58. Avdeef, A.; Bendels, S.; Di, L.; Faller, B.; Kansy, M.; Sugano, K.; Yamauchi, Y. *J. Pharm. Sci.* **2007**, *96*, 2893.
59. Mulvey, M. A.; Schilling, J. D.; Hultgren, S. *J. Infect. Immun.* **2001**, *69*, 4572.
60. VCCLAB, Virtual Computational Chemistry Laboratory, <http://www.vcclab.org>, 2005.; (b) Tetko, I. V.; Gasteiger, J.; Todeschini, R.; Mauri, A.; Livingstone, D.; Ertl, P.; Palyulin, V. A.; Radchenko, E. V.; Zefirov, N. S.; Makarenko, A. S.; Tanchuk, V. Y.; Prokopenko, V. V. *J. Comput. Aid. Mol. Des.* **2005**, *19*, 453.

3 Summary and outlook

The goal of the present thesis was the physicochemical and pharmacokinetic characterization of carbohydrate mimetics within the development process of a highly potent, orally available FimH antagonist. For this purpose, various *in vitro* assays predictive for drug absorption, distribution, metabolism, and excretion (ADME) were established. Procedures for the determination of the aqueous solubility, the octanol-water distribution coefficient, and the acid dissociation constant were implemented in order to elucidate the physicochemical determinants of the ADME properties. The parallel artificial membrane permeability assay and the Caco-2 cell monolayer model were used for predicting the permeation through the membranes lining the small intestine by passive diffusion or carrier mediated transport. The Caco-2 model was moreover used for elucidating the enzyme-mediated bioactivation of phosphate ester prodrugs. Plasma protein binding – a determinant of compound distribution and elimination – was assessed by an equilibrium dialysis experiment. The metabolic stability assay using liver microsomes or plasma was established for estimating a compound's propensity to cytochrome P450-mediated metabolism and for assessing the esterase-mediated bioactivation of ester prodrugs. The various *in vitro* assays were integrated into a flowchart (see Figure 3.1) that we used as a guideline for the optimization of our FimH antagonists towards oral bioavailability and sustained renal excretion as the major route of drug elimination.

Starting from the highly soluble but poorly permeable biphenyl α -D-mannopyranoside with a *para*-carboxylate on the terminal aromatic ring of the aglycone, we optimized the physicochemical and pharmacokinetic properties following various strategies.

An ester prodrug approach proved successful for masking the polar carboxylate and, hence, for increasing the membrane permeability. Preliminary results *in vitro* and *in vivo* suggested that the methyl ester was advantageous for intestinal absorption and rapid bioactivation by hepatic esterases. However, the aqueous solubility of the ester prodrug was in the low $\mu\text{g/mL}$ range. Since low solubility constrains the oral absorption potential, further optimization of the alkyl promoiety was required.

Alkyl promoiety functionalized with oxygenated and nitrogenated substituents were shown to effectively shield the polar carboxylate and to confer higher aqueous solubility than the methyl ester. Consequently, higher oral doses should be dissolvable in the intestinal fluids, which enhances the concentration gradient across the intestinal mucosa and supports the

absorptive flux. We furthermore observed that the alkoxyethyl esters were recognized by the carboxylesterase expressed in hepatocytes while the aminoethyl esters were rapidly cleaved by the plasma-borne butyrylcholinesterase. Indeed, bioactivation by plasma-borne enzymes implies immediate availability of the active principle in the bloodstream and low non-renal clearance by phase II metabolic reactions and hepatobiliary excretion.

Disruption of the molecular planarity and symmetry of the biphenyl mannoside by modifying the substitution pattern was considered as an alternative strategy for optimizing the physicochemical profile of the methyl ester. With this approach, solubility and membrane permeability in the range for high oral absorption was achieved. However, shifting the substituents markedly decreased the affinity to the FimH-CRD, overriding the gain in the intestinal uptake potential. Furthermore, the introduction of triazole, pyrazole or six-membered aromatic heterocycles proved beneficial to the aqueous solubility but in turn drastically reduced the membrane permeability. By contrast, the phenyl-*IH*-pyrrole aglycone conferred markedly higher aqueous solubility than the biphenyl analogue and similarly high permeability, suggesting an improvement in systemic availability of the prodrugs upon oral administration. Surprisingly, those compounds containing a phenyl-*IH*-pyrrole aglycone showed high microsomal stability and therefore do not act as prodrugs but are renally excreted unchanged.

While exploring the substitution pattern on the aromatic ring adjacent to the anomeric oxygen, we realized that chloro, methyl, or trifluoromethyl substituents in the *ortho*-position – they are advantageous for the binding to the FimH-CRD – increased the lipophilicity of the biphenyl mannoside and consequently the membrane permeability. They otherwise had negligible effects on the low aqueous solubility, namely of the methyl ester prodrug. Nonetheless, we identified these substituents as a useful tool for optimizing the absorption potential of hydrophilic, highly soluble biaryl mannosides.

While modifying the substitution pattern on the terminal ring of the biphenyl aglycone following the *Topliss* operational scheme, we recognized further effects of the substituents' nature and position on aqueous solubility, lipophilicity, and membrane permeability. Indeed, only a few biphenyl derivatives (*o*-methyl, *o*-methoxy, *m*- & *p*-cyano, and *p*-nitro) showed aqueous solubility above the critical limit of 50 µg/ml. Nevertheless, all of these compounds exhibited substantial permeability, which, in combination with high aqueous solubility, suggests high systemic availability upon oral dosing.

With a series of bioisosteres, *i.e.* alternative electron-withdrawing substituents on the terminal aromatic ring of the biphenyl aglycone, a substantial improvement of the affinity and the relevant pharmacokinetic parameters (solubility, permeability, renal excretion) could be achieved. With 3'-chloro-4'-(α -D-mannopyranosyloxy)biphenyl-4-carbonitrile, a FimH antagonist with an optimal *in vitro* PK/PD profile was identified. The *para*-cyano substituent conferred lipophilicity and high binding to plasma proteins, which slowed the rate of renal excretion. Despite higher lipophilicity, the antagonist was unsusceptible to CYP450-mediated metabolism and therefore predominantly eliminated via the renal pathway. *In vivo* experiments in a mouse model confirmed the excellent PK profile.

Further bioisosteres, *e.g.* the *para*-methylsulfone substituent, proved promising regarding affinity and their propensity to renal excretion but were – unlike the *para*-cyano analogue – too polar for oral absorption. Nonetheless, the introduction of acyl promoieties in the C-6 position of the mannoside turned out successful for addressing low lipophilicity and permeability. Hydrolysis by the carboxylesterase isozyme expressed in the enterocytes (hCE2) was identified as primary mechanism of bioactivation. This might be unfavorable for the intestinal uptake since hydrolysis within the enterocytes yields the polar active principle supposed as likely to be effluxed back into the gut lumen as it is to proceed into the portal blood. The half-life should therefore be long enough to enable the majority of the prodrug to be absorbed in unchanged form. For proving the benefits of the prodrug approach on oral bioavailability and for assessing whether the intestinal uptake is affected by concomitant hydrolysis, *in vivo* pharmacokinetic studies in a mouse model shall be performed in a further step.

We further focused our efforts on a phosphate prodrug strategy to optimize the physicochemical profile of indolinyphenyl and biphenyl mannosides. Indeed, the introduction of a phosphate promoiety proved advantageous for improving the otherwise low aqueous solubility of the parent compound. In a Caco-2 cell model, the phosphate esters displayed susceptibility to hydrolysis mediated by the alkaline phosphatase on the apical brush border membrane. Rapid bioconversion was shown to provide a high concentration gradient of the mannoside antagonists across the cell monolayer, promoting the absorptive flux and saturating the apparent efflux carrier activity. *In vivo* experiments in a mouse model showing high oral availability and sustained renal excretion of the antagonists confirmed the excellent profile of the phosphate prodrugs.

In summary, the physicochemical and pharmacokinetic characterization has become a vital tool for the development of carbohydrate mimetics towards oral bioavailability and sustained renal excretion as main route of drug elimination. As a result of our thorough studies, two approaches were identified as most advantageous for the design of orally available FimH antagonists: first the prodrug approach, *i.e.* the introduction of heteroalkyl or phosphate promoieties, and second the replacement of the *para*-carboxylate on the terminal ring of the biphenyl aglycone with bioisosteres, such as the cyano substituent.

Given our impressive progress in improving the oral absorption, the focus shall now be moved to renal excretion, which is the second crucial step in the FimH antagonist's delivery to the therapeutic target in the urinary bladder. This task requires a deepened understanding of the compound secretion and reuptake mechanisms in the renal tubules. *In vitro* assays focusing on passive permeation and carrier-mediated transport through the tubular membranes shall therefore be established.¹⁴ Moreover, the metabolic stability assay implemented in our laboratory suggests a high stability of the most active biaryl α -D-mannopyranosides against cytochrome P450-mediated metabolism. Establishing more advanced *in vitro* models considering Phase II metabolic reactions and the identification of metabolic soft spots will nonetheless be an important task.¹⁵ The toxicity of the carbohydrate mimetics will be a further field of interest. An MTT assay¹⁶ for screening the cytotoxicity has already been implemented in our laboratory and is regularly performed for validating the outcome of cell-based assays (*e.g.* activity assay, cell monolayer permeation assays). Further assays focusing on the cardiotoxicity (*i.e.* screening for hERG K⁺ channel blocking¹⁷) or the mutagenicity (*e.g.* Ames test¹⁸) will provide a deeper insight into the toxic potential of the carbohydrate mimetics.

This thorough ADMET characterization will finally support the further development of the biaryl α -D-mannopyranosides towards a marketed drug for the prevention and treatment of urinary tract infection.

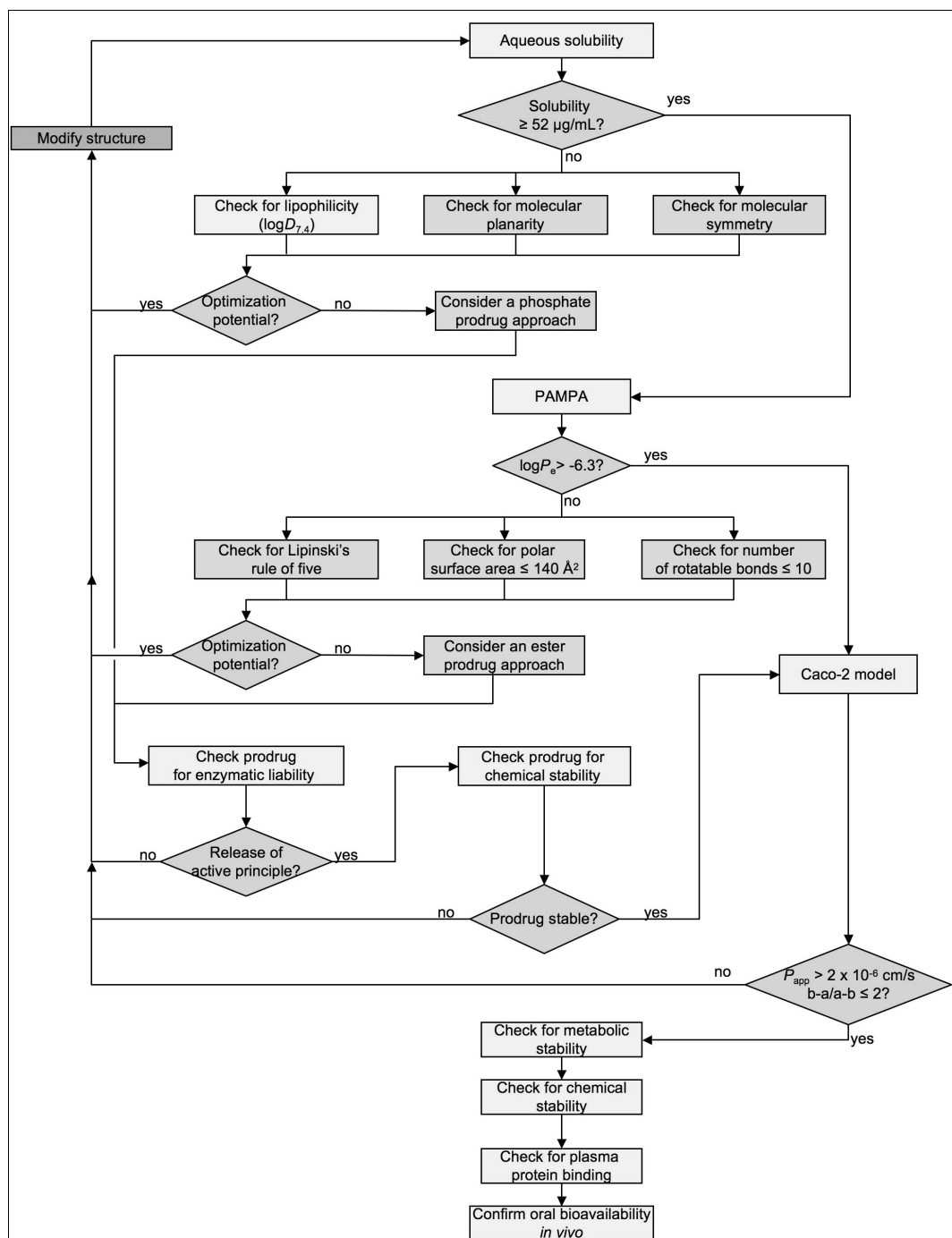


Figure 3.1. Flowchart guiding the optimization of the FimH antagonists towards oral bioavailability and sustained renal excretion as major route of drug elimination. The scheme includes assays for determining the aqueous solubility and the octanol-water distribution coefficient ($\log D_{7.4}$), the artificial membrane permeability assay (PAMPA), the Caco-2 cell monolayer model, an equilibrium dialysis experiment for determining plasma protein binding, and the metabolic stability assay using microsomal preparations or plasma.¹⁻⁷ The strategies for increasing the aqueous solubility (*i.e.* disruption of molecular planarity and symmetry) are according to the study by Ishikawa *et al.*⁸ The strategies for increasing the permeability are based on the seminal publications by Lipinski *et al.* and Veber *et al.*^{9, 10} The minimum solubility criteria are based on the maximum absorbable dose (MAD) concept introduced by Johnson and Swindell.¹¹ The effective permeability ($\log P_e$) criteria were adopted from Avdeef *et al.* and the apparent permeability criteria (P_{app}) from Kerns *et al.*^{12, 13}

REFERENCES

1. Avdeef, A. High-throughput measurements of solubility profiles. In *Pharmacokinetic Optimization in Drug Research; Biological, Physicochemical and Computational Strategies*, Testa, B.; Van de Waterbeemd, H.; Folkers, G.; Guy, R. Eds. Helvetica Chimica Acta, Zurich **2001**, 305-326.
2. Dearden, J. C.; Bresnen, G. M. The measurement of partition coefficients. *QSAR Comb. Sci.* **1988**, *7*, 133-144.
3. Kansy, M.; Senner, F.; Gubernator, K. Physicochemical high throughput screening: parallel artificial membrane permeation assay in the description of passive absorption processes. *J. Med. Chem.* **1998**, *41*, 1007-1010.
4. Artursson, P.; Karlsson, J. Correlation between oral drug absorption in humans and apparent drug permeability coefficients in human intestinal epithelial (Caco-2) cells. *Biochem. Biophys. Res. Commun.* **1991**, *175*, 880-885.
5. Banker, M. J.; Clark, T. H.; Williams, J. A. Development and validation of a 96-well equilibrium dialysis apparatus for measuring plasma protein binding. *J. Pharm. Sci.* **2003**, *92*, 967-974.
6. Obach, R. Prediction of human clearance of twenty-nine drugs from hepatic microsomal intrinsic clearance data: An examination of in vitro half-life approach and nonspecific binding to microsomes. *Drug Metab. Dispos.* **1999**, *27*, 1350-1359.
7. Di, L.; Kerns, E. H.; Hong, Y.; Chen, H. Development and application of high throughput plasma stability assay for drug discovery. *Int. J. Pharm.* **2005**, *297*, 110-119.
8. Ishikawa, M.; Hashimoto, Y. Improvement in aqueous solubility in small molecule drug discovery programs by disruption of molecular planarity and symmetry. *J. Med. Chem.* **2011**, *54*, 1539-54.
9. Lipinski, C. A.; Lombardo, F.; Dominy, B. W.; Feeney, P. J. Experimental and computational approaches to estimate solubility and permeability in drug discovery and development settings. *Adv. Drug Deliv. Rev.* **2001**, *46*, 3-26.
10. Veber, D. V.; Johnson, S. R.; Cheng, H. Y.; Smith, B. R.; Ward, K. W.; Kopple, K. D. Molecular properties that influence the oral bioavailability of drug candidates. *J. Med. Chem.* **2002**, *45*, 2615-2623.
11. Johnson, K. C.; Swindell, A. C. Guidance in the setting of drug particle size specifications to minimize variability in absorption. *Pharm. Res.* **1996**, *13*, 1795-1798.
12. Avdeef, A.; Bendels, S.; Di, L.; Faller, B.; Kansy, M.; Sugano, K.; Yamauchi, Y. PAMPA – critical factors for better predictions of absorption. *J. Pharm. Sci.* **2007**, *96*, 2893-2909.
13. Kerns, E. H.; Di, L. *Drug-like-properties: concepts, structure design and methods: from ADME to toxicity optimization*. Academic Press, Amsterdam, London **2008**, 287-310.
14. Giacomini, K. M.; Huang, S. M.; Tweedie, D. J.; Benet, L. Z.; Brouwer, K. L.; Chu, X.; Dahlin, A.; Evers, R.; Fischer, V.; Hillgren, K. M.; Hoffmaster, K. A.; Ishikawa, T.; Keppler, D.; Kim, R. B.; Lee, C. A.; Niemi, M.; Polli, J. W.; Sugiyama, Y.; Swaan, P. W.; Ware, J. A.; Wright, S. H.; Yee, S. W.; Zamek-Gliszczynski, M. J.; Zhang, L. Membrane transporters in drug development. *Nat. Rev. Drug Discov.* **2010**, *9*, 215-236.
15. Lin, J. H.; Rodrigues, A. D. *In vitro* models for early studies of drug metabolism. In *Pharmacokinetic Optimization in Drug Research; Biological, Physicochemical and Computational Strategies*, Testa, B.; Van de Waterbeemd, H.; Folkers, G.; Guy, R. Eds. Helvetica Chimica Acta, Zurich **2001**, 217-243.
16. Rapid colorimetric assay for cellular growth and survival: application to proliferation and cytotoxicity assays. *J. Immunol. Methods.* **1983**, *65*, 55-63.
17. Netzer, R.; Ebnet, A.; Bischoff, U.; Pongs, O. Screening lead compounds for QT interval prolongation. *Drug Discov. Today* **2001**, *6*, 78-84.

18. Ames, B. N.; McCann, J.; Yamasaki, E. Methods for detecting carcinogens and mutagens with the Salmonella/mammalian-microsome mutagenicity test. *Mutat. Res.* **1975**, *31*, 347-364.

